2-Day Workshop on

Fundamental Issues and Future Research Directions for Parallel Mechanisms and Manipulators

October 2-4, 2002,
Quebec City, Quebec, Canada

Organized by

UNIVERSITÉ LAVAL

Georgia Institute of Technology

Sponsored by

Recherche, Science et Technologie Québec

National Science Foundation

WORKSHOP ON FUNDAMENTAL ISSUES & FUTURE RESEARCH DIRECTIONS FOR PARALLEL MECHANISMS & MANIPULATORS

PREFACE

This workshop is bringing together experts in the area of parallel manipulators from around the globe for two days in order to disseminate recent research progress and to identify the most promising future research directions for parallel manipulators. This meeting is not a routine conference, wherein the primary responsibility of the participant is to present his or her paper. Instead, the purpose of this workshop is to create **significant opportunity for dialog** between the participants.

Therefore the workshop contains not only focused keynote presentations, an industrial panel, an educational panel and a poster session on white papers, but also focused paper sessions of a fairly unusual format: Each presenter serves not only as a speaker, but also as a panelist. Specifically, 20 minutes are reserved for each speaker, but they are used as follows:

1. Each regular paper session starts with 10-minute presentations by all speakers back-to-back, with only 1-2 minutes in between for immediate questions.
2. The remaining time is used for a panel discussion in which all speakers of the session serve on the panel. The discussions are moderated by the session chairs.

Furthermore, workshop secretaries will take notes throughout the workshop to keep track of the discussions. They will report at the workshop summary on Friday afternoon. (We will *try* to make written summaries of the discussions available after the workshop at http://robot.me.gatech.edu/WORKSHOP/workshop.html .)

The paper submission process was open to anybody interested in parallel manipulators. 41 regular papers were received, and, after a rigorous peer-review process, 29 were accepted. In addition, 10 non-refereed white papers were submitted and are included in the proceedings.

By trying a new (and untested) format for the regular paper sessions of this workshop we are of course taking a certain risk. We hope that when you leave this workshop you will find that this format was beneficial to your experience and that it created an entirely different atmosphere that encouraged open discussion and the exchange of ideas. We will certainly appreciate your feedback on how you think this format worked out and incorporate any suggestions you may have in future events.

Last but not least, we hope that you do enjoy your stay in beautiful Québec City.

With best regards,

Imme Ebert-Uphoff
Clément M. Gosselin

ACKNOWLEDGEMENTS

This workshop would not have been possible without the help of many of our colleagues. We would like to thank the members of the technical program committee for their invaluable help in the review process and the organization of the workshop. We would also like to thank the keynote speakers and panel members for their participation.

Furthermore, Terri Keita at Georgia Tech did an incredible job of handling all paper submissions, assembling the proceedings, etc. Colombe Dalpé, at Laval University, is deeply acknowledged for coordinating the local arrangements. Richard Martineau, also at Laval, designed the workshop logo and the layout of the program brochure.

The Georgia Institute of Technology and Université Laval are acknowledged for their support of this event.

The financial support from our sponsors was crucial to make this workshop possible and to keep the registration cost at a reasonable level. The National Science Foundation (Program for Manufacturing Machines and Equipment) and the Ministry of Research, Science and Technology of the Québec Government both provided generous support. In addition, the NSF funds made it possible to provide travel grants to four students who would otherwise not have been able to attend.

Imme Ebert-Uphoff
Clément M. Gosselin

Conference Chairs

Dr. Imme Ebert-Uphoff, Georgia Institute of Technology, US
Dr. Clément M. Gosselin, Université Laval, Canada

Technical Program Committee

Dr. Sunil Agrawal, University of Delaware, US
Dr. Jian Dai, King's College London, UK
Dr. Tian Huang, Tianjin University, P.R. China
Dr. Just Herder, Delft University of Technology, The Netherlands
Dr. Venkat Krovi, SUNY Buffalo, US
Dr. John McPhee, University of Waterloo, Canada
Dr. Vincenzo Parenti-Castelli, University of Bologna, Italy
Dr. Francois Pierrot, LIRMM, France
Dr. Moshe Shoham, Technion, Israel
Dr. Yukio Takeda, Tokyo Institute of Technology, Japan
Dr. Philippe Wenger, IRCCynN, France
Dr. Gloria Wiens, Univ. of Florida, US

Educational Committee

Dr. Michael McCarthy, University of California, Irvine, US
Dr. Just Herder, Delft University of Technology, The Netherlands

Conference Coordinator

Terri Keita, Georgia Institute of Technology

Local Arrangements

Colombe Dalpé, Université Laval, Canada

Sponsors

National Science Foundation, Program for Manufacturing Machines and Equipment (MME)
The Québec Government, Ministry of Research, Science and Technology

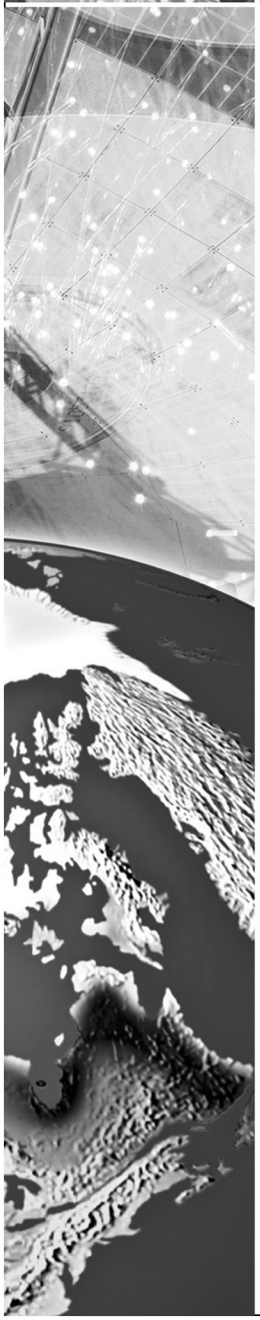

Le ministère de la Recherche, de la Science et de la Technologie
soutien résolument la tenue du congrès

«Les manipulateurs et mécanismes parallèles:
synthèse des travaux accomplis et perspectives futures»

et souhaite la bienvenue à tous les congressistes.

Cet événement donnera lieu à des rencontres des plus fructueuses
et connaîtra sûrement un franc succès.

Bon colloque à tous et bon séjour à Québec!

The Ministère de la Recherche, de la Science et de la Technologie
is proud to support

«The Fundamental Issues and Future Research Directions
for Parallel Mechanisms and Manipulators convention»

and extends a warm welcome to all convention delegates.

This undisputedly successful event will also lead to promising
exchanges and encounters.

Enjoy both the convention and your stay in Québec!

Recherche, Science
et Technologie
Québec
On prépare l'avenir

www.mrst.gouv.qc.ca

WORKSHOP ON FUNDAMENTAL ISSUES & FUTURE RESEARCH DIRECTIONS FOR PARALLEL MECHANISMS & MANIPULATORS

PROGRAM

WEDNESDAY - OCTOBER 2

2:30PM – Bus leaves from Montreal (DETC Hotel)

5:15PM – Bus arrives at Hotel Classique (Québec City)

6:15PM – Bus leaves hotel for reception at Université Laval

6:30PM – Registration and reception at Université Laval, including a visit of the robotics lab and demos

9:30PM – Bus returns to Hotel Classique

THURSDAY – OCTOBER 3

8:00AM – Bus leaves from Hotel to Université Laval

8:20AM – Welcoming address (C. Gosselin and I. Ebert-Uphoff)

8:30AM – Keynote Address I

J.-P. Merlet, *"An Initiative for the Kinematic Study of Parallel Manipulators"*

9:30AM – Regular Papers: New Architectures 1

Session Chairs: S. Agrawal and F. Pierrot

1. I. Zabalza, J. Ros, J.J. Gil, J.M. Pintor, J.M. Jimemez
   "TRI-SCOTT. A MICABO like 6-DOF Quasi-Decoupled Parallel Manipulator".

2. P. Wenger, D. Chablat
   "Design of a Three-Axis Isotropic Parallel Manipulator for Machining Applications: The Orthoglide"

3. X. Kong, C.M. Gosselin
   "A Class of 3-DOF Translational Parallel Manipulators with Linear I-O Equations"

10:30AM – Coffee Break

10:45AM – Regular Papers: Kinetostatic Analysis

Session Chairs: J. Dai and T. Huang

1. U.A. Tol, J.-P. Clerc, G.J. Wiens, 3-08-02/13
   "Micro/Macro Approach for Dexterity Enhancement of PKM's".

2. J.L. Herder
   "Some Considerations Regarding Statically Balanced Parallel Mechanisms (SBPM's)".

3. S. Krut, O. Company, F. Pierrot
   "Velocity Performance Indexes for Parallel Mechanisms with Actuation Redundancy".

4. M.J.D. Hayes
   "Architecture Independent Workspace Analysis of Planar Three-Legged Manipulators"

12:00PM – Lunch with Keynote Address II

T. Brogårdh, *"PKM Research – Important Issues as seen from a Product Development Perspective at ABB Robotics"*

1:30PM – Industrial Panel

Panelists:

- Torgny Brogardh, ABB Robotics, Sweden
- Ed Dougherty, August Design Inc., US
- Adam Jacoff, NIST, US
- Gerhard Serapins, CAE, Montreal, Canada

2:25PM – Regular Papers: Design and Optimization

Session Chairs: V. Krovi and P. Wenger

1. A.S. Sorensen, H.G. Petersen, O.G. Jakobsen, J. Steinicke
   "Towards the Industrial Usage of Parallel Kinematic Chain Modules in a Fully Modular Robotic Manipulator".

2. J. Yoon, J. Ryu
   "Reconfigurability of a Parallel Manipulator: A Case Study".

3. E. Ottaviano, M. Ceccarelli
   "Optimum Design of Parallel Manipulators for Workspace and Singularity Performances".

4. G.F. Liu, Z.X. Li
   "General Geometric Algorithms for Optimal Design of Parallel Manipulators".

5. K. Kozak, P.A. Voglewede, I. Ebert-Uphoff, W. Singhose
   "Concept Paper: On the Significance of the Lowest Linearized Natural Frequency of a Parallel Manipulator as a Performance Measure for Concurrent Design".

4:00PM – Coffee Break

4:15PM – Regular Papers: Kinematics and Singularities

Session Chairs: M. Shoham and G. Wiens

1. A. Meschini, R. Sinatra, S. Pirrotta
   "A Parallel Mechanism for a Satellite Antenna with Double Reflector".

2. M.L. Husty, A. Karger
   "Self Motions of Stewart-Gough-Platforms – An Overview".

3. Y. Takeda, U. Spaelter, H. Funabashi
   "Forward Displacement and Singularity Analysis of a Crank-Type 6-3 In-Parellel Actuated Mechanism".

4. A. Perez, J.M. McCarthy
   "Dual Quaternion Synthesis of a 2-TPR Constrained Parallel Robot".

5:30PM – Bus leaves Univ. Laval for guided tour of City and Banquet downtown.

9:30PM – Bus returns to Hotel Classique

FRIDAY – October 4

8:00AM – Bus leaves from Hotel to Université Laval

8:30AM – Keynote Address III

J. Angeles, *"The Qualitative Synthesis of Parallel Manipulators"*

9:30AM – Regular Papers: New Architectures and Wire-Driven Manipulators

Session Chairs: V. Parenti-Castelli and Y. Takeda

1. X-J. Liu, J. Kim, J. Wang
   "Two Novel Parallel Mechanisms with Less than Six DoFs and the Applications".

2. J. Kim, J.C. Hwang, J.S. Kim, C.C. Iurascu, F.C. Park, Y.M. Cho
   "Analysis and Design of a New 6 D.O.F. Full Tilting Parallel Mechanism".

3. P. Lafourcade, M. Llibre, C. Reboulet
   "Design of a Parallel Wire-Driven Manipulator for Wind Tunnels".

4. A. Fattah, S.K. Agrawal
   "Design of Cable-Suspended Planar Parallel Robots for an Optimal Workspace".

10:45AM – Coffee Break

11:00AM – Regular Papers: Calibration and Applications

Session Chairs: J. Herder and J.-P. Merlet

1. I. Fassi, G. Legnani
   "Automatic Identification of a Minimum, Complete and Parametrically Continuos Model for the Geometrical Calibration of Parallel Robots".

2. V. Parenti-Castelli, S. Venanzi
   "On the Joint Clearance Effects in Serial and Parallel Manipulators"

3. M. Krefft, M. Frindt, J. Hesselbach, F.M. Wahl
   "Robotic Systems for Handling and Assembly -- High Dynamic Parallel Structures with Adaptronic Components --".

12:00PM – Lunch with Panel on Education

Session Chairs: J.L. Herder, J.M. McCarthy

J.L. Herder, *"Proposal for a Self-Developing Practical Course in Parallel Mechanisms"*. *(Additional details to be announced.)*

1:30PM – White Papers – Poster Session

Session Chairs: C. Gosselin and I. Ebert-Uphoff

1. C. Lange, J-C Piedboeuf, E. Martin, J. Kövecses
   "Towards Docking Emulation using Hardware-in-the-Loop Simulation with Parallel Platforms".

2. R.L. Williams, II
   "Parallel Robot Projects at Ohio University".

3. B. Dasgupta
   "Redundancy Resolution Schemes for Parallel Manipulators with Force Redundancy".

4. K. Mianowski
   "On Some Properties of POLMAN-3L Parallel Manipulator to the Use as a 3-D Measuring System for Industrial/Educational Applications".

5. A.M. Hay, J.A. Snyman
   "Design of Parallel Manipulators for Optimal Conditioning Throughout a Prescribed Workspace".

6. Z. Huang, Q.C. Li
   "On the Type Synthesis of Lower-Mobility Parallel Manipulators".

7. J.M. Herve, M. Karouia
   "The Novel 3-RUU Wrist with No Idle Pair".

8. Y-Q Zheng
   "Workspace Analysis of a Six DOF Wire-Driven Parallel Manipulator".

9. Z. Xu, F. Xi, C.K. Mechefske
"Kinetostatic Analysis and Optimization of a Tripod Attachment for Machine Tools".

10. P. Zsombor-Murray
"Planar Point & Line Transformation with Blaschke-Grünwald Image Space Coordinates".

2:50PM – Coffee Break

3.00PM – Regular Papers: Dynamics

Session Chairs: J. McPhee and J. Angeles

1. Y. Wu, C.M. Gosselin
"On the Synthesis of a Reactionless 6-DOF Parallel Mechanism Using Planar Four-Bar Linkages".

2. W.A. Khan, V. Krovi
"Comparison of Two Alternate Methods for Distributed Forward Dynamic Simulation of a Four-Bar Linkage".

3. I. Ebert-Uphoff, K. Kozak
"Review of the Role of Quasi-Coordinates for the Kinematic and Dynamic Modeling of Parallel Manipulators".

4. J. Kövecses, J-C. Piedboeuf, C. Lange
"Methods for Dynamic Models of Parallel Robots and Mechanisms".

5. T. Geike, J. McPhee
"On the Automatic Generation of Inverse Dynamic Solutions for Parallel Manipulators with Full and Reduced Mobility".

4.40PM – Workshop Summary – Reports from Workshop Secretaries

Workshop secretaries summarize key issues and action items identified throughout the workshop.

5.30PM – Workshop Ends

6:00PM – Bus leaves for Montreal

6:30PM – Informal dinner for participants who are staying in Québec City (not included in workshop registration fees)

TABLE OF CONTENTS

Preface..... iii
Acknowledgements..... iv
Committees..... v
Message from Québec Government..... vi
Program.....vii

Keynote Address I

An Initiative for the Kinematic Study of Parallel Manipulators
Jean-Pierre Merlet.....2

Regular Papers: New Architectures 1

TRI-SCOTT. A MICABO like 6-DOF Quasi-Decoupled Parallel Manipulator
I. Zabala, J. Ros, J.J. Gil, J.M. Pintor, J.M. Jimemez..... 12

Design of a Three-Axis Isotropic Parallel Manipulator for Maching Applications: The Orthoglide
P. Wenger, D. Chablat..... 16

A Class of 3-DOF Translational Parallel Manipulators with Linear I-O Equations
X. Kong, C.M. Gosselin.....25

Regular Papers: Kinetostatic Analysis

Micro/Macro Approach for Dexterity Enhancement of PKM's
U.A. Tol, J-P. Clerc, G.J. Wiens.....34

Some Considerations Regarding Statically Balanced Parallel Mechanisms (SBPM's)
J.L. Herder.....40

Velocity Performances Indexes for Parallel Mechanisms with Actuation Redundancy
S. Krut, O. Company, F. Pierrot.....46

Architecture Independent Workspace Analysis of Planar Three-Legged Manipulators
M.J.D. Hayes.....57

Keynote Address II

PKM Research – Important Issues as seen from a Product Development Perspective at ABB Robotics
T. Brogårdh.....68

Regular Papers: Design and Optimization

Towards the Industrial Usage of Parallel Kinematic Chain Modules in a Fully Modular Robotic Manipulator
A.S. Sorensen, H.G. Petersen, O.G. Jakobsen, J. Steinicke.....86

Reconfigurability of a Parallel Manipulator: A Case Study
J. Yoon, J. Ryu..... ..94

Optimum Design of Parallel Manipulators for Workspace and Singularity Performances
E. Ottaviano, M. Ceccarelli.....98

General Geometric Algorithms for Optimal Design of Parallel Manipulators
G.F. Liu, Z.X. Li..... 106

Concept Paper: On the Significance of the Lowest Linearized Natural Frequency of a Parallel Manipulator as a Performance Measure for Concurrent Design
K. Kozak, P.A. Voglewede, I. Ebert-Uphoff, W. Singhose..... 112

Regular Papers: Kinematics and Singularities

A Parallel Mechanism for a Satellite Antenna with Double Reflector
A. Meschini, R. Sinatra, S. Pirrotta..... 120

Self Motions of Stewart-Gough-Platforms – An Overview
M.L. Husty, A. Karger..... 131

Forward displacement and Singularity Analysis of a Crank-Type 6-3 In-Parallel Actuated Mechanism
Y. Takeda, U. Spaelter, H. Funabashi..... 142

Dual Quaternion Synthesis of a 2-TPR Constrained Parallel Robot
A. Perez, J.M. McCarthy.....150

Keynote Address III

The Qualitative Synthesis of Parallel Manipulators
J. Angeles..... .160

Regular Papers: New Architectures and Wire-Driven Manipulators

Two Novel Parallel Mechanisms with Less than Six DoFs and the Applications
X-J. Liu, J. Kim, J. Wang.....172

Analysis and Design of a New 6 D.O.F. Full Tilting Parallel Mechanism
J. Kim, J.C. Hwang, J.S. Kim, C.C. Iurascu, F.C. Park, Y.M. Cho..... 178

Design of a Parallel Wire-Driven Manipulator for Wind Tunnels
P. Lafourcade, M. Llibre, C. Reboulet..... 187

Design of Cable-Suspended Planar Parallel Robots for an Optimal Workspace
A. Fattach, S.K. Agrawal..... 195

Regular Papers: Calibration and Applications

Automatic Identification of a Minimum, Complete and Parametrically Continuous Model for the Geometrical Calibration of Parallel Robots
I. Fassi, G. Legnani.....204

On the Joint Clearance Effects in Serial and Parallel Manipulators
V. Parenti-Castelli, S. Venanzi.....215

Robotic Systems for Handling and Assembly – High Dynamic Parallel Structures with Adaptronic Components
M. Krefft, M. Frindt, J. Hesselbach, F.M. Wahl..... 224

Panel on Education

Proposal for a Self-Developing Practical Course in Parallel Mechanisms
J.L. Herder..... 238

White Papers

Towards Docking Emulation using Hardware-in-the-Loop Simulation with Parallel Platforms
C. Lange, J.C. Piedboeuf, E. Martin, J. Kövecses.....244

Parallel Robot Projects at Ohio University
R.L. Williams, II.....248

Redundancy Resolution Schemes for Parallel Manipulators with Force Redundancy
B. Dasgupta..... 257

On Some Properties of POLMAN-3L Parallel Manipulator to the Use as a 3-D Measuring System for Industrial/Educational Applications
K. Mianowski.....261

Design of Parallel Manipulators for Optimal Conditioning Throughout a Prescribed Workspace
A.M. Hay, J.A. Snyman.....267

On the Type Synthesis of Lower-Mobility Parallel Manipulators
Z. Huang, Q.C. Li.....272

The Novel 3-RUU Wrist with No Idle Pair
J.M. Herve, M. Karouia.....284

Workspace Analysis of a Six DOF Wire-Driven Parallel Manipulator
Y-Q. Zheng.....287

Kinetostatic Analysis and Optimization of a Tripod Attachment for Machine Tools
Z. Xu, F. Xi, C.K. Mechefske.....294

Planar Point & Line Transformation with Blaschke-Grünwald Image Space Coordinates
P. Zsombor-Murray..... 304

Regular Papers: Dynamics

On the Synthesis of a Reactionless 6-DOF Parallel Mechanism Using Planar Four-Bar Linkages
Y. Wu, C.M. Gosselin.....310

Comparison of Two Alternate Methods for Distributed Forward Dynamic Simulation of a Four-Bar Linkage
W.A. Khan, V. Krovi.....317

Review of the Role of Quasi-Coordinates for the Kinematic and Dynamic Modeling of Parallel Manipulators
I. Ebert-Uphoff, K. Kozak.....328

Methods for Dynamic Models of Parallel Robots and Mechanisms
J. Kövecses, J-C Piedboeuf, C. Lange..... 339

On the Automatic Generation of Inverse Dynamic Solutions for Parallel Manipulators with Full and Reduced Mobility
T. Geike, J. McPhee.....348

AUTHOR INDEX **359**

Keynote Address I
Thursday, October 3, 2002, 8:30AM

Jean Pierre Merlet
INRIA, Sophia-Antipolis, France
"An Initiative for the Kinematic Study of Parallel Manipulators"

Proceedings of the WORKSHOP on
Fundamental Issues and Future Research Directions for Parallel Mechanisms and Manipulators
October 3–4, 2002, Quebec City, Quebec, Canada
Clément M. Gosselin and Imme Ebert-Uphoff, editors

An initiative for the kinematics study of parallel manipulators

JEAN-PIERRE MERLET

INRIA Sophia-Antipolis
France
Jean-Pierre.Merlet@sophia.inria.fr

Abstract:

Although it is has been largely demonstrated in specific applications that parallel manipulators offer very good performances there are still domains (e.g. the machine-tool industry) in which this type of structure is not yet completely accepted. This may be explained by two main reasons:

- *at the end-user level the intrinsic non-linearity of these structures is still not well understood and previous works on the subject has been overlooked. This has led to the development of prototypes whose performances where not the expected one, which in turn has led to negative opinions among some communities*
- *at the academic level they are still many open problems, even at the most basic levels. A direct consequence is that there is still no simulation tool that allow to design efficiently parallel structures whatever is their topology, while this is a key issue as the performances of these structures are highly dependent on the topology and dimensioning of the mechanism.*

We will review what are the main problems that are still to be solved in the field of kinematics for parallel mechanisms, focusing especially on the optimal design problem, and try to outline possible approaches to solve this problem, the purpose being to clearly separate what part of the problem is architecture dependent from what may be dealt with by generic tools.

Finally we will present the Parallel Structure Initiative PSI *proposed by the Computational Kinematics Committee of IFToMM that intend to initiate a collaborative work between academics, companies and end-users to solve the kinematics problems for parallel structures.*

1 Introduction

Historically, closed-chain structures have attracted the interest mostly of mathematicians as they offer interesting problems. Some theoretical problems linked to this type of structure were mentioned as early as 1645 by Christopher Wren, then in 1813 by Cauchy (Cauchy 13) and in 1867 by Lebesgue (Lebesgue 67). One of the main theoretical problems in this field, called the *spherical motion problem*, related to what is now called singularity analysis, was the central point of a competition called *Le Prix Vaillant*, that took place in France in the 1900's and was organized by the Académie des Sciences. The prize was won on equal terms by Borel (Borel 08) and Bricard (Bricard 06).

But clearly at this time the technology was not able to deal with any practical applications of this type of structure. Although the very first application was proposed by Gough for a tire test machine (Gough 57; Gough Whitehall 62) parallel structure were really put in practice in the 70's for flight simulator (Baret 78; King 73; Koevermans $^+$75; Parrish $^+$73) (a very specific area where mostly acceleration are of interest) and in the early 80's for robotics application (McCallion Pham 79; Reboulet Robert 85) (with an interest in a larger panel of performances).

Starting in the 90's parallel kinematic structure (PKS) have started either to be put in use in various domains such as fine positioning devices or to be considered for potential applications such as machine-tool. Among these applications, some of them were not as successful as expected. The clearest illustration of this fact is the use of PKS in the machine-tool industry. Although the first presentation of such PKS dates from 1994 with the Variax of Giddings, we have still to see PKS in current use for such application.

I see three main reasons for this failure in this particular domain:

1. with very few exceptions there is no interaction with the laboratories having worked in this field for many years and the developers in the industry; hence problems that were familiar for researchers are completely overlooked by the developers, while researchers may miss important points for a specific application.

2. the inherent non-linearity of PKS and its consequences on the design and on the control of such structure is highly unfamiliar to people working in the field of machine-tool, accustomed to a linear world,

3. developers in the industry focus first on the development of the basic mechanical elements of a PKS, such as ball-and-socket joints. Although this work was necessary as these components in the right size were not commercially available, this type of development is only *local*, missing the point that these elements are part of a *global system* that has to be considered as such.

I must also be noted that these failures have a negative influence on the development of PKS, as they comfort a trend that states that these structures are too complex to work in practice (a trend that completely ignore past success stories in this field).

On a larger level I intend to show that *claiming that a PKS offers better performances than more usual structures is* **wrong** *. . . except if the PKS is the result of an optimal design methodology*

To support this claim I will try to emphasize the difficulties with which we are confronted to build efficient PKS and outline a possible approach to solve these difficulties.

2 Topology synthesis

Although I will focus on the dimensional synthesis problem, it is easy to show that the topology synthesis problem, i.e. finding the most appropriate mechanical architecture for a given task, is difficult for PKS.

Assume for a simplicity that for a given task we have to design a mechanism with 6 d.o.f. and that the comparison between different mechanical architectures has to be done based only on the volume of the workspace that can be reached by the end-effector. A further assumption is that actuated joints will only be of the prismatic (P) or revolute (R) type.

For classical serial structure, only the first three joints have an influence on the location of the end-effector. All the possible architectures will be obtained by considering all the possible set of three elements, each element being either P or R. For example a Cartesian robot is defined as the set PPP, while the spherical robot is RRR. Now affect a standard length L to each element of the robot: each link of the robots will have length L, prismatic joint have a retracted length of L and an extended length of $2L$ etc...

Under that assumption the workspace volume of a PPP robot is L^3 while the RRR workspace volume is roughly $85L^3$, *for any value of* L. Hence as far has workspace is concerned it is clear that the RRR structure is better than the PPP, whatever is the final dimensioning.

Now let us introduce two different PKS, namely a classical Gough platform and an Hexa robot (Pierrot Dauchez Fournier 91). A first problem is that for these type of structure the translation ability is not decoupled from the orientation. Then according to our hypothesis we will assume that the radii of the base and platform is identical and equal to L. This is clearly a very restrictive assumption, which will have a large effect on the workspace volume. Finally even for a given orientation we do not know what will be the workspace volume of both PKS as a function of L. It seems only that for a given geometry of Gough platform the workspace volume is roughly $k\rho^3$ where ρ is the extension of the leg (Masory Wang 95), where k is a factor that depend on the geometry of the robot (hence under our assumption the workspace volume will be written as $k(L)L^3$). A similar result has never been established for the Hexa robot but imagine that in that case the workspace may be written as $g(L)L^3$. Comparison of the two PKS in term of workspace volume based on the previous formula may lead only to the conclusion that for some ranges on L the Gough platform has a larger workspace than the Hexa, the opposite being true for other ranges for L.

Hence at this time we are only able to compare the generic workspace volume of 2 serial structures but not to compare either a serial and a parallel structure or 2 PKS.

Hence topology synthesis for PKS is a much more complex problem than for serial structure and cannot be disconnected from the dimensional synthesis problem.

There is also an important open problem related both to the topology and dimensional synthesis of PKS with less than 6 d.o.f. Having less than 6 d.o.f. may be interesting for some tasks (such as using a PKS for a milling machine for which the rotation around the normal of the platform is not necessary) and allows for a reduction in the cost of the machine. Numerous PKS with between 3 and 5 d.o.f. have been proposed in the literature. We may classify them into two different categories:

- *externally constrained mechanism*: the PKS has less than 6 d.o.f because a passive mechanism restricts the motion of the platform. A typical example of such type of PKS is the Tricepts robot.

- *geometrically constrained mechanism*: the geometry of the legs imposes constraints on the motions of the platform. A typical example of such type of PKS is the Delta robot or the ”Agile Eye”.

In both cases the platform will have less than 6 d.o.f. only in theory. Indeed due to the manufacturing tolerances, clearance in the joints, . . . the platform will exhibit motions in all 6 d.o.f. The problem to be addressed is the following: being given a threshold on the maximal amplitude of the undesired motion what are the amplitude of the errors that are allowed for the manufacturing of the robot?. Clearly this is a very important issue: if the amplitude of the errors are lower than reasonable manufacturing tolerances, then the mechanical architecture cannot be used in practice. This important subject has almost never been addressed (Parenti-Castelli Di Gregorio 00).

3 Dimensional synthesis

Finding the dimensions of a given mechanism so that it is optimal with respect to some requirements is a very old problem in mechanism theory. Before describing the existing methods let us examine what are the requirements that may be imposed on PKS and what is their complexity.

3.1 Requirements

The COPRIN project of INRIA has a lot of practical experience in the optimal design of PKS, which has been gained from the development of our own prototype and from several industrial contracts. We have been dealing especially with:

- fine positioning devices for heavy loads (with the European Synchrotron Radiation Facility, the Institut Laue Langevin, Alcatel),
- machine-tools (with Constructions Mécaniques des Vosges),
- medical robots.

Very early we have established an evaluation form for the design of Gough platform type PKS that both allows the end-user to describe his requirements (either as trends or with numerical values) and enable the designer to get all the necessary information to perform the design study.

The end-user may provide information and requirements that may be classified as:

- *kinematics*: workspace, accuracy, maximal motion of the passive joints, dexterity,
- *statics*: load on the platform, stiffness of the robot,
- *dynamics*: maximal velocity and acceleration of the actuator and of the platform, inertia and center of mass,
- *geometrical*: overall size of the robot, of the mechanical components,
- *technological*: overall information on the actuator, on the sensors and on the passive joints. Indeed the context of the application may impose the use of restricted classes of such components.

Note that most of the time the requirements provided by the end-user will only be subset of the requirements used by the designer. For example the end-user may provide only requirements on the workspace and on the load carrying ability but the designer will also consider, for example, singularities and maximal passive joint motions. Among the list of requirements, workspace and accuracy are almost always provided.

The end-user has also to classify his requirements according to their importance: this is crucial as in some case we have to relax some requirements in order to be able to satisfy some other requirements. Hence we will have to consider first *strict requirements* that cannot be relaxed and then other criterion that can be relaxed to some extent.

It must also be mentioned that some requirements may involve a fixed value (e.g. the accuracy of the positioning of the platform for a unit value of the sensor error must not greater than a given threshold) and will be called *fixed value requirements*. On the other hand, we may have *a maxima requirements* (e.g. the positioning error of the platform for a unit value of the sensor error must be as low as possible).

First of all it must be noticed that for PKS most of these performances are *pose dependent*. For example, the workspace of the end-effector is dependent upon its orientation, while the accuracy is dependent both upon the orientation and the location of the end-effector. This dependency is usually quite complex: for example the accuracy $\Delta\mathbf{X}$ of the positioning of a Gough platform is related to the accuracy $\Delta\rho$ of the sensor by:

$$\Delta\rho = J^{-1}(X)\Delta\mathbf{X}$$

The inverse Jacobian matrix J^{-1} has a relatively simple analytical form, but establishing the positioning accuracy of the platform as a function of the sensor accuracy will require the use of J, which is highly complex.

Most of these requirements are of the *worst case* type with respect to the workspace: as the performances are pose dependent, the limits imposed on the requirements have to be considered for the whole workspace. For example an accuracy requirement ΔX_d indicates that the positioning error must not exceed ΔX_d *over the whole workspace of the robot*.

But the designer may have also to deal with other cases. Imagine for example that two robots A and B with different geometries have equivalent worst case accuracy. Clearly this does not imply that they are equivalent. Indeed, for example, the *average value* of the positioning error over the whole workspace may be quite different or alternatively we may have to consider the *best case* (when some crucial part of the task requires a high accuracy).

Determining the the best and worst case accuracy is obtained by solving a difficult constrained optimization problem. We will see later on that although difficult the problem is tractable. This is not the case for determining *exactly* (we will explain later on what is our meaning of the word exactly) the average value of the positioning error over a given workspace which is a problem without known solution at this time. Using in the design process criterion for which best or worst case are difficult to calculate, however appropriate or pertinent they may be, clearly complicate the process. Another example of such complex criteria is the family of *dexterity index* such as the absolute value of the determinant of the inverse jacobian or the *condition number*, i.e. the ratio of the minimal eigenvalue over the maximal eigenvalue of the matrix $J^{-1}J{-}T$. The analytical form of such index is in the best case very difficult to calculate and very often even not possible (for example the condition number is the ratio of the roots of a polynomial whose degree is equal to the number of

d.o.f. of the robot and hence cannot be calculated analytically as soon as this number exceed 4). The average value of these criterion (often called the *global conditioning index*) is very difficult to calculate exactly. Furthermore we must mention the lack of significance of this type of index as soon as the motion of the platform mixes translation and rotation.

Finally it must be emphasized that all the requirements in the above list are highly sensitive to the geometry of the robot. Such sensitivity is the first reason for the failure of some prototype of PKS which have been designed using a local approach instead of a global one, the second one being that some properties of PKS have been overlooked. For example changing the radius of the platform of a Gough platform by 10% may modify the worst case stiffness by 700%. Clearly such ratio imply that a robot with a poor topology but optimally designed will present largely better performances than a robot with an appropriate topology but poorly designed. Hence **dimensional synthesis is crucial when designing a PKS**.

3.2 Workspace requirements

As mentioned previously, most of the design requirements have to be verified over the workspace of the robot. This workspace may be defined in various terms:

1. a workspace defined with respect to a global reference frame
2. the whole workspace of the robot. For example, for a Gough platform, this workspace may be defined as the set of poses that the robot can reach with the leg lengths ρ satisfying the inequalities $\rho_{min} \leq \rho \leq \rho_{max}$ where ρ_{min}, ρ_{max} are given constants. A general definition will be all the reachable poses such that n inequality constraints $F_i(X, \rho) \leq 0$ $(i = 1, \ldots, n)$ are satisfied.
3. a workspace, where the z component specification is defined relatively to some unknown quantity z_d. For example the z motion ability may be specified as $\pm$ 50 mm relatively to some unknown design parameter z_d.

These three different possibilities may co-exist for a given design problem. For example, the accuracy requirement may be defined for a workspace of type 1, while singularity analysis has to be performed in the type 2 workspace. For the type 3 workspace we have to include z_d as a design parameter.

3.3 Design methodology and performance verification

The most well known design methodology is the cost-function approach (Erdman 93). To each design requirement j is associated a numerical index I_j that is minimal for the best robot. The cost function $\mathcal{C}$ is defined as:

$$\mathcal{C} = \sum w_j I_j,$$

where the w_j are weight associated to the I_j. In some sense, the cost function is an indicator of the global behavior of the mechanism with respect to the requirements. As $\mathcal{C}$ is clearly a function of the set of design parameters $\mathcal{P}$, a numerical procedure is used to find the value of the design parameters that minimize $\mathcal{C}$. This approach has several drawbacks:

- the result is heavily dependent upon the weights that are used in the cost-function, and there is no automatic way to find the right weights,
- defining the index I is not always an easy task, for example if we have constraints on the shape of the workspace. Furthermore, as mentioned earlier, some of these index are even very difficult to estimate (for example the global conditioning index).
- introducing strict requirements in the minimization is difficult, and in any case computer intensive,
- as for any optimization problem, it is difficult to guarantee that the global extremum has been found. Error at this level put in jeopardy the whole design methodology.
- some of the requirements are antagonistic; for example, it is well known that dexterity is antagonistic with the workspace volume (Ma Angeles 91); using both criterion in a weighted sum does not have any physical meaning

But the main difficulty is that the computation of the index for a given geometry must be very efficient as the minimization procedure will use these calculations extensively. Unfortunately, verifying that a PKS of given geometry satisfies a single requirement is usually a very complex task.

3.4 Performance verification

3.4.1 Standard verification form

In my opinion, any optimal design methodology will use a performance verification module that takes as its input a robot geometry and verify whether this geometry satisfy a list of requirements. Hence **the development of an efficient performance verification module is a key point for the optimal design of PKS**.

Ideally, such module should be able to

1. deal with any type of PKS, although optimized version for the most usual PKS may exist,
2. deal with almost any type of requirements, especially worst and best cases,
3. provide *guaranteed* results.

A given requirement usually defines an implicit set of constraints $\mathcal{I}$ that is only dependent upon the topology of the robot. Assume now that we have a generic tool $\mathcal{T}$ that is able to deal with any $\mathcal{I}$ as soon as $\mathcal{I}$ is expressed in a standard form (that we will call the *standard verification form* (SVF)). A generic performance verification module may reach the first two objectives if

1. we first preprocess all the $\mathcal{I}$ for each requirement to put them in the standard form, probably using a symbolic computation software,

2. we use then the generic tool $\mathcal{T}$ to verify all the requirements either in sequence or simultaneously.

In my opinion, many mathematical tools offer the possibility of designing $\mathcal{T}$ (see the Annex for one possibility). But the key point on this issue is **a collaborative work of researchers in the field of mechanism theory and mathematicians**. The first part of this effort is the development of the SVF: the researchers in mechanism theory will provide the description of all the requirements that may be of interest for PKS; the mathematicians will analyze them to obtain a very reduced set of problems to solve. For example, although dealing with very different quantities, determining the worst case accuracy of a robot and the maximal joint forces are strictly equivalent mathematical problems.

The second part of the collaborative work is the design of the tool $\mathcal{T}$ that allow to solve the reduced set of problems.

3.4.2 The meaning of exact

Designing $\mathcal{T}$ will be clearly a difficult job but **a key point on this issue is the meaning of getting an *exact* result**. We must take advantage of the fact that exact means in our community that the result must be *guaranteed* and this may strongly be different than the mathematical meaning of the word exact (or even approximatively exact in the computer science signification of this term). A guaranteed result means that we are able to determine error bounds on the result, so that a decision based on this result will be justified. In the worst case the algorithm will indicate that the result cannot be calculated safely in a standard manner on a computer (this will usually happen when we are at the limits on the requirements and neglecting the design results that may be provided at this point should not cause any problem as these solutions will have an error margin that will be well below the manufacturing tolerances). Guaranteed result is therefore much less stringent than exact result: hence we must design our algorithm to use this freedom in view of reducing the computation time. Note also that getting a guaranteed result excludes the use of discretization methods that just sample the workspace and verify the requirement only at the sampling points.

In the optimal design process mostly guaranteed results are needed, as for many requirements it will not be necessary to obtain exactly result.

Let us consider for example the determination of the accuracy of the sensor that must be used to reach a given accuracy for the positioning of the platform. We will first determine what will be the accuracy ΔX_1 of the positioning of the platform for a unit value of the sensor error. Then, as the relationship between these two quantities is linear, we will be able to determine what must be the sensor error $\Delta\rho_s$ so that the accuracy of the platform reaches a given value ΔX_d. The important point is that *in many cases only a restricted set of accuracy for the sensor will be available*. Hence the accuracy of the platform need to be determined only to the extent that it will result in a unique possible value for the accuracy of the sensor. For example if the available sensor accuracy are 0.1, 0.2 and 0.5 and if $\mathcal{T}$ is able to compute a range for ΔX_1 such that $\Delta\rho_s$ is in the range [0.3,0.4], then we are able to decide that we have to use the sensor with the accuracy 0.2. Hence, although we have not determined *exactly* what will be the worst case accuracy, we can still guarantee that this choice of sensor error will satisfy the requirement.

Clearly $\mathcal{T}$ must be designed so that it only guarantees the result, especially if getting a guaranteed result is less computer intensive than getting the exact result.

3.4.3 Exact methods

In some favorable cases it will be possible to solve exactly the performance evaluation problem. Unfortunately in my experience this happen only for very simple problems (robot with 2 d.o.f. and very simple requirements). But if such an approach is possible it should be clearly favored as soon as the computation time is small.

3.4.4 Hybrid methods

Let us assume that we have to solve a n dimensional performance evaluation problem (i.e. that the number of unknowns in the problem is n) and that we are able to solve the same problem exactly when the number of unknowns is $m < n$, i.e. when the unknowns $x_{m+1}, \ldots x_n$ have a fixed value. As we have in most case to solve an optimization problem (i.e. determine the extremal value F_m of a given function) we may be able to determine what may be the maximal change in the unknowns $x_{m+1}, \ldots x_n$ such that these changes will not result in a change of F_m greater than a given threshold ϵ. Hence using the exact method with as value for $x_{m+1}, \ldots x_n$ these new values ensures that we will determine the optimal value of F_m with an accuracy less than ϵ. Repeating this process until the whole workspace has been explored will ensure that in the worst case the optimum has been found with an accuracy ϵ. Such method has been proven to be very efficient for the analysis of some requirements for PKS over some specific workspace (Merlet 98a; Merlet 98b).

3.5 Alternative optimal design methodologies

3.5.1 Genetic algorithms

Assume now that an efficient performance verification module is available. This open the door to alternative design methodologies such as the use of genetic algorithms (GA). In this type of algorithm individuals have genes that represent values for the design parameters. An initial population of individuals is initially selected as parents and they are crossed-over to generate children, some of them having genes that are obtained as mutation of the genes of their parents. Each individual is evaluated with respect to the design requirements, and selection rules allow to select only the "more promising" children that will constitute the next generation.

GA's are well known optimization procedures that may

be used when the function to be optimized are complex. They have been already used in the field of planar PKS (Boudreau Gosselin 99), although the lack of an efficient performance verification has restricted their use to simple PKS. In my opinion GA may be interesting only if we have only fixed value requirements and cannot be used for a maxima requirements as they give guarantee on the result.

3.6 The parameter space approach

Let m be the number of design parameters in $\mathcal{P}$. We define an m dimensional space, the *parameter space* $\mathcal{S}$, in which each dimension is associated to one design parameter (hence each point in the parameter space defines an unique robot geometry). The purpose of the parameter space approach is to determine the regions of $\mathcal{S}$ that include all the possible solutions of the design problem.

To reach this goal, the following approach may be used:

1. select a particular requirement R_j, or a relaxed version of this requirement (for example if the requirement is that the workspace of the PKS includes a specific Cartesian box we may relax the requirement by verifying only that the workspace includes the 8 corners of the box).
2. determine the region $\mathcal{S}_j$ of $\mathcal{S}$ which include all the robots satisfying R_j.
3. repeat the process for another requirement.
4. after completing the 3 first steps of this process we have obtained m regions $\mathcal{S}_j$. If there is a solution to the optimal design problem, then it will lie in the intersection of the regions. At this step we compute this intersection $\mathcal{S}_i$.
5. at this point we have determined all the robots that satisfy a subset of the requirements. A local approach is then used to determine the solutions within $\mathcal{S}_i$ that satisfy all the requirements.

A key issue in this approach is step 2. We must develop a generic method that is able to deal with most common requirements. This method will rely on an extended version of the standard verification form, called the *standard design verification form (SDVF)*, that takes also into account the design parameters and will have basically the same structure than the performance verification module:

- transform the requirements into a SDVF,
- apply a generic tool $\overline{\mathcal{T}}$ to determine the region $\mathcal{S}_j$. Note that the generic tool $\mathcal{T}$ is a special instance of $\overline{\mathcal{T}}$ in which all the design parameters have a fixed value.

Although the problem may seem to be quite complex, we have already obtained some result in this area, especially for the workspace requirement, either by using a geometrical approach (Merlet 97) or an interval analysis approach (Merlet 01).

4 Conclusion

Optimal design can be divided into two main topics: topology synthesis and dimensional synthesis, although it is unclear if topology synthesis can be separated from dimensional synthesis for PKS. Performances of PKS are highly sensitive to both type of synthesis; hence optimal design is a crucial issue for the development of efficient PKS.

We propose to develop a generic method for the optimal design of PKS, based on the transformation of the requirement into a reduced set of generic problems that may be treated by an universal solver. The development of this generic method is a huge project and can only be the result of a collaborative work between the researchers working in this field, mathematicians interested in this type of problems, and end-users. This effort must be coordinated: hence the Computational Kinematics technical Committee of IFToMM (the International Federation on the Theory of Machine and Mechanisms) has proposed to coordinate this effort. Researcher from academy and industry willing to participate to this research effort are encouraged to look at the Parallel Structure Initiative (PSI) web site:

`http://www-sop.inria.fr/coprin/EJCK/PSI.html`

A further problem that has to be taken into account is control: there is a crucial need for robot controller that are able to deal efficiently with the inherent non-linearity of PKS and with its consequence on control, on-line and off-line motion planning, ... In my opinion current controller are not very effective for PKS. But this is another story ...

Annex: Interval analysis

Interval analysis is a powerful method initially proposed by Moore (Moore 79). Let us illustrate this method on a simple example: let f be the function $x^2 - 2x$ and assume that we are looking for the solutions of $f = 0$ when x is in the range $[3, 4]$. Intuitively it is easy to see that if x is in [3,4], then x^2 is in [9,16]: this means that if x has a particular value in the range [3,4], then $f(x)$ has a value in the range [9,16] (similarly $-2x$ is in the range [-8,-6]). Now consider the sum of 2 intervals $A = [\underline{a}, \overline{a}]$, $B = [\underline{b}, \overline{b}]$. It may be seen that $A + B = [\underline{a} + \underline{b}, \overline{a} + \overline{b}] = C$, which means that for any value of x in A and y in B, then $x+y$ lie in C. In our case we will write $f([3, 4]) = [9, 16]+[-8, -6] = [1, 10]$. The resulting interval defines therefore lower and upper bound for the values of f: we may guarantee that for any x is [3,4] $1 \leq f(x) \leq 10$. As 0 is not included in the final interval we may state that there is no zero of f for x in the range [3,4]. Note that the bounds provided by interval analysis are overestimated, the true range of $f(x)$ being [3,8]. However, this does not affect the validity of the conclusion.

This method works for all the classical mathematical functions such as $\sin, \cos, \sinh, \ldots$. Furthermore this method may be

implemented to take into account numerical round-off errors and is therefore safe from a numerical view point.

Let us apply this method for a classical problem for PKS. Assume that we want to verify that a particular Cartesian box $\mathcal{B}_0$ is included in the workspace of a Gough platform, the orientation of the platform being constant. If the leg lengths ρ of the robot are restricted to lie in the interval $[\rho_{min}, \rho_{max}]$ we have to verify that for any X in $\mathcal{B}_0$ we have $\rho_{min} \leq \rho(X) \leq \rho_{max}$. As we know an analytical form for $\rho(X)$ we may determine by using interval arithmetics a lower and an upper bound $\underline{\rho(X)}, \overline{\rho(X)}$ for $\rho(X)$ if X lie in a given Cartesian box. The algorithm uses a list of Cartesian box $\mathcal{L}$ which is initialized to be $\mathcal{L} = \{\mathcal{B}_0\}$ at the start and $\mathcal{L}_i$ will denote the i-th box in $\mathcal{L}$. The algorithm is then, starting with $i = 1$:

1. compute $\left[\underline{\rho(\mathcal{L}_i)}, \overline{\rho(\mathcal{L}_i)}\right]$ using interval arithmetics.

2. if $\underline{\rho(\mathcal{L}_i)} > \rho_{max}$ or $\overline{\rho(\mathcal{L}_i)} < \rho_{min}$, then $\mathcal{B}_0$ is not included in the workspace, as every point of $\mathcal{L}_i$, which is included in $\mathcal{B}_0$, is outside the workspace. Send the message "BOX IS OUT".

3. if $\underline{\rho(\mathcal{L}_i)} \geq \rho_{min}$ and $\overline{\rho(\mathcal{L}_i)} \leq \rho_{max}$, then $\mathcal{L}_i$ is included in the workspace, as for any point in this box the leg lengths are within the limits. Restart at 1 with the $i = i + 1$.

4. otherwise bisect $\mathcal{L}_i$ along one of its dimension (either x, y or z) to create two new Cartesian boxes that will be stored at the end of $\mathcal{L}$. Restart at 1 with the $i = i + 1$.

The algorithm either exits at step 2, in which case part of $\mathcal{B}_0$ is outside the workspace, or it stops when all the boxes of $\mathcal{L}$ have been processed, in which case $\mathcal{B}_0$ is fully included in the workspace. Note that the previous algorithm is just an outline of what can be done, and may be improved in many different aspects.

Acknowledgment

This paper is dedicated to Claude Reboulet, a pioneer in the research on parallel structure. Claude was a discrete gentleman whose early works has open the way to this exciting field of research. I am personnaly indebted to Claude which has motivated my interest in this subject. At a time were almost all was to be invented Claude has always offered me the most gentle advice and has always supported me in the difficult moments where the difficulties were overwhelming.

Many proposals of this paper are the result of numerous discussions with Arnold Neumaier from Wien University, to which I am deeply indebted.

References

[Baret 78] Baret M. Six degrees of freedom large motion system for flight simulators, piloted aircraft environment simulation techniques. In *AGARD Conference Proceeding* n°249, *Piloted aircraft environment simulation techniques*, pages 22–1/22–7, Bruxelles, April, 24-27, 1978.

[Borel 08] Borel E. Mémoire sur les déplacements à trajectoire sphériques. *Mémoire présentés par divers savants*, 33(1):1–128, 1908.

[Boudreau Gosselin 99] Boudreau R. and Gosselin C.M. The synthesis of planar parallel manipulators with a genetic algorithm. *ASME J. of Mechanical Design*, 121(4):533–537, December 1999.

[Bricard 06] Bricard R. Mémoire sur les déplacements à trajectoire sphériques. *Journal de l'École Polytechnique*, 11(2):1–96, 1906.

[Cauchy 13] Cauchy A. Deuxième mémoire sur les polygones et les polyèdres. *Journal de l'École Polytechnique*, pages 87–98, May 1813.

[Erdman 93] Erdman A.G. *Modern Kinematics*. Wiley, New-York, 1993.

[Gough 57] Gough V.E. Contribution to discussion of papers on research in automobile stability, control and tyre performance, 1956-1957. Proc. Auto Div. Inst. Mech. Eng.

[Gough Whitehall 62] Gough V.E. and Whitehall S.G. Universal tire test machine. In *Proceedings 9th Int. Technical Congress F.I.S.I.T.A.*, volume 117, pages 117–135, May 1962.

[King 73] King R.F. A flight simulator for advanced aircraft-servo: design to realization.

In *Summer Computation Simulation Conf.*, pages 248–253, Montréal, July, 13-19, 1973.

[Koevermans +75] Koevermans W.P. and others . Design and performance of the four d.o.f. motion system of the NLR research flight simulator. In *AGARD Conf. Proc. No 198, Flight Simulation*, pages 17–1/17–11, La Haye, October, 20-23, 1975.

[Lebesgue 67] Lebesgue H. Octaèdre articulé de Bricard. *L'enseignement mathématique*, (13):150–160, 1967.

[Ma Angeles 91] Ma O. and Angeles J. Optimum architecture design of platform manipulator. In *ICAR*, pages 1131–1135, Pise, June, 19-22, 1991.

[Masory Wang 95] Masory O. and Wang J. Workspace evaluation of Stewart platforms. *Advanced robotics*, 9(4):443–461, 1995.

[McCallion Pham 79] McCallion H. and Pham D.T. The analysis of a six degrees of freedom work station for mechanized assembly. In *Proc. 5th World Congress on Theory of Machines and Mechanisms*, pages 611–616, Montréal, July 1979.

[Merlet 97] Merlet J-P. Designing a parallel manipulator for a specific workspace. *Int. J. of Robotics Research*, 16(4):545–556, August 1997.

[Merlet 98a] Merlet J-P. Efficient computation of the extremum of the articular velocities of a parallel manipulator in a translation workspace. In *IEEE Int. Conf. on Robotics and Automation*, pages 1976–1981, Louvain, May, 18-20, 1998.

[Merlet 98b] Merlet J-P. Efficient estimation of the extremal articular forces of a parallel manipulator in a translation workspace. In *IEEE Int. Conf. on Robotics and Automation*, pages 1982–1987, Louvain, May, 18-20, 1998.

[Merlet 01] Merlet J-P. An improved design algorithm based on interval analysis for parallel manipulator with specified workspace. In *IEEE Int. Conf. on Robotics and Automation*, Seoul, May, 23-25, 2001.

[Moore 79] Moore R.E. *Methods and Applications of Interval Analysis*. SIAM Studies in Applied Mathematics, 1979.

[Parenti-Castelli Di Gregorio 00] Parenti-Castelli V. and Di Gregorio R. Influence of manufacturing errors on the kinematic performance of the 3-UPU parallel mechanism. In *2nd Chemnitzer Parallelkinematik Seminar*, pages 85–99, Chemnitz, April, 12-13, 2000.

[Parrish +73] Parrish R.V. and others . Motion software for a synergistic six-degree-of-freedom motion base. Technical Report D-7350, NASA, December 1973.

[Pierrot Dauchez Fournier 91] Pierrot F., Dauchez P., and Fournier A. Hexa: a fast six-dof fully parallel robot. In *ICAR*, pages 1159–1163, Pise, June, 19-22, 1991.

[Reboulet Robert 85] Reboulet C. and Robert A. Hybrid control of a manipulator with an active compliant wrist. In *3rd ISRR*, pages 76–80, Gouvieux, France, October, 7-11, 1985.

Regular Papers: New Architectures 1

Thursday, October 3, 2002, 9:30AM

Session Chairs: S. Agrawal and F. Pierrot

1. Zabalza, J. Ros, J.J. Gil, J.M. Pintor, J.M. Jimemez
   "TRI-SCOTT. A MICABO like 6-DOF Quasi-Decoupled Parallel Manipulator".

2. P. Wenger, D. Chablat
   "Design of a Three-Axis Isotropic Parallel Manipulato r for Machining Applications: The Orthoglide"

3. X. Kong, C.M. Gosselin
   "A Class of 3-DOF Translational Parallel Manipulators with Linear I-O Equations"

Proceedings of the WORKSHOP on
Fundamental Issues and Future Research Directions for Parallel Mechanisms and Manipulators
October 3–4, 2002, Quebec City, Quebec, Canada
Clément M. Gosselin and Imme Ebert-Uphoff, editors

TRI-SCOTT. A New Kinematic Structure for a 6-DOF Decoupled Parallel Manipulator

ISIDRO ZABALZA, JAVIER ROS, JOSE J. GIL, JESUS M. PINTOR, and JOSE M. JIMENEZ
Mechanical, Energy and Materials Engineering Department
Public University of Navarra
Campus Arrosadia, 31006, Pamplona, Spain
izavi@unavarra.es

Abstract: *This paper describes a new structure for a six-DOF decoupled parallel manipulator. The decoupled movement of the moving platform is analyzed and its degrees of freedom is calculated. The inverse and direct kinematics of the manipulator are presented, and the assembly modes determined.*

1 Introduction

The kinematic structure of most contemporary robots is an open kinematic chain structure (serial manipulators). However, robots with closed kinematic chains (parallel manipulators) have some advantages compared to serial ones:

- Higher payload to weight ratio, since the payload is supported by several legs in parallel.
- Higher accuracy due to non-cumulative joint error.
- Higher structural rigidity due to closed kinematic structure.
- Insensitivity positions (singular configurations) with very high position precision for the output link.
- Usually, actuators are located on the fixed platform.
- Simple solution of the inverse kinematics equations.
- Conversely, they suffer from smaller work space, uncertainty position, singular configurations and more complicated direct kinematic solution.

One of the first parallel manipulators, patented by Pollard (1942), was used for car painting. Later, Gough and Whitehall (1962) presented a parallel manipulator for tire testing and Stewart (1965) another one used in a fly simulator, both manipulators having linear actuators. Hunt (1983) presented a new parallel manipulator structure with 6 rotary actuators. During these last decades many authors have shown different parallel kinematic structures, some of them with linear actuators, others with rotary actuators and some with a mixture of linear and rotary actuators. Several of these parallel manipulators can be seen in (Merlet 2000). Also, these and other examples and references can be found in the following web sites:

- [http://www-sop.inria.fr/coprin/equipe/merlet/merlet.html].
- [http://www.parallemic.org/].

In most parallel manipulators, actuator movement influences both position and moving platform direction, but for some it influences only in the position or direction, these are called **decoupled manipulators**.

Examples of different decoupled parallel manipulator structures are presented for Innocenti and Parenti-Castelli (1991), Zlatanov et al. (1992), Patarinski and Uchiyama (1993), Wohlhart (1994), Geng and Haynes (1994), Bernier et al. (1995), Lee (1995), Lallemand et al. (1997), Ben-Horin et al. (1998), Brodski et al. (1998), Mianowski (1998) and Lee and Park (1999).

According to the previous references the **Tri-Scott** structure, that is going to be presented, has not been described before.

2 Tri-Scott structure

The parallel manipulator (Fig. 1) is composed of one fixed platform with three masts, three modified Scott's mechanisms sliding on the masts, and a triangular moving platform.

The masts are fixed and perpendicular to the fixed platform and are located in the vertexes of a triangle. Two of each Scott's mechanisms turning pairs have been replaced by two universal joints (K) allowing them to have a spatial movement instead of a planar one. Each complete Scott's mechanism can slide on its corresponding mast. The three vertexes of the moving platform are attached to the three

ending points of the Scott's mechanisms (points 41, 42 and 43).

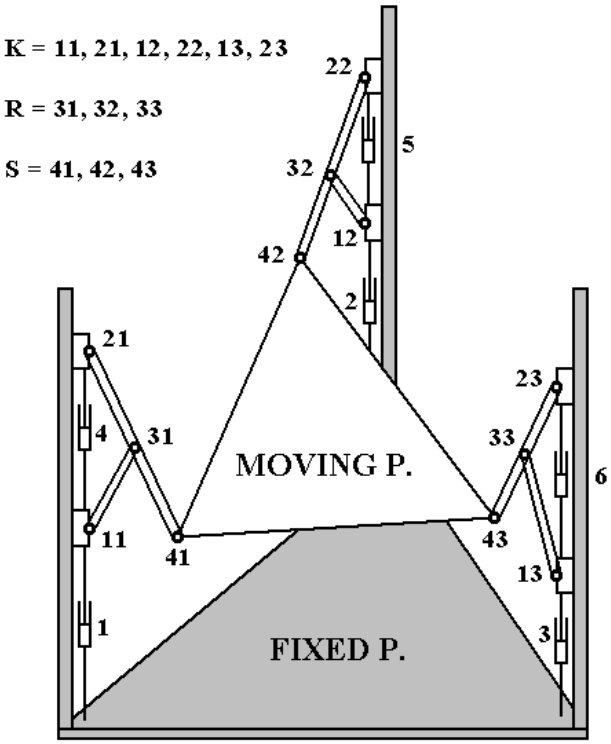

Figure 1. Tri-Scott parallel manipulator

At each mast, the overall movement of the complete Scott's mechanism is introduced by one linear actuator (actuators 1, 2 and 3), attaching the mechanism to the fixed platform. The intrinsic movement in each Scott's mechanism is introduced by one linear actuator (actuators 4, 5 and 6), attaching both mechanism sliders.

3 Tri-Scott kinematics

The original Scott's mechanism (Fig. 2) is a planar straight-line mechanism. With appropriate dimensions point "P" describes a straight line. In this mechanism, the pairs "A", "B" and "C" are revolutes.

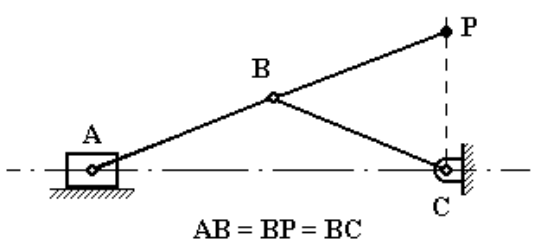

Figure 2. Original Scott's mechanism

Replacing the original Scott's mechanism turning pairs "A" and "C" by two spherical pairs (S) or by two universal joints (K) with two of their turning pairs aligned, a spatial mechanism is obtained in which point "P" moves on a plane. Placing pair "C" on a slider, the complete mechanism can have an overall sliding motion on the mast, (Fig. 3).

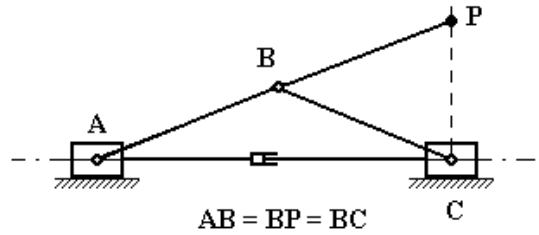

Figure 3. Modified Scott's mechanism

Due to the characteristics of such modified Scott's mechanisms, a decoupled movement of the moving platform is obtained. For example, if movement is only introduced by actuators "4", "5" and "6", a **planar movement** of the moving platform is obtained.

Using the Kutzbach criterion, having into account that pairs 11, 21, 12, 22, 13 and 23 can be spherical or universal joints with two of their turning pairs aligned, the moving platform degrees of freedom are easily found:

$$DOF = 6 \cdot (14 - 1) - 5 \cdot 9 - 3 \cdot 9 = 6 \quad (1)$$

3.1 Tri-Scott notation and topology

The notation used to describe the topology of this parallel manipulator is summarized in the following items and shown in figures 1, 4 and 5.

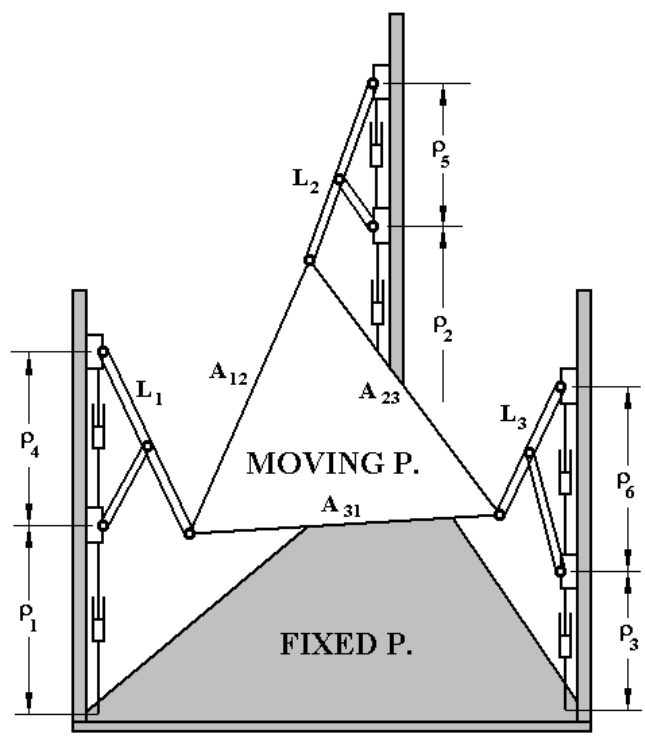

Figure 4. Notation of parallel manipulator, perspective

- *i* Linear actuator.
- ρ_i Articular coordinate of the *i-th* actuator.
- *1i* Center of universal joint in the lower slider of the *i-th* Scott's mechanism.
- *2i* Center of universal joint in the upper slider of the *i-th* Scott's mechanism.
- *3i* Center of turning pair in the *i-th* Scott's mechanism.
- *4i* Center of the spherical joint, vertex of moving platform attached to *i-th* Scott's mechanism.
- *Li* Length between centers *2i* and *4i*, or lengh of the longer link of the *i-th* Scott's mechanism.
- *Aij* Length moving platform edge that links the *i-th* and *j-th* Scott's mechanisms.
- *L'i* Length of the horizontal projection of *Li*, or length between centers *1i* and *4i*.
- *A'ij* Length of the horizontal projection of the edge *Aij*.

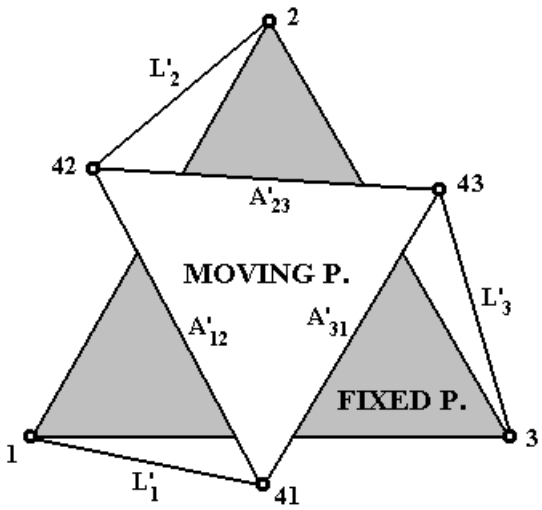

Figure 5. Notation of parallel manipulator, horizontal projection

4 Inverse kinematics

Inverse kinematics deals with the determination of the articular coordinates in terms of the moving platform position.

The moving platform position is expressed in terms of the value of the coordinates of the moving platform vertexes (X_{4i}, Y_{4i}, Z_{4i}).

It must be noted that although the position of the moving platform can be stated in a different way, for example by means of the coordinates of its gravity center and three Euler angles, it is always easy to determine the coordinates of its three above mentioned vertexes in terms of the alternative set of coordinates.

It is evident that in the Scott's mechanism the articular coordinates of "1", "2" and "3" actuators are de "Z" coordinates of the moving platform vertexes, so

$$\rho_i = Z_{4i} \quad ; \quad i = 1,2,3 . \tag{2}$$

And, as

$$L'_i = \sqrt{L_i^2 - \rho_{i+3}^2} \ , \tag{3}$$

the articular coordinates of "4", "5" and "6" actuators will be:

$$\rho_4 = \sqrt{L_1^2 - (X_{41} - X_1)^2 - (Y_{41} - Y_1)^2} \tag{4}$$

$$\rho_5 = \sqrt{L_2^2 - (X_{42} - X_2)^2 - (Y_{42} - Y_2)^2} \tag{5}$$

$$\rho_6 = \sqrt{L_3^2 - (X_{43} - X_3)^2 - (Y_{43} - Y_3)^2} \tag{6}$$

5 Direct kinematic

Direct kinematic deals with the determination of moving platform position in terms of the input (actuator) coordinates.

Given the articular coordinates "ρ_i", the "Z_{4i}" coordinates of the of moving platform vertexes are directly determined:

$$Z_{4i} = \rho_i \quad ; \quad i = 1,2,3. \tag{7}$$

The lengths of the horizontal projections of the longer links in the Scott's mechanisms will be:

$$L'_1 = \sqrt{L_1^2 - \rho_4^2} \tag{8}$$

$$L'_2 = \sqrt{L_2^2 - \rho_5^2} \tag{9}$$

$$L'_3 = \sqrt{L_3^2 - \rho_6^2} \tag{10}$$

And the lengths of the horizontal projections of the edges of moving platform will be:

$$A'_{12} = \sqrt{A_{12}^2 - (Z_{42} - Z_{41})^2} \tag{11}$$

$$A'_{23} = \sqrt{A_{23}^2 - (Z_{43} - Z_{42})^2} \tag{12}$$

$$A'_{31} = \sqrt{A_{31}^2 - (Z_{41} - Z_{43})^2} \tag{13}$$

Taking into acount the lengths of the projections, ecuations (8 to 13), the coordinates "X" and "Y" of the vertexes of moving platform can be determined with the polynomial method proposed by Gosselin et al. (1992) for planar parallel manipulators.

Gosselin et al. obtained a sixth degree polynomial which could get six real solutions, corresponding to the different assembly modes of the manipulator.

As Tri-Scott is a spatial mechanism, its moving platform can turn upside down, for this reason, the Tri-scott have another six degree polynomial with another six possible solutions.

As a consequence, the direct kinematics of the Tri-Scott parallel manipulator presents two sixth degree polynomials with twelve possible solutions associated with different assembly modes of the manipulator.

6 Conclusions

In this paper the structure of a new six DOF decoupled parallel manipulator has been presented. The kinematic structure is based on three modified Scott's mechanisms. With this structure a decoupled movement of the moving platform is obtained. It is verified that it is a six degree of freedom mechanism. The inverse kinematics of the manipulator is presented. Finally, it is presented a closed form direct kinematics in terms of two polynomials of sixth degree that have associated twelve different assembly modes.

References

Ben-Horin R., Shoham M, and Djerassi S., 1998, "Kinematics, dynamics and construction of a planarly actuated parallel robot", Robotics and Computer-Integrated Manufacturing, Vol. 14, Nº 2, pp. 163-172.

Bernier D., Castelain J.M., and Li X., 1995, "A new parallel structure with six degree of freedom", 9th World Congress on the Theory of Machines and Mechanisms", Milan, August 30-September 2, pp. 8-12.

Brodski V., Glozman D., and Shoham M., 1998, "Double circular-triangular six-degree-of-freedom parallel robot", ARK, Strobl, June 29-July 4, pp. 155-164.

Geng Z., and Haynes L.S., 1994, "A 3-2-1 kinematic configuration of a Stewart platform and its application to six degree of freedom pose measurements", Robotics & Computer-Integrated Manufacturing, Vol. 11, Nº 1, pp. 23-34.

Gosselin C.M., Sefrioui J., and Richard M.J., 1992, " Solutions polynomiales au problème de la cinématique directe des manipulateurs parallèles plans à trois degrés de liberté", Mechanism and Machine Theory, Vol. 27 Nº 2, pp. 107-119.

Gough V.E., and Whitehall S.G., 1962, "Universal tire test machine", Proc. 9th Int. Technical Congres F.I.S.I.T.A., Vol. 117, pp. 117-135.

Hunt K.H., 1983, "Structural kinematics of in-parallel-actuated robot-arms", J. of Mechanisms, Transmissions, and Automation in Design, Vol. 105, Nº 4, pp. 705-712.

Innocenti C., and Parenti-Castelli V., 1991, "Direct kinematics of the 6-4 fully parallel manipulator with position and orientation uncoupled" European Robotics and Intelligent Systems Conf., Corfu, June 23-28.

Lallemand J.P., Goudali A., and Zeghloul S., 1997, "The 6-dof 2-Delta parallel robot", Robotica, Vol. 15, Nº 4, pp. 407-416.

Lee M.K., 1995, "Design of a high stiffness machining robot arm using double parallel mechanism", IEEE Int. Conf. on Robotics and Automation, Nagoya, May 25-27, pp. 234-240.

Lee M.K., and Park K.W., 1999, "Kinematics and dynamics analysis of a double parallel manipulator for enlarging workspace and avoiding singularities", IEEE Trans. on Robotics and Automation, Vol. 15, Nº 6, pp. 1024-1034.

Merlet J.P., 2000, "Parallel robots", Kluwer Academic Publishers.

Mianowski K., 1998, Dextrous fully parallel manipulator with six degrees of freedom", 12th RoManSy, Paris, July 6-9, pp. 253-260.

Patarinski S.P., and Uchiyama M., 1993, "Position/ orientation decoupled parallel manipulator", ICAR, Tokio, November 1-2, pp. 153-158.

Pollard W.L.V., 1942, "Position controlling apparatus", United States Patent Nº US2286571.

Stewart D., 1965, "A platform with 6 degree of freedom", Proc. of the Institution of Mechanical Engineers, Vol. 180, Pt. 1, Nº 15, pp. 371-386.

Wohlhart K., 1994, "Displacement analysis of the general spherical Stewart platform", Mechanisms and Machine Theory, Vol. 29, Nº 4, pp. 581-589.

Zlatanov D., Dai M.Q., Fenton R.G., and Benhabib B., 1992, "Mechanical design and kinematic analysis of a three-legged six degree-of-freedom parallel manipulator", Robotics, Spatial Mechanisms, and Mechanical Systems, ASME, DE-Vol 45, pp. 529-536.

Proceedings of the WORKSHOP on
Fundamental Issues and Future Research Directions for Parallel Mechanisms and Manipulators
October 3–4, 2002, Quebec City, Quebec, Canada
Clément M. Gosselin and Imme Ebert-Uphoff, editors

Design of a Three-Axis Isotropic Parallel Manipulator for Machining Applications: The Orthoglide

PHILIPPE WENGER, DAMIEN CHABLAT
Institut de Recherche en Communications et Cybernétique de Nantes (IRCCyN)
1, rue de la Noë, 44321 Nantes, France
email: Philippe.Wenger@irccyn.ec-nantes.fr
email: Damien.Chablat@irccyn.ec-nantes.fr

Abstract: *The orthoglide is a 3-DOF parallel mechanism designed at IRCCyN for machining applications. It features three fixed parallel linear joints which are mounted orthogonally and a mobile platform which moves in the Cartesian x-y-z space with fixed orientation. The orthoglide has been designed as function of a prescribed Cartesian workspace with prescribed kinetostatic performances. The interesting features of the orthoglide are a regular Cartesian workspace shape, uniform performances in all directions and good compactness. A small-scale prototype of the orthoglide under development is presented at the end of this paper.*

1 Introduction

Parallel kinematic machines (PKM) are interesting alternative designs for high-speed machining applications and have been attracting the interest of more and more researchers and companies. Since the first prototype presented in 1994 during the IMTS in Chicago by Gidding&Lewis (the Variax), many other prototypes have appeared.

However, the existing PKM suffer from two major drawbacks, namely, a complex Cartesian workspace and highly non linear input/output relations. For most PKM, the Jacobian matrix which relates the joint rates to the output velocities is not constant and not isotropic. Consequently, the performances (e.g. maximum speeds, forces accuracy and rigidity) vary considerably for different points in the Cartesian workspace and for different directions at one given point. This is a serious drawback for machining applications (Kim (1997); Treib *et al.* (1998); Wenger *et al.* (1999)). To be of interest for machining applications, a PKM should preserve good workspace properties, that is, regular shape and acceptable kinetostatic performances throughout. In milling applications, the machining conditions must remain constant along the whole tool path (Rehsteiner (1999); Rehsteiner *et al.* (1999)). In many research papers, this criterion is not taking into account in the algorithmic methods used for the optimization of the workspace volume (Luh *et al.* (1996); Merlet (1999)).

The orthoglide optimization is conducted to define a 3-axis PKM with the advantages a classical serial PPP machine tool but not its drawbacks. Most industrial 3-axis machine-tool have a serial PPP kinematic architecture with orthogonal linear joint axes along the x, y and z directions. Thus, the motion of the tool in any of these directions is linearly related to the motion of one of the three actuated axes. Also, the performances are constant in the most part of the Cartesian workspace, which is a parallelepiped. The main drawback is inherent to the serial arrangement of the links, namely, poor dynamic performances.

The orthoglide is a PKM with three fixed linear joints mounted orthogonally. The mobile platform is connected to the linear joints by three articulated parallelograms and moves in the Cartesian x-y-z space with fixed orientation. Its workspace shape is close to a cube whose sides are parallel to the planes xy, yz and xz respectively. The optimization is conducted on the basis of the size of a prescribed cubic workspace with bounded velocity and force transmission factors. Two criteria are used for the architecture optimization of the orthoglide, (i) the conditioning of the Jacobian matrix of the PKM (Golub *et al.* (1989); Salisbury *et al.* (1982); Angeles (1997)) and (ii) the manipulability ellipsoid (Yoshikawa (1985)).

The first criterion leads to an isotropic architecture and to homogeneous performances in the workspace. The second criterion permits to optimize the actuated joint limits and the link lengths of the orthoglide with respect to the aforementioned two criteria.

Next section presents the orthoglide. The kinematic equations and the singularity analysis is detailed in Section 3. Section 4 is devoted to the optimization process of the orthoglide and to the presentation of the prototype.

2 Description of the Orthoglide

Most existing PKM can be classified into two main families. The PKM of the first family have fixed foot points and variable length struts and are generally called "hexapods". They have a Stewart-Gought parallel kinematic architecture. Many prototypes and commercial hexapod PKM already exist like the Variax-Hexacenter (Gidding&Lewis), the CMW300 (Compagnie Mécanique des Vosges), the TORNADO 2000 (Hexel), the MIKROMAT 6X (Mikromat/IWU), the hexapod OKUMA (Okuma), the hexapod G500 (GEODETIC). In this first family, we find also hybrid architectures with a 2-axis wrist mounted in series to a 3-DOF tripod positioning structure (the TRICEPT from Neos Robotics).

The second family of PKM has been more recently investigated. In this category we find the HEXAGLIDE (ETH Zürich) which features six parallel (also in the geometrical sense) and coplanar linear joints. The HexaM (Toyoda) is another example with non coplanar linear joints. A 3-axis translational version of the hexaglide is the TRIGLIDE (Mikron), which has three coplanar and parallel linear joints. Another 3-axis translational PKM is proposed by the ISW Uni Stuttgart with the LINAPOD. This PKM has three vertical (non coplanar) linear joints. The URANE SX (Renault Automation) and the QUICKSTEP (Krause & Mauser) are 3-axis PKM with three non coplanar horizontal linear joints. The SPRINT Z3 (DS Technology) is a 3-axis PKM with one degree of translation and two degrees of rotations. A hybrid parallel/serial PKM with three parallel inclined linear joints and a two-axis wrist is the GEORGE V (IFW Uni Hanover).

PKMs of the second family are more interesting because the actuators are fixed and thus the moving masses are lower than in the hexapods and tripods.

The orthoglide presented in this article is a 3-axis translational parallel kinematic machine with variable foot points and fixed length struts. Figure 1 shows the general kinematic architecture of the orthoglide.

The orthoglide has three parallel $PRPaR$ identical chains (where P, R and Pa stands for Prismatic, Revolute and Parallelogram joint, respectively). The actuated joints are the three orthogonal linear joints. These joints can be actuated by means of linear motors or by conventional rotary motors with ball screws. The output body is connected to the linear joints through a set of three parallelograms of equal lengths $L = B_iC_i$, so that it can move only in translation. The first linear joint axis is parallel to the x-axis, the second one is parallel to the y-axis and the third one is parallel to the z-axis. In figure 1, the base points A_1, A_2 and A_3 are fixed on the ith linear axis such that $A_1A_2 = A_1A_3 = A_2A_3$, B_i is at the intersection of the first revolute axis $\mathbf{i}_i$ and the second revolute axis $\mathbf{j}_i$ of the ith parallelogram, and C_i is at the intersection of the last two revolute joints of the ith parallelogram. When each B_iC_i is aligned with the linear joint axis A_iB_i , the orthoglide is in an isotropic configuration (see 4.4) and the tool center point P is located at the intersection of the three linear joint axes. In this configuration, the base points A_1, A_2 and A_3 are equally distant from P. The symmetric design and the simplicity of the kinematic chains (all joints have only one degree of freedom, Fig. 2) should contribute to lower the manufacturing cost of the orthoglide.

The orthoglide is free of singularities and self-collisions. The workspace has a regular, quasi-cubic shape. The input/output equations are simple and the velocity transmission factors are equal to one along the x, y and z direction at the isotropic configuration, like in a serial PPP machine (Wenger *et al.* (2000)).

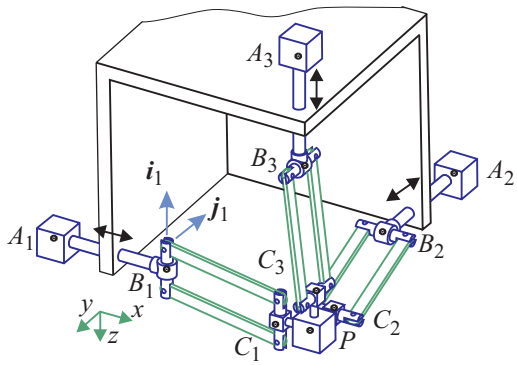

Figure 1: Orthoglide kinematic architecture

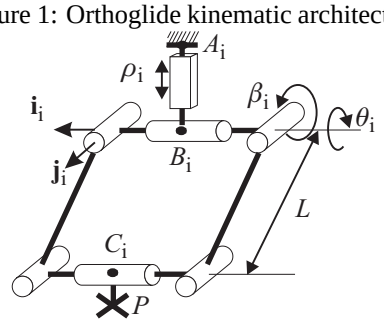

Figure 2: Leg kinematics

3 Kinematic Equations and Singularity Analysis

3.1 Static Equations

Let θ_i and β_i denote the joint angles of the parallelogram about the axes $\mathbf{i}_i$ and $\mathbf{j}_i$, respectively (fig. 2). Let ρ_1, ρ_2, ρ_3 denote the linear joint variables, $\rho_i = A_iB_i$. In a reference frame (O, x, y, z) centered at the intersection of the three linear joint axes (note that the reference frame has been translated in Fig. 1 for more legibility) , the position vector $\mathbf{p}$ of the tool center point P can be defined in three different ways:

$$\mathbf{p} = \begin{bmatrix} a + \rho_1 + \cos(\theta_1)\cos(\beta_1)L + e \\ \sin(\theta_1)\cos(\beta_1)L \\ -\sin(\beta_1)L \end{bmatrix} \tag{1a}$$

$$\mathbf{p} = \begin{bmatrix} -\sin(\beta_2)L \\ a+\rho_2+\cos(\theta_2)\cos(\beta_2)L+e \\ \sin(\theta_2)\cos(\beta_2)L \end{bmatrix} \quad (1b)$$

$$\mathbf{p} = \begin{bmatrix} \sin(\theta_3)\cos(\beta_3)L \\ -\sin(\beta_3)L \\ a+\rho_3+\cos(\theta_3)\cos(\beta_3)L+e \end{bmatrix} \quad (1c)$$

where $a = OA_i$, $e = C_iP$ and we recall that $L = B_iC_i$, $\rho_i = A_iB_i$.

3.2 Kinematic Equations

Let $\dot{\boldsymbol{\rho}}$ be referred to as the vector of actuated joint rates and $\dot{\mathbf{p}}$ as the velocity vector of point P:

$$\dot{\boldsymbol{\rho}} = [\dot{\rho}_1\ \dot{\rho}_2\ \dot{\rho}_3]^T, \quad \dot{\mathbf{p}} = [\dot{x}\ \dot{y}\ \dot{z}]^T$$

$\dot{\mathbf{p}}$ can be written in three different ways by traversing the three chains $A_iB_iC_iP$:

$$\dot{\mathbf{p}} = \mathbf{n}_1\dot{\rho}_1 + (\dot{\theta}_1\mathbf{i}_1 + \dot{\beta}_1\mathbf{j}_1) \times (\mathbf{c}_1 - \mathbf{b}_1) \quad (2a)$$
$$\dot{\mathbf{p}} = \mathbf{n}_2\dot{\rho}_1 + (\dot{\theta}_2\mathbf{i}_2 + \dot{\beta}_2\mathbf{j}_2) \times (\mathbf{c}_2 - \mathbf{b}_2) \quad (2b)$$
$$\dot{\mathbf{p}} = \mathbf{n}_3\dot{\rho}_3 + (\dot{\theta}_3\mathbf{i}_3 + \dot{\beta}_3\mathbf{j}_3) \times (\mathbf{c}_3 - \mathbf{b}_3) \quad (2c)$$

where $\mathbf{b}_i$ and $\mathbf{c}_i$ are the position vectors of the points B_i and C_i, respectively, and $\mathbf{n}_i$ is the direction vector of the linear joints, for $i = 1, 2, 3$.

3.3 Singular configurations

We want to eliminate the two idle joint rates $\dot{\theta}_i$ and $\dot{\beta}_i$ from Eqs. (2a–c), which we do upon dot-multiplying Eqs. (2a–c) by $\mathbf{c}_i - \mathbf{b}_i$:

$$(\mathbf{c}_1 - \mathbf{b}_1)^T\dot{\mathbf{p}} = (\mathbf{c}_1 - \mathbf{b}_1)^T\mathbf{n}_1\dot{\rho}_1 \quad (3a)$$
$$(\mathbf{c}_2 - \mathbf{b}_2)^T\dot{\mathbf{p}} = (\mathbf{c}_2 - \mathbf{b}_2)^T\mathbf{n}_2\dot{\rho}_2 \quad (3b)$$
$$(\mathbf{c}_3 - \mathbf{b}_3)^T\dot{\mathbf{p}} = (\mathbf{c}_3 - \mathbf{b}_3)^T\mathbf{n}_3\dot{\rho}_3 \quad (3c)$$

Equations (3a–c) can now be cast in vector form, namely

$$\mathbf{A}\dot{\mathbf{p}} = \mathbf{B}\dot{\boldsymbol{\rho}}$$

where **A** and **B** are the parallel and serial Jacobian matrices, respectively:

$$\mathbf{A} = \begin{bmatrix} (\mathbf{c}_1 - \mathbf{b}_1)^T \\ (\mathbf{c}_2 - \mathbf{b}_2)^T \\ (\mathbf{c}_3 - \mathbf{b}_3)^T \end{bmatrix} \quad (4a)$$

$$\mathbf{B} = \begin{bmatrix} \eta_1 & 0 & 0 \\ 0 & \eta_2 & 0 \\ 0 & 0 & \eta_3 \end{bmatrix} \quad (4b)$$

with $\eta_i = (\mathbf{c}_i - \mathbf{b}_i)^T\mathbf{n}_i$ for $i = 1, 2, 3$.

The parallel singularities (Chablat *et al.* (1998)) occur when the determinant of the matrix **A** vanishes, *i.e.* when $det(\mathbf{A}) = 0$. In such configurations, it is possible to move locally the mobile platform whereas the actuated joints are locked. These singularities are particularly undesirable because the structure cannot resist any force. Eq. (4a) shows that the parallel singularities occur when:

$$(\mathbf{c}_1 - \mathbf{b}_1) = \alpha(\mathbf{c}_2 - \mathbf{b}_2) + \lambda(\mathbf{c}_3 - \mathbf{b}_3)$$

that is when the points B_1, C_1, B_2, C_2, B_3 and C_3 are coplanar (Fig. 3). A particular case occurs when the links B_iC_i are parallel (Fig. 4):

$$(\mathbf{c}_1 - \mathbf{b}_1) \ // \ (\mathbf{c}_2 - \mathbf{b}_2) \quad \text{and}$$
$$(\mathbf{c}_2 - \mathbf{b}_2) \ // \ (\mathbf{c}_3 - \mathbf{b}_3) \quad \text{and}$$
$$(\mathbf{c}_3 - \mathbf{b}_3) \ // \ (\mathbf{c}_1 - \mathbf{b}_1)$$

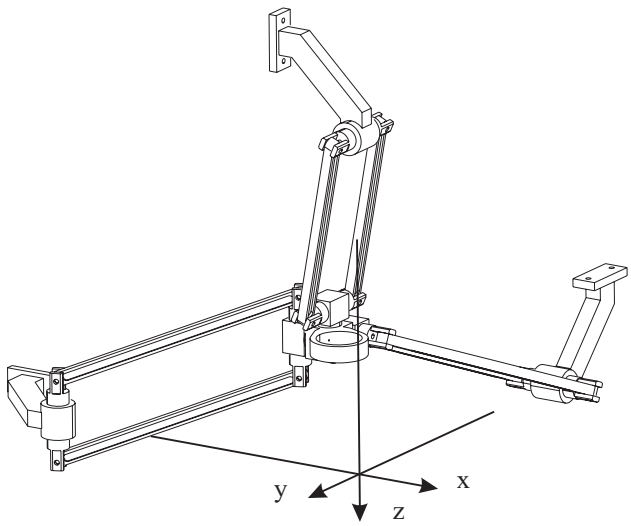

Figure 3: Parallel singular configuration when B_iC_i are coplanar

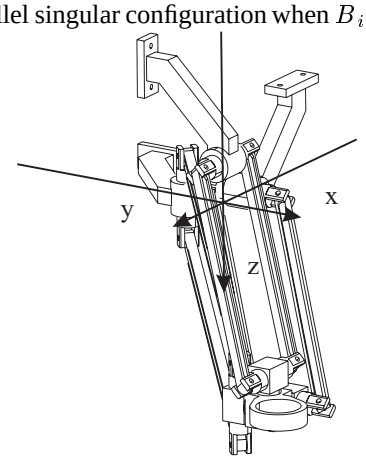

Figure 4: Parallel singular configuration when B_iC_i are parallel

Serial singularities arise when the serial Jacobian matrix **B** is no longer invertible *i.e.* when $det(\mathbf{B}) = 0$. At a serial singularity a direction exists along which any cartesian velocity cannot be

produced. Eq. (4b) shows that $\det(\mathbf{B}) = 0$ when for one leg i, $(\mathbf{b}_i - \mathbf{a}_i) \perp (\mathbf{c}_i - \mathbf{b}_i)$.

The optimization of the orthoglide will put the serial and parallel singularities far away from the workspace (see 4.4).

4 Design and Performance Analysis of the Orthoglide

For usual machine tools, the Cartesian workspace is generally given as a function of the size of a right-angled parallelepiped. Due to the symmetrical architecture of the orthoglide, the Cartesian workspace has a fairly regular shape in which it is possible to include a cube whose sides are parallel to the planes xy, yz and xz respectively (Fig. 5).

The aim of this section is to define the dimensions of the orthoglide as a function of the size $L_{Workspace}$ of a prescribed cubic workspace with bounded transmission factors. We first show that the orthogonal arrangement of the linear joints is justified by the condition on the isotropy and manipulability: we want the orthoglide to have an isotropic configuration with velocity and force transmission factors equal to one. Then, we impose that the transmission factors remain under prescribed bounds throughout the prescribed workspace and we deduce the link dimensions and the joint limits.

4.1 Condition Number and Isotropic Configuration

The Jacobian matrix is said to be isotropic when its condition number attains its minimum value of one (Angeles (1997)). The condition number of the Jacobian matrix is an interesting performance index which characterises the distortion of a unit ball under the transformation represented by the Jacobian matrix. The Jacobian matrix of a manipulator is used to relate (i) the joint rates and the Cartesian velocities, and (ii) the static load on the output link and the joint torques or forces. Thus, the condition number of the Jacobian matrix can be used to measure the uniformity of the distribution of the tool velocities and forces in the Cartesian workspace.

4.2 Isotropic Configuration of the Orthoglide

For parallel manipulators, it is more convenient to study the conditioning of the Jacobian matrix that is related to the inverse transformation, $\mathbf{J}^{-1}$. When $\mathbf{B}$ is not singular, $\mathbf{J}^{-1}$ is defined by:

$$\dot{\boldsymbol{\rho}} = \mathbf{J}^{-1}\dot{\mathbf{p}} \text{ with } \mathbf{J}^{-1} = \mathbf{B}^{-1}\mathbf{A}$$

Thus:

$$\mathbf{J}^{-1} = \begin{bmatrix} (1/\eta_1)(\mathbf{c}_1 - \mathbf{b}_1)^T \\ (1/\eta_2)(\mathbf{c}_2 - \mathbf{b}_2)^T \\ (1/\eta_3)(\mathbf{c}_3 - \mathbf{b}_3)^T \end{bmatrix} \tag{5}$$

with $\eta_i = (\mathbf{c}_i - \mathbf{b}_i)^T\mathbf{n}_i$ for $i = 1, 2, 3$.

The matrix $\mathbf{J}^{-1}$ is isotropic when $\mathbf{J}^{-1}\mathbf{J}^{-T} = \sigma^2\mathbf{1}_{3\times3}$, where $\mathbf{1}_{3\times3}$ is the 3×3 identity matrix. Thus, we must have,

$$\frac{1}{\eta_1}||\mathbf{c}_1 - \mathbf{b}_1|| = \frac{1}{\eta_2}||\mathbf{c}_2 - \mathbf{b}_2|| = \frac{1}{\eta_3}||\mathbf{c}_3 - \mathbf{b}_3|| \tag{6a}$$

$$(\mathbf{c}_1 - \mathbf{b}_1)^T(\mathbf{c}_2 - \mathbf{b}_2) = 0 \tag{6b}$$

$$(\mathbf{c}_2 - \mathbf{b}_2)^T(\mathbf{c}_3 - \mathbf{b}_3) = 0 \tag{6c}$$

$$(\mathbf{c}_3 - \mathbf{b}_3)^T(\mathbf{c}_1 - \mathbf{b}_1) = 0 \tag{6d}$$

Equation (6a) states that the orientation between the axis of the linear joint and the link B_iC_i must be the same for each leg i. Equations (6b–d) mean that the links B_iC_i must be orthogonal to each other. Figure 6 shows the isotropic configuration of the orthoglide. Note that the orthogonal arrangement of the linear joints is not a consequence of the isotropy condition, but it stems from the condition on the transmission factors at the isotropic configuration (see next section).

4.3 Manipulability Analysis

For a serial PPP machine tool, Fig. 7, a motion of an actuated joint yields the same motion of the tool (the transmission factors are equal to one). In the purpose on our study, this factor is calculated from linear joint to the end-effector.

For a parallel machine, these motions are generally not equivalent. When the mechanism is close to a parallel singularity, a small joint rate can generate a large velocity of the tool. This means that the positioning accuracy of the tool is lower in some directions for some configurations close to parallel singularities because the encoder resolution is amplified. In addition, a velocity amplification in one direction is equivalent to a loss of rigidity in this direction.

The manipulability ellipsoids of the Jacobian matrix of robotic manipulators was defined several years ago (Salisbury *et al.* (1982)). This concept has then been applied as a performance index to parallel manipulators (Kim (1997)). Note that, although the concept of manipulability is close to the concept of condition number, these two concepts do not provide the same information. The condition number quantifies the proximity to an isotropic configuration, *i.e.* where the manipulability ellipsoid is a sphere, or, in other words, where the transmission factors are the same in all the directions, but it does not inform about the value of the transmission factor.

The manipulability ellipsoid of $\mathbf{J}^{-1}$ is used here for (i) justifying the orthogonal orientation of the linear joints and (ii) defining the joint limits of the orthoglide such that the transmission factors are bounded in the prescribed workspace.

We want the transmission factors to be equal to one at the isotropic configuration like for a PPP machine tool. This condition implies that the three terms of Eq. (6) must be equal to one:

$$\frac{1}{\eta_1}||\mathbf{c}_1 - \mathbf{b}_1|| = \frac{1}{\eta_2}||\mathbf{c}_2 - \mathbf{b}_2|| = \frac{1}{\eta_3}||\mathbf{c}_3 - \mathbf{b}_3|| = 1 \tag{7}$$

which implies that $(\mathbf{b}_i - \mathbf{a}_i)$ and $(\mathbf{c}_i - \mathbf{b}_i)$ must be collinear for each i.

Since, at this isotropic configuration, links B_iC_i are orthogonal, Eq. (7) implies that the links A_iB_i are orthogonal, *i.e.* the linear joints are orthogonal. For joint rates belonging to a unit

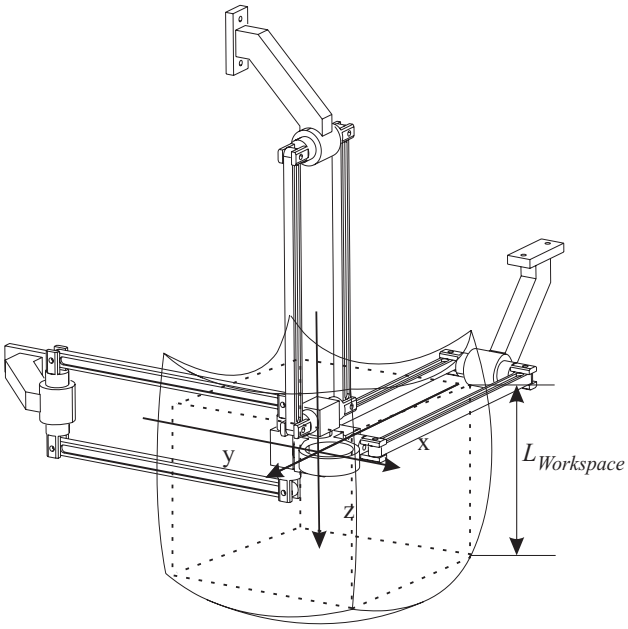

Figure 5: Cartesian workspace

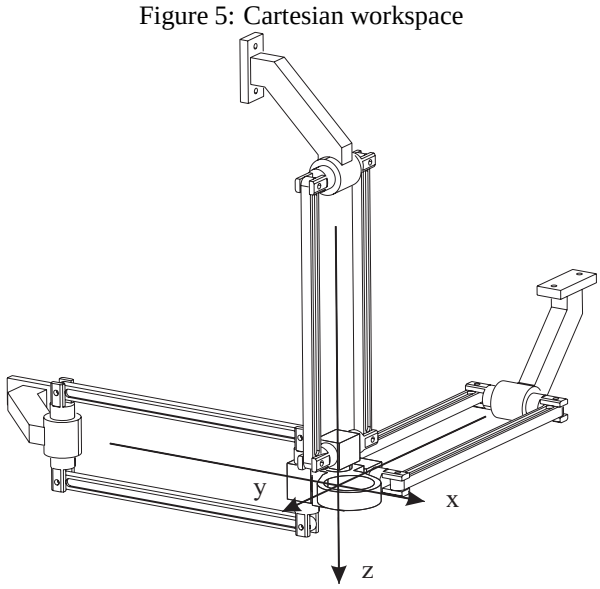

Figure 6: Isotropic configuration of the Orthoglide mecanism

ball, namely, $||\dot{\boldsymbol{\rho}}|| \leq 1$, the Cartesian velocities belong to an ellipsoid such that:

$$\dot{\boldsymbol{p}}^T(\mathbf{J}\mathbf{J}^T)\dot{\boldsymbol{p}} \leq 1$$

The eigenvectors of matrix $(\mathbf{J}\mathbf{J}^T)^{-1}$ define the direction of its principal axes of this ellipsoid and the square roots ξ_1, ξ_2 and ξ_3 of the eigenvalues of $(\mathbf{J}\mathbf{J}^T)^{-1}$ are the lengths of the aforementioned principal axes. The velocity transmission factors in the directions of the principal axes are defined by $\psi_1 = 1/\xi_1$, $\psi_2 = 1/\xi_2$ and $\psi_3 = 1/\xi_3$. To limit the variations of this factor

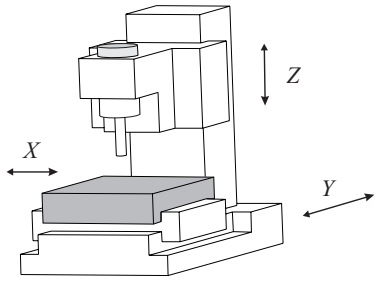

Figure 7: Typical industrial 3-axis PPP machine-tool

in the Cartesian workspace, we impose

$$\psi_{min} \leq \psi_i \leq \psi_{max} \tag{8}$$

throughout the workspace. This condition determines the link lengths and the linear joint limits. To simplify the problem, we set $\psi_{min} = 1/\psi_{max}$.

4.4 Design of the Orthoglide for a Prescribed Workspace

The aim of this section is to define the position of the fixed point A_i, the link lengths L and the linear actuator range $\Delta\rho$ with respect to the limits on the transmission factors defined in Eq. (8) and as a function of the size of the prescribed workspace $L_{Workspace}$.

Our process of optimization is divided into three steps.

1. First, we determine two points Q_1 and Q_2 in the prescribed cubic workspace such that if the transmission factor bounds are satisfied at these points, they are satisfied in all the prescribed workspace.

2. The points Q_1 and Q_2 are used to define the leg length L as function of the size of the prescribed cubic workspace.

3. Finally, the positions of the base points A_i and the linear actuator range $\Delta\rho$ are calculated such that the prescribed cubic workspace is fully included in the Cartesian workspace of the orthoglide.

Step 1: The transmission factors are equal to one at the isotropic configuration. These factors increase or decrease when the tool center point moves away from the isotropic configuration and they tend towards zero or infinity in the vicinity of the singularity surfaces. It turns out that the points Q_1 and Q_2 defined at the intersection of the workspace boundary with the axis $x = y = z$ (figure 8) are the closest ones to the singularity surfaces, as illustrated in figure 9 which shows on the same top view the orthoglide in the two parallel singular configurations of figures 3 and 4. Thus, we may postulate the intuitive result that if the prescribed bounds on the transmission factors are satisfied at Q_1 and Q_2, then these bounds are satisfied throughout the prescribed cubic workspace. Although we could not derive a simple

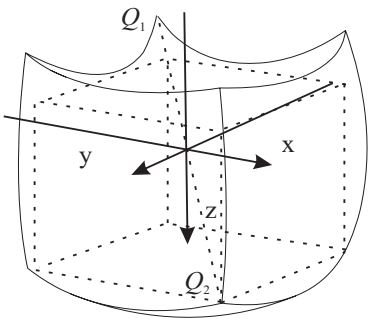

Figure 8: Points Q_1 and Q_2

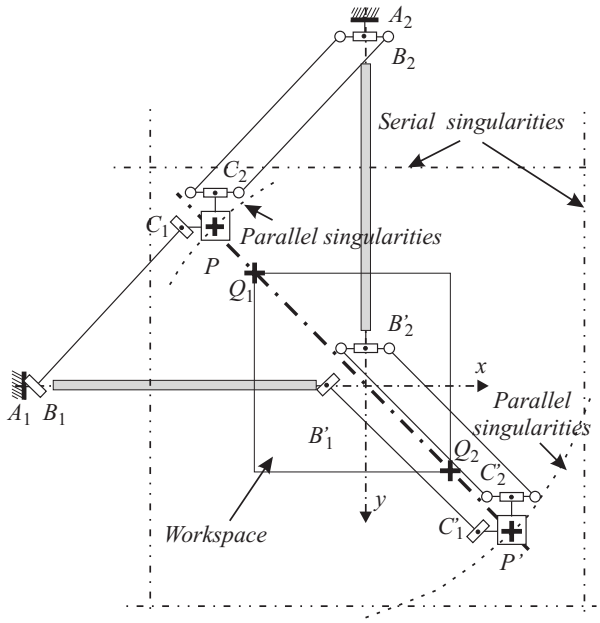

Figure 9: Points Q_1 and Q_2 and the singular configurations (top view)

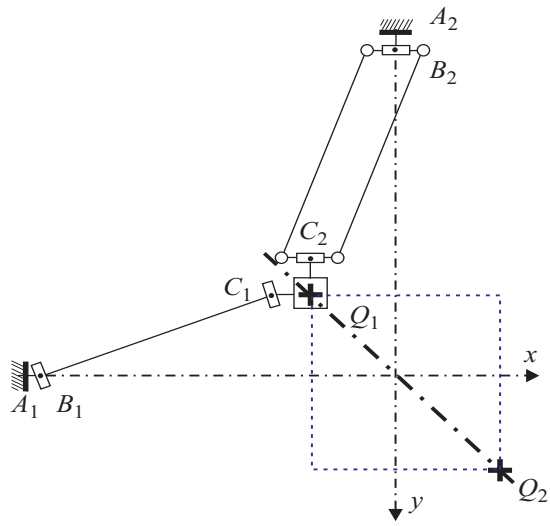

Figure 10: Q_1 configuration

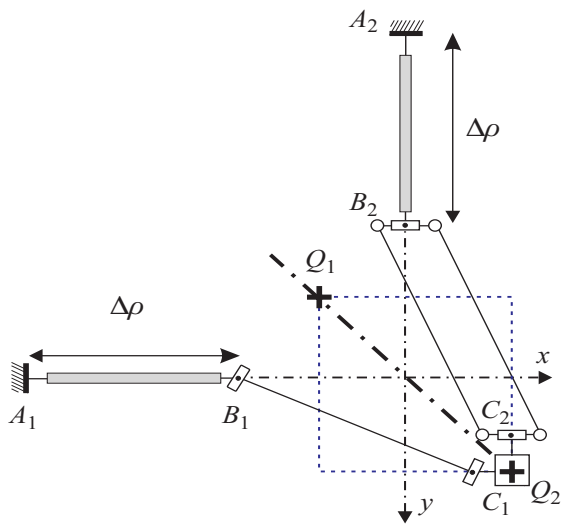

Figure 11: Q_2 configuration

formal proof, we have verified numerically that this result holds.

Step 2: At the isotropic configuration, the angles θ_i and β_i are equal to zero by definition. When the tool center point P is at Q_1, $\rho_1 = \rho_2 = \rho_3 = \rho_{min}$ (Fig. 10). When P is at Q_2, $\rho_1 = \rho_2 = \rho_3 = \rho_{max}$ (Fig. 11).

We pose $\rho_{min} = 0$ for more simplicity.

On the axis (Q_1Q_2), $\beta_1 = \beta_2 = \beta_3$ and $\theta_1 = \theta_2 = \theta_3$. We note,

$$\beta_1 = \beta_2 = \beta_3 = \beta \quad \text{and} \quad \theta_1 = \theta_2 = \theta_3 = \theta \tag{9}$$

Upon substitution of Eq. (9) into Eqs. (1a–c), the angle β can be written as a function of θ,

$$\beta = -\arctan(\sin(\theta)) \tag{10}$$

Finally, by substituting Eq. (10) into Eq. (5), the inverse Jacobian matrix $\mathbf{J}^{-1}$ can be simplified as follows

$$\mathbf{J}^{-1} = \begin{bmatrix} 1 & -\tan(\theta) & -\tan(\theta) \\ -\tan(\theta) & 1 & -\tan(\theta) \\ -\tan(\theta) & -\tan(\theta) & 1 \end{bmatrix}$$

Thus, the square roots of the eigenvalues of $(\mathbf{J}\mathbf{J}^T)^{-1}$ are,

$$\xi_1 = |2\tan(\theta) - 1| \quad \text{and} \quad \xi_2 = \xi_3 = |\tan(\theta) + 1|$$

And the three velocity transmission factors are,

$$\psi_1 = \frac{1}{|2\tan(\theta) - 1|} \quad \text{and} \quad \psi_2 = \psi_3 = \frac{1}{|\tan(\theta) + 1|} \tag{11}$$

Figure 12 depicts ψ_1, ψ_2 and ψ_3 as function of θ along the axis (Q_1Q_2).

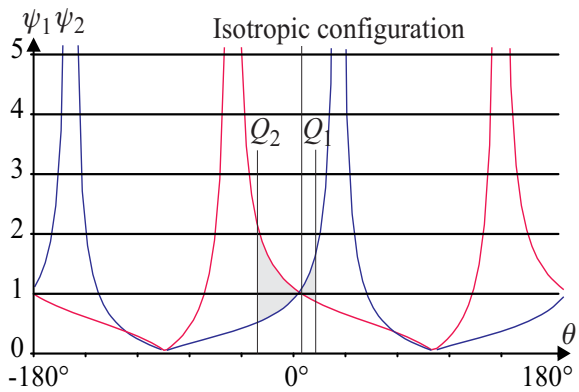

Figure 12: The three velocity transmission factors as function of θ along the axis (Q_1Q_2)

The joint limits on θ are located on both sides of the isotropic configuration. To calculate the joint limits, we solve the following inequations,

$$\frac{1}{\psi_{max}} \leq \frac{1}{|2\tan(\theta) - 1|} \leq \psi_{max} \tag{12a}$$

$$\frac{1}{\psi_{max}} \leq \frac{1}{|\tan(\theta) + 1|} \leq \psi_{max} \tag{12b}$$

where the value of ψ_{max} depends on the performance requirements. Two sets of joint limits ($[\theta_{Q_1}\ \beta_{Q_1}]$ and $[\theta_{Q_2}\ \beta_{Q_2}]$) are found. The detail of this calculation is given in the Appendix.

The position vectors $\mathbf{q}_1$ and $\mathbf{q}_2$ of the points Q_1 and Q_2, respectively, can be easily defined as a function of L (Figs. 10 and 11),

$$\mathbf{q}_1 = [q_1\ q_1\ q_1]^T \quad \text{and} \quad \mathbf{q}_2 = [q_2\ q_2\ q_2]^T \tag{13a}$$

with

$$q_1 = -\sin(\beta_{Q_1})L \quad \text{and} \quad q_2 = -\sin(\beta_{Q_2})L \tag{13b}$$

The size of the Cartesian workspace is,

$$L_{Workspace} = |q_2 - q_1|$$

Thus, L can be defined as a function of $L_{Workspace}$.

$$L = \frac{L_{Workspace}}{|\sin(\beta_{Q_2}) - \sin(\beta_{Q_1})|}$$

Step 3: We want to determine the positions of the base points, namely, a. When the tool center point P is at Q'_1 defined as the projection onto the y-axis of Q_1, $\rho = 0$ and, (Fig. 13)

$$OA_2 = OQ'_1 + Q'_1C_2 + C_2A_2$$

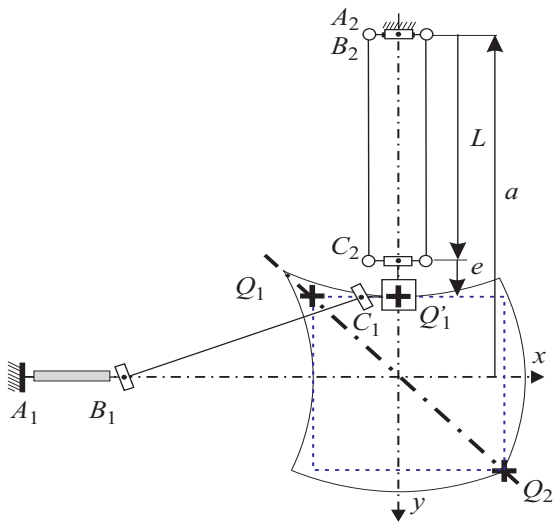

Figure 13: The point Q'_1 used for the determination of a

with $OA_2 = a$, $OQ'_1 = q_1$, $Q'_1C_2 = PC_2 = -e$ and since $\rho = 0$, $C_2A_2 = C_2B_2 - L$. Thus,

$$a = q_1 - e - L$$

Since q_1 is known from Eqs. (13a) and (19b), a can be calculated as function of e, L and ψ_{max}.

Now, we have to calculate the linear joint range $\Delta\rho = \rho_{max}$ (we have posed ρ_{min}=0).

When the tool center point P is at Q_2, $\rho = \rho_{max}$. The equation of the direct kinematics (Eq. (1b)) written at Q_2 yields,

$$\rho_{max} = q_2 - a - \cos(\theta_{Q_2})\cos(\beta_{Q_2})L - e$$

4.5 Prototype

Using the aforementioned two kinetostatic criteria, a small-scale prototype is under development in our laboratory. The mechanical structure is now finished, (Fig. 14). The actuated joints used for this prototype are rotative motors with ball screws. The prescribed performances of the orthoglide prototype are a Cartesian velocity of $1.2m/s$ and an acceleration of $14m/s^2$ at the isotropic point. The desired payload is $4kg$. The size of its prescribed cubic workspace is $200 \times 200 \times 200\ mm$. We limit the variations of the velocity transmission factors as,

$$1/2 \leq \psi_i \leq 2 \tag{14}$$

The resulting length of the three parallelograms is $L = 310\ mm$ and the resulting range of the linear joints is $\Delta\ \rho = 257\ mm$. Thus, the ratio of the range of the actuated joints to the size of the prescribed Cartesian workspace is $r = 200/257 = 0.78$. This ratio is high compared to other mechanisms. The three velocity transmission factors are depicted in Fig. 15. These factors are given in a z-cross section of the Cartesian workspace passing through Q_1.

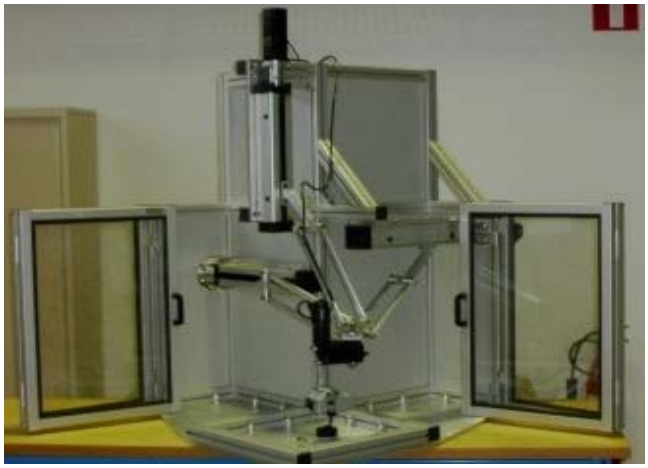

Figure 14: The orthoglide prototype

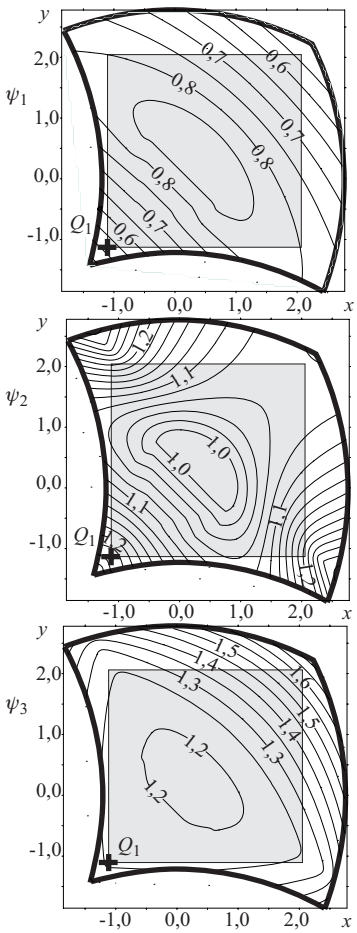

Figure 15: The three velocity transmission factors in a z-cross section of the Cartesian workspace passing through Q_1

5 Conclusions

Presented in this paper is a new kinematic structure of a PKM dedicated to machining applications: the Orthoglide. The main feature of this PKM design is its trade-off between the popular serial PPP architecture with homogeneous performances and the parallel kinematic architecture with good dynamic performances.

The workspace is simple, regular and free of singularities and self-collisions. The Jacobian matrix is isotropic at a point close to the center point of the workspace. Unlike most existing PKMs, the workspace is fairly regular and the performances are homogeneous in it. Thus, the entire workspace is really available for tool paths. In addition, the orthoglide is rather compact compared to most existing PKMs. A small-scale prototype of this mechanism is under construction at IRCCyN. First experiments with plastic parts will be conducted. The dynamic analysis has not been reported in this article. A rigid dynamic model has been proposed in (Guegan *et al.* (2002) and an elastic dynamic model is now being developed with the software package Meccano.

Acknowledgments

The authors would like to acknowledge the financial support of Région Pays-de-Loire, Agence Nationale pour la Valorisation de la Recherche, and École des Mines de Nantes.

References

Treib, T. and Zirn, O. “Similarity laws of serial and parallel manipulators for machine tools”, Proc. Int. Seminar on Improving Machine Tool Performance, pp. 125–131, Vol. 1, 1998.

Wenger, P. Gosselin, C. and Maille. B. “A Comparative Study of Serial and Parallel Mechanism Topologies for Machine Tools”, Proc. PKM’99, Milano, pp. 23–32, 1999.

Kim J. , Park C., Kim J. and Park F.C., 1997, “Performance Analysis of Parallel Manipulator Architectures for CNC Machining Applications”, Proc. IMECE Symp. On Machine Tools, Dallas.

Wenger, P. Gosselin, C. and Chablat. D. “A Comparative Study of Parallel Kinematic Architectures for Machining Applications”, Proc. Workshop on Computational Kinematics’2001, Seoul, Korea, pp. 249–258, 2001.

Rehsteiner, F., Neugebauer, R.. Spiewak, S. and Wieland, F., 1999, “Putting Parallel Kinematics Machines (PKM) to Productive Work”, Annals of the CIRP, Vol. 48:1, pp. 345–350.

Tlusty, J., Ziegert, J, and Ridgeway, S., 1999, “Fundamental Comparison of the Use of Serial and Parallel Kinematics for Machine Tools”, Annals of the CIRP, Vol. 48:1, pp. 351–356.

Luh C-M., Adkins F. A., Haug E. J. and Qui C. C., 1996, “Working Capability Analysis of Stewart platforms”, Transactions of ASME, pp. 220–227.

Merlet J-P., 1999, “Dertemination of 6D Workspace of Gough-Type Parallel Manipulator and Comparison between Different Geometries”, The Int. Journal of Robotic Research, Vol. 19, No. 9, pp. 902–916.

Golub, G. H. and Van Loan, C. F., Matrix Computations, The John Hopkins University Press, Baltimore, 1989.

Salisbury J-K. and Craig J-J., 1982, “Articulated Hands: Force Control and Kinematic Issues”, The Int. J. Robotics Res., Vol. 1, No. 1, pp. 4–17.

Angeles J., 1997, Fundamentals of Robotic Mechanical Systems, Springer-Verlag.

Yoshikawa, T., “Manipulability of Robot Mechanisms”, 1985, The Int. J. Robotics Res., Vol. 4, No. 2, pp. 3–9.

Wenger, P., and Chablat, D., 2000, “Kinematic Analysis of a new Parallel Machine Tool: the Orthoglide”, in Lenarčič, J. and Stanišić, M.M. (editors), *Advances in Robot Kinematic*, Kluwer Academic Publishers, June, pp. 305–314.

Chablat D. and Wenger P., 1998, “Working Modes and Aspects in Fully-Parallel Manipulator”, IEEE Int. Conf. On Robotics and Automation, pp. 1964–1969.

Guegan S. and Khalil W., 2002, “Dynamic Modeling of the Orthoglide”, to appear in *Advances in Robot Kinematic*, Kluwer Academic Publishers, June.

6 Appendix

To calculate the joint limits on θ and β, we solve the followings inequations, from the Eqs. 12,

$$|2\tan(\theta) - 1| \leq \psi_{max} \tag{15a}$$

$$\frac{1}{|2\tan(\theta) - 1|} \leq \psi_{max} \tag{15b}$$

Thus, we note,

$$f_1 = |2\tan(\theta) - 1| \quad f_2 = 1/|2\tan(\theta) - 1| \tag{16a}$$

Figure (16) shows f_1 and f_2 as function of θ along (Q_1Q_2). The four roots of $f_1 = f_2$ in $[-\pi\ \pi]$ are,

$$s_1 = -\arctan\left((1+\sqrt{17})/4\right) \tag{17a}$$

$$s_2 = -\arctan(1/2) \tag{17b}$$

$$s_3 = 0 \tag{17c}$$

$$s_4 = \arctan\left((-1+\sqrt{17})/4\right) \tag{17d}$$

with

$$f_1(s_1) = (-3+\sqrt{17})/4 \quad f_1(s_2) = 2 \tag{17e}$$

$$f_1(s_3) = 1 \quad f_1(s_4) = (3+\sqrt{17})/4 \tag{17f}$$

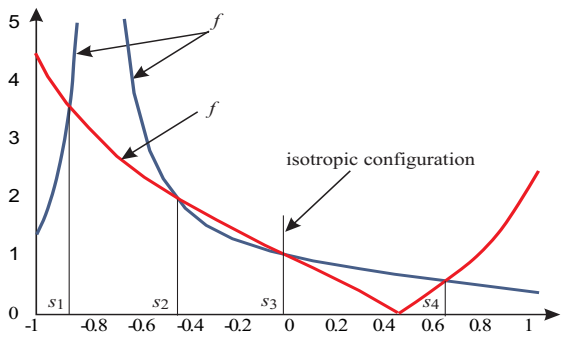

Figure 16: f_1 and f_2 as function of θ along (Q_1Q_2)

and

$$f_1(\theta) = 0 \quad \text{when} \quad \theta = \arctan(1/2) - \pi \tag{18a}$$

$$f_2(\theta) = 0 \quad \text{when} \quad \theta = \arctan(1/2)) \tag{18b}$$

The isotropic configuration is located at the configuration where $\theta = \beta = 0$. The limits on θ and β are in the vicinity of this configuration. Along the axis (Q_1Q_2), the angle θ is lower than 0 when it is close to Q_2, and greater than 0 when it is close to Q_1.

To find θ_{Q_1}, we study the functions f_1 and f_2 which are both decreasing on $[0\ \arctan(1/2)]$. Thus, we have,

$$\theta_{Q_1} = \arctan\left(\frac{\psi_{max} - 1}{2\psi_{max}}\right) \tag{19a}$$

$$\beta_{Q_1} = -\arctan\left(\frac{\psi_{max} - 1}{\sqrt{5\psi_{max}^2 - 2\psi_{max} + 1}}\right) \tag{19b}$$

In the same way, to find θ_{Q_2}, we study the functions f_1 and f_2 on $[s_1\ 0]$. The three roots s_1, s_2 and s_3 define two intervals. If $\psi_{max} \in [f_1(s_1)\ f_1(s_2)]$, we have,

$$\theta_{Q_2} = -\arctan\left(\frac{\psi_{max} - 1}{\psi_{max}}\right) \tag{20a}$$

$$\beta_{Q_2} = \arctan\left(\frac{\psi_{max} - 1}{\sqrt{2\psi_{max}^2 - 2\psi_{max} + 1}}\right) \tag{20b}$$

otherwise, if $\psi_{max} \in [f_1(s_2)\ f_1(s_3)]$,

$$\theta_{Q_2} = -\arctan\left(\frac{\psi_{max} - 1}{2}\right) \tag{20c}$$

$$\beta_{Q_2} = \arctan\left(\frac{\psi_{max} - 1}{\sqrt{{\psi_{max}}^2 - 2\psi_{max} + 5}}\right) \tag{20d}$$

Proceedings of the WORKSHOP on
Fundamental Issues and Future Research Directions for Parallel Mechanisms and Manipulators
October 3–4, 2002, Quebec City, Quebec, Canada
Clément M. Gosselin and Imme Ebert-Uphoff, editors

A Class of 3-DOF Translational Parallel Manipulators with Linear Input-Output Equations

XIANWEN KONG
Département de Génie Mécanique
Université Laval
Québec, Québec, Canada, G1K 7P4
xwkong@gmc.ulaval.ca

CLÉMENT M. GOSSELIN
Département de Génie Mécanique
Université Laval
Québec, Québec, Canada, G1K 7P4
gosselin@gmc.ulaval.ca

Abstract: *A class of LTPMs (3-legged 3-DOF translational parallel manipulators with linear Input-Output equations) is first proposed. The proposed LTPMs may or may not contain some inactive joints or redundant DOFs. The inverse kinematics, the forward kinematics, and the kinematic singularity analysis of the LTPMs are then performed. The analysis shows that the proposed LTPMs have the following kinematic merits, namely: (1) The forward displacement analysis and the inverse displacement analysis can be performed by solving a set of linear equations; (2) The Jacobian matrix of the LTPMs is constant. The inverse of the Jacobian matrix can be pre-calculated, and there is no need to calculate repeatedly the inverse of the Jacobian matrix in performing the forward displacement analysis and the forward velocity analysis; (3) There exists no rotation singularity; (4) There exists no uncertainty singularity. Finally, the geometric condition for a LTPM to be isotropic is also revealed. Two additional kinematic merits exist for the isotropic LTPM. The first is that an isotropic LTPM is isotropic in any of its configurations within its workspace. The second is that fewer calculations are needed in order to pre-determine the inverse of the Jacobian matrix.*

Key words: *Translational parallel manipulator, Kinematics, Singularity analysis, Isotropic manipulator, Screw theory, Linear Input-Output equations*

1 Introduction

Three-DOF translational parallel manipulators (TPMs) have a wide range of applications such as assembly and machining. Several types of TPMs have been proposed (Clavel, 1990; Appleberry, 1992; Hervé and Sparacino, 1991; Hervé, 1995; Di Raffaele and Parenti-Castelli, 1998; Tsai, 1999a,b; Zhao and Huang, 2000; Carricato and Parenti-Castelli, 2001; Jin and Yang, 2001). Systematic studies on the generation of 3-DOF TPMs are performed using respectively the displacement group theory (Hervé and Sparacino, 1991; Hervé, 1995), screw algebra (Frisoli et al., 2000) or screw theory (Kong and Gosselin, 2001a). It is revealed in (Di Raffaele and Parenti-Castelli, 1999) that there exists rotation singularities for the 3-UPU TPMs.

In fact, previous works on the systematic type synthesis of TPMs (Hervé and Sparacino, 1991; Frisoli et al., 2000; Kong and Gosselin, 2001a) deal mainly with the systematic type synthesis of translational parallel kinematic chains. [1] Some important issues in obtaining TPMs such as the selection of inputs (Kong (1999)), have not been dealt with systematically.

Recently, Kong and Gosselin (2001b, 2002) revealed the condition for all the translational degrees of freedom of the C (cylindrical) joints of the 3-CRR translational parallel kinematic chain, which is proposed in Hervé and Sparacino (1991), to be actuated and thus proposed a 3-$\underline{C}$RR TPM with linear actuators. Here and throughout, $\underline{C}$, $\underline{P}$ and R are used to denote a C joint whose translational DOF is actuated, an actuated prismatic joint and an unactuated revolute joint respectively. It has been revealed that both the forward displacement analysis and the inverse displacement analysis of the 3-$\underline{C}$RR TPM can be solved by solving a set of linear equations.

This paper tries to perform a systematic study on LTPMs (3-legged 3-DOF translational parallel manipulators with linear Input-Output equations) based on the results of type synthesis of translational parallel kinematic chains (Hervé and Sparacino, 1991; Hervé, 1995; Frisoli et al., 2000; Kong and Gosselin, 2001a) as well as our previous work (Kong and Gosselin, 2002). In Section 2, the geometric description of a class of LTPMs is first given. The inactive joints, the dependent joint groups and the redundant DOFs of LTPMs are revealed. The rotation singularity analysis is also performed. The inverse kinematics and forward kinematics is dealt with in Section 3. In Section 4, the kinematic singularity analysis of the LTPMs is investigated. The geometric condition for the isotropic LTPMs is revealed in Section 5. Finally, conclusions are drawn.

[1] A translational parallel kinematic chain differs from a translational parallel manipulator in that the inputs have not been selected in the former while the inputs have been selected in the latter.

2 Description of the LTPMs

2.1 Proposed LTPMs

Each of the proposed LTPMs (Kong and Gosselin (2001b)) is composed of a base and a moving platform connected by three legs[2] in parallel (Fig. 1, Here and throughout, each of the $\underline{R}$ joints with parallel axes within a leg for LTPMs is denoted by $\overline{R}$.) . The proposed LTPMs satisfy the following conditions.

(a1) Each leg for parallel manipulators is composed of a group of at least three R joints with parallel axes and at most one R joint whose axis is not parallel to the axes of the R joints in the group of R joints with parallel axes, while the axis of the P joint is not perpendicular to the axes of the R joints in the group of R joints with parallel axes.

(a2) For a parallel manipulator in which all the axes of the R joints in each of its legs are parallel, the axes of all the R joints of the parallel manipulator should not be parallel to a line. For a parallel manipulator in which not all the axes of the R joints in each of its legs are parallel and for which the R joints not belonging to the groups of R joints with parallel axes are connected to the moving platform or the base through a P joint or located on the moving platform or the base, then the three lines, each of which is perpendicular to the axes of all the R joints of one leg, should not be parallel to a plane.

(b) The axes of all the R joints in all the groups of R joints with parallel axes are not parallel to a plane.

(c) All P joints are actuated.

As will be proved in the following sections, the PMs satisfying the above conditions are LTPMs.

2.2 Working principle of LTPMs

2.2.1 Proposed PMs are TPMs

In screw theory, the motion and constraints of a kinematic chain are represented by screw systems, which are termed as twist systems and wrench systems respectively (see Hunt (1978) and Kumar et al. (2000) for example).

Under condition (a1), the wrench system of a leg will be a 2-system of ∞-pitch [3] in the case of a leg in which the axes of the R joints are all parallel or a 1-system of ∞-pitch in the case of a leg in which not all the axes of the R joints are parallel. It is noted that the axis of each wrench of a leg is perpendicular to the axes of all the R joints within the same leg.

Under conditions (a1) and (a2), the wrench system of the parallel manipulator, which is the union of the wrench systems of all its legs, will be a 3-system of ∞-pitch. The 3 DOFs of rotation of the moving platform are thus eliminated, and the moving platform can only translate with respect to the base.

[2] A leg in a parallel manipulator is a serial kinematic chain connecting the base and the moving platform. It is also called a limb.

[3] A ∞-pitch wrench is actually a couple in common usage.

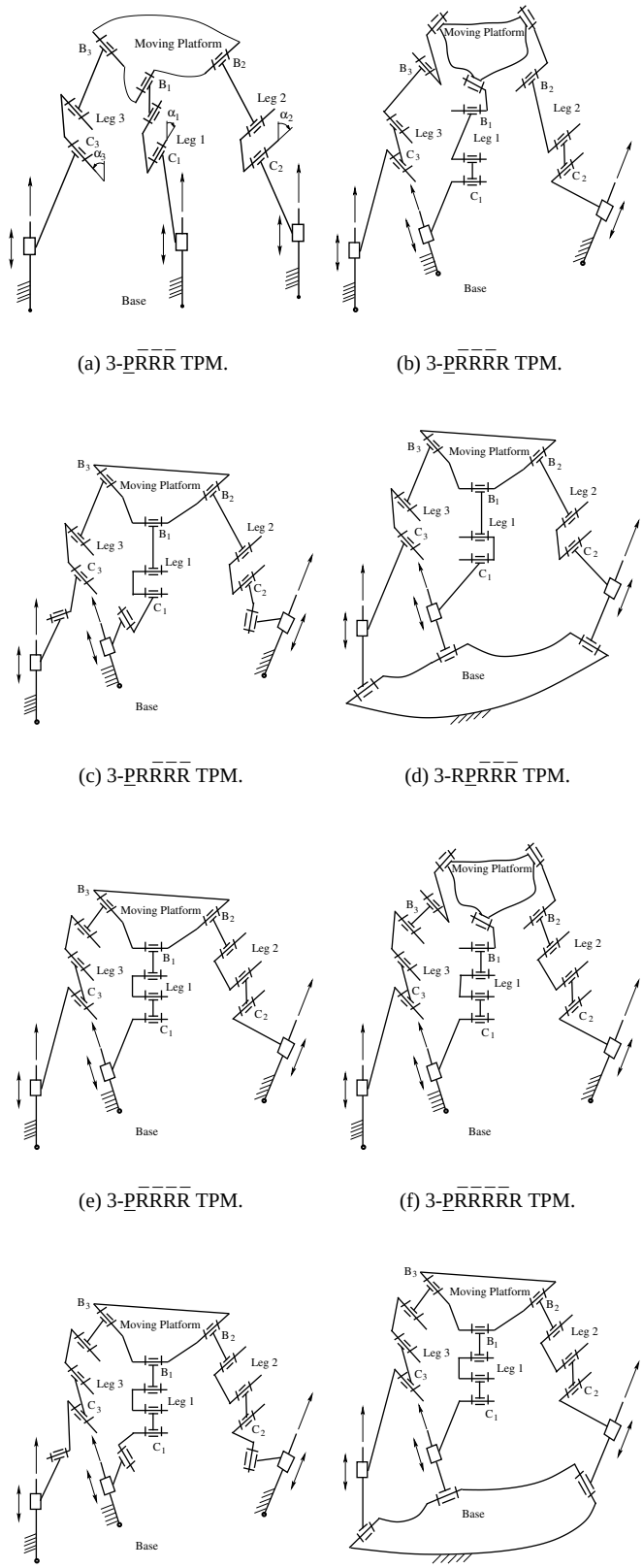

(a) 3-$\underline{P}\overline{RRR}$ TPM. (b) 3-$\underline{P}\overline{RRRR}$ TPM.

(c) 3-$\underline{P}\overline{RRRR}$ TPM. (d) 3-R$\underline{P}\overline{RRR}$ TPM.

(e) 3-$\underline{P}\overline{RRRR}$ TPM. (f) 3-$\underline{P}\overline{RRRRR}$ TPM.

(g) 3-$\underline{P}\overline{RRRRR}$ TPM. (h) 3-R$\underline{P}\overline{RRRR}$ TPM.

Figure 1: Proposed LTPMs.

2.2.2 *All P joints can be actuated*

Under condition (b), the union of the effective wrenches of all legs form a 3-system of 0-pitch. Once the inputs of the P joints are given, the translation of the moving platform can be determined.

The effective wrenches [4] of a leg are the wrenches reciprocal to all the twist of its joints except the twist of the actuators. It is noted that the axes of the effective wrenches of a leg for LTPM is parallel to the axes of the R joints in the group of R joints with parallel axes.

2.3 Inactive joints, dependent joint groups, redundant DOFs of a LTPM

2.3.1 *Inactive joints and dependent joint groups of a LTPM*

A general leg for LTPMs is composed of $(n-1)$ R joints and 1 P joint. For the purposes of simplification, the P joint is labeled with 1, while the R joints are labeled with 2, 3, $\cdots$, and n in the sequence from the base to the moving platform.

The infinitesimal change of orientation of the moving platform in a serial kinematic chain undergoing infinitesimal joint motion is

$$\Delta R = \sum_{i=2}^{n} (\Delta\theta_i \mathbf{s}_i) \tag{1}$$

where ΔR and $\Delta\theta_i$ denote the infinitesimal change of orientation of the moving platform and the infinitesimal joint motion of joint i respectively; $\mathbf{s}_i$ denotes the unit vector along the axis of joint i before the infinitesimal motion.
For a TPM, there exists

$$\Delta R = \mathbf{0} \tag{2}$$

Substitution of Eq. (1) into Eq. (2) yields

$$\sum_{i=2}^{n} (\Delta\theta_i \mathbf{s}_i) = 0 \tag{3}$$

Case 1 Legs in which all the axes of the R joints are parallel.

For a leg in which all the axes of the R joints are parallel, there exists

$$\mathbf{s}_n = \mathbf{s}_{n-1} = \cdots = \mathbf{s}_2 \tag{4}$$

Substitution of Eq. (4) into Eq. (3) yields

$$\sum_{i=2}^{n} \Delta\theta_i \mathbf{s}_2 = 0 \tag{5}$$

Solving Eq. (5), we have

$$\sum_{i=2}^{n} \Delta\theta_i = 0 \tag{6}$$

[4] Similar terms have been defined previously by several authors (e.g., Agrawal (1991)).

Case 2 Legs in which not all the axes of the R joints are parallel.

For the purposes of simplification, we make the assumption that the only R joint whose axis is not parallel to the axes of the other R joints are labeled with 2. For a leg in which not all the axes of the R joints are parallel, there exists

$$\mathbf{s}_n = \mathbf{s}_{n-1} = \cdots = \mathbf{s}_3 \neq \mathbf{s}_2 \tag{7}$$

Substitution of Eq. (7) into Eq. (3) yields

$$\Delta\theta_2 \mathbf{s}_2 + \sum_{i=3}^{n} \Delta\theta_i \mathbf{s}_3 = 0 \tag{8}$$

Solving Eq. (8), we have

$$\Delta\theta_2 = 0 \tag{9}$$

and

$$\sum_{i=3}^{n} \Delta\theta_i = 0 \tag{10}$$

Eqs. (6) and (10) show that the R joints with parallel axes within the same leg constitute a dependent joint group (Fig. 1). Eq. (9) shows that in a leg in which not all the axes of the R joints are parallel, the only R joint whose axis is not parallel to the axes of the other R joints is inactive (Figs. 1(b)–1(d) and 1(f)–1(h)).

Inactive joints have been intensionally used in Kong and Gosselin (2001b) to reduce the number of over-constraints of a TPM. Kim also proposed a TPM containing an inactive joint in each of its legs (Kim, 2001). However, he may not have realized that these joints were inactive since he didn't mention the inactive joint.

2.3.2 *Redundant DOFs of a LTPM*

For a LTPM, if there exist $n(n>3)$ R joints with parallel axes in one of its leg, there exist $(n-3)$ redundant DOFs within the n R joints.

The redundant DOFs do not affect the Input-Output equations of the LTPMs (Figs. 1(c) and 1(d)). However, they can be used in link-interference avoidance or in auxiliary operation of the LTPM.

2.4 Rotation singularity analysis of the LTPM

The rotation singularity (Di Raffaele and Parenti-Castelli, 1999) occurs when the moving platform of a TPM can rotate instantaneously.

It is clear that the rotation singularity occurs for a TPM if and only if its wrench system (a 3-system of ∞-pitch) degenerates into a 2-system or 1-system.

For those LTPMs with no inactive joints and those LTPMs in which all the inactive joints are connected to the moving platform or the base through a P joint or located on the moving platform or the base, the wrench system of a leg for LTPMs is invariant (Section 2.2). The order of the wrench system of these LTPM is

thus a constant. Thus, the moving platform cannot rotate at any instant. That is to say, there is no rotation singularity for these LTPMs.

For other LTPMs, the wrench system of a leg for LTPMs is not invariant. When the three lines, each of which is perpendicular to the axes of all the R joints within one leg, are parallel to a plane, the rotation singularity occurs.

2.5 Preferred LTPMs

By changing the order of different joints, many types of LTPMs can be obtained. For practical reason, LTPMs should satisfy the following conditions.

- (1) All the legs of a LTPM are of the same type.
- (2) Each of the actuators is located on or connected through an inactive joint to the base.
- (3) The LTPM has no rotation singularity.
- (4) The number of redundant DOF of a leg is not greater than 1.
- (5) The number of inactive joint of a leg is not greater than 1.

The LTPMs satisfying the above conditions are shown in Fig. 1. The number of inactive joints, the redundant DOF and the number of over-constraints of these LTPMs are listed in Table 1.

Table 1: LTPMs

No	Type	Number of inactive joints	Redundant DOFs	Number of over-constraints
1	3-$\underline{\mathrm{P}}\overline{\mathrm{R}}\overline{\mathrm{R}}\overline{\mathrm{R}}$	0	0	3
2	3-$\underline{\mathrm{P}}\overline{\mathrm{R}}\overline{\mathrm{R}}\overline{\mathrm{R}}\mathrm{R}$	3	0	0
3	3-$\underline{\mathrm{P}}\mathrm{R}\overline{\mathrm{R}}\overline{\mathrm{R}}$	3	0	0
4	3-$\mathrm{R}\underline{\mathrm{P}}\overline{\mathrm{R}}\overline{\mathrm{R}}$	3	0	0
5	3-$\underline{\mathrm{P}}\overline{\mathrm{R}}\overline{\mathrm{R}}\overline{\mathrm{R}}$	0	3	3
6	3-$\underline{\mathrm{P}}\overline{\mathrm{R}}\overline{\mathrm{R}}\overline{\mathrm{R}}\mathrm{R}$	3	3	0
7	3-$\underline{\mathrm{P}}\mathrm{R}\overline{\mathrm{R}}\overline{\mathrm{R}}\overline{\mathrm{R}}$	3	3	0
8	3-$\mathrm{R}\underline{\mathrm{P}}\overline{\mathrm{R}}\overline{\mathrm{R}}\overline{\mathrm{R}}$	3	3	0

When a combination of one R joint and one P joint with parallel axes arises, or a combination of two R joints with intersecting non-parallel axes arises, they can be replaced with a C joint and U (universal) joint respectively. Many specific cases of LTPMs can be obtained in this way. For brevity reason, we only give the specific cases of LTPMs when necessary.

2.6 Equivalent LTPM

It is clear that the removal of the inactive joints and redundant joints from a LTPM does not affect the Input-Output equations of the LTPM. The LTPM thus obtained from a LTPM by removing all the inactive joints and redundant joints is termed as the equivalent LTPM of the original LTPM.

It is found that the LTPMs proposed above have the same equivalent LTPM, namely, the 3-$\underline{\mathrm{P}}\overline{\mathrm{R}}\overline{\mathrm{R}}\overline{\mathrm{R}}$ LTPM [5] described above.

3 Kinematic analysis of LTPMs

As all the LTPMs are kinematically equivalent to the 3-$\underline{\mathrm{P}}\overline{\mathrm{R}}\overline{\mathrm{R}}\overline{\mathrm{R}}$ LTPM, the kinematic analysis of all the LTPMs can be performed in the same way as that of the 3-$\underline{\mathrm{P}}\overline{\mathrm{R}}\overline{\mathrm{R}}\overline{\mathrm{R}}$ LTPM.

To study the kinematics of the 3-$\underline{\mathrm{P}}\overline{\mathrm{R}}\overline{\mathrm{R}}\overline{\mathrm{R}}$ LTPM, two coordinate systems, $P - X_P Y_P Z_P$ and $O - XYZ$, are attached to its moving platform and base respectively. In leg i (denoted by the subscript i), let B_i denote a point on the axis of the R joint on the moving platform, C_i denote a point on the axis of the R joint adjacent to the P joint, A_i denote a point on the axis of the P joint on the link connected to the base by the P joint, A_{i0} denote the point on the base which is coincident with the initial position of A_i, $\mathbf{s}_{i2}$ denote the unit vector along the R joint, $\mathbf{s}_{i1}$ denote the unit vector along the P joint, $\mathbf{b}_{Pi}$ denote the vector from P to B_i, $\mathbf{c}_{Ai}$ denote the vector from A_i to C_i, $\mathbf{a}_i$ and $\mathbf{a}_{i0}$ denote respectively the position vectors of A_i and A_{i0} in the coordinate system $O - XYZ$, and S_i denote the input i of the 3-$\underline{\mathrm{P}}\overline{\mathrm{R}}\overline{\mathrm{R}}\overline{\mathrm{R}}$ LTPM.

For purposes of simplification and without loss of generality, the X_P-, Y_P-, Z_P-axes of the coordinate system $P - X_P Y_P Z_P$ are respectively parallel to the X-, Y-, Z-axes of the coordinate system $O - XYZ$, B_i and C_i are chosen in such a way that $A_i C_i$ is perpendicular to $\mathbf{s}_{i2}$.

3.1 Inverse kinematics of the 3-$\underline{\mathrm{P}}\overline{\mathrm{R}}\overline{\mathrm{R}}\overline{\mathrm{R}}$ LTPM

3.1.1 Inverse displacement analysis

The inverse displacement analysis of the 3-$\underline{\mathrm{P}}\overline{\mathrm{R}}\overline{\mathrm{R}}\overline{\mathrm{R}}$ LTPM consists in determining the required inputs, S_i (i=1, 2, 3), for a given position, $\mathbf{p}$, of the moving platform, where $\mathbf{p}$ is the vector directing from point O to point P.

As there exists no rotation singularity for the 3-$\underline{\mathrm{P}}\overline{\mathrm{R}}\overline{\mathrm{R}}\overline{\mathrm{R}}$ LTPM, $C_i B_i$ (i=1, 2, 3) is perpendicular to the axis of the R joint i at any instant, i.e.,

$$\mathbf{s}_{i2}^T[\mathbf{p} + \mathbf{b}_{Pi} - (\mathbf{a}_{i0} + S_i \mathbf{s}_{i1} + \mathbf{c}_{Ai})] = 0 \quad i=1, 2, 3 \tag{11}$$

Expanding Eq. (11), we have

$$\mathbf{s}_{i2}^T \mathbf{s}_{i1} S_i = \mathbf{s}_{i2}^T(\mathbf{p} + \mathbf{b}_{Pi} - \mathbf{a}_{i0} - \mathbf{c}_{Ai}) \quad i=1, 2, 3 \tag{12}$$

From condition (a1) in Section 2.1, we have $\mathbf{s}_{i2}^T \mathbf{s}_{i1} \neq 0$. Solving Eq. (12), we obtain the solution to the inverse displacement

[5] The 3-PRRR translational parallel kinematic chain was implicitly proposed by Hervé and Sparacino (1991).

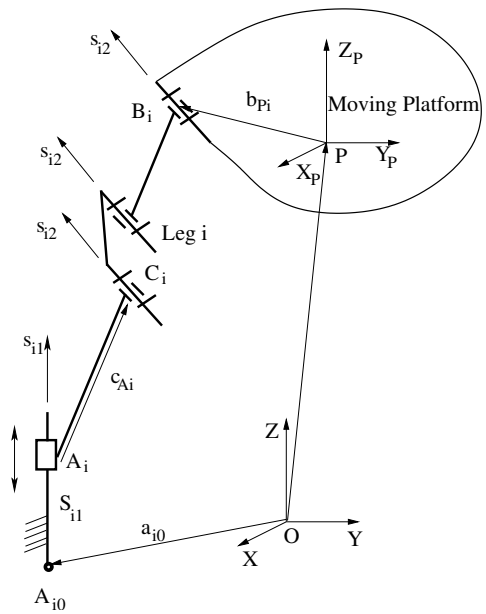

Figure 2: $\underline{\text{P}}\overline{\text{RRR}}$ leg for a LTPM.

analysis

$$S_i = \mathbf{s}_{i2}^T(\mathbf{p} + \mathbf{b}_{Pi} - \mathbf{a}_{i0} - \mathbf{c}_{Ai})/\mathbf{s}_{i2}^T\mathbf{s}_{i1} \quad i\text{=1, 2, 3} \tag{13}$$

For any $\mathbf{p}$ within the workspace, the distance between points B_i and C_i is no greater than the total of the lengths of all the RR binary links in leg i. In the case the distance between points B_i and C_i is greater than the total of the lengths of all the RR binary links in leg i, the set of inputs are invalid as the LTPM cannot be assembled.

Let $\Delta\mathbf{p}$ denote an increment of $\mathbf{p}$ and ΔS_i denote the corresponding increment of S_i. From Eq. (13), we have

$$S_i + \Delta S_i = \mathbf{s}_{i2}^T(\mathbf{p} + \Delta\mathbf{p} + \mathbf{b}_{Pi} - \mathbf{a}_{i0} - \mathbf{c}_{Ai})/\mathbf{s}_{i2}^T\mathbf{s}_{i1} \quad i\text{=1, 2, 3} \tag{14}$$

Subtracting Eq. (13) from Eq. (14), we obtain the solution to the inverse displacement analysis in incremental form

$$\Delta S_i = \mathbf{s}_{i2}^T\Delta\mathbf{p}/\mathbf{s}_{i2}^T\mathbf{s}_{i1} \quad i\text{=1, 2, 3} \tag{15}$$

3.1.2 Inverse velocity analysis

The inverse velocity analysis of the 3-$\underline{\text{P}}\overline{\text{RRR}}$ LTPM consists in determining the required velocities of the actuators, $\dot{S}_i$(=dS_i/dt), for a given velocity, $\mathbf{v}$=($d\mathbf{p}/dt$), of the moving platform in a given configuration.

Differentiating Eq. (13) with respect to time, we obtain the solution to the inverse velocity analysis

$$\dot{S}_i = \mathbf{s}_{i2}^T\mathbf{v}/\mathbf{s}_{i2}^T\mathbf{s}_{i1} \quad i\text{=1, 2, 3} \tag{16}$$

3.2 Forward kinematics of the 3-$\underline{\text{P}}\overline{\text{RRR}}$ LTPM

3.2.1 Forward displacement analysis

The forward displacement analysis of the 3-$\underline{\text{P}}\overline{\text{RRR}}$ LTPM consists in determining the position, $\mathbf{p}$, of the moving platform for a given set of inputs, S_i.

From Eq. (11), we have

$$\mathbf{s}_{i2}^T\mathbf{p} = \mathbf{s}_{i2}^T(\mathbf{a}_{i0} + \mathbf{c}_{Ai} + S_i\mathbf{s}_i - \mathbf{b}_{Pi}) \quad i\text{=1, 2, 3} \tag{17}$$

Rewriting Eq. (17) in matrix form, we have

$$\mathbf{J}_1\mathbf{p} = \begin{bmatrix} \mathbf{s}_{12}^T(\mathbf{a}_{10} + \mathbf{c}_{A1} + S_1\mathbf{s}_{11} - \mathbf{b}_{P1}) \\ \mathbf{s}_{22}^T(\mathbf{a}_{20} + \mathbf{c}_{A2} + S_2\mathbf{s}_{21} - \mathbf{b}_{P2}) \\ \mathbf{s}_{32}^T(\mathbf{a}_{30} + \mathbf{c}_{A3} + S_3\mathbf{s}_{31} - \mathbf{b}_{P3}) \end{bmatrix} \tag{18}$$

where

$$\mathbf{J}_1 = \begin{bmatrix} \mathbf{s}_{12}^T \\ \mathbf{s}_{22}^T \\ \mathbf{s}_{32}^T \end{bmatrix} \tag{19}$$

Solving Eq. (18), we obtain the solution to the forward displacement analysis

$$\mathbf{p} = \mathbf{J}_1^{-1} \begin{bmatrix} \mathbf{s}_{12}^T(\mathbf{a}_{10} + \mathbf{c}_{A1} + S_1\mathbf{s}_{11} - \mathbf{b}_{P1}) \\ \mathbf{s}_{22}^T(\mathbf{a}_{20} + \mathbf{c}_{A2} + S_2\mathbf{s}_{21} - \mathbf{b}_{P2}) \\ \mathbf{s}_{32}^T(\mathbf{a}_{30} + \mathbf{c}_{A3} + S_3\mathbf{s}_{31} - \mathbf{b}_{P3}) \end{bmatrix} \tag{20}$$

It should be pointed out that for a vector $\mathbf{p}$ obtained using Eq. (20) with a set of valid inputs, the distance between points B_i and C_i is no greater than the total of the lengths of all the RR binary links in leg i. In the case the distance between points B_i and C_i is greater than the total of the lengths of all the RR binary links in leg i, the set of inputs are invalid as the LTPM cannot be assembled.

Rewriting Eq. (15) in matrix form, we have

$$\mathbf{J}\Delta\mathbf{p} = \begin{bmatrix} \Delta S_1 \\ \Delta S_2 \\ \Delta S_3 \end{bmatrix} \tag{21}$$

where

$$\begin{aligned} \mathbf{J} &= \begin{bmatrix} \mathbf{s}_{12}^T/\mathbf{s}_{12}^T\mathbf{s}_{11} \\ \mathbf{s}_{22}^T/\mathbf{s}_{22}^T\mathbf{s}_{21} \\ \mathbf{s}_{32}^T/\mathbf{s}_{32}^T\mathbf{s}_{31} \end{bmatrix} \\ &= diag(1/\mathbf{s}_{12}^T\mathbf{s}_{11} \quad 1/\mathbf{s}_{22}^T\mathbf{s}_{21} \quad 1/\mathbf{s}_{32}^T\mathbf{s}_{31})\mathbf{J}_1 \end{aligned} \tag{22}$$

Solving Eq. (21), we obtain the solution to the forward displacement analysis in incremental form

$$\Delta\mathbf{p} = \mathbf{J}^{-1} \begin{bmatrix} \Delta S_1 \\ \Delta S_2 \\ \Delta S_3 \end{bmatrix} \tag{23}$$

where

$$\mathbf{J}^{-1} = \mathbf{J}_1^{-1} diag(\mathbf{s}_{12}^T\mathbf{s}_{11} \quad \mathbf{s}_{22}^T\mathbf{s}_{21} \quad \mathbf{s}_{32}^T\mathbf{s}_{31}) \tag{24}$$

3.2.2 *Forward velocity analysis*

The forward velocity analysis of the 3-$\underline{P}\overline{R}\overline{R}\overline{R}$ LTPM consists in determining the velocity, $\mathbf{v}$, of the moving platform for a given set of velocities of the actuators, $\dot{S}_i$, in a given configuration.

Rewriting Eq. (16) in matrix form, we have

$$\begin{bmatrix} \dot{S}_1 \\ \dot{S}_2 \\ \dot{S}_3 \end{bmatrix} = \mathbf{J}\mathbf{v} \tag{25}$$

Solving Eq. (25), we obtain the solution to the forward velocity analysis

$$\mathbf{v} = \mathbf{J}^{-1} \begin{bmatrix} \dot{S}_1 \\ \dot{S}_2 \\ \dot{S}_3 \end{bmatrix} \tag{26}$$

3.3 Discussion on the Jacobian Matrix J

From Eq. (22), it can be found that each row of the Jacobian matrix, $\mathbf{J}$, is proportional to the unit vector along the axes of the R joints within one leg. As the unit vector along the axes of all the R joints are invariant, the Jacobian matrix, $\mathbf{J}$, is constant.

For a given 3-$\underline{P}\overline{R}\overline{R}\overline{R}$ LTPM, the inverse of $\mathbf{J}$ is therefore also constant and can be pre-calculated. Thus, there is no need to calculate $\mathbf{J}^{-1}$ repeatedly in performing the forward position analysis and forward velocity analysis of the 3-$\underline{P}\overline{R}\overline{R}\overline{R}$ LTPM. This simplifies to a great extent the real-time control of the 3-$\underline{P}\overline{R}\overline{R}\overline{R}$ LTPM.

As $\mathbf{J}$ and $\mathbf{J}^{-1}$ are constant, from Eqs. (21) and (23), there will be a same $\Delta\mathbf{p}$ corresponding to a given ΔS_i in any configuration of a LTPM, and vice visa. Thus, both the inverse displacement analysis and the forward displacement analysis will be further simplified if the LTPM is used with relative position control.

4 Kinematic singularity analysis of the LTPMs

4.1 Inverse kinematic singularity analysis

The inverse kinematic singularities occur for a parallel manipulator when the order of the twist system of any one of the legs decreases instantaneously. For a leg for LTPMs, an inverse kinematic singularity occurs if and only if the axes of all the R joints with parallel axes are coplanar. In this case, the distance between points B_i and C_i is equal to the total of the lengths of all the RR binary links in leg i. These configurations correspond to a boundary of the workspace. The inverse kinematic singularities at the boundary of the workspace can be eliminated by limiting the range of motion of the actuated joints.

4.2 Uncertainty singularity analysis

When uncertainty singularities occur for a parallel manipulator, the moving platform can undergo infinitesimal or finite motion when the inputs are locked. It will be proved below that there exists no uncertainty singularity for the LTPMs.

From Section 2.4, it is known that there exists no rotation singularity for the LTPMs. Thus, Eq. (25) is always satisfied. Uncertainty singularities for the LTPMs occur if and only if $\mathbf{J}$ is singular.

From Section 3.3, it is known that each row of the Jacobian matrix, $\mathbf{J}$, is proportional to the unit vector along the axes of the R joints of the group of R joints with parallel axes of one leg. As the axes of the R joints belong to the groups of R joints with parallel axes are not all parallel to a common plane (see Section 2), $\mathbf{J}$ is always non-singular. There thus exists no uncertainty singularity for the LTPMs.

4.3 Discussion on the choice of working mode

The working mode of a parallel manipulator is introduced in Chablat and Wenger (1998) for a better control and application of parallel manipulators. However, the definition of working mode given in Chablat and Wenger (1998) does not apply to the LTPMs proposed here since it is defined based on the Input-Output velocity equation and the unactuated joint variables are neglected. In this section, the working mode of parallel manipulators is generalized to cover the LTPMs with no redundant DOF. The choice of working mode of LTPMs is also discussed.

In performing the inverse displacement analysis of a parallel manipulator, any one of its legs can be treated as a serial manipulator. The concept of postures of serial manipulator can also be applied to a leg in a parallel manipulator. A working mode of a parallel manipulator is defined as a combination of the postures of all its legs. For a parallel manipulator having multiple solutions to its inverse displacement analysis, there are multiple working modes. The postures of at least one leg are different in different working modes of a parallel manipulator.

Consider a LTPM with no redundant DOF. For a given position of the moving platform, there usually exist two sets of solutions to the joint variables of the unactuated joints for each leg and eight solutions to the inverse displacement analysis of the LTPM. The LTPM has thus 8 working modes. The joint variables of the unactuated joints in at least one leg are different between two working modes while the inputs are the same for a given position of the moving platform. Different working modes are separated by the inverse singularity of one or more legs. If the link interference is neglected and the ranges of joint motions are not limited, the workspaces of the manipulator under the different working modes are the same.

In practice, the assembly mode with higher stiffness and in which link interference can be easily avoided should be selected to perform a required task. If the inverse kinematic singularities at the boundary of the workspace are eliminated by limiting the range of motion of the actuated joints, a LTPM will always remains in the working mode in which it was first assembled.

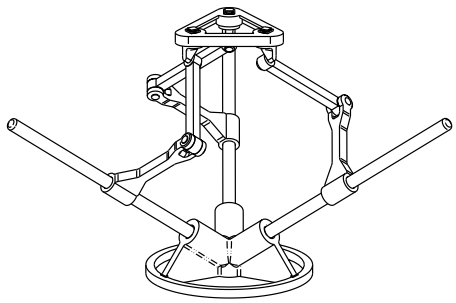

Figure 3: Isotropic 3-$\underline{C}\overline{R}\overline{R}\overline{R}$ TPM (Kong and Gosselin, 2002).

5 Isotropic LTPMs

An isotropic manipulator (Angeles, 1997) is a manipulator whose Jacobian matrix has a condition number equal to 1 in at least one of its configurations. In isotropic configurations, the manipulator performs very well with regard to the force and motion transmission. Except the 3-CRR TPM proposed in Kong and Gosselin (2002), isotropic manipulators proposed so far are isotropic only in a small portion of their workspace. In the following, the geometric condition which renders the LTPMs isotropic will be revealed and it will be proved that the isotropic LTPMs are isotropic in their whole workspace.

As each row of the Jacobian matrix, $\mathbf{J}$, is proportional to the unit vector along the axes of R joints in the group of R joints with parallel axes of one leg (Section 3.3), it can be easily found that when the axes of the three R joints are orthogonal and the $abs(\mathbf{s}_{i2}^T\mathbf{s}_{i1})$ for all three legs are equal, the LTPM is isotropic, i.e., the condition number of the Jacobian matrix is 1. As the Jacobian matrix, $\mathbf{J}$, of the LTPM is constant (Section 3.3), the isotropic LTPM is isotropic in its whole workspace.

In this case, $\mathbf{J}_1$ (see Eq. (19)) is an orthogonal matrix. One has

$$\mathbf{J}_1^{-1} = \mathbf{J}_1^T \tag{27}$$

Substitution of Eq. (27) into Eq. (24) yields

$$\mathbf{J}^{-1} = \left[\begin{array}{ccc} \mathbf{s}_{12}^T\mathbf{s}_{11}\mathbf{s}_{12} & \mathbf{s}_{22}^T\mathbf{s}_{21}\mathbf{s}_{22} & \mathbf{s}_{32}^T\mathbf{s}_{31}\mathbf{s}_{32} \end{array}\right] \tag{28}$$

Thus, fewer calculations are needed in obtaining the inverse of the Jacobian matrix when performing the forward kinematic analysis of isotropic LTPM. Moreover, if the coordinate system $O-XYZ$ fixed to the base is defined such that vectors $\mathbf{s}_{12}$, $\mathbf{s}_{22}$, and $\mathbf{s}_{32}$ are respectively aligned with the X-, Y-, and Z-axes of $O-XYZ$, then the Jacobian matrix becomes a constant diagonal matrix with identical elements. Hence the inverse displacement analysis as well as the forward displacement analysis and the associated velocity problems are further simplified.

In order to make a comprehensive comparison of the LTPMs, several prototypes are being developed in the Robotics Laboratory at Laval University. In addition to the isotropic 3-$\underline{C}$RR LTPM shown in Fig. 3, the isotropic 3-$\underline{P}\overline{R}\overline{R}\overline{R}\overline{R}$ LTPM

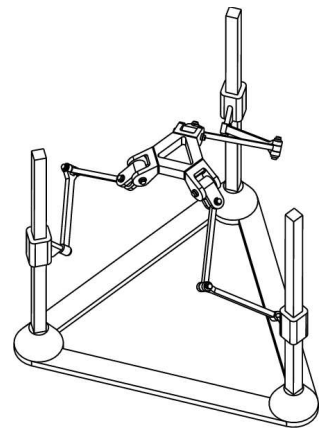

Figure 4: Isotropic 3-$\underline{P}\overline{R}\overline{R}\overline{R}\overline{R}$ TPM.

with the axes of actuators arranged in parallel (Fig. 4) is another potential application. As compared with the isotropic 3-$\underline{C}$RR LTPM, the isotropic 3-$\underline{P}\overline{R}\overline{R}\overline{R}\overline{R}$ LTPM is not-overconstrained and has a larger workspace along the the direction parallel to the axes of the P joints.

6 Conclusions

A class of LTPMs has been proposed. The LTPMs may or may not contain some inactive joints and redundant DOFs. The inverse kinematics, the forward kinematics, and the kinematic singularity analysis of the LTPMs have been performed. It has been shown that the proposed LTPMs have the following kinematic merits, namely: (1) Both the forward displacement analysis and the inverse displacement analysis can be performed by solving a set of linear equations. There exists only one solution to the position of the moving platform for a given set of inputs, and vice versa; (2) The Jacobian matrix of the LTPMs is constant. The inverse of the Jacobian matrix can be pre-calculated, and there is no need to calculate repeatedly the inverse of the Jacobian matrix in performing the forward displacement analysis and forward velocity analysis; (3) There exists no rotation singularity; (4) There exists no uncertainty singularity.

The geometric condition which makes the LTPMs isotropic has also been revealed. Two additional kinematic merits exist for the isotropic LTPMs. The first is that an isotropic LTPM is isotropic in its whole workspace. The second is that fewer calculations are needed to pre-determine the inverse of the Jacobian matrix.

Two approaches have been adopted in the work of this paper, i.e., the approach based on screw theory and the method based on the differentiation of the constraint equations. The first approach is used in the rotation singularity analysis and the inverse singularity analysis while the second approach is used in the velocity analysis and the uncertainty singularity analysis. In this way, the above problems are solved in the most concise manner.

The results of this paper should be of great interest in the

development of fast TPMs and high-performance parallel kinematic machines.

7 Acknowledgments

The authors would like to acknowledge the financial support of the Natural Sciences and Engineering Research Council of Canada (NSERC). Clément M. Gosselin is holding a Canada Research Chair and would like to acknowledge the financial support of the Chair program. The financial support of Innovatech through the PVR Program is also acknowledged. Finally, the authors thank Pierre-Luc Richard, Thierry Laliberté and Mathieu Goulet for building the CAD and plastic models of the isotropic LTPMs.

References

Agrawal, S. K., 1991, "Study of an In-Parallel Mechanism Using Reciprocal Screws," *Proceedings of the Ninth World Congress on the Theory of Machines and Mechanisms*, Prague, August 26-31, Vol. 2, pp. 405-408.

Angeles, J., 1997, *Fundamentals of Robotic Mechanical Systems*, Springer-Verleg New York Inc., pp. 174-190.

Appleberry, W. T., 1992, "Anti-Rotation Positioning Mechanism," *United States Patent*, No. 5156062.

Carricato, M., and Parenti-Castelli, V., 2001, "Position Analysis of a New Family of 3-DOF Translational Parallel Robot Manipulators," DETC2001/DAC-21036, *Proceedings of the 2000 ASME Design Engineering Technical Conferences*,

Chablat, D. and Wenger, Ph., 1998, "Working Modes and Aspects in Fully Parallel Manipulators," *Proceedings of the 1998 IEEE International Conference on Robotics & Automation*, Leuven, Belgium, pp. 1964 - 1969.

Clavel, R., 1990, "Device for the Movement and Positioning of an Element in Space," *United States Patent*, No. 4976582.

Di Raffaele, R., and Parenti-Castelli V., 1998, "A Translational 3-DOF Parallel Manipulator," *Advances in Robot Kinematics: Analysis and Control*, J. Lenarčič and M. L. Husty, eds., Kluwer Academic Publishers, pp. 49-58.

Di Raffaele, R., and Parenti-Castelli, V., 1999, "Mobility Analysis of the 3-UPU Parallel Mechanism Assembled for a Pure Translational Motion," *Proceedings of 1999 IEEE/ASME International Conference on Advanced Intelligent Mechatronics*, pp. 520-525.

Frisoli, A., Checcacci, D., Salsedo, F. , and Bergamasco, M., 2000, "Synthesis by Screw Algebra of Translating In-parallel Actuated Mechanisms," *Advances in Robot Kinematics*, J. Lenarčič and M. M. Stanišić, eds., Kluwer Academic Publishers, pp. 433-440.

Hervé, J. M., and Sparacino F., 1991, "Structural synthesis of parallel robots generating spatial translation," *Proceedings of the fifth Int. Conf. on Adv. Robotics*, Pisa, Italy, Vol. 1, pp. 808-813.

Hervé, J. M., 1995, "Design of Parallel Manipulators via the Displacement Group," *Proceedings of the Ninth World Congress on the Theory of Machines and Mechanisms*, Milan, Italy, Vol. 3, pp. 2079-2082.

Hunt, K. H., 1978, *Kinematic Geometry of Mechanisms*. Cambridge University Press.

Jin, Q., and Yang, T.L., 2001, "Position Analysis for a Class of Novel 3-DOF Translational Parallel Robot Mechanisms," DETC2001/DAC-21151, *Proceedings of the 2000 ASME Design Engineering Technical Conferences*.

Kim, D., 2001., *Analytical Formulation of Kinematics of Parallel Manipulators*, Ph. D thesis, Pohang University of Science and Technology, Korea.

Kong, X., 1999, *Detection of input interference in spatial linkages*, Journal of Mechanical Transmission (in Chinese), **23(4)**, pp. 23-25

Kong, X., and Gosselin, C. M., 2001a, "Generation of Parallel Manipulators with Three Translational Degrees of Freedom Based on Screw Theory," *Proceedings of 2001 CCToMM Symposium on Mechanisms, Machines and Mechatronics*, Saint-Hubert (Montreal), URL: http://www.cim.mcgill.ca/˜alexvit/SM3/Content.htm.

Kong, X., and Gosselin, C. M., 2001b, "Analytical parallel manipulators with three translational degreed of freedom," *Canadian Provisional Patent Application* (Submitted).

Kong, X., and Gosselin, C. M., 2002, Kinematics and Singularity Analysis of a Novel Type of 3-CRR 3-DOF Translational Parallel Manipulator," *International Journal of Robotics Research* (To appear).

Kumar, V., Waldron, K. J., Chrikjian, G., and Lipkin, H., 2000, "Applications of Screw System Theory and Lie Theory to Spatial Kinematics: A Tutorial," *2000 ASME Design Engineering Technical Conferences.*

Tsai, L. W., 1999, *Robot Analysis: the Mechanics of Serial and Parallel Manipulators*, John Willey & Sons Inc..

Tsai, L. W., 1999, "The Enumeration of a Class of Three-DOF Parallel Manipulators," *Proceedings of the Tenth World Congress on the Theory of Machines and Mechanisms*, Oulu. Vol. 3, pp. 1121-1126.

Zhao, T. S., and Huang, Z., 2000, "A novel Three DOF Translational Platform Mechanism and Its Kinematics," DETC2000/MECH-14101, *Proceedings of 2000 ASME Design Engineering Technical Conferences*.

Regular Papers: Kinetostatic Analysis

Thursday, October 3, 2002, 10:45AM

Session Chairs: J. Dai and T. Huang

1. U.A. Tol, J.-P. Clerc, G.J. Wiens, 3-08-02/13
   "Micro/Macro Approach for Dexterity Enhancement of PKM's".

2. J.L. Herder
   "Some Considerations Regarding Statically Balanced Parallel Mechanisms (SBPM's)".

3. S. Krut, O. Company, F. Pierrot
   "Velocity Performance Indexes for Parallel Mechanisms with Actuation Redundancy".

4. M.J.D. Hayes
   "Architecture Independent Workspace Analysis of Planar Three-Legged Manipulators"

Proceedings of the WORKSHOP on
Fundamental Issues and Future Research Directions for Parallel Mechanisms and Manipulators
October 3–4, 2002, Quebec City, Quebec, Canada
Clément M. Gosselin and Imme Ebert-Uphoff, editors

Micro/Macro Approach for Dexterity Enhancement of PKM's

Umesh Avadhut Tol
Department Mechanical Engineering
University of Florida
Gainesville, Florida 32611-6300
umesh@ufl.edu

Jean-Philippe Clerc
Department of Mechanical Engineering
University of Florida
Gainesville, Florida 32611-6300
jpsclerc@lycos.com

Gloria J. Wiens
Department of Mechanical Engineering
University of Florida
Gainesville, Florida 32611-6300
gwiens@ufl.edu

Abstract: *The Stewart-Gough, extendable strut type parallel kinematic mechanism (PKM) tends to lack sufficient dexterity over any sizeable workspace volume. This is particularly true for applications such as robotic deburring and machining. This paper describes the concept of micro/macro system integration of a PKM and a two-degree of freedom micro-manipulator. The particular application focus is on automated deburring and finishing systems.*

1 Introduction

Roots of development of parallel structures can be found in the late 1800's when the first theoretical article on parallel structures was published by Maxwell in 1890. In 1965, Stewart developed a 6-degree of freedom parallel structure for use as a flight stimulator called the 'Stewart platform'. Since this time parallel kinematics is seen as a promising research area, with a wide range of applications. A recent survey shows PKM's used in robotics, measuring machines, machine tools, positioning devices, and other special applications related to production. Equipped with today's fast computing devices, implementation of advanced controllers is also being achieved on PKM's (Tönshoff, 1998).

However, at the onset of parallel kinematic mechanisms used as machine tools, great claims were made regarding their dexterity, stiffness and range of motion. Many of these claims were an over statement of the PKM designs capabilities (Fassi and Wiens, 2000). Inspite of recent developments, PKM's have some inherent drawbacks like low work volume to size ratio, limited dexterity and shrinking of work volume with tilt in platform angles, see Figure 1. Furthermore, PKMs generally do not have ability for continuous rotation about its platform's vertical axis. These limitations become a particular problem for applications such as finishing and deburring which require controlled forces normal to an edge or surface contour. A limited number of PKM's have been developed for such applications, e.g. 3 dof Tricept PKM with deburring head attached and shoe deburring PKM (Molinari-Tosatti, et al., 2000). To overcome these drawbacks, the University of Florida System Automation and Mobility in Manufacturing (SAMM) Laboratory has designed a 2-degree of freedom micro-manipulator system operating under hybrid controller. This paper presents the 2-degree of freedom micro-manipulator as a subsystem of a micro/macro parallel kinematic mechanism as a new approach for increasing the dexterity of PKM's therefore, providing a vectorized rotational dexterity for finishing complex shapes and contours, see Figure 2.

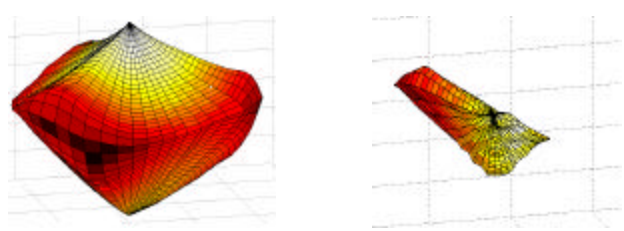

Horizontal Platform Platform Tilted 15 degrees

Figure 1. Workspace Reduction with Dexterity

2 Background

Deburring operations are expensive and increase the cost of manufacturing. Burrs are sharp and relatively small

projections that form along the edges on the work piece that is machined or stamped. In most cases, these burrs must be removed for improved product/system performance, safety, cost, ease of assembly, elimination of stress risers, proper tolerancing, appearance, etc.

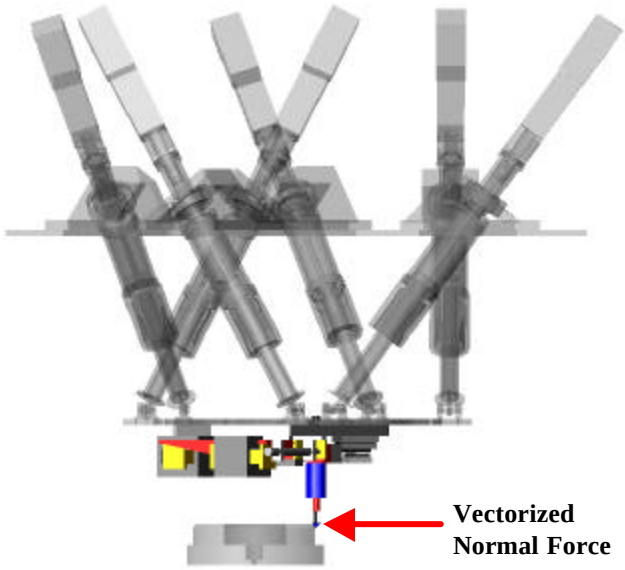

(a) Side View

(b) Final Assembly

Figure 2. UF-SAMM Laboratory Micro/Macro Automated PKM Finishing System

In manual deburring a person moves a deburring knife/file or a high-speed cutting tool along the desired edges of the work piece, maintaining a constant normal force on the tool. This process is time consuming and involves risk of part rejection, especially in cases of complex and thin walled sections. Due to repetitive task injuries and the hostile environment associated with manual deburring, corporations also suffer from large turnover rates. This has promoted the increased interest in automatic deburring and chamfering machines, as seen during the past decade.

Existing robots/machine tools typically operate as positioning devices, moving a cutter through a programmed trajectory. They generally lack the ability to control proper direction and force with respect to burr variation. Attaching an active micro-manipulator as end-effector tooling has been found to be effective in providing existing systems controlled compliance in the direction of burr variation. However for varying contours, the positioning device has to change its orientation continuously to maintain the constant normal force along the desired trajectory. This can result in long cycle time and tedious CNC/robot programming. The SAMM Laboratory's macro/micro system eliminates the orientation issues through controlled vectorized chamfering and deburring forces. In addition, this system uses event-driven control yielding tighter toleranced edges and surfaces and a reduction in the need for multiple passes for finishing.

3 New Micro/Macro PKM Design

The SAMM Laboratory PKM is divided into two-sub systems: Nominal Positioning Device (PKM) and Force Control Device (Two DOF).

3.1 PKM

The PKM of the SAMM Laboratory is a modular machine that can be easily assembled and dismantled. It is capable of producing sufficient forces needed for moving the finishing component while performing chamfering and deburring operations (refer to Figures 2 and 3). Design criteria for the PKM were it should be small to medium-size, maintain structural rigidity, and produce enough force to carry out finishing operation. The SAMM Laboratory's PKM adheres to a special 6-6 layout patented by Griffis and Duffy (1989). To accommodate cost restrictions, the PKM was designed using as many off the shelf components as possible. This PKM has limited rotation about its platform's vertical axes, and at a cost in workspace volume.

The main components of the PKM are a base, moving platform and six struts. Each strut consists of a telescopic cylinder. To adjust the length of the struts, one cylinder slides inside the other and this is achieved and controlled using a servomotor and ball screw arrangement. Selection, arrangement and alignment of the base and moving platform joints connecting the struts was made so that the maximum range of motion within the joints is achieved, full range of actuated motion is not restricted due to a joint limit, and each joint has sufficient static and dynamic load capacity. Six degrees of freedom of the moving platform is achieved through each of the six struts having a six degree of freedom kinematic chain of a spherical, prismatic and Hooke joint

pair. A ball spline is used to form the prismatic pair. The base platform joints are hollowed spherical bearings, through which passes the ball screw/motor shaft. The joints connecting the struts to the moving platform are designed to serve two purposes. First is to allow angular motion while transmitting the linear strut forces and motion to platform and second is to provide a means to perform minor adjustments to the moving platform upon PKM setup. To accommodate both these features, simple rod ends are used.

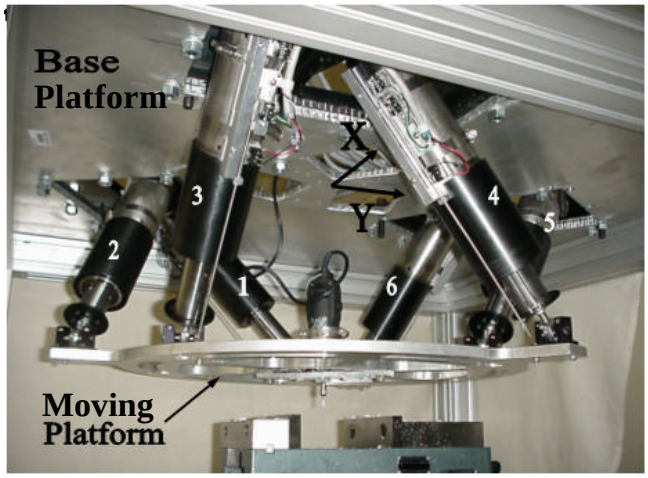

Figure 3. UF-SAMM Parallel Kinematic Mechanism

3.2 Two Degree of Freedom

The two degree of freedom micro-manipulator is designed to be attached to the moving platform of the PKM forming an automated finishing system (refer to Figures 2 and 4). It controls both normal force so as to maintain constant chamfer depth and controls tangential position of spindle along the feed direction. Due to its compliance in two directions, the application of this micro-manipulator is very effective for chamfering and deburring of parts with geometries in which the edge contours vary two dimensionally in the plane of movement of positioning device. That is providing a vectorized normal force vector. Machines equipped with this micro-manipulator do not have to change its orientation (e.g., minimizes robotic wrist/platform rotation) to maintain desired normal force. Hence, greatly saves cycle time and eliminates tedious programming.

The main components of this manipulator are two VCA's (Voice Coil Actuator), two LVDT's, two single axis force tranducers, and spindle mounting bracket. The two VCA's are aligned along x and y directions at 90 degrees to each other. The spindle mounting bracket is attached to VCA-X and VCA-Y through a ball spline, ball nut and a force transducer. The assembly is done in such a way that movement of the VCA-X does not reflect the applied VCA-X force on VCA-Y and vise versa. Two cross-slides are provided to prevent moments on the force transducers. The VCA assembly base can be mounted on PKM or a stationary frame.

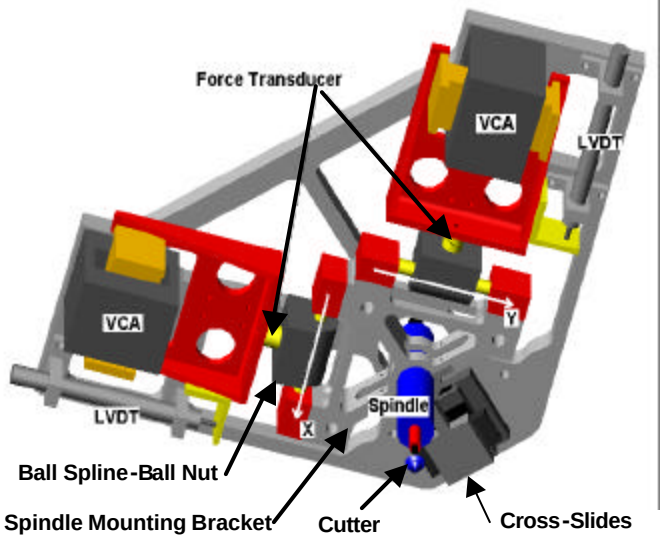

Figure 4. UF-SAMM Micro-Manipulator

3.3 Macro/Micro Assembly

The assembly of the macro/micro components allow for an easy deburring operation. The micro-manipulator has a high-speed spindle mounted at the center of its platform. Depending on the force experienced by the spindle, the controller reacts in real-time to maintain a desired normal force. If no burrs are experienced, then this force is constant. Figure 2 shows a 3-D model of the assembled machine with the cutter in contact with a sample part.

The micro-manipulator assembly is located so that the spindle is also at the center of the platform of the PKM. The PKM provides the motion along the edges of the part where the chamfering and deburring operation is required, see Figure 2. The PKM's motion does not need to take into account the presence and or shape of a burr in the plane of motion because those are already dealt with in real-time by the micro-manipulator controller. So theoretically any shape or contour within the range of the PKM can be submitted to a deburring operation by simply deriving the proper nominal (ideal) path for the PKM.

3.4 Control System

Around-the-arm force control is a method that is based on using the macro-manipulator (here PKM) for nominal positioning and motion only and a micro-manipulator for higher bandwidth force control (Proctor and Murphy, 1989; Whitney, 1987). This method decouples the micro-manipulator's controller from the macro-manipulator's controller. The hybrid position/force control micro-manipulator can be either mounted to a stationary base or on the macro-manipulator. The micro-manipulator performs as

an auxiliary tool that adds additional axes of motion to the system. Along these axes of motion, the required compliance for automated finishing tasks is provided.

There are two methods used to implement around-the-arm force control: passive and active. Passive force control is an open loop control system with no mechanism to adjust for force errors. The advantages of this micro-manipulator system are its simplicity and the cost. Closing the force loop, the active around-the-arm control maintains a constant normal force inspite of burr variations. Typically these micro-manipulators have been instrumented to sense the position, enabling these constant force devices to automatically determine the tool wear, part misalignment, and sudden process changes due to the presence of burrs.

The UF-SAMM PKM uses the active around-the-arm control approach. The PKM's controller is the National Institute of Standards and Technology Enhanced Motion Controller modified to accommodate six axis non-orthogonal systems, and running under Real-time Linux. The micro-manipulator is an event-driven hybrid position/force controller. This controller uses a process based logic module to instantaneously modify the constant force reference value (F_n) in accordance to sensed burr variations. Thus yielding a higher precision edge and a reduction in the need for multiple deburring passes (Wiens, Musuner and Walker, 1997).

In the design of the event-driven hybrid controller, the VCA-X and VCA-Y are orthogonal to each other but are in general not aligned with the normal and tangent directions relative to the cutter's trajectory along the part's edge. The PKM provides the nominal motion of the cutter such that the VCA-X and VCA-Y frame is in a parallel plane to the normal and tangent frame of the part's edge. Ideally, the origins of these two frames will coincide. Referring to Figure 5, the micro-manipulator's controller takes measured LVDT signals in X and Y directions and force transducer signals and converts them to normal and tangent components relative to the part's edge (directions as defined by the ideal part contour and process plan). The converted signals are then fed into corresponding comparator and controller (position and force) followed by another transformation back to the VCA axes directions. The signals from both the position and force controller are then combined generating the appropriate VCA-X and VCA-Y input commands. The hybrid position/force controller is designed in such way that tangential position is controlled to keep spindle at center of VCA stroke while at the same time maintaining the normal force required to maintain the desired chamfer depth. This controller also uses the position feedback to detect the presence of burrs and part misalignment. If a burr is detected, the process plan's normal force is adjusted using a process based "Logic Module". Without this module the finished edge would be a replica of the original surface prior to the deburring and chamfering operations, i.e., have the same waviness of the original edge. If the burrs are small than the edge would be within tolerance with the use of the appropriate normal force. More aggressive action is required if this is not the case, e.g. the 'logic module' is needed.

3.5 Results

Figures shows simulation results achieved on hole processing. The VCA rotates the force vector electronically to follow the normal to the work piece edge and thus maintain the constant desired chamfer depth. Experimental results are very close to theoretical values, see Figures 6 and 7. This is easiest to visualize by comparing the VCA forces in x and y to the normal when either the x or y force component is zero. Figures 6 shows the experimental result of the force vectorization done by the micro-manipulator. In this particular case, the movement along the edges was simulated using a 2dof machine (U500). Figure 7 shows the same force vectorization done by the micro/macro manipulator final assembly. In Figure 7, the error observed between the simulated and the experimental can be attributed to an observed increase in friction in the ball screw, ball nut and counter balance slides.

4 Conclusions

In conclusion, the integration of the two devices into one macro/micro machine takes advantage of the two manipulators while canceling their drawbacks. For example the small movements in 2-D by the 2 degree of freedom micro-manipulator are compensated by an ability of the PKM to follow 3-D nominal paths through out its work volume; and the relative low precision of the PKM is compensated by the ability of the micro-manipulator to apply greater precision with its hybrid position/force control. Combining these 2 manipulators and the process based, event-driven controller results in a new machine that is superb for low cost and high precision deburring operations.

Acknowledgment

The authors would like to acknowledge the contributions of J. Fitcher, M. Heger, N. Jhaveri, M. Lindstrom, R. Register, S. Shamblin, J. Steene, in the design, fabrication, and implementation of the various subcomponents of the UF SAMM PKM automated finishing system. Funding has been provided in part by the National Science Foundation/Grant Opportunities for Academic Liaisons with Industry Program (NSF/GOALI) and matching funds from Sandia National Laboratories (SNL): Grant Nos. DMI-9800806, and NSF Equipment Grant No. DMI-9622328.

References

Fassi, I., and Wiens, G.J., 2000, "Multiaxis Machining: PKM's and Traditional Machining Centers", Journal of Manufacturing Processes, Vol. 1., No. 2, pp. 1-14.

Griffis, M., and Duffy, J., 1989, "A Forward Displacement Analysis of a Class of Stewart Platforms", Journal of Robotic Systems, John Wiley, 6(6), pp. 703-729.

Gillespie, L.K., 1999, Deburring And Edge Finishing Handbook, SME Dearborn, Michigan.

Jhaveri, N., 2000, "Design of a Controller For a Platform-Based Automated Finishing System", Master Thesis, University of Florida, Gainesville, FL.

Molinari-Tosatti, L., Bianchi, G., Fassi, I., and Maj, R., 2000, "Analysis and Design of a Translational 3 Dof Tripod for Light Deburring Operations", International MATADOR Conference 33, D.R. Hayhurst (Editor), Springer, pp. 501-506.

Proctor, F. M., and Murphy, K.N., 1989, "Advanced Deburring System Technology," Symposium on the Mechanics of Deburring and Surface Finishing, ASME Winter Annual Meeting.

Tönshoff, H.K, 1998, "A Systematic Comparison of Parallel Kinematics", First European-American Forum on Parallel Kinematic Machines: Theoretical Aspects and Industrial Machines, 1998, pp. 21.

Whiteny, D.E., 1987, "Historical Perspective and State of the Art in Robot Force Control," The International Journal of Robotics Research.

Wiens, G.J., Musunur, L.P., and Walker, C.W., 1997 " Process Model- Based Force Chamfering and Deburring", Journal of Vibration and Control, Special Issue on Machining and Finishing Process, Vol. 3 , No. 3, pp. 331-350.

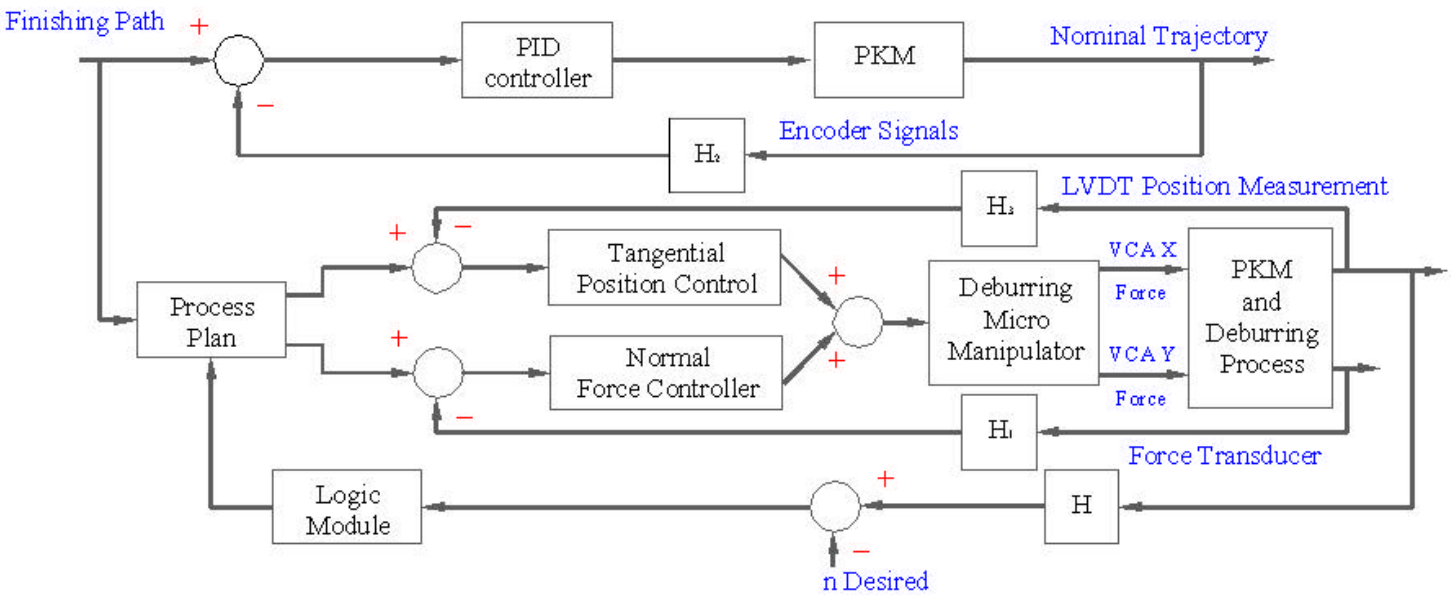

Figure 5. Controller for the Macro/Micro Automated PKM Finishing System

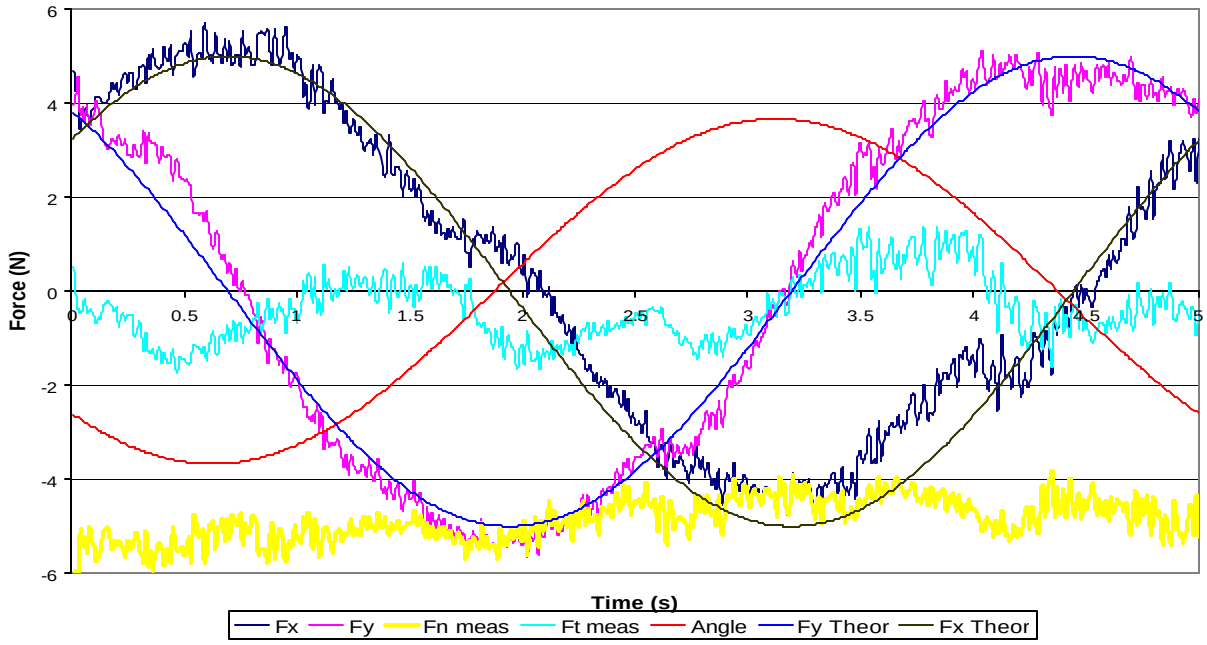

Figure 6, Experimental Results on U500

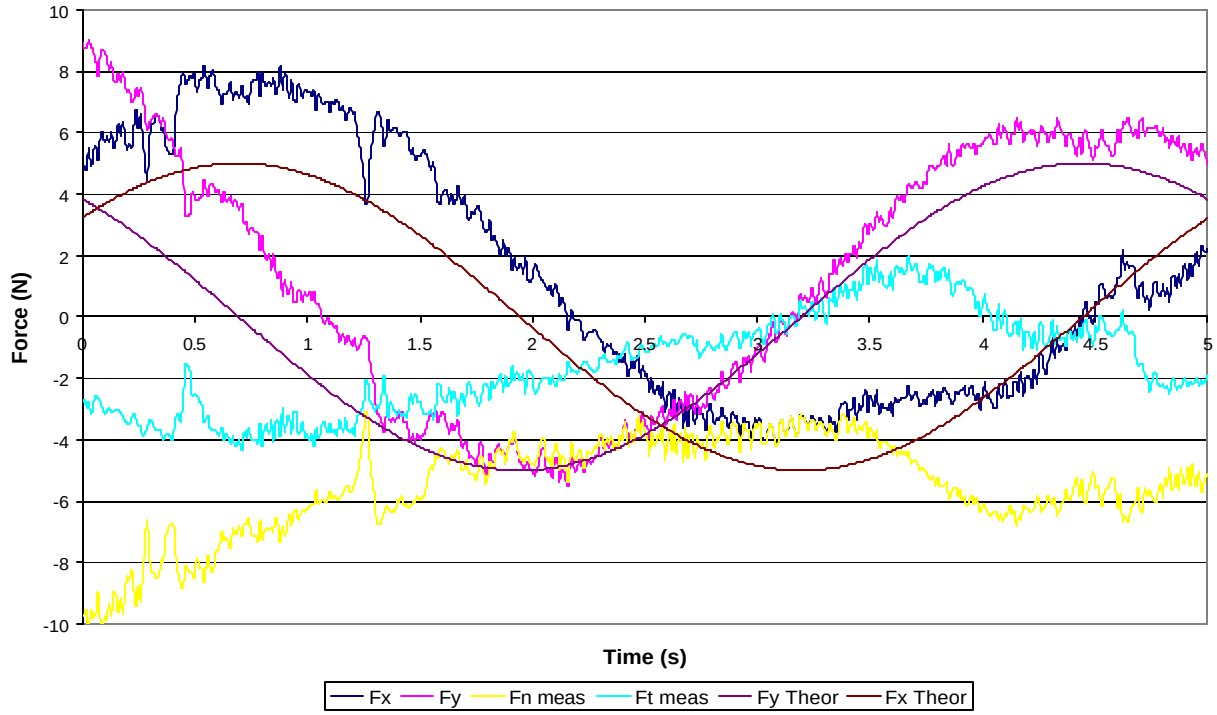

Figure 7, Experimental Results on PKM

Proceedings of the WORKSHOP on
Fundamental Issues and Future Research Directions for Parallel Mechanisms and Manipulators
October 3–4, 2002, Quebec City, Quebec, Canada
Clément M. Gosselin and Imme Ebert-Uphoff, editors

Some considerations regarding Statically Balanced Parallel Mechanisms (SBPM's)

JUST L. HERDER
Delft University of Technology
Department of Mechanical Engineering
Section of HuMan-Machine Systems (mms.tudelft.nl)
Mekelweg 2, 2628 CD Delft, The Netherlands
j.l.herder@wbmt.tudelft.nl

Abstract: *Gravity compensation in parallel mechanisms by mechanical means bears great advantages in system behavior, including increased bandwidth and accuracy, and reduced energy consumption, overall weight, and friction. As not many statically balanced parallel mechanisms exist, this short paper aims to give an overview of possible approaches and proposes possible research directions.*

1 Introduction

This paper discusses some fundamental questions and possible research directions regarding the application of static balance in parallel mechanisms.

The most striking feature of statically balanced mechanisms is their static equilibrium in all possible configurations, also in case no friction is present. This implies that no operating effort, apart from acceleration and deceleration, is needed to move the system from one configuration to another. Consequently, a mechanism with perfect static balance has constant potential energy throughout its range of motion. To achieve static balance in a pre-existing non-balanced mechanism, a balancing mechanism including energy storage devices needs to be added to complement the total system's potential energy to a constant value. In principle, any conservative force can be statically balanced (Herder, 2001).

A well-known application of static balancing is the compensation of gravity forces. Gravity compensation yields many advantages, including reduced energy consumption, smaller actuators, improved performance and inherent safety in case of power failure. An overview of literature on static balancing using counterweights, static balancing using springs, dynamic balancing using counterweights which implies static balancing, and gravity compensation in robotics is given in Herder (2001).

Also in the field of parallel mechanisms gravity compensation is receiving increasing attention, as realization of the advantages of static balancing may increase their use. The first statically balanced parallel mechanisms are currently under construction at Laval University (http://wwwrobot. gmc.ulaval.ca). Associated references include Jean and Gosselin (1996), Gosselin (1999), Gosselin and Wang (2000), and Ebert-Uphoff *et al.* (2000). Specific advantages are mentioned for a parallel haptic master device, where mechanical counterbalancing would reduce the compexity and time consumption of the controller, which improves accuracy of force feedback (Birglen, 2002). In addition it would also increase its mechanical performance. Also in cable-actuated parallel mechanisms the use of springs is proposed to decrease the effect of gravity in static mode or to contribute to the efforts of the cables in the directions where maximum accelerations are needed (Barette and Gosselin, 2000).

This paper focuses on the application of gravity compensation in parallel mechanisms. First, an inventory of fundamental questions is made. Without claiming completeness, it turns out that important issues are readily encountered. Subsequently, these issues are addressed in some detail.

2 Inventory

From the definition of statically balanced systems it is seen that any gravity balancer must apply forces to the system to be balanced, in this case the moving platform of the parallel mechanism. Principally, the balancing system must provide some connection between the (center of mass of the) moving platform and Earth, generally in the form of one or more

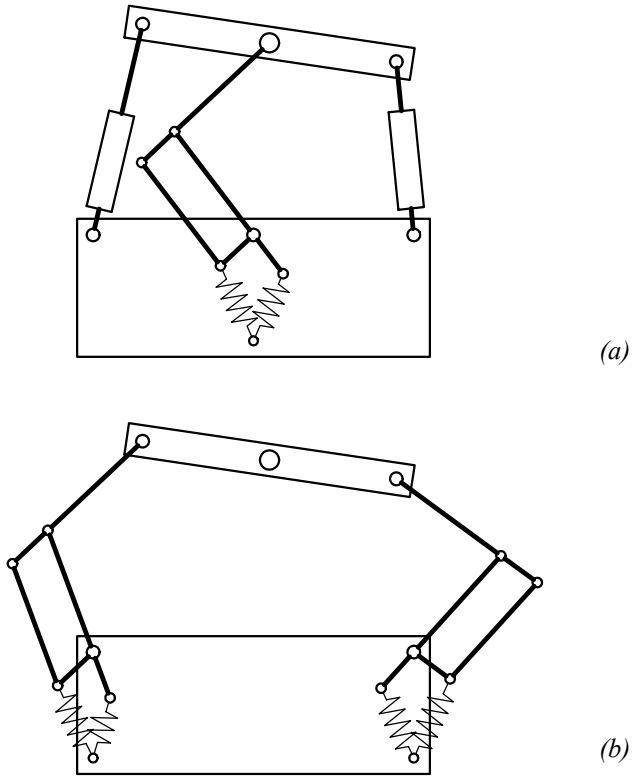

Figure 1 Two planar 3DoF parallel mechanisms with gravity compensation: (a) separate compensation system, (b) integrated compensation system.

linkage chains between the moving platform and the fixed ground. Furthermore, the balancing system must include potential energy storage devices. These observations lead to several questions. A first question to be answered is whether to use the balancing system for actuation or not. A second question is which kind of energy stores to use. A third associated question concerns the number of energy storage elements.

In addition to gravity compensation, static balancing may also be useful in compliant parallel mechanisms, such as the one by Canfield *et al*. (2001). Compliant mechanisms gain at least some of their mobility from the deflection of their flexible members rather than from movable joints only (Howell, 2001). To offset the elastic forces induced by these deformations, the addition of a static balancer may be advantageous (Herder and van den Berg, 2000).

The questions posed above, together with some practical considerations will be briefly discussed in the following sections.

3 Combination of actuation and balancing systems

A gravity compensation mechanism can be integrated with the actuator legs of the platform or can be added as a separate

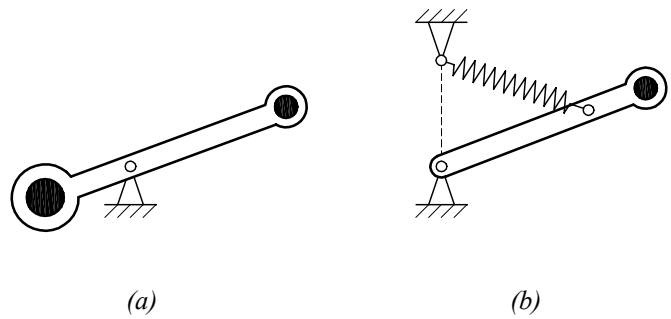

Figure 2 Two constant force mechanisms, both in use as gravity compensation mechanism: (a) mass-lever element, (b) spring-lever element with zero-free-length spring.

system. An *integrated compensation system* will be defined as a compensation system which makes use of the actuation system's chains between the moving platform and ground, whereas a *separate compensation system* adds one or more chains between the moving platform and ground to those of the actuation system. A fully separate compensation system is passive, in that it contains no actuators, only passive (requiring no external energy) energy storage devices such as springs or counterweights.

Figure 1 shows two versions of a planar three-degrees-of-freedom parallel linkage with gravity compensation. The system in figure 1a uses one Anglepoise-type gravity balancer (Carwardine, 1935) which applies at the center of mass of the moving platform. This ensures perfect gravity compensation (for proof see Herder, 2001). For the actuation of the platform, the original system (in this example the linear actuators) are retained. Therefore, the compensation system is fully separate. In the system of figure 1b, two Anglepoise-type gravity balancers are used as legs which perfectly balance the moving platform against gravity (proof of this statement is straightforward if it is realized that each leg carries half of the platform mass, see also Ebert-Uphoff *et al.*, 2000, who provide a more general proof). Each leg, as a separate system, has two degrees of freedom. If, in the total system, actuators are placed in three of the four joints associated with these degrees of freedom, the moving platform can be fully controlled using the legs of the balancing system. Therefore, this system has an integrated compensation system.

Most gravity balancers designed to date have revolute joints. This is due to the fact that both a mass-lever element and a spring-lever element incorporating a zero-free-length spring (figure 2) are constant force generators (Nathan, 1985). The technology for many of these systems is based on the *equipoising mechanisms* designed by George Carwardine (1932, 1935). Many parallel mechanisms, however, are equipped with linear actuators, for which much less balancers have been developed. In these cases the *equipoised lazy-tongs mechanism* by Carwardine (1938) and the similar *parallel-link equilibrator* by Streit an Shin (1993) can be used, but these are not very practical. Cable-driven parallel

mechanisms require yet other balancers. An integrated compensation system would be particularly desirable to not reduce their large workspace. The design of integrated balancing systems for parallel mechanisms with linear actuators and cable-driven parallel mechanisms seems to be in its early infancy.

4 Energy storage devices

Any source of conservative force qualifies for use as potential energy storage device. In practice, the choice is often limited to masses (counterweights) or springs. A mechanism that is gravity balanced using counterweights has the advantage that it has become insensitive for its orientation with respect to the gravity accerelation vector. Advantages of the use of springs are that the additional mass and inertia associated with counterweights is avoided, which results in increased accelerations. Several authors support this statement (references to general robotics are included in Herder (2001), while references to parallel mechanisms include Gosselin, 1999, and Gosselin and Wang, 2000).

Although perhaps intuitively less than a counterweight, the mass of springs is not always negligible. This section will show that under certain conditions a spring may actually be heavier than a counterweight.

The energy $U_{\max}$ that can be stored in a prismatic beam loaded in pure tension or compression equals:

$$U_{\max} = \int_0^{x_{\max}} F dx \tag{1}$$

where F is the axial force acting on the prismatic body (the spring), and x is the elongation. Assuming linear elastic material behavior, Hooke's law applies which yields:

$$dx = \frac{dFL}{AE} \tag{2}$$

where L is the (initial) length of the spring, A its (initial) cross-section, and E is Young's modulus. Substitution of equation (2) into equation (1) yields:

$$U_{\max} = \int_0^{F_{\max}} \frac{FL}{EA} dF = \frac{F_{\max}^2 L}{2AE} = \frac{\sigma_{\max}^2}{2E} AL = \frac{\sigma_{\max}^2}{2E} V \tag{3}$$

where V is the (initial) volume of the spring. Thus, the energy stored in the spring is proportional with its material volume. The elastic energy per volume can be expressed as a function of the material properties σ (yield strength) and E (Young's modulus), and a type factor α :

$$\frac{U_{\max}}{V} = \alpha \frac{\sigma^2}{E} \tag{4}$$

For axially loaded prismatic beams, the type factor α =1/2, according to equation 3. For other springs, this factor is less. Cool (1992) provides a table of type factors (table 1).

Spring type		Type factor
Prismatic beam with pure tension or compression load	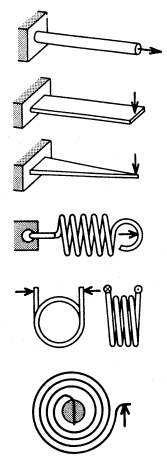	1/2
Rectangular cantilever with perpendicular load		1/18
Triangular cantilever with perpendicular load		1/6
Helical tension or compression spring with circular wire cross section		1/4
Coiled torsion spring with circular wire cross section		1/8
Spiral spring with rectangular wire cross section		1/6

Table 1 Type factors (coefficient relating maximum elastic energy to material properties of a spring) for some springs.

Let for example a weight of 100 kg be statically balanced by a helical extension spring, as in figure 2b. If the arm length r_o is 1 m (vertical displacement h of the mass 2 m), than at least a potential energy of $U_m = mgh$ = 2*981 Nm needs to be stored in the spring. If the spring is manufactured out of steel (σ=1200 MN/m^2, E=210 GN/m^2), then the material volume is:

$$V = U_{\max} \frac{E}{\alpha\sigma^2} = 2 \cdot 981 \frac{210e9}{\frac{1}{4}(1.2e9)^2} = 1.14e-3 \tag{5}$$

With a density of ρ=7800 kg/m^3 this example yields a spring mass of 9 kg or around 10% of the payload. This is much less than the mass of a counterweight, which, depending on the lever arm length (usually smaller than the arm of the mass to be balanced) may be factors greater than the payload. In this example, a springs seems the favorable option, however, the outcome of the comparison is dependent on the circumstances.

The outcome of the comparison of counterweight and spring is, among other factors, depending on the scale of the application. The ratio of energy storage to mass of a counterweight is given by:

$$\frac{U_{cw}}{m_{cw}} = \frac{mgh}{m} = gh \tag{6}$$

This expression implies that in case all of the geometry is scaled by a scaling factor S_l (being equal to the ratio of scaled length measure to original length measure), then the scaling factor of energy storage to mass of a counterweight is equal

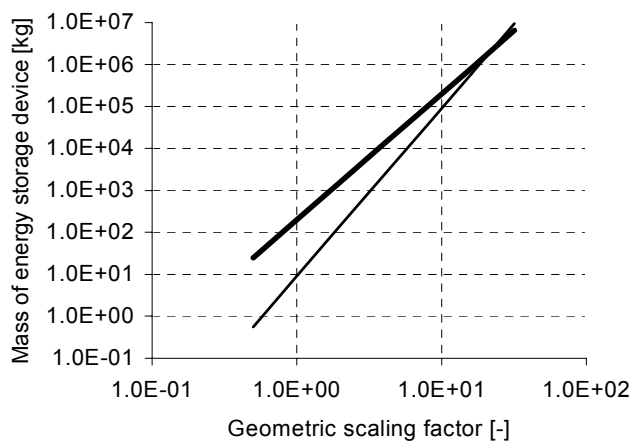

Figure 3 Relation between the scaling factor and the mass of the energy storage device for the example in the text. The thin line corresponds with the compensation spring, the thick line corresponds with the counterweight. In this case the break-even point occurs at a scaling factor of 22.

to the geometric scaling factor S_l. The ratio of energy storage to mass of a spring, using equation (4), is given by:

$$\frac{U_s}{m_s} = \frac{\alpha \frac{\sigma^2}{E} V}{\rho V} = \alpha \frac{\sigma^2}{E\rho} \tag{7}$$

This expression implies that the scaling factor of energy storage to mass of a spring is unity, in other words that the ratio of energy storage to mass of a spring is independent of the geometric scaling factor. This result indicates that as the geometric scale increases, the ratio of stored energy over mass increases (which is desirable) for counterweights, while it remains constant for springs. In this case there is a point where the counterweight becomes lighter than the compensation spring. It is interesting to locate this break-even point, and investigate other criteria (such as the size of the lever arms) affecting the choice. In the example the lever arm of the counterweight was selected half as long as the lever arm of the mass to be balanced. Consequently, the mass of the counterweight in the original situation is 200 kg. For this example, figure 3 suggests the relation between the scaling factor and the mass of the energy storage device. The diagram shows that a counterweight becomes lighter when the configuration is scaled up by a factor greater than 22.

Finally, it is noted that the zero-free-length spring behavior that is often required is not easily obtained. Either the initial tension of the spring itself should be increased, or a special mechanism is required, such as the pulley and string (Herder, 2001). Special mechanisms may increase friction, which is highly undesirable for instance in motion simulators. To circumvent these problems, it is worthwhile to investigate

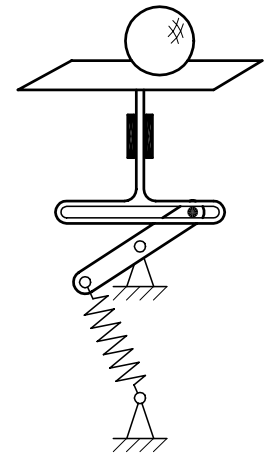

Figure 4 Six-degrees-of-freedom gravity compensation mechanism incorporating one zero-free-length spring.

design methods for compensation mechanisms incorporating normal springs, to investigate low-friction mechanisms, and to investigate methods to reduce loading of joints or even eliminate joints themselves. Some initial efforts in these directions are included in Herder (2001) and also in Te Riele and Herder (2001).

5 Number of potential energy storage devices

A gravity compensation device may need as many degrees of freedom as the mechanism to be balanced to accommodate its motion, but when the potential energy of the center of mass of the moving platform is considered (and the masses of the legs are neglected), essentially the only degree of freedom of concern for the balancing energy storage device is its vertical movement. Therefore, one energy storage device should be sufficient for the static balancing of this mass. It has been suggested that the number of energy storage devices should equal the degrees of freedom of the mechanism (Hilpert, 1968), but in fact there is no straightforward relation between the degrees of freedom of a linkage and the required number of energy storage devices.

In figure 4, a solution for the six-degree-of-freedom static balancing of a mass by a single spring is suggested. It consists of a ball which can slide an spin without friction on a horizontal platform. The platform can move up and down while being suspended by a spring mechanism providing static balance for the vertical movement. Clearly, this is not a practical mechanism, but it raises the challenge of reducing the number of springs.

Currently, parallel mechanisms having an integrated compensation system exist with six degrees of freedom and six springs (Gosselin, 1999). One balancing system has been reported previously (Herder and Tuijthof, 2000; Herder 2001) which may well be applied as separate compensation system in a six-degrees-of-freedom parallel mechanism with linear actuators. This system, called a general suspension

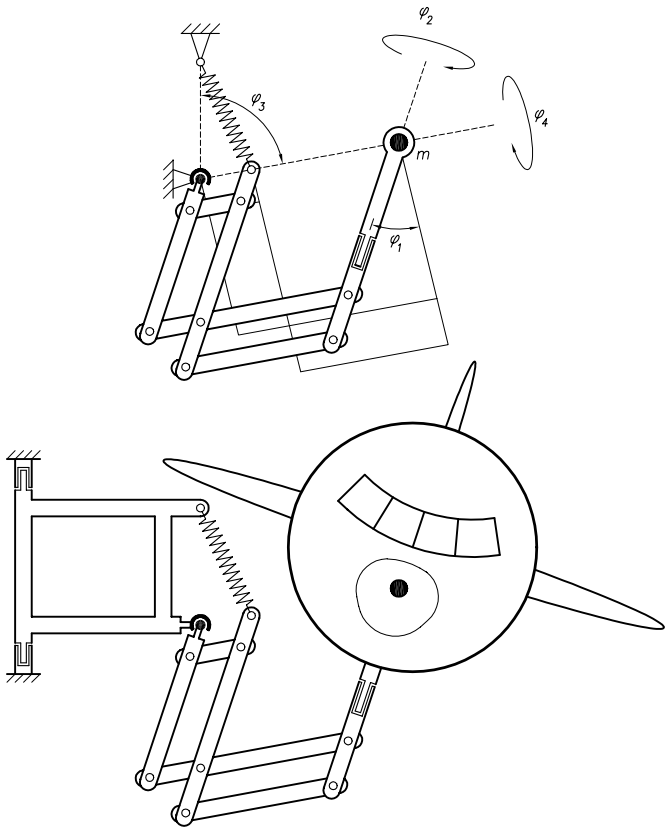

Figure 4 General suspension unit: (a, top) parallelogram mechanism, (b, bottom) addition of a rectangular segment (not in the plane of drawing) to obtain three independent translations.

unit, is shown in figure 5. From a potential energy perspective, this mechanism is essentially equal to the gravity balancer in figure 2b. However, the multiple-parallelogram mechanism provides additional degrees of freedom, which are very useful when the center of mass of the body to be suspended is not accessible for cardanic suspension. The addition of the rectangular link in figure 5b (for convenience shown in the plane of drawing, however the plane of the rectangle is to make a considerable angle with the plane of the rest of the mechanism to allow for sufficient x-, y-, and z-translation).

As has become apparent, there is scope for conceptional design improvements in several directions. Other interesting directions include the extension of the work by Agrawal *et al.* (2001), who use auxiliary parallelograms to trace the center of mass of series chains, a technique which may well work in parallel mechanisms too.

7 Conclusion

This paper has made an inventory of some fundamental questions and possible research directions regarding the application of static balance in parallel mechanisms. Primarily gravity compensation was considered, but also the compensation of the elastic forces in compliant parallel mechanisms was mentioned. The issues of separate or integrated compensation, the kind and number of energy storage devices, their weight as a function of the geometric scale, and the conceptional design of statically balanced parallel mechanisms were addressed in some detail.

Acknowledgements

This paper was originally submitted as a short paper intended for presentation as a poster.

Nomenclature

a = distance between fixed spring attachment and pivot
A = area
E = Young's Modulus
F = force
g = acceleration of gravity
k = stiffness
L = length
m = mass
r = link length
S = scaling factor
U = potential energy
V = volume
x = displacement
α = type factor
ρ = density
σ = yield strength

References

Agrawal, S. K., Gardner, G., Pledgie, S., 2001, "Design and fabrication of an active gravity balanced planar mechanism using auxiliary parallelograms, *Journal of Mechanical Design,* Vol. 123, p525-528.

Birglen, L., 2002, "Haptic devices based on parallel mechanisms, state of the art", http://parallemic.org/reviews/review003p.html.

Barette, G., Gosselin, C. M., 2000, "Kinematic analysis and design of planar parllel machanisms acutated with cables", *Proc. of the 2000 ASME Design engineering Technical Conferences*, DETC2000/MECH-14091.

Canfield S. L., Beard J. W., Parsons, R. D., Lobontiu, N., Paine, M., Paine, J., 2001, "Development of parallel architecture spatial compliant manipulators", *Proc. of the 2001 ASME Design engineering Technical Conferences*, DETC2001/DAC-21033.

Carwardine, G., 1932, "Improvements in elastic force mechanisms", UK Patent 379.680, *Specifications of Inventions*, Vol. 2729, Patent Office Sale Branch, London.

Carwardine, G., 1935, "Improvements in equipoising mechanism", UK Patent 433.617, *Specifications of Inventions*, Vol. 3337, Patent Office Sale Branch, London.

Carwardine, G., 1938, "Improvements in and relating to elastic force and equipoising mechanisms", UK Patent 489.547, *Specifications of Inventions*, Vol. 3896, Patent Office Sale Branch, London.

Cool J. C., 1992, "Mechanical systems", (in Dutch), DUM, Delft, The Netherlands.

Ebert-Uphoff, I., Gosselin, C. M., Laliberté, T., 2000, "Static balancing of spatial parallel platform mechanisms – revisited", *Journal of Mechanical Design*, 122(1)43/51.

Gosselin CM (1999) Static balancing of spherical 3-dof parallel mechanisms and manipulators, *The International Journal of Robotics Research,* 18(8)819/29.

Gosselin, C. M., Wang, J., 2000, "Static balancing of spatial six-degree-of-freedom parallel mechanisms with revolute actuators", *Journal of Robotic Systems,* 17(3)159/70.

Herder, J. L., van den Berg, F. P. A., 2000, "Statically balanced compliant mechanisms (SBCM's), an example and prospects, *Proc. ASME DETC 26th Biennial Mechanisms and Robotics Conference*, DETC2000/MECH-14144.

Herder, J. L., 2001, "*Energy-free systems; theory, conception and design of statically balanced spring mechanisms*", PhD-Thesis, Delft University of Technology, The Netherlands.

Hilpert H (1968) Weight balancing of precision mechanical instruments, *Jnl Mechanisms,* (3)289/302.

Howell, L. L., 2001, "*Compliant mechanisms*", John Wiley & Sons, Inc., New York.

Jean, M., Gosselin, C. M., 1996, "Static balancing of planar parallel manipulators", *Proceedings of the IEEE International Conference on Robotics and Automation*, Minneapolis, Minnesota, USA, p3732/7.

Nathan, R. H., 1985 "A constant force generating mechanism", *Journal of Mechanisms, Transmissions, and Automation in Design*, 107(12)508/12.

Riele FLS te, Herder JL (2001) Perfect static balance with normal springs, *Proceedings ASME Design Engineering Technical Conferences*, Sept 9-12, Pittsburgh, Pennsylvania, paper number DETC2001/DAC21096.

Streit, D. A., Shin, E., 1993, "Equilibrators for planar linkages", *Journal of Mechanical Design*, 115(3)604/11.

Proceedings of the WORKSHOP on
Fundamental Issues and Future Research Directions for Parallel Mechanisms and Manipulators
October 3–4, 2002, Quebec City, Quebec, Canada
Clément M. Gosselin and Imme Ebert-Uphoff, editors

Velocity Performance Indexes for Parallel Mechanisms with Actuation Redundancy

SEBASTIEN KRUT, OLIVIER COMPANY, FRANÇOIS PIERROT
LIRMM, UMR 5506
CNRS - Université Montpellier II
161, rue Ada
34392 Montpellier Cedex 5, France
<krut, company, pierrot>@lirmm.fr

Abstract: *This paper analyses the velocity isotropy of Parallel Mechanism with Actuation Redundancy. The limits of classical indexes based on the Jacobean matrix condition number is shown. Two new indexes are proposed, and the ways to computed them efficiently are given.*

1 Introduction

When designing a machine, optimization processes are often run aiming at pointing out the machine of "best performances". For this task, quality indexes are used. According to the machine purpose, one index is selected, and that will lead to the machine which provides the best score, *i.e.* which offers the best index value. Actually, optimization is often more delicate and often ends with a compromise of several abilities because of the antagonist evolution of various abilities that are essential to the correct behavior of the mechanism,.

Among all the quality indexes, the Jacobean matrix condition number is often used; it is supposed to characterize the velocities isotropy of the mechanism. Due to the forces-velocities duality, it is also said to be representative of forces isotropy. The mathematical basics which are the foundations of the isotropy concept for robots have been first defined for serial robots [1][2], and it turns out that a deeper analysis is required when considering more complex mechanisms.

This paper aims at offering such an analysis of isotropy concept when considering PMAR (**P**arallel **M**echanisms with ***A**ctuation **R**edundancy)*, *i.e.* mechanisms where a given operational force does not correspond to a unique set of joint forces. This type of redundancy differs from the *kinematic redundancy* case where a given operational velocity does not correspond to a unique set of joint velocities. It has been shown [3][4] that actuation redundancy may help to overcome over-mobility singularities, and it seems important to offer tools to correctly analyze the velocity performances of such machines.

In section 2, some basic issues related to condition number are firstly recalled and one of its important limitations is pointed out when considering PMAR: this index does not provide a proper measure of kinematic isotropy. Section 3 is dedicated to the definition of a new index which is consistent with the classical condition number since it refers to measures made on a velocity ellipsoid; however this ellipsoid is rather different from the usual one. Two different algorithms are given: one is based on derivations made in joint space, and the other one on derivations made in operational space. Section 4 is a discussion about different possible indexes and the relevant algorithms: they are based on an analysis of the velocity polytop.

2 Condition number and its application to PMAR

In the following a mechanism is characterized by its inverse Jacobean, $\mathbf{J_m}$, which links joints velocities $\dot{\mathbf{q}}$ to operational speed, $\dot{\mathbf{x}}$, as follows[1]:

$$\dot{\mathbf{q}} = \mathbf{J_m}\ \dot{\mathbf{x}} \tag{1}$$

2.1 Is a two-dof X-Y table an isotropic device?

In order to illustrate the following discussion, let us consider the simple case of a serial 2-dof X-Y table in fig. 1.

For this mechanism, $\mathbf{J_m}$ is the identity matrix, and for the robotics community, this mechanism is often considered as perfectly isotropic; that is to say, velocity performances are said to be identical in all directions of the operational space. This is clearly not true, as shown in fig. 2 and fig. 3.

[1] the notation $\dot{\mathbf{x}}$ does not mean it is the derivative of operational position vector with respect to time.

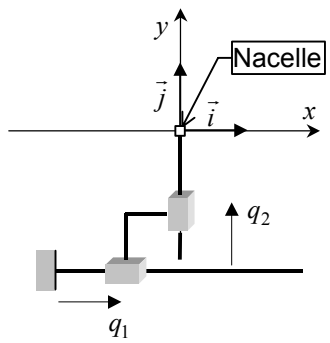

fig. 1 – X-Y table geometry

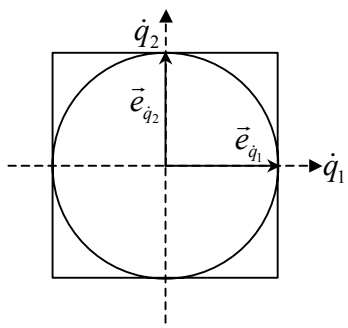

fig. 2 – Reachable joint space of the X-Y table

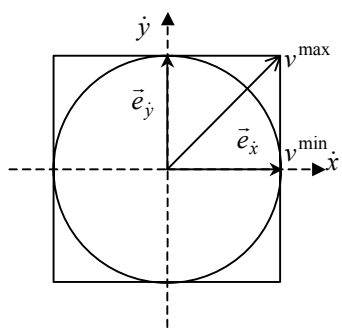

fig. 3 – Reachable operational space of the X-Y table

Reachable velocity joint is actually a square defined by $|\dot{q}_i| \le \dot{q}^{\max}$. This square remains a square once mapped in the operational space, using matrix $\mathbf{J_m}^{-1}$. Therefore the highest velocity reachable by the nacelle is $v^{\max} = \sqrt{2} \times \dot{q}^{\max}$. Such a speed is only accessible for a very specific motion direction. Moreover, $v^{\min} = \dot{q}^{\max}$ is always reachable for all operational directions. Graphically, this results in the circle of radius $v^{\min}$ inscribed in the square. This circle is the image of the joint space circle of radius $\dot{q}^{\max}$ by the linear mapping represented by matrix $\mathbf{J_m}^{-1}$. Interestingly enough, even if this is not an isotropic device strictly speaking, designers often refer to the deformation of a velocity joint space circle (or hyper-sphere for higher orders) by the Jacobean matrix to measure the "quality" of velocity mapping in terms of isotropy…

2.2 Analysis of a basic non-redundant parallel mechanism

The simple parallel mechanism in fig. 4 is made of two connecting rods linking two identical linear motors to the nacelle. Obviously, the nacelle can move in translation along two directions.

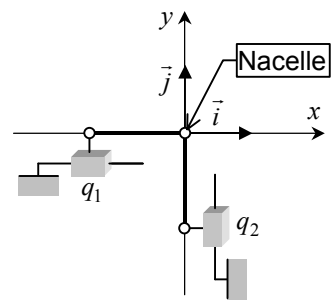

fig. 4 – V shape mechanism geometry

The inverse Jacobean matrix $\mathbf{J_m}$ of this mechanism in this centered position is the same as for the X-Y table (joint and operational reachable domains are those represented in fig. 2 and fig. 3). When the mechanism is not more in its centered position, the inverse Jacobean matrix is not equal to the identity matrix anymore; so if the reachable joint domain remains the same, the reachable operational domain becomes a polytop (see fig. 5).

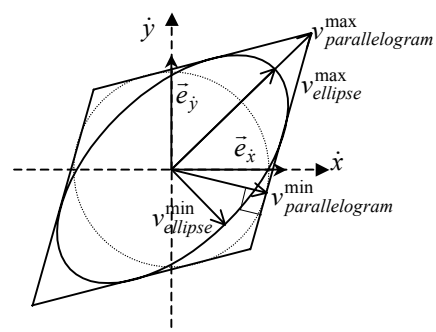

fig. 5 – Reachable operational space for a simple parallel mechanisms.

The image of the joint circle is an ellipse inscribed in the polytop. This ellipse is entirely characterized by the SVD[2] of $\mathbf{J_m}$; the SVD provides in particular the lengths of the ellipse's axes. A usual isotropy index is derived as the ratio of extreme operational velocities: $v^{\max}_{ellipse}$ and $v^{\min}_{ellipse}$; this index is a measure of the ellipse's distortion. The lower the distortion is (index value close to 1), the more the ellipse tends towards the circle, considered as the "ideal case" from the isotropy point of view.

Rather than considering the ellipse, one could be interested in the more realistic polytop that may be analyzed in terms of ratio between the absolute maximal speed ($v^{\max}_{parallelogram}$) and the maximum speed that the mechanism can reach in all

[2] Singular Value Decomposition

operational space directions ($v^{\min}_{parallelogram}$). The latter graphically corresponds to the radius of the largest circle inscribed in the operational polytop.

In this paper, discussions related to PMAR are made for both cases, velocity ellipsoid and velocity polytop; however, the usual inverse Jacobean matrix condition number cannot be used straightforward, as shown in the next section.

2.3 A basic PMAR – 3 actuators / 2 dof

Let us consider the PMAR in fig. 6., made up of three connecting rods and three identical linear actuators. Here, two actuators are colinear.

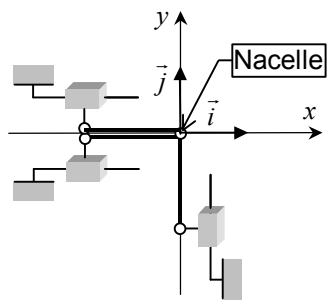

fig. 6 – Geometry of a specific PMAR

This mechanism produces in term of velocities the same effects that the former non-redundant parallel mechanism (fig. 4). So, in this centered position, this mechanism is as isotropic from the velocity point of view as the previous mechanism or even the X-Y table; operational velocities explore the same field as previously: a square (fig. 3).

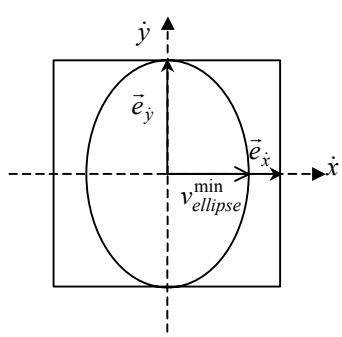

fig. 7 – Reachable operational space for this specific PMAR

For this mechanism the inverse Jacobean matrix, $\mathbf{J_m}$, is given by:

$$\mathbf{J_m} = \begin{bmatrix} 1 & 0 \\ 1 & 0 \\ 0 & 1 \end{bmatrix}$$

… and its condition number is equal to $\sqrt{2}$. Thus, the ratio between extreme singular values does not represent anymore the ratio of extreme dimensions of the ellipse of maximum surface inscribed in the operational polytop, since this ratio should be equal to 1. Indeed, the operational ellipse obtained using the SVD, has two half-axes which length are $\dot{q}_{\max}$ and $\dot{q}_{\max}/\sqrt{2}$ as depicted in fig. 7.

In different words, the usual isotropy index says such a machine is far from being isotropic, when a common sense analysis says it is as isotropic as an X-Y table. Indeed in such cases, the condition number may give a rough estimate of the anisotropy in force (in reality the machine maximum force along x is twice the maximum force along y), but it does not represent anything related to velocity isotropy.

As a matter of fact, for PMAR the "duality" between force and velocity does not hold anymore for this simple fact: a set of joint forces can be chosen freely within the actuators capacity boundaries, while the components of the joint velocities vector must respect kinematic constraints and thus cannot be chosen freely.

In order to be consistent with the interpretation of the condition number established for non-redundant mechanisms, the ellipse of larger surface inscribed into the operational polytop will be determined. Its characteristics, length of the largest and the smallest half-axis, will lead to a more significant isotropy index which can cope with PMAR.(section 3). Moreover, the way to establish the extreme velocities related to the operational space polytop will be described as well (section 4).

3 Construction of an isotropy index based on ellipses

3.1 Preliminary remarks

- To be simple, different domains of space will be named circle, ellipse, polytop, square, cube. One should keep in mind that those terms must be generalized when considering spaces whose dimensions are higher than 2 or 3 (hyper-circle, hyper-ellipse, and so on).

- Only a-dimensional problems are considered here. In other cases, weighting matrices, $\mathbf{W}_{\dot{\mathbf{x}}}$ and $\mathbf{W}_{\dot{\mathbf{q}}}$, can be used as follows [9]:

$$\mathbf{W}_{\dot{\mathbf{x}}} = \begin{bmatrix} 1/\dot{x}_1^{\max} & & 0 \\ & \ddots & \\ 0 & & 1/\dot{x}_n^{\max} \end{bmatrix}, \tilde{\dot{\mathbf{x}}} = \mathbf{W}_{\dot{\mathbf{x}}}\ \dot{\mathbf{x}},\ \left|\tilde{\dot{x}}_i\right| \le 1,$$

$$\mathbf{W}_{\dot{\mathbf{q}}} = \begin{bmatrix} 1/\dot{q}_1^{\max} & & 0 \\ & \ddots & \\ 0 & & 1/\dot{q}_n^{\max} \end{bmatrix}, \tilde{\dot{\mathbf{q}}} = \mathbf{W}_{\dot{\mathbf{q}}}\ \dot{\mathbf{q}},\ \left|\tilde{\dot{q}}_i\right| \le 1.$$

Weighting matrices help in managing issues such as: non-homogeneity (coexistence of linear and angular velocities), differences in actuators' performances ($\dot{q}_i^{\max} \neq \dot{q}_j^{\max}$), differences in desired performances along various operational axes ($\dot{x}_i^{\max} \neq \dot{x}_j^{\max}$).

- The next sub-sections are organized as follows: (i) in section 3.2 linear algebra tools are briefly recalled and the limits of their use for PMAR is pointed out; (ii) in section 3.3, a way to compute the largest admissible ellipse included in the joint polytop and to map it into the operational space; (iii) in section 3.4 it is proven that the resulting ellipse is actually the largest one in the operational space.

3.2 Analyze of the SVD for a redundant mechanism

For illustration purpose the planar mechanism shown in fig. 8 will be used here. It is a 3 actuators / 2 dof PMAR, which geometry is more general than the one in section 2.3. However, formulas will be established any type of joint and operational spaces, as long as they respect the following condition:

$$m > n \text{, with } \dim(\dot{\mathbf{q}}) = m \text{ and } \dim(\dot{\mathbf{x}}) = n$$

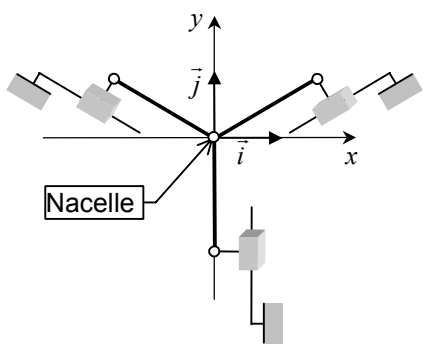

fig. 8 – Geometry of a typical parallel redundant mechanism

The SVD of the inverse Jacobean matrix gives [5]:

$$\mathbf{J_m} = \mathbf{U}\,\mathbf{S}\,\mathbf{V^T}, \qquad (2)$$

where:

- $\mathbf{V^T}$ is a $n \times n$ orthogonal matrix, representing a linear application in the operational space;

- $\mathbf{S}$ is a rectangular matrix whose upper part includes the singular values of $\mathbf{J_m}$, $\sigma_1, \cdots, \sigma_n$,:

$$\mathbf{S} = \begin{array}{c} \overleftrightarrow{\quad n \quad} \\ \left[\begin{array}{ccc} \sigma_1 & & 0 \\ & \ddots & \\ 0 & & \sigma_n \\ \hdashline & 0 & \end{array}\right] \end{array} \begin{array}{l} \updownarrow n \\ \updownarrow m \end{array}$$

It characterizes the linear application that links a operational velocity vector to a joint velocity vector.

- $\mathbf{U}$ is a $m \times m$ orthogonal matrix, representing a linear application in the joint space. The n first columns, vectors $U_1, \ldots, U_n$ ($n < m$) span the range of $\mathbf{J_m}$. The $m - n$ following columns correspond to the actuators velocities which can never be produced by a movement of the nacelle. They span the kernel of $\mathbf{J_m}$.

$$\mathbf{U} = \begin{array}{c} \overleftrightarrow{\quad m \quad} \\ \overleftrightarrow{\quad n \quad} \\ \left[\begin{array}{ccc} U_1 & \ldots & U_n \\ & & \\ & & \end{array}\right] \end{array} \updownarrow m$$

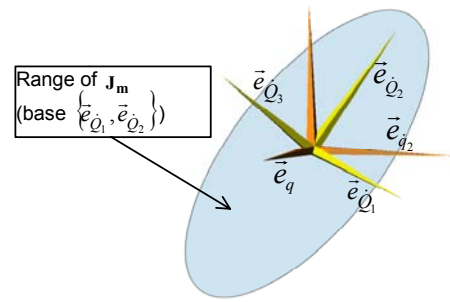

fig. 9 – Graphical representation of $\dot{\mathbf{q}} = \mathbf{U}\,\dot{\mathbf{Q}}$

To be acceptable, *i.e.* to be admissible by the mechanism, a joint velocity vector must belongs to the range of $\mathbf{J_m}$,. Let us note:

$\{\vec{e}_{\dot{Q}_1}, \ldots, \vec{e}_{\dot{Q}_n}\}$, a base for this type of vector;

$\tilde{\dot{\mathbf{Q}}}$ ($\dim(\tilde{\dot{\mathbf{Q}}}) = n$), a column matrix representative of the joint velocity vector in this base;

$\mathbf{S_1}$, a matrix representing a mapping from the operational space to the restriction of the joint space to the range of $\mathbf{J_m}$:

$$\mathbf{S_1} = \begin{array}{c} \overleftrightarrow{\quad n \quad} \\ \left[\begin{array}{ccc} \sigma_1 & & 0 \\ & \ddots & \\ 0 & & \sigma_n \end{array}\right] \end{array} \updownarrow n$$

The following equation links an admissible joint velocity vector to an operational velocity vector:

$$\dot{\mathbf{x}} = \mathbf{V}\,\mathbf{S_1}^{-1}\,\tilde{\dot{\mathbf{Q}}} \qquad (3)$$

The restriction of the unit sphere to the range of $\mathbf{J_m}$ is a circle of radius 1 (*cf.* fig. 10). This circle if transformed into an ellipse in the operational space; the ellipse's half-axes length are $1/\sigma_i, i \in \{1, \ldots, n\}$. The condition number of $\mathbf{J_m}$ is an image of this ellipse's shape.

Obviously, the entire acceptable joint space is not a sphere but a cube defined by the following inequalities:

$$-1 \le \dot{q}_i \le 1, i \in \{1, \ldots, m\}$$

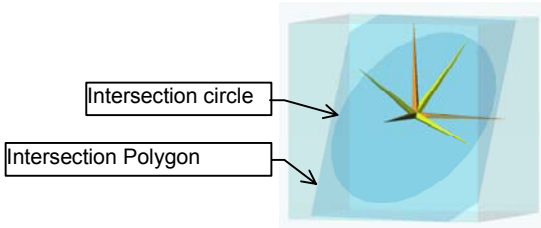

fig. 10 – Intersection of the unit cube and the unit sphere with the range of $\mathbf{J_m}$

The restriction of this cube to the range of $\mathbf{J_m}$ (*cf.* fig. 10) is a polygon, or polytop. All acceptable motors velocities vectors must be located inside this polygon. In fig. 11, the circle and the polygon are depicted. It is to be noted that the circle could be larger and still acceptable because it is not tangent with the polygon. *That implies that the opposite of the singular values are not enlightening maximum speeds which can be reached by the nacelle.*

fig. 11 – Joint polygon and circle

For a non-redundant mechanism, the joint circle and the operational ellipse are the greatest ellipses respectively included into the joint square and the operational polytop; for a PMAR, this is no more the case.

It is proposed in this paper to determine the largest ellipse included in the operational polytop. The ratio of the extreme half-axis of this ellipse can be a really significant isotropy index.

It is proposed as well to consider another index constituted from the ratio between the extreme velocities measured at the polytop level, $v^{\max}_{polytop}$ and $v^{\min}_{polytop}$.

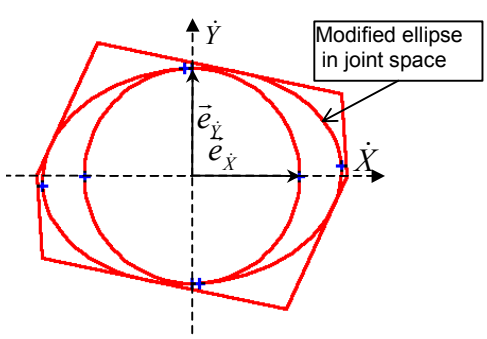

fig. 12 – Joint velocities for a PMAR

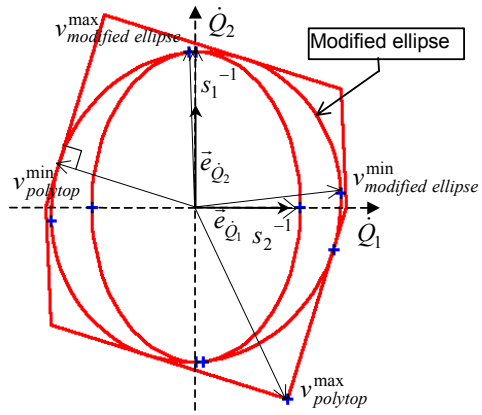

fig. 13 – Operational velocities for a PMAR

Case study.

The complete situation is depicted in fig. 14 for a given geometry [120° between each actuators, length of arms = 100, position of the nacelle (-40,-10)].

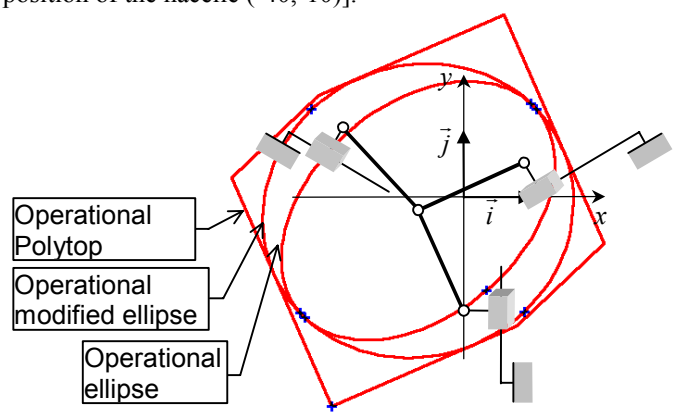

fig. 14 – Operational velocity situation centered on the nacelle.

The obtained results are given in table 1. Clearly the modified operational ellipse is a better representation of the machine velocity capability than the ellipse associated with the restriction of joint space unit sphere (operational ellipse in fig. 14).

$cond(\mathbf{J_m})$	1.49
Largest ellipse index	1.08
$v^{\max}_{modified\ ellipse}$	$1.35 \times \dot{q}_{\max}$
$v^{\min}_{modified\ ellipse}$	$0.97 \times \dot{q}_{\max}$
Polytop index	1.48

table 1 – Results and indexes values

The following sub-sections are dedicated to the derivation of both indexes in a general case.

3.3 Search of the operational ellipse of greatest surface included into the admissible operational polytop

This search can be made:

- by reasoning in joint space, i.e. finding the largest ellipse in joint space and then mapping it into the operational space (section 3.3.1);
- by reasoning directly in the operational space (section 3.3.2).

3.3.1 Reasoning in joint space

The application which transforms the joint unitary circle of the subspace image of $\mathbf{J_m}$ into the joint ellipse of largest surface included in the joint polytop will be determined here. This ellipse, once mapped into the operational space by the linear application of matrix $\mathbf{S_1}^{-1}$ gives the ellipse of largest surface included into the operational polytop (this point will be proved in section 3.3.2). The conditions which must be respected by the joint ellipse to be located inside the joint polytop will be firstly presented; then the conditions to find the largest ellipse will be formulated as an optimization problem.

General approach

Let M be a point of the range of $\mathbf{J_m}$ and belonging to the unitary circle. Vector $\overrightarrow{OM}$ (where O is the origin of the frame) is a linear combination of vectors $\vec{e}_{\dot{Q}_1},\ldots,\vec{e}_{\dot{Q}_n}$. Let $\mathbf{M}$ be the column matrix representative of this vector in the base of the range $\mathrm{B}_{\mathrm{Im}(\mathbf{J_m})} = (\vec{e}_{\dot{Q}_1},\ldots,\vec{e}_{\dot{Q}_n})$. The relation $\left\|\overrightarrow{OM}\right\| = 1$ results in:

$$\mathbf{M}^{\mathbf{T}}\ \mathbf{M} = \mathbf{1}. \tag{4}$$

The largest ellipse in joint space is calculated with two transformations: (i) the original unitary circle is expanded (point M is transformed in point $\widetilde{M}$), (ii) the expanded ellipse is rotated (point $\widetilde{M}$ is transformed in point in M'). Thus:

- $\widetilde{M}$ belongs to an ellipse whose axis are the vectors of $\mathrm{B}_{\mathrm{Im}(\mathbf{J_m})}$, and whose half-axes length are $d_1,\ldots,d_n$,

The column matrix representative of point $\widetilde{M}$ in frame of origin O and base $\mathrm{B}_{\mathrm{Im}(\mathbf{J_m})}$, is noted $\widetilde{\mathbf{M}}$, and verifies:

$$\widetilde{\mathbf{M}} = \mathbf{D}\,\mathbf{M} \tag{5}$$

where $\mathbf{D} = diag(d_1,\cdots,d_n)$

- M' belongs to the ellipse of greatest surface.
  $\mathbf{M}'$, the matrix associated to point M' verifies:

$$\mathbf{M}' = \mathbf{R}\ \widetilde{\mathbf{M}}, \tag{6}$$

with $\mathbf{R}$ an orthogonal matrix.

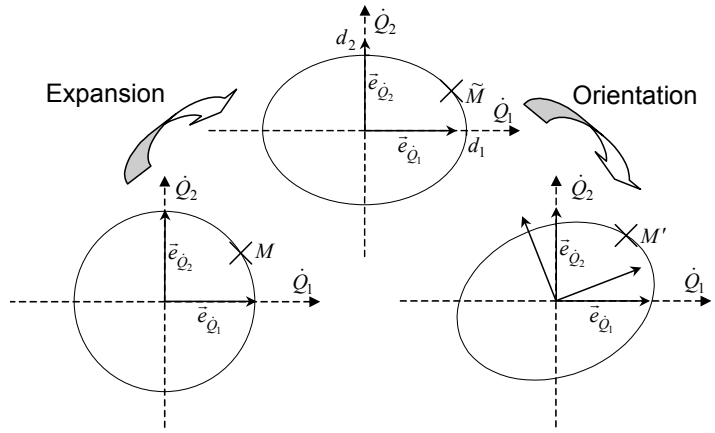

fig. 15 – From the unitary circle to the largest ellipse

Expansion and orientation are combined to get the largest ellipse. To be included in the joint polytop, the ellipse must verify:

- the ellipse is located inside the unitary cube;
- it belongs to the range of $\mathbf{J_m}$ (true by construction),

To belong to the joint cube, point M' must respect the following condition:

$$\vec{e}_{\dot{q}_i} \cdot \overrightarrow{OM'} \le 1 \quad i = 1,\cdots,m$$

Indeed, the cube is defined by $2m$ faces. However, the problem is symmetric with respect to point O, and only m faces have to be considered. Such faces are directed by vectors $\vec{e}_{\dot{q}_i}$ $i = 1,\cdots,m$, of the joint space canonic base. This expresses the fact that M' belongs to the ith admissible domain of space, delimited by the plan perpendicular to $\vec{e}_{\dot{q}_i}$. , such that the distance from point O to the plan is equal to 1. This can be written in matrix form as follows:

$$\mathbf{E_i}^{\mathbf{T}}\ \mathbf{M}' \le 1, \tag{7}$$

where $\mathbf{E_i}$ is the column matrix associated to vector $\vec{e}_{\dot{q}_i}$ in base $\mathrm{B}_{\mathrm{Im}(\mathbf{J_m})} = (\vec{e}_{\dot{Q}_1},\ldots,\vec{e}_{\dot{Q}_n})$.

Finding the vectors perpendicular to the ellipse and the polytop.

To guarantee that all ellipse points belong to the ith admissible domain, it is sufficient to verify that the point closest to the ith face is inside this domain. For such a point, the vector perpendicular to the ellipse, $\vec{n'}$, is collinear to the vector, $\vec{e}'_{\dot{q}_i}$, perpendicular to the considered face of the polytop (*cf.* fig. 16).

Let be $\vec{e}'_{\dot{q}_i}$ the projection of vector $\vec{e}_{\dot{q}_i}$ in the range of $\mathbf{J_m}$. Because $\mathrm{B}_{\mathrm{Im}(\mathbf{J_m})}$ does only direct a subpart of the articular space it has to be noticed that $\mathbf{E_i}$ is also the column matrix associated to vector $\vec{e}'_{\dot{q}_i}$.

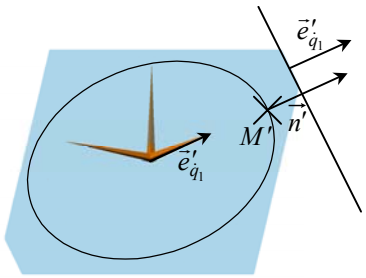

fig. 16 – Colinearity normal to the ellipse / normal to the frontier

The colinearity relationship is expressed as:

$$\exists k \,/\quad \mathbf{N}' = k \times \mathbf{E_i}\,, \tag{8}$$

Where:

- $\mathbf{N}'$ is the column matrix associated to vector $\vec{n}'$ in base $\mathrm{B}_{\mathrm{Im}(\mathbf{J_m})}$,
- $\mathbf{E_i}$ is the column matrix associated to vector $\vec{e}'_{\dot{q}_i}$.

Let point $\widetilde{M}$ be defined in the frame $\left\langle O, \mathrm{B}_{\mathrm{Im}(\mathbf{J_m})} \right\rangle$ by the following set of coordinates:

$$(x_1, \ldots, x_n)$$

Then the ellipse whose axis are the vectors of $\mathrm{B}_{\mathrm{Im}(\mathbf{J_m})}$, and whose half-axes length are $d_1, \ldots, d_n$ is defined by:

$$f(\widetilde{M}) = \frac{x_1^{\,2}}{d_1^{\,2}} + \ldots + \frac{x_n^{\,2}}{d_n^{\,2}} - 1 = 0$$

Then the vector perpendicular to the ellipse at point $\widetilde{M}$, $\vec{\tilde{n}}$, is defined by:

$$\vec{\tilde{n}} = [\overrightarrow{grad} f](\widetilde{M}) = \frac{2\,x_1}{d_1^{\,2}} \vec{e}_{\dot{Q}_1} + \ldots + \frac{2\,x_n}{d_n^{\,2}} \vec{e}_{\dot{Q}_n}\,.$$

With matrix in base $\mathrm{B}_{\mathrm{Im}(\mathbf{J_m})}$, this results in relation:

$$\widetilde{\mathbf{N}} = \mathbf{D^{-2}}\ \widetilde{\mathbf{M}}\,. \tag{9}$$

In fact, because $\mathbf{D}$ is a diagonal matrix, $\mathbf{D^{-2}}$ is defined by:

$$\mathbf{D^{-2}} = \begin{bmatrix} 1/d_1^{\,2} & & 0 \\ & \ddots & \\ 0 & & 1/d_n^{\,2} \end{bmatrix}.$$

Then $\vec{n}'$ is obtained as:

$$\mathbf{N}' = \mathbf{R}\ \widetilde{\mathbf{N}}\,. \tag{10}$$

with:

$\mathbf{R}$ a rotation matrix

<u>Defining the admissible ellipses</u>

To summarize the situation, the system of matrix equations to be solved is the following:

$$\forall \mathbf{i} \in \{1, \ldots, m\}, \quad \begin{cases} \mathbf{M^T\ M = 1} & (4) \\ \widetilde{\mathbf{M}} = \mathbf{D\ M} & (5) \\ \mathbf{M}' = \mathbf{R}\ \widetilde{\mathbf{M}} & (6) \\ \mathbf{E_i^{\,T}\ M}' \le 1 & (7) \\ \exists k \,/\quad \mathbf{N}' = k \times \mathbf{E_i} & (8) \\ \widetilde{\mathbf{N}} = \mathbf{D^{-2}}\ \widetilde{\mathbf{M}} & (9) \\ \mathbf{N}' = \mathbf{R}\ \widetilde{\mathbf{N}} & (10) \end{cases}$$

(5) and (6) imply that:

$$\mathbf{M}' = \mathbf{R\ D\ M}\,. \tag{11}$$

(9) and (10) lead to:

$$\mathbf{N}' = \mathbf{R\ D^{-2}}\ \widetilde{\mathbf{M}}\,, \tag{12}$$

(12) and (5) lead to:

$$\mathbf{N}' = \mathbf{R\ D^{-1}\ M}\,. \tag{13}$$

Inverting (13) leads to:

$$\mathbf{M} = \mathbf{D\ R^T\ N}' \tag{14}$$

Combining (11) and (7) gives:

$$\mathbf{E_i^{\,T}\ R\ D\ M} \le 1 \tag{15}$$

Combining (8) and (14) gives:

$$\exists k \,/\quad \mathbf{M} = k \times \mathbf{D\ R^T\ E_i} \tag{16}$$

Combining (16) and (4), knowing that $\mathbf{D}$ is diagonal, can be written as follows:

$$\exists k \,/\quad k^2\ \mathbf{E_i^{\,T}\ R\ D^2\ R^T\ E_i} = 1 \tag{17}$$

In the same way, combining (16) and (7) leads to:

$$\exists k \,/\quad k\ \mathbf{E_i^{\,T}\ R\ D^2\ R^T\ E_i} \le 1 \tag{18}$$

While making sure that $0 \le k\ \mathbf{E_i^{\,T}\ R\ D^2\ R^T\ E_i}$, (18) gives:

$$\exists k \,/\, k^2\ \mathbf{E_i^{\,T}\ R\ D^2\ R^T\ E_i} \times \mathbf{E_i^{\,T}\ R\ D^2\ R^T\ E_i} \le 1 \tag{19}$$

Knowing (17), (19) simplifies in the inequality:

$$\mathbf{E_i^{\,T}\ \Sigma\ E_i} \le 1 \tag{20}$$

with $\mathbf{\Sigma} = \mathbf{R\ D^2\ R^T}$, a symmetrical matrix.

Of course, (20) has to be verified for all $i = 1, \cdots, m$.

As a matter of fact, a relation exists between vectors $\mathbf{E_i}$ and matrix $\mathbf{U}$. Matrix $\mathbf{U}$ can be expressed as follows:

$$\mathbf{U} = \left[\mathbf{U_1} \;\vdots\; \mathbf{U_2}\right]$$

with

$$\mathbf{U_1} = \begin{bmatrix} \vec{e}_{\dot{q}_1} \cdot \vec{e}_{\dot{Q}_1} & \cdots & \vec{e}_{\dot{q}_1} \cdot \vec{e}_{\dot{Q}_n} \\ & \cdots & \\ \vec{e}_{\dot{q}_m} \cdot \vec{e}_{\dot{Q}_1} & \cdots & \vec{e}_{\dot{q}_m} \cdot \vec{e}_{\dot{Q}_n} \end{bmatrix}$$

$$\mathbf{U}_2 = \begin{bmatrix} \vec{e}_{\dot{q}_1} \cdot \vec{e}_{\dot{Q}_{n+1}} & \cdots & \vec{e}_{\dot{q}_1} \cdot \vec{e}_{\dot{Q}_m} \\ & & \\ \vec{e}_{\dot{q}_m} \cdot \vec{e}_{\dot{Q}_{n+1}} & \cdots & \vec{e}_{\dot{q}_m} \cdot \vec{e}_{\dot{Q}_m} \end{bmatrix}$$

And since $\mathbf{E_i} = \begin{bmatrix} \vec{e}_{\dot{q}_i} \cdot \vec{e}_{\dot{Q}_1} \\ \vdots \\ \vec{e}_{\dot{q}_i} \cdot \vec{e}_{\dot{Q}_n} \end{bmatrix}$ $\mathbf{U_1}$ is expressed as follows:

$$\mathbf{U_1} = \begin{bmatrix} \mathbf{E_1}^{\mathbf{T}} \\ \vdots \\ \mathbf{E_m}^{\mathbf{T}} \end{bmatrix}. \qquad (21)$$

Noting $\mathbf{U_1}(i)$ the ith line of matrix $\mathbf{U_1}$ equation (20) can be rewritten as:

$$\forall i \in \{1, \cdots, m\} \quad \mathbf{U_1}(i)\, \mathbf{\Sigma}\, \mathbf{U_1}(i)^{\mathbf{T}} \le 1 \qquad (22)$$

<u>Finding the largest admissible ellipse</u>

Among all those ellipses respecting (22), the one of maximal surface still have to be found. This problem is described here as an optimization problem.

The surface of an hyper-ellipse equals to:

$$A = k \times \prod_{i=1}^{n} d_i \ ,$$

with $k = \pi$ for $n = 2$, $k = \frac{4}{3}\pi$ for $n = 3$, etc.

Maximizing A is equivalent to maximizing the product of the ellipse half-axes length. It is also equivalent to minimize the following expression:

$$-\prod_{i=1}^{n} d_i^{\,2}$$

It can be seen that the determinant of $\mathbf{\Sigma}$ is:

$$\det(\mathbf{\Sigma}) = \det(\mathbf{R}) \times \det(\mathbf{D^2}) \times \det(\mathbf{R^{-1}}) = \det(\mathbf{D^2})$$

$$\det(\mathbf{\Sigma}) = \prod_{i=1}^{n} d_i^{\,2} \qquad (23)$$

To conclude, determining the ellipse of greatest surface included in the joint polytop, consists in finding the *symmetrical* matrix $\mathbf{\Sigma}$ which verifies:

$$-\det(\mathbf{\Sigma}) \text{ minimum}$$

under constraints

$$\mathbf{U_1}(i)\, \mathbf{\Sigma}\, \mathbf{U_1}(i)^{\mathbf{T}} \le 1 \quad \forall i \in \{1, \cdots, m\}.$$

The eigen value decomposition of the *real symmetric* $\mathbf{\Sigma}$ gives:

$$\mathbf{\Sigma} = \mathbf{R}\, \mathbf{\Delta}\, \mathbf{R}^{\mathbf{T}} \qquad (24)$$

With

- $\mathbf{R}$ is the orientation matrix (note that $\mathbf{R}^{\mathbf{T}} = \mathbf{R}^{-1}$)
- $\mathbf{\Delta} = diag(\delta_1, \cdots, \delta_n)$
- $d_i = \sqrt{\delta_i}$

The knowledge of $\mathbf{R}$ and $\mathbf{D}$ characterizes entirely the ellipse of greatest surface included inside the joint polytop. This matrix is then mapped by matrix $\mathbf{S_1}^{-1}$ to the ellipse of largest surface included in the operational polytop (This point will be proven in next section).

The sought matrix which represents the transformation of a unitary circle in the admissible part of joint space into the largest ellipse included inside the operational space polytop is given by:

$$\mathbf{X} = \mathbf{S_1}^{-1}\, \mathbf{R}\, \mathbf{D}$$

The proposed index is then related to singular values of this matrix, *e.g.* $cond(\mathbf{X})$ **, or** $\min(\sigma(\mathbf{X}))$ **, etc.**

3.3.2 Reasoning in operational space

Rather than seeking the ellipse of maximum surface included inside the joint polytop, and then computing its image in the operational space, it is possible to find the ellipse of greatest surface included inside the operational polytop.

The following relation describes the mapping between the operational space and the range of $\mathbf{J_m}$:

$$\mathbf{M}' = \mathbf{S_1}\ \mathbf{K}' \tag{25}$$

With:

$M' \in range(\mathbf{J_m})$

K' a point in operational space

$\mathbf{M}'$ the column matrix associated with M' in $B_{Im(\mathbf{J_m})}$

$\mathbf{K}'$ the column matrix associated with K' in the singular vectors base.

M' belongs to the joint polytop:

$$\mathbf{E_i}^{\mathbf{T}}\ \mathbf{M}' \leq 1 \quad i = 1, \cdots, m \tag{26}$$

Thanks to relation (25), equation(26) becomes in operational space:

$$\mathbf{E_i}^{\mathbf{T}}\ \mathbf{S_1}\ \mathbf{K}' \leq 1 \tag{27}$$

Since equation (27) is the only equation that differs from the system of equations of the previous section, the resolution of the system leads to:

$$\forall i \in \{1, \cdots, m\} \quad \mathbf{U_1}(i)\, \mathbf{S_1} \mathbf{\Sigma}' \mathbf{S_1}^{\mathbf{T}} \mathbf{U_1}(i)^{\mathbf{T}} \leq 1 \tag{28}$$

where $\mathbf{\Sigma}'$ is a symmetrical matrix defined as follows:

$$\mathbf{\Sigma}' = \mathbf{R}'\, \mathbf{D}'^{\mathbf{2}}\ \mathbf{R}'^{\mathbf{T}}$$

Those equations express the constraints that must be fulfilled by the operational ellipse to be located inside the operational polytop. Those relations are very similar to those obtained in the joint space.

In the operational space, the optimization problem consists in fining a *symmetrical* matrix $\mathbf{\Sigma}'$ which verifies:

$$-\det(\mathbf{\Sigma}') \text{ minimum}$$

under constraints

$$\mathbf{U_1}(i)\, \mathbf{S_1} \mathbf{\Sigma}' \mathbf{S_1}^{\mathbf{T}} \mathbf{U_1}(i)^{\mathbf{T}} \leq 1 \quad \forall i \in \{1, \cdots, m\}$$

The eigen values decomposition of $\mathbf{\Sigma}'$ leads to matrix $\mathbf{R}'$ and $\mathbf{D}'$. Matrix $\mathbf{X}' = \mathbf{R}'\, \mathbf{D}'$ characterizes the linear application that transforms a unitary circle in the ellipse of maximum surface included into the operational polytop. The ratio of extreme diagonal values of $\mathbf{D}'$ constitutes the isotropy index built previously.

One can check that $\mathbf{X} = \mathbf{X}'$, that is to say that the ellipses obtained with both methods are the same. In fact referring to the definitions of $\mathbf{X}$ and $\mathbf{X}'$, it can be verified that:

$$\mathbf{\Sigma} = \mathbf{S_1}\ \mathbf{X}\, \mathbf{X}^{\mathbf{T}}\ \mathbf{S_1}^{\mathbf{T}}$$

$$\mathbf{\Sigma}' = \mathbf{X}'\, \mathbf{X}'^{\mathbf{T}}.$$

So the admissible domains constraints can be written as:

Reasoning in joint space

$$\mathbf{U_1}(i)\, \mathbf{S_1}\, \mathbf{X}\, \mathbf{X}^{\mathbf{T}}\ \mathbf{S_1}^{\mathbf{T}}\, \mathbf{U_1}(i)^{\mathbf{T}} \leq 1$$

Reasoning in operational space

$$\mathbf{U_1}(i)\, \mathbf{S_1}\, \mathbf{X}'\, \mathbf{X}'^{\mathbf{T}}\ \mathbf{S_1}^{\mathbf{T}}\, \mathbf{U_1}(i)^{\mathbf{T}} \leq 1$$

In joint space, $-\det(\mathbf{\Sigma})$ has to be minimized, that is $-\det(\mathbf{X}\, \mathbf{X}^{\mathbf{T}})$, because:

$$-\det(\mathbf{\Sigma}) = -2\det(\mathbf{S_1})\det(\mathbf{X}\, \mathbf{X}^{\mathbf{T}})$$

$$\det(\mathbf{S_1}) > 0$$

In operational space $-\det(\mathbf{\Sigma}')$ has to be minimized, that is: $-\det(\mathbf{X}'\, \mathbf{X}'^{\mathbf{T}})$. Thus, both entities are obtained as results of the same optimization problem under the same constraints.

4 Determination of extreme velocities of the operational polytop

In this section, the extreme velocities of the operational polytop will be determined. The "lowest" velocity is defined as the minimum velocity always reachable by the nacelle in all directions of the operational space. The "highest" velocity is the maximum velocity that can be reached by the nacelle in a very particular direction.

The highest velocity $v_{polytop}^{\max}$ belongs necessary to a vertex of the polytop; the lowest value $v_{polytop}^{\min}$ is located on one of the faces (cf. fig. 13).

Finding $v_{polytop}^{\max}$

Referring to (27), a point K_i' belonging to the ith face can be described by:

$$\mathbf{E_i}^{\mathbf{T}}\ \mathbf{S_1}\ \mathbf{K_i'} = 1 \tag{29}$$

A point K_{m+i}', $i \in \{1, \ldots, m\}$, belonging to the opposite face (the $(m+i)^{th}$ face) can be described by:

$$-\mathbf{E_i}^{\mathbf{T}}\ \mathbf{S_1}\ \mathbf{K'_{m+i}} = 1 \tag{30}$$

In the optimization problem faces of type (30) had not been considered; here they must be taken into account. A vertex of the polytop is a point of the *n*-dimensional operational space. The *2m* frontier equations (*m* of type (29) and *m* of type (30)) will be seek, to find all the combinations of *n* faces which generate a vertex. For this, all C_{2m}^{n} possible systems will be considered.

If the ith system can be solved, the fact that point K_i', $i \in \{1, \ldots, 2m\}$ belongs to the polytop will have to be verified. The system might have no solution, for example when

two vectors $\vec{e}_i$ et $\vec{e}_j$ have the same projection in the range of $\mathbf{J_m}$: $\mathbf{E_i} = \mathbf{E_j}$. Moreover, when a point K'_i is established, this point might be located outside the admissible space (*cf.* fig. 17).

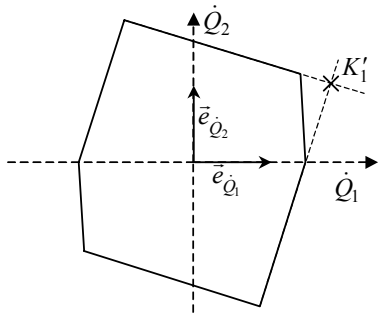

fig. 17 – Determination of a point outside from the admissible polytop

Once all vertices are determined, the highest distance between the center and points K'_i is given by:

$$v^{\max}_{parallelogram} = \max_{\mathbf{i}\in\{1,\ldots,2m\}} \|\mathbf{K'_i}\| \tag{31}$$

Finding $v^{\min}_{polytop}$

The lowest distance $v^{\min}_{polytop}$ is measured between the center and a point located on one of the side of the polytop. Let us note H'_i the closest point on side i . OH'_i is collinear with the normal of this side.

Relation (29) for H'_i and i^{th} face is the following:

$$\mathbf{E'_i}^{\mathbf{T}}\ \mathbf{H'} = 1 \tag{32}$$

Where
$\mathbf{E'_i} = \mathbf{S_1}\ \mathbf{E_i}$. is the normal vector to the side.

The colinearity relation can be written as follows:

$$\exists k / \quad \mathbf{H'_i} = k\ \mathbf{E'_i}\,. \tag{33}$$

So, combining (33) and (32) implies:

$$\mathbf{E'_i}^{\mathbf{T}}\ k\ \mathbf{E'_i} = 1\,. \tag{34}$$

Thus k is:

$$k = 1/\|\mathbf{E'_i}\|^2\,. \tag{35}$$

By replacing the value of k in relation (33) and by calculating the distance from point $H'_i, i \in \{1,\ldots,m\}$ to the center, this leads to:

$$\|\mathbf{H'_i}\| = 1/\|\mathbf{E'_i}\|, \tag{36}$$

That is to say, by using expression of $\mathbf{E'_i}$:

$$\|\mathbf{H'_i}\| = 1/\|\mathbf{S_1}\ \mathbf{E_i}\|\,. \tag{37}$$

Then, the sought value is given by:

$$v^{\min}_{parallelogram} = \min_{\mathbf{i}\in\{1,\ldots,m\}} \|\mathbf{H'_i}\| \tag{38}$$

5 Conclusion

In this paper we have firstly shown the limits of classical indexes based on the Jacobean matrix condition number when Parallel Mechanisms with Actuation Redundancy are considered in terms of velocity isotropy. We have introduced new tools to analyze and optimize such mechanisms. The first set of tools offers measures based on a classical point of view, a velocity ellipsoid, with an important feature: the sought ellipsoid is much closer to the real machine capability than the one usually considered. The second set of tools is based on velocity polytop: the ways to efficiently compute such a polytop and, more important, its extreme values have been described. It is expected that indexes based on both analysis can be usefully implemented in optimization processes for new redundant parallel mechanisms.

References

[1] T. Yoshikawa, "Manipulability of robotic mechanisms", in *Robotics Research: The second International Symposium,* eds. H. Hanafusa and H. Inoue, MIT Press, Cambridge (MA), USA, 1985

[2] T. Yoshikawa, "Dynamic manipulability of robot manipulators", in *Journal of Robotic Systems*, Vol. 2, No. 1, pp. 113-124, 1985.

[3] F. Marquet, S. Krut, O. Company, F. Pierrot, "Archi, a redundant mechanism for machining with unlimited rotation capacities", in *Proc. of ICAR*, Budapest, Aug. 2001.

[4] S.J. Ryu, J.W. Kim, J.C. Hwang, C. Park, H.S. ho, K. Lee, Y. Lee, U. Cornel, F.C. Park and J. Kim, "ECLIPSE: An Overactuated Parallel Mechanism for Rapid Machining", in *Proc. ASME Int. Mechanical Engineering Congress and Exposition*, USA, 1998, Vol. 8, pp. 681-689.

[5] V. C. Klema and A. J. Laub, "The singular value decompostion: its computation and some applications," in *IEEE Transactions and Automatic Control*, Vol. AC-25, No. 2, pp. 164-176, 1980.

[6] P. Chiacchio, Y. Bouffard-Vercelli and F. Pierrot, "Evaluation of Force Capabilities for Redundant Manipulators", in *Proc. of IEEE ICR&A*, Minneapolis (Minnesota), USA, April 1996.

[7] F. Pierrot and P. Chiacchio, "Evaluation of Velocity Capabilities for Redundant Parallel Robots", in *Proc. of IEEE ICR&A*, Albuquerque, New Mexico, April 1997.

[8] J. Kirchner and R. Neugebauer, "How to optimize parallel link mechanisms – proposal of new strategy", in *Proc. of IEEE ICR&A*, Albuquerque, New Mexico, April 1997.

[9] L. Stocco, S. E. Salcudean and F. Sassani, ,"Matrix Normalization for Optimal Robot Design", in *Proc. of IEEE ICR&A*, Leuven, Belgium, May 16-21, 1998.

[10] L. J. Stocco, S. E. Salcudean, F. Sassani, "Mechanism Design for Global Isotropy with Applications to Haptic Interfaces", in *Proc. of ASME Int. Mechanical Engineering Congress and Exhibition*, Vol. 61, pp. 115-122, 1997.

[11] S. E. Salcudean and L. Stocco, "Isotropy and Actuator Optimization in Haptic Interface Design", in Proc. of IEEE *ICR&A*, San Francisco, CA, USA, April 22-28, 2000.

[12] C. M. Gosselin and J. Angeles, "A global performance index for the kinematic optimization of robotic manipulators", in *ASME Journal of Mechanical Design*, Vol. 113, No. 3, pp. 220-226, 1991.

[13] J. Kirchner, R. Neugebauer, "How to Optimize Parallel Link Mechanisms - Proposal of a New Strategy", in Proc. of *2000-PKM-IC*, Ann Arbor (MI), USA, September 13-15, 2000.

[14] J. Lee, J. Duffy and K. H. Hunt, "The Optimum Quality Index for Some Spatial In-parallel Devices", in Proc. of *Florida Conference on Recent Advances in Robotics*, Miami (Florida), USA, April 10-11, 1997.

Proceedings of the WORKSHOP on
Fundamental Issues and Future Research Directions for Parallel Mechanisms and Manipulators
October 3–4, 2002, Quebec City, Quebec, Canada
Clément M. Gosselin and Imme Ebert-Uphoff, editors

Architecture Independent Workspace Analysis of Planar Three-Legged Manipulators

M.J.D. HAYES
Mechanical & Aerospace Engineering
Carleton University
1125 Colonel By Drive
Ottawa, ON, Canada, K1S 5B6
jhayes@mae.carleton.ca

Abstract: *A method for determining the reachable workspace of general planar three degree of freedom platforms with three legs of arbitrary architecture is presented, where only the active joints are in the presence of limits. A brief review of kinematic mapping is given. The kinematic image of the workspace consists of solid regions bounded by the intersection of minimum and maximum joint input constraint surfaces, a pair for each platform leg. The condition that the leg joining the moving platform to the fixed base be connected with three independent one degree of freedom lower pair joints is employed. Because the procedure uses position-level constraint surfaces in a kinematic image space, it additionally allows for the analysis of some platforms containing holonomic higher pairs.*

1 Introduction

Research interest in parallel manipulators has grown steadily over the last twenty-five years. This is partly due to their inherent advantages over serial manipulators where accuracy, stiffness, load-to-weight-ratio and operating speeds are concerned [1]. One major disadvantage of parallel manipulators in general, compared to serial ones, is that their reachable workspace is small and may contain a high density of interior singularities [2, 3]. Although the workspace analysis of planar three-legged manipulators is well established, see [4, 5, 6] for example, there exists no unified approach that is architecture independent. This gives the motivation for the work presented herein.

In this paper kinematic mapping is used to analyze the reachable workspace planar three-legged platforms of arbitrary architecture in the presence of joints limits on only the actuated joints. Such a *general planar three-legged platform* (GP3LP) consists of a moving platform connected to a fixed base by three kinematic chains. Each chain is connected by three independent one degree-of-freedom (DOF) joints, one of which is active, see [7, 8]. The method employed is based on that found in [6], wherein platforms consisting of three revolute-prismatic-revolute (RPR) legs, the actuated joint being the P-pair, are analyzed. This approach can be generalized to all possible GP3LP due to the results presented in [9] and [10]. It can also be adapted for analysis of a sub-class of platforms with actuated holonomic higher pairs [11].

For GP3LP with three DOF we consider the motions of the platform by examining the motions of each leg separately. The kinematic mapping transforms distinct planar displacements of a reference frame rigidly attached to the platform to distinct points in a three dimensional projective image space. When the joints are restricted to lower-pairs, *prismatic* (P) and *revolute* (R) pairs, then depending on the details of how the kinematic chain is arranged the image space point sets can be one of only two types: 1) if the constraint is linear (a point on the moving platform remains on a fixed line, or the inversion of a line on the platform moving on a fixed point) the corresponding image space point set is an hyperbolic paraboloid; 2) if the constraint is circular (a point on the moving platform remains on a fixed circle) the corresponding image space point set is an hyperboloid of one sheet [9]. Because these quadric surfaces contain the images of the constrained displacements, it is natural to call them *constraint surfaces*. Kinematic analysis of GP3LP reduces to intersection problems between the constraint surfaces for each leg.

Because of the illustrative description of all possible positions of the end-effector system as a surface-bound solid region in an image space, it is believed that this is a useful tool for designers. Moreover, it facilitates computations when the reachable workspace of more than one reference point in the end-effector system has to be determined.

2 Classifying General Planar Three-Legged Platforms

A GP3LP with three DOF consists of a moving platform connected to a fixed base by three simple kinematic chains. Each

chain is connected by three independent one DOF joints, one of which is active. Thus each chain provides the control of one of three DOF of the moving platform. Since the displacements of the platform are confined to the plane, only R- and P-pairs are used. But, in certain cases a holonomic higher gear pair (G) can replace a lower R-, or P-pair (one such platform is considered in Section 5.3. Platform motions are characterized by the motion of reference frame E, attached to the moving platform, relative to frame Σ, attached to the non-moving base, see Figure 1.

The possible combinations of R- and P-pairs which connect the moving platform to the fixed base and constrain the independent open kinematic chains, consisting of successions of three joints starting from the fixed base, in a GP3LP are [7]:

$$RRR,\ RPR,\ RRP,\ RPP,\ PRR,\ PPR,\ PRP,\ PPP.$$

We must, however, exclude the PPP chain because no combination of pure planar translations can cause a change in orientation. Thus, there are seven possible kinematic chains, which may be combined in either topologically symmetric or asymmetric groups of three. Figure 2 illustrates topologically symmetric platforms, each characterized by one of the seven allowable simple kinematic chains. For our working definitions of topological symmetry and asymmetry, see the last paragraph in Section 2.1.

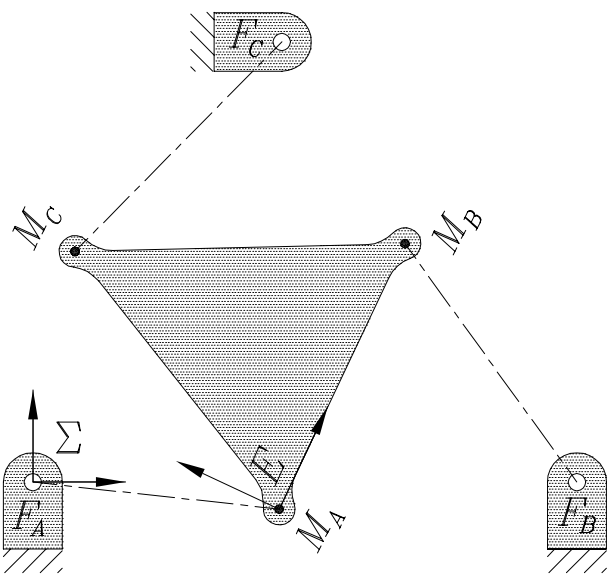

Figure 1: The moving frame E and fixed frame Σ for any combination of legs from Table 1.

2.1 Passive Sub-chains

The active joint in a leg is identified with an underscore, $R\underline{P}R$, for example. Since any one of the three joints in any of the seven allowable simple kinematic chains may be actuated there are twenty-one possible leg architectures.

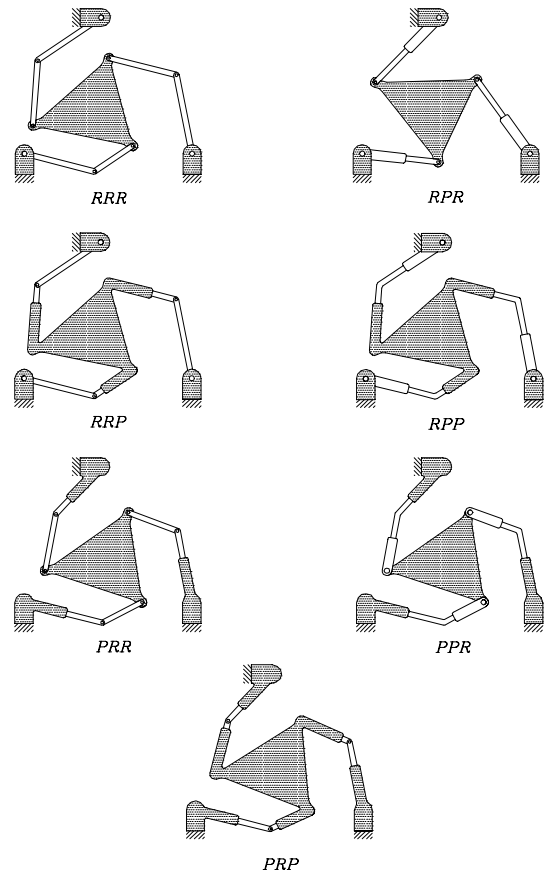

Figure 2: The seven possible leg topologies in *symmetric* platforms. When the legs are not all the same, the platform is *asymmetric*.

When the value of the activated joint coordinate in a leg is specified, the joint is effectively locked and may be temporarily removed from the chain. What remains is a kinematic chain connected with two passive joints. Examining Figure 2, it is to be seen that the resulting passive sub-chain is one of only four types: either RR, PR, RP, or PP. For now we exclude PP-type legs from the enumeration since platforms containing two or three such legs either move uncontrollably or are not assemblable when the actuated joint variables are specified [7, 12]. Nonetheless, platforms containing one PP-type leg are feasible. They are discussed in Section 4.4, but are not included in the enumeration because the expression of their constraints in a way that is compatible with the kinematic mapping remains an open, but likely straightforward, problem. This reduces the number of possible leg architectures to eighteen. They are listed, according to passive sub-chain, in Table 1.

The platform is considered to be *symmetric* when all three legs are the same type, each possessing the same type of actuated joint at the same location in the kinematic chain. The leg is otherwise considered to be *asymmetric*.

RR-type	PR-type	RP-type
$\underline{R}RR$	$\underline{R}PR$	$\underline{R}RP$
$R\underline{R}R$	$P\underline{R}R$	$R\underline{R}P$
$RR\underline{R}$	$PR\underline{R}$	$RP\underline{R}$
$\underline{P}RR$	$\underline{P}PR$	$\underline{P}RP$
$R\underline{P}R$	$P\underline{P}R$	$R\underline{P}P$
$RR\underline{P}$	$PR\underline{P}$	$RP\underline{P}$

Table 1: The 18 possible leg architectures.

2.2 Enumerating the GP3LP

How many distinct GP3LP with three DOF are there? This number is arrived at by considering that there are 18 possible kinematic chains to choose from for each leg. A selection of r different elements taken from a set of n, without regard to order, is a combination of the n elements taken r at a time. If the elements are allowed to be counted more than once the number of possible combinations is given by

$$\begin{aligned} C(n,r) &= \frac{(n+r-1)!}{r!(n-1)!} \\ \Rightarrow C(18,3) &= 1140. \end{aligned} \tag{1}$$

3 Planar Mapping

Consider the reference frame E which can undergo general planar displacements relative to reference frame Σ, as illustrated in Figure 1. Let the homogeneous coordinates of points in the moving frame E be the ratios $(x : y : z)$, and homogeneous coordinates of the same point, but expressed in the fixed frame Σ, be the ratios $(X : Y : Z)$. The homogeneous transformation that maps points in E to Σ can be written as

$$\begin{bmatrix} X \\ Y \\ Z \end{bmatrix} = \begin{bmatrix} \cos\varphi & -\sin\varphi & a \\ \sin\varphi & \cos\varphi & b \\ 0 & 0 & 1 \end{bmatrix} \begin{bmatrix} x \\ y \\ z \end{bmatrix}. \tag{2}$$

Equation (2) underscores the fact that a general planar displacement is characterized by the three parameters a, b, and φ, where a and b are the (X, Y) coordinates of the origin of E expressed in Σ and φ is the orientation of E relative to Σ, respectively.

The essential idea of the kinematic mapping, introduced simultaneously but independently by Blashke [13] and Grünwald [14] in 1911, is to map the three homogeneous coordinates of the pole of a planar displacement, in terms of (a, b, φ), to the points of a three dimensional projective image space. The kinematic mapping image coordinates are defined as:

$$\begin{aligned} X_1 &= a\sin(\varphi/2) - b\cos(\varphi/2) \\ X_2 &= a\cos(\varphi/2) + b\sin(\varphi/2) \\ X_3 &= 2\sin(\varphi/2) \\ X_4 &= 2\cos(\varphi/2). \end{aligned} \tag{3}$$

Since each distinct displacement described by (a, b, ϕ) has a corresponding unique image point, the inverse mapping can be obtained from Equation (3): for a given point of the image space, the displacement parameters are

$$\begin{aligned} \tan(\varphi/2) &= X_3/X_4, \\ a &= 2(X_1X_3 + X_2X_4)/(X_3^2 + X_4^2), \\ b &= 2(X_2X_3 - X_1X_4)/(X_3^2 + X_4^2). \end{aligned} \tag{4}$$

Equations (4) give correct results when either X_3 or X_4 is zero. Caution is in order, however, because the mapping is injective, not bijective: *there is at most one pre-image for each image point*. Thus, not every point in the image space represents a displacement. It is easy to see that any image point on the real line $X_3 = X_4 = 0$ has no pre-image and therefore does not correspond to a real displacement of EE. From Equation (4), this condition renders φ indeterminate and places a and b on the line at infinity.

By virtue of the relationships expressed in Equation (3), the transformation matrix from Equation (2) may be expressed in terms of the homogeneous coordinates of the image space. This yields a linear transformation to express a displacement of E with respect to Σ in terms of the image point [15]:

$$\begin{bmatrix} X \\ Y \\ Z \end{bmatrix} = \boldsymbol{T} \begin{bmatrix} x \\ y \\ z \end{bmatrix}, \tag{5}$$

where

$$\boldsymbol{T} = \begin{bmatrix} X_4^2 - X_3^2 & -2X_3X_4 & 2(X_1X_3 + X_2X_4) \\ 2X_3X_4 & X_4^2 - X_3^2 & 2(X_2X_3 - X_1X_4) \\ 0 & 0 & X_3^2 + X_4^2 \end{bmatrix}.$$

The inverse transformation can be obtained with the inverse of the matrix in Eq. (5) as follows.

$$\begin{bmatrix} x \\ y \\ z \end{bmatrix} = \boldsymbol{T}^{-1} \begin{bmatrix} X \\ Y \\ Z \end{bmatrix}, \tag{6}$$

with

$$\boldsymbol{T}^{-1} = \begin{bmatrix} X_4^2 - X_3^2 & 2X_3X_4 & 2(X_1X_3 - X_2X_4) \\ -2X_3X_4 & X_4^2 - X_3^2 & 2(X_2X_3 + X_1X_4) \\ 0 & 0 & X_3^2 + X_4^2 \end{bmatrix}.$$

Thus, the coordinates of a point $(x, : y : z)$ in the (relatively) moving frame has coordinates $(X, : Y : Z)$ in the (relatively) fixed frame:

$$
\begin{aligned}
X &= (X_4^2 - X_3^2)x - (2X_3X_4)y + 2(X_1X_3 + X_2X_4)z, \\
Y &= (2X_3X_4)x + (X_4^2 - X_3^2)y + 2(X_2X_3 - X_1X_4)z, \\
Z &= (X_3^2 + X_4^2)z. \qquad (7)
\end{aligned}
$$

While the inverse, coordinates of a point $(X, : Y : Z)$ in the (relatively) moving frame has coordinates $(x, : y : z)$ in the (relatively) fixed frame are given by:

$$
\begin{aligned}
x &= (X_4^2 - X_3^2)X + (2X_3X_4)Y + 2(X_1X_3 - X_2X_4)Z, \\
y &= -(2X_3X_4)X + (X_4^2 - X_3^2)Y + 2(X_2X_3 + X_1X_4)Z, \\
z &= (X_3^2 + X_4^2)Z. \qquad (8)
\end{aligned}
$$

4 Constraint Surfaces

The lower-pair constraints on the motion of any particular leg in an arbitrary GP3LP involve only one of the following.

1. A point with fixed coordinates in the moving frame moves on a fixed circle of fixed radius in the fixed frame (*RR*-type constraint).
2. A point with fixed coordinates in the moving frame moves on a fixed line in the fixed frame (*PR*-type constraint).
3. A line with fixed coordinates in the moving frame moves on a fixed point in the fixed frame (*RP*-type constraint).

The last two constraints are kinematically equivalent when considered inversions of each other. It may additionally be argued that the circular constraint is the most general, since a line can always be considered as a circle of infinite radius.

4.1 Implicit Equation of General Constraint Surface

A clearer picture of the image space constraint surface that corresponds to the kinematic constraints emerges when $(X : Y : Z)$, or $(x : y : z)$ from Equations (7), or (8) are substituted into the general equation of a circle, the form of the most general constraint:

$$
K_0(X^2 + Y^2) + 2K_1XZ + 2K_2YZ + K_3Z^2 = 0, \quad (9)
$$

where $[K_0 : K_1 : K_2 : K_3]$ are the *circle coordinates*, with $K_1 = -X_c$, $K_2 = -Y_c$, $K_3 = X_c^2 + Y_c^2 - r^2$, with X_c and Y_c being the coordinates of the circle centre of radius r, and K_0 is an arbitrary homogenising constant. One obtains the following implicit equation of a constraint surface in the image space:

$$
\begin{aligned}
&K_0z^2(X_1^2 + X_2^2) + (-K_0x + K_1z)zX_1X_3 \\
&+(-K_0y + K_2z)zX_2X_3 \mp (K_0y + K_2z)zX_1X_4 \\
&\pm(K_0x + K_1z)zX_2X_4 \mp (K_1y - K_2x)zX_3X_4 \\
&+\frac{1}{4}[K_0(x^2 + y^2) - 2z(K_1x + K_2y) + K_3z^2]X_3^2 \\
&+\frac{1}{4}[K_0(x^2 + y^2) + 2z(K_1x + K_2y) + K_3z^2]X_4^2 = 0. \qquad (10)
\end{aligned}
$$

If the kinematic constraint is a fixed point in E bound to a circle ($K_0 = 1$), or line ($K_0 = 0$) in Σ, then $(x : y : z)$ are the coordinates of the platform reference point in E and the upper signs apply. On the other hand, if the kinematic constraint is a fixed point in Σ bound to a circle ($K_0 = 1$), or line ($K_0 = 0$) in E, then $(X : Y : Z)$ are substituted for $(x : y : z)$, and the lower signs apply.

The K_i are functions of the variable joint input parameter. The constraint surfaces defined by the joint input are not arranged arbitrarily in the image space. It turns out that the image of the workspace for a particular leg is bounded by the two constraint surfaces corresponding to the minimum and maximum variable joint input parameters. Moreover, it can be shown that the hyperboloid of one sheet and the hyperbolic paraboloid are the only possible constraint surfaces for such planar three-legged platforms [9].

4.2 Circle Constraints

When one sets $K_0 = 1$, together with $X_4 = z = 1$ in Eq. (10) the result is the implicit equation of a hyperboloid of one sheet in terms of the image space coordinates (X_1, X_2, X_3)[9, 10]:

$$
\begin{aligned}
&(X_1^2 + X_2^2) + (K_1 - x)X_1X_3 + (K_2 - y)X_2X_3 \\
&\mp(K_2 + y)X_1 \pm (K_1 + x)X_2 \pm (K_2x - K_1y)X_3 \\
&+\frac{1}{4}[(x^2 + y^2) - 2(K_1x + K_2y) + K_3]X_3^2 \\
&+\frac{1}{4}[(x^2 + y^2) + 2(K_1x + K_2y) + K_3] = 0. \qquad (11)
\end{aligned}
$$

This hyperboloid has the property that planes parallel to $X_3 = 0$ intersect it in circles, though its axis is not necessarily perpendicular to $X_3 = 0$. For planar three-legged platforms, the inversion of a fixed circle in the moving frame moving on a fixed point in the fixed frame never arises.

All points on this constraint hyperboloid represent displacements of the platform for the given input in the given leg when the remaining two legs have been disconnected from the platform. It can be easily parameterized [9], an example illustrated in Figure 3 shows the minimum and maximum constraint hyperboloids for the three legs of a symmetric $R\underline{P}R$ platform, similar to the one shown in Figure 9.

4.3 Line Constraints

If $K_0 = 0$ in Eq. (9) we obtain a line, which is a real degenerate circle, with *line coordinates* determined by the relation $[L_1 : L_2 : L_3] = [2K_1 : 2K_2 : K_3]$. Setting $K_0 = 0$, together with $X_4 = z = 1$ in Eq. (10) one obtains the implicit equation of a hyperbolic paraboloid in the image space [9, 10]:

$$
\begin{aligned}
&K_1X_1X_3 + K_2X_2X_3 \mp K_2X_1 \pm K_1X_2 \pm (K_2x - K_1y)X_3 \\
&-\frac{1}{4}[2K_1x + 2K_2y - K_3]X_3^2 + \frac{1}{4}[2K_1x + 2K_2y + K_3] = 0. \qquad (12)
\end{aligned}
$$

The kinematic inversion between PR- and RP-type legs, unlike the RR case, is a concern here. Equation (12) is used to

represent both. For PR-type legs a point with fixed coordinates in the moving frame moves on a fixed line in the fixed frame. In this case the corresponding constraint equation is given by Equation (12) the upper signs are used. However, for RP-type legs, where the constraint is a line with fixed coordinates in the moving frame moving on a fixed point in the fixed frame, the lower signs are used and x, y, or z is substituted whenever X, Y, or Z are encountered. A parameterized example is illustrated in Figure 5, showing the minimum and maximum constraint hyperbolic paraboloids for the three legs of a symmetric $P\underline{P}R$, similar to the one shown in Figure 4.

4.4 PP-Type Legs

The image space constraint surface corresponding to possible displacements of a PP-type leg is a degenerate quadric that splits into a real and an imaginary plane. This is because only curvilinear motion of the platform can result when the other two platform attachment joints are disconnected: once the angular input of the active R-pair is fixed no rotation of leg or platform is possible. Still, the image of a two parameter family of displacements must be a two parameter constraint manifold, but because φ is constant, the image space coordinates $X_3 = f(\varphi)$ and $X_4 = g(\varphi)$ must also be constant. Hence, the finite part of the two dimensional constraint manifold is linear and must be a hyper-plane.

Moreover, all planes corresponding to possible displacements of the PP-type leg are parallel to $X_3 = 0$. If the platform consists of two, or three PP-type legs, the constraint planes may be distinct, but parallel thereby having no finite points in common; or the planes will be coincident, indicating infinite assembly modes yielding uncontrollable self motions.

There is no practical design merit associated with platforms containing two, or three PP-type legs. This, however, does not preclude designs of topologically asymmetrical three legged planar platforms with at most one PP-type leg. On the other hand, the self-motion property provides possibilities to design very stiff one DOF planar platforms which are relatively easy to actuate.

5 Examples

5.1 Workspace of *R$\underline{P}$R*-Symmetric Platforms

The first use of kinematic mapping for workspace analysis of planar three-legged platforms was in [6]. However, the particular approach is suitable only for $R\underline{P}R$-symmetric platforms, similar to that found in Figure 9.

The first step is to parameterize Equation (11). One possibility is [9]

$$\begin{bmatrix} X_1 \\ X_2 \\ X_3 \end{bmatrix} = \frac{1}{2} \begin{bmatrix} [(\mathcal{K}_1 + x)t - \mathcal{K}_2 + y] + (r_i\sqrt{t^2+1})\cos\zeta \\ [(\mathcal{K}_2 + y)t + \mathcal{K}_1 - x] + (r_i\sqrt{t^2+1})\sin\zeta \\ 2t \end{bmatrix},$$

$$\begin{aligned} &\zeta \in \{0, \ldots, 2\pi\}, \\ &t \in \{-\infty, \ldots, \infty\}, \\ &i_{min} \le i \le i_{max}, \end{aligned} \tag{13}$$

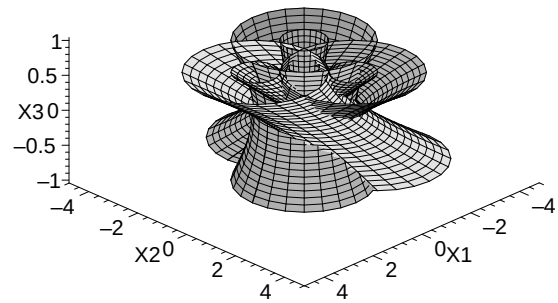

Figure 3: Workspace image of an $R\underline{P}R$-symmetric platform.

where K_1 and K_2 are two circle coordinates, as defined previously, x and y are the coordinates of the platform attachment point expressed in E, r_i is the length of the prismatic joint in the ith leg, t is the tangent of half the orientation angle of the platform, $\tan\varphi/2$, and ζ is an angular parameter arising from the derivation of the parametric equation.

For each leg in the $R\underline{P}R$ platform, the active P-pair has a minimum and a maximum extention. Examining Equation (13) one immediately sees this corresponds to a minimum and a maximum pair of coaxial hyperboloids.

The minimum and maximum constraint hyperboloids for each $R\underline{P}R$ leg must be determined. The image of the reachable workspace of a specific platform reference point is the solid bounded by the six hyperboloids. To obtain the image of the workspace we consider all positions of the reference point for fixed platform orientations for each leg. This involves intersecting the three surface bound solids with the planes X_3 = constant. The corresponding curves are three pairs of concentric circles. The area common to the six circles, if any, is the image of the reachable workspace of the reference point for the specific orientation.

It is a simple matter to determine the pre-image, giving the Cartesian workspace for the reference point. This is done by selecting a reference point, $(x : y : 1)$, then substituting the expressions for the three sets of hyperboloid circles into Equation (7). Again, the area common the the six pre-image curves, if any, is the Cartesian reachable workspace of the reference point for the given platform orientation. The entire Cartesian reachable workspace is the union of all orientation layers. An example of the workspace image is illustrated in Figure 3, while a detailed example is given in [6].

It is easy to see computing the image for another reference point is not difficult. Note, the platform reference point is completely arbitrary: the pre-image depends on the choice for the platform reference point. Examples for the $RR\underline{G}$ and the $P\underline{P}R$ symmetric platforms follow in the next sections.

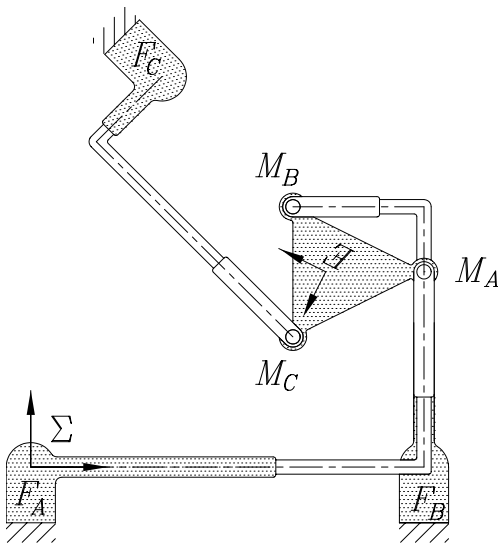

Figure 4: A $P\underline{P}R$-symmetric platform.

5.2 *P<u>P</u>R*-Symmetric Platforms

For each leg in the $P\underline{P}R$ platform the active P-pair has a minimum and a maximum extension. The only variable quantities are the length of the P-pair, and the platform reference point coordinates, $(x : y : z)$; all other quantities are design constants. Hence, for a selected platform reference point there is a minimum and a maximum hyperbolic paraboloid constraint surface corresponding to the minimum and maximum length of the P-pair. It turns out that every pair of hyperbolic paraboloids in a given family have the same curve of intersection because terms dependent on the length of the P-pair can be factored out. This can be seen when the intersection curve is projected into the planes $X_1 = 0$, $X_2 = 0$, $X_3 = 0$ and $X_4 = 0$. Therefore, the whole set of hyperbolic paraboloids in a family forms a pencil of quadrics. The solid bounded by the minimum and maximum hyperbolic paraboloid in each leg is the kinematic image of the platform workspace when the other two legs are disconnected.

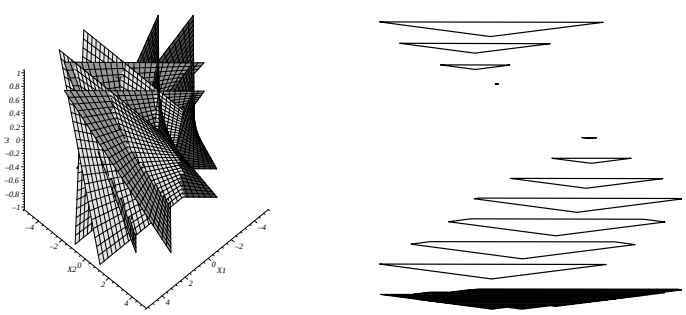

Figure 5: Workspace image; 3D view of workspace layers of a $P\underline{P}R$-symmetric platform.

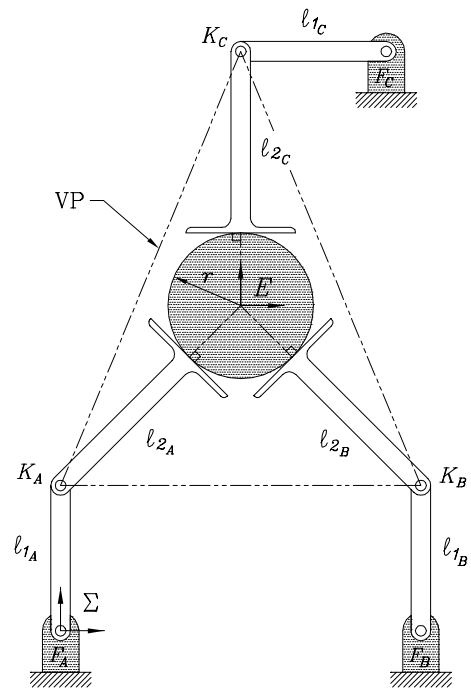

Figure 6: An $RR\underline{G}$-symmetric platform.

The left-hand side of Figure 5 shows the minimum and a maximum hyperbolic paraboloid constraint surfaces corresponding to the minimum and maximum length of the active P-pair in each of the symmetric $P\underline{P}R$ platform legs. Exploiting some geometric properties of the constraint manifold, we can derive the following parametric form [9]:

$$\begin{bmatrix} X_1 \\ X_2 \\ X_3 \end{bmatrix} = \begin{bmatrix} f(t)+s \\ g(t,s) \\ t \end{bmatrix}, \quad \begin{array}{l} -\infty \le t \le \infty, \\ -\infty \le s \le \infty, \end{array} \tag{14}$$

where t and s are linear parameters and

$$f(t) = \frac{(K_3+2K_1x+2K_2y)t^2+(K_1y-K_2x)4t-2(K_1x+K_2y)+K_3}{4(K_1t-K_2)},$$
$$g(t,s) = \frac{(K_2-K_1t)s}{K_1+K_2t}.$$

The right-hand side of Figure 5 shows different layers of the reachable Cartesian reachable workspace. There are 13 layers, each representing a $30°$ increment in φ. The top layer represents a platform orientation of $180°$, the second from the bottom is that of $-180°$, while the shaded bottom layer is the union of all the layers. The platform has orientation singularities between approximately $10°$ and $70°$, hence the layers representing $30°$ and $60°$ are empty.

5.3 *RR<u>G</u>*-Symmetric Platforms

Perhaps the most interesting, from a geometric perspective, is a three-legged platform possessing an active higher-pair as the

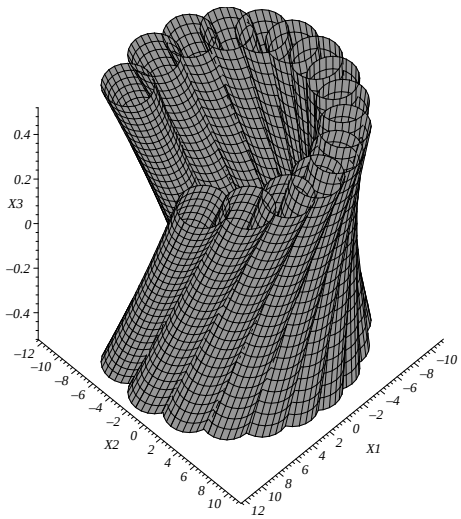

Figure 7: Workspace image of one leg of an $RR\underline{G}$-symmetric platform.

third joint in each kinematic chain. For this type of platform it can be shown, see [16, 11], that the workspace image for each leg consists of the solid bounded by an envelope of hyperboloids of one sheet possessing identical shape parameters, but unique axis. For every value of the higher pair input there corresponds an hyperboloid axis, all belonging to a ruled surface. The solid bounded by the envelope of these hyperboloids is the image of the workspace for that leg when the other two have been disconnected from the pinion. The image of the workspace of the entire platform is the solid region bounded by the intersection of these three envelopes. For the example found in [11], the reachable workspace image of one leg is shown in Figure 7.

The left-hand side of Figure 8 shows different layers of the reachable Cartesian workspace for the reference point taken to be the centre of the pinion. There are 13 layers, each representing a $30°$ increment in the orientation of the pinion. In right-hand side of Figure 8, the different layers are given different elevations according to the pinion orientation. The top layer is the reachable workspace for a pinion orientation of $180°$ while the second layer from the bottom is that of $-180°$ orientation. The bottom is the union of all the layers.

The dextrous workspace of a manipulator is usually defined as the set of all points within the reachable workspace that the end-effector can reach with any orientation. Examining the left-hand side of Figure 8, the boundary of the dextrous workspace is seen to be the shaded region that is common to all layers. An area computation reveals that the dextrous workspace comprises 31.71% of the reachable workspace. Moreover, the reachable and dextrous workspace contain no holes; a remarkable result when compared with lower pair jointed three-legged platforms, see [2, 17], or [6], for example.

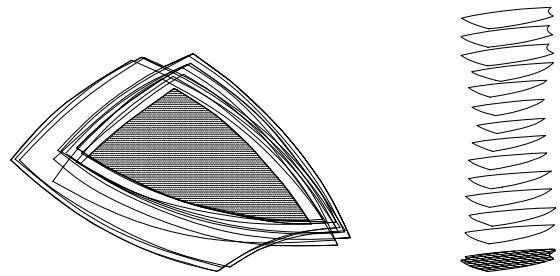

Figure 8: Overlay of workspace layers; 3D view of workspace layers.

5.4 RPR Platform: Different Active Joint in Each Leg

The general case of a three-legged platform can be demonstrated using a platform possessing three RPR legs where the active joint is different in each of the three legs: leg A is RR-type, leg B is PR-type, leg C is RP-type. This platform is illustrated in Figure 9.

5.4.1 FK Example

Here we use the general FK procedure [10] to solve the FK problem of a platform with one each of $\underline{R}PR$, $R\underline{P}R$, and $RP\underline{R}$ legs, shown in Figure 9. The relevant kinematic mapping parameters, listed in Table 2, are the fixed base points $(X : Y : Z)$ expressed in Σ, the relatively moving platform points $(x : y : z)$ expressed in E, the variable joint inputs (the subscripts on β and γ indicate the frame in which the angle is measured counter-clock-wise relative to the X or x axis, respectively), and the corresponding circle coordinates for the platform illustrated in Figure 9.

i	$(X : Y : Z)$	$(x : y : z)$	Input
A	$(0 : 0 : 1)$	$(0 : 0 : 1)$	$d = 2.5$
B	$(6 : 0 : 1)$	$(2 : 0 : 1)$	$\beta_\Sigma = 135°$
C	$(3 : 6 : 1)$	$(1 : 2 : 1)$	$\gamma_E = 45°$

i	$(K_0 : K_1 : K_2 : K_3)$
A	$(1 : 0 : 0 : -4)$
B	$(0 : -\sqrt{2}/4 : -\sqrt{2}/4 : 3\sqrt{2})$
C	$(0 : -\sqrt{2}/4 : -\sqrt{2}/4 : -\sqrt{2}/2)$

Table 2: Kinematic mapping parameters.

The corresponding three constraint surfaces are a hyperboloid of one sheet for the $\underline{R}PR$ leg A, a hyperbolic paraboloid for the $R\underline{P}R$ leg B, and an inversion hyperbolic paraboloid for the $RP\underline{R}$ leg C. The univariate in X_3 (see Eq. 15) is computed together with corresponding values of X_1 and X_2 for the real roots of the univariate, which in this case is 5th order:

$$45X_3^5 - 77X_3^4 + 56X_3^3 + 120X_3^2 - 53X_3 + 5. \qquad (15)$$

The solutions must be carefully inspected. There are three real and one pair of complex conjugate roots. One root, $X_3 =$

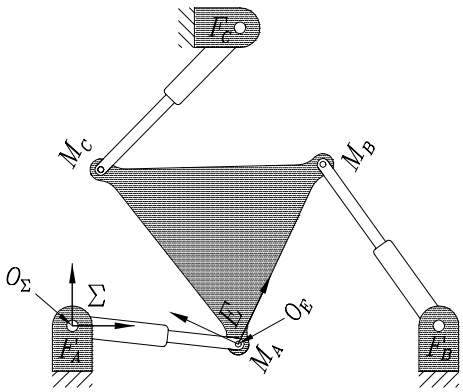

Figure 9: A platform with one each of *$\underline{R}$PR, R$\underline{P}$R, and RP$\underline{R}$* legs.

-1, represents a line that is a common generator between the two hyperbolic paraboloids, but that does not intersect the hyperboloid in any finite points.

The two real roots that lead to solutions are listed in Table 3. The kinematic mapping image of the two solutions can be seen as the two points common to the three surfaces in Figure 10, while the corresponding configurations are illustrated in Figure 11. Note that the common line bewteen the two hyperbolic paraboloids is visible in the same figure.

Solution	a	b	φ (deg)
1	2.2993	0.9814	29.0303
2	1.5837	1.9344	16.3404

Table 3: The two real Cartesian solutions.

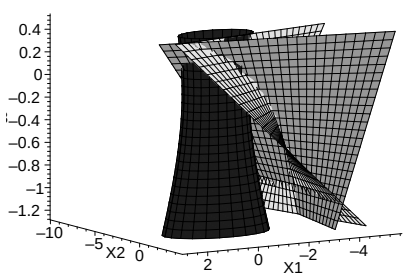

Figure 10: The image of the two real FK solutions.

5.4.2 Workspace

The strategy for determining the kinematic image of the reachable workspace for arbitrary mixed-leg platforms is an extension of the approach to solving the FK. For each leg we determine the constraint surfaces corresponding to the minimum and maximum variable joint inputs. For RR-type legs, the constraint surfaces are hyperboloids of one sheet all sharing the same axis. For RP- and PR-type legs the constraint surfaces are hyperbolic paraboloids, however, the relationship between the minimum and maximum surfaces depends on the type of active joint in the kinematic chain.

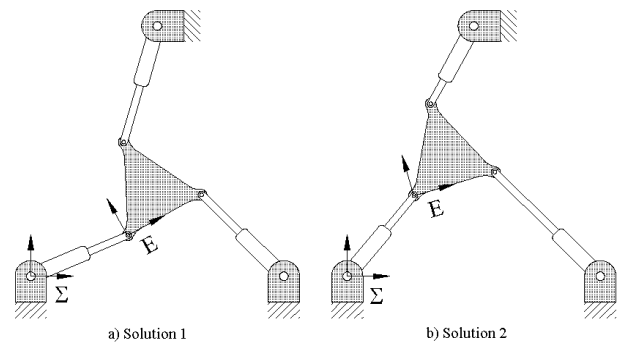

Figure 11: The two real FK solutions.

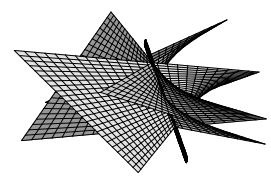

Figure 12: Three hyperbolic paraboloid for three input angles in an *$\underline{R}$PR* leg, and *axis*.

When the active joint is an R-pair, pairs of hyperbolic paraboloids in a family still intersect in the same type of degenerate quadratic: a real and imaginary line pair. Figure 12 illustrates three hyperbolic paraboloid constraint surfaces for an $\underline{R}PR$ leg for three distinct input angles. They all share the line shown in the figure, in a sense the *axis* of the family of hyperbolic paraboloids. The working conjecture is that the the real image space line is finite. Figure 13 shows the hyperboloid family for leg A and the lines of intersection of the hyperbolic paraboloid families belonging to legs B and C.

Summarizing the discussion in Section 5.2, if the active joint is a P-pair, its reach is limited by its minimum and maximum extention. Hence, for a selected platform reference point there is a minimum and a maximum hyperbolic paraboloid constraint surface corresponding to the minimum and maximum length of

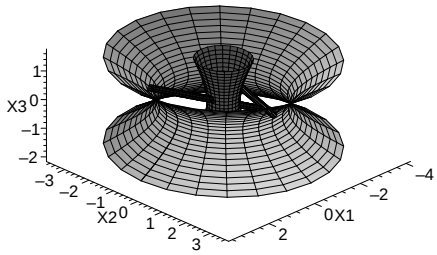

Figure 13: The concentric hyperboloids for leg A and hyperbolic paraboloid axes for legs B and C.

the active P-pair. Every pair of hyperbolic paraboloids in a given family have the same curve of intersection, which degenerates to a real and imaginary line pair. Therefore, the whole set of hyperbolic paraboloids in a family forms a pencil of quadrics. The current working conjecture is that the real line is on the plane at infinity, thus no two hyperbolic paraboloids in one family have finite image points in common, recall the left-hand side of Figure 5. The solid bounded by the minimum and maximum hyperbolic paraboloid in each leg is the kinematic image of the platform workspace when the other two legs are disconnected.

The Cartesian reachable workspace, not shown here, is the pre-image obtained by substituting X_1, X_2, X_3 from either parametric Equations (13), or (14) into either Equations (5), or (6), depending upon the nature of the constraint. The general rules are as follows:

1. RR-type: substitute X_1, X_2, X_3 from Equation (13) into Equation (5).

2. PR-type: substitute X_1, X_2, X_3 from Equation (14) into Equation (5).

3. RP-type: substitute X_1, X_2, X_3 from Equation (14) into Equation (6), being careful to define the coefficients as described in the discussionin Section 4.

6 Conclusions and Future Work

A unified method for determining the reachable workspace of GP3LP, including a sub-class of three-legged platforms with actuated holonomic higher pairs, has been presented. The current state of the determination allows for only the joint limits on the active pairs. In order to be a truly useful tool for designers the passive joint limits must be included in the constraint equations. We are now working with some formulations that could provide this crucial missing component. PP-type leg constraints must also be formulated so as to complete the generalization.

References

[1] J-P. Merlet. Parallel Manipulators: State of the Art and Perspectives. http://www-sop.inria.fr/saga/personnel/merlet/merlet.html, Inst. Nat. de Rech. en Inf. et en Auto, France, 1999.

[2] J. Sefrioui and C.M. Gosselin. "Singularity Analysis and Representation of Planar Parallel Manipulators". *Robotics and Autonomous Systems*, vol. 10: pages 209–224, 1992.

[3] C.L. Collins and J.M. McCarthy. "The Quartic Singularity Surface of Planar Platforms in the Clifford Algebra of the Projective Plane". *Mech. Mach. Theory*, vol. 33, no. 7: pages 931–944, 1998.

[4] C. Gosselin. *Kinematic Analysis, Optimization and Programming of Parallel Robotic Manipulators*. PhD thesis, Dept. of Mech. Eng., McGill University, Montréal, Qc., Canada, 1988.

[5] J-P. Merlet. *Les Robots Parallèles*. Hermès Publishers, Paris, France, 1990.

[6] M.L. Husty. "On the Workspace of Planar Three-legged Platforms". *Proc. World Automation Conf., 6th Int. Symposium on Rob. and Manuf.* (ISRAM 1996), Montpellier, France, vol. 3: pages 339–344, 1996.

[7] J-P. Merlet. "Direct Kinematics of Planar Parallel Manipulators". *IEEE Int. Conf. on Robotics and Automation*, Minneapolis, U.S.A., pages 3744–3749, 1996.

[8] M.J.D. Hayes, M.L. Husty, and P.J. Zsombor-Murray. "Kinematic Mapping of Planar Stewart-Gough Platforms". *Proc. 17th Canadian Congress of Applied Mechanics (CANCAM 1999)*, Hamilton, On., Canada, pages 319–320, 1999.

[9] M.J.D. Hayes and M.L. Husty. "On the Kinematic Constraint Surfaces of General Three-Legged Planar Robot Platforms". Accepted for publication April 2002 in *Mechanism and Machine Theory*, 2002.

[10] P.J. Zsombor-Murrary, C. Chen, and M.J.D. Hayes. "Direct Kinematic Mapping for General Planar Parallel Manipulators". *Proc. CSME Forum 2002*, Kingston, On., Canada, May 21-24, 2002.

[11] M.J.D. Hayes and M.L. Husty. "Workspace Characterization of Planar Three-legged Platforms With Holonomic Higher Pairs". *Advances in Robotic Kinematics*, eds. Lenarčič, J., Stanišić, Kluwer Academic Publishers, Dordrecht, The Netherlands, pages 267–276, 2000.

[12] M.J.D. Hayes. *Kinematics of General Planar Stewart-Gough Platforms*. PhD thesis, Dept. of Mech. Eng., McGill University, Montréal, Qc., Canada, 1999.

[13] W. Blaschke. “Euklidische Kinematik und Nichteuklidische Geometrie”. *Zeitschr. Math. Phys.*, vol. 60: pages 61–91 and 203–204, 1911.

[14] J. Grünwald. “Ein Abbildungsprinzip, welches die ebene Geometrie und Kinematik mit der räumlichen Geometrie verknüpft”. *Sitzber. Ak. Wiss. Wien*, vol. 120: pages 677–741, 1911.

[15] O. Bottema and B. Roth. *Theoretical Kinematics*. Dover Publications, Inc., New York, N.Y., U.S.A., 1990.

[16] M.J.D. Hayes, M.L. Husty, and P.J. Zsombor-Murray. “Solving the Forward Kinematics of a Planar 3-legged Platform With Holonomic Higher Pairs”. *ASME, Journal of Mechanical Design*, vol. 121, no. 2: pages 212–219, 1999.

[17] J. Sefrioui and C.M. Gosselin. “On the Quadric Nature of the Singularity Curves of Planar Three-Degree-of-Freedom Parallel Manipulators”. *Mech. Mach. Theory*, vol. 30, no. 4: pages 533–551, 1995.

[18] M.J.D. Hayes, M.L. Husty, and P.J. Zsombor-Murray. “Towards Workspace Analysis of Platforms with Three Arbitrary Legs”. *Proc. 18th Canadian Congress of Applied Mechanics (CANCAM)*, St. John’s NF. Canada, pages 355–356, 2001.

Keynote Address II

Thursday, October 3, 2002, Noon (throughout lunch)

Torgny Brogårdh

ABB Robotics, Sweden

"PKM Research – Important Issues as seen from a Product Development Perspective at ABB Robotics"

Proceedings of the WORKSHOP on
Fundamental Issues and Future Research Directions for Parallel Mechanisms and Manipulators
October 3–4, 2002, Quebec City, Quebec, Canada
Clément M. Gosselin and Imme Ebert-Uphoff, editors

PKM Research - Important Issues, as seen from a Product Development Perspective at ABB Robotics

TORGNY BROGÅRDH
ABB Automation Technology Products / Robotics
SE 721 68 Västerås
Sweden

Abstract: *This paper will address some of the most important PKM research issues as seen from a robot manufacturer's point of view. In section 2 the importance of linking research activities to the application requirements is discussed and in section 3, which is the most important part of this paper, the urgent need for a systematic topology synthesis is put forward. The rest of the paper is structured according to a proposed development process for industrial parallel kinematic robots. Thus, the optimization of the mechanical design with respect to kinematics and dynamics is discussed in section 4. In section 5 some problems related to the selection of components for parallel kinematic robots are put forward and in section 6 the importance of drive and control system performance is discussed. Finally, the most important research topics as seen from an industrial point of view are discussed in section 7.*

1 Introduction

In spite of the high performance potential of manipulator structures based on parallel kinematics, this technology has not yet made a dramtatic impact on industrial automation. However, there is an interesting trend towards the use of general purpose industrial robots for applications with higher demands on accuracy, stiffness, eigenfrequency, cycle time etc. Thus, significant efforts are now being made to use industrial robots for such applications as measurements, laser cutting, laser welding, high precision assembly, grinding, deburring, milling etc. Because of the inefficient robot performance for these applications, several compensation methods are used, which add cost and make installation, programming, maintenance etc. difficult. Moreover, in most cases the industrial robots of today will never reach the application requirements for these high performance applications. One way to solve these problems could be to make use of robots based on parallel kinematics, but it is not easy to challenge the mature industrial robot technology, even if some successful structures find increasing market shares already now. However, parallel kinematic structures provide such high performance potential that it is important for the research community to come up with concepts and technologies which will make parallel kinematic robots a natural choice when designing flexible automation systems.

2 Analysis of application requirements on parallel kinematic robot structures

One example of a successful parallel kinematic structure as seen from an industrial point of view is the Delta structure. The reason for this success is that the features of this structure fit into applications requiring very fast handling of light weight products, for example in the consumer goods, food and electronics industries. Thus, to be able to succeed with the transfer of results from PKM research to industrial product development, it is very important to understand the application requirements. Morever, it is important to understand what PKM features provide advantages in potential applications. For example, parallel kinematic robot structures may give higher speed and acceleration, higher static and dynamic accuracy and higher stiffness than what is possible with the industrial robots used today. Starting with these competitive features, potential applications and end users can be evaluated, beginning with a first simple overview as exemplified by the diagram in Figure 1.

For each application and for each type of installation in the manufacturing plants of the end users, a detailed study is needed to find out if the parallel kinematic robot will satisfy all requirements. The first topic in such a study is to match the kinematics of the parallel robot with the customer requirements. This means that simulations must be made to make sure that the number of degrees of freedom, the working range, the accessibility and the motion type of the parallel kinematic structure fulfil the requirements. For example, in pick and place applications on a flat surface, where only 3 or 4 degrees of freedom are needed, the working range and the accessibility are

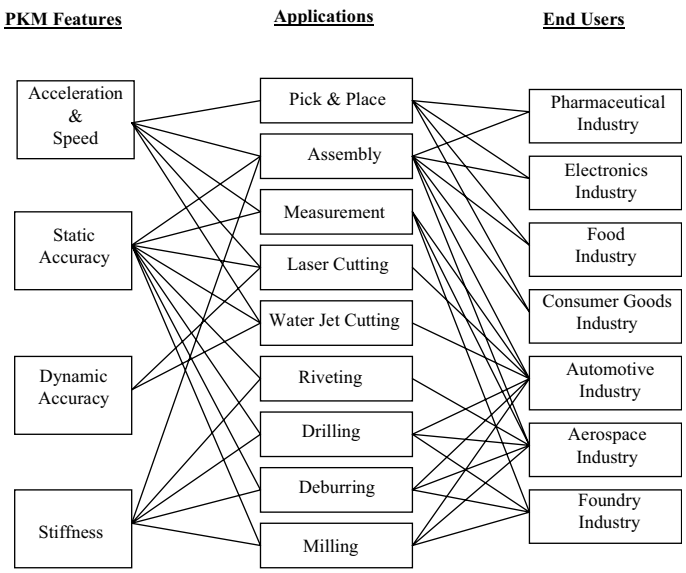

Figure 1: Diagram exemplifying the relations between potential performance features of a parallel kinematic robot and the applications and industries needing this performance for improved flexible automation.

usually not critical and the kinematics of the Delta structure can do the job. In the same way, there are applications of laser cutting and water jet cutting 2D objects out of metal sheets for which the Delta kinematics might be useful. However, in these applications large rectangular horizontal working areas are usually needed (typically 1.5 x 3 meters), which could make a Gantry type of parallel manipulator more competitive. For other applications, such as assembly of components for automotive transmission lines, a cylindrical workspace may match the tasks better and for these applications a 6 DOF robot is usually needed. In Figure 2 some examples are given of kinematic requirements from the applications in figure 1 concerning motion type and the number of degrees of freedom.

3 Synthesis of PKM Structures for Robot Applications

This is the most important section of this paper (from the author's point of view) since new PKM structures must be synthesized to obtain a broader use of parallel robots in industry. Systematic topology methods may be needed and the purpose of this section is to show that there still exist unused parallel structures with high industrial potential.

When searching for a new PKM structure or when analyzing an already discovered PKM structure, the motion type and the number of DOF needed for the applications under investigation are basic kinematic features that must be determined (Figure 2). It is then a good strategy to start looking at the motion type since the motion type will give useful constraints on the actuating structure, reducing the number of possible PKM topologies.

3.1 Synthesis of Actuating Structures for Positioning

To be able to synthesize parallel kinematic structures for positioning with Scara, Gantry and antropomorphic motion patterns according to the application demands in Figure 2, one way is to start with parallel actuating structures giving rotation symmetric (for Scara and antropomorphic robots) and Cartesian (Gantry robots) motion patterns. How this can be made in the 3 DOF case (for positioning) is shown in Figure 3. For the parallel actuation in the rotation case, 3 arms are actuated independent of each other around a central column. The actuators, which are mounted on the central column, drive the actuating arms, mounted on horizontal bearings. For the parallel actuation in the Cartesian case, 3 actuating platforms are independently driven along 3 linear tracks.

3.2 Synthesis of Actuating Structures for Orientation Control

As can be seen in Figure 2, usually more than 3 DOF are needed. To achieve a 4th DOF with full rotation capability, a parallel independent transmission link in addition to the positioning links is used in the Delta robot case [1]. This link must transmit torque and does not have the same performance as the rest of the Delta structure and can be looked upon as a transmission link for rotation. In the H4 robot structure [2] the same link structure is used for the 4th DOF, but a gear transmission is used on the platform to convert and amplify a linear motion to a rotational motion. This solution does not give infinite rotation capability and the torque amplification in the gear will reduce the orientation performance in comparison with the positioning performance. The most promising way to obtain a 4th DOF seems to use a redundant actuation [3]. However, the need of an extra actuator and a redundant link will increase cost and manipulator volume. Thus, it seems very difficult to find parallel structures giving full orientation performance as for the serial robots used in industry today. It will then be even more difficult to find PKM structures with 5 or 6 DOF with the same orientation capability as for serial robots. Of course, there might still be 4 DOF - 6 DOF parallel structures not discovered and searching for such structures and also developing systematic search methods would be very interesting. However, with the present experience of the orientation capability of known PKM structures, it seems in the general case necessary to separate the rotation generating structure from the positioning structure and connect these structures in series. Such a configuration makes modularization easier since a basic positioning PKM can then be combined with different wrists for different applications. These wrists may then be either serial or parallel [11] and in the parallel case new structures with improved orientation performance are needed.

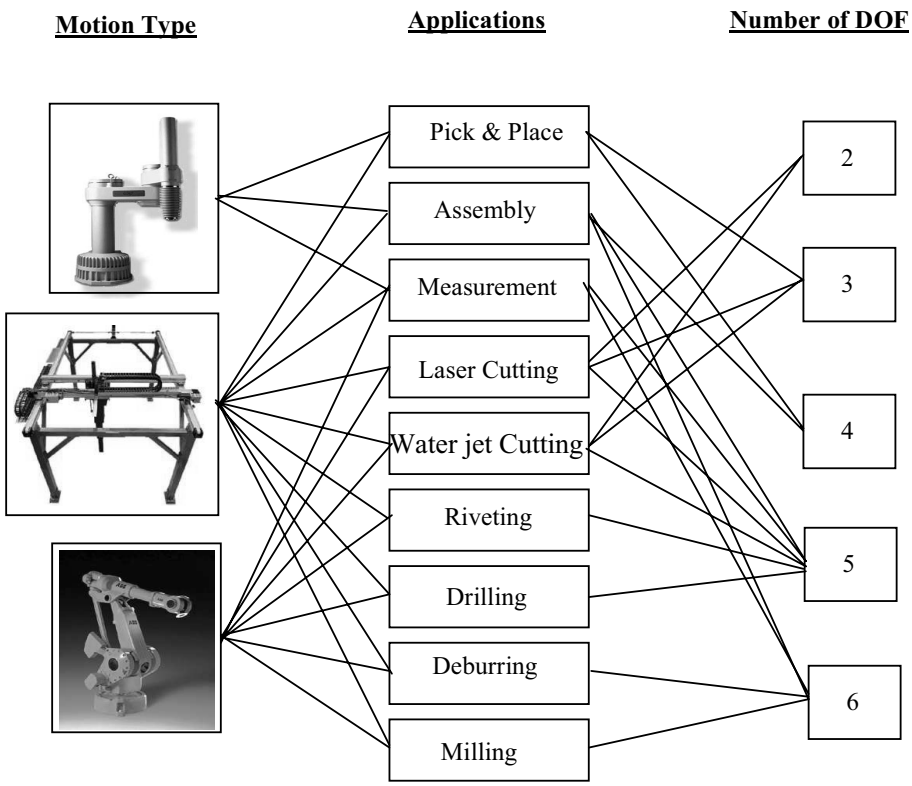

Figure 2: Requirements on motion types and number of degrees of freedom for the applications in Figure 1.

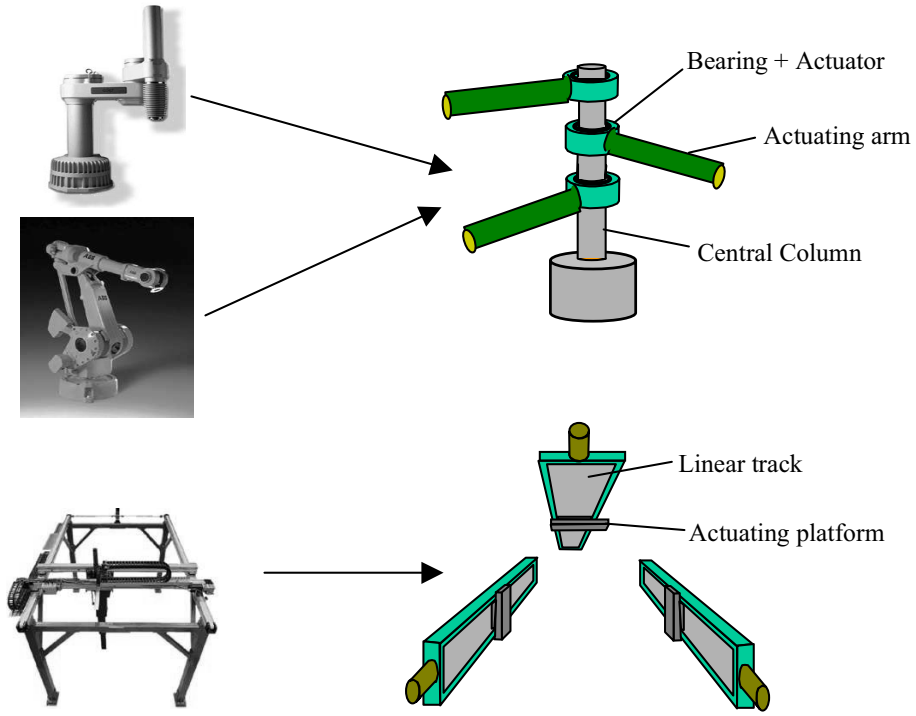

Figure 3: Examples of parallel actuating arrangements to obtain positioning PKM motion patterns similar to the serial manipulators used today.

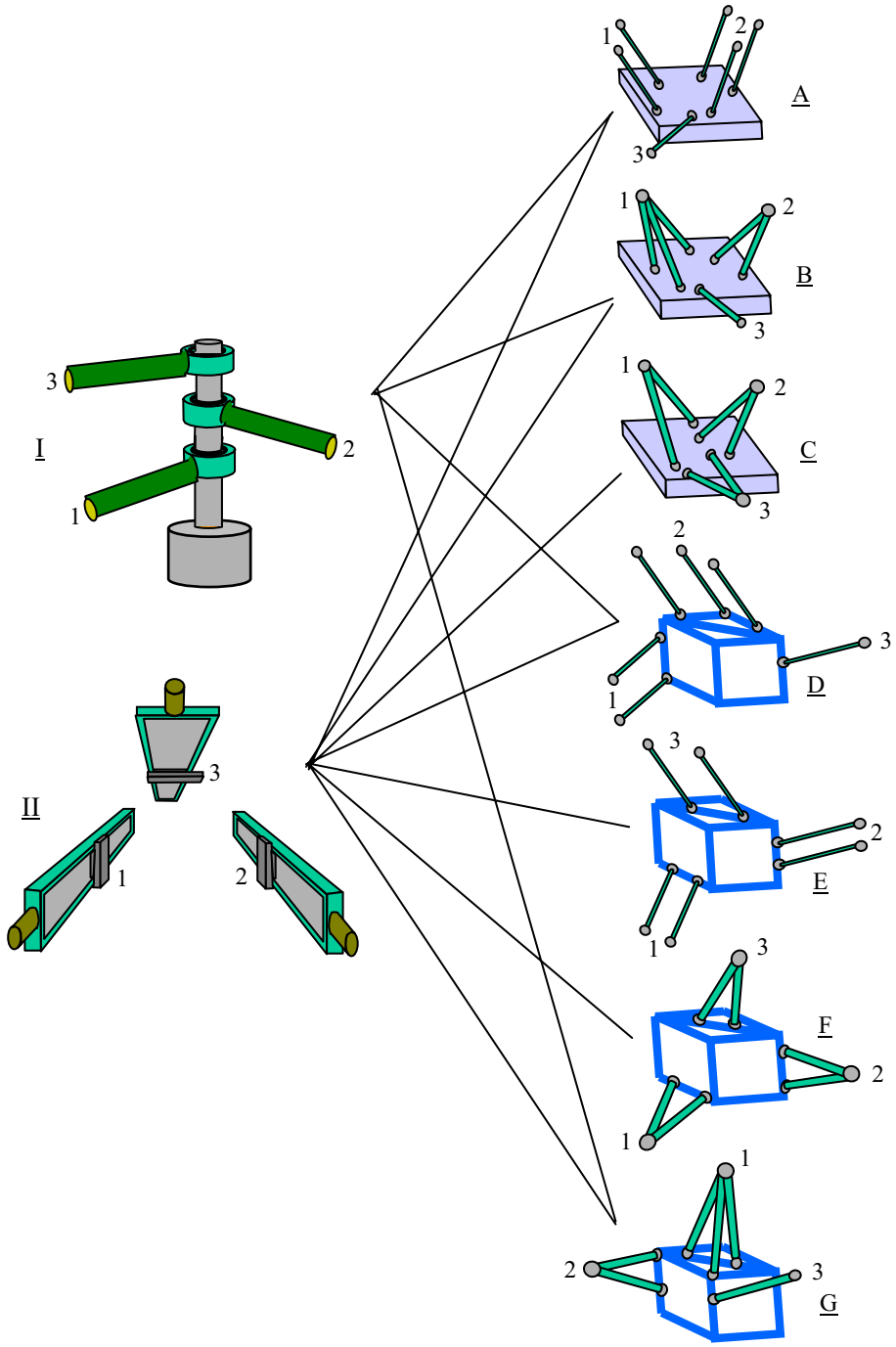

Figure 4: Examples of useful combinations between 6 link parallel structures (A - G) and the actuating parallel structures (I and II) from Figure 3.

3.3 Synthesis of Parallel 6 Link Structures for Positioning

Using the modularization approach discussed above, the next step is to find the parallel structures between the actuating arms or linear tracks in Figure 4 and the manipulated platform, on which a wrist could be mounted. These parallel structures should then be selected to obtain the potential advantages of a parallel kinematic robot as listed on the left in Figure 1.

To obtain the lowest possible moving mass in relation to the stiffness of the robot structure, there should be at least 6 links between the actuating structures and the manipulated platform. The links should be configured to transmit only axial forces, just like the struts of Hexapod, Delta and Hexaglide [3] structures.

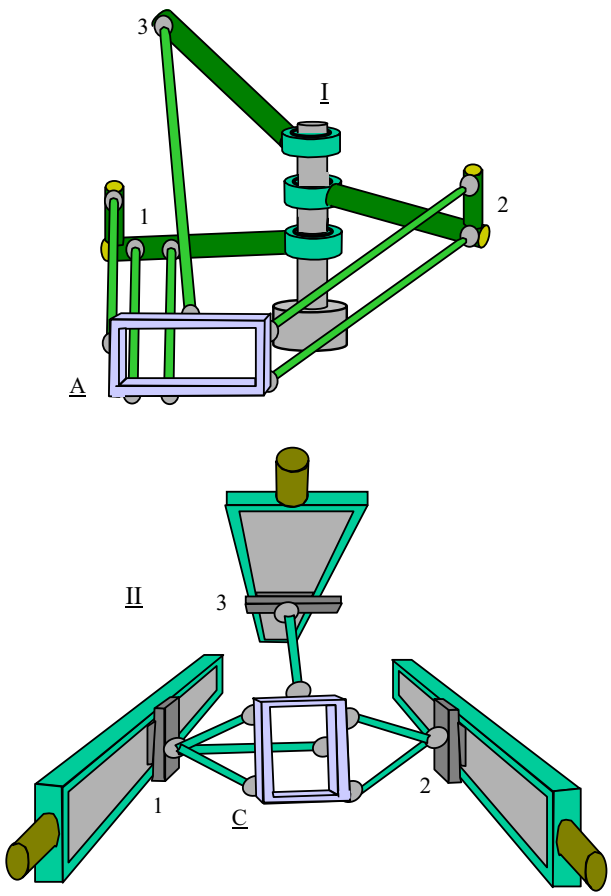

Figure 5: Robot structures when combining the actuating structure I with the link structure A (upper figure) and the actuating structure II with the link structure C in Figure 4 (lower figure). In the same way the other useful combinations in figure 4 can be assembled to study the kinematic properties of the resulting 3 DOF manipulator.

This will also give high acceleration potential and it will be easier to obtain high dynamic and static accuracy.

Figure 4 shows some useful combinations between 6 link structures and the 2 actuating parallel structures in Figure 3. Each link has a 3 DOF spherical joint in each end and the links are clustered in different configurations for 3 DOF (positioning) manipulation of the platforms. The links are mounted either with a 2D (A - C) or a 3D (D - G) pattern on the manipulated platform [5, 6].

Figure 5 shows examples of assembled positioning robots for two combinations in Figure 4. The upper combination (IA) gives a motion pattern as for a Scara robot while the lower combination (2C) gives a workspace like a Gantry robot but with a motion pattern more like an antropomorphic robot.

3.4 Synthesis of Parallel Structures with less than 6 Links for Positioning

Even if 6 link structures, where the links only transmit axial forces, are optimal from the mass/stiffness point of view, there may be design advantages by using fewer links between the actuating structure and the manipulated platform. This means that at least one link will have to transmit bending or twisting and a manipulator design can be made by combining different link types [7, 8], for example such link types as shown in figure 6.

In Figure 6 the number of DOF indicated (in parentheses) for each link type tells how many DOF constraints the link type will impose on the moving platform. For example, link type a3 will give 3 DOF constraints by transmitting bending torque in 2 radial directions and compression/expansion force in axial direction. When a cardan joint is used as in a4 - a6 and b4 - b6, the links will also constrain 1 DOF by transmitting twisting torque. The link type a8 will impose 5 DOF constraints and can thus only be used in a 2 DOF manipulator. In the link types b2 - b8 the DOF transmitted by the compression/expansion force is disabled by a linear joint, which will, however, transmit twisting torque. In b2 - b8 the linear joints can be replaced by rotational joints having the rotation axis either in parallel (not useful for b2 -b3) or with an angle relative the axial link direction.

When not only the link type a1 in figure 6 is used, a way to find useful PKM structures using other link types is to find link types that will take over the DOF constraints of two or more of the links of type a1. One example of this is shown in figure 7, where a 6 link structure is transformed to a 3 link structure.

3.5 Adding Passive Parallel Links to the Structures

From a stiffness/mass point of view, especially when using carbon epoxy struts in the links, it is an advantage to find structures as in Figure 7, where no torque will appear in the link struts. However, when the acceleration performance is not essential and heavy stiff steel struts and large bearings can be used, solutions with cardan joints may satisfy the application needs. An example of such a structure is shown in Figure 8. This figure also exemplifies the possibility of having a passive connection to the moving platform to constraint a number of platform DOF without having the link connected to any actuating structure. From a product cost point of view a passive link may be a disadvantage, but simultaneously the extra passive links can be used to carry cables, mechanical transmissions etc. to the wrist and tool equipment. In principle more than one passive link can be used and in principle all the link types in Figure 6 can be used as passive parallel links.

3.6 Synthesis of Parallel Structures for Orientation Control

When we adopt the modularization principle mentioned in 3.2 (meaning that one positioning parallel kinematic robot is connected in series with a structure responsible for the orientation

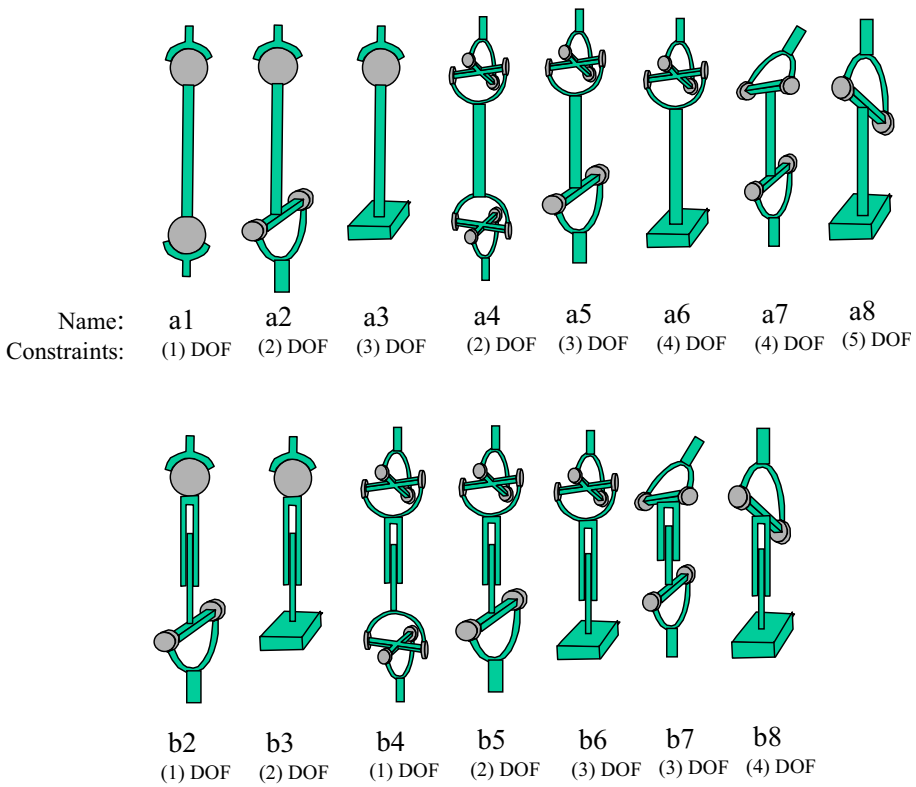

Figure 6: Link types that can be used for the synthesis for new parallel robot structures with working envelopes and motion types as for the serial industrial robots used today.

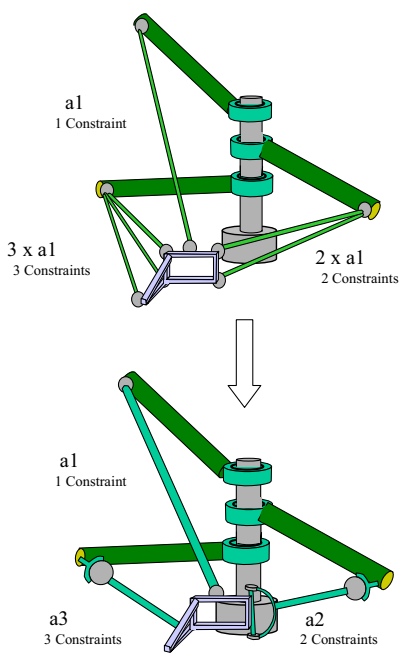

Figure 7: An example of how the a1 link type in figure 6 can be replaced by other link types (a2, a3) to obtain the same kinematics. The identical transformation can of course be made for the Gantry actuator structure in figure 5.

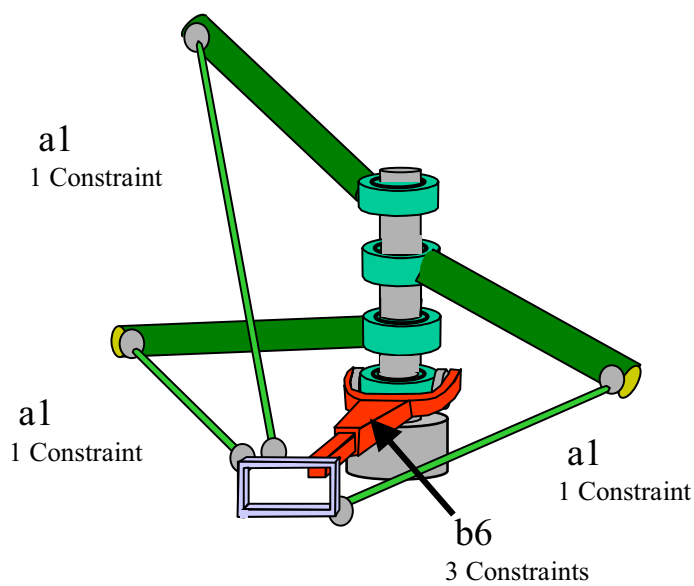

Figure 8: An example of how a link (type b6 according to Figure 6) transmitting a torque can be used to form a PKM. This is an example of the use of an extra passive link between the moving platform and the base of the robot.

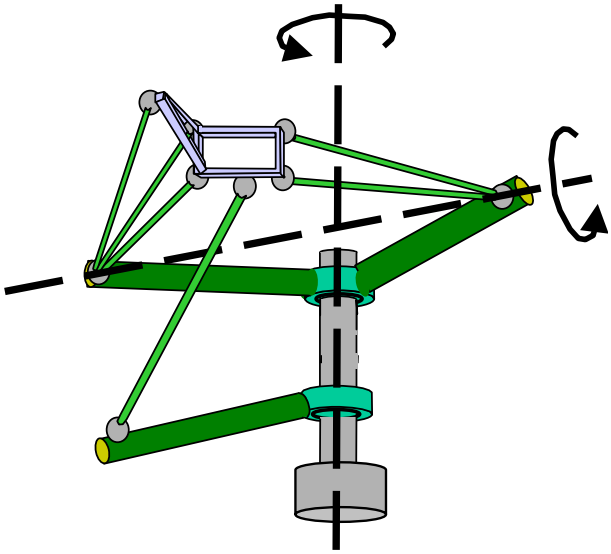

Figure 9: An example of a 2DOF parallel kinematic wrist to be used for tool orientation. The mechanism is simply a 2 DOF version of the upper positioning structure in Figure 7. The dashed lines in the figure indicate the 2 axes, around which the tool is rotated. This structure could be built with 3DOF by a rotation transmission (for example with a cardan joint) to the manipulated platform.

control) it is interesting to find out if there are any parallel structures for tool orientation, which could compete with the simple wrist structures used in industrial robots today. Two examples of parallel wrist structures, which could be competitive for applications where very fast 2 DOF tool orientation is required are shown in Figures 9 and 10.

Orientation generating parallel structures, much like positioning structures, should also be 6 link structures to optimize the stiffness/mass ratio. Looking at Figure 4, it is easy to conclude that candidates could be found with the link structures B, C, F and G. Thus, Figure 9 shows a variant combining a 2 DOF version of the actuating structure I in Figure 4 with the link structure B in the same figure. Relaxing the stiffness to mass requirement, a 6 link structure could be abandoned and a much simpler 2 DOF orientation generating version can be made with the same kinematics, as exemplified in Figure 10.

It should be emphasised that parallel as well as serial structures can be actuated via transmission links (as with the fourth axis of the Delta robot). Such transmission links will usually lower the mass of the positioning platform but simultaneously it is difficult to maintain the stiffness and the dynamic accuracy as in the case when the actuator is directly coupled to the orientation generating mechanism.

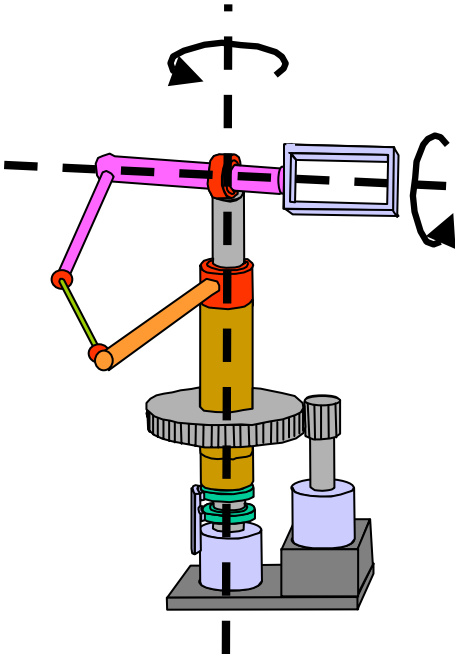

Figure 10: An example of a simple parallel 2 DOF wrist structure, which is not of the 6 link type, but which has the same kinematic features as the structure in Figure 9. The dashed lines in the figure indicate the 2 axes around which the tool is rotated.

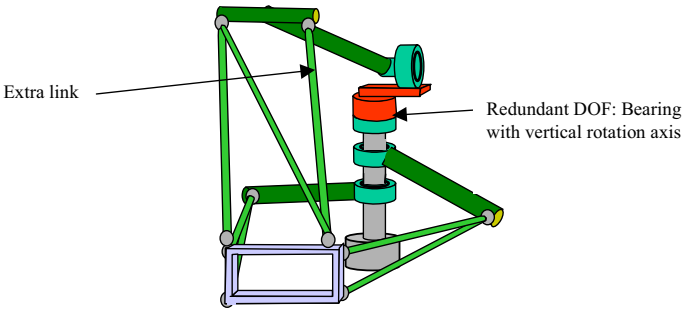

Figure 11: A parallel robot structure where 1 redundant DOF has been added to the actuating system and where one extra link has been introduced to constrain this extra DOF. It should be pointed out that the links connected to the lower and middle actuating arms could be replaced by a2 links according to Figure 6.

3.7 Adopting Redundancy With Respect to the Number of DOF

Besides using different types of links and using passive links, there is also the possibility to add DOF to the actuating structure or to the manipulated platform [9] and compensating these extra DOF with a corresponding set of constraints with extra links or with links constraining more DOF. Thus, Figure 11 shows an example where one redundant DOF has been added to the actuating system and Figure 12 an example where one redundant DOF has been added to the manipulated platform.

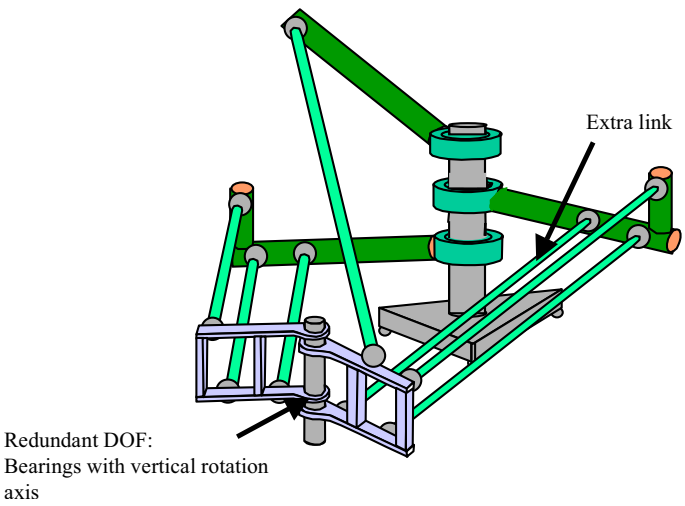

Figure 12: A robot structure where 1 redundant DOF has been added to the manipulated platform and where one extra link has been introduced to constrain this redundant DOF.

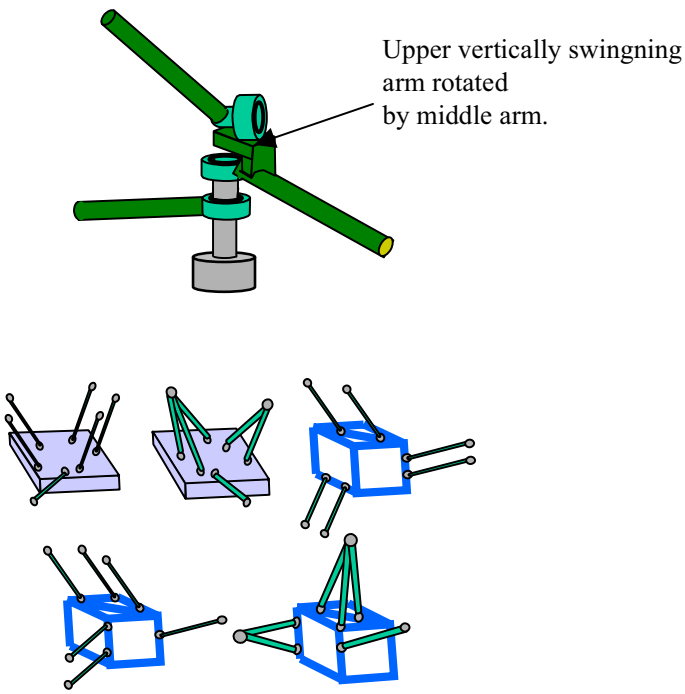

Figure 13: A semi-parallel actuating structure with serial kinematics between middle and upper actuating arms. In the lower part of the figure some link structures, which are useful together with this actuating structure.

3.8 Relaxing the Demands on Full Parallel Structures

It should be pointed out that a pure parallel structure is not always optimal and it could sometimes be worth while to be less stringent in the PKM synthesis and introduce some serial parts in the structures. For example, very good performance can be

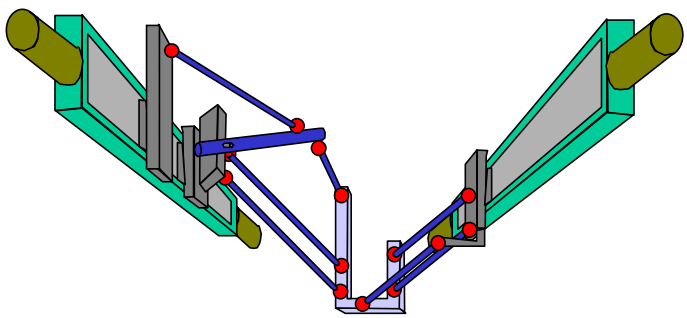

Figure 14: A semi-parallel actuating structure with serial kinematics between the 2 couriers at the left linear track. This is also an example of the possibilities to mix linear tracks with swinging arms to achieve useful kinematic properties.

achieved by mounting the upper actuated arm in the actuating structure I in Figure 4 in series with the middle arm, as shown in figure 13. Figure 13 also shows which 6 links structures that will give useful motion pattern and workspace for this type of partly serial actuating system. In Figure 14 it is shown that introducing a serial part in the actuating structure can also be useful for a gantry type PKM, whereby only 2 linear tracks are needed for 3 DOF positioning. This figure also exemplifies the possibility to mix rotating and linear actuating structures.

3.9 Concluding Remarks on the Synthesis of Parallel Robot Structures

It is well known that there are thousands of possibilities to build working PKM structures, but most of these will not fit into the requirements for flexible industrial automation. It is therefore very important to have constraints in the search for new structures. Simultaneously, it is important to have design rules to follow and to know basic structural possibilities. Thus, this section has pointed out some important issues to consider when synthesising parallel mechanisms for flexible automation. These issues are summarised in figure 15, which could be a starting point for the development of a more systematic topology method for PKM synthesis.

4 Design Optimization of Parallel Kinematic Mechanics for Robot Applications

In the previous section the important and difficult problem of PKM synthesis have been discussed. When a new structure that seems to be suitable for a target application has been found, then a mechanical design optimization procedure will take place, which will contain several interesting problems.

4.1 Simulation of Application Tasks

The first step in the mechanical design optimization procedure should be to analyze the application and set up a robot CAD environment to be able to simulate a robot together with the

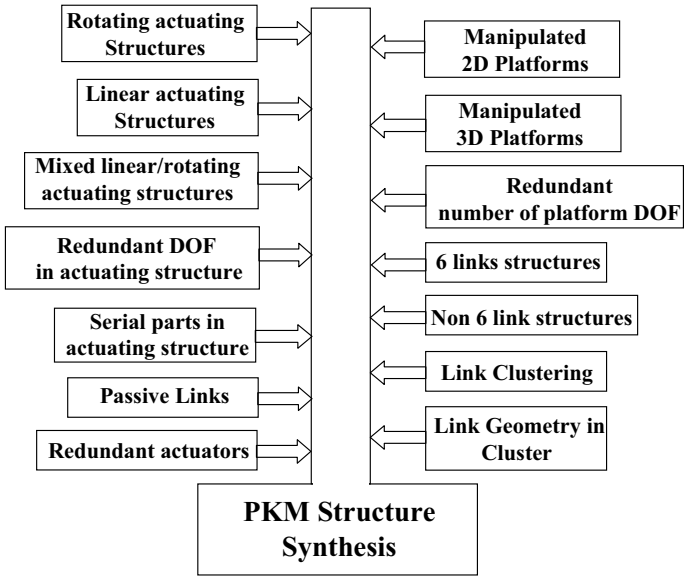

Figure 15: Examples of different issues that have been put forward as important to be aware of when synthesising a suitable PKM concept for a given application.

equipment and the process that the robot will serve. This will give the demands on the robot with respect to workspace, number of DOF, accessibility, collision avoidance, singularity avoidance, motion pattern etc. Knowing these kinematic requirements, suitable PKM concepts may be selected and tested by simulation of the real robot tasks. This means that kinematic models are needed for all the tentative parallel kinematic robots and that these models must be included in the CAD simulation environment, for example Robcad, Envision or Robot Studio.

These simulations of the application tasks should then be used in the following steps of the robot optimization. When dynamic optimization is made, usually other simulation tools are needed (ADAMS, DADS etc.) and then the trajectories obtained from the application task simulations can be used as input to the dynamic model simulations.

4.2 Optimization of Robot Kinematics

When suitable robot concepts have been selected by kinematic task simulation, the next step is to find out which of these selected concepts produces optimal kinematic performance for the application. To do this, the kinematics of each selected PKM structure should be optimized with objective functions such as workspace, accessibility, motion pattern, kinematic error propagation and kinematic error identification performance (for best possible robot calibration). Some of these object functions could of course also serve as constraints in the optimization process. The design parameters for the optimization could be actuating arm lengths, distance between actuating arms, distance between linear tracks, lengths of linear tracks, link lengths, joint angle ranges, manipulated platform dimensions, backlash in components, manufacturing tolerances and assembly accuracy. How to make this multi-objective optimization is a very important robot design issue. One approach is to start with manually optimized kinematics and then tune the structure by means such as genetic algorithms for global optimization and gradient searching methods for local optimization. Some design parameters and objective functions/ constraints for kinematic design optimization are summarised in Figure 16.

4.3 Optimization of Rigid Body Dynamics

The next step in the design should be to optimize the rigid body dynamics. The input to this design could be a simplified FEM model of the structure. However, since it is often possible to obtain a good approximation of a parallel robot structure with beams, tubes and plates, FEM modeling could wait until a later more accurate stage in the design process. Just as for the kinematic optimization, rigid body optimization also has multiple objectives. Examples of rigid body objective functions are robot max acceleration and robot max speed while the torque and forces on bearings and the torque and forces in structural elements as arms, links and manipulated platform could be handled as constraints. Design parameters are actuator torque and forces, arm and link dimensions and geometry, arm and link material, joint mass, platform dimensions, platform material etc. For this design, the most demanding robot motion trajectories must be found and to make a safe optimization the objective functions should be studied for different trajectories in different parts of the workspace. This is a very time consuming task, especially since the maximum acceleration and speed and the maximum load on different components and structural elements will be different for different motion types in different parts of the workspace. This is of course a very challenging R&D topic and just as for the kinematic optimization, one could start with a design relying on the experience of a skilled designer and then tune the design by different optimization methods. In a long term perspective one could also think of using some kind of more general method for topology optimization. Some design parameters and objective functions/constraints for the rigid body optimization can be found in Figure 17.

4.4 Optimization of Robot Flexibility

In the optimization of the rigid body dynamics as described above, the approximation is made that the flexibility of the robot does not affect the rigid body optimization. This is of course not true, but in a first design iteration this separation of rigid body and elastic body design could be a way to make the design process easier to handle. One could argue that a first pure rigid body optimization is made to learn the desired actuator performance to fulfill the acceleration and speed demands without exceeding the fatigue limits. In the flexible body design optimization it is then the objective to find out if the pure rigid body design must be tuned to obtain the stiffness objectives given by the application. Thus, such objective functions as

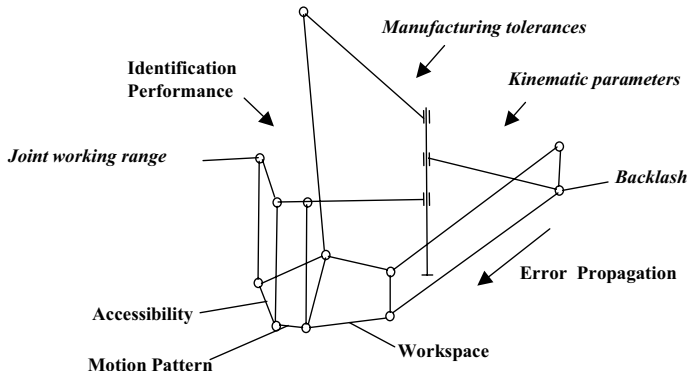

Figure 16: Some design parameters (in cursive) and design objective functions (or constraints) for the optimization of the kinematics of a parallel kinematic robot.

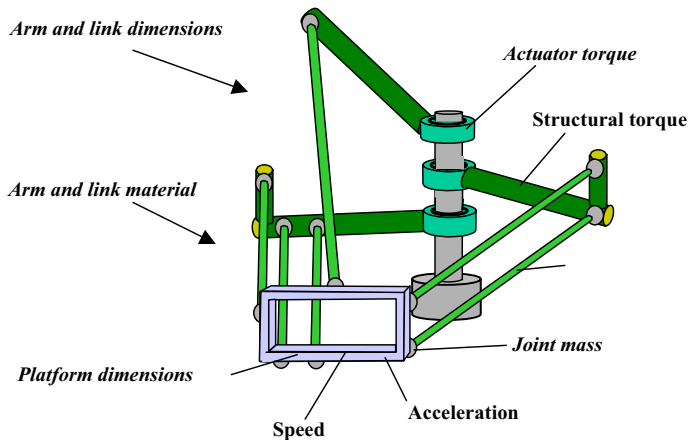

Figure 17: Some design parameters (in cursive), design objective functions and constraints for the optimization of the rigid body dynamics of a parallel kinematic robot.

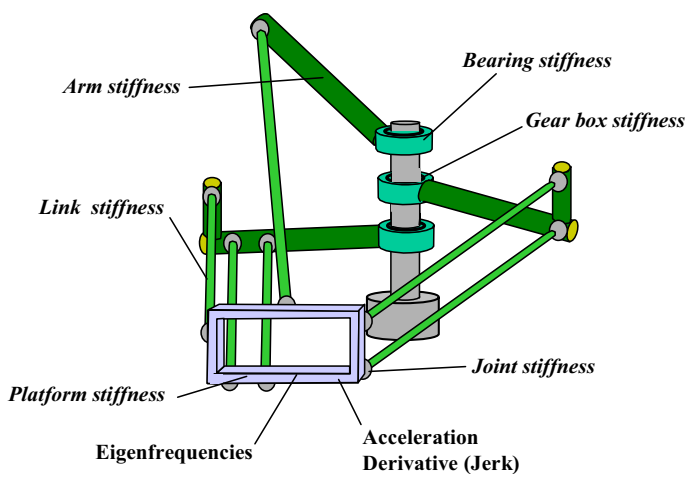

Figure 18: Some design parameters (in cursive) and design objective functions and constraints for the optimization of the flexible body dynamics of a parallel kinematic robot.

robot stiffness and robot eigenfrequencies must be used and the relation between the rigid body properties of the robot components and the stiffness of the robot components must be known. To run the flexibility optimization the rigid multibody dynamic models must be expanded to also include the stiffness of bearings, arms, links and the manipulated platform. This model with flexibilities is also needed for the compensation of static position errors caused by gravity. When a gear box or another transmission unit is used, the stiffness of this component should also be included in the model, as summarized in Figure 18.

4.5 Optimization Iteration Sequence

In summary, the mechanical design of a parallel kinematic robot for a given application could be divided into 4 steps:

1. Analyze the application requirements and select the optimal concepts with respect to kinematic requirements.
2. Optimize the parallel kinematic structures to find a globally optimal structure.
3. Optimize the rigid body performance.
4. Optimize the elasticity performance.

In the same way as mentioned for steps 3) and 4), an iteration is needed between all the steps to find an optimal robot for the tasks defined by the application. Usually, a general purpose robot is needed from robot business point of view and the optimization has to be made for a spectrum of applications. One problem to then solve is finding applications that are similar to each other with respect to the performance potential of the parallel robot structure that has been selected. This problem also relates to the robot modularization issue. Probably, parallel structures will be easier to modularize than serial robot structures because of simpler components with smaller dynamic interdependence.

5 Selection of Components for a Parallel Kinematic Robot

In the mechanical design optimization process discussed in section 4 above, one important issue is to select the most suitable components for the parallel kinematic robot. A first component discrimination is of course made when the parallel robot concept is selected. However, also in the other design steps there will be opportunities to select between different component solutions.

5.1 Kinematic Requirements on Components

In the kinematic optimization it is important to find out the requirements on the working range for the joints. If, for example, large working angles are needed in a 2 DOF joint, then a cardan type of joint may be needed, but if large joint angles are needed only in one direction, then a ball and socket joint can do the job. The kinematic analysis also includes the kinematic error propagation and the identification performance. If it is important to design the structure with low sensitivity to temperature changes in the robot environment, then the components giving the highest error propagation and the lowest calibration accuracy should be made of a material with a low temperature coefficient (as for example carbon reinforced epoxy). Also the error propagation and the identification performance with respect to backlash in actuators and joints must be analyzed kinematically, which may put demands on these components and even make it necessary to exclude certain types of components. The error propagation and identification performance analysis will also give information on the demands on the accuracy needed for the manufacturing and assembly of the components and the robot.

5.2 Dynamic Requirements on Components

In the rigid and flexible dynamic design optimization, the dynamic requirements on the components and the robot are obtained and a final component selection should be made. Starting with the actuator selection, the first question is if a direct drive (linear direct drive or a ring motor) is needed. This selection depends on the requirements on the stiffness and, as pointed out for the kinematic analysis, also on the demands on maximum allowed backlash (more generally lost motion). At this stage of the design the cost optimization will also enter the design procedure and the high cost of a direct drive solution must be weight against the performance/cost ratio for a drive with a gear box or band/screw transmission. If it is necessary to go for a low cost solution, as used in industrial robots today, backlash-free highly pre-stressed transmissions may be needed, which will however give the drawback of adding friction. Some of these problems with a low cost actuator solution can be compensated for by the servo, and the optimization problem will thus be extended to cover also the servo optimization, which will be covered in the next section. As a consequence the actuator selection could have to wait until the servo is designed and optimized.

Also of significant importance for the dynamic design is the selection of the bearing technology for the actuating structure and for the link joints. Important bearing features besides the working range are stiffness, load capacity, friction and backlash. For high stiffness and high load capacity, pre-stressed ball bearings or roller bearings may be used, which will, however, give high bearing friction. Moreover, when these bearing concepts are used in the link joints, the moving mass will become high, giving high load in the structure for applications needing high acceleration and speed. In applications with these high motion demands it may then be better to implement the joints with low weight ball and socket bearings. This means that the bearings cannot be bought off shelf, but a custom design must be made, whereby the best material combination in the sliding interfaces of the bearings must be found. It might also be needed to have an interface medium (air, oil) to obtain low friction and long lifetime of the joints. It should be pointed out that the passive joints of a parallel kinematic robot are the key mechanical elements that distinguish it from a serial robot.

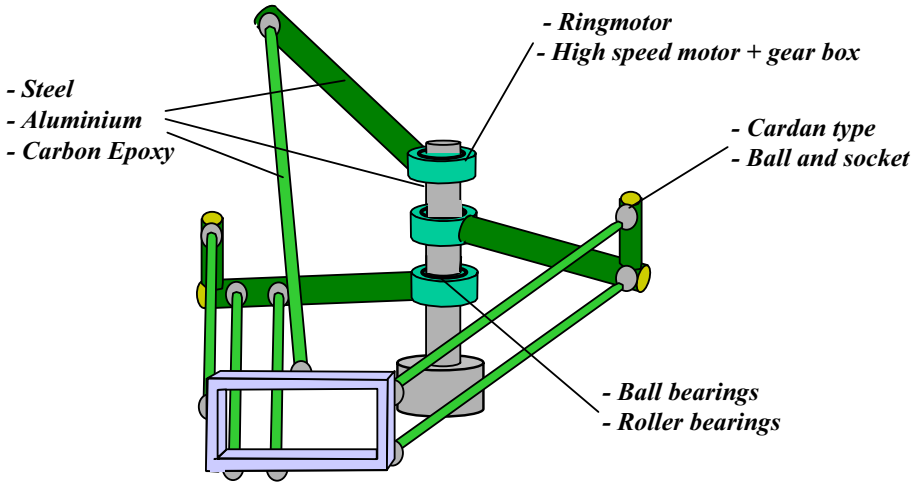

Figure 19: Some examples of component technologies to investigate during the design optimization of a parallel kinematic robot.

In addition to the actuator and bearing components, the arms, linear tracks, links and the manipulated platform must also be optimized. Linear tracks may be selected off the shelf, but arms, links and manipulated platform must be customized. For the dynamic optimization the weight/stiffness relation is of course most important and for this both the geometry and the type of material must be considered. What is also important is the technology and methods used for joining the components. If for example carbon epoxy is used, then gluing may be favorable, but a lot of experience is needed to optimize this process to the demands on stiffness, load, accuracy and lifetime.

Some of the component technologies important for a parallel kinematic robot are summarized in Figure 19.

6 Drive System and Control Optimization

The mechanical robot optimization cannot be made independent of the drive system design and the controller design. Thus, the rigid body dynamics optimization will give requirements on the actuator performance and it will be necessary to find drive system solutions that will satisfy these requirements.

6.1 Drive System Design

For the drive system optimization it is not enough to calculate the values of the maximum torque needed, but it is just as important to know the duty cycle to be able to calculate the thermal demands on the actuators. Thus, applications such as pick and place and 2D laser and water jet cutting will usually run with high frequency and the nominal motor torque and the nominal drive current must be designed at a higher level than for applications such as assembly and measurement. To be able to optimize the drive system with respect to the thermal situation, robot programs having the highest frequency for the applications under consideration must be simulated using the rigid body model. If the demands on the cooling then become too high, there could be a need to make a redesign of the mechanics. However, compared with a serial kinematic robot, the dependence between the rigid body design and the drive system design is smaller since the actuators do not contribute to the moving mass of the robot. For optimal use of the actuators, a real time running thermal model should be used together with the rigid body model and drive system model to calculate the thermal load on the actuators. Then it is possible to make on line tuning of the acceleration and the speed of the robot to avoid overheating. This model-based control scheme will adapt the actuator performance of the PKM to the actual tasks, giving shorter cycle times and a more cost efficient drive system design. The same idea can be used for on line fatigue control. Then the dynamic models are extended to contain critical interfaces, in which force and torque are supervised. The force and torque levels of the dynamic models are then supervised by the controller to avoid passing the fatigue limits given by the lifetime of the PKM. These adaptive control schemes are good examples of the need of an optimization including both mechanical and control design.

6.2 Static Control

Of utmost importance is to design control schemes that are optimized for the mechanical design. It is also important to design the robot structure such that it will not be too difficult to control. For the static control it is necessary to compensate for errors caused by the deviations from a nominal kinematic model and errors induced by sagging of the structure due to gravity. For these compensations a kinematic error model is needed as well as the flexibility model discussed earlier. Since the kinematic errors are different for each individual robot, identification of the errors must be performed. This identification may consist of measurements of critical components before robot assembly and then a kinematic identification of the whole robot structure to get the errors not measured in advance. The difficulty level for the identification will depend on the measuring method used. If an

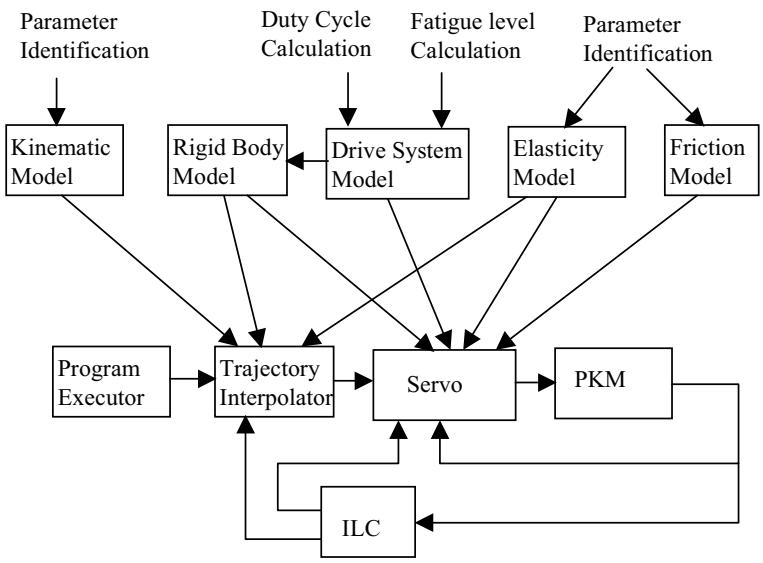

Figure 20: Controller structure overview for model-based control of a parallel kinematic robot. The controller design may start with nominal models, but to achieve maximum robot performance, deviations from nominal models must be identified, especially for the kinematic and elasticity and friction models. To obtaind shortest possible cycle time, the drive system should be adapted to the actual duty cycle and mechanical stress levels.

advanced 6 DOF measurement system is used, the identification will be easier than if, for example, a 1 DOF measurement system such as a double ball bar is used. It is certainly interesting to find methods to optimize the identification of the robot structure under investigation with the constraints given by the available measurement system.

6.3 Dynamic Control

The compensation of static errors can be made in such a way that the programmed and interpolated positions are moved, which is not too difficult. It is much more difficult to handle the dynamic effects of the parallel kinematic structure to obtain low dynamic path errors as well when large acceleration and acceleration derivative (jerk) are needed. To obtain high performance control with respect to cycle time and accuracy, model-based control is needed. Of the models already mentioned, the controller needs the rigid body model, the flexibility model and the drive system model. Moreover, a friction model is needed and the quality of the control will of course depend on the accuracy of the models. The rigid body model and the drive system model are usually well defined for a robot type, while the flexibility model and the friction model will usually be very difficult to predict. Moreover, these models may be different for different individual robots and therefore the model parameters must be identified. For the flexibility model, black box or grey box identification is made (see Identification toolbox in Matlab) by exciting the robot with different frequencies (chirp, PRBS, discrete sinusoidal, white noise etc.) to find eigenfrequencies and damping parameters. For the friction, special movements are used to identify at least the Stribeck, Coulomb and viscous friction parameters, which may differ at different positions of the robot and in different motion directions. The control loops may be designed using such optimization methods as LQG and H_∞ and the servo may make use of model-based feed forward control, computed torque control, MIMO control, input shaping and parameter scheduling. The accuracy of the models will be limited, so to improve the control performance further the control loops can be extended to contain such sensors as encoders, accelerometers, strain gauges and force sensors in the arm and link system. Some of these sensors could be used for redundant measurements to obtain on line parameter error identification and compensation. The sensors in the mechanical structure can also be used to increase the stiffness, bandwidth and accuracy of the control [12]. Moreover, non-model based control methods such as iterative learning control (ILC) can be adopted to decrease the control errors below the level determined by the accuracy of the dynamic models. It could also be possible to use adaptronics - using high bandwidth actuators and sensors in the robot structure to compensate for mechanical deflections.

Figure 20 gives an overview of a model-based control system useful for parallel kinematic robot control. Advanced control will do a lot for the robot performance, but simultaneously it is very important to design the robot in such a way that the control will not be too difficult. This means that the mechanical eigenfrequencies should be as high as possible, eigenfrequencies should not be too close to each other, friction should be kept as low as possible etc. Thus, it is important to have the control requirements in consideration when the mechanical optimization is made. For this a simulation environment is needed, where

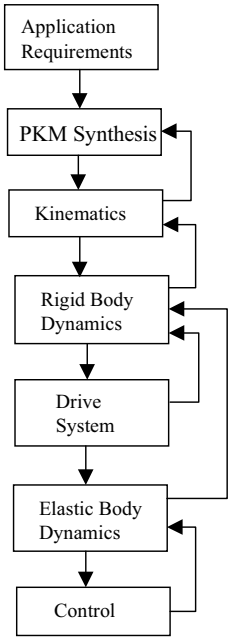

Figure 21: Possible development process for a PKM, as seen in an industrial perspective. Each box contains an optimization activity as described in this paper and to achieve a global optimization of the PKM product, iterations are needed between the different activities as shown by the arrows.

control developers meet the mechanical developers in an early stage of the robot development to optimize the mechanics with respect to the control requirements. In such an environment it will also be possible to get accurate performance predictions, which is very important to get industry interested in starting product development.

7 Summary

The purpose of this paper is to give an overview of the need of PKM research as seen in an industrial perspective. It is then important to stress the fact that at first when all the steps in the robot design optimization are made, as summarised in Figure 21, the industrial potential of the concept can be judged. This means that besides new methods to synthesize parallel structures, new methods are also needed to make a fast and accurate robot optimization [10] to such a level that the risk of starting a high cost product development will be low. The most difficult topic then is to predict the control performance. Next to the synthesis of new parallel kinematic structures, the most important issue seems to be the issue of automatic control. More than likely, the only way for the PKM technology to compete with the very rigid and accurate Cartesian machines used today for such high performance applications as machining and laser cutting, is to make use of advanced model based control, and if needed, add more sensors and also learning control concepts.

Summing up, below is a proposal for a list of the most important research topics from an industrial point of view (in priority order):

1. Methods and tools for a systematic synthesis of new parallel kinematic structures.
2. Advanced automatic control technology for the control of parallel kinematic robots (including different sensor loops and adaptronics).
3. Methods and tools for fast and accurate parallel kinematic robot optimization and performance prediction (optimization and prediction by virtual prototyping: application requirements, kinematics, dynamics, drive system, controller)
4. Further development of bearing technology for link joints
5. Methods for adaptive thermal and fatigue control

To succeed with this research, close collaboration is probably needed between researchers from different fields such as automatic control, applied mathematics, computer science, kinematic and dynamic modelling, system identification, optimization, sensor technology, drive system technology, material technology, tribology and mechanical design. There are many interdisciplinary research topics just as for research in serial robotics, but the requirement on the research depth is probably higher since the target of the parallel robots are applications needing much higher performance than can be obtained with the industrial robots used today.

Acknowledgements

The author would like to thank Paul Bosscher, doctoral student at Georgia Tech, for editing and formatting this article.

References

[1] R. Clavel. Dispositif pour le déplacement et le positionnement d'un élément dans l'espace, 1985. Patent CH 672 089.

[2] F. Pierrot, F. Marquet, O. Company, and T. Gil. H4 parallel robot: Modelling, design, and preliminary experiments. In *Proceedings of 2001 IEEE International Conference on Robotics and Automation*, Seoul, Korea, May 2001. http: www.lirmm.fr/rdc/pm/papers/lirmm_icra2001.pdf.

[3] F. Marquet, S. Krut, O. Company, and F. Pierrot. ARCHI, a redundant mechanism for machining with unlimited rotation capacities. In *ICAR 2001*, Budapest, August 2001.

[4] M. Honegger, A. Codourey, and E. Burdet. Adaptive control of the Hexaglide, a 6 dof parallel manipulator. http: www.ifr.mavt.ethz.ch/publications/honegger97a.pdf.

[5] T. Brogårdh. Design of high performance parallel arm robots for industrial applications. In *Proceedings of the Symposium Commemorating the Legacy, Works, and Life of Sir Robert Stawell Ball Upon the 100th Anniversary of A Treatise on the Theory on the Screws*, University of Cambridge, Trinity College, July 9-11, 2000.

[6] T. Brogårdh and CY Gu. Parallel robot development at ABB. In *Proceedings of the First International Colloquium of the Collaborative Research Centre 562*, University of Braunschweig, May 29-30, 2002.

[7] K.H. Hunt. Constant-velocity shaft couplings: A general theory. *Transactions of the ASME: Journal of Engineering for Industry*, 95, Series B:455–464, 1973.

[8] K.H. Hunt. Structural kinematics of in-parallel-actuated robot arms. *Transactions of the ASME: Journal of Mechanisms, Transmissions, and Automation in Design*, 105:705–712, 1983.

[9] F. Pierrot. Parallel mechanisms and redundancy. In *Proceedings of the First International Colloquium of the Collaborative Research Centre 562*, University of Braunschweig, May 29-30, 2002.

[10] J.-P. Merlet. The need for systematic methodology for the evaluation and optimal design of parallel manipulators. In *Proceedings of the 3rd Chemnitz Parallel Kinematics Seminar*, April 23-25, 2002.

[11] M. Karouia and Hervé. An orientational3-DOF parallel mechanism. In *Proceedings of the 3rd Chemnitz Parallel Kinematics Seminar*, April 23-25, 2002.

[12] G. Pritschow, C. Eppler, and W.-D. Lehner. Highly dynamic drives for parallel kinematic machines with constant arm lengths. In *Proceedings of the First International Colloquium of the Collaborative Research Centre 562*, University of Braunschweig, May 29-30, 2002.

Industrial Panel

Thursday, October 3, 2002, 1:30PM

Panelists:

- Torgny Brogardh, ABB Robotics, Sweden
- Ed Dougherty, August Design Inc., US
- Adam Jacoff, NIST, US
- Gerhard Serapins, CAE, Montreal, Canada

Regular Papers: Design and Optimization

Thursday, October 3, 2002, 2:25PM

Session Chairs: V. Krovi and P. Wenger

1. A.S. Sorensen, H.G. Petersen, O.G. Jakobsen, J. Steinicke
   "Towards the Industrial Usage of Parallel Kinematic Chain Modules in a Fully Modular Robotic Manipulator".

2. J. Yoon, J. Ryu
   "*Reconfigurability of a Parallel Manipulator: A Case Study*".

3. E. Ottaviano, M. Ceccarelli
   "*Optimum Design of Parallel Manipulators for Workspace and Singularity Performances*".

4. G.F. Liu, Z.X. Li
   "*General Geometric Algorithms for Optimal Design of Parallel Manipulators*".

5. K. Kozak, P.A. Voglewede, I. Ebert-Uphoff, W. Singhose
   "*Concept Paper: On the Significance of the Lowest Linearized Natural Frequency of a Parallel Manipulator as a Performance Measure for Concurrent Design*".

Proceedings of the WORKSHOP on
Fundamental Issues and Future Research Directions for Parallel Mechanisms and Manipulators
October 3–4, 2002, Quebec City, Quebec, Canada
Clément M. Gosselin and Imme Ebert-Uphoff, editors

Towards the industrial usage of parallel kinematic chain modules in a fully modular robotic manipulator

ANDERS S. SØRENSEN AND HENRIK G. PETERSEN
The Mærsk McKinney Møller Institute for Production Technology
University of Southern Denmark
Campusvej 55, DK-5230 Odense M
Denmark
zaphod@mip.sdu.dk, hgp@mip.sdu.dk

OLE G. JAKOBSEN AND JAKOB STEINICKE
Meganic ApS
Forskerparken 10
DK-5230 Odense M
Denmark
ogj@meganic.dk, jakob@meganic.dk

Abstract: *One of the main advantages of parallel robots is that they can be applied as modules in long-reach (snake-like) robotic manipulators enabling robotic automation of unhealthy work in confined spaces. However, before parallel kinematic robotic modules (PKRM's) can be widely used in such applications a variety of technological tasks must be accomplished such as design issues, precise model based calibration, modular control and process control. It is the purpose of this paper to address our work within each of these tasks aimed at developing robust reconfigurable PKRM's for long reach welding applications within e.g. shipbuilding.*

1 Introduction

The industrial usage of the classical 5 or 6 axis robots has now matured over 20-30 years. However, the use is almost always limited to situations where the base of the robot is either fixed or mounted on a gantry with easy access from above. This leads to severe demands on the production system as the items that the robot is supposed to process must be moved to the robot as for example in the assembly lines of the automobile industry or in the panel lines in shipbuilding. This leads again to severe constraints on the logistics of the production process. In many potential applications, it would be desirable for the robot to have a long horizontal reach, enabling it to creep into confined areas, such as "rooms" closed from above. The usage of robots in such confined areas where the working environment is often very unpleasant is impossible with the classical robot installations. There is therefore a strong demand for new types of industrial robotic systems where the robots have the following new properties:

- Have a much longer horizontal reach
- Can handle tasks in confined areas
- Are lightweight and movable
- Are reconfigurable

Rather than approaching these new robotic systems as a few types of new robotic manipulators, we believe that they will be a product of increased reconfigurabilility, in the way that the systems will consist of robotic modules (subunits) which can be plugged together in various ways. Each module has it's own embedded controller which is linked to a network when the modules are assembled into a manipulator. The manipulator can be specified and designed in advance, based on information about available modules and the tasks the manipulator is going to perform. Another advantage is that if one module fails during operation, it may quickly be replaced with another module of a similar type. The modules will often be subsets of a long robotic arm, but they may also be moving platforms, such as fork-lifts or other vehicles. Once the task is accomplished, the modules can be reconfigured for the next task.

In this paper, we will discuss the reach as being horizontal (perpendicular to the gravitational force). There are two reasons for this choice.First, horizontal reach enables a new range of applications. Second, horizontal reach is the worst case application for designers, because of the torque due to gravity is at its maximum. Thus, all our results for our PKRM's at given horizontal reach hold for the same reach in other directions.

Given the desire for a long horizontal reach and low weight, it is obvious that PKRM's will be very suitable as components in such robotic systems. There has been a lot of research in connection with mechanical design, kinematics, calibration and dynamics of a single PKRM consisting of a fixed platform and a moving platform which are connected together by more than one kinematic chain. However, there have been only few studies on the problems connected with using the PKRM's as components in a modular manipulator. This leads to new problems within more or less all the research areas within parallel robots and also to some additional problems concerning embedded modular control. It is

the purpose of this paper to address these problems and to present our solutions and how they have been incorporated into a prototype of a PKRM. The paper is organized in the following way: In section 2 the problems within mechanical design is discussed. In section 3, we discuss problems within kinematics and in section 4 we discuss the related problems with calibration. Both sections give a somewhat detailed review of the literature. Much of the results are also summarized in (Merlet00). In section 5, we discuss the development of an embedded controller for a PKRM. In section 6, we discuss the incorporation of the PKRM prototype into a long reach manipulator that is being developed for welding in confined areas in shipbuilding. Section 7 concludes the paper with some topics for future research.

2 Mechanical design and implementations

In this section, we describe our design considerations and choices used in the implementation of our PKRM prototype. Due to the desire of high modularity, which may be achieved by plugging small PKRM's with few degrees of freedom together in linear chain, we have decided to only consider 3DOF modules. One should thus view these modules as rather small bending modules in a "snake" like robot rather than modules with high longitudinal extension possibilities.

Choice of kinematic topology

The most popular 3DOF PKRM kinematic topology studied for use in long reach applications has been the VGT (Variable Geometry Truss). Among these the Double Octahedron (DO) has been the most appealing (Salerno94). Close to industrial prototypes have been designed and demonstrated at NASA Langley and at Odense Steel Shipyard Ltd. These designs have revealed major practical problems when designing DO-VGT's (Jakobsen98). The main problems are expensive, complicated joints and a large reduction in workspace (WS) due to mechanical limitations in practical joint- and actuator design.

To overcome these limitations in WS the Double Tripod (DT) was examined as an alternative mechanical structure (Canfield97). The DT structure is basically a DO-VGT structure where the actuators have been removed from the symmetry plane of the mechanism and consequently the mathematically spherical joints at the symmetry plane can be mechanically built out of 3 simple rotational joints (roll-pitch roll). When using the DT structure as a module in a long reach manipulator it is important to minimize the torque loads in all members. For this reason our design is as far as practical possible a truss-structure and referred to as the Double Tripod VGT (DT-VGT).

Design criteria

The main aim in the mechanical design of the DT-VGT has been to work on the following design goals:

- Increase the workspace
- Decrease weight and size
- Increase stiffness
- Minimize costs
- Increase accuracy

A severe contradiction in the design goals exists and the best compromise has to be chosen based on the demands of the specific application.

Workspace optimization

One of the main parameters used in the design of the DT-VGT has been the ratio between the height of the triangle created by the rotation axes of the leg and the width of the triangle created by the rotation axes of the distal plate (See Figure 1). The ratio is referred to as the H/W-ratio. This ratio has a great affect on the WS.

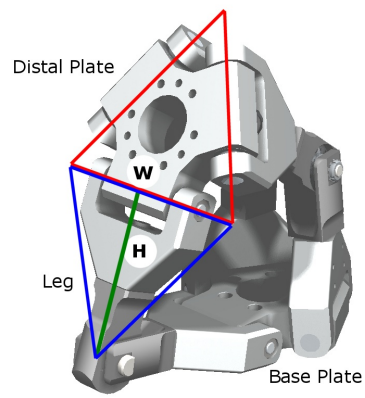

Figure 1: The distal plate and the leg in a DT-VGT design

The advantages gained by shifting from the DO-VGT to the DT-VGT can be demonstrated by comparing the maximum achievable angle between the base plate and the distal plate. Figure 2 shows the maximum achievable angle between the base plate and the distal plate for different H/W ratios for a certain actuator stroke. The current DT-VGT prototype has a H/W ratio of 0.75. This has proven to be a reasonable ratio in practical design.

With the chosen joint limits and H/W ratio the maximum angle between the distal plate and the top plate is 80°. It should be noticed that this angle is limited to only 30° in known DO-VGT designs.

Forces

Due to the joint limitations, the DO-VGT's have never been operating close to singularities or extreme positions of the legs. This is not the case with the DT-VGT. The larger WS requires the mechanism to operate close to singularities and extreme positions, and the design has to cope with the internal forces occurring in these positions. Force curves have been examined and an

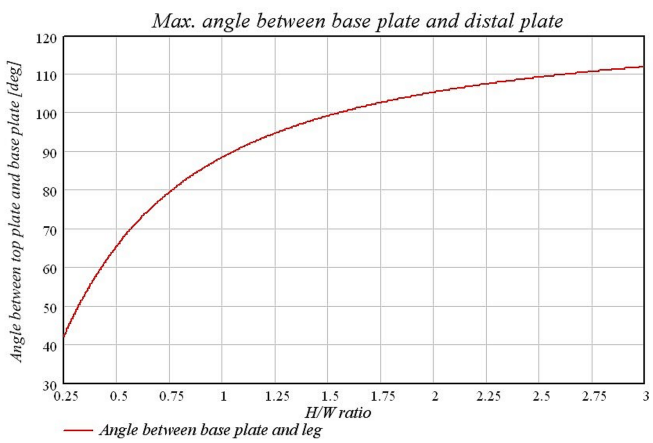

Figure 2: Max. angle between fixed and moving plate as function of the H/W ratio

example from the current prototype can be seen in Figure 3. The curves have been produced by applying a force-couple system to the distal plate and calculating the forces in the joints when moving all 3 legs of the mechanism from one limit to the other.

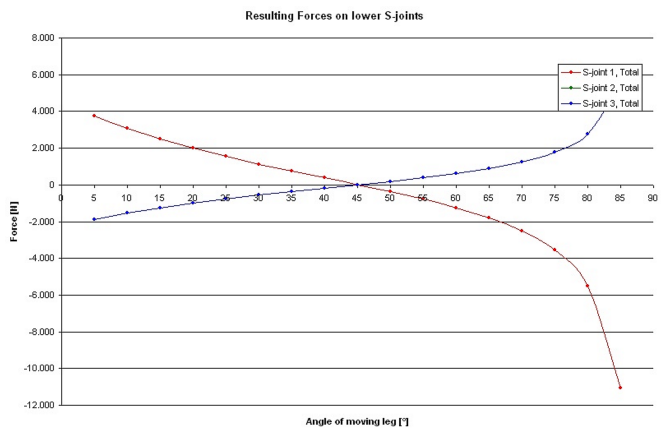

Figure 3: The figure illustrates the forces when one lower leg is moved from $5°$ to $85°$ (measured from the plane of the base plate), and the other 2 legs are in position $5°$. The curves for those two legs therefore coincides.

As can be seen, the magnitudes of the forces increase dramatically when the mechanism is completely contracted.

The current DT-VGT prototype

The current prototype represents the latest in DT-VGT development. The prototype is shown in Figure 4.

The data for the prototype are:

- Mass of Prototype: 65 kg
- Payload: 65 kg at 500mm from the distal plate

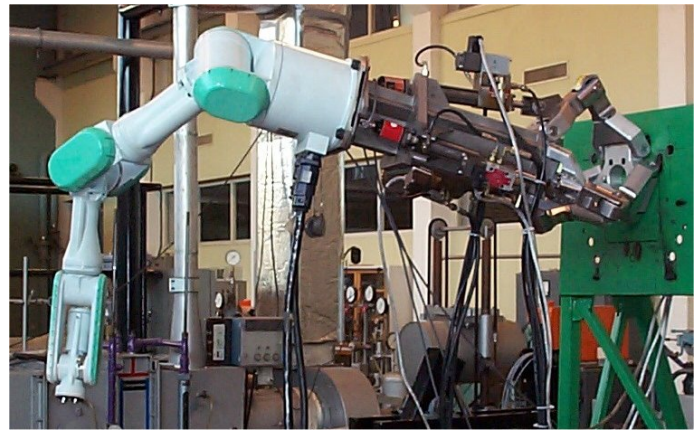

Figure 4: Present DT-VGT prototype carrying a Mitsubishi PA-10 robot

- Max angle: 80 deg
- Max diameter: 600 mm
- Min diameter: 425 mm
- Max length: 945 mm
- Min length: 688 mm

The DT-VGT is designed as a modular mechanism with an integrated modular control system. One of the advantages is that the mechanism can be configured to fit a specific application. In Figure 4, the DT-VGT can be seen carrying a Mitsubishi PA10 robot where the PA10 robot has been attached to the base part of the DT-VGT and the tool of the DT-VGT is attached to the foundation, hereby increasing the reach of the complete manipulator.

3 Kinematics

The direct kinematics problem for parallel robots (deriving the pose of the moving platform given the actuator values) has received very high attention. Many results are based on the elimination idea (Faugere95) where the solutions for the pose can be derived from the real roots of a univariate polynomial. The elimination process may lead to polynomials of different degrees and therefore research has also been carried out towards deriving bounds for the number of solutions for the pose as for example in (Raghavan95) where a bound of 40 was found for the Gough platform. This bound was actually later shown to be tight (Dietmaier98). From a mathematical point of view, the results are beautiful, but from an application point of view, they are not so important as the huge amount of work may indicate. The reason is, that other methods are typically available in applications for keeping track of the initial pose of a movement of the manipulator, so the often criticized Newton-Raphson approach will be very efficient as the robot is then moving incrementally and an initial guess close to the solution therefore exists. Problems with

the Newton-Raphson approach then only occurs near singularities, but the singularities can often be determined in advance and subsequently avoided by the control software to also avoid the corresponding mechanical problems with passing nearby a singularity. Also the problems outlined in (Innocenti95)(Wenger98) cause no practical problems with the small step sizes used in the Newton-Raphson approach.

Although the main focus on kinematics of parallel robots has been on the direct kinematics problem, the main interest in applications is on the inverse kinematics problem. The inverse kinematics problem for parallel robots with a moving platform suspended from a fixed platform through several legs is essentially at most as complicated as the inverse kinematics for a serial robot corresponding to each of the legs and seems therefore to need no treatment. The inverse kinematics problem leads often again to a polynomial equation describing the solutions. However, in many applications parallel robots of this type may be modules inside a highly redundant robot. When this is the case, this classical analytical approach for the inverse kinematics is useless as it is not suitable for being incorporated in an overall inverse kinematics for the whole robot.

Rather than trying to develop and implement sophisticated methods using the analytical approach for the forward and inverse kinematics, we have considered the situation within applications. The advantages are as mentioned that singularities are avoided and that the movement is incremental. However, there is a demand for the kinematics to be modular and thus easily reconfigurable. Moreover, it is desirable to have an easy to understand user definition of the kinematics within each new module.

Our chosen approach is a straightforward generalization of the inverse Jacobian method for serial robots. Recall, that the classical Jacobian for serial robots relates an infinitesimal joint angle change dq to an infinitesimal translation and rotation of the tool through the Jacobian J as

$$J(q(t))dq = dY \tag{1}$$

where dY is a vector of dimension $\lambda \leq 6$ where λ is the dimension of the space in which the tool link can move with respect to the base (e.g. $\lambda = 3$ for planar substructures and $\lambda = 6$ for general movements in 3 dimensional space). For the typical case $\lambda = 6$, one may write $dY = (dp, d\phi)^T$ where dp is the displacement of the tool frame with respect to the base frame and $d\phi$ is the desired tool frame rotation around the base frame given as a signed vector along the rotation axis (fixed in the base frame) with length equal to the size of the rotation. This method can be generalized directly to a parallel manipulator consisting of a moving platform suspended from a fixed platform through $L > 1$ independent legs. Throughout this paper we assume that the way the moving platform is suspended satisfies the classical mobility criteria

$$\beta \equiv \sum_{k=1}^{L} \beta^{(k)} = F + \lambda(L-1)$$

$$\lambda \geq \beta^{(k)} \geq F \tag{2}$$

where $\beta^{(k)}$ denotes the total number of one degree of freedom joints in each leg k, F is the number of degrees of freedom of the moving platform with respect to the fixed platform and β is the total number of joints.

We may now consider the serial kinematics from a reference frame in the fixed platform to a reference frame in the moving platform through each of the legs. We then get

$$\begin{aligned} J_1(q^{(1)})dq^{(1)} &= J_2(q^{(2)})dq^{(2)} = \dots \\ &= \dots = J_L(q^{(L)})dq^{(L)} = dY \end{aligned} \tag{3}$$

where dY is defined in the same way as above and $J_k(q^{(k)})$ is the Jacobian matrix for the kinematics through link k given by the joint angles $q^{(k)})$ of link k. Writing $(q^{(1)}, \dots, q^{(L)})^T \equiv q$ and $(dq^{(1)}, \dots, dq^{(L)})^T \equiv dq$, we may formally establish the equation, which is equivalent to Eq.(1) for serial robots as

$$J(q)dq = dx_\lambda \tag{4}$$

where

$$dx_\lambda = \begin{bmatrix} 0_{\lambda(L-1)} \\ dY \end{bmatrix}$$

and where we can write $J(q)$ as a block matrix:

$$J(q) = \begin{bmatrix} J_1 & -J_2 & 0 & \dots & \dots & \dots & 0 \\ 0 & J_2 & -J_3 & 0 & \dots & \dots & 0 \\ & & & \dots & & & \\ & & & \dots & & & \\ & & & \dots & & & \\ 0 & \dots & \dots & \dots & 0 & J_{L-1} & -J_L \\ 0 & \dots & \dots & \dots & 0 & 0 & J_L \end{bmatrix}$$

We thus have λL equations in the β unknowns in dq. From Eq.(2), we get that $\beta \leq \lambda L$ and that $\beta = \lambda L$ if and only if $F = \lambda$. There are thus at least as many rows in $J(q)$ as there are columns, so $J(q)$ has full rank if and only if the columns are linearly independent. It is easy to see that the columns of $J(q)$ are linearly independent if and only if the columns of each of the $J_k(q^{(k)})$'s are linearly independent. Thus, $J(q)$ has full rank if and only if each of the $J_k(q^{(k)})$'s have full rank, which is equivalent to a situation where none of the legs are in a singular configuration. When using the Jacobian formulation for the inverse kinematics problem in connection with incremental movements we thus always obtain a set of non-singular linear equations with a unique solution for the joint changes. Notice that when $F < \lambda$, this solution must be obtained using a pseudo inverse such as e.g. the Moore-Penrose inverse. In practice, the incremental steps are small but finite. Therefore, the above formulation is incorporated into an iterative (Newton-Raphson like) scheme where we need to compute the forward kinematics through each leg in each step to derive a new right hand side. As the linearized model has a unique solution and as the increments are small, the true nonlinear kinematic model will also in practice always have a unique

solution. It should be noticed that the matrix for determining the un-actuated joints in the forward kinematics is the square matrix obtained by removing the last λ rows and the F columns corresponding to the actuated joints from $J(q)$. It is then easily seen that this matrix is nonsingular whenever $J(q)$ has full rank meaning that also the forward kinematics problem has a unique solution when considering incremental moves.

Consider now the situation, where N modules (some of them may have open loop kinematics) are connected in a chain. Let now $J^{(i)}(q^{(i)})$ denote the Jacobian of the i'th module as defined above. Assume now that we write this Jacobian as

$$J^{(i)}(q^{(i)}) \equiv \begin{bmatrix} J_1^{(i)}(q^{(i)}) \\ J_2^{(i)}(q^{(i)}) \end{bmatrix}$$

where $J_2^{(i)}$ contains the last λ rows of $J^{(i)}$ and $J_1^{(i)}$ the remaining $\lambda(L-1)$ rows (thus there are no rows in $J_1^{(i)}$ if the i'th module has open loop kinematics). Let now $H^{(i)}(q)$ be the matrix that relates a given tool displacement dY seen in the base frame of the i'th module to the same displacement seen in the overall base frame. It can then easily seen that we may obtain an overall relation

$$j(q)dq = dx_\lambda$$

where the $\lambda L \times \beta$ dimensional matrix $j(q)$ now is defined as

$$j(q) = \begin{bmatrix} j_1^{(1)} & 0 & 0 & \dots & \dots & \dots & 0 \\ 0 & j_1^{(2)} & 0 & 0 & \dots & \dots & 0 \\ & & & \dots & & & \\ & & & \dots & & & \\ & & & \dots & & & \\ 0 & \dots & \dots & \dots & 0 & 0 & j_1^{(N)} \\ j_2^{(1)} & j_2^{(2)} & \dots & \dots & \dots & \dots & j_2^{(N)} \end{bmatrix}$$

where the 6 last elements in dx_λ contain the displacement and rotation of the overall tool frame measured in the overall base frame and where all the other elements are zero. Furthermore, we have defined $j_1^{(i)}(q^{(i)}) = J_1^{(i)}(q^{(i)})$ and $j_2^{(i)}(q^{(i)}) = H^{(i)}(q)J_2^{(i)}(q^{(i)})$.

Although the formulation may seem complicated, it has not been difficult to implement. Furthermore, it should be observed that once it is implemented, it is easy to reconfigure for new parallel manipulators. To illustrate how simple the configuration is, we wish to point out that the whole kinematics of each module is configured through a file interface where we use the well known Denavit-Hartenberg formulation. The file has the following simple format

L
$\beta^{(1)}\ \beta^{(2)}$ ... $\beta^{(L)}$

$\theta_1^{(1)}\ d_1^{(1)}\ a_1^{(1)}\ \alpha_1^{(1)}\ \xi_1^{(1)}$
....
$\theta_{\beta^{(1)}}^{(1)}\ d_{\beta^{(1)}}^{(1)}\ a_{\beta^{(1)}}^{(1)}\ \alpha_{\beta^{(1)}}^{(1)}\ \xi_{\beta^{(1)}}^{(1)}$
....
....
....
$\theta_1^{(L)}\ d_1^{(L)}\ a_1^{(L)}\ \alpha_1^{(L)}\ \xi_1^{(L)}$
....
$\theta_{\beta^{(L)}}^{(L)}\ d_{\beta^{(L)}}^{(L)}\ a_{\beta^{(L)}}^{(L)}\ \alpha_{\beta^{(L)}}^{(L)}\ \xi_{\beta^{(L)}}^{(L)}$

$T_{Fixed,1}$
$T_{Fixed,2}$
...
$T_{Fixed,L}$

$T_{Moving,1}$
$T_{Moving,2}$
...
$T_{Moving,L}$

where $T_{Fixed,j}$ is the fixed transformation from the reference frame of the fixed platform to the Denavit-Hartenberg coordinate system for the base of the j'th leg and $T_{Moving,j}$ is the fixed transformation from the frame of the reference frame of the moving platform to the Denavit-Hartenberg coordinate system for the tool of the j'th leg and where the $\theta_i^{(j)}$,$d_i^{(j)}$,$a_i^{(j)}$,$\alpha_i^{(j)}$'s are the Denavit-Hartenberg parameters for the transformation from $T_{Fixed,j}$ to $T_{Moving,j}$ through the j'th leg viewed as a serial arm. Finally, it should be noticed that $xi_i^{(j)}$ is one if joint i in the j'th leg is rotational and zero if it is prismatic.

4 Calibration

An important problem that must be solved before a parallel robot is of any use for industrial applications is the calibration of the robot. For serial robots there are various excellent methods that all give good results. However, for parallel robots the result has been not quite so promising. The reason is that the impact of parameter change on the configuration of the moving platform may be low, which makes it difficult to estimate that parameter. However, the main goal is not necessarily to find accurate estimates of all parameters. The goal is rather to find parameters that lead to a sufficiently accurate result for the position and orientation of the moving platform. Various methods for such calibration using an external measurement system have been proposed (see e.g. (Geng94), (Nahvi96), (Oliviers95), (Vischer98), (Zhuang96)). In our work, we have used the precise external measurement system Rodym 6D manufactured by the company Krypton Ltd. which for our purpose is sufficiently accurate. We have used a large number of poses to suppress noise and to ensure that all important parameters are approximated sufficiently well. We shall now give a brief outline of our chosen calibration method.

The first step is to consider each leg as a serial manipulator connecting the base to the tool and to derive a set of independent

calibration parameters for that leg using the classical approaches for serial robots. It should be pointed out that these are essentially a subset of the parameters from the kinematic input file of the previous section. The result of the calibration will therefore be extremely easy to incorporate into the kinematics. Let now $p^{(j)}$ denote these parameters for the j'th leg. By considering the forward kinematics for the j'th leg, we may derive an extended Jacobian

$$J(q^{(j)}, p^{(j)})[dq^{(j)} dp^{(j)}]^T = dY$$

where dY is defined as in the previous section and we now have allowed the static kinematic parameters to vary. We may then establish a Jacobian for the whole manipulator $J(q, p)$ using exactly the same idea as in the previous section. If the number of components in p is denoted by M, the matrix $J(q, p)$ will be $\lambda L \times \beta + M$ dimensional. Assume now that we make K measurements where we obtain deviations $dY_1, \ldots, dY_K$ between the moving platform configuration from the un-calibrated model and the moving platform configuration from the measurements. For each of the unknown un-actuated joint values, the deviation must be assumed to be different from experiment to experiment. We thus get $K\lambda L$ equations in $(\beta - F)K + M$ unknowns. By choosing K so that $K(\lambda L - \beta + F)/M >> 1$, we get a strongly over determined set of equations for a good determination of the parameter modifications dp. We use Singular value decompositions to suppress problems due to indeterminable or dependent parameter changes.

In the DT-VGT module, we have as mentioned $F = L = 3$ and $\lambda = 6$. The number of independent parameters in a single chain was 19, so the total number of parameters $M = 57$. As $\lambda L - \beta + F = 6$, we get that $6K >> 57$ and we have therefore chosen $K = 50$ random configuration of the actuator positions. As model validation, we have used $K = 50$ other actuator positions. We were capable of using the calibration to suppress all errors that had some regularity (correlation with the configuration of the PKRM). However, we still have some errors of size approximately $1/3$ of the size before calibration. These errors have a structure that very much looks like white noise. We expect them to be due to vibrations in the PKRM during the calibration experiment - a problem that as described in the next section will be solved very much.

5 Embedded modular control

The purpose of embedded modular control is to establish the PKRM as fully modular components that can be assembled into manipulators in various ways. When designing a control system for a potentially industrial robot system based on different mechanical modules, we are faced with various demands:

- The control system must be based on a network of embedded control modules, in order to utilize the inherent mechanical modularity.
- The technology of the embedded modules must be flexible enough to adapt to a wide range of sensors and actuators in order to ensure compatibility with current and future mechanical modules.
- It must be feasible to minituarize the technology of the embedded controller, in order to ensure compatibility with physically small mechanical modules.
- The embedded technology must have sufficient *real-time* computing and communication bandwidth to support demanding control systems.
- It must be feasible to use the embedded computer technology in industrial environments.
- The network technology and embedded software should support self configuration of the system, when the mechanical modules have been configured and turned on.

We have not been able to identify any existing standard system, capable of supporting all these demands. Typical industrial computer systems rely on physical modules, eg. C-PCI, VME, IP and PC-104. to establish a flexible and reconfigurable system, but this method is space consuming, and often results in redundant functionality, as there is seldom a one-to-one mapping between requirements and capabilities of existing modules.

In order to meet the technological demands, we are looking towards a combination of technology from conventional industrial automation, Programmable Gate Arrays (FPGA's), and the multimedia industry.

We are implementing the analog/digital front-end towards sensors and actuators, using conventional industrial components, such as buffers, A/D and D/A converters, transceivers etc.

Instead of using conventional peripheral units, we are implementing the digital part of our I/O system with programmable gate arrays (FPGA's), using the specification language VHDL. By implementing an array of VHDL modules, for different I/O applications, we have made a 'virtually modular I/O system', that can be adapted to new sensors and actuators. As the FPGA technology allows us to implement very complex digital state machines, we are actually using the FPGA as a customizable I/O processor, relieving the embedded computer of many of the traditional CPU intensive I/O tasks.

Using FPGA technology instead of conventional peripheral units, gives us a great flexibility when choosing CPU architecture. The FPGA can easily be configured to work with virtually any CPU on the market. An independence we are using to experiment with state of the art DSP technology for the embedded control computers.

The control algorithm running on the embedded controllers has until now been a simple PD-control, where we have had to sacrifice accuracy in order to obtain stability at the eigenfrequencies of the mechanism. We have now been able to model the complicated behavior of the hydraulic actuators leading to these

eigenfrequencies and are going to design a new model-based control strategy that will increase accuracy.

6 Incorporation into a manipulator

One of the main objectives for the DT-VGT development has been to create them as fully modular subcomponents that can be incorporated into a long reach manipulator which will be used for welding in confined areas in shipbuilding (Sørensen01). The development of this manipulator is carried out in the collaborative R&D project ”Dockwelder” funded by the European Commission under the 5th framework program. The project consortium consists (apart from us) of Odense Steelshipyard, the Italian shipyard Fincantieri and technology providing companies from France and Germany. The manipulator consists of a telescopic placer mechanism. Mounted at the tip of the placer mechanism is two DT-VGT modules. At the tip of the outermost DT-VGT module, a conventional welding robot is placed. This will probably be a Motoman SV3 robot. All the problems discussed in the previous sections (design, kinematics, calibration, embedded control) are crucial for the DT-VGT modules to operate in the Dockwelder manipulator.

In Figure 5, we show a CAD model of the two DT-VGT modules and the conventional robot without the placer mechanism. This manipulator is currently being developed and it will be tested for its potential industrial reliability and accuracy ultimo 2002 as a subgoal of the Dockwelder project which will terminate ultimo 2003.

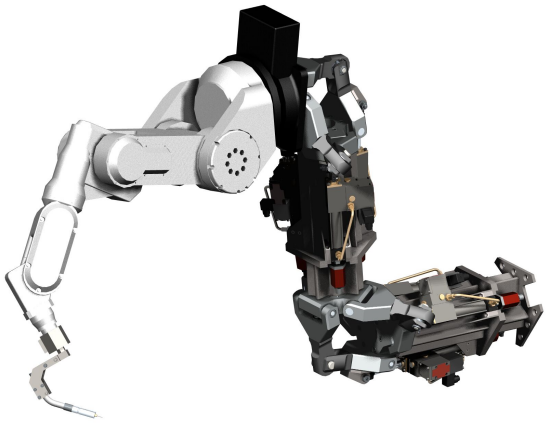

Figure 5: A sketch of the Dockwelder manipulator

7 Conclusion

We have presented our technological achievements towards the industrial usage of PKRM’s. We have shown a successful design using the DT-VGT topology that takes workspace as well as payload considerations and requirements into account. We have presented the kinematics used based on the Jacobian approach which has been proven to be an excellent choice with respect to generic and modular properties. We have discussed the incorporation of our PKRM technology into a modular industrial long-reach manipulator.

Future important research areas will be the modeling of deflections and vibrations of the PKRM’s. The problem of deflection modeling can actually be viewed as a generalization of the calibration problem where the static parameters estimated during calibration are allowed to be strain able. A deflection model is already being developed in connection with the Dockwelder project. Vibration modeling is on the other hand a rather different issue which is coupled much more to the process control and is an issue for future research.

References

[Merlet00] J-P Merlet, “Parallel robots”, ISBN 0-7923-6308-6, Kluwer, 2000

[Salerno94] R.J. Salerno and C.F. Reinholtz, “A modular, Long-Reach, Truss-Type Manipulator for Waste Storage Tank Remediation”, *Robotics: Kinematics, Dynamics and Controls*, DE-Vol. 72, pp. 153-159, 1994

[Jakobsen98] O.G. Jakobsen, S.A. Larsen, N. J. Jacobsen and A. S. Srensen, “Design of Double-octahedral VGT Manipulators”, *VDI BERICHTE 1427, Neue Maschinekonzepte Mit Parallelen Strukturen Fur Handhabung Und Produktion*, pp. 201-220, 1998

[Canfield97] S.L. Canfield, “Development of the Carpal Robotic Wrist”, Ph.D. dissertation, Department of Mechanical Engineering, Virginia Polytechnic and State University Blacksburg, 1997

[Faugere95] J.C. Faugere and D. Lazard, “The combinatorial classes of parallel manipulators”, *Mechanism and Machine Theory*, 30(6), pp. 765-776, 1995

[Raghavan95] M. Raghavan and B. Roth, “Solving polynomial systems for the kinematic analysis of robot manipulators”, *ASME J. of Mechanical Design*, 117(2):71-79, 1995

[Dietmaier98] P. Dietmaier, “The Stewart-Gough platform of general geometry can have 40 real postures”, *ARK (Strobl)*, pp. 7-16, 1998

[Innocenti92] C. Innocenti,“Algorithms for kinematic calibration of fully parallel manipulators”, *In Computational kinematics (edited by J-P Merlet and B. Ravani)*, pp. 241-250, Kluwer 1995

[Innocenti95] C. Innocenti and V. Parenti-Castelli,“Singularity free evolution from one configuration to another in serial and fully parallel manipulators”, *22nd Biennial Mechanisms Conf.*, pp. 553-560, 1992

[Wenger98] P. Wenger and D. Chablat,"Workspace and assembly models in fully parallel manipulators: a descriptive study", *ARK (Strobl)*, pp. 117-126, 1998

[Geng94] Z. Geng and L.S. Haynes, "An effective kinematics calibration method for Stewart platform" *ISRAM (Hawaii)*, pp. 87-92, 1994

[Nahvi96] A. Nahvi and J.M. Hollerbach, "The noise amplification index for optimal pose selection in robot calibration", *IEEE Int. Conf. on Rob. and Aut.*, pp. 647-654, 1996

[Oliviers95] M.P. Oliviers and J.R.R. Mayer, "Global kinematic calibration of a Stewart platform", *ASME DSC*, 57(1), pp. 129-136, 1995

[Vischer98] P. Vischer and R. Clavel, "Kinematic calibration of the parallel Delta robot", *Robotica*, 16(2), pp. 207-218, 1998

[Zhuang96] H. Zhuang and L. Liu, "Self calibration of a class of parallel manipulators", *IEEE Int. Conf. on Rob. and Aut.*, pp. 994-999, 1996

[Sørensen01] ,"A.S. Sørensen, H.G. Petersen, N.J. Jacobsen and O.G. Jakobsen", *A development of parallel robotic modules for long reach applications*, In Proc. of the 32nd Int. Symposium on Robotics, Korea, 2001

Proceedings of the WORKSHOP on
Fundamental Issues and Future Research Directions for Parallel Mechanisms and Manipulators
October 3–4, 2002, Quebec City, Quebec, Canada
Clément M. Gosselin and Imme Ebert-Uphoff, editors

Reconfigurability of a Parallel Manipulator: A Case Study

Jungwon Yoon and Jeha Ryu
Department of Mechatronics
KwangJu Institute of Science and Technology (K-JIST)
1 Oryong-dong, Puk-gu, Kwangju 500-712, Korea
Tel: +82-62-970-2389, Fax: +82-62-970-2384, E-mail: ryu@kjist.ac.kr

Abstract: *This paper describes a case study for reconfigurability of a parallel manipulator, which had been suggested as a haptic device. A parallel mechanism can be reconfigured only by relocating actuators and/or by changing the direction of a revolute joint with adding a simple extra part. The motivation for this investigation is to select the best layout that best fits the task requirements among several rearrangeable configurations.*

1 Introduction

Advanced robot application may demand high versatility of a manipulator system for accommodating a wide range of tasks. Reconfiguration of manipulator mechanism hardware can be one solution to satisfy these needs by using modular type links and joints. Modular design has already been pursued for serial mechanism robots [1-5] and for parallel mechanism robots [6,7]. Ji and Song [6] addressed design and construction of the Stewart-Gough platform manipulator and discussed such issues as its adjustment, calibration, and operation. Yang et al. [7] also presented design consideration and kinematic modeling for modular reconfigurable parallel robots.

Among many robot system applications, haptic interface has been one popular application area with the development of the virtual reality (VR) technology [8]. Many types of haptic mechanisms have been developed [9]. Among these, Long and Collins [10] and Iwata [11] proposed 6-dof tool type haptic devices with a parallel mechanism, which has 3-pantograph linkages, each of which is attached to one mid-point of an equilateral base triangle through a passive revolute joint so that motors must rotate together with the mechanism. At the top, each pantograph is connected with one vertex of a top equilateral triangle through a three-dof ball-and–socket joint. Woo et al. [12] made a force feedback device for telesurgery. This device has five bars instead of pantograph linkages for easier construction.

Recently, Yoon and Ryu [13] designed a parallel mechanism (K-Joystick I) with the motors fixed on the ground for low inertia in order to improve dynamic characteristics. Basically, this mechanism has the same parts as those of predecessor mechanisms. Main difference lies in the location of spherical and revolute joints (see Fig. 1), which causes big difference in kinematic and dynamic characteristics.

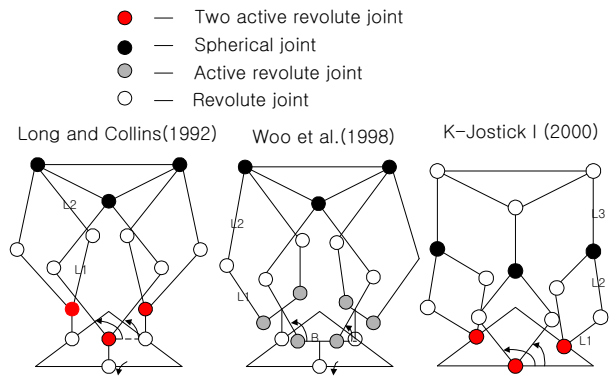

Fig 1. Different Mechanisms by Different Joint Layouts

One particular feature of the Yoon and Ryu's mechanism is that the mechanism can easily be reconfigured only by adding extra part or by changing the joints or the positions of actuators. This rearrangeable parallel manipulator consists of a collection of individual standard actuators, passive joints, rigid links, and end-effectors so that its kinematic characteristics can be adjusted by reconfiguration for a diversity of task requirements.

This paper describes briefly a case study for reconfigurability of a parallel manipulator. The following section describes a schematic diagram of what we call "base configuration" as well as detailed joints. Section 3 presents modular links and additional parts for reconfiguration. Then Section 4 discusses mechanism rearrangement from the base

configuration. Finally, the last section presents conclusions and discussions.

2. Mechanism description of base configuration

A base configuration of the parallel mechanism (K-Joystick I) that is designed for haptic device is composed of three-pantograph mechanisms that are driven by six base-fixed servomotors (Fig.2). The pantograph mechanisms move perpendicularly to the base plate. There are three RRR type spherical joints (Fig.3) between the top of the pantograph mechanisms and connecting bars, and three revolute joints connect bars with a mobile platform.

The three pantographs have 2-dof motions on the $Y_{pi}-Z_{pi}$ plane. Lower links of pantograph are denoted by L_1 and upper links by L_2. A connecting bar is denoted by L_3. Circle radius of the top plate is defined by R_1. The points M_i, Q_i, and E_i denote the positions of active revolute, passive spherical, and passive revolute joints, respectively. The three revolute joints are attached to the top plate and centered on a circle of radius R_1 with the angle γ_i (0, 2π/3, and 4π/3 radians), which specifies rotation angles about the $Z_{o'}$-axis from the $X_{o'}$-axis.

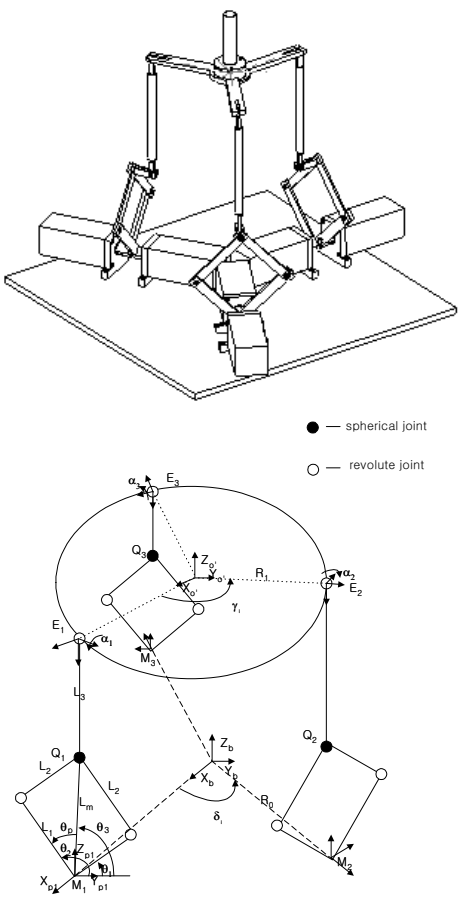

Fig 2. Base Configuration (K-Joystick I)

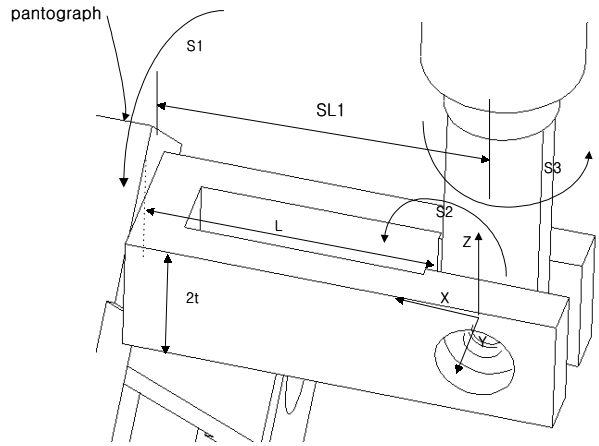

Fig 3. RRR type Spherical Joint

3.Modular parts of parallel manipulator

The modular rigid links are designed to connect modular ball bearing joints so that a set of links with a few geometrical shapes and dimensions may be assembled for different manipulator arrangements. A pantograph or five-bar mechanism can be made of part A and part B shown in Fig. 4(a)-(b). The lower part of the pantograph mechanism is composed of part A while the upper part of pantograph mechanism is composed of part B. Part A is used to connect actuator and part B is used to connect spherical joint. A connecting bar (Fig. 4(c)) is designed to connect a spherical joint with the mobile platform. A RRR type spherical joint is designed to enhance the operating range of 3-axis rotation. Fig. 5 shows that an additional part that can be inserted to the mobile platform is designed to change the direction of a revolute joint at the mobile platform for mechanism rearrangement.

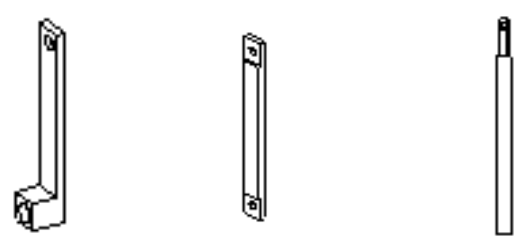

(a) Part A (b) Part B (c) Connecting bar

Fig 4. Modular Links

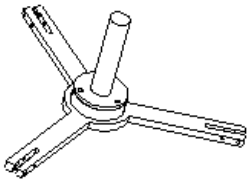

(a) base mobile platform

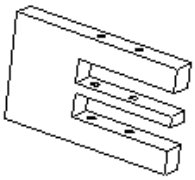

(b) additional part

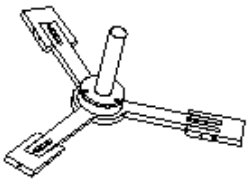

(c) mobile platform with aditional part

Fig 5. Additional part to change direction of revolute joint

4.Mechanism rearrangement

The base configuration of a parallel manipulator can be rearranged with the modular links, joints, and additional parts. Consider first the 6-DOF and nonredundant parallel mechanism rearrangement. For example, the base mechanism with pantograph (Fig.6 (a): type 1) can be rearranged to five bar arrangement (Fig.6 (b): type 2) only by reorienting actuators. This rearrangement is good for more compact design in base because all actuators are located inside a base circle. This rearrangement has similar structure with the haptic device of Woo [12] in array of fivebar mechanisms. In the case of haptic device of Long and Collins [10], they will have more difficulty to rearrange this configuration due to the use of cable transmissions to drive pantograph mechanism.

Moreover, since all joints of the parallel mechanism are revolute joints, the direction of the revolute joint can be changed with an additional part. Using these properties, other arrangement such as type 3 (Fig.6 (c)) can be assembled from the base mechanism. This rearrangement has similar structure with the haptic device of Iwata [11] in the array of pantograph mechanisms.

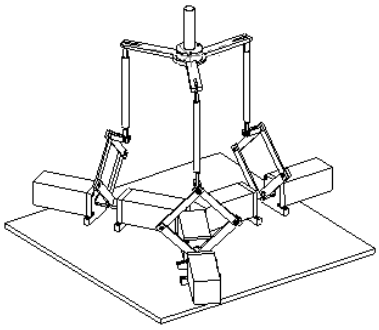

(a) type 1

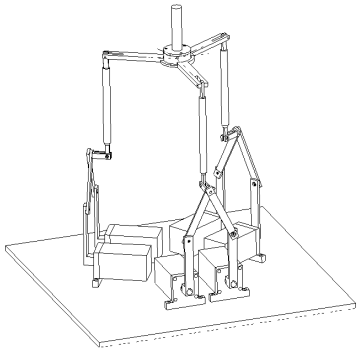

(b) type 2

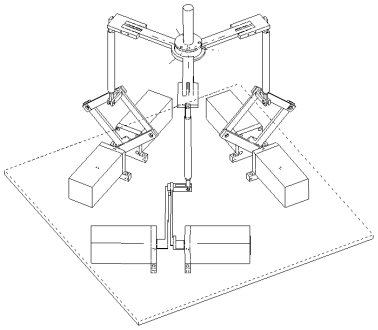

(c) type 3

Fig 6. 6 dof Reconfiguration

Second, some parts from the 6dof mechanisms are removed to make lower dof mechanisms. Some 3dof examples of this reconfiguration are shown in Fig. 7. Note that for the haptic device of Woo et. al [12], this kind of rearrangeability is difficult due to the ball and socket type spherical joint that can not separated into three individual axes.

This rearrangeability of a parallel mechanism is good for more versatile usage of the mechanism in different situations where different performance is required. Note that even though we presented rearrageability of a particular mechanism, many other parallel mechanisms can be rearranged easily in a similar fashion.

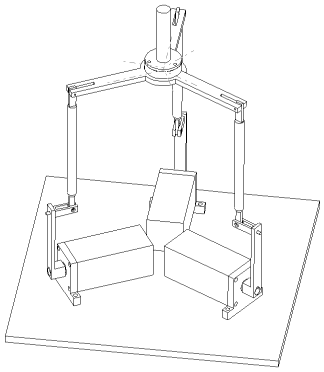

(Case1)

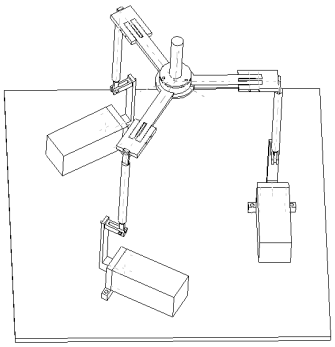

(Case 2)

Fig 7. 3 dof Reconfiguration

The motivation for this investigation is to select a haptic mechanism that best fits the conditions of the haptic mechanism among several reconfigurable configurations (mechanism architecture layout and operation pose). For this purpose, the Jacobian matrix of each parallel mechanism had been derived by using the screw theory and performance analyses such as GPI (Glo bal Payload Index), GCI (Global Conditioning Index), orientation workspace, translation workspace, and singularity had been performed to investigate kinematic characteristics. Based on the kinematic performance indices, we could select a mechanism with the best kinematic characteristics [14].

5. Conclusions and Discussions

We showed several types of a rearangeable manipulator, which are made only by relocating actuators and/or by changing the direction of a revolute joint with adding a simple extra part. In order for these reconfigurable mechanisms to be used in practical environment, many issues such as rapid and efficient calibration, easily modifiable control software environment, ease and comprehensive evaluation of kinematic and dynamic characteristic changes, etc. must be resolved.

Acknowledgement
Research reported here was supported by BK21 grant in 2002

6. References

[1] J. Albus, R. Bostelman, and N.Dagalakis, "The NIST ROBOCRANE," J.Robot. Syst., 10(5), 709-724, 1993.

[2] K. Cleary and T. Brooks, " Kinematic analysis of a novel 6-DOF parallel manipulator," Proceedings of the IEEE International Conference on Robotics and Automation, Altlanta, GA. 1993, pp. 708-713.

[3] D. Schmitz, P. K. Khosla, and T. Kanade, "The CMU reconfigurable modular manipulator system, " Thchnical Report, Carnegie Mellon University, CMU-RI-TR-88-7, 1998.

[4] C. J. J. Paredis, H. B. Brown, and P. K. Khosla, " A rapidly deployable manipulator system," Proceedings of the IEEE international Conference on Robotics and Automation, Minneapolis, MN, 1996, pp. 1434-1439.

[5] R. Cohen, M. G. Lipton, M. Q. Dai, and B. Benhabib, "Conecptual design and a modular robot, " ASME J. Mech. Des., 114, 117-125, 1992.

[6] Ji Z. and Song P., " Design of a Reconfigurable Platform Manipulator," J. of Robotic Systems, Vol. 15, No. 6, pp. 341-346, 1998.

[7] Yang G., Chen I-M., and Yeo S. H., " Design Consideration and Kinematic Modeling for Modular Reconfigurable Parallel Robots," 10th World Congress on the Theory of Machines and Mechanisms, pp. 1079-1084, Oulu, June 20-24, 1999.

[8] G.C. Burdea and P. Coiffect, *Virtual Reality Technology*, John Wiley & Sons, Inc. 1994

[9] G.C. Burdea, *Force and Touch Feedback for Virtual Reality*, John Wiley & Sons, Inc. 1996

[10] G. L. Long and C. L. Collins, "A pantograph linkage parallel platform master hand controller for force-reflection," *Proc. IEEE Int. Conf. on Robotics and Automation*, pp. 390-396, 1992.

[11] H. Iwata, "Artificial reality with force–feedback: development of desktop virtual space with compact master manipulator," *Computer Graphics*, Vol. 24, No. 4, pp. 165-170, 1990.

[12] K. Y. Woo, B. D. Jin, and D-S. Kwon, "A 6 DOF Force-Reflecting Hand Controller using the Fivebar Parallel Mechanism, " *Proc. IEEE Int. Conf. on Robotics and Automation*, pp.1597-1602, 1998.

[13] J. Yoon and J. Ryu, "Design and Analysis of a New Haptic Device Using a Parallel Mechanism", IROS, Takamatsu, Japan 2000.

[14] J. Yoon and J. Ryu, "Kinematic Performance Compariso n of Rearrangeable Parallel Manipulator," Proc. Of the3 2nd International Sysmposium on Robotics, Seoul, April 1

Proceedings of the WORKSHOP on
Fundamental Issues and Future Research Directions for Parallel Mechanisms and Manipulators
October 3–4, 2002, Quebec City, Quebec, Canada
Clément M. Gosselin and Imme Ebert-Uphoff, editors

Optimum Design of Parallel Manipulators for Workspace and Singularity Performances

ERIKA OTTAVIANO AND MARCO CECCARELLI
Laboratory of Robotics and Mechatronics
DiMSAT – University of Cassino
Via Di Biasio 43 - 03043 Cassino (Fr), Italy
ottaviano/ceccarelli@ing.unicas.it

Abstract: *This paper presents analysis and design considerations for parallel manipulators. Kinematics properties such as workspace and singularity have been analyzed and then considered for design purposes. Novel formulations are proposed for analysis algorithms and then for optimum design procedures combining the above-mentioned main characteristics. The proposed algorithm has been applied to CaPaMan, a spatial 3-Degree of Freedom (DOF) parallel manipulator.*

1 Introduction

The design of parallel manipulators is one of the challenging subjects of Robotics research in recent years. Indeed, with the development of parallel manipulators for performing several tasks, the introduction of performance index or criteria, which are used to characterize the manipulator, has become of great interest.
Typically a parallel manipulator consists of a moving platform connected by several legs to a fixed platform, usually called base. The paradigm of parallel manipulators is the Gough-Stewart platform, which has 6 DOF, but recently machine industry has discovered the potential applications of parallel manipulators with less DOF, usually 3, 4 or 5. Indeed, the study of this type of parallel manipulators is important. They exhibit interesting features if compared to 6-DOF mechanisms, such as simpler architecture, simpler control system, high-speed performance, low manufacturing and operations cost.
Furthermore, for several parallel manipulators with reduced number of DOF kinematic and singularity analyses can be solved to obtain algebraic expressions, which are well suited for an implementation in optimum design problems.
In general, parallel manipulators performances highly depends on their geometry so that it is of great interest the design problem but only few work can be found in the literature.
Several researchers have already proposed optimum design procedures. Nevertheless, the proposed procedures are focused only on the optimization of one main characteristic of the manipulator, such as dexterity (Gosselin, 1992), kinematic isotropy (Zanganeh and Angeles, 1997), workspace (Parenti-Castelli et al., 1999).
Optimum design procedures have been proposed in order to optimize both position and orientation workspaces in (Ottaviano and Ceccarelli, 2001a; Ottaviano and Ceccarelli, 2001b).
In this work a novel optimum design formulation is proposed to take into account position and orientation workspaces and singularities. The first attempt to combine the above-mentioned design criterion has been proposed in (Ottaviano, 2002).
A numerical example is presented in this work to show the feasibility of the proposed formulation as applied to a spatial 3-DOF parallel manipulator CaPaMan (Cassino Parallel Manipulator), whose prototype has been designed and built at the Laboratory of Robotics and Mechatronics (LARM) in Cassino.

2 A Formulation for an Optimum Design Regarding Workspace and Singularity Performances

A design problem is presented in this paragraph in which multiple criterion have been considered. Three performances have been taken into account: position workspace, orientation workspace and singularity. The aim is to design a parallel manipulator whose position and orientation workspaces are as close as possible to prescribed ones and free from singularity.
In general, a multi-objective optimization problem can be formulated for the optimum design of parallel manipulators as the minimization of a function vector **f** in the form

$$\min \mathbf{f}(\mathbf{X}) \tag{1}$$

subjected to

$$g_k(\mathbf{X}) < 0$$
$$h_l(\mathbf{X}) = 0 \qquad (2)$$

where **X** is the vector of design variables and each component of the objective function is an expression of a design optimum criterion, (Ottaviano, 2002). Each component g_k (k=1,…,m) describes an inequality design constraint, and each component h_l (l=1,…, n) describes en equality design constraint.

Referring to workspace and singularity conditions for parallel manipulators, one can express one or more measures for each of them in the components of **f**.

Therefore, in this paper the general optimum design problem of Eqs. (1) and (2) can be formulated using a multi-objective function with three components f_i that take into account a measure evaluation of position and orientation workspaces, and singularity condition.

One can evaluate workspace by means of its volume and singularity conditions by means measures of the Jacobian matrices.

The analysis of the workspace of parallel manipulators is a difficult problem since the workspace boundary is defined by a set of highly non-linear equations. Indeed, in most of cases, it is very difficult to exactly calculate the workspace volume of parallel manipulator. Discretization methods may be efficient and useful, especially during the design stage.

A formulation for an optimum design of parallel manipulators has been presented in (Ottaviano e Ceccarelli, 2001a). The authors have proposed a numerical approximation for the workspace volume by considering the smallest parallelepiped, which completely contains the actual workspace.

The workspace volume can be numerically approximated by considering a parallelepiped workspace volume V*, which can be evaluated by considering the extreme reaches, maximum and minimum, along X, Y and Z-axis, if one consider the position workspace, or the extreme reaches along Euler angles axes, for the orientation workspace.

The proposed procedure has been considered for an optimum design of parallel manipulators with prescribed position and orientation workspaces. In this case the two prescribed parallelepiped volumes for position and orientation workspaces volumes are denoted with V' in Figs. 1 and 2.

An approximation for the evaluation of those workspaces can be obtained by considering V_{pos}* and V_{or}*. Figures 1 and 2 show the proposed numerical approximation of position and orientation workspaces respectively, for the case of CaPaMan manipulator.

The numerical approximation has been used for optimum design purposes. The advantages of this formulation are that it can be used for any type of robot, even serial, by solving its Kinematics and can take into account constraints such as mobility limitation of passive joints and legs interference.

The workspace volume can be numerically approximated by considering the parallelepiped workspace volume V*, which can be evaluated as

$$V^* = \Delta l \, \Delta m \Delta n \qquad (3)$$

in which Δl, Δm and Δn are respectively the difference between the extreme reaches, maximum and minimum, along X, Y and Z-axis, (Ottaviano e Ceccarelli, 2001a), if one consider the position workspace. If the orientation workspace is considered Δl, Δm and Δn in Eq. (1) are respectively the difference between the extreme reaches along Euler angles axes, (Ottaviano e Ceccarelli, 2001b). Reachable positions of the reference point are computed by a suitable scanning of the input joint angles within the mobility range.

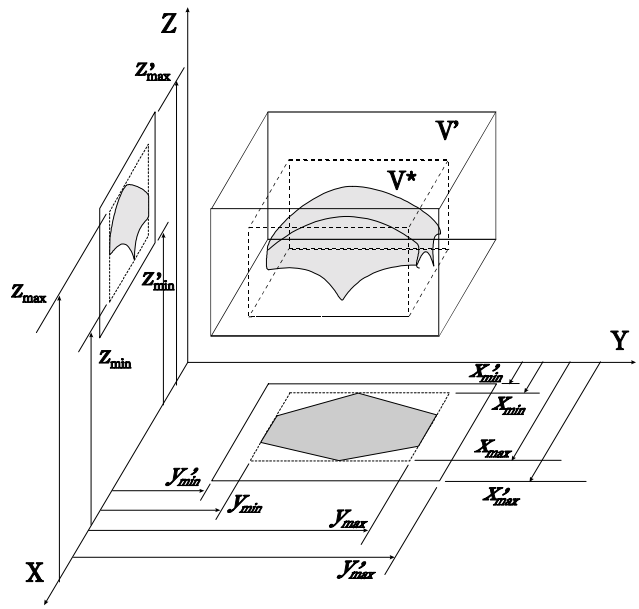

Fig. 1 The proposed numerical approximation for the position workspace volume of CaPaMan manipulator.

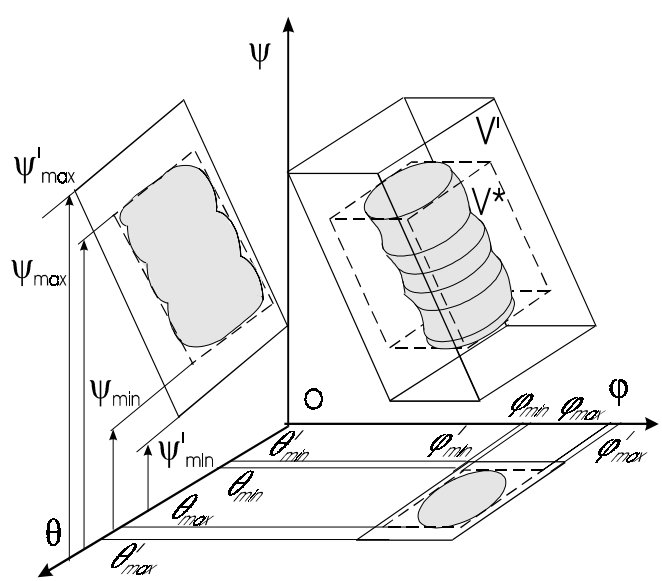

Fig. 2 The proposed numerical approximation for the orientation workspace volume of CaPaMan manipulator.

If one consider the position workspace, Δl, Δm and Δn in Eq. (3) can be evaluated as

$$\Delta l = x_{max} - x_{min}\ ;\ \ \Delta m = y_{max} - y_{min}\ ;\ \ \Delta n = z_{max} - z_{min} \quad (4)$$

If the orientation workspace is considered Δl, Δm and Δn in Eq. (3) can be evaluated similarly to Eq. (4).
One of the important drawbacks of parallel manipulators is that they may lead to singular configurations in which the number of DOFs of the mechanism changes instantaneously. This property has attracted the attention of several researchers because it represents a crucial issue in the context of analysis and design.
Usually singular configurations are represented by surfaces in the configuration space and they can be obtained vanishing the determinant of the two Jacobian matrices J and K. In particular, matrix J is related to the Inverse Kinematics singularities; K is related to the Direct Kinematics singularities, as described in (Gosselin and Angeles, 1990). Last ones are considered to be critical, since they are inside the workspace and in such configurations the manipulator loses its rigidity becoming locally movable, even if the actuate joints are locked. Indeed, in this work Direct Kinematics singularities have been considered for the formulated optimum design.
Analytical expressions for the Direct Kinematics singularities have been obtained for planar parallel manipulators, (Sefrioui and Gosselin, 1992) and for parallel manipulators with reduced number of DOFs, (Parenti-Castelli et al., 1999; Ottaviano et al., 2001).
Usually analytical expressions are difficult to obtain for 6 DOF parallel manipulators, but an interesting algorithm for the determination of the singularities of the general Gough-Stewart platform has been presented in (Mayer St-Onge and Gosselin, 2000). This method gives an analytical expression for the determinant of the Jacobian matrix K.
Therefore, for a general design problem one can consider the analytical expression of the determinant for the Direct Kinematics singularities as a performance criteria. Since the determinant of the Jacobian matrix is configuration dependent, one can obtain design conditions suitably based on its analytical expression.
Therefore, the multi-objective optimization problem can be re-formulated as

$$\mathbf{f}(\mathbf{X}) = \min\left(\max\left(f_1(\mathbf{X}), f_2(\mathbf{X}), f_3(\mathbf{X})\right)\right) \quad (5)$$

with

$$f_1(X) = \left| 1 - \frac{V_{pos}\,*}{V_{pos}\,'} \right|$$
$$f_2(X) = \left| 1 - \frac{V_{or}\,*}{V_{or}\,'} \right| \quad (6)$$
$$f_3(X) = \text{fun}\,(\det\,(K)\,)$$

where "fun" expresses a function of the determinant matrix K and can be conveniently determined for the considered parallel manipulator.
Function **f** (**X**) of Eq. (5) can be subject to design constraints such as

$$a_m \le a_k \le a_M \quad (7)$$

when a_k is a dimensional design parameter that is limited within practical values.
In the proposed formulation it has been considered the two smallest parallelepiped volumes V_{pos}' and V_{or}', which completely contain position and orientation workspaces volumes. An approximation for the evaluation of those workspaces has been considered by considering V_{pos}* and V_{or}*, which can be evaluated by Eqs. (3) and (4), together with the kinematic analysis of the manipulator.
The optimum design problem for objective functions f_1 (X) and f_2 (X) can be formulated as finding the optimal design parameters values such as the position and orientation workspaces are as close as possible to prescribed ones.
Regarding to f_3 (X) a function of the determinant of matrix K. In particular, design considerations can be made in order to obtain architecture free or sufficiently far from Direct Kinematics singularities. These considerations can be deduced by analyzing matrix K, through a function of the its determinant, which has been synthetically expressed by "fun" in Eq. (6).

3 A Case of Study: CaPaMan Architecture

A schematic representation of the CaPaMan manipulator is shown in Fig.1, where the fixed platform is FP and the moving platform is MP. MP is connected to FP through three identical leg mechanisms and is driven by the corresponding articulation points H_1, H_2, H_3.
An articulated parallelogram AP, a prismatic joint SJ and a connecting bar CB compose each leg mechanism. AP's coupler carries the SJ and CB transmits the motion from AP to MP through SJ; CB is connected to the MP by a spherical joint BJ, which is installed on MP. CB may translate along the prismatic guide of SJ keeping its vertical posture and BJ allows MP to rotate in the space. Each plane, which contains AP, is rotated of π/3 with respect to the neighbor one.
Particularly, design parameters of the k-th leg are identified through a_k, which is the length of the frame link; b_k, which is the length of the input crank; c_k, which is the length of the coupler link; d_k, which is the length of the follower crank. The length of the connecting bar is h_k.
The kinematic variables are α_k, which is the input crank angle and s_k , which is the stroke of the prismatic joint. Finally, the size of MP and FP are given by r_p and r_f, respectively, H is the center point of MP, O is the center point of FP, H_k is the center point of the k-th BJ and O_k is the middle point of the frame link a_k, Fig.1.
The motion of MP with respect to FP can be described by considering a world frame O-XYZ, which is fixed to FP, and

a moving frame H-$X_pY_pZ_p$, which is fixed to MP.
To specify position and orientation of the MP with respect to the fixed frame it is necessary to consider six variables, that can be chosen as the Cartesian coordinates of the reference point H and Euler angles φ, θ and ψ, as shown in Fig.1.
A built prototype is shown in Fig. 2 and dimensions of design variables for the built prototype are reported in Table 1.

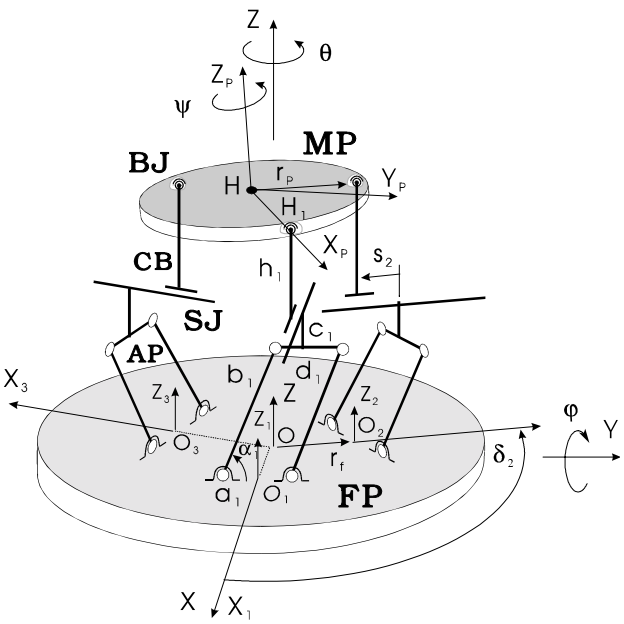

Fig. 1 Kinematic chain and design parameters of CaPaMan.

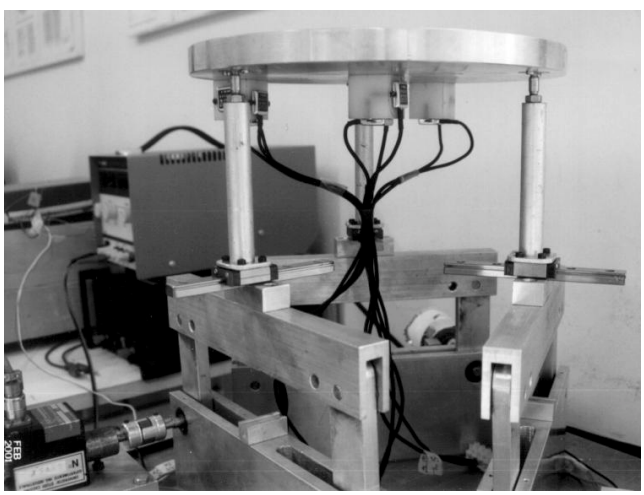

Fig. 2. Prototype of CaPaMan at LARM in Cassino.

Table 1. Design parameters of the built prototype at LARM in Cassino.

$a_k = c_k$ (mm)	$b_k = d_k$ (mm)	h_k (mm)	$r_p = r_f$ (mm)	α_k (deg)	s_k (mm)
200.00	80.00	100.00	109.50	45 ;135	60.00

Velocity equations represent the linear mapping between joint and Cartesian velocities. The differential kinematic relation for parallel manipulators can be expressed in the form

$$\mathbf{J}\dot{\vartheta} = K\mathbf{t} \tag{7}$$

where J and K are two Jacobian matrices of the manipulator. Moreover $d\vartheta/dt$ is the vector of joint rates, $d\vartheta/dt=[d\alpha_1/dt;d\alpha_2/dt;d\alpha_3/dt]^T$. $\mathbf{t}$ is the twist array, a six-dimensional array for spatial tasks given by $\mathbf{t}=[\mathbf{v}_H^T;\boldsymbol{\omega}^T]^T$. The three-dimensional angular velocity vector of the moving platform is $\boldsymbol{\omega}$ and $\mathbf{v}_H$ is the three-dimensional velocity of the operation point H of the moving platform.
Since the mechanism has 3-DOF, only three of the six variables can be specified as function of the input crank angles α_k, (k=1,2,3), for describing the configuration of CaPaMan.
The independent coordinates can be chosen as two rotations about two perpendicular axes intersecting at the mobile platform center, φ and ψ, and a vertical translation, z.
The other dependent coordinates x, y and θ, can be specified by using a proper formulation of the kinematic analysis.
Thus, Eq. (7) can be rewritten as, (Ottaviano et al., 2001)

$$\mathbf{J}\dot{\boldsymbol{\vartheta}} = K\ A\ A_R\ \mathbf{t}_r \tag{8}$$

where A_R expresses the relationship between $\mathbf{t}_r=[d\varphi/dt;d\psi/dt;d\theta/dt]^T$ and dependent coordinates x, y and θ. A is a transformation matrix, (Ottaviano, 2002).
Independent coordinates can be specified as function of the input crank angles only as, (Ceccarelli, 1997)

$$\begin{aligned} z &= \frac{z_1 + z_2 + z_3}{3} \\ \varphi &= \cos^{-1}\left[\pm\frac{2}{3r_P}\sqrt{E}\right] \qquad (z \geq z_1 \Rightarrow +\,;\, z < z_1 \Rightarrow -) \\ \psi &= \tan^{-1}\left[\sqrt{3}\frac{D-F}{D+F}\right] \end{aligned} \tag{9}$$

with

$$\begin{aligned} E &= z_1^2 + z_2^2 + z_3^2 - z_1z_2 - z_2z_3 - z_1z_3 \\ D &= 2z_2 - z_1 - z_3 \\ F &= 2z_3 - z_1 - z_2 \end{aligned} \tag{10}$$

when for k = 1,2,3, one consider

$$z_k = b_k \sin\alpha_k \tag{11}$$

Thus, the Jacobian matrices associated with the CaPaMan manipulator can be written as

$$K_r = K\,A\,A_R = \begin{bmatrix} \frac{6E}{\sqrt{3}} & 0 & 0 \\ 0 & \sqrt{E\left(9r_p^2 - 4E\right)} & 0 \\ 0 & 0 & 3 \end{bmatrix} \qquad (13)$$

$$J = \begin{bmatrix} (D-F)\,b_1 c\alpha_1 & (D+2F)\,b_2 c\alpha_2 & -(2D+F)\,b_3 c\alpha_3 \\ (D+F)\,b_1 c\alpha_1 & -D b_2 c\alpha_2 & -F\,b_3 c\alpha_3 \\ b_1 c\alpha_1 & b_2 c\alpha_2 & b_3 c\alpha_3 \end{bmatrix} \qquad (14)$$

Singularity analysis for CaPaMan manipulator has been carried out in (Ottaviano et al., 2001).
From matrix Kr in Eq. (13) the singularity condition can be expressed as (Ottaviano, 2002)

$$\frac{2\sqrt{E}}{3r_p} = 1 \qquad (15)$$

If $b_i=b_j$, for $i\neq j$, $i,j=1,2,3$, and assuming $u=s\alpha_1$; $v=s\alpha_2$; $w=s\alpha_3$, with $k=1,2,3$, Eq. (15), together with Eqs.(10) and (11), can be written as

$$(u-v)^2 + (u-w)^2 + (v-w)^2 = G \qquad (16)$$

with

$$G = \frac{9r_p^2}{2b_k^2} \qquad (17)$$

Eqs. (16) represent an elliptic cylinder, which divides the configuration space into two regions free from singularities: the region inside and outside the cylinder. Indeed, by properly choosing design parameters values r_p and b_k, it is possible to decide the manipulator to work inside or outside of the cylinder.
Furthermore, Eqs. (16) and (17) give feasible solutions if and only if G is minor or equal to 8. This is due to sine function limitation.
Indeed, by properly sizing the moving platform and crank length to obtain a G value major than 8 one can obtain an architecture for CaPaMan manipulator which is free from singularities.
If one considers an architecture with design parameters of Table 2 it is possible verify by using Eqs. (16) and (17) that the considered architecture has Direct Kinematics singular configurations.
Therefore, a representation of those singular configurations is shown in Fig. 3.

Table 2. Design parameters of a singular architecture of the CaPaMan manipulator.

$a_k = c_k$ (mm)	$b_k = d_k$ (mm)	h_k (mm)	$r_p = r_f$ (mm)	α_k (deg)	s_k (mm)
27.85	90.00	100.00	60.00	45;135	50.00

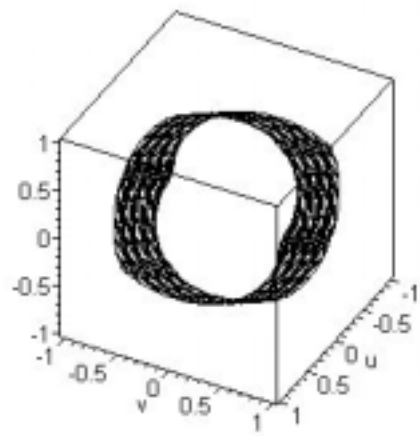

Fig. 3. Direct Kinematics singular configurations in the configuration space for CaPaMan manipulator with design parameters of Table 2.

4 A Numerical Example

The proposed formulation has been applied for the optimum multi-objective design of CaPaMan manipulator by using the vector objective function of Eq. (6) and results of the position and orientation workspaces computations, together with the singularity analysis, which have been reported in (Ottaviano e Ceccarelli, 2001b; Ottaviano et al., 2001).
The design problem can be formulated as contemporaneously minimizing three different objective functions, which for the case of the CaPaMan manipulator assume the form

$$\begin{aligned} f_1(X) &= \left| 1 - \frac{V_{pos}^{\,*}}{V_{pos}^{\,'}} \right| \\ f_2(X) &= \left| 1 - \frac{V_{or}^{\,*}}{V_{or}^{\,'}} \right| \\ f_3(X) &= 8 - G \end{aligned} \qquad (18)$$

The optimum multi-objective design can be subjected to constraints for the position workspace as

$$x_{max} \le x'_{max}\,;\; y_{max} \le y'_{max}\,;\; z_{max} \le z'_{max}\,; \qquad (19)$$

and for orientation workspace

$$\varphi_{max} \le \varphi'_{max}\ ;\ \psi_{max} \le \psi'_{max}\ ;\ \left(\theta_{max}\right)_{\psi} \le \left(\theta'_{max}\right)_{\psi}\ ; (20)$$

We assume $r_p = r_f$, $a_k = c_k$, $b_k = d_k$, so that fixed and movable plates have the same dimensions, and links of the APs have the same dimensions, in order to ensure the characteristic CaPaMan design.

The design value $r_p = r_f$ has also been assumed to avoid prismatic joints with too large values of the strokes s_k. The size of the prismatic guides can be conveniently designed through s_k. a_k parameter has been properly chosen to avoid link interference, as reported in [Ceccarelli e Ottaviano, 2000]. Indeed, design parameters for the optimum design of CaPaMan manipulator are b_k, h_k, r_p, α_{kmin},α_{kmax} and s_k.

The optimum design problem has been defined by Eqs. (18) to (20) and it is highly non-linear. A critical issue for proposed optimum design procedure is the choice of a proper initial guess solution.

For the proposed numerical example we have chosen as initial guess solution an architecture which is quite different from the built prototype and for which exists Direct Kinematics singular configurations.

Indeed, for the initial guess solution the computed value of G given by Eq. (17) is equal to 2.

Position and orientation workspaces volumes can be computed by using the proposed numerical approximation of Eqs. (3) and (4) and the Kinematics of the CaPaMan manipulator, (Ceccarelli, 1997), to give the values of V^*_{pos} and V^*_{or}.

The prescribed position workspace volume V'_{pos} is 192,000 mm^3. The prescribed constraints on position workspace are x_{min} = -40 mm, y_{min} = -40 mm, z_{min} = 150 mm, x_{max} = 40 mm, y_{max} = 40 mm, z_{max} =180 mm.

The prescribed orientation workspace volume V'_{or} is 108,000 deg^3. The prescribed constraints on orientation workspace are ψ_{min} = -90 deg, φ_{min} = 85 degi, θ_{min}= - 90 deg, ψ_{max} = 90 deg, φ_{max} = 95 deg e θ_{max} = 90 deg.

These constraints allow taking into account size and dimensions of the position and orientation workspaces volumes.

The proposed algorithm described in the previous section has been developed in MATLAB code (The Math Works, 1995) for its convenience for manipulating multi-dimensional arrays and for its wide range of visualization capabilities. The "minimax" optimization algorithm of the MATLAB Optimization Toolbox (The Math Works, 1995) has been used to solve optimal parameter values.

The used optimization algorithm minimizes the worst case values of the f_i functions of Eq. (18) at each iteration, by taking into account the constraint equations given by Eqs. (19) and (20). The used optimization algorithm uses a Sequential Quadratic Programming (The Math Works, 1995).

Figures 4 and 5 show the position and orientation workspaces for the optimal architecture of CaPaMan manipulator, whose design parameters are reported in Table 3.

Figure 6 shows the objective functions f_1 (X), f_2 (X) and f_3 (X) during the process which takes 40 iterations.

By observing Fig. 6 it is possible to note that functions f_1 and f_2 are close to zero, indeed the position and orientation workspaces of the optimum designed architecture are close to prescribed ones. In fact, for the optimum designed architecture the position workspace volume is 191,183 mm^3 and the orientation workspace volume is 90,030 deg^3.

Figure 7 shows the position and orientation workspace volumes for the optimum designed architecture.

Figures 8 and 9 show the evolution of design parameters b_k, h_k, r_p, α_{kmin},α_{kmax} and s_k, and parameter a_k.

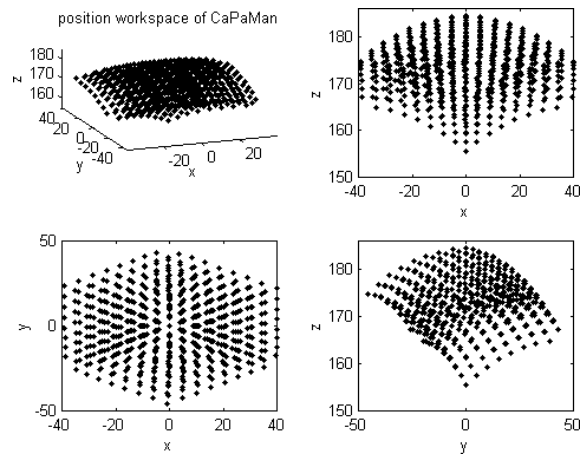

Fig. 4. The position workspace of the optimum designed CaPaMan architecture.

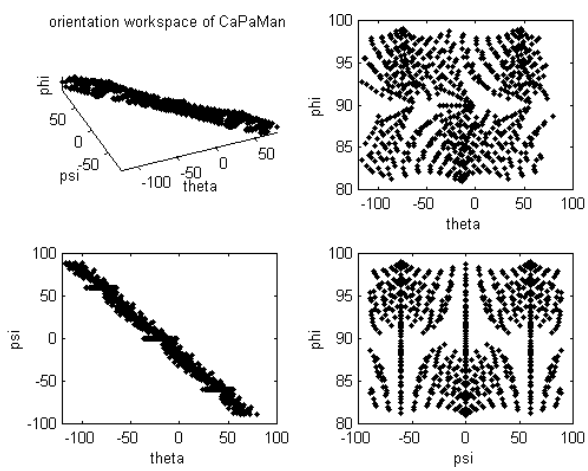

Fig. 5. The orientation workspace of the optimum designed CaPaMan architecture.

Table 3. Design parameters of the optimum designed CaPaMan of Figs.4 and 5.

$a_k = c_k$ (mm)	$b_k = d_k$ (mm)	h_k (mm)	$r_p = r_f$ (mm)	α_k (deg)	s_k (mm)
209.03	108.60	76.33	122.80	93 ;135	50.00

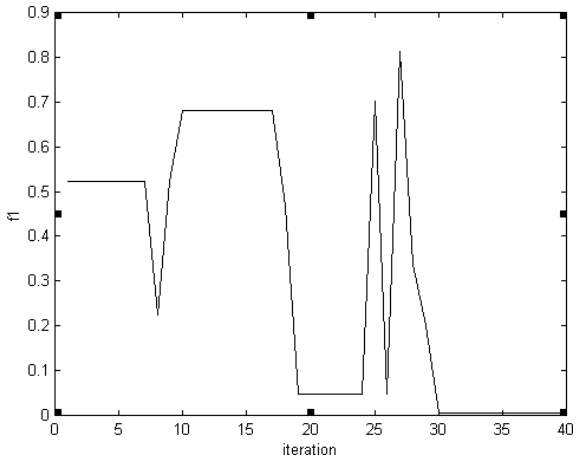

a)

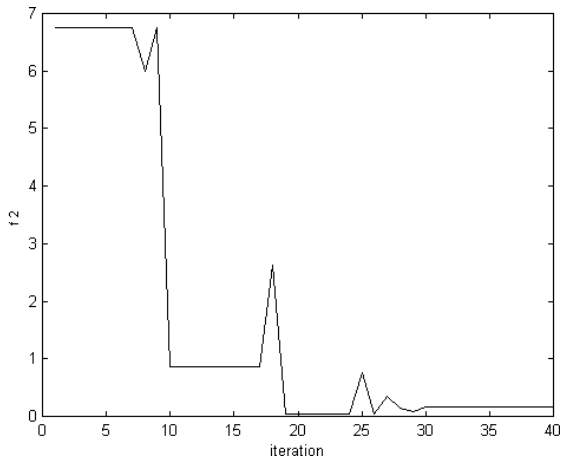

b)

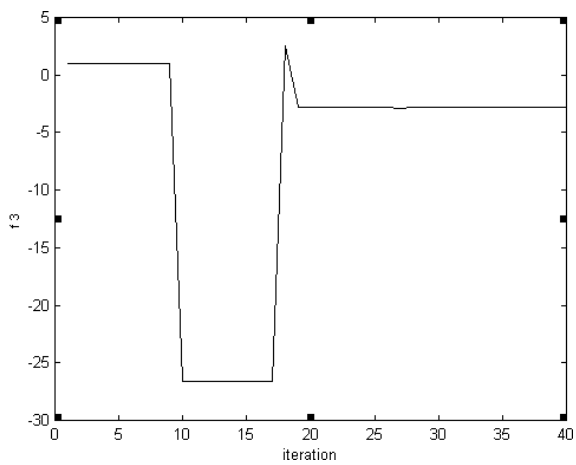

c)

Fig. 6. Evolution of the objective functions versus number of iterations of the case of Figs.4 and 5: a) $f_1=|1-V_{pos}*/V_{pos}'|$; b) $f_2=|1-V_{pos}*/V_{pos}'|$; c) $f_3=8-G$.

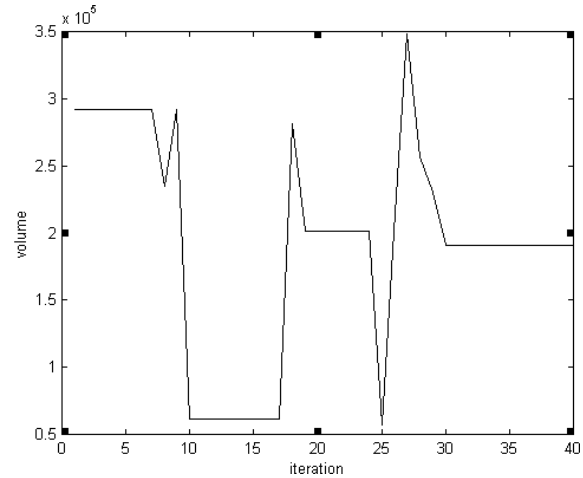

a)

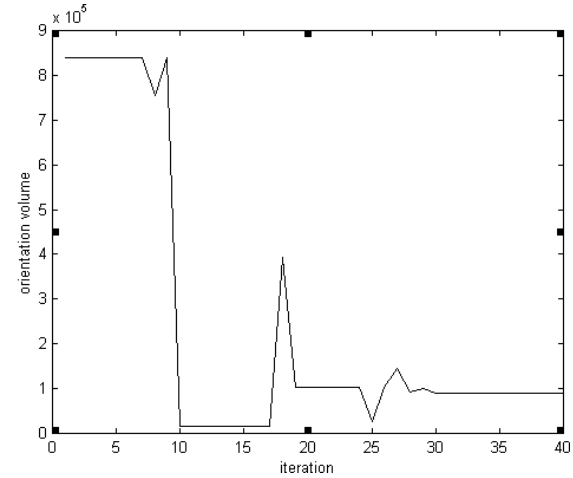

b)

Fig. 7. Evolution versus number of iterations of the case of Figs.4 and 5: a) position workspace volume; b) orientation workspace volume.

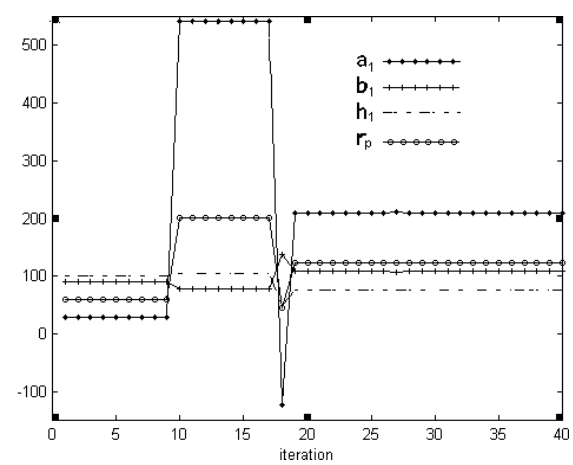

Fig. 8. Evolution of design parameters for the case of Fig.4 and 5: link length a_1; link length b_1; link length h_1; platform size r_p. (lengths are expressed in mm).

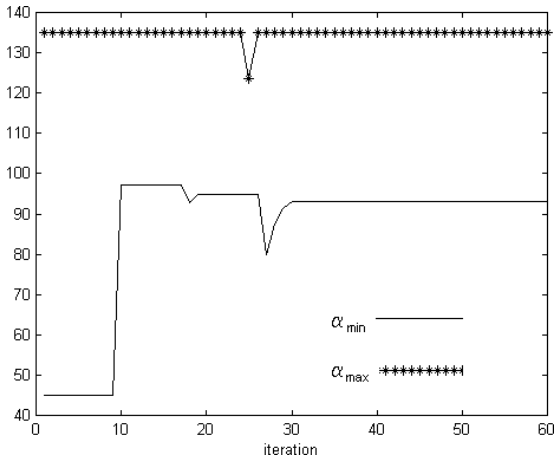

Fig. 9. Evolution of design parameters for the case of Fig.4 and 5: minimum and maximum values for α. (angles are expressed in deg).

5 Conclusion

In this paper a design algorithm for the optimal design of parallel manipulators has been presented. In particular, the proposed formulation represents an integration of the relevant aspects of the dimensional design of parallel manipulators in a multi-objective optimization design by using workspace characteristics and singularity analysis results. A numerical example referring to the architecture of the CaPaMan has been presented to show the feasibility and soundness of the proposed formulation.

References

Ceccarelli M., 1997, “A New 3 dof Spatial Parallel Mechanism”, Mechanism and Machine Theory, Vol.32, No.8, pp. 895-902.

Ceccarelli, M. Ottaviano, E., 2000, “An Analytical Design for CaPaMan with Prescribed Position and Orientation”, Proceedings of the ASME Design Engineering Technical Conference and Computers and Information in Engineering Conference, Baltimore, Paper DETC2000/MECH-14099.

Gosselin C., Angeles J., 1990, "Singularity Analysis of Closed-Loop Kinematic Chains", IEEE Transactions on Robotics and Automation, Vol.6, No.3, pp.281-290.

Gosselin C. M., 1992, “The Optimum Design of Robotic Manipulators Using Dexterity Indices”, Robotics and Autonomous Systems, Vol.9, pp.213-226.

Mayer St-Onge B., Gosselin C. M., 2000, "Singularity Analysis and Representation of the General Gough-Stewart Platform", The International Journal of Robotics Research, Vol.19, No.3, pp.271-288.

Ottaviano E., 2002, ” Optimum Design of Parallel Manipulators", Ph.D. Dissertation, University of Cassino, Cassino, Italy. (in Italian)

Ottaviano E., Ceccarelli M., 2001, “Optimal Design of CaPaMan (Cassino Parallel Manipulator) with Prescribed Workspace”, Proceedings of Computational Kinematics, Seoul, pp35-44.

Ottaviano E., Ceccarelli M., 2001, ”Optimal Design of CaPaMan (Cassino Parallel Manipulator) With Prescribed Position and Orientation Workspace”, 9th International Conference on Control and Automation MED 2001, Dubrovnik, 2001, CD Proceedings, Paper No. Med01-009.

Ottaviano E., Gosselin C. M., Ceccarelli M., 2001, “Singularity Analysis of CaPaMan: A Three-Degree of Freedom Spatial Parallel Manipulator”, IEEE International Conference on Robotics and Automation ICRA2001, Seoul, pp.1295-1300.

Parenti-Castelli V., Di Gregorio R., Bubani F., 1999, “Workspace and Optimal Design of a Pure Tranlation Parallel Manipulator”, Proceedings of the XIV National Congress AIMETA ‘99, Como, Paper No. 17.

Sefrioui J., Gosselin C. M., 1992, "Singularity Analysis and Representation of Planar Parallel Manipulators", Robotics and Autonomous Systems, Vol.10, pp.209-224.

The Math Works, 1995, “Matlab Optimization Toolbox”.

Zanganeh K. E., Angeles J., 1997, “Kinematic Isotropy and the Optimum Design of Parallel Manipulators”, The International Journal of Robotics Research, Vol.16, No.2, pp.185-197.

Proceedings of the WORKSHOP on
Fundamental Issues and Future Research Directions for Parallel Mechanisms and Manipulators
October 3–4, 2002, Quebec City, Quebec, Canada
Clément M. Gosselin and Imme Ebert-Uphoff, editors

General Geometric Algorithms for Optimal Design of Parallel Manipulators

G.F. Liu and Z.X. Li
EE. Department
Hong Kong University of Science and Technology
Clear Water Bay, Kowloon, Hong Kong
Liugf@ust.hk

Abstract: *This paper deals with the problem of optimal design of parallel manipulators which are singularityless, of high stiffness and manipulability and the most economic. By observing that those requirements can be cast into Linear Matrix Inequalities (LMIs), we formulate the design problem as a convex optimization problem subject to LMIs with either a linear function or a max-det function as the objective function. The variables x associated with LMIs are nonlinear functions of some key kinematic parameters α. If the dimension of x, t, is equal to the number of kinematic parameters, l_0, a two level algorithm can be applied to solve for a set of optimal kinematic parameters: (1) Applying the interior point algorithm for solving of x; (2) Applying Newton method to a set of nonlinear algebraic equations for solving of α. If the dimension of x is greater than the number of kinematic parameters (i.e., x are not linearly independent), we consider the constrained semi-definite programming problems and the constrained max-det problems by taking account of an additional set of nonlinear constraints. We propose a simplified constrained gradient algorithm for solving of x in such cases. α derives from x using Newton method. Simulation results verifies the effectiveness of the proposed algorithms.*

1 Introduction

Parallel manipulators with its high stiffness, high accuracy and low inertia characteristics have attracted many researchers in the robotics society. In the past several decades, lots of effort has been spent on design, analysis and control of various types of parallel manipulators [1, 2, 3, 4, 5]. Those work paved ways for design of a parallel manipulator with desired quality.

Optimization the workspace of a manipulator was one of the first considerations when designing a parallel manipulator. Oblak and Kohi [6] studied the manipulator workspace based on the local Jacobian analysis and the boundary surface technic. Stamper, Tsai, and Walsh [7] exploited the Monte Carlo method in determining a set of design variables that result in the largest total manipulator workspace. However, such obtained manipulators may not have good dexterity, good manipulability, and high stiffness. Gosselin and Angeles [8] considered to optimize the local condition number in addition to the workspace of a spherical three DOF parallel manipulator. Park and Brockett [9] proposed global dexterity indices for design of parallel manipulators with the optimal global dexterity. However, the requirement of singularitylessness and high stiffness was not or little considered in those previous research works. Efficient algorithms for design of economic, reliable, and efficient manipulators based on a comprehensive consideration of all those requirements are needed. The main purpose of this paper is to provide such an algorithm. First, we observe that the requirements of singularitylessness, high stiffness and good manipulability can be cast into LMIs. Second, design of a most economic manipulator while satisfying those LMIs can be formulated as a convex optimization problem with a linear function or a max-det function as the objective function. Both cases can be solved by efficient algorithms.

2 Problem Statement

A parallel manipulator as shown in Fig. 1 is regarded as a set of open-chains connected in parallel to a common rigid body, known as the end-effector. The ambient space E of the manipulator is given by the Cartesian product of the joint spaces of all the joints that make up the manipulator. We denote by $\theta \in \mathbb{R}^n$ the local coordinates of E. The loop (or closure) constraints of the manipulator are denoted by

$$H : E \longrightarrow \mathbb{R}^m, \theta \longmapsto H(\theta) = \begin{bmatrix} h_1(\theta) \\ \vdots \\ h_m(\theta) \end{bmatrix} = 0. \quad (1)$$

Note that the loop constraints are obtained by equating pairwise the end-effector positions from each of the open-chains. The preimage $Q := H^{-1}(0)$ is referred to as the configuration space of the manipulator. h_i, $i = 1, \cdots, m$,

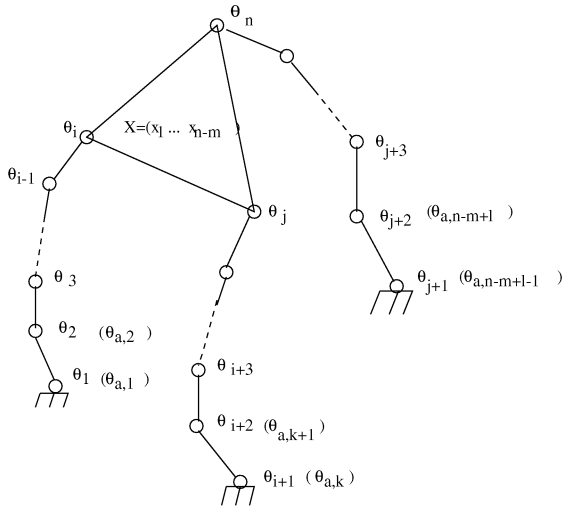

Figure 1: Coordinate systems for a parallel manipulator

are uniquely characterized by a set of kinematic parameters, e.g, the length of links, the position of base joints, and the size of the end-effector. In practice, we may only focus on a subset of those parameters, known as design kinematic parameters (or key kinematic parameters) while fixing the remaining parameters due to some practical restrictions. Note that the design kinematic parameters affect the singularity, stiffness and manipulability properties of a manipulator. Based on this, we state the following optimal design problem. Let $\alpha \in \mathbb{R}^{l_0}$ be the set of design kinematic parameters, $\gamma > 0$, $\Gamma > 0$ be two thresholds. Let $f(\alpha)$ be the objective function which measures the cost of material of the manipulator (may also include some other terms). We denote by K_p, M_p the Cartesian stiffness matrix and the manipulability function of the manipulator, respectively.

Problem 1 Optimal design problem
Find a set of optimal design parameters α such that $f(\alpha)$ is minimal and the manipulator is singularityless while satisfying $K_p \geq \gamma I$, and $M_p \geq \Gamma$. The inequality sign in $K_p \geq \gamma I$ means that $K_p - \gamma I$ is positive semi-definite.

3 Formulating Constraints as Linear Matrix Inequalities

In this section, we transform the constraints due to singularitylessness, high stiffness and good manipulability into Linear Matrix Inequalities as well as a set of additional nonlinear constraints.

3.1 Singularityless Constraints

In this subsection, the distribution of configuration space singularity (or constraint singularity, CS singularity) is found to a function of the key kinematic parameters. Singularityless constraints are then cast as linear inequalities of those parameters which can be sequentially transformed into LMIs.

Given a function $h : E \longrightarrow \mathbb{R}$, its differential, denoted dh and given in local coordinates by

$$dh = \sum_{i=1}^{n} \frac{\partial h}{\partial \theta_i} d\theta_i$$

is a one-form, i.e., $dh(\theta) \in T_\theta^* E$. Physically, an element in $T_\theta^* E$ has the meaning of a generalized force, and its pairing with a generalized velocity vector v in $T_\theta E$ gives the virtual power. In particular, for $v = \sum_{i=1}^{n} v_i \frac{\partial}{\partial \theta_i} \in T_\theta E$,

$$\langle dh, v \rangle = \sum_{i=1}^{n} v_i \frac{\partial h}{\partial \theta_i} := v(h)$$

is the directional derivative of h in the direction v.

We refer the readers to [10] for the definition of $dh_1 \wedge dh_2$, a two-form, known as the wedge product of dh_1 with dh_2, and similarly that of $dh_1 \wedge \cdots \wedge dh_m$, a m-form. In local coordinates,

$$dh_1 \wedge dh_2 = \sum_{i<j} \left(\frac{\partial h_1}{\partial \theta_i}\frac{\partial h_2}{\partial \theta_j} - \frac{\partial h_2}{\partial \theta_i}\frac{\partial h_1}{\partial \theta_j}\right) d\theta_i \wedge d\theta_j.$$

Two functions h_1 and h_2 are said to be linearly independent at $\theta \in E$ if $dh_1(\theta)$ and $dh_2(\theta)$ are linearly independent as two covectors. The latter is translated exactly into the requirement that

$$dh_1 \wedge dh_2 \mid_\theta \neq 0.$$

When $dh_1 \wedge dh_2 = 0$, the intersection of $h_1^{-1}(0)$ with $h_2^{-1}(0)$ is not transversal [11].

Definition 1 *A point $\theta \in Q$ is called a configuration space singularity (or CS singularity) if*

$$dh_1 \wedge \cdots \wedge dh_m \mid_\theta = 0. \tag{2}$$

A basic result of differentiable manifolds [10] shows that if $\forall \theta \in Q$, $dh_1 \wedge \cdots \wedge dh_m \mid_\theta \neq 0$, then Q is a submanifold of dimension $n - m$ of E. To develop a general understanding of CS singularities and their relations with some key kinematic parameters of a parallel manipulator, we apply Morse theory [11] where CS singularities are viewed as the critical points of an appropriately defined function with its value being the design parameter. By varying the design parameter from one critical value to another, we obtain the homotopy classes of the configuration space and useful information on suitable ranges of the design parameter. We assume, for simplicity, that the first $(m-1)$ functions are linearly independent for all $p \in \tilde{Q}$, where $\tilde{Q} = \tilde{H}^{-1}(0)$ and

$$\tilde{H} : E \longrightarrow \mathbb{R}^{m-1}, \theta \longmapsto \begin{bmatrix} h_1(\theta) \\ \vdots \\ h_{m-1}(\theta) \end{bmatrix}.$$

Then, $\tilde{Q}$ is a manifold of dimension $(n - m + 1)$. Let $h_m(\theta) = c$, and define

$$\tilde{h}_m : \tilde{Q} \longrightarrow \mathbb{R}, \theta \longmapsto h_m(\theta) = c$$

to be the restriction of h_m to $\tilde{Q}$. Since the tangent space $T_p\tilde{Q}$ has the form

$$T_p\tilde{Q} = \{v \in T_pE \mid \langle v, dh_i \rangle = 0, \quad i = 1, \cdots m-1\},$$

it is not difficult to see that a point $p \in \tilde{Q}$ is a critical point of $\tilde{h}_m$ if and only if it is a CS singularity. The study of CS singularities is translated into study of the critical points of the Morse function $\tilde{h}_m$. By varying the parameter c over $\mathbb{R}$, we obtain homotopy classes of the configuration space. In the case that the first $(m-1)$ functions are not linearly independent, i.e. $\tilde{Q}$ may be singular, the former procedure can still be performed according to stratified Morse theory [12]. As a matter of fact, an alternate subset of constraint functions may be used to define an alternate $\tilde{Q}$, and the remaining one as a new Morse function for the study of other CS singularities and their related kinematic parameters.

We state the following useful result from [11]:

Proposition 1 *Let $a < b$ and suppose that the set $\tilde{h}_m^{-1}[a,b]$, consisting of all $p \in \tilde{Q}$ with $a \leq \tilde{h}_m(p) \leq b$, is compact, and contains no critical points of $\tilde{h}_m$. Then, $\tilde{Q}^a$ is diffeomorphic to $\tilde{Q}^b$. Furthermore, $\tilde{Q}^a$ is a deformation retract of $\tilde{Q}^b$, so that the inclusion map $\tilde{Q}^a \longrightarrow \tilde{Q}^b$ is a homotopy equivalence.*

In other words, the parameter c should be chosen to lie in a range $[a,b]$ so that $\tilde{h}_m^{-1}[a,b]$ contains no critical points of $\tilde{h}_m$.

To summarize the above analysis, we have the following linear inequalities for achieving singularityless design

$$\mu_i \in (a_i, b_i) \rightarrow \mu_i - a_i > 0 \text{ and } -\mu_i + b_i > 0$$

where μ_i, $i = 1, \cdots, l$, are nonlinear functions of the design parameters: $\mu_i = \mu_i(\alpha)$, $\mu = [\mu_1, \cdots, \mu_l]^T$, and a_i, b_i, $i = 1, \cdots, l$, are the lower and upper bound of the interval of μ_i where the configuration spaces of the manipulator are homotopic and without CS singularity. As can be easily seen that these constraints can be further cast as LMIs [13]

$$A(\mu) = A_0 + A_1\mu_1 + \cdots + A_l\mu_l > 0 \tag{3}$$

where A_i $(i = 1, \cdots, l)$ are constant symmetric base matrices. To use the semi-definite programming method introduced later, we consider nonstrict inequalities

$$\mu_i \in [a_i + \epsilon, b_i - \epsilon]$$

where ϵ is a pre-specified small value. Then, the inequalities are cast into nonstrict LMIs and for simplicity (without using additional notations), denoted as

$$A(\mu) = A_0 + A_1\mu_1 + \cdots + A_l\mu_l \geq 0.$$

3.2 Constraints of Cartesian Stiffness

For a general parallel manipulator, its kinematics can be described as

$$Zv = \dot{\theta}_a$$

where v is the Cartesian velocity of the moving platform (end-effector), $\dot{\theta}_a$ the velocities of actuators, and Z the map relating the two quantities. We associate a joint stiffness matrix to the joint space, K_θ. The Cartesian stiffness matrix of the manipulator at an equilibrium is given by

$$K_p = Z^T K_\theta Z. \tag{4}$$

The requirement of high stiffness amounts to

$$K_p \geq \gamma I, \gamma > 0$$

in the whole workspace. Substituting (4) into it yields

$$Z^T K_\theta Z \geq \gamma I. \tag{5}$$

Since the Jacobian matrix Z is a function of the key kinematic parameters, (5) can be rewritten as a LMI

$$B_0 + B_1\beta_1 + \cdots + B_p\beta_p \geq 0 \tag{6}$$

where B_i $(i = 0, \cdots, p)$ are symmetric base matrices which are independent on the key kinematic parameters, and β_i some nonlinear functions of the key kinematic parameters: $\beta_i = \beta_i(\alpha)$. Since B_i are functions of the configurations of the manipulator, different constraints as (6) can be constructed at different configurations. In practice, we usually discretize the whole workspace and form the LMI constraints at all nodes. Augment all the LMI together using diagonal matrix technic, we obtain a new set of LMI, for simplicity, still denoted as (6).

3.3 Constraints of Manipulability

Manipulability is another index measuring the ability of the manipulator in manipulating the end-effector, and mathematically formulated as

$$M_p = \frac{1}{\det(Z^T Z)}. \tag{7}$$

The requirement of good manipulability is translated to

$$M_p \geq \Gamma > 0$$

in the whole workspace. Substituting (7) into it yields

$$det(Z^T Z) \leq \frac{1}{\Gamma}. \tag{8}$$

This inequality is still LMI as

$$cc_0 + cc_1\xi_1 + \cdots + cc_q\xi_q \geq 0$$

where $cc_i \in \mathbb{R}$ $(i = 0, \cdots, q)$ are only dependent on the configurations of the manipulator, and ξ_i some nonlinear functions of the key kinematic parameters $\xi_i = \xi(\alpha)$. Similar as the previous discussion, through discretizing the workspace, we obtain the global constraints as

$$C_0 + C_1\xi_1 + \cdots + C_q\xi_q \geq 0 \tag{9}$$

where C_i are diagonal matrices with the diagonal elements be cc_i at different nodes of the workspace. Note that this constraint is also LMI.

3.4 Objective functions Based on the Expense

Considering the restrictions on the expense, the value of the key kinematic parameters can not be limitless large. We consider to minimize the following linear function which measures the total expense:

$$\min \phi = e^T x \tag{10}$$

where $e = (e_1, \cdots, e_t)^T$ is a constant vector, and $x = [x_1, \cdots, x_t]^T$ with $x_i \in \{\mu_1, \cdots, \mu_l, \beta_1, \cdots, \beta_p, \xi_1, \cdots, \xi_q\}$, $i = 1, \cdots, t$. Let

$$G(x) = G_0 + G_1 x_1 + \cdots + G_t x_t \geq 0 \tag{11}$$

be the LMI representing all the above LMIs (using the diagonal matrix technic). One may consider that the final optimal solution of (10) should not be too close to the boundary of the constrained set. So we add one determinant term $\log\det G^{-1}$ to (10) as

$$\min \phi = e^T x + \log\det G^{-1}. \tag{12}$$

4 Constrained Semi-definite Programming Problem and Constrained Max-det Problem Subject to LMIs

In this section, we first give a general description of the constrained semi-definite programming problem and the constrained max-det problem subject to LMIs by taking account of an additional set of nonlinear constraints. we propose a simplified algorithm based on constrained gradient flow methods.

4.1 Constrained Semi-definite Programming Problem and Constrained Max-det Problem

The variables x_i, $i = 1, \cdots, t$, associated with LMIs may not be linearly independent, as seen from (3), (6), and (9). If $t = l_0$, x_i, $i = 1, \cdots, t$, are linearly independent and α can be simply solved as functions of x using Newton method.

$$\alpha = \alpha(x).$$

If $t > l_0$, we need to take account of an additional set of nonlinear constraints:

$$g(x) = \begin{bmatrix} g_1(x) \\ \vdots \\ g_{t-l_0}(x) \end{bmatrix} = 0.$$

Based on this, we introduce the following constrained semi-definite programming problem

$$\min \quad e^T x \tag{13}$$

subject to

$$\begin{aligned} G(x) &= G_0 + \sum_{i=1}^{t} G_i x_i \geq 0 \\ g(x) &= 0 \end{aligned} \tag{14}$$

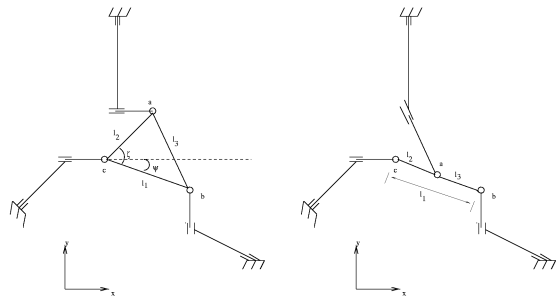

(a) (b)

Figure 2: (a)A 3-PPR planar parallel manipulator (b)A CS singularity

and constrained max-det problem

$$\min_x \phi(x) = e^T x + \log\det G(x)^{-1} \tag{15}$$

subject to

$$\begin{aligned} G(x) &= G_0 + \sum_{i=1}^{t} G_i x_i \geq 0 \\ g(x) &= 0. \end{aligned}$$

4.2 Geometric Algorithms

In this subsection, we propose a simplified gradient algorithm for the constrained semi-definite programming problem and the constrained max-det problem based on their special properties.

Algorithm 1 A Simplified Algorithm
Input: An initial point x_0, step size $0 < \eta < 1$, tolerance $\epsilon_1, \epsilon_2 > 0$;
Output: The optimal solution x^*;
1: Initialization: $x(0) = x_0$, $G(0) = G(x(0))$ and $k = 0$;
2: If $\lambda_{\min}(G(k)) < \epsilon_1$, apply the constrained gradient algorithm:

$$x(k+1) = x(k) + \eta(I - A^T(AA^T)^{-1}A)\nabla\lambda_{\min}(G(x))|_{x(k)}.$$

else apply the constrained gradient algorithm

$$x(k+1) = x(k) - \eta(I - A^T(AA^T)^{-1}A)\nabla\phi|_{x(k)}.$$

3: If $\|\phi(x(k+1)) - \phi(x(k))\| < \epsilon_2$ output $x^* = x(k+1)$ else set $k = k+1$ and go to step 2.

where $\lambda_{\min}(G(x))$ denotes the minimal eigenvalue of $G(x)$,

$$\nabla\lambda_{\min}(G(x)) = \begin{bmatrix} \omega^T G_1 \omega \\ \vdots \\ \omega^T G_t \omega \end{bmatrix}$$

, $\nabla(\phi(x) = e^T x) = e$, and

$$\nabla(\phi(x) = e^T x + \log\det G(x)^{-1}) = \begin{bmatrix} e_1 - \mathbf{Tr}(G^{-1}G_1) \\ \vdots \\ e_t - \mathbf{Tr}(G^{-1}G_t) \end{bmatrix}.$$

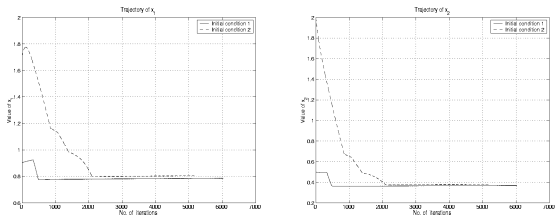

(a) (b)

Figure 3: (a)Trajectory of x_1 (b) Trajectory of x_2

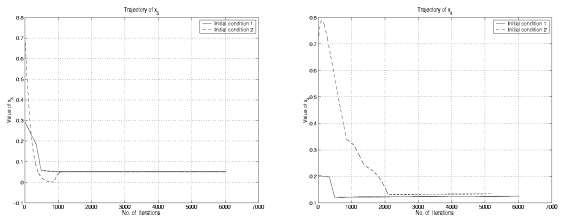

(a) (b)

Figure 4: (a)Trajectory of x_3 (b) Trajectory of x_4

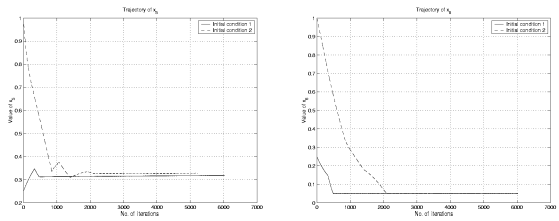

(a) (b)

Figure 5: (a)Trajectory of x_5 (b) Trajectory of x_6

$A = \frac{\partial g}{\partial x}$.
After we obtain the x^*, we can solve α: (1) If $t = l_0$, we use Newton method; (2) If $t > l_0$, we pick l_0 linearly independent nonlinear equations and use the Newton method for solving of α.

5 Simulation Results

In this section, we apply the simplified algorithm to optimal design of a three-DOF planar parallel manipulator, as shown in Fig. 2-(a). To simplify the problem and focus on the design of the shape and size of the moving platform, the manipulator is assumed to be 3-PPR.

Because of the simple kinematic structure of the manipulator, we refer to the coordinates of vertex a, b, c as the joint variables

$$\theta = (x_c, y_c, x_b, y_b, x_a, y_a)^T,$$

which are also considered to be active in the following analysis. The manipulator kinematics derives from the loop closure equations of three loops :

$$\begin{aligned} h_1 = (x_a - x_b)^2 + (y_a - y_b)^2 &= l_3^2 \\ h_2 = (x_b - x_c)^2 + (y_b - y_c)^2 &= l_1^2 \\ h_3 = (x_c - x_a)^2 + (y_c - y_a)^2 &= l_2^2 \end{aligned}$$

where l_1, l_2 and l_3 are lengths of three sides of the moving platform. Its CS singularities are derived according to (2):

$$dh_1 \wedge dh_2 \wedge dh_3 = 0 \rightarrow l_i + l_j = l_k, 1 \leq i, j, k \leq 3.$$

In other words, the triangle degenerates to a line, as shown in Fig. 2-(b). Let ζ be the angle between ca and cb, and the triangle is uniquely determined by l_1, l_2 and ζ. To design a CS singularityless manipulator, we impose the following constraints:

$$l_1 \sin\zeta \geq \epsilon. \tag{16}$$

Sometimes, we may want the end-effector to be obtuse-triangle according to some practical restrictions, then, we need three additional constraints:

$$l_1 l_2 \cos\zeta \geq \epsilon \ , \ l_1 l_2 \cos\zeta - l_2^2 \geq \epsilon \ , \ l_1^2 - l_1 l_2 \cos\zeta \geq \epsilon. \tag{17}$$

Second, we compute the Jacobian matrix Z in

$$\dot{\theta} = Zv = Z[\dot{x}_c, \dot{y}_c, \dot{\psi}]^T,$$

where the configuration of the end-effector is parameterized by $Y = [x_c, y_c, \psi]^T$. Z is given by

$$Z = \begin{bmatrix} 1 & 0 & 1 & 0 & 1 & 0 \\ 0 & 1 & 0 & 1 & 0 & 1 \\ 0 & 0 & -l_1 \sin\psi & l_1 \cos\psi & -l_2 \sin(\psi+\zeta) & l_2 \cos(\psi+\zeta) \end{bmatrix}^T.$$

Let the joint stiffness matrix be $K_\theta = I$, then, (5) can be reorganized into

$$\begin{aligned} K_p &= \begin{bmatrix} 0 & 0 & -\sin\psi \\ 0 & 0 & \cos\psi \\ -\sin\psi & \cos\psi & 0 \end{bmatrix} (l_1 + l_2 \cos\zeta) \\ &+ \begin{bmatrix} 3 & 0 & 0 \\ 0 & 3 & 0 \\ 0 & 0 & 0 \end{bmatrix} + + \begin{bmatrix} 0 & 0 & 0 \\ 0 & 0 & 0 \\ 0 & 0 & 0 \end{bmatrix} (l_1^2 + l_2^2) \\ &+ \begin{bmatrix} 0 & 0 & -\cos\psi \\ 0 & 0 & -\sin\psi \\ -\cos\psi & -\sin\psi & 0 \end{bmatrix} l_2 \sin\zeta \\ &\geq \gamma I. \end{aligned} \tag{18}$$

Substituting Z into (8) yields

$$6(l_1^2 + l_2^2) - 6 l_1 l_2 \cos\zeta \leq \frac{1}{\Gamma}. \tag{19}$$

To stack (16), (17), (18), and (19) together, we introduce variables $x_1 = l_1 + l_2 \cos\zeta$, $x_2 = l_1^2 + l_2^2$, $x_3 = l_2 \sin\zeta$,

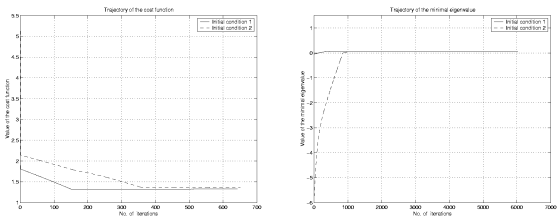

(a) (b)

Figure 6: (a)Trajectory of the cost function (b) Trajectory of the minimal eigenvalue

$x_4 = l_1 l_2 \cos\zeta$, $x_5 = l_1^2$, and $x_6 = l_2^2$. x_i, $i = 1, \cdots, 6$ are subject to the following nonlinear constraints:

$$\begin{aligned} g_1(x) &:= x_1^2 - x_2 + x_3^2 - 2x_4 = 0 \\ g_2(x) &:= x_2 - x_5 - x_6 = 0 \\ g_3(x) &:= x_5 x_3^2 + x_4^2 - x_5 x_6 = 0 \end{aligned}$$

and two additional inequalities $x_5 \geq \epsilon$ and $x_6 \geq \epsilon$. We use the linear function $\phi = [1, 1, 1, 1, 0, 0]x$ as the objective function. The other parameters are $\gamma = 0.1$, $\Gamma = 0.5$, $\epsilon = 0.001$, $\eta = 0.001$, $\epsilon_1 = 0.005$ and $\epsilon_2 = 1e-7$.

In the simulation, we test the convergence of Algorithm 1 under two different initial conditions: (1). $x(0) = \begin{bmatrix} 0.9045 & 0.5 & 0.2939 & 0.2023 & 0.25 & 0.25 \end{bmatrix}^T$ or $l_1(0) = 0.5$, $l_2(0) = 0.5$, $\zeta(0) = \frac{\pi}{5}$; (2). $x(0) = \begin{bmatrix} 1.7071 & 2.0 & 0.7071 & 0.7071 & 1.0 & 1.0 \end{bmatrix}^T$ or $l_1(0) = 1.0$, $l_2(0) = 1.0$, $\zeta(0) = \frac{\pi}{4}$. We discretize the workspace by simply dividing the range of ψ into 8 intervals. The 8 nodes are $\psi_i = (i-1)\frac{1}{4}\pi$, $i = 1, \cdots, 8$. For each node, we calculate the LMIs (18) and (19). Finally, by stacking all those LMIs together, we have the following global LMI:

$$G(x) = G_0 + G_1 x_1 + \cdots + G_6 x_6 \geq 0 \tag{20}$$

where G_i can be found in [14]. Fig. 3, 4 and 5 show the trajectories of x. x_i will converge to almost the same optimal value for the two initial conditions:(1). $x^* = [0.7858, 0.3675, 0.0506, 0.1254, \ 0.3108, 0.0495]^T$ or $l_1^* = 0.5640$, $l_2^* = 0.2225$,$\zeta^* = 0.2293$; (2). $x^* = [0.8045, 0.3779, 0.0506, 0.1340, \ 0.3283, 0.0496]^T$ or $l_1^* = 0.5729$, $l_2^* = 0.2227$, $\zeta^* = 0.2293$. Fig. 6-(a) and 6-(b) give the trajectory of the cost function and the minimal eigenvalue of $G(x)$.

6 Conclusion

This paper discussed the problem of optimal design of parallel manipulators. Requirements on singularitylessness, Cartesian stiffness and manipulability are cost into LMIs where the variables are nonlinear functions of key kinematic parameters. To limit the cost of the material of the manipulator in addition to these constraints, the optimal design problem are tranformed into either a constrained semi-definite programming problem or a constrained max-det problem. A simplified gradient algorithm is proposed for solving of the two problems. Simulation results verify the effectiveness of the proposed algorithm.

References

[1] D. Stewart. A platform with six degrees of freedom. In *Proc. Institute of Mechanical Engr., London, England, vol. 180*, pages 371–386, 1965.

[2] V.E. Gough and S.G. Whitehall. Universal tyre test machine. In *Proc. of the* 9th *International Tech. Congress, F.I.S.I.T.A.*, 1962.

[3] S. Kock and W. Schumacher. A mixed elastic and rigid-body dynamic model of an actuation redundant parallel robot with high-reduction gears. In *Proceedings of IEEE International Conference on Robotics and Automation*, pages 1918–1923, 2000.

[4] S. Kock and W. Schumacher. A parallel x-y manipulator with actuation redundancy for high-speed and active-stiffness applications. In *Proceedings of IEEE International Conference on Robotics and Automation*, volume 3, pages 2295–2300, 1998.

[5] J.P. Merlet. *Parallel Robots.* Kluwer Academic Publishers, 2000.

[6] D. Oblak and D. Kohli. Boundary surfaces, limit surfaces, crossable and noncrossable surfaces in workspace of mechanical manipulators. *ASME Journal of mechanisms, Transmissions, and Automation in Design*, 110, 1988.

[7] R.E. Stamper, L.W. Tsai, and G.C. Walsh. Optimization of a three dof translational platform for well-conditioned workspace. In *Proceedings of IEEE International Conference on Robotics and Automation*, pages 3250–3255, 1997.

[8] C. Gosselin and J. Angeles. The optimum kinematic design of a spherical three-dof-of-freedom parallel manipulator. *ASME Journal of mechanisms, Transmissions, and Automation in Design*, 111, 1989.

[9] F. Park and R. Brockett. Kinematic dexterity of robotic mechanisms. *International Journal of Robotics Research*, 13:1–15, 1994.

[10] W. Boothby. *An Introduction to Differentiable Manifolds and Riemannian Geometry.* Academic Press, 1975.

[11] J. Milnor. *Morese Theory.* Princeton University Press, Princeton, N.J., 1963.

[12] Mark Goresky and Robert MacPherson. *Stratified Morese Theory.* Springer-Verlag, Berlin, 1988.

[13] Y. Nesterov and A. Nemirovsky. *Interior-Point Polynominal Methods in Convex Programming.* Vo. 13 of Studies in App. Math., SIAM, 1994.

[14] G.F. Liu and Z.X. Li. Geometric algorithms for optimal design of parallel manipulators. Technical report, Department of Electrical Engineering, HKUST, 2002.

Proceedings of the WORKSHOP on
Fundamental Issues and Future Research Directions for Parallel Mechanisms and Manipulators
October 3–4, 2002, Quebec City, Quebec, Canada
Clément M. Gosselin and Imme Ebert-Uphoff, editors

Concept Paper: On the Significance of the Lowest Linearized Natural Frequency of a Parallel Manipulator as a Performance Measure for Concurrent Design

KRIS KOZAK
Woodruff School of Mechanical Engineering
Georgia Institute of Technology
Atlanta, GA 30332-0405, USA
gt3141a@prism.gatech.edu

IMME EBERT-UPHOFF
Woodruff School of Mechanical Engineering
Georgia Institute of Technology
Atlanta, GA 30332-0405, USA
ebert@me.gatech.edu

PHILIP A. VOGLEWEDE
Woodruff School of Mechanical Engineering
Georgia Institute of Technology
Atlanta, GA 30332-0405, USA
gte611w@prism.gatech.edu

WILLIAM SINGHOSE
Woodruff School of Mechanical Engineering
Georgia Institute of Technology
Atlanta, GA 30332-0405, USA
william.singhose@me.gatech.edu

Abstract: *This concept paper proposes the use of the lowest linearized natural frequency of a parallel manipulator (PM) as a performance measure for concurrent design of the kinematics, dynamics and control of a PM. Some interesting properties of the lowest linearized natural frequency are discussed to illustrate its potential benefits, while potential shortcomings and open research questions are enumerated for future work.*

1 Introduction

A basic problem in the study of parallel manipulators is how to best design a manipulator to perform a certain task. A typical approach to manipulator design might be described by the following: after a class of manipulators is selected, optimization techniques are employed to select the best architecture and/or to select kinematic parameters. The first step of the optimization is to specify a cost function that captures the desired manipulator performance characteristics and expresses them in a mathematical form. Depending upon what is required of a manipulator, different cost functions are devised, and secondary criteria can be added as constraints on the optimization. After the optimization is performed, the resulting mechanism is usually analyzed to ensure that the optimization produced an acceptable mechanism. If the results of the optimization do not lead to an acceptable design, the cost function can be modified and the process iterated.

In this paper we propose a new performance measure as an alternative that may simultaneously capture characteristics of a manipulator's kinematic *and* dynamic properties: the lowest linearized natural frequency. Linearized natural frequency can serve as a measure of the dynamic performance of a nonlinear system about an operating point. By observing linearized natural frequency at various points in the operating space an overall picture of the configuration based performance of the mechanism can be obtained, and thus the linearized natural frequency can seemingly be used to establish the overall dynamic performance of a nonlinear system. This paper outlines properties of the lowest natural frequency that illustrate its potential as a performance measure, discusses advantages and disadvantages of this measure, and enumerates open research questions to be addressed.

Most design strategies utilized currently look at the kinematics and the dynamics of the manipulator separately. Usually, some aspect of the kinematics of the manipulator are optimized first and then the dynamics are analyzed. Sometimes the dynamics are optimized after the kinematic parameters are defined. This is typically done because the analysis tools for both realms are different, and dynamic analysis is usually very difficult to perform. Additionally, the dynamics of a manipulator can be "modified" using different control techniques, thus diminishing the need to perform dynamic analysis before the kinematic parameters are selected. Because of these issues, most research has refrained from optimizing the dynamics of PMs during the hardware design phase.

This paper proposes a way to merge the two realms into a single performance measure:[1] the lowest linearized natural

[1] It is understood that secondary cost functions are still required to capture other aspects, such as workspace, etc. Nevertheless, a reduction of the total

frequency. By integrating the kinematics and dynamics in the design process, more efficient manipulators can be constructed. However, it should be noted that these are only thoughts on directions for research. The ideas contained herein are proposals and have not been thoroughly researched. Given this caveat, we hope to present sound reasoning for why this topic should be investigated further.

2 Literature Review

For parallel manipulators, there exists a great deal of literature on their kinematic analysis, including the workspace [1, 2] and singularities [3, 4, 5, 6]. Merlet [7] provides an excellent overview of the optimization of parallel manipulators in his book. Another good starting point for optimization is provided by Angeles [8]. The majority of the methods cited by Angeles are for serial mechanisms, but are applicable to parallel mechanisms as well. Some of the more popular optimization techniques are discussed below.

Yoshikawa [9] proposed several measures of manipulability. Lipkin and Duffy [10] and Doty et al. [11] discussed problems with the scale and frame invariance of those manipulability measures. Gosselin [12] used the inverse of the condition number (aka the dexterity) with a characteristic length to address the problem of scale invariance. Kurtz and Hayward [13] investigated several different objective functions including dexterity, dexterity uniformity, and forces to design a redundant spherical mechanism.

Gosselin and Angeles [14] optimized a three degree of freedom manipulator for global workspace and Merlet [15] designed a PM to have a specific workspace. Chakarov [16] optimized the stiffness of a PM, while Bhattacharya et al. [17] designed a Gough-Stewart platform for optimal stiffness.[2]

As a separate topic, the dynamics of PMs [18] have not received much attention for optimal design. A possible reason for this is that parallel manipulators are dominated by their kinematics as opposed to serial manipulators which are dominated by their dynamics. One of the very few papers actually defining dynamic performance measures and using them for optimization is by Khatib and Bowling [19]. In this article, the inertial and acceleration properties of a PM are optimized using a weighted cost function.

Numerous papers have used one or more of the performance measures above to design PMs. For example, Lückel et al. [20] used a computer model with an iterative routine to design the TRIPLANAR robot. Company et al. [21] also used an iterative technique to come up with a 3 axis machine tool. Numerous other references exist, but are not included here because of length.

number of cost functions to be used is still advantageous.

[2] Note that the method used by Bhattacharya et al. can suffer from the same problems with frame invariance, but is included here because of its relevance to this problem.

3 Review of Singularities

A significant portion of this paper focuses on the ability of the linearized natural frequency to detect kinematic singularities. This section provides a brief review of the notation and terminology of kinematic singularities. Utilizing the formulation in Gosselin and Angeles [4], one can write the relationship between the joint velocities, $\dot{\boldsymbol{\theta}}$, and end effector twist, $\mathbf{\$}_t$, as:

$$\mathbf{A}\dot{\boldsymbol{\theta}} = \mathbf{B}\begin{bmatrix}\mathbf{v}\\ \boldsymbol{\omega}\end{bmatrix} \equiv \mathbf{B}\mathbf{\$}_t \tag{1}$$

where $\mathbf{A}, \mathbf{B}$ are called Jacobian matrices and are most conveniently written as functions of both, the joint angles, θ_i, and the end-effector position and orientation. Assuming a non-redundant, fully constrained manipulator, the number of outputs is equal to the number of inputs, and thus, $\mathbf{A}$ and $\mathbf{B}$ are square. If $\mathbf{A}$ is non-singular, then Equation (1) can be written as:

$$\dot{\boldsymbol{\theta}} = \mathbf{J}\mathbf{\$}_t \qquad \text{where} \qquad \mathbf{J} \equiv \mathbf{A}^{-1}\mathbf{B} \tag{2}$$

Using the principle of virtual work (a complete derivation can be found in Craig [22]), a relationship can be derived between the input torques, $\boldsymbol{\tau}$, and output wrench, $\mathbf{\$}_w$ as follows:

$$\boldsymbol{\tau} = \mathbf{J}^{\intercal}\mathbf{\$}_w. \tag{3}$$

Singular configurations occur if either matrix $\mathbf{A}$ or $\mathbf{B}$ is singular [4]. If $\mathbf{A}$ is singular, a *leg singularity* is encountered and the end-effector is over-constrained, i.e. it instantaneously loses at least one degree-of-freedom. This type of singularity is due to the serial nature of the legs and has been well discussed for serial manipulators. If $\mathbf{B}$ is singular, a *platform singularity* is encountered and the end-effector is under-constrained, i.e. the end-effector can move instantaneously even if all actuators are locked.

4 Proposed Optimization Procedure

Typically, one designs a PM using a standard procedure. One picks an architecture, creates a cost function from a suitable performance measure(s), and then iteratively changes the kinematic parameters until the cost function is either minimized or maximized such that the optimum design is found. After the kinematic parameters are defined, typically a dynamic analysis is performed so that a suitable controller can be designed.

The method proposed in this paper is to combine the kinematic, dynamic, and control parameters into one encompassing cost function. In this way, the mechanism is concurrently designed. Specifically, the base performance measure for this cost function is the lowest linearized natural frequency, ω_1. Examples of the different types of cost functions that could be devised using ω_1 are:

1. $\min_{\mathcal{W}}(\omega_1)$

2. $\min_{\mathcal{W}}(\omega_1\zeta_1)$

3. $\max_{\mathcal{W}}|\omega_1 - \omega_{avg}|$

where $\mathcal{W}$ is the workspace, ζ_1 is the lowest linearized damping ratio and ω_{avg} is an average desired natural frequency. Likewise, any other norm based cost functions might be appropriate. These cost functions are then either minimized or maximized to find an optimal set of kinematic (leg lengths, actuator placement, etc.), dynamic (inertias), and control (gains) parameters.

5 Properties of the Natural Frequency

In this section some of the advantages and disadvantages of using a parallel manipulator's lowest linearized natural frequency as a performance measure are enumerated. Before discussing the these advantages and disadvantages, a review of some of the relevant concepts from linear system theory is in order.

5.1 Review of Linear System Parameters

The linear system parameters of interest in this paper are a system's natural frequencies and damping ratios. However, for much of the discussion only the lowest natural frequency, denoted by ω_1, will be considered. Note that the use of natural frequencies and damping ratios assumes that the modes of the mechanism are underdamped, which implies that there are as many natural frequencies as there are degrees of freedom.

The linearized natural frequency and damping ratio can be used to estimate a number of local, low speed characteristics of the system performance. For example, system response times, such as rise time or settling time can often be estimated using the smallest quantity $|\zeta_i\omega_i|$, where i is a mode index. The lowest quantity ζ_1 determines whether the system will tend to vibrate and how much vibration might be expected. The natural frequencies and damping ratios together can be used to predict a variety of local response characteristics. Finally, the real part of the linearized system's eigenvalues, $-\zeta_i\omega_i$, determines the local stability of the system, i.e. the system is unstable if $-\zeta_i\omega_i > 0$ for any i.

The following two subsections will highlight some of the key advantages and disadvantages to using the linearized parameters as performance measures for parallel manipulators.

5.2 Advantages

There are a number of advantages of using the linearized, quasi-static natural frequencies and damping ratios. Some of these advantages are as follows:

1. Important kinematic elements are embedded in the natural frequencies (e.g. platform singularities appear as zero natural frequencies – this will be discussed in more detail in Section 6.2).

2. Natural frequencies are physically meaningful measures of performance (at least in the linearized sense).

3. As a consequence of item 2 (above), the natural frequencies and damping ratios, or any relevant function of the two measures, are frame and scale invariant measures of the dynamic performance of the parallel manipulator.

4. The use of natural frequencies and damping ratios is a holistic approach to design, in that it combines kinematic, dynamic and controller parameters into the same cost function.

5. When allowing controller gains to vary as design parameters, then (at least for low speeds) the mechanism can be guaranteed to be stable by ensuring that the quantities $-\zeta_i\omega_i$ are negative for all i.

6. A natural frequency measure can indicate regions of poor dynamic performance that kinematic measures alone may not detect.

Additionally, natural frequency can potentially be used for the design of redundantly actuated parallel manipulators. In particular, cost functions based on natural frequencies could be used to design redundant manipulators that have fewer singularities, posses faster response times, and behave more linearly than their non-redundant counterparts. However, there are some open questions regarding the computation of natural frequencies for redundant manipulators that must be answered before such design strategies can be developed.

5.3 Disadvantages

There are some apparent drawbacks to the use of natural frequencies and damping ratios as base performance measures in a design cost function. It should be noted however that most of these drawbacks are related more to implementation difficulty than to the value of the measure.

1. Equations of motion must be derived symbolically, and then linearized about an arbitrary point in the workspace. Since the dynamic equations rely on the kinematic equations, derivation of the dynamic equations must be done in addition to, not instead of, the kinematics.

2. The best cost function to use is not obvious. Several examples of possible cost functions were shown in Section 4, but none of them captures all aspects of the mechanism.

3. There are more parameters to vary, thus the computational expense of an optimization is increased.

4. There has not yet been any research, at least to these authors' knowledge, regarding the linearization of a set of dynamic equations corresponding to a parallel manipulator with more than one degree of rotation at the end effector (the general form of the dynamic equations of most parallel manipulators provide unique challenges for linearization and eigenvalue computation).

5. Natural frequency does not reveal any information about the size of the workspace.

6 Dynamic-Kinematic Relationships

As already mentioned, the dynamics and kinematics of a mechanism are inherently related, so it might seem reasonable that an ideal performance measure would exist that incorporates both the kinematics and dynamics. Initial research indicates that the linearized natural frequency of a parallel manipulator synthesizes key elements of both the kinematics and dynamics in a way that may make it a good performance measure. An exposition of some of the relationships between natural frequency and the Jacobian are provided in the following subsections to support this idea.

6.1 Numerical Example for Linearized Natural Frequency

We will start with a numerical example for a simple parallel manipulator. Figure 1 shows a 2R<u>P</u>R planar parallel manipulator. To compute the natural frequencies of this manipulator throughout its workspace the following assumptions were made:

1. the manipulator is controlled by independent joint PD controllers;
2. the mechanism lies in the horizontal plane, so gravity has no effect;
3. the link inertias are *not* negligible;
4. the mechanism is linearized about static equilibrium points;
5. the mechanism is underdamped.

Note that for the mechanism to be in static equilibrium, the end-effector velocities and accelerations must be zero, and the end-effector position must be at the desired position. Also note that the desired position is simply the input to the controller, so any point in the workspace can be an equilibrium point.

The natural frequency can be calculated for various positions in the workspace by linearizing the equations of motion about an arbitrary desired position, computing the eigenvalues of the system and extracting the natural frequency information from the eigenvalues. For more detailed information on this process see [23]. Figure 2 shows the lowest natural frequency of the manipulator as the position of the end-effector varies over a portion of the x-y plane. Note that due to practical joint limitations the mechanism would tend to be restricted to a smaller reachable workspace than the region shown. Note also that the frequency plot corresponds to the manipulator in Figure 1 for $L = 1$.

There are two characteristics that are of particular interest in Figure 2. First, the natural frequency along the straight line, $y = 0$, in the workspace is zero. This line corresponds exactly to the manipulator's platform singularities. This characteristic illustrates a connection between a platform singularity and a

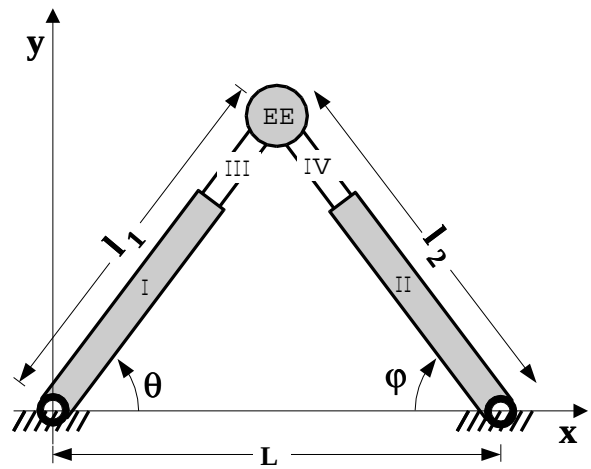

Figure 1: Two degree-of-freedom Parallel Manipulator

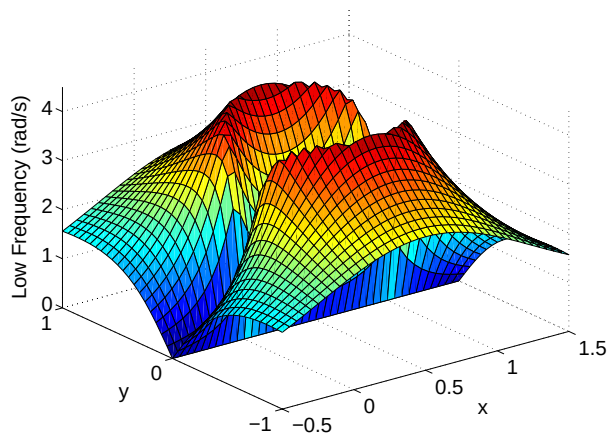

Figure 2: Low Natural Frequency Plot

natural frequency of zero, which will be discussed in Section 6.2. Second, notice that near the points $(x, y) = (0, 0)$ and $(1, 0)$, which are the locations of the base revolute joints and leg singularities, the natural frequency surface is steep but continuous. The continuity of the surface, which is assured only if the leg inertias are not neglected, will become important in Section 6.3.

6.2 Properties of the Natural Frequency

The fact that a vanishing natural frequency of the parallel manipulator from Figure 1 corresponds to the platform singularities of the mechanism suggests that perhaps there exists an important relationship between the dynamic measure of natural frequency, and the kinematics of a mechanism. In fact, this relationship leads directly to the recognition that a zero natural frequency is a condition of diminished dynamic performance, which is encapsulated by the following definition:

Definition 1: A *Dynamic Singularity* of a parallel manipulator is a configuration for which the natural frequency associated with

at least one mode is zero, i.e. $\min(\omega_n) = 0$.

In essence a dynamic singularity is a location where the dynamic performance of a manipulator degenerates, and the manipulator becomes incapable of moving via its own actuators in the direction (or mode) associated with the zero natural frequency.

Clearly, a dynamic singularity is an undesirable configuration of a mechanism. An appropriate question is then: under what conditions will a mechanism be in a dynamic singularity? While this is an open research question that is not fully answered in this paper, the following discussion is intended to give some insight into this problem.

As a motivation consider a simple, single-degree-of-freedom system with no damping, that when linearized has the form

$$m(x_0)\Delta\ddot{x} + k(x_0)\Delta x = \tau \tag{4}$$

where x_0 is a point in the workspace. To examine the characteristic dynamics of the system, only the homogeneous system needs to be considered, i.e. $\tau = 0$. The natural frequency for this system at x_0 is

$$\omega_n = \sqrt{k(x_0)/m(x_0)} \tag{5}$$

For the natural frequency of the system to be zero, one or both of the following statements must be true: either the stiffness, $k(x_0)$, must be zero, or the inertia, $m(x_0)$, must be infinite. As it turns out, the latter case can actually arise, and will be discussed in Section 6.3

Hypothesis 1: If the determinant of the combined Jacobian, $\mathbf{J} = \mathbf{A}^{-1}\mathbf{B}$, at a given configuration is well-defined, but singular, then the manipulator is in a dynamic singularity. In other words, if $\det \mathbf{B} = 0$ and $\det \mathbf{A} \neq 0$, then $\min(\omega_n) = 0$.

Reasoning:

Consider the linearized equations of motion of a parallel manipulator without damping. A common form of these equations can be written as

$$\underbrace{(\mathbf{M} + \sum_i \mathbf{J}_i^\intercal \mathbf{M}_i \mathbf{J}_i)}_{\widehat{\mathbf{M}}} \ddot{\mathbf{x}} + \mathbf{J}^\intercal \mathbf{K} \mathbf{J} \mathbf{x} = \mathbf{0} \tag{6}$$

where $\mathbf{M}$ is the linearized inertia matrix and $\mathbf{J}^\intercal\mathbf{K}\mathbf{J}$ represents the linearized stiffness matrix. $\widehat{\mathbf{M}}$ is the effective mass matrix as seen at the end effector. Note that $\mathbf{K}$ is the stiffness of the mechanism (in joint space) due to the actuators under a control law, and perhaps also the structural stiffness of the links (also in joint space). The terms $\mathbf{J}_i^\intercal \mathbf{M}_i \mathbf{J}_i$ are the linearized leg inertia terms, where $\mathbf{M}_i$ is the inertia matrix of the ith leg with respect to a body fixed coordinate frame and $\mathbf{J}_i$ is the leg Jacobian matrix that relates the velocities of the leg in the leg coordinate frame to the end effector velocities.

Based on Equation (6) the lowest natural frequency of the manipulator is found by solving the following eigenvalue problem for ω:

$$\det(\mathbf{I}\omega^2 - \widehat{\mathbf{M}}^{-1}\mathbf{J}^\intercal\mathbf{K}\mathbf{J}) = 0 \tag{7}$$

But if $\det \mathbf{J} = 0$ (implying that the manipulator is in a platform singularity), then $\widehat{\mathbf{M}}^{-1}\mathbf{J}^\intercal\mathbf{K}\mathbf{J}$ is singular which implies that at least one root of Equation (7) is zero, and thus $\min(\omega_n) = 0$. □

This hypothesis indicates a useful relationship between the kinematics and dynamics of a parallel manipulator[3]. However, a number of open questions need to be addressed to fully reveal the relationship between the kinematics and the natural frequency.

Research Questions:

Question 1: If $\det \mathbf{A} = 0$ and $\det \mathbf{B} = 0$ then is $\min(\omega_n) = 0$?

Question 2: If $\det \mathbf{A} = 0$ and $\det \mathbf{B} \neq 0$ then what can be said about $\min(\omega_n)$?

Question 3: Does $\min(\omega_n) = 0$ imply that $\det \mathbf{B} = 0$?

Though the answers to these questions are not known, it may be useful to discuss an example that confronts a situation in which the assumptions of Question 1 hold. In the following section a special configuration of the 2R<u>P</u>R manipulator shown in Figure 1 is addressed.

6.3 Interesting Example

The 2R<u>P</u>R manipulator from Figure 1 can be in a leg and platform singularity simultaneously only at the points $(x, y) = (0, 0)$ and $(L, 0)$. Only one point needs to be considered because the manipulator is symmetric.

Consider the case where the end effector is near the leg/platform singularity $(x, y) = (L, 0)$. Clearly when the end effector approaches the point $(x, y) = (L, 0)$ along the path (L, ϵ) as $\epsilon \to 0$ (assuming that such a point is reachable), where $0 < \epsilon \ll L$, $\mathbf{A}$ and $\mathbf{B}$ both become singular:

$$\mathbf{A} = \begin{bmatrix} \ell_1 & 0 \\ 0 & \ell_2 \end{bmatrix} \approx \begin{bmatrix} L & 0 \\ 0 & \epsilon \end{bmatrix} \to \begin{bmatrix} L & 0 \\ 0 & 0 \end{bmatrix} \tag{8}$$

$$\mathbf{B} = \begin{bmatrix} x & y \\ -(L-x) & y \end{bmatrix} = \begin{bmatrix} L & \epsilon \\ 0 & \epsilon \end{bmatrix} \to \begin{bmatrix} L & 0 \\ 0 & 0 \end{bmatrix} \tag{9}$$

This result confirms that $(L, 0)$ is both a leg and a platform singularity. Now consider what happens to the combined Jacobian $\mathbf{J}$. The limit as $\epsilon \to 0$ of the combined Jacobian, $\mathbf{J}$, is not a singular matrix:

$$\mathbf{J} = \begin{bmatrix} \frac{x}{\ell_1} & \frac{y}{\ell_1} \\ \frac{-(L-x)}{\ell_2} & \frac{y}{\ell_2} \end{bmatrix} \approx \begin{bmatrix} \frac{L}{L} & \frac{\epsilon}{L} \\ \frac{0}{\epsilon} & \frac{\epsilon}{\epsilon} \end{bmatrix} \to \begin{bmatrix} 1 & 0 \\ 0 & 1 \end{bmatrix} \tag{10}$$

Along *this* path $\mathbf{J}$ is well-conditioned, but the limit of $\mathbf{J}$ along another path, such as $(x, y) = (L - \epsilon, 0)$ where $\epsilon \to 0$ gives a different result. Specifically,

$$\mathbf{J} = \begin{bmatrix} \frac{L-\epsilon}{L-\epsilon} & \frac{0}{L-\epsilon} \\ \frac{\epsilon}{\epsilon} & \frac{0}{\epsilon} \end{bmatrix} \to \begin{bmatrix} 1 & 0 \\ 0 & 0 \end{bmatrix} \tag{11}$$

[3] It is only a hypothesis, rather than a proposition, since Equation (6) may not sufficiently represent the relevant dynamics of all parallel manipulators

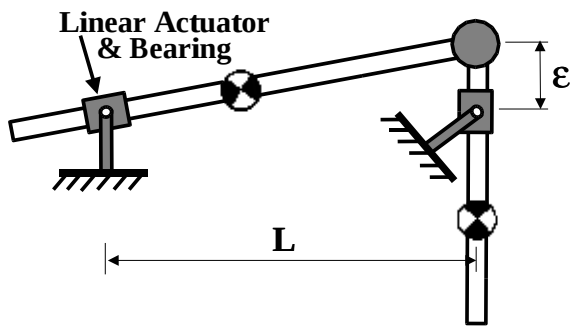

Figure 3: Two Degree of Freedom Parallel Manipulator Near a Combined Leg and Platform Singularity

These results indicate a discontinuity in the stiffness[4] at the actual location $(L, 0)$. So the question remaining is: what happens to the natural frequency? By numerical calculation of the natural frequency from the linearized equations of motion it was found that the lowest natural frequency converges to zero along any trajectory that goes to $(L, 0)$. This trend can be seen in Figure 2 (recall that $L = 1$ in Figure 2).

Though the numerical calculations seem to confirm that the natural frequency can detect such a problem, it would help to have a more intuitive example to see what is actually happening. As suggested by the discussion in section 6.2, in particular by Equation (5), there are two possible manners by which the natural frequency can tend to zero. Either some component of the stiffness must degenerate or some component of the inertia must become infinite. Since the stiffness was shown not to degenerate along the path (L, ϵ) for $\epsilon \to 0$, while the natural frequency does, in fact, go to zero, the effective inertia must become infinite. In fact, this was confirmed numerically, but it is difficult to see how this can be the case from Figure 1.

It is easier to see how the effective inertia becomes infinite for the mechanism seen in Figure 3. Figure 3 shows a 2R$\underline{\text{P}}$R manipulator that shares the same velocity kinematics (and thus the same Jacobian relations given by Equations (8)–(11)) with the manipulator from Figure 1. However, the manipulator from Figure 3 has been contrived in such a manner as to allow the end effector to (nearly) reach the leg/platform singularity described above. Specifically, the links I–IV from Figure 1 have been modified to allow for more freedom of motion. Note that since both of these manipulators have the same combined Jacobian $\mathbf{J}$ and leg Jacobians $\mathbf{J}_i$, though the quantities $\mathbf{M}$ and $\mathbf{M}_i$ (from Equation (6)) may differ, the natural frequency will still tend to zero at $(x, y) = (0, L)$.

To see physically why the natural frequency tends to zero consider again the position $(x, y) = (L, \epsilon)$ in Figure 3. As $\epsilon \to 0$, the effective rotational inertia of the right-hand leg as seen by a horizontal force applied to the end-effector by the left prismatic actuator goes to infinity, because the length of the moment arm for the horizontal force tends to zero as $\epsilon \to 0$. Note that in reality this infinite inertia may be prevented due to joint motion restrictions. However, in any case, it seems clear that natural frequency can indicate a degradation of the dynamic performance of the manipulator in a region near the leg/platform singularity, while the combined Jacobian $\mathbf{J}$ does not.

[4]This example illustrates that any property of the $\mathbf{J}$ matrix along a given trajectory may not detect closeness to a singular configuration of this type. In fact, in the Jacobian matrix the effect of the leg singularity appears to *cancel* the effect of the platform singularity.

7 Conclusions

The purpose of this paper was to show the usefulness of the linearized natural frequency of a parallel manipulator. In particular we proposed the use of natural frequency (and damping ratio) as a flexible performance measure upon which to build cost functions for the optimum concurrent design of a parallel manipulator and to obtain the optimal kinematic, dynamic and controller parameters of that manipulator. In addition, we motivated the use of natural frequency in this regard by introducing a concept known as a dynamic singularity, which is a configuration of a parallel manipulator where the dynamic performance (at least locally) goes to zero, and gave a simple example that indicates a relationship between a dynamic singularity and a kinematic singularity.

ACKNOWLEDGEMENTS

This work was supported by an NDSEG doctoral fellowship awarded to the first author. Furthermore, this work was partly supported by the National Science Foundation under Grant No. 9984279.

References

[1] J.-P. Merlet, C.M. Gosselin, and N. Mouly. Workspaces of planar parallel manipulators. *Mechanism and Machine Theory*, 33(1/2):7–20, January-February 1998.

[2] C. Gosselin. Determination of the workspace of 6-DOF parallel manipulators. *Journal of Mechanical Design*, 112:331–336, September 1990.

[3] J.-P. Merlet. Singular configurations of parallel manipulators and Grassman geometry. *International Journal of Robotics Research*, 8(5):45–56, October 1989.

[4] C. Gosselin and J. Angeles. Singularity analysis of closed loop kinematic chains. *IEEE Transactions on Robotics and Automation*, 6(3):281–290, June 1990.

[5] H.R. Mohammadi Danialli, P.J. Zsombor-Murray, and J. Angeles. Singularity analysis of planar parallel manipulators. *Mechanism and Machine Theory*, 30(5):665–678, July 1995.

[6] F.C. Park and J.W. Kim. Singularity analysis of closed kinematic chains. *Journal of Mechanical Design, Transactions of the ASME*, 121(1):32–38, March 1999.

[7] J.-P. Merlet. *Parallel Robots*. Kluwer Academic Publishers, Dordrecht, 2000.

[8] J. Angeles. *Fundamentals of Robotic Mechanical Systems: Theory, Methods and Algorithms*. Springer-Verlag, New York, 1997.

[9] T. Yoshikawa. *Foundations of Robotics: Analysis and Control*. The MIT Press, Cambridge, Massachusetts, 1990.

[10] H. Lipkin and J. Duffy. Hybrid twist and wrench control for a robotic manipulator. *Journal of Mechanisms, Transmissions, and Automation in Design*, 110:138–144, June 1988.

[11] K. Doty, C. Melchiorri, E. Schwartz, and C. Bonivento. Robot manipulability. *IEEE Transactions on Robotics and Automation*, 11:462–468, June 1995.

[12] C. Gosselin. On the design of efficient parallel mechanisms. In *Proceedings of the NATO Advanced Study Institute on Computational Methods in Mechanics*, volume 1, pages 157–186, Bulgaria, June 1997.

[13] R. Kurtz and V. Hayward. Multiple-goal kinematic optimization of a parallel spherical mechanism with actuator redundancy. *IEEE Transactions on Robotics and Automation*, 8(5):644–651, October 1992.

[14] C. Gosselin and J. Angeles. The optimum kinematic design of a planar three-degree-of-freedom parallel manipulator. *Journal of Mechanisms, Transmissions, and Automation in Design*, 110:35–41, March 1988.

[15] J.P. Merlet. Designing a parallel manipulator for a specific workspace, April 1995. INRIA Research Report No. 2527.

[16] D. Chakarov. Study of the passive compliance of parallel manipulators. *Mechanism and Machine Theory*, 34:373–389, 1999.

[17] S. Bhattacharya, H. Hatwal, and A. Ghosh. On the optimum design of Stewart platform type parallel manipulators. *Robotica*, 13(2):133–140, March-April 1995.

[18] S. Shamblin and G. Wiens. Characterization of dynamics in PKMs. In *Parallel Kinemtic Machines International Conference*, pages 24–33, Ann Arbor, MI, September 2000.

[19] O. Khatib and A. Bowling. Optimization of the inertial and acceleration characteristics of manipulators. In *International Conference on Robotics and Automation*, pages 2883–2889, Minneapolis, Minnesota, April 1996.

[20] J. Lückel, T. Moritz, W. Kuhlbusch, S. Toepper, F. Scharfeld, P. Maisser, H. Freudenberg, E. Kallenbach, J. Zentner, and E. Saffert. Iterative model-based design of the parallel robot, TRIPLANAR. In *International Conference on Advanced Intelligent Mechatronics*, pages 135–140, Como, Italy, July 2001.

[21] O. Company, F. Pierrot, F. Launay, and C. Fioroni. Modeling and preliminary design issues of a 3-axis parallel machine tool. In *Parallel Kinemtic Machines International Conference*, pages 14–23, Ann Arbor, MI, September 2000.

[22] J. Craig. *Introduction to Robotics: Mechanics and Control*. Addison-Wesley Publishing Company, Reading, MA, 1989.

[23] K. Kozak, I. Ebert-Uphoff, and W. Singhose. Analysis of varying natural frequencies and damping ratios of a sample parallel manipulator throughout its workspace using linearized equations of motion. In *Proceetings of ASME DETC 2001*, number VIB-21529, Pittsburgh, PA, September 2001.

Regular Papers: Kinematics and Singularities

Thursday, October 3 2002, 4:15PM

Session Chairs: M. Shoham and G. Wiens

1. A. Meschini, R. Sinatra
   "A Parallel Mechanism for a Satellite Antenna with Double Reflector".

2. M.L. Husty, A. Karger
   "Self Motions of Stewart-Gough-Platforms – An Overview".

3. Y. Takeda, U. Spaelter, H. Funabashi
   "Forward Displacement and Singularity Analysis of a Crank-Type 6-3 In-Parellel Actuated Mechanism".

4. A. Perez, J.M. McCarthy
   "Dual Quaternion Synthesis of a 2-TPR Constrained Parallel Robot".

Proceedings of the WORKSHOP on
Fundamental Issues and Future Research Directions for Parallel Mechanisms and Manipulators
October 3–4, 2002, Quebec City, Quebec, Canada
Clément M. Gosselin and Imme Ebert-Uphoff, editors

A Parallel Mechanism for a Satellite Antenna with double reflector

ALBERTO MESCHINI
Alenia Spazio s.p.a.
Space Division
Via Saccomuro, 24, Roma, Italy,
a.meschini@roma.alespazio.it

ROSARIO SINATRA
Dipartimento di Ingegneria Industriale e Meccanica
Università di Catania
Viale A. Doria n. 6, 95125 Catania, Italy
rsinatra@diim.unicxt.it

SIMONE PIRROTTA
Dipartimento di Ingegneria Industriale e Meccanica
Università di Catania
Viale A. Doria n. 6, 95125 Catania, Italy
simonepirrotta@tin.it

Abstract: *This paper presents the study of a parallel mechanism for the Gregorian offset antenna with double reflector developed by Alenia Aerospazio. The architecture of the mechanical system can rightly be considered a six-degree-of-freedom platform-type parallel manipulator with six prismatic legs connected to the base and moving platform. A reflector with appropriate surfaces for the transmission of signals is fixed to each platform. The alternative tracking system studied is based on the analogy of the Stewart platform mechanism actuated by prismatic joints on the legs. First, a three-dimensional vector optical analysis was performed on the system relative to the reciprocal position of the reflectors. Varying the incidence conditions of the electromagnetic signal on the fixed surface, the position and orientation of the upper reflector, called sub-reflector, are found for the best optical configuration. The kinematic relations of the system in terms of the displacement, velocity and acceleration of the linear prismatic actuators are derived and used to minimise tracking errors due to disturbances effecting the satellite in orbit. The implementation of the equations is illustrated by computer simulation, and numerical results are obtained for two input conditions of disturbance.*

1 Introduction

Various configurations are possible for satellite antenna, each with different characteristics. In the antennas which adopted Gregorian configuration, shown in Figure 1, the geometric parameters of the paraboloid and ellipsoid are considered. The geometry of the ellipsoid is such that rays emitted by a

Fig. 1 – Gregorian offset antenna *W24*.

source placed at one of the two focuses, F_1, are reflected in a direction passing through the other focus, F_2. If the ellipsoid is positioned relative to the paraboloid in such a way that its focus F_2 coincides with the focus of the paraboloid itself, well-known geometric properties result in any ray emitted by F_1 being propagated, after the two reflections, in a direction parallel to the axis of the paraboloid.

In particular, the antenna under study has a configuration defined *offset,* shown in Figure 2, because it does not present the axial-symmetry of the correlated *onset* configuration, as in Figure 3.

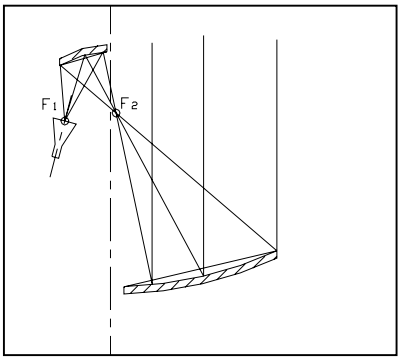

Fig. 2 – Gregorian offset

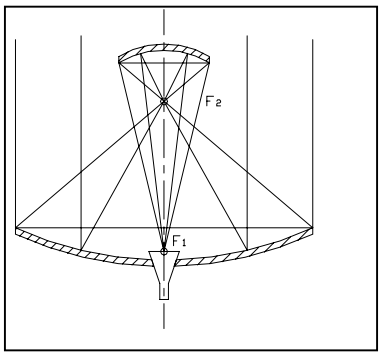

Fig. 3 – Gregorian onset

In the Gregorian type satellite antenna, the system optics are invariable and optimised under conditions of standard reception. Here the *boresight*, i.e. the central beam of the incident signal, is parallel to the axis of the reflector with paraboloid surface. Any corrections necessary are made using a tracking system based on a biaxial positioning mechanism, APM *Antenna Positioner Mechanism,* to move the platform carrying the antenna, and a coaxial actuator, *Sub-reflector Actuator Mechanism,* consisting of a stepper motor to rotate the upper reflector, termed *sub-reflector*. The principle is to use the APM system to point the lower reflector and, therefore, the whole antenna, given that the relative positions of the components making up the optical system are invariable, as seen in Figure 4.

The concept developed in this study is to track the antenna using linear actuators on its legs to modify the position and orientation of the sub-reflector and obtain the desired optical configuration. This suggests schematising the antenna mechanical system as a 6-6 platform-type parallel mechanism, commonly called a *Stewart platform*. This model consists of six telescopic legs, a base and a mobile platform. One end of each leg is connected to the base platform by a universal joint, while the other end is connected to the moving platform by a spherical joint. Six actuators on the legs are used to control the motion of the manipulator, as in Figure 5.

The relations of the system at the displacement, velocity and acceleration level of the prismatic joint variables are derived from the kinematic model, and used to control the position of the moving platform and, consequently, of the sub-reflector integral with to it.

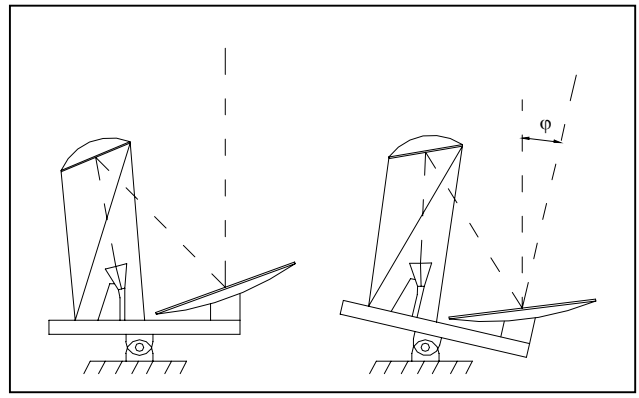

Fig. 4 – Tracking of the *Gregorian offset* antenna using an APM system to move all components.

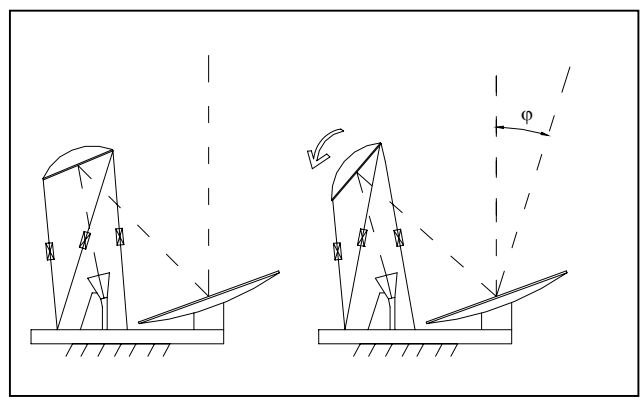

Fig. 5 – Tracking of the *Gregorian offset* antenna using a system of actuators on legs to move the sub-reflector alone.

2 Vector analysis of reflection

The aim of the following analysis is to determine the position and orientation of the sub-reflector centre, C, which guarantees a correct reception even when the direction of incidence differs from the condition of standard reception, i.e. when the *boresight* is no longer parallel to the paraboloid axis. This means that focus F_2, common with the lower reflector, is shifted because of disturbances while focus F_1 remains fixed and coincident with the emitter/receiver element, termed *feed* (Silver, 1986)

The input of this analysis is the geometry of the upper and lower reflectors. While the lower surface is assumed coincident with the theoretical surface, i.e. the paraboloid cross-section, the sub-reflector is schematised as a spherical

mirror, except for subsequent corrections to take surface irregularities into account.

Referring to Figure 6, three co-ordinate frames are defined:

fixed frame $\mathcal{F}_P$ (X_P, Y_P, Z_P) with its origin at the point O_P integral with the antenna base;

frame $\mathcal{F}_1$ (X_1, Y_1, Z_1) not rotating with respect to frame $\mathcal{F}_P$ and with its origin at the point O_1, centre of the parabolic reflector, whose co-ordinates are known in frame $\mathcal{F}_P$;

frame $\mathcal{F}_S$ (X_S, Y_S, Z_S) with its origin at the centre of the sub-reflector, such that the Z_S-axis is directed along the sub-reflector axis.

The plane in which reflection occurs, π_1, is tangent to the paraboloid at point O_1; it is then possible to define frame $\hat{\mathcal{F}}_1$, obtained by rotating $\mathcal{F}_1$ around the axis Y_1 by an angle $\theta/2$ such that π_1 coincides with the plane $\hat{X}_1\hat{Y}_1$.

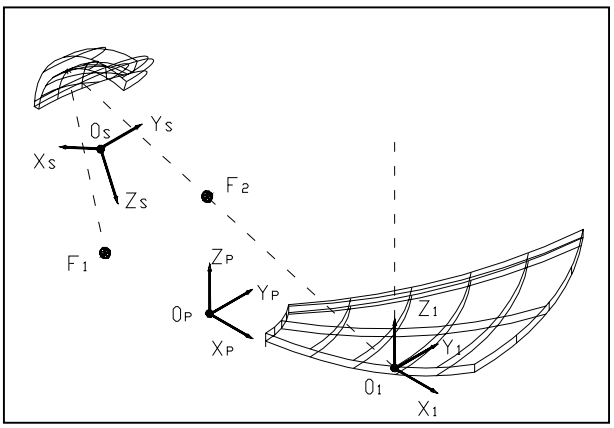

Fig. 6 – The frame notations.

Let $\mathbf{e}_i$ be the versor indicating the direction of incidence of the *boresight*. Due to variation in the direction of incidence with respect to standard conditions, the versor $\mathbf{e}_i$ will form two, non zero, angles θ_1 e θ_2, defined in Figure 7.

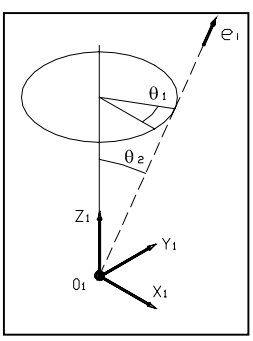

Fig. 7 – Versor and angles of incidence.

To perform the reflections, it is first necessary to express $\mathbf{e}_i$ with respect to $\hat{\mathcal{F}}_1$:

$$\hat{\mathbf{e}}_i = \mathbf{R}_Y \cdot \mathbf{e}_i \tag{1}$$

where $\mathbf{R}_Y$ is the 3×3 matrix transforming $\mathcal{F}_1$ co-ordinates into $\hat{\mathcal{F}}_1$ ones:

$$\mathbf{R}_Y = \begin{bmatrix} \cos(\theta/2) & 0 & \sin(\theta/2) \\ 0 & 1 & 0 \\ -\sin(\theta/2) & 0 & \cos(\theta/2) \end{bmatrix} \tag{2}$$

To obtain the reflected versor $\hat{\mathbf{e}}_{ir}$ it is enough to invert the signs of the X and Y co-ordinates of $\hat{\mathbf{e}}_i$, recalling the matrix:

$$\hat{\mathbf{e}}_{ir} = \begin{bmatrix} -1 & 0 & 0 \\ 0 & -1 & 0 \\ 0 & 0 & 1 \end{bmatrix} \cdot \hat{\mathbf{e}}_i \tag{3}$$

The unit vector $\hat{\mathbf{e}}_{ir}$ is expressed in the rotated reference system $\hat{\mathcal{F}}_1$. The unit vector of the direction of reflection in frame $\mathcal{F}_1$ is found by:

$$\mathbf{e}_{ir} = \mathbf{R}_Y^{-1} \cdot \hat{\mathbf{e}}_{ir} \tag{4}$$

Assuming that the geometric position of F_2 on varying the angles of incidence θ_1 and θ_2 is a sphere with centre at O_1 and a radius r_1, as in Figure 8, the vector identifying the new position of focus F_2' is calculated by multiplying the versor $\mathbf{e}_{ir}$ by its modulus, i.e. the focal distance r_1:

$$\overrightarrow{O_1F_2'} = r_1 \cdot \mathbf{e}_{ir} \tag{5}$$

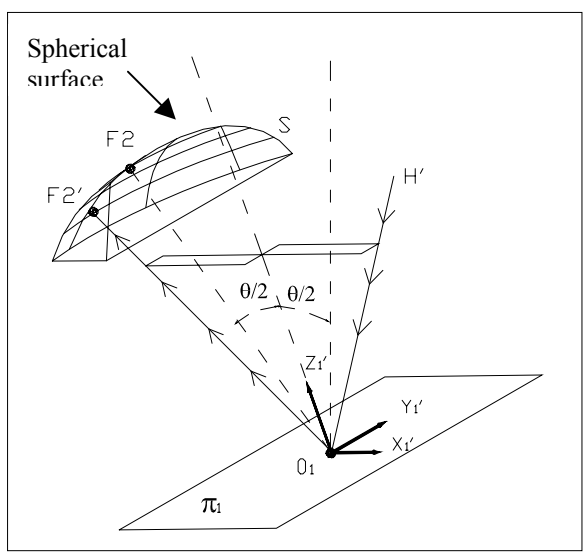

Fig. 8 – Reflection on parabolic surfaces.

This simplified hypothesis is a good optical-geometric approximation of the antenna behaviour in the radio-frequency domain. In fact, if phenomena caused by diffraction and edge effects are excluded, geometrical optics are a good approximation of physical optics. This procedure makes it possible to determine the direction in which the beam emerges from the parabolic reflector and, in particular, the new position of the reflector focus F_2', which, due to the properties of the Gregorian optical system, coincides with one of the sub-reflector focuses.

The next step consists of positioning and orienting the sub-reflector to obtain a correct reflection, knowing the new position of focus F_2 and maintaining focus F_1 fixed at the position of the antenna *feed*. The plane π_2 is defined as belonging to the beam carried by the vector $\overrightarrow{O_1F_2'}$ and passing through point F_1, or as belonging to the carrier beam $\overrightarrow{O_1F_1}$ and passing through F_2'.

The phenomenon of reflection takes place entirely in the plane π_2 and this allows laws of geometrical optics to be used. In particular, using the reference system $\mathcal{F}_3$, defined rotating $\mathcal{F}_1$ so that Z_1 coincides with the versor of the reflected ray $\mathbf{e}_{ir}$, the problem is further simplified. The associated rotation matrix $\mathbf{R}_t$ has the Z_3 axis coincident with the versor of $\mathbf{e}_{ir}$, the Y_3 axis is the versor orthogonal to the plane π_2, and the X_3 axis is obtained from the vector product of the first two to complete the right-handed triplet

$$\mathbf{R}_3 = [X_3; Y_3; Z_3] \tag{6}$$

where

$$Z_3 = \mathbf{e}_{ir}, \qquad Y_3 = \frac{\mathbf{n}}{\|\mathbf{n}\|}, \qquad X_3 = Y_3 \times Z_3 \tag{7}$$

and $\mathbf{n}$ is the orthogonal vector to the plane π_2, defined by the co-ordinates of points F_1 and F_2' as:

$$\mathbf{n} = \begin{bmatrix} 1 \\ -x_{F_1} / z_{F_1} \\ (((x_{F_1} - x_{F_2}) / (-x_{F_2}) / y_{F_2} \end{bmatrix} \tag{8}$$

Multiplying from the left the vectors $\overrightarrow{O_1F_1}$ and $\overrightarrow{O_1F_2'}$ by the matrix $\mathbf{R}_3$ gives their expressions in the reference system $\mathcal{F}_3$, or better, as a result of how $\mathcal{F}_3$ was defined, in the plane Z_3X_3 which coincides with π_2. It should be noted that point F_2 belongs to the Z_3 axis.

Having brought the problem to the aptly chosen plane π_2, the laws of geometrical optic can be used. In particular, the condition must always hold:

$$1/f_1 + 1/f_2 = 2/r \tag{9}$$

where f_1 and f_2 are the distances on the Z_3 axis of the two foci from the vertex V, and r is the radius of the spherical mirror. The other relation connecting variables f_1 and f_2 is obtained from the condition that point C must be situated at the conjunction of points F_1 and F_2, as shown in Figure 9:

$$z_1 - z_2 = h = f_2 - f_1 \tag{10}$$

Referring to Figure 9 and eqs. (9 & 10), the variables f_1 and f_2 can be calculated, and consequently the co-ordinates of the centre C of the sub-reflector:

$$z_c = z_2 + f_2 - r \tag{11}$$

$$x_c = (-x_1)(f_2 - r) / h \tag{12}$$

$$\overrightarrow{O_1C} = \overrightarrow{O_1O_S} = [x_C; 0; z_C] \tag{13}$$

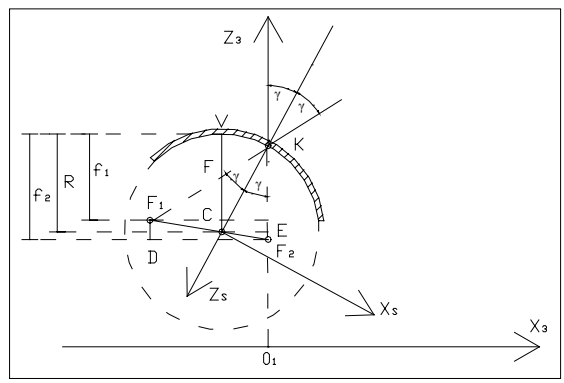

Fig. 9 – Geometry of reflection in the π_2 plane on the sub-reflector considered spherical.

The 6×6 rotation matrix **S** of the sub-reflector is defined as:

$$\mathbf{S} = \begin{bmatrix} 1 & 0 & 0 \\ 0 & -1 & 0 \\ 0 & 0 & -1 \end{bmatrix} \cdot \begin{bmatrix} \cos\gamma & 0 & \sin\gamma \\ 0 & 1 & 0 \\ -\sin\gamma & 0 & \cos\gamma \end{bmatrix} \tag{14}$$

where

$$\gamma = \arcsin(-x_C / r) \tag{15}$$

Referring to the inertial frame:

$$\mathbf{p} = \overrightarrow{O_PO_S} = (\mathbf{R}_3^{-1} \cdot \overrightarrow{O_1O_S}) + \overrightarrow{O_PO_1} \tag{16}$$

$$\mathbf{Q} = \mathbf{R}_3^{-1} \cdot \mathbf{S} \tag{17}$$

Eqs.(16 & 17) represent the analytical expression of the position and orientation of the sub-reflector C in the case of non-zero angles of incidence.

To validate the procedure, trials were conducted to study the behaviour of the input/output electromagnetic signal of the antenna with the support of *GRASP8* software used by the electromagnetic design group of the *Alenia Spazio* Antenna Department.

With *GRASP8* it is possible to obtain radiation diagrams using the physics-optics description to calculate the electromagnetic field of the antenna under examination. In more detail, the program calculates the electrical currents generated on the reflectors by the feed, and then the corresponding long-range radiation produced. Figure 10 shows a graphical output of this software.

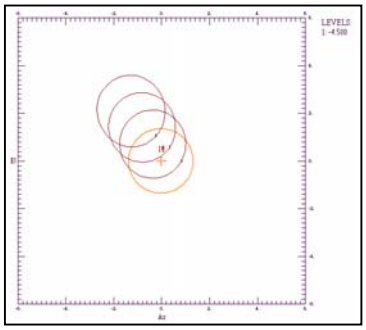

Fig. 10 – Graphical output of the simulator. Displacement of coverage with θ_1=120°, θ_2=1°, 2°, 3°.

The trials consist of supplying the simulator with the position of the sub-reflector centre and its rotation matrix for given angles of incidence and then verifying the behaviour of the radiation beam, in particular the difference between the given angle of incidence values, termed *mechanical*, and those actually obtained with the beam, termed *electrical*. This difference is taken as an index of the integrity of the procedure developed. Simulations for given values of θ_1 and θ_2 showed significant differences and an irregular behaviour which can be imputed to the excessive simplification of assuming the sub-reflector surface to be spherical.

Greater precision in determining the position of the sub-reflector centre is possible if the non-spherical geometry of the surface is taken into account by refining the law of reflection with the expression:

$$1/f_1 + 1/f_2 = k/r \tag{18}$$

where the constant k is found by applying the equation inversely when the antenna is in the fixed configuration of optimal reflection. The values of f_1 and f_2 can then be calculated, and from these the constant k defined in eq. (18):

$$k = r\,(1/f_1 + 1/f_2\,) \tag{19}$$

In this geometry, $k = 2.12$.

In the light of this new value, the geometry of reflection becomes that shown in Figure 11, for which the equation obtained previously cannot be used.

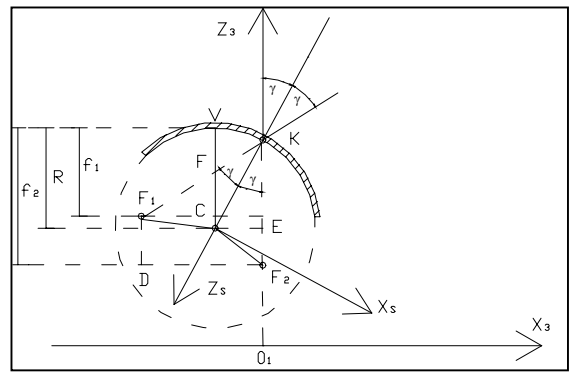

Fig. 11 – Geometry of reflection in the π_2 plane on sub-reflector with corrected surface

Since the line KC bisects the angle $O\hat{K}F_1$, it follows that:

$$tg(2\cdot\varphi) = \frac{-x_{F_1}}{x_P - z_{F_1}} = \frac{-x_{F_1}}{(z_C + r\cdot\cos(\varphi)) - z_{F_1}} \tag{20}$$

This transcendental equation can be solved by various methods: for example by substituting the variable, letting tg $\varphi = y$ gives:

$$\frac{2\cdot y}{1-y^2} = \frac{(-x_{F_1})\cdot\sqrt{1+y^2}}{\sqrt{1+y^2}\cdot(z_C - z_{F_1}) + r} \tag{21}$$

For simplicity, let:

$$x_{F_1} = A \tag{22}$$

$$z_C - z_{F_1} = B \tag{23}$$

where A and B are known constants, since x_{F_1} and z_{F_1} are fixed and z_C is calculated from eq. (11). Eq. (21) becomes:

$$\sqrt{1+y^2}\,(y^2 - 2yB - A) = 2y\cdot r \tag{24}$$

This equation in y can be rendered in polynomial form with coefficients which are known terms:

$$y^6 + c_5\cdot y^5 + c_4\cdot y^4 + c_3\cdot y^3 + c_2\cdot y^2 + c_1\cdot y + c_0 = 0 \tag{25}$$

Among the possible solutions of y_i, for i = 1,…,6, imaginary solutions are ignored and the only admissible positive solution is used to calculate the value of φ.

Starting from this angle, the co-ordinates of C are found:

$$z_C = z_P - r\cos\varphi \tag{26}$$

$$x_C = -\,r\sin\varphi \tag{27}$$

and also the rotation matrix **S** of the reference system integral with the sub-reflector with respect to the system $\mathcal{F}_3$, which expresses a rotation of φ around the Y_3 axis:

$$\mathbf{S} = \begin{bmatrix} 1 & 0 & 0 \\ 0 & -1 & 0 \\ 0 & 0 & -1 \end{bmatrix} \cdot \begin{bmatrix} \cos\gamma & 0 & \sin\gamma \\ 0 & 1 & 0 \\ -\sin\gamma & 0 & \cos\gamma \end{bmatrix} \tag{28}$$

The vectors and matrices so found are then expressed in the reference system $\mathcal{F}_1$, again using the inverse of matrix $\mathbf{R}_3$, as in eqs.(16 & 17).

Figure 12 shows the results of this simulation, evidencing a greater precision in terms of difference between electrical obtained angles and mechanical imposed ones, and above all a greater regularity in the behaviour on varying the angles of incidence. However, these errors are neither negligible nor avoidable, but depend on the irregularity of the sub-reflector surface.

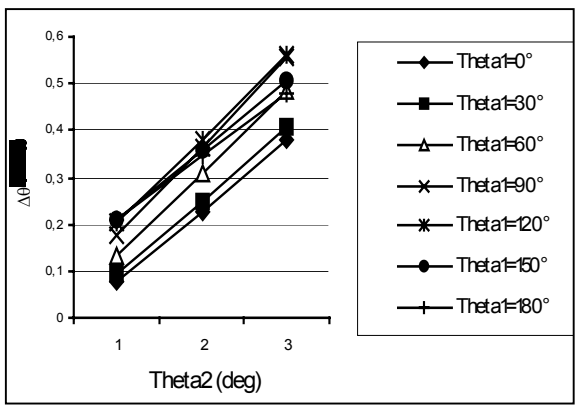

Fig. 12 – Difference between theoretical and obtained angles on varying the angles of incidence.

3 Kinematics

The antenna mechanism can be schematised as a conventional six-degrees-of-freedom platform-type parallel mechanism, known as a Stewart-Gough platform. The slender elements can in fact be considered six telescopic legs connecting the two platforms, one fixed with respect to an inertia system, and the other mobile, named respectively FB and MB. The joints are the result of the deformation capacity of the elements placed at the extremities of the legs, termed *spindles*. Since the deformation is localised in a limited zone, it can reasonably be schematised as point constraints placed on the mid-line of the axis of the cylindrical section. For each leg, one end is connected to the base platform by universal joint, while the other end is connected to the moving platform by a spherical joint. Six actuators on the legs are used to control the motion of the manipulators.

Having defined the co-ordinate inertial frame $\mathcal{F}_P$ (X_P, Y_P, Z_P) fixed at point O_P on the inertial platform BP, and the frame $\mathcal{F}_S$ (X_S, Y_S, Z_S), fixed to the sub-reflector and, consequently, to the mobile platform MP with its origin at the point O_S, it is possible to define points O_{1i} and C_i connecting, respectively, the legs and the fixed and mobile platforms, where i characterises the leg. Since these points must coincide with the universal and spherical point constraints, they will be located, as evidenced above, at the centre of the section in which the deformation is imagined to be located, as shown in Figures 13 & 14.

The kinematics are studied using the schematisation indicated as *simple legs* (Ma, 1991). Each leg therefore consists of two prismatic elements, constrained at the extremities by a spherical and a universal joint, and whose relative movement is associated with the prismatic joint variable q_j with i = 1,…6. The values of q_j for each leg are grouped in the 6×1 vector **q**.

The solution to the inverse kinematic problem is now possible: the vector **q** is determined on varying the position and orientation of the system associated with the sub-reflector.

Referring to Figure 13, the kinematic constraint equations for each leg can be written:

$$\mathbf{p} = \overrightarrow{O_P O_S} = \overrightarrow{O_P O_{1i}} + \overrightarrow{O_{1i} C_i} + (\mathbf{Q} \cdot \overrightarrow{C_i O_S}) \quad i = 1,\ldots,6 \tag{29}$$

from which it is possible to calculate the unknown vector $\overrightarrow{O_{1i} C_i}$ on varying $\mathbf{p}(t) = \overrightarrow{O_P O_S}$ and $\mathbf{Q}(t)$, and in which all other vectors and matrices are known and depend on the geometry of the system.

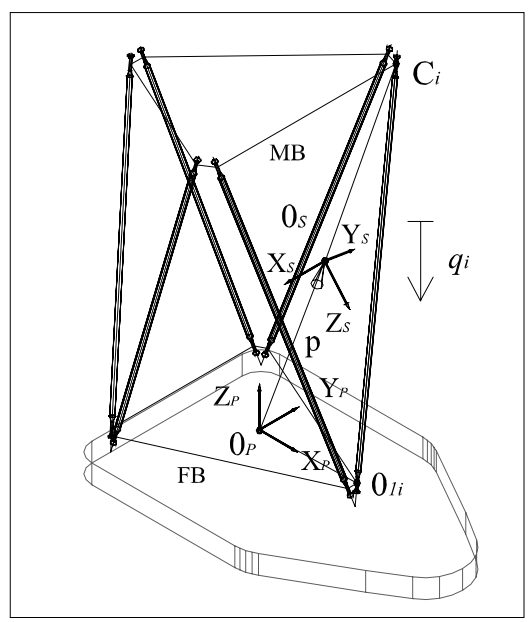

Fig. 13 – Reference system and base points.

Moreover, referring to kinematic notation for simple legs shown in Figure 14, we have:

$$\mathbf{l}_i(t) = \overrightarrow{O_{1i} C_i}(t) = q_i \cdot \mathbf{e}_i\,, \quad \mathbf{u}_i = \overrightarrow{O_P O_{1i}}\,, \quad \mathbf{r}_i = \overrightarrow{C_i O_S} \quad i=1,..,6 \tag{30}$$

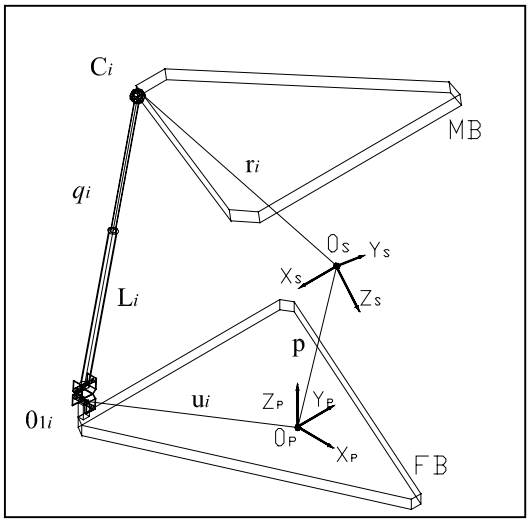

Fig. 14 – Kinematic notation for simple legs.

The modulus of vector $\overrightarrow{O_{1i}C_i}$ then gives the joint variable q_i, which characterises the length of each leg:

$$q_i = \left|\overrightarrow{O_{1i}C_i}\right| = \sqrt{[\mathbf{p} + \mathbf{Q}\mathbf{r}_i^{'} - \mathbf{u}_i]^{\mathrm{T}}[\mathbf{p} + \mathbf{Q}\mathbf{r}_i^{'} - \mathbf{u}_i]} \quad \text{for } i = 1,\ldots,6 \tag{31}$$

and thus:

$$\mathbf{q} = [q_1, q_2, q_3, q_4, q_5, q_6]^{\mathrm{T}} \tag{32}$$

The velocity problem is defined by the equation:

$$\mathbf{J}\,\mathbf{t} = \dot{\mathbf{q}} \tag{33}$$

where **J** is the Jacobian matrix 6×6 (Gosselin, 1988) and $\mathbf{t} = \begin{bmatrix} \boldsymbol{\omega} \\ \dot{\mathbf{p}} \end{bmatrix}$ is the twist vector of the MB, while is possible to solve the acceleration problem by the time derivative of eq.(33):

$$\mathbf{J}\,\dot{\mathbf{t}} + \dot{\mathbf{J}}\,\mathbf{t} = \ddot{\mathbf{q}} \tag{34}$$

where $\dot{\mathbf{t}} = \begin{bmatrix} \dot{\boldsymbol{\omega}} \\ \ddot{\mathbf{p}} \end{bmatrix}$ is the time derivative of vector **t**.

To solve the inverse problems at the velocity and acceleration level, it is necessary to know the generalised velocity vector, i.e. the twist **t** and its time derivative. Since the analytical law for the input $\mathbf{p}(t) = \overrightarrow{O_P O_S}$ and $\mathbf{Q}(t)$ is not available, it is necessary to obtain the time derivative in approximate form, using the derivative definition:

$$\dot{\mathbf{p}} = \frac{\mathbf{p}(t+\Delta t) - \mathbf{p}(t)}{\Delta t} \tag{35}$$

$$\dot{\mathbf{Q}} = \frac{\mathbf{Q}(t+\Delta t) - \mathbf{Q}(t)}{\Delta t} \tag{36}$$

Thus it is possible to calculate the angular velocity vector of the MB $\boldsymbol{\omega}$:

$$\boldsymbol{\omega} = \mathrm{vect}(\boldsymbol{\Omega}) = \mathrm{vect}(\dot{\mathbf{Q}} \cdot \mathbf{Q}^T) \tag{37}$$

and also calculate $\dot{\mathbf{t}}$, from $\ddot{\mathbf{p}}$ e $\dot{\boldsymbol{\omega}}$, by:

$$\ddot{\mathbf{p}} = \frac{\dot{\mathbf{p}}(t+\Delta t) - \dot{\mathbf{p}}(t)}{\Delta t} \tag{38}$$

$$\dot{\boldsymbol{\Omega}} = \frac{\boldsymbol{\Omega}(t+\Delta t) - \boldsymbol{\Omega}(t)}{\Delta t} \tag{39}$$

$$\dot{\boldsymbol{\omega}} = \mathrm{vect}(\dot{\boldsymbol{\Omega}}) \tag{40}$$

Let α_{ji}, θ_{ji}, b_{ji}, a_{ji}, the Denavit-Hartenberg parameters, defined (as in Angeles, 1997) for the *j*-th joint of the *i*-th leg. For simple legs, actuated joints are prismatic joints, whose parameters are the variables b_{3i}, previously defined as q_i.

For this application, it is also important to calculate the variables of non-actuated joints: in fact the values of θ_{1i} and θ_{2i} are the angles of flexion in plane $X_P Z_P$ and $Y_P Z_P$ and θ_{4i} is the torque angle of the *i*-th leg. As in Angeles, 1997:

$$\theta_{1i} = \tan^{-1}(y_{Ci} / x_{Ci}) \tag{41}$$

$$\theta_{2i} = \tan^{-1}[(x_{Ci} \cdot \cos\theta_{1i} + y_{Ci} \cdot \sin\theta_{1i}) / (-z_{Ci})] \tag{42}$$

We now define the versor of the *j*-th joint $[\mathbf{e}_{ji}]_{ki}$, in the frame $\mathcal{F}_{ki}$, for $i = 1,\ldots,6$:

$$[\mathbf{e}_{5i}]_{4i} = \begin{bmatrix} \mu_{4i} \sin\vartheta_{4i} \\ -\mu_{4i} \cos\vartheta_{4i} \\ \lambda_{4i} \end{bmatrix} \tag{43}$$

where:

$$\mu_{ji} = \sin\alpha_{ji} \tag{44}$$

$$\lambda_{ji} = \cos\alpha_{ji} \tag{45}$$

It is then possible to calculate:

$$[\mathbf{e}_{6i}]_{4i} = \mathbf{Q}_{3i}^{\mathrm{T}} \cdot \mathbf{Q}_{2i}^{\mathrm{T}} \cdot \mathbf{Q}_{1i}^{\mathrm{T}} \cdot [\mathbf{e}_{6i}]_{1i} \tag{46}$$

in which $[\mathbf{e}_{6i}]_{1i}$ is the third column of the matrix **Q**.

Thus θ_{4i} derives from the following equation:

$$[\mathbf{e}_{6i}]_{4i}^{\mathrm{T}} \cdot [\mathbf{e}_{5i}]_{4i} = \lambda_{5i} \tag{47}$$

which can be rewritten in the form:

$$(\lambda_{5i} - \eta_i \cdot \mu_{4i} - \zeta_i \cdot \lambda_{4i})\tau_{4i}^2 - 2 \cdot \xi\mu_{4i}\tau_{4i} + (\lambda_{5i} + \eta_i \cdot \mu_{4i} - \varsigma_i \cdot \lambda_{4i}) = 0 \quad (48)$$

where:

$$\tau_{4i} = \tan(\theta_{4i} / 2) \quad (49)$$

3.1 Numerical Simulations

The kinematics modelling above was implemented in an algorithm, named *Subreflector Positioning Algorithm*, to evaluate the kinematics of the system under different end-effector conditions. A numerical example of the application both in the angular oscillations effected to minimise tracking errors caused by disturbances, *objective 1#*, and to re-point the antenna, *objective 2#*, is reported.

To evaluate the dynamic phenomena conditioning the operation of a satellite, measurements made by *Alenia Spazio* on *ITALSAT* were analysed. Continuous records are made of angular movements effected by the antenna actuators to zero tracking errors caused by a series of natural, or in any case unavoidable, phenomena. These are *thermal distortion*; *residual rotation*, i.e. residual satellite tracking errors in *roll/pitch*; *normal mode*, the effect of firing the thrusters to correct satellite orientation; and *station keeping*, due to accelerations of the satellite. For simulation purposes, the steps of the *Subreflector Positioning Algorithm* are shown schematically in Figure 15.The equations corresponding to each block of the diagram have been described above. Simulations were conducted under two conditions: *normal mode* and *station keeping* mode, shown respectively in Figures 16 and 17, and for a particular model of antenna, named *W24* developed and certified by *Alenia Spazio*.

The time-histories of displacement, velocity and acceleration of the actuated joints, named $q_i, \dot{q}_i, \ddot{q}_i$, are reported in Figures 18 and 19, respectively for *normal mode* and *station keeping* mode and for i =1,…,6.

It is then possible to obtain the non-actuated prismatic variables, i.e. the flexion and torsion of the spindles, which are titanium elements connecting legs to platforms, as shown in Figure 20. Instead Figures 21 and 22 show the time-histories of flexion angles ϑ_{1i} and ϑ_{2i} and of torsion angles ϑ_{4i}, for *normal mode* and *station keeping* mode, respectively, and for i =1,…,6.

It is then possible to consider whether the maximum strain values are supported by the spindles: for objective 1#, spindle resistance is sufficient in terms of both static and fatigue resistance, but insufficient if the antenna must be re-pointed. In fact in this case the angles of *tracking error* increase.

4 Conclusions

In this paper, the mechanism of the *Gregorian offset* antenna is considered as a *Stewart platform* actuated by six prismatic joints.

A preliminary phase analysed the optics of the system deriving the laws of motion for the sub-reflector which act as input for the inverse kinematics problem, already largely solved.

Modifying the optical system is of particular interest in an attempt to reduce tracking errors due to disturbances to which the satellite is subjected and which, in any case, are in the order of hundredths of a degree, but also for any greater re-orientations with Earth that may be necessary. In this case, the errors increase in order of magnitude, as evidenced by the electrical simulation, as shown in Figure 10, with the manifestation of optical aberration phenomena due to external causes.

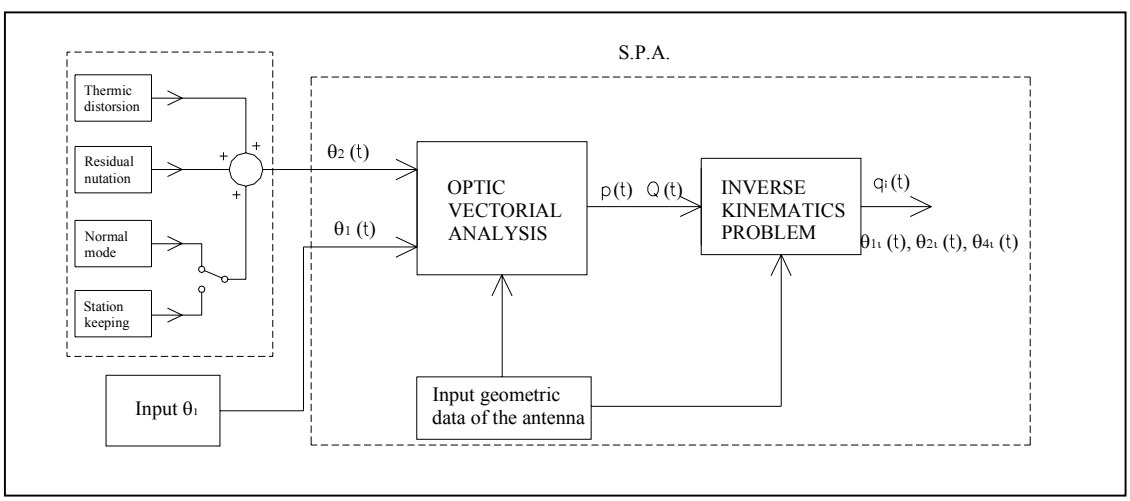

Fig. 15 – Block diagram of the algorithm calculating the joint variables for different disturbance modes.

Thus the *Subreflector Positioning Algorithm* was developed to simulate the pointing of the antenna, both to minimise tracking errors caused by disturbances acting on the satellite and to re-tracking the antenna toward Earth.

Results regarding actuated joints can be used to dimension linear actuators for the legs, while those concerning non-actuated joints determine whether the strains produced are tolerated by the antenna structure, above all by the spindles.

In particular, the spindles were found to be inadequate for the performance of *objective 2#*, namely the re-pointing of the antenna.

Future developments include the construction of antenna prototypes where motion is controlled by the extension of telescopic legs. The most interesting aspect is the development of linear actuators, with their functioning based on the resonance induced by piezoelectric phenomena.

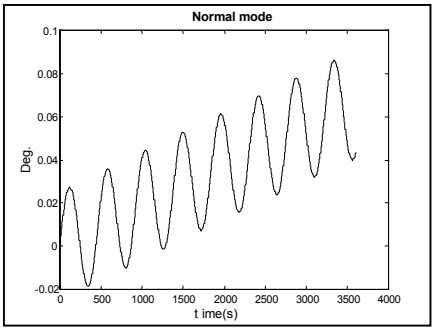

Fig. 16 – Disturbance in *normal mode*.

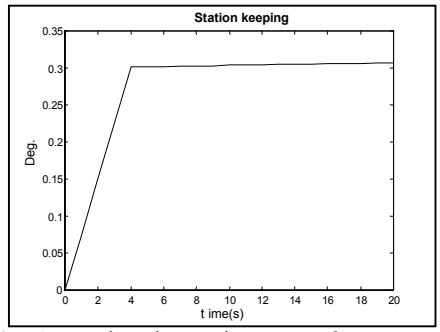

Fig. 17 – Disturbance in *station keeping* mode.

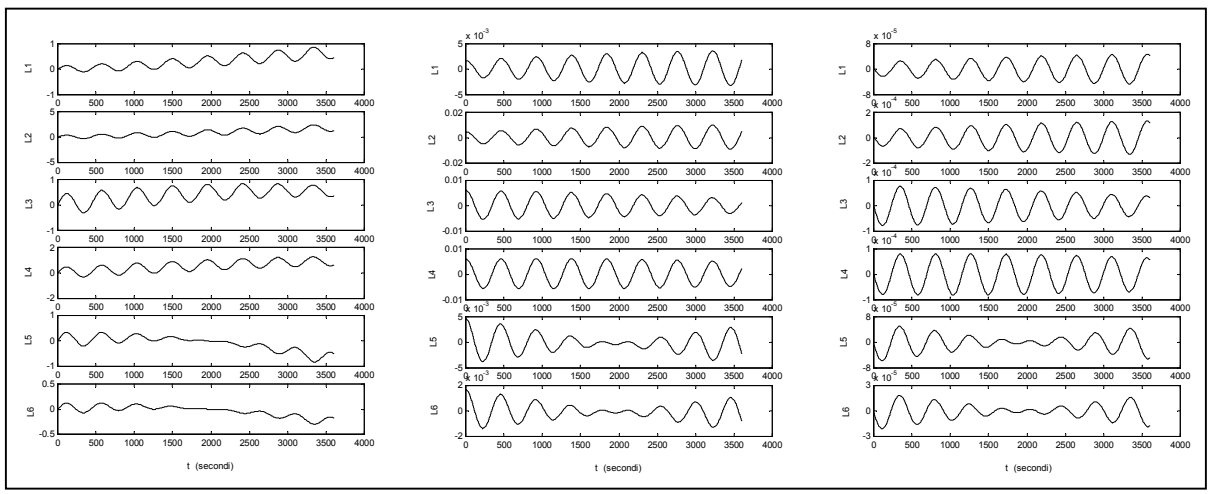

Fig. 18 – Displacements, velocities and accelerations ($q_i, \dot{q}_i, \ddot{q}_i$ for i = 1,…,6) in *normal mode*.

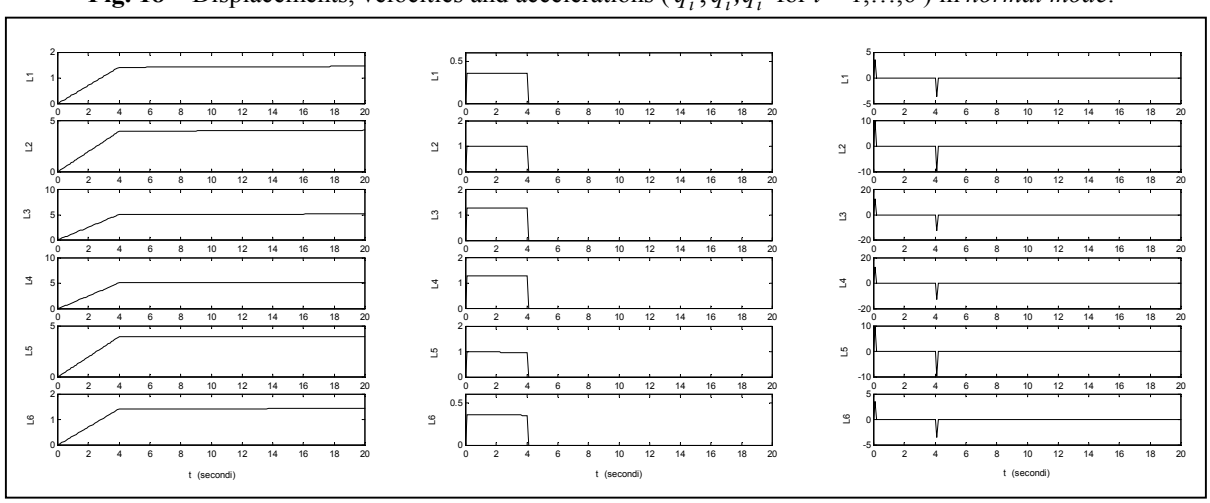

Fig. 19 – Displacements, velocities and accelerations ($q_i, \dot{q}_i, \ddot{q}_i$ for i = 1,…,6) in *station keeping*.

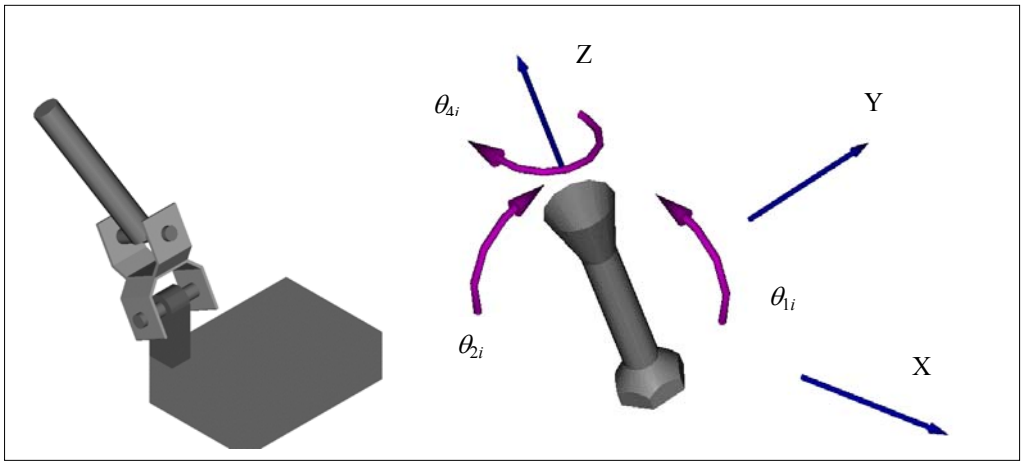

Fig. 20 – Strains on the spindle.

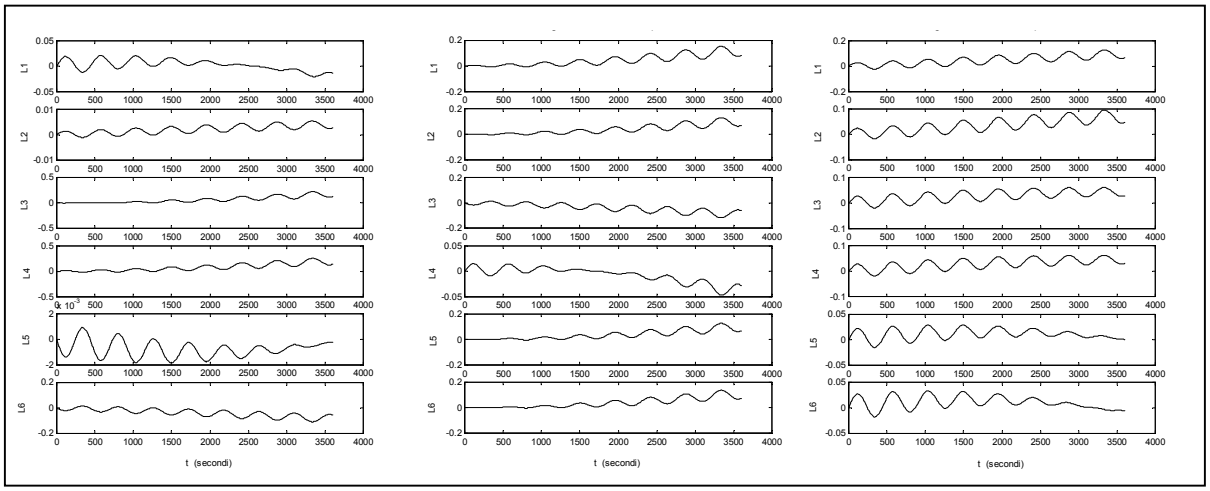

Fig. 21 – Torsions and flexions in planes XZ and YZ (ϑ_{4i} , ϑ_{1i} , ϑ_{2i} for i = 1,…,6) in *normal mode*.

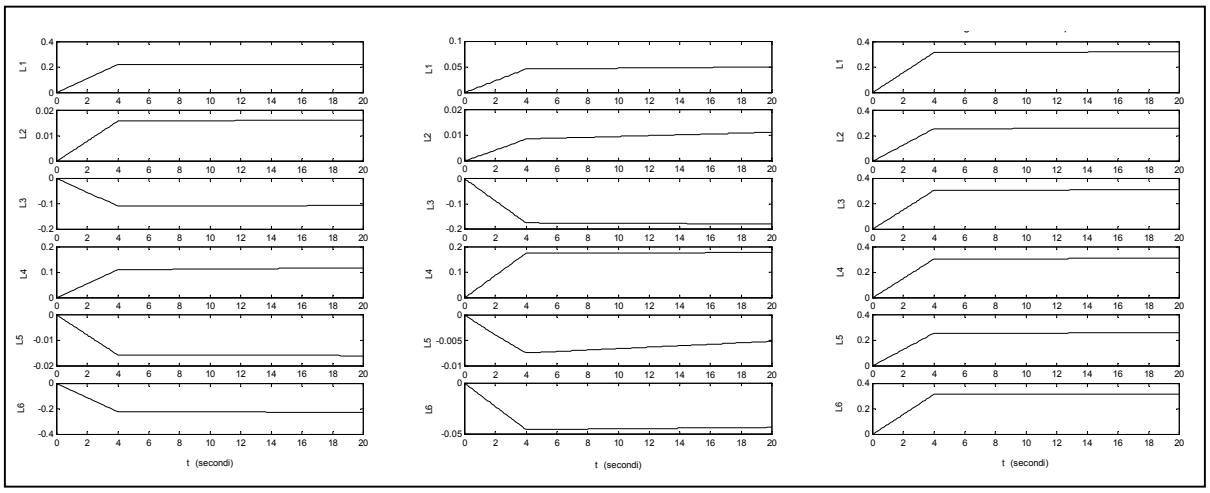

Fig. 22 – Torsions and flexions in planes XZ and YZ (ϑ_{4i} , ϑ_{1i} , ϑ_{2i} for i = 1,…,6) in *station keeping*.

References

Agrawal, S.K., Desmier, G., 1993, "Fabrication and analysis of a novel 3 DOF parallel wrist mechanism", Journal of Applied mechanics, Asme.

Angeles, J., 1997 "Fundamentals of robotic mechanical systems", Springer, New York.

Di Benedetto, A., Pennestrì, E., 1997, "Introduzione alla cinematica dei meccanismi Vol. 1 e 2", Casa Editrice Ambrosiana, Milano.

Fichter, E.F., 1986, "A Stewart Platform-Based Manipulator: General Theory and Practical Construction". Int. J. Robot. Res. 5 (2), 157-182.

Fu, Gonzales, Lee, 1989, "Robotica", Mc Graw-Hill, New York.

Goldstein, H., 1974, "Classical mechanics", Harward University, Addison-Wesley Publishing.

Gosselin, C., Perreault, L., Vaillancourt, C., 1995, "Simulation and computer aided kinematic design of three-degree of freedom spherical parallel manipulators". J. Robot. Syst.. 12 (12), 857-869.

Huang Z. and Wang, H.B., 1992, "Dynamic Force Analysis of n-d.f. Multiloop Complex Spatial Mechanism", *Mech. Mach. Theory* 27, No. 1, 97-105.

Hudgens, J.C., Tesar, D., 1988, "A fully parallel six degree of freedom micromanipulator: kinematic analysis and dynamic model", Proc. ASME Design Tech., pp.29-37.

Innocenti, C., Parenti Castelli, V., 1992, "Echelon form of direct kinematics for the general fully-parallel spherical wrist", Mech. Mach. Theory Vol.28, No4. pp 553-561.

Innocenti, C., Parenti Castelli, V., 1998, "Exhaustive enumeration of fully-parallel kinematic chains", Mech. Mach. Theory Vol.29, No5.

Lilly K.W. and Orin, D.E., 1994, "Efficient Dynamic Simulator of Multiple Chain Robotic Mechanism" *ASME J. Dynamic Systems, Measurement, and Control* 116, 223-231.

Kokkins, T., Millies, P., 1991, "A Parallel Robot-Arm Regional Structure with Actuational Redundancy", Mech. Mach. Theory, Vol. 26, No. 6, pp.629-641.

Kourosh, E., Sinatra, R., Angeles, J., 1997, "Kinematics and dynamics of a six-degree-of-freedom parallel manipulator with revolute legs", Robotica volume 15, pp 385-394, Cambridge University Press, United Kingdom.

Kurtz, R., Hayward, V., 1992, "Multiple-Goal Kinematic Optimization of a Parallel Spherical Mechanism with Actuator Redundancy", IEEE J. Robotics Automat., Vol. 8, No. 5, pp.664-651.

Ma, O., 1991, "Mechanical Analysis of Parallel Manipulators with Simulation, design and Control Applications", Ph.D. Thesis, McGill University, Montreal.

Merlet J.-P., 1990, "Les Robots Paralléles", Hèrmes, Paris, France.

Pfreundschuh, G.H., Sugar, T.G., Kumar, V.,1994, "Design and Control of a Three-Degrees-of-Freedom in-Parallel actuated Manipulator" J. Robotic Systems 11, No. 2 103-115.

Pierrot, F., Fournier, A., Dauchez, P., 1992, "Toward a Fully Parallel 6-DOF Robot for High-Speed Applications" Int. J. Robotics and Automation 7, No. 1, 15-22.

Silver S., 1986, "Micro wave antenna: theory and Design", IEE, Electromagnetic waves series.

Stewart, D., 1965, "A Platform with six degrees of freedom", Proc. Inst. Mech. Engr. 180, Part.1, No. 15, 371-378.

Sugimoto, K., 1987, "Kinematic and Dynamic Analysis of Parallel Manipulators by Means of Motor Algebra", ASME Mechanisms, Transmissions, and Automation in Design, Vol. 109, pp. 3-7.

Zanganeh, K. E., Angeles, J., 1994, "Instantaneous Kinematics and Design of a Novel Redundant Parallel Manipulator", IEEE Int. Conference on Robotics and Automation.

Proceedings of the WORKSHOP on
Fundamental Issues and Future Research Directions for Parallel Mechanisms and Manipulators
October 3–4, 2002, Quebec City, Quebec, Canada
Clement M. Gosselin and Imme Ebert-Uphoff, editors

SELF MOTIONS OF STEWART-GOUGH-PLATFORMS
An overview

MANFRED L. HUSTY
Inst. f. Engineering Mathematics, Geometry and Computer Science, University of Innsbruck, Austria
manfred.husty@uibk.ac.at

ADOLF KARGER
Mathematics Institute
Charles University, Praha
karger@karlin.mff.cuni.cz

Abstract: *Two rigid bodies linked by six general constraints form a new rigid body which may have different assemblies depending on the type of constraints which are used. It might occur that some of the assemblies are infinitesimal mobile, shaky, snapping or even mobile with one or more degrees of freedom. In this paper we investigate the so called Stewart-Gough platform, which consists of two rigid bodies linked by six legs and give an overview of results concerning self mobility of this mechanism. In the first three sections we give an overview on the work done on self motions, introduce the mathematical framework and give classical and more recently discovered examples. In the fourth section of the paper we give a complete listing of all designs of Stewart-Gough platforms that have Schönflies self motions.*

1 Introduction

Stewart-Gough parallel manipulators (SGP) are under investigation since more than twenty years. Many different types have found various applications (see section 2.5 in Merlet (2000)). A typical SGP consists of a base and a platform joined by six linearly actuated legs. The legs are mounted to base and platform via ball and socket joints. Using the SGP as robot manipulator the six legs are actuated and allow by changing their length a free motion of the platform within certain ranges. When on the other hand all six actuators are locked and the legs have certain lengths, then the SGP is a rigid structure in most cases. Depending on the geometry of the anchor points of the legs and the pose in which the platform is, it can happen that the mechanism gains an infinitesimal degree of freedom (the SGP is in a singular configuration, see Merlet (2000), chapter 5). Ma and Angeles (1992) introduced the notion of architecture singularity, defining that a SGP is architecture singular when it is singular in every configuration it can obtain. But only recently the complete list of all architecture singular designs was given by Karger (1998) and Husty and Karger (2001). It turns out that for a general SGP (anchor points not in a plane) only trivial designs can be architecturally singular, but when the anchor points of platform and base are in a plane (SGPS), then we have many non trivial examples. The general case is completely solved in Karger (1998). In Husty and Karger (2001) the nontrivial case of SGPS is completely solved and it was shown that architecture singularity of SGPS is governed by a set of four simple equations for the design parameters. These four equations have a nice geometric interpretation which also can be found in Husty and Karger (2001). Surprisingly there are well known designs, e.g the Griffis left hand (Griffis *et al.*, 1994) (see also Merlet (2000), page 40, Griffis and Duffy (1993)), among these structures. All architecture singular manipulators have self motions, although one has to be careful, because it can happen that the self motion is complex and only some isolated points of it are real. Then one might be tempted to say that the manipulator has only a finite number of assembly modes. Self motion has to be viewed from point of algebraic geometry and the roots have to be counted in algebraic way, because as we will show self motions are determined by a set of algebraic equations.

When a SGP admits a one parameter self motion, then this motion is determined by the geometry of the manipulator and the length of five legs. The sixth leg has to fulfill an assembly condition to fit into the motion. Once this condition is fulfilled the leg will take part in the motion prescribed by the five other. In many of the cases on can add even more legs without disturbing the motion. This fact was already shown in the first paper which mentioned self motions of SGP (Husty and Zsombor-Murray, 1994). Platform types with two parameter self motions have been discussed in Zsombor-Murray *et al.* (1995a) and Zsombor-Murray *et al.* (1995b). A complete classification of the self motions of the classical SGP is given in Karger and Husty (1998). "Classical SGP" was named that case where the anchor points are located on a semi regular hexagon, which is obtained by cutting the vertices of a regular triangle with a circle centered at the centroid and radius smaller than the radius of the circum-circle. This is the design used in the most applications. The subcase

of linearly related platform and base anchor points was treated in Kong and Gosselin (2001). This case was already known to Bricard (1906) (and even earlier to Chasles, see page 3 in Bricard (1906)). Sommese *et al.* (2002) show that an extended version of numerical continuation can be useful to find the complete solution set of self motions of SGP .

From the remark in the last paragraph it is clear that the problem of self motions of parallel manipulators has also a historical dimension. Self motions are related to the spherical motion problem, which was addressed in a mathematical competition (Le Prix Vaillant) organized by the French Academy of science in 1904. Borel and Bricard won both prizes but did not solve the problem completely. Nevertheless all examples they found in their thorough studies are examples of self motions of parallel manipulators. In Bricard's paper one can even find a figure of the Griffis left hand. An overview on the history of the problem can be found in Husty (2000).

This paper is organized as follows: In Section 2 we set up the mathematical framework and all the notions we will use. In Section 3 we show some examples of self motions to explain the methods which are used to find the geometric conditions for the design parameters. Section 4 gives a complete investigation of all SGP which can have a Schönflies self motion[1].

2 Mathematical framework

For the description of the pose of the platform with respect to the base we use Study's parameterizations of Euclidean displacements. The transformation from the platform coordinate system (Σ , position vectors $\mathbf{x}$) to the base coordinate system (Σ_0 , position vectors $\mathbf{x_0}$) is written

$$\mathbf{x_0} = \mathbf{Q}\mathbf{x}$$

using the 4×4 - transformation matrix

$$\mathbf{Q} = \frac{1}{\Delta}\begin{bmatrix} x_1^2+x_2^2+x_3^2+x_0^2 & 0 & 0 & 0 \\ 2(y_0x_1-y_3x_2+y_2x_3-y_1x_0) & x_1^2-x_2^2-x_3^2+x_0^2 & 2(x_1x_2-x_3x_0) & 2(x_1x_3+x_2x_0) \\ 2(y_3x_1+y_0x_2-y_1x_3-y_2x_0) & 2(x_1x_2+x_3x_0) & x_2^2-x_1^2-x_3^2+x_0^2 & 2(x_2x_3-x_1x_0) \\ 2(y_1x_2-y_2x_1+y_0x_3-y_3x_0) & 2(x_1x_3-x_2x_0) & 2(x_2x_3+x_1x_0) & x_0^2-x_1^2-x_2^2+x_3^2 \end{bmatrix}, \tag{1}$$

where

$$\Delta = x_1^2+x_2^2+x_3^2+x_0^2. \tag{2}$$

The x_i are the Euler parameters and they have to fulfill an orthogonality condition with the remaining four parameters y_i

$$x_0y_0 + x_1y_1 + x_2y_2 + x_3y_3 = 0. \tag{3}$$

[1]This section gives a new and complete investigation of a special case of self motion to show how complicated the computations are. The reader only interested in an introduction to the topic can skip this section and read only the theorem at the very end of section 4.

This parameterization is essentially (up to a double covering) the dual quaternion parameterization of the Euclidean motion group and it has the following geometric interpretation (due to Study). Eq.3 can be viewed as a six dimensional quadric S_6^2 in a seven dimensional projective space P^7. This space is called kinematic image space or Study parameter space.[2] S_6^2 is known as the Study-quadric. Every point on S_6^2 (with the exception of one generator space $x_1 = x_2 = x_3 = x_0 = 0$) represents a valid position and orientation of a given coordinate frame with respect to an arbitrarily chosen reference frame.

It was shown in Husty (1996) that the direct kinematics of all SGPs is governed by a set of seven quadratic equations, one of them being Eq. 3 and the other six having the general form

$$\begin{aligned} h =& R(x_0^2+x_1^2+x_2^2+x_3^2) + 4(y_0^2+y_1^2+y_2^2+y_3^2) - \\ & 2x_0^2(Aa+Bb+Cc) + 2x_1^2(-Aa+Bb+Cc) + \\ & 2x_2^2(Aa-Bb-Cc) + 2x_3^2(Aa+Bb+Cc) + \\ & 2x_3^2(Aa+Bb-Cc) + 4[x_0x_1(Bc-Cb) + \\ & x_0x_2(Ca-Ac) + x_0x_3(Ab-Ba) - \\ & x_1x_2(Ab+Ba) - x_1x_3(Ac+Ca) - \\ & x_2x_3(Bc+Cb) + (x_0y_1-y_0x_1)(A-a) + \\ & (x_0y_2-y_0x_2)(B-b) + (x_0y_3-y_0x_3)(C-c) + \\ & (x_1y_2-y_1x_2)(C+c) - (x_1y_3-y_1x_3)(B+b) + \\ & (x_2y_3-y_2x_3)(A+a)] = 0, \end{aligned} \tag{4}$$

where (a, b, c) are the coordinates of a point in the platform frame, (A, B, C) are coordinates of a point in the base frame, r is the joint parameter (leg length). Furthermore it was set

$$R := A^2 + B^2 + C^2 + a^2 + b^2 + c^2 - r^2$$

The solutions of the seven quadratic equations constitute an affine variety $V(h_i, S_6^2)$. This variety V represents the solutions of the direct kinematics in the kinematic image space. The polynomials determining V generate an ideal, whose elements are obtained by linear combination and multiplication of the seven polynomials with coefficients from $\mathbb{R}$. In the general situation the variety V will be zero dimensional, because we have seven equations and seven unknowns. It is well known, that this system has maximal 40 real solutions (Wampler (1996), Raghavan (1991)). An algorithm to solve the system was presented in Husty (1996). Quite recently it was shown, that within the ideal one can generate additional polynomials which represent additional constraints between the rigid bodies. The zeros of these additional polynomials determine quadrics which pass through all forty solutions. From this follows that one can construct redundant SGP (more than six legs, for SGPP even infinitely many) having all solutions of the direct kinematics in common. This has also the consequence that adding leg would not change the singularities of such a SGP. It shows that one has to be careful in adding to avoid singularities.

[2]For a more detailed explanation see Bottema and Roth (1990), Ravani and Roth (1984) and Husty (1996).

It is not surprising that for special platform and base geometries it can happen that the solution variety V is not zero dimensional. Then $V(h_i, S_6^2)$ no longer consists of discrete points, but of a curve, or even of a surface, on S_6^2.[3]

Remark: This is now the point to report more on the work which was done by Borel and Bricard more than 90 years ago. The question of the French Academy was to determine all motions which have as many spherical paths as possible. Bricard presented many examples which he got pursuing a very geometrical approach. Borel used analytic and algebraic methods. Both were essentially starting with the same equation (Eq. 4) we have presented in this section. Because of the lack of algebraic manipulation systems they had to make an important restriction. They assumed for all motions that they should have linear relations between the direction cosines, which yields quadratic or linear relations between the Euler parameters. All their results are classified with respect to the type of relation which can exist between the Euler parameters. There are only the following possibilities:

1. Three relations: the Euler parameters are determined, the motion can only be a translation. This yields only trivial cases, e.g. Platform and base anchor points congruent and all legs of the same length.

2. Two linear relations, then the motion is represented by a line in the Euler parameter space and the motion preserves one direction; this is a Schönflies motion. They give some examples without claim of completeness. Within this case there are some interesting and well known motions. One example is the motion where all points of the moving body travel on spherical paths (see e.g. Bottema and Roth (1990) (page 324), Bricard (1896) or Krames (1937)). This type of motion was the first reported self motion of a parallel manipulator (Husty and Zsombor-Murray, 1994).

3. A linear and a quadratic relation. The motion is represented by a conic in the Euler parameter space. Into this type of motion belong the self-motions of platforms investigated in Zsombor-Murray *et al.* (1995a) and Zsombor-Murray *et al.* (1995b).

4. Two special quadratic relations. The motion is represented by a cubic in the Euler parameter space.

5. Two general quadratic relations. The motion is represented by a quartic in the Euler parameter space.

6. One linear relation. The motion is two parametric and represented by a plane in the Euler parameter space.

7. One quadratic relation. The motions is two parametric and represented by a quadric in the Euler parameter space.

8. No (linear or quadratic) relation between the Euler parameters. The general case. Borel and Bricard have almost no results, but in the investigations of self motions of parallel manipulators many motions which belong to this type have been discovered (Karger and Husty (1998), Husty and Karger (2000), Husty and Karger (2000b), Karger and Husty (1997)) .

[3] Examples of 2-DOF self motions are known. If non-trivial 3-DOF self motions are possible is not known. They would correspond to solids on S_6^2.

3 Examples of Self Motions

3.1 Self motions of 3-3 Stewart-Gough Platforms

The anchor points of this platform type are on the vertices of triangles. Each vertex of the base is joined to two vertices of the platform and vice versa. This platform type can be considered as a polyhedron consisting of eight triangular shaped faces (a general octahedron). From this fact it is clear that any assembly mode of the 3-3-platform which forms a convex octahedron is a rigid body. This proposition follows from an old theorem due to

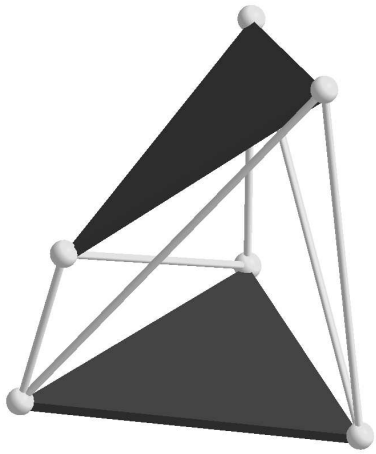

Figure 1: 3-3 Platform

Cauchy (1813), which states that a convex polyhedron with rigid faces, but hinged at the edges, is completely rigid. A convex assembly of a 3-3 platform can neither be singular (infinitesimal mobile) nor mobile. So, if a 3-3 platform has a self motion it must be non-convex. In 1897 Bricard gave a complete list of all flexible octahedra (Bricard, 1897). From the remark above it is clear that therefore the self motions of the 3-3 platforms are known (see also Stachel (1987), Conelly (1978) and Wunderlich (1965)). Bricard identified in a thorough and nice geometric investigation 3 different types of such flexible octahedra. In the language of 3-3 SGP they can be characterized in the following way:

- Type 1: Platform and base have an axial symmetry.

- Type 2: Platform and base are symmetric with respect to a plane.

- The manipulator has a position where it is completely folded in one plane.

A particularly nice version of type one was found by Blaschke (1920). The anchor points of the manipulator are on a closed hexagon consisting of six edges of a cube. It is relatively easy to see that the three anchor points on the platform are free to move on circles. Fig.2 shows this platform in a starting position, an intermediate position and an end position. For a practical application it is clear that the manipulator cannot reach the end position because of leg intersection and the start position because of intersection of the leg with the base and the platform plate. This sequence of positions of Blaschke's 3-3-Platform was already published in Blaschke (1948).

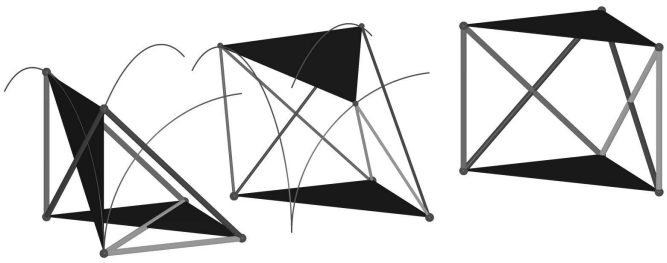

Figure 2: Blaschke 3-3 Platform

Fig. 3 and Fig. 4 show photographs of a simple model of Bricard's type 3 flexible octahedron in a general and a flat position.

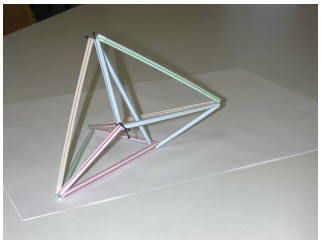

Figure 3: 3-3 Platform (Bricard Type 3)

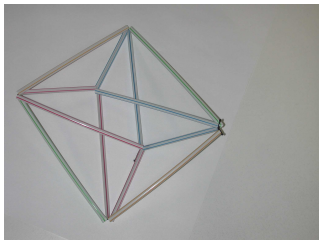

Figure 4: Bricard Type 3 flat position

3.2 Griffis-Duffy Platforms

In Griffis and Duffy (1993) and Griffis *et al.* (1994) two types of mechanisms are proposed which will be called Griffis-Duffy Platforms (GDP). Both are special types of SGP. One of them is called "midline to apex" embodiment and the other "apex to apex" embodiment. The anchor points of the spherical joints on platform and base are arranged on the vertices of a triangle and the remaining three each on the edges of the triangle. Here we will summarize briefly the results of Husty and Karger (2000) on the "midline to apex" embodiment (Fig. 5). Base and platform consist of an equilateral triangle and the remaining anchor points are the mid points of the three edges. This special case of GDP will be called a "Special Griffis-Duffy-Platform" (SGDP). Using the coordinate systems shown in Fig. 5 coordinates of both

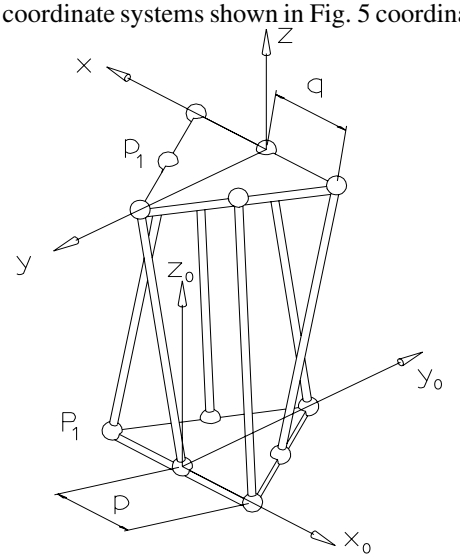

Figure 5: Manipulator coordinate systems

anchor points in base and platform are listed in Table 1.

	A	B	C		a	b	c
P_1	-p	0	0	p_1	$\frac{q}{2}$	$\frac{q\sqrt{3}}{2}$	0
P_2	0	0	0	p_2	0	$q\sqrt{3}$	0
P_3	p	0	0	p_3	$-\frac{q}{2}$	$\frac{q\sqrt{3}}{2}$	0
P_4	$\frac{p}{2}$	$\frac{p\sqrt{3}}{2}$	0	p_4	$-q$	0	0
P_5	0	$p\sqrt{3}$	0	p_5	0	0	0
P_6	$-\frac{p}{2}$	$\frac{p\sqrt{3}}{2}$	0	p_4	q	0	0

Table 1: Coordinates of anchor points

3.2.1 *Architecture Singularity*

For an arbitrary SGP the transformation of the joint velocities into the infinitesimal twist of the produced motion is written as

$$\mathbf{Jq} = \mathbf{t}, \tag{5}$$

where $\mathbf{q}$ is the vector of joint velocities and $\mathbf{t}$ is the twist of the platform. $\mathbf{J}$ is a 6×6-matrix and it is well known that its rows consist of the axis coordinates of the linear actuator axes $\overline{P_i p_i}$.

$\mathbf{p_i}^0$ denotes the position of a joint center of the platform measured in the base coordinate system and $\mathbf{Q}$ is the transformation matrix from platform to base.

$$\mathbf{p_i^0} = \mathbf{Q}\mathbf{p_i}. \tag{6}$$

To compute the Jacobian matrix $\mathbf{J}$ for the SGDP we substitute the coordinates of Table 1 into Eq. 6, compute $\mathbf{p_i}^0$ and the axis coordinates of the legs. For the first leg we get

$$\begin{aligned}
&(0 : p\,(2y_0x_3 - 2y_3x_0 + 2y_2x_1 - 2y_1x_2 + qx_1x_3 + qx_0x_2 - \\
&q\sqrt{3}x_2x_3q\sqrt{3}x_0x_1) : -p\,(2y_0x_2 - 2y_2x_0 + 2y_1x_3 - 2y_3x_1 + \\
&(x_1x_2 - x_0x_3)q + \frac{1}{2}(x_0^2 - x_1^2 + x_2^2 - x_3^2)q\sqrt{3}) : \\
&2y_0x_1 - 2y_1x_0 + 2y_3x_2 - 2y_2x_3 + \\
&\frac{1}{2}(x_0^2 + x_1^2 - x_2^2 - x_3^2)q + (x_1x_2 + x_0x_3)q\sqrt{3} + p : \\
&2y_0x2 - 2y_2x_0 + 2y_1x_3 - 2y_3x_1 + \\
&(x_1x_2 - x_0x_3)q + \frac{1}{2}(x_0^2 - x_1^2 + x_2^2 - x_3^2)q\sqrt{3} : \\
&2y_0x_3 - 2y_3x_0 + 2y_2x_1 - 2y_1x_2 + \\
&qx_1x_3 + qx_0x_2 + q\sqrt{3}x_2x_3 - q\sqrt{3}x_0x_1\Big)\,.
\end{aligned} \tag{7}$$

Similar expressions build up the whole matrix $\mathbf{J}$. Using an algebraic manipulation system to compute the determinant of $\mathbf{J}$ we get $\det \mathbf{J} = 0$. This tells that $\mathbf{J}$ is singular independently of the joint parameters and therefore of the pose of the platform. The SGDP is architecture singular.

3.2.2 Self Motions of SGDP

In this section we will show that the SGDP platform is not only architecture singular but also movable from every point of its workspace. To show this we will go back to the constraint equation Eq. 4 and the equation for S_6^2 (Eq.3). Because of the six legs there are six constraint equations $h_j, j = 1, \ldots, 6$ and S_6^2. They make a system $\mathcal{A}$ of seven quadratic equations that has to be solved for the eight homogeneous unknowns $x_i, y_i,\ (i = 0, \ldots, 3)$. The affine variety $V(h_j, S_6^2)$ consisting of the zeros of the polynomial equations $h_j = 0, x_0y_0 + x_1y_1 + x_2y_2 + x_3y_3 = 0$ is at least one dimensional. We will show that V is a curve. This curve represents in the kinematic image space the one parameter motion in which the platform can move without changing leg lengths. Substituting the coordinates of Table 1 into Eq. 4 we get six constraint equations $h_j,\ (j = 1, \ldots, 6)$ one of them, h_1, is displayed below, all the other five have a similar structure.

$$\begin{aligned}
h_1 : {} & qx_0^2p + 4y_0x_1p - 4y_1x_0p - 4y_3x_2p + 4y_2x_3p - \\
& qx_3^2p - 2q\sqrt{3}x_0x_3p + qx_1^2p - qx_2^2p + 2q\sqrt{3}x_1x_2p + \\
& (x_3^2 + x_1^2 + x_0^2 + x_2^2)R_1 + 2x_2y_3q - 2y_2x_3q + \\
& 2y_0x_1q - 2y_1x_0q + 2y_1x_3q\sqrt{3} + 2x_2y_0q\sqrt{3} - \\
& 2y_2x_0q\sqrt{3} - 2y_3q\sqrt{3}x_1 + 4(y_3^2 + y_2^2 + y_0^2 + y_1^2) = 0.
\end{aligned} \tag{8}$$

From the six constraint equations five difference equations are produced: $U_1 = h_1 - h_3, U_2 = h_2 - h_5, U_3 = h_4 - h_6, U_4 = h_1 - h_2, U_5 = h_1 - h_4$. The equations U_i have the characteristic property that they are all linear in y_i. We take three of the difference equations U_1, U_2, U_3 and Eq. 3 and solve this linear system $\mathcal{LS}$ for y_i. Substitution of the solutions of $\mathcal{LS}$ into U_4, U_5 and h_1 yields a system $\mathcal{S}$ of three nonlinear equations for the four remaining homogeneous unknowns x_i. It is easy to show that no more independent equations can be generated from the original system $\mathcal{A}$. A close inspection of the new system $\mathcal{S}$ shows that U_4 is of degree four, h_1 is of degree eight and U_5 takes the form

$$\begin{aligned}
U_5 : \ & (x_3^2 + x_0^2 + x_1^2 + x_2^2)(3q^2 - 3p^2 - \\
& R4 - R2 - R6 + R3 + R1 + R5) = 0.
\end{aligned} \tag{9}$$

The first factor in U_5 cannot be zero because the x_i are the Euler parameters of an Euclidean displacement and the second factor depends only on the design of the manipulator and the leg lengths. We will call the second factor an *assembly condition*, because U_5 allows only for one interpretation: Either U_5 is fulfilled, which means one linear condition on the legs is fulfilled, or this condition is not fulfilled, but then the manipulator cannot be assembled with the six given legs. Let us assume that U_5 is fulfilled. Then only two equations remain in $\mathcal{S}$ for four homogeneous unknowns. One of the unknowns e.g. x_1 can be eliminated and the remaining equation $L(x_0, x_2, x_3, R_2, R_3, R_4, R_5, R_6) = 0$ represents the affine solution variety V of the original set of seven nonlinear equations. After specifying a set of joint parameters $(R_2, R_3, R_4, R_5, R_6)$ the equation $L(x_0, x_2, x_3) = 0$ represents a curve in the Study parameter space which corresponds to a one parameter motion which the platform will perform without changing the joint inputs. Inspection of L reveals that it has special algebraic (and geometric) properties because it can be factored into

$$L : \ p^{20}(x_0, x_2, x_3)(q^6(x_0, x_2, x_3))^2 = 0. \tag{10}$$

q^6 is a sixth degree polynomial (which is squared) and it is the determinant D of coefficients of the linear system $\mathcal{LS}$ which has been used to solve for y_i. This polynomial cannot vanish in the case in discussion, so the motion is represented by the polynomial of degree 20. Different subcases can occur for different values of leg lengths because then D could vanish and the elimination process has to be modified . A detailed discussion can be found in Husty and Karger (2000). Note that the polynomial of degree 20 in Eq. 10 does not necessarily show the order of the overall motion curve because it represents only a projection of this curve onto the x_2x_3 plane of the Euler parameter space. A detailed discussion on this fact is in Sommese *et al.* (2002) where continuation methods are used to find all components of different dimensions of the solution variety V.

4 Schönflies Motions

In this section a complete discussion on the Schönflies case of self motions of SGP is presented. The essential question is: how

does the geometry (the design) of a SGP have to look like, so that the manipulator is able to perform a Schönflies motion. This case essentially has been discussed in detail by Borel (1908), but there was no proof of the completeness of the results.

Schönflies motions (S-motions) constitute a four dimensional subgroup $\mathcal{S}_4$ of the six dimensional group of Euclidean motions. It consists of all translations combined with all rotations about one fixed direction. In what follows we will suppose that coordinate systems are chosen in such a way that this fixed direction coincides with the z-axis of the coordinate systems. With this choice of the coordinate system any element $\mathbf{G}$ of the Schönflies group $\mathcal{S}_4$ can be written in the following form

$$\mathbf{G} = \begin{pmatrix} 1 & 0 & 0 & 0 \\ t_1 & \cos\varphi & -\sin\varphi & 0 \\ t_2 & \sin\varphi & \cos\varphi & 0 \\ t_3 & 0 & 0 & 1 \end{pmatrix} \tag{11}$$

For the following it is convenient to parameterize $\mathcal{S}_4$ with help of Study parameters $x_0, x_1, x_2, x_3, y_0, y_1, y_2, y_3$. The group $\mathcal{S}_4$ is then characterized by the equations $x_1 = x_2 = 0$. In the following we are only interested in non trivial cases, so we suppose $x_0 \neq const.$ and $x_3 \neq const.$ The Study parameters are homogeneous parameters so we can normalize $x_0 = 1$. With this assumptions the Study condition yields $y_0 = -x_3 y_3$.

Points of the moving space, being on lines parallel to the z-axis have congruent trajectories in a S-motion which has the z-axis as fixed direction. This means that if one point moves on a spherical path in such a motion all points on the line parallel to the z-axis through the point move also on spherical paths. For this reason it is enough to study trajectories of the points of one plane in the moving space. Without any restriction we choose the plane $z = 0$ in the moving space.

By a Schönflies-Borel-Bricard motion (SBB-motion) we understand any S-motion, which has at least four lines parallel to the z-axis and all points of these four lines move on spherical trajectories. As $\mathcal{S}_4$ is four parametric, one can choose three spherical constraints arbitrarily to obtain a one parametric S-motion with three one parameter sets of spherical paths (trivial case, the similar to a general space motion with just five spherical paths). The natural question arises now: Given three spherical constraints, are there any other points which move on spherical paths? To answer this question the problem has to be formulated more precisely. Let us take three lines (l_1, l_2, l_3) in the moving space and three lines (L_1, L_2, L_3) in the fixed space, all of them parallel to the z-axis (i.e. the fixed direction of the S-motion). Now three points $m_1, m_2, m_3, (m_i \in l_i, i = 1, \ldots 3)$ and three points $M_1, M_2, M_3, (M_i \in L_i, i = 1, \ldots 3)$ are chosen. According to the statements above we can prescribe three distances between points $m_i M_i$ to obtain a one parametric S-motion. Now we have to look for constraints for the geometry of the anchor points and the distances between them, so that more than three points move on spherical paths. We will show within this section that such constraints can be imposed and therefore SBB-motions exist for any choice of $m_i, M_i, l_i, L_i,\ i = 1, \ldots, 3$.

We denote $m_i = (a_i, b_i, c_i)$ and $M_i = (A_i, B_i, C_i),\ i = 1, \ldots, 3$. Without restriction the coordinate systems in moving and fixed spaces can be specialized so that $c_i = 0, a_1 = b_1 = b_2 = 0, A_1 = B_1 = B_2 = 0, C_1 = 0$ holds.

4.1 Equations for SBB-motions

Let us suppose that we have a SBB-motion with points $m_i, i = 1, \ldots, 4$ having spherical trajectories with centers at M_i. Let h_i be the constraint equation expressing the fact that the distance r_i between $m_i M_i$ is constant during the motion(Eq.4). Having a S-motion this equation simplifies to:

$$\begin{gathered} h_i = 4y_1[A_i - a_i + x_3(b_i + B_i)] + \\ 4y_2[B_i - b_i - x_3(a_i + A_i)] + 4x_3(A_i b_i - B_i a_i) + \\ 2(x_3^2 - 1)(B_i b_i + A_i a_i) + (R_i + 4y_3 C_i + 4y_3^2)(1 + x_3^2) + \\ 4(y_1^2 + y_2^2) = 0, \end{gathered} \tag{12}$$

Substituting the coordinates for the points m_i and M_i into Eq. 12 we obtain four constraint equations $h_i = 0$. From these equations we can derive the following difference equations $U_j = h_j - h_1, j = 2, 3, 4$. SBB-motions are now the one parametric solutions of the system of polynomial equations $\mathcal{S} = \{h_1, U_2, U_3, U_4\}$. Furthermore we denote $S_j = R_j - R_1$. As we have excluded translations, we can take x_3 for the parameter of the motion. Now we have four equations for three unknowns y_1, y_2, y_3. This means we have to have constraints on $A_i, B_i, C_i, a_i, b_i, c_i, r_i$ to obtain a solution.

4.2 The singular case

Equations $U_j = 0, j = 2, 3, 4$ are linear non-homogeneous equations in the unknowns $y_i, i = 1, 2, 3$. Let M be the matrix of this system. Then we have (up to nonzero factors)

$$M = \begin{pmatrix} A_2 - a_2 & -x_3(A_2 + a_2) & C_2 \\ x_3(B_3 + b_3) + A_3 - a_3 & -x_3(A_3 + a_3) + B_3 - b_3 & C_3 \\ x_3(B_4 + b_4) + A_4 - a_4 & -x_3(A_4 + a_4) + B_4 - b_4 & C_4 \end{pmatrix}. \tag{13}$$

From now on we shall suppose that the points m_1, m_2, m_3 are not collinear, which means that $a_2 b_3 \neq 0$. Moreover, we can rotate the coordinates systems in such a way that we have $a_2 > 0, A_2 \geq 0$. There are now two basic possibilities, either M is regular or M is singular.

At first we will treat the singular case. Let the rank of the matrix M be equal to one for all x_3. Then computing suitable sub-determinants of M, we obtain $B_3 = -b_3,\ B_4 = -b_4,\ A_2 = a_2,\ A_3 = a_3, A_4 = a_4,\ C_2 = C_3 = C_4 = 0$, which means that points $M_1, \ldots. M_4$ lie in a plane perpendicular to z-axis and configurations $m_1, \ldots, m_4$ and $M_1, \ldots, M_4$ are indirectly congruent. Substitution into the remaining equations shows that we have no solution in this case. So let us suppose that this case is excluded. (Either one of C_i is not equal to zero or configurations are not indirectly congruent). This means that M has rank two iff

$\det(M) = 0$. Computation shows that $\det(M)$ is a polynomial of degree two in x_3, which must identically vanish. This yields three equations $q_0 = 0, q_1 = 0, q_2 = 0$ for the geometry of the configuration from the coefficients of the different powers of x_3. From the last column of the matrix M we see that these equations are linear homogeneous in C_2, C_3, C_4. Let P be matrix of the system $q_i = 0$. Then we have (up to linear combinations)

$$P = \begin{pmatrix} a_3B_4 - A_4b_3 - B_3a_4 + A_3b_4 & -a_2B_4 - A_2b_4 & b_3A_2 + a_2B_3 \\ a_3A_4 - b_4B_3 - A_3a_4 + b_3B_4 & -a_2A_4 + A_2a_4 & A_3a_2 - A_2a_3 \\ A_3B_4 - a_4b_3 - B_3A_4 + a_3b_4 & -a_2b_4 - A_2B_4 & b_3a_2 + A_2B_3 \end{pmatrix} \quad (14)$$

We have to distinguish again different cases according to the rank of the matrix P.

Case A: Let Let P be regular. Then the only possible solution of the system $q_i = 0$ is $C_2 = C_3 = C_4 = 0$. From equations $U_2 = 0, U_3 = 0$ we can solve for y_1, y_2 uniquely, as the rank of M is equal to two. We substitute the result into $U_4 = 0$ and we obtain a polynomial of degree four in x_3 which must vanish. This yields five equations from the coefficients of the different powers of x_3. Let us denote by K_l the coefficient of x_3^l. Then the equations $K_2 - K_4 - K_0 = 0, K_3 - K_1 = 0$ are linear in A_4 and B_4 and we solve for them. The solution depends quadratically on the coordinates a_4, b_4 of the fourth point in the moving system. The obtained relation is an inversion. This inversion will be discussed later in the regular case, so we skip here the details. But here there are still three more equations. We substitute the solutions for A_4, B_4 into equations $K_0 = 0, K_3 = 0, K_4 = 0$, and see that the resulting equations are linear in S_2, S_3, S_4. The determinant of this system of equations is nonzero unless $A_3/a_3 = A_2/a_2 = -B_3/b_3$,. Singularity of this system would cause that P is singular and this was excluded. This means that we can always compute S_2, S_3, S_4 without any constraint for the geometry and for any choice of a_4, b_4 (except for the center of inversion). The obtained motion is the known Borel-Bricard motion (BB-motion)where all points (with exception of the points of the z-axis) are running on spherical paths. Platform manipulators with this type of self motion were treated in Husty and Zsombor-Murray (1994). The motion is a line symmetric motion, a fact which was discovered by Krames (see Bottema and Roth (1990), pp.324).

Case B: The rank of the matrix P is equal to one. This means that all sub-determinants of order two of the matrix P must be equal to zero. Let the configurations of points m_i and projections of M_i onto $Z = 0$ be not congruent. Then by rearranging points m_i we obtain $a_2 \neq A_2$. Sub-determinants of the second and third column yield

$$A_4 = \frac{A_2b_3a_4 + (A_3a_2 - A_2a_3)b_4}{a_2b_3}, \; B_4 = \frac{B_3b_4}{b_3}, \quad C_4 = \frac{C_2b_3a_4 + (C_3a_2 - C_2a_3)b_4}{a_2b_3}. \quad (15)$$

Points $M_1, ..., M_4$ lie in a plane and the conditions mean that the configurations of points m_i and M_i are affinely equivalent. If the configurations of points m_i and projections of M_i are directly congruent, we obtain a special case of the previous equations.

Case B1: Let $J = (a_2B_3 - b_3A_2)^2 + (A_2a_3 - A_3a_2) \neq 0$. Then we solve for y_1, y_2 from $U_2 = 0, U_3 = 0$ and substitute the result into the equation $U_4 = 0$. We obtain a polynomial of degree two in x_3 which must vanish. This yields

$$\begin{aligned} a_4 =& a_2(a_3B_3 - b_3A_3)[-A_2A_3(a_2 + a_3) + \\ & a_2(A_3^2 + B_3^2) + A_2(a_3A_2 - b_3B_3)]/[B_3J], \\ b_4 =& -a_2A_2(a_3B_3 - b_3A_3)[B_3(a_2 - a_3) + \\ & b_3(A_3 - A_2)]/[B_3J]. \end{aligned} \quad (16)$$

We have obtained a SBB-motion where the points of exactly four lines move on spherical trajectories. The fourth point in the moving system is given by Eq.16.

Case B2: Let $J = 0$. Then configurations of points m_i and projections of M_i on the $Z = 0$ plane are similar, $A_3/a_3 = B_3/b_3 = A_4/a_4 = B_4/b_4 = A_2/a_2$, and only one condition remains, which is the condition that the points $m_1, ..., m_4$ lie on a circle. This means that all points of the cylinder with the circumscribed circle of points m_1, m_2, m_3 as directing circle have spherical trajectories.

Denote ς the cylinder of revolution which passes through m_1, m_2, m_3 with generators parallel to the $z-$axis and ζ the equivalent cylinder in the fixed space. We take arbitrary plane sections λ in the moving space of ς and plane section Λ of ζ in the fixed space. Now we join points corresponding in the affinity f and obtain a movable system with infinitely many spherical trajectories. This is a special case of a well known Bricard case with two conic sections in projective correspondence. These structures are always movable, what is interesting here is that the motion is a S-motion. This finishes the discussion of the case B.

Case C:. The rank of the matrix P is equal to two. This happens iff the determinant D of the matrix P is equal to zero and the previous case is excluded. Let us suppose that this is the case. From equations $U_2 = 0, U_3 = 0$ we express y_1, y_2 and substitute the result into $U_4 = 0$. The coefficient with y_3 in U_4 must be equal to zero because the rank of the linear system for y_1, y_2, y_3 is equal to two. U_4 is then a polynomial of degree four in x_3, let K_i be the coefficient with x_3^i in U_4. We obtain five equations $K_0 = 0, ..., K_4 = 0$. Equations $K_5 = K_3 - K_1 = 0$, $K_6 = K_4 - K_0 + 2K_2 = 0$ do not contain S_2, S_3, S_4, we can express from them A_4, B_4 and obtain the inversion described below. Remaining equations are $K_0 = 0, K_1 = 0, K_2 = 0$, they

are linearly dependent and we can always express from them S_3, S_4. We are now left with equations $q_0 = 0, q_1 = 0, q_2 = 0$, which are linear homogeneous equations for C_2, C_3, C_4 and we know that exactly two of them are linearly independent. From one of them we express C_4 and one linear equation of the form $K = k + \lambda h = 0$, remains, where $\lambda = C_3/C_2$. k and h are cubic expressions in b_4, a_4, which means that we can choose λ arbitrarily, but then the point m_4 is bound to lie on a certain cubic. What remains is the equation $D = 0$. It factorizes into two factors. One of them is an expression of degree six in a_4, b_4, let us denote it $D_1 = 0$. Let us treat this case at first. We can show that

$$HD_1 = k_1 k_2,$$

where $k_i = k + \lambda_i h$, H is a constant and λ_i are roots of the quadratic equation

$$(a_2^2 - A_2^2)\lambda^2 + 2(A_2A_3 - a_2a_3)\lambda + b_3^2 + a_3^2 - B_3^2 - A_3^2 = 0.$$

This has the following consequences: We can choose points m_1, m_2, m_3 and M_1, M_2, M_3 quite free ($C_2 \neq 0$). Then all points which are common to cubics $k = 0, h = 0$ run on spherical paths, moreover, if $\lambda = \lambda_1$ or $\lambda = \lambda_2$ are roots of the quadratical equation, we have a whole cubic of points running on spherical paths. Cubics $k = 0, h = 0$ have always five common points (as they are circular, we have four common points at infinity), they are points m_1, m_2, m_3, the center of inversion and one more point, given by the same formulas as in the case B1, and the rank of P is equal to one, we obtain the solution from $B1$. Special case happens, if $B_3^2 = b_3^2$. In that case cubic curves $h = 0$ and $k = 0$ are the same, the value of λ is given and we have the whole cubic of spherical points. The case of the second factor of D being equal to zero leads to the case where configurations of m_1, m_2, m_3 and projection of M_1, M_2, M_3 are indirectly similar and the rank of P is one.

4.3 General Case

Now we suppose that $\det(M) \neq 0$ holds. We express y_1, y_2, y_3 from $U_2 = 0, U_3 = 0, U_4 = 0$. We substitute the result into h_1 and obtain a polynomial of degree eight which has to vanish identically to obtain a SBB-motion with four points moving on spherical paths. We denote by $f_i, i = 0, \ldots 8$ the coefficients at the respective powers i of x_3 in this polynomial. This yields nine equations $f_i = 0$ as necessary and sufficient conditions for the geometry and distances of possible points moving on spherical paths for general SBB motions. Unfortunately these equations are quite involved (e.g. f_8 and f_0 have 1425 terms, f_7 and f_1 have 1880 terms, f_6 and f_2 have 1819 terms, f_5 and f_3 have 2048 and f_4 has 1172 terms). To simplify these equations we use suitable linear combinations. We denote

$$g_i = f_i + f_{8-i}, \quad g_{8-i} = f_{8-i} - f_i, i = 0, \ldots, 3 \qquad (17)$$

Then the following equations are the most significant ones:

$$Z_1 = g_2 - g_0 - f_4 = 0, \qquad Z_2 = g_7 - g_5 = 0$$
$$Z_3 = g_6 - 2g_8 = 0, \qquad Z_4 = g_3 - 3g_1 = 0. \qquad (18)$$

Together with equations $g_0 = 0, g_1 = 0, g_2 = 0, g_7 = 0, g_8 = 0$ the form a system equivalent to the original system of equations $f_i = 0, i = 0, \ldots, 8$. The equations Z_1 and Z_2 do not contain distances and z-coordinates and factorize into:

$$Z_1 = Z_{11}Z_{12} = 0, \qquad Z_2 = Z_{21}Z_{22} = 0 \qquad (19)$$

Z_{ij} are linear in A_4 and B_4. To solve the system $Z_1 = 0, Z_2 = 0$ we have to combine one factor from each and solve it. This way we obtain four systems consisting of two equations for two unknowns A_4, B_4. Surprisingly all four systems have the same solution. This means that we have got a correspondence between the points of the moving system and projections of the points in the fixed system onto the plane $Z = 0$ of the fixed space. By translating the coordinate system in the plane $z = 0$ in the moving and $Z = 0$ in the fixed spaces this correspondence can be written in the following form:

$$P = \frac{m_2p + m_3q}{m_1(p^2 + q^2)}, \qquad Q = \frac{-m_3p + m_2q}{m_1(p^2 + q^2)} \qquad (20)$$

It is easy to show that by a suitable rotation of the coordinate system in the moving space and identifying both spaces the correspondence becomes an inversion ι

$$\iota : x' = \frac{kx}{x^2 + y^2} \qquad y' = \frac{kd}{x^2 + y^2}. \qquad (21)$$

Looking at Eq.20 we see that this procedure cannot be done if $m_1 = 0$ holds. As $m_1 = (A_2a_3 - A_3a_2)^2 + (B_3a_2 + A_2b_3)^2$, we have $A_3 = \dfrac{A_2a_3}{a_2}$, $B_3 = \dfrac{-A_2b_3}{a_2}$. The correspondence becomes a similarity and a reflection about x-axis. Careful inspection of the remaining equations shows that there is only one more point which could move on a spherical path and for this point we obtain $Y = 0$,a contradiction.

A similar situation appears if the inversion is degenerated $m_2 = 0, m_3 = 0, m_1 \neq 0$. Taking the resultants of $m_2 = 0, m_3 = 0$ with respect to A_3 and A_2 we obtain $m_1 = 0$, a contradiction.

We assume that non of the above mentioned special cases occur, solve for A_4, B_4 and substitute the solution into remaining expressions Z_3, Z_4, g_0, g_1, g_2, g_7, g_8. Equations $Z_3 = 0, Z_4 = 0$ are homogeneous quadratical in unknowns C_2, C_3, C_4, therefore they express two conic sections in the plane of the homogeneous coordinates C_2, C_3, C_4 and we are looking for their common points. Surprisingly, equations $Z_3 = 0, Z_4 = 0$ factorize into four lines, $Z_3 = Z_{31}.Z_{32} = 0, Z_4 = Z_{41}.Z_{42}$, which pass in general through one point. This statement could not be proved in general because equations are too complex, but sufficiently general examples show that this is really the case. Substitution into

remaining equation shows that the only possibility for solution is that the rank of M is less than three, a case which was already discussed. For this reason we have no solution in this case. A special case appears if the conic sections $Z_3 = 0, Z_4 = 0$ have one line in common. This happens iff two of the lines $Z_{31} = 0, Z_{32} = 0$ and $Z_{41} = 0, Z_{42} = 0$ coincide. Let us investigate this possibility. We denote

$$\begin{aligned} Z_3 &= (C_2 + gC_3 + hC_4)(r_2C_2 + r_3C_3 + r_4C_4) = \\ &= (a_{22}C_2^2 + 2a_{23}C_2C_3 + 2a_{24}C_2C_4 + 2a34C_3C_4 + \\ &\quad a_33C_3^2 + a_{44}C_4^2) \\ Z_4 &= (C_2 + gC_3 + hC_4)(s_2C_2 + s_3C_3 + s_4C_4) = \\ &\quad (b_{22}C_2^2 + 2b_{23}C_2C_3 + 2b_{24}C_2C_4 + \\ &\quad 2b34C_3C_4 + b_33C_3^2 + b_{44}C_4^2) \end{aligned} \tag{22}$$

Comparison of coefficients yields the following necessary conditions for the factorization:

$$(b_{22}a_{44} - a_{22}b_{44})^2 + 4(a_{44}b_{24} - b_{44}a_{24})(a_{22}b_{24} - b_{22}a_{24}) = 0.$$

$$(a_{22}b_{33} - a_{33}b_{22} + 4(a_{33}b_{23} - b_{33}a_{23})(a_{23}b_{22} - a_{22}b_{23}) = 0.$$

Fortunately, these conditions can be expressed explicitly, they yield two equations for a_4 and b_4 of third degree. Taking the resultants of these two equations, we obtain four solutions for a_4, b_4, the given points m_1, m_2, m_3 and the fourth solution is given by Eq.16 as in the singular case. Substitution into the determinant of the matrix M shows that it must be equal to zero, a contradiction. We cannot express a_4, b_4 in the similarity case, $B_3 = b_3A_2/a_2, A_3 = a_3A_2/a_2$. This case must be treated separately, but with the same result. This finishes the discussion of all possible cases.

As the result we obtain the following cases of SBB- motions. (We shall discuss only points in the $z = 0$ plane, to each such a point we have a whole line parallel to z-axis of points with a spherical paths):

Theorem 1 *Given three points m_i in the moving system and three points in the fixed system M_i (centers of spheres on which the points m_i run). Then there are the following possibilities for additional pairs of points which take part in a Schönflies-Borel-Bricard motion so that the distance M_im_i is constant:*

1. *Four points, the fourth point is given by $m_1, m_2, m_3, M_1, M2, M_3$, centers of spheres are in a plane.*
2. *All points of the circumscribed circle of the points m_1, m_2, m_3 have spherical trajectory, centers are on an ellipse.*
3. *All points of a cubic run on spherical paths, centers lie on a space curve. The cubic can split into a line and a circle.*
4. *All points run on spherical paths, centers are in the plane $C = 0$. In all cases points m_i and projections of points M_i to $z = 0$ are in an inversion.*

Note that this theorem essentially gives all the design information which is necessary to design (or avoid) platform mechanisms which are able to perform SBB self motions.

4.4 A general example:

Let us choose $a_2 = 3, A_2 = 5, a_3 = 7, b_3 = 17, A_3 = 13, B_3 = 11$. Then we obtain

$$A_4 = 5[1993(a_4^2 + b_4^2) + 20556a_4 - 8673b_4]/W,$$

$$B_4 = 5[2891(a_4^2 + b_4^2) - 8673a_4 - 20556b_4]/W,$$

where

$$W = 1394[(a_4 + \frac{3594}{2788})^2 + (b_4 - \frac{17346}{2788})^2].$$

This yields the expression for the inversion. Further we obtain

$$C_3 = -C_2/2,\ C_3 = 6C_2.$$

For the second possibility we obtain the equation of the cubic in the form

$$\begin{aligned} K &= 41(5a_4 - 3b_4)(a_4^2 + b_4^2) + 1775a_4^2 + 2777b_4^2 - \\ &\quad 2868a_4b_4 - 7170a_4 - 16254b_4 = 0. \end{aligned} \tag{23}$$

Expressions for y_1, y_2 are too complicated to be given here, y_3 is computed from the remaining equation $h_1 = 0$. If we choose $a_4 = 1458/187, b_4 = 1242/187$, we obtain

$$C_4 = \frac{5364C_2 + 1242C_3}{3179} \quad \mathrm{S}_4 = \frac{5364S_2 + 1242S_3}{3179}. \tag{24}$$

This yields the previous case with exactly four points with spherical trajectories, points M_i are in one plane.

5 Conclusion

I this paper we have tried to give an overview on the results which have been obtained for self motions and architecture singularity of Stewart-Gough manipulators. Although the listing of the references is as complete as possible, the examples can only be exemplarily. We emphasized to demonstrate the mathematical and geometrical methods which can be used to derive results in this field.

That the discussion of all possible cases can be very long and involved is shown in the new and complete analysis of the Schönflies-Borel-Bricard platform motions. Although all cases of SBBM-motions were known already to Borel, a prove of completeness was missing until now. A kinematic and geometric discussion of all these cases is open.

An open problem is also the discussion of many cases listed already by Borel (Type 5,7 and 8). All of these cases would lead to self motions of SGP, but maybe with strange designs of the mechanisms.

6 Acknowledgments

The research of this paper was supported by the Grant no 201/02/0616 of the Czech Grant Agency and partially by the Grant MSM113200007 of the Ministery of Education of the Czech Republic and by grant no P14982 of the Austrian FWF.

References

Blaschke, W., 1920, Wackelige Achtflache [transl. M. Husty: Shaky polyhedra with eight faces], *Math. Zeitschrift*, vol.6, 85–93.

Blaschke, W. 1948, *Analytische Geometrie*, Wolfenbüttler Verlagsanstalt.

Bottema, O., Roth, B., 1990, *Theoretical Kinematics*, Dover Publishing.

Bricard, R., 1896, "Déplacement remarquable", *Comptes rendues*, vol 123, 939-940.

Bricard, R., 1897, Mémoire sur la théorie de l'octaédre articulé, *J. math. pur appl., Liouville*, 3, 113-148.

Bricard, R. ,1906, "Mémoire sur les déplacements à trajectoires sphériques", *Journ. École Polyt.*, (2), cahier 11, 1-96.

Borel, E., 1908 "Mémoire sur les déplacements à trajectoires sphériques", Mém. présentés par divers savants, Paris (2), 33, pp. 1-128.

Cauchy, A. L., 1813, Sur les polygones et les polyèdres, *J. École polytech*,XVIe Cahier IX, 87-89.

Conelly, R., 1978, "The rigidity of suspensions", *J. differential Geometry*, vol.13, 399–408.

Dasgupta, B., Mruthyunjaya, T. S., "The Stewart Platform manipulator: a review", *Mechanism and Machine Theory*, vol. 34, No. 1, pp. 15-40, 2000.

Griffis, M., Crane, C., Duffy, J., 1994, "A smart kinestatic interactive platform", in: Lenarcic, J. and Ravani, B.: *Advances in Robot Kinematics*, Kluwer Acad. Pub., 459 – 464, ISBN 0-7923-2983-X.

Griffis, M., Duffy, J., 1993, "Method and Apparatus for Controlling Geometrically Simple Parallel Mechanisms with Distinctive Connections", US Patent # 5,179, 525, 1993.

Husty, M. L., 1996, "An Algorithm for Solving the Direct Kinematic of General Stewart-Gough Platforms",*Mechanism and Machine Theory*, vol. 31, No. 4, pp. 365-380.

Husty, M., 2000, "E. Borel's and R. Bricard's Papers on Displacements with Spherical Paths and their Relevance to Self-Motions of Parallel Manipulators", in: *International Symposium on History of Machines and Mechanisms-Proceedings HMM 2000*, Ed. M. Ceccarelli, Kluwer Acad. Pub., 163 – 172, ISBN 0-7923-6372-8.

Husty, M. - Karger, A., 1996, "Self-Motions of Stewart-Gough Platforms", *Proceedings VIIth International Congress on the Theory of Machines and Mechanisms*, Liberec, 245 – 250.

Husty, M., and Karger, A., 2000 "Self-Motions of Griffis-Duffy Type Platforms", *Proceedings of IEEE conference on Robotics and Automation (ICRA 2000)*, San Francisco, 7–12.

Husty, M. and Karger, A., 2000, "Architecture Singular Parallel Manipulators and their Self-Motions", *Proceedings of VIII. Int. Conf. on the Theory of Machines and Mechanisms*, Sept. 2000, Liberec, 219–222.

Husty, M.- Karger, A.: "Architecture singular parallel manipulators and their self-motions", in: Lenarcic, J. and Stanisic, M. M.: *Advances in Robot Kinematics*, Kluwer Acad. Pub., (2000), 355 – 364, ISBN 0-7923-6426-0.

Husty, M. and Karger, A., 2001, "Architecture singular planar Stewart-Gough platforms", Proceedings of the 10th workshop RAAD, Vienna, (2001), 6 pages (CD-Proceedings).

Husty, M. - Zsombor-Murray, P., 1994, "A Special Type of Singular Stewart Gough Platform", in: Lenarcic, J. and Ravani, B.: *Advances in Robot Kinematics*, Kluwer Acad. Pub., (1994), 439 – 449, ISBN 0-7923-2983-X.

Karger, A., 1998, "Architecture singular parallel manipulators", in: Lenarcic, J. and Husty, M.: *Advances in Robot Kinematics*, Kluwer Acad. Pub., 445 – 454, ISBN 0-7923-5169-X.

Karger, A. - Husty, M., 1997, "Singularities and Self-Motions of Stewart-Gough Platforms", *NATO-ASI Workshop on Comuputational Methods in Mechanism Design*, vol. 2, Varna, 270 – 289.

Karger, A. and Husty, M., 1998, "Classification of All Self-Motions of the Original Stewart-Gough Platform", *Computer Aided Design*, vol. 30, 205 – 215.

Krames, J., 1937, Zur Bricardschen Bewegung, deren sämtliche Bahnkurven auf Kugeln liegen (Über symmetrische Schrotungen II), [transl. On Bricard's motion, with all paths on spheres. (On line symmetric motions II)], *Monatsh. Math. Phys.*, vol. 45, 407–417.

Kong, X. and Gosselin, C., 2001, "Generation of Architecturally Singular 6-SPS Parallel Manipulators with Linearly Related Planar Platforms", *Proceedings of CK2001*, 67–75.

Ma, O. and Angeles, J., 1992, "Architecture Singularities of Parallel Manipulators". *Int. Journal of Robotics and Automation*, vol. 7, 23-29.

Merlet, J. P., 2000, *Parallel Robots*, Kluwer Academic Publishers, Dordrecht, The Netherlands.

Mick, S. and Röschel, O., "Geometry and architecturally shaky platforms" in: Lenarcic, J. and Husty, M.: *Advances in Robot Kinematics*, Kluwer Acad. Pub., 445 – 454, ISBN 0-7923-5169-X.

Raghavan, M., 1991, "The Stewart platform of general geometry has 40 configurations", *ASME Design and Automation Conf., Chicago, 1991*, vol. 32-2, 397–402.

Ravani, B. Roth, B., 1984, "Mappings of Spatial Kinematics",*ASME, J. of Mechanisms, Transmissions and Autom. in Design*, Vol. 106, pp. 341–347.

Röschel, O. and Mick, S., "Characterization of of architecturally shaky platforms", in: Lenarcic, J. and Husty, M.: *Advances in Robot Kinematics*, Kluwer Acad. Pub., 445 – 454, ISBN 0-7923-5169-X.

Sommese, A, Verschelde, Wampler, Ch., 2002, ”Advances in Polynomial Continuation for Solving problems in Kinematics”, preprint.

Stachel, H., 1987, "Zur Einzigartigkeit der Bricardschen Oktaeder" [transl. by M. Husty: On the Uniqueness of Bricard’s Octahedra], *Journal of Geometry*, vol. 28, 41–56.

Wampler, C., 1996, "Forward displacement analysis of general six-in-parallel SPS (Stewart) platform manipulators using soma coordinates", *Mech. Mach. theory*, vol.31 (3), 331-337.

Wohlhart, K., 2000, "A spinning platform mechanism", *Proceedings of VIII. Int. Conf. on the Theory of Machines and Mechanisms*, Sept. 2000, Liberec, 829–838.

Wohlhart, K., 2000, "Architectural shakliness or architectural mobility of platforms" in: Lenarcic, J. and Stanisic, M. M.: *Advances in Robot Kinematics*, Kluwer Acad. Pub., (2000), 365 – 374, ISBN 0-7923-6426-0.

Wunderlich, W., 1965, Starre, kippende, wackelige und bewegliche Achtflache, [transl. M. Husty: "Rigid, snapping, shaky and flexible polyhedra with eight faces"], *Elemente Math.*, vol. 20, 25-32.

Zsombor-Murray, P., Husty, M., Hartmann, D., 1995a, "Singular Stewart-Gough Platforms with Spherocylindrical and Spheroconical Hip Joint Trajectories", *Proc. 9th World Congress on the Theory of Machines and Mechanisms*, Milano, vol. 3, (1995b), 1886 – 1890.

Zsombor-Murray, P., Husty, M., Hartmann, D., 1995b, "Surface Symmetries in Overconstrained Mechanisms", Proc. Robotics in Alpe Adria, Pörtschach, 125 – 129.

Proceedings of the WORKSHOP on
Fundamental Issues and Future Research Directions for Parallel Mechanisms and Manipulators
October 3–4, 2002, Quebec City, Quebec, Canada
Clément M. Gosselin and Imme Ebert-Uphoff, editors

Forward Displacement and Singularity Analysis of a Crank-Type 6-3 In-Parallel Actuated Mechanism

YUKIO TAKEDA
Department of Mechanical Sciences and Engineering
Tokyo Institute of Technology
2-12-1, O-okayama, Meguro-ku, Tokyo 152-8552, Japan
takeda@mech.titech.ac.jp

ULRICH SPAELTER
Department of Mechanical Sciences and Engineering
Tokyo Institute of Technology
2-12-1, O-okayama, Meguro-ku, Tokyo 152-8552, Japan

HIROAKI FUNABASHI
Department of Mechanical Engineering
Shibaura Institute of Technology
3-9-14, Shibaura, Minato-ku, Tokyo 108-8548, Japan

Abstract: *We propose a closed-form solution of the forward displacement analysis (FDA) for a crank type 6-3 in-parallel actuated mechanism. From the derived FDA-equations both real and complex solutions are numerically determined for given example input angles. It is pointed out, that the FDA for the 6-3 crank-type mechanism is described by a polynomial of* 16th *degree also including uneven terms. Root diagrams are introduced in order to show the behavior of real and complex equation solutions for changing input angles. We prove that forward kinematic singularities of parallel mechanisms can be identified by characteristic patterns in the root diagram, which is verified with the determinant of the Jacobian and the previously introduced Transmission Index (TI). An algorithm for sorting solutions to obtain the root-curves of identical assembly modes of FDA using the root diagram is discussed as well.*

1 Introduction

The crank-type in-parallel actuated mechanism shown in Figure 1 (Hunt,1983) (Funabashi,*et al.* 1991) (Uchiyama,*et al.* 1992) (Takeda,*et al.* 1997) (Arai,*et al.* 1997) (Takeda,*et al.* 1999) has advantageous characteristics in larger working space, higher-speed motion, etc. compared with slider-type in-parallel actuated mechanisms (Stewart,1965) (Arai,*et al.*1996) (Ota,*et al.* 2000). However, methods to support the design of mechanism and controller for crank-type mechanism have not been developed so much compared with the case of slider-type mechanisms such as the Stewart Platform mechanism, though working space(Bonev,*et al.* 2000), static balancing (Gosselin,*et al.* 2000), motion transmissibility (Takeda,*et al.*1995) (Takeda,*et al.* 1997) and output isotropy (Takeda,*et al.* 1999JRM) have been already investigated. Especially, as far as the authors know, the forward displacement analysis (FDA) of crank-type mechanism has not ever been discussed though numerous articles on the FDA of the Stewart Platform have been published and some knowledges for mechanism design from the view point of the easiness of FDA have been proposed (Griffs,*et al.* 1994).

With the closed-form FDA of the in-parallel actuated mechanisms, all possible poses can be determined for given input displacements, thus enabling a better understanding of the entire mechanism. The FDA is not only important for mechanism control, but also for identifying working space properties and assembly modes, which opens a wider range of applications. As will be pointed out, also singular points, which limit working space, can be determined from FDA-results. The detection of both inverse kinematic singularities (IKS), forward kinematic singularities (FKS) and their neighborhood is especially important for control purposes, as singular points either result in high forces, which can destroy the mechanism (IKS), or increase the degree of freedom thus making mechanism control impossible (FKS). Therefore, we must investigate the following aspects as well as to obtain the closed-form equation in order to use FDA in the mechanism design and control of the crank-type in-parallel actuated mechanisms:

- nature of the equations and solutions of FDA
- sort algorithm of solutions

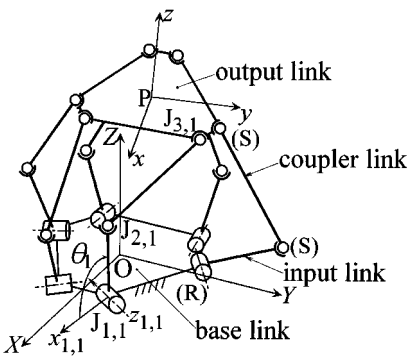

Figure 1: Crank-type spatial in-parallel actuated mechanism with six dof with general joint-arrangement

- relationship between the kinematic parameters of the mechanism and FDA problem
- relationship between singular points and the FDA solutions

In the present paper, as the first step of our investigations on FDA of the crank-type in-parallel actuated mechanism, the equations of FDA for a crank-type in-parallel actuated mechanism with a simplified joint arrangement are derived. The change of the FDA-solutions is analyzed for changing input angles and characteristics of FDA using the root diagram with relation to singular points are treated. An algorithm for sorting solutions to obtain the root-curves of identical assembly modes of FDA using the root diagram is discussed.

2 Mechanism Configuration

The crank-type spatial in-parallel actuated mechanism with six degrees of freedom(dof) with general joint-arrangement is shown in Figure 1. The output link is supported by six connecting chains of identical structure. The connecting chain is composed of one revolute (R) joint and two spherical (S) joints. In this mechanism, the revolute joints on the base are active joints. As described in the Introduction, as the first investigation of our FDA problem, we deal with a crank-type mechanism with a simple joint-arrangement as shown in Figure 2 in which the spherical joints on the output link are located on the vertices of an equilateral triangle with sidelength s. We call this mechanism the crank-type spatial 6-3 in-parallel actuated mechanism.

The joints in each connecting chain are denoted by $\mathrm{J}_{1,i}$, $\mathrm{J}_{2,i}(i = 1, 2, \cdots, 6)$ and $\mathrm{J}_{3,j}(j = 1, 2, 3)$, and the axis of rotation of the input link is denoted by $z_{1,i}$, as shown in Figure 2. The input angle θ_i is defined as the angle between $\overrightarrow{\mathrm{J}_{1,i}\mathrm{J}_{2,i}}$ and the axis $x_{1,i}$ around $z_{1,i}$. The revolute joints on the base link are symmetrically located as shown in Figure 3, and their locations are described by the radius R and the angles β_1 and β_2. The lengths of the input and coupler links are denoted by f and l, respectively.

Once all the input angles are given, the FDA problems of the mechanism shown in Figures 1 and 2 will essentially be-

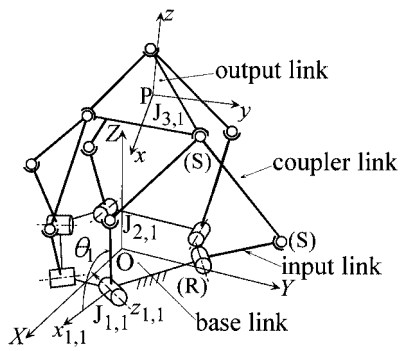

Figure 2: Crank-type spatial 6-3 in-parallel actuated mechanism with six dof

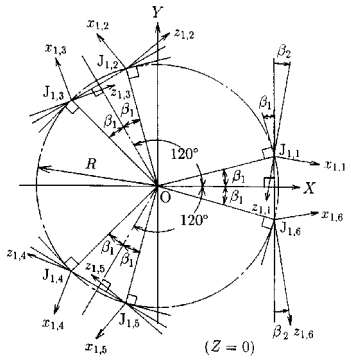

Figure 3: Location of joints on the base

come the same as that of Stewart Platforms with general joints arrangements ("non-planar case") (Husty,1996) (Innocenti,2001) (Lee,*et al.* 2001) (Selfridge,*et al.* 2000) (Kong,*et al.* 2001). In literatures, however, important problems related to FDA of parallel mechanisms mentioned in Introduction have not been investigated though the equations for FDA have been generally derived and an example solution has been numerically presented.

3 Forward Kinematics

First the forward displacement analysis is derived for a crank-type spatial in-parallel actuated mechanism with a simplified joints arrangement on the output link shown in Figure 2. Given the crank length f and the coupler link length l, the vector for the i-th crank to one edge of the triangular platform is described by as there are three pairs of links with one unknown remaining for each, the position of the output link of the 6-3 mechanism can be entirely described by three angular variables.

The FDA in closed form is derived via three loop equations. ${}_{\mathbf{R}}\mathbf{r}_{\mathbf{J_{2,i}J_{1,i}}}$ represents the crank end-point vector in coordinate system R relative to the crank,

$$ {}_{\mathbf{R}}\mathbf{r}_{\mathbf{J_{1,i}J_{2,i}}} = \begin{pmatrix} f\cos\theta_i \\ 0 \\ f\sin\theta_i \end{pmatrix} \tag{1} $$

This vector is transformed into I-coordinate(base-coordinate

system) with transformation matrix $\mathbf{A_{IR}}$.

$$
\begin{aligned}
{}_{\mathbf{I}}\mathbf{r}_{\mathbf{J_{1,i}J_{2,i}}} &= \mathbf{A_{IR}}\,{}_{\mathbf{R}}\mathbf{r}_{\mathbf{J_{1,i}J_{2,i}}} \\
&= \begin{pmatrix} \cos\beta_2 & \sin\beta_2 & 0 \\ -\sin\beta_2 & \cos\beta_2 & 0 \\ 0 & 0 & 1 \end{pmatrix} \begin{pmatrix} f\cos\theta_i \\ 0 \\ f\sin\theta_i \end{pmatrix} \\
&= \begin{pmatrix} f\cos\theta_i\cos\beta_2 \\ -f\cos\theta_i\sin\beta_2 \\ f\sin\theta_i \end{pmatrix}
\end{aligned} \tag{2}
$$

$$
\mathbf{A_{IR}} = \begin{pmatrix} \cos\beta_2 & \sin\beta_2 & 0 \\ -\sin\beta_2 & \cos\beta_2 & 0 \\ 0 & 0 & 1 \end{pmatrix} \tag{3}
$$

Adding ${}_{\mathbf{I}}\mathbf{r}_{\mathbf{OJ_{1,i}}}$ that expresses position vector of $\mathrm{J}_{1,i}$ in the base coordinate system.

$$
{}_{\mathbf{I}}\mathbf{r}_{\mathbf{OJ_{1,i}}} = \begin{pmatrix} a_i \\ b_i \\ 0 \end{pmatrix} \tag{4}
$$

$$
\begin{aligned}
{}_{\mathbf{I}}\mathbf{r}_{\mathbf{OJ_{2,i}}} &= {}_{\mathbf{I}}\mathbf{r}_{\mathbf{OJ_{1,i}}} + {}_{\mathbf{I}}\mathbf{r}_{\mathbf{J_{1,i}J_{2,i}}} \\
&= \begin{pmatrix} a_i \\ b_i \\ 0 \end{pmatrix} + \begin{pmatrix} f\cos\theta_i\cos\beta_2 \\ -f\cos\theta_i\sin\beta_2 \\ f\sin\theta_i \end{pmatrix} \\
&= \begin{pmatrix} a_i + f\cos\theta_i\cos\beta_2 \\ b_i - f\cos\theta_i\sin\beta_2 \\ f\sin\theta_i \end{pmatrix}
\end{aligned} \tag{5}
$$

${}_{\mathbf{I}}\mathbf{r}_{\mathbf{J_{2,2j-1}J_{2,2j}}}(j = 1,2,3)$ represents the vector between two cranks of one crank-pair.

$$
\begin{aligned}
{}_{\mathbf{I}}\mathbf{r}_{\mathbf{J_{2,2j-1}J_{2,2j}}} &= {}_{\mathbf{I}}\mathbf{r}_{\mathbf{OJ_{2,2j}}} - {}_{\mathbf{I}}\mathbf{r}_{\mathbf{OJ_{2,2j-1}}} \\
&= \begin{pmatrix} a_{2j} - a_{2j-1} + f(\cos\theta_{2j}\cos\beta_2 - \cos\theta_{2j-1}\cos\beta_2) \\ b_{2j} - b_{2j-1} + f(\cos\theta_{2j-1}\sin\beta_2 - \cos\theta_{2j}\sin\beta_2) \\ f(\sin\theta_{2j} - \sin\theta_{2j-1}) \end{pmatrix}
\end{aligned} \tag{6}
$$

The two links of length l of one crank-pair meet at one point. As the two links limit each other to one rotational dof, they can only perform circular movement around a circle with the rotation center P_j half in between both cranks as shown in Figure 4. The radius r_j of the circle is calculated via the relation:

$$
r_j^2(\theta_{2j-1}, \theta_{2j}) = l^2 - \frac{1}{4}\left|{}_{\mathbf{I}}\mathbf{r}_{\mathbf{J_{2,2j}J_{2,2j-1}}}\right|^2 \tag{7}
$$

The position of the point, where the two links meet (therefore one edge-point of the output link) can be uniquely described by only one (unknown) angle ψ_j of the circular plane. The polar coordinate of the circular plane can be expressed in base coordinate via two coordinate transformations, which first rotate the circle around its x_j-axis (angle γ_j) and then around the z_j-axis (angle ϵ_j):

$$
{}_{\mathbf{K}}\mathbf{r}_{\mathbf{P_jJ_{3,j}}} = r_j(\theta_{2j}, \theta_{2j-1}) \begin{pmatrix} \cos\psi_j \\ 0 \\ \sin\psi_j \end{pmatrix} \tag{8}
$$

$$
\begin{aligned}
{}_{\mathbf{I}}\mathbf{r}_{\mathbf{P_jJ_{3,j}}} &= [\mathbf{D_{1,j}}(\epsilon_\mathbf{j})\mathbf{D_{2,j}}(\gamma_\mathbf{j})]_{IK}\,{}_{\mathbf{K}}\mathbf{r}_{\mathbf{P_jJ_{3,j}}} \\
&= r_j \begin{pmatrix} \cos\epsilon_j & \sin\epsilon_j & 0 \\ -\sin\epsilon_j & \cos\epsilon_j & 0 \\ 0 & 0 & 1 \end{pmatrix} \begin{pmatrix} 1 & 0 & 0 \\ 0 & \cos\gamma_j & -\sin\gamma_j \\ 0 & \sin\gamma_j & \cos\gamma_j \end{pmatrix} \begin{pmatrix} \cos\psi_j \\ 0 \\ \sin\psi_j \end{pmatrix} \\
&= r_j \begin{pmatrix} \cos\psi_j\cos\epsilon_j - \sin\psi_j\sin\epsilon_j\sin\gamma_j \\ -\cos\psi_j\sin\epsilon_j - \sin\psi_j\cos\epsilon_j\sin\gamma_j \\ \sin\psi_j\cos\gamma_j \end{pmatrix}
\end{aligned} \tag{9}
$$

Here, the angles ψ_j and γ_j are defined in Figure 4. $\mathbf{J_{3,j}}$ is expressed as follows with only ψ_j remaining unknown.

$$
\begin{aligned}
{}_{\mathbf{I}}\mathbf{r}_{\mathbf{OJ_{3,j}}} &= {}_{\mathbf{I}}\mathbf{r}_{\mathbf{OP_j}} + {}_{\mathbf{I}}\mathbf{r}_{\mathbf{P_jJ_{3,j}}} \\
&= {}_{\mathbf{I}}\mathbf{r}_{\mathbf{OJ_{2,2j}}} + \tfrac{1}{2}{}_{\mathbf{I}}\mathbf{r}_{\mathbf{J_{2,2j+1}J_{2,2j}}} + [\mathbf{D_{1,j}}(\epsilon_\mathbf{j})\mathbf{D_{2,j}}(\gamma_\mathbf{j})]_{IK}\,{}_{\mathbf{K}}\mathbf{r}_{\mathbf{P_jJ_{3,j}}} \\
&= \tfrac{1}{2}\begin{pmatrix} a_{2j} + a_{2j-1} + f(\cos\theta_{2j}\cos\psi_{2j} + \cos\theta_{2j-1}\cos\psi_{2j-1}) \\ b_{2j} + b_{2j-1} - f(\cos\theta_{2j-1}\sin\psi_{2j-1} + \cos\theta_{2j}\sin\psi_{2j}) \\ f(\sin\theta_{2j} + \sin\theta_{2j-1}) \end{pmatrix} \\
&\quad + r_j \begin{pmatrix} \cos\psi_j\cos\epsilon_j - \sin\psi_j\sin\epsilon_j\sin\gamma_j \\ -\cos\psi_j\sin\epsilon_j - \sin\psi_j\cos\epsilon_j\sin\gamma_j \\ \sin\psi_j\cos\gamma_j \end{pmatrix}
\end{aligned} \tag{10}
$$

$$
{}_{\mathbf{I}}\mathbf{r}_{\mathbf{OJ_{3,j}}} = \begin{pmatrix} A_j \\ B_j \\ C_j \end{pmatrix} + r_j \begin{pmatrix} \cos\psi_j D_j - \sin\psi_j E_j \\ -\cos\psi_j F_j - \sin\psi_j G_j \\ \sin\psi_j H_j \end{pmatrix} \tag{11}
$$

Altogether there are three link pairs with three $\psi_{1,2,3}$ remaining unknown, thus the FDA for the 6-3 mechanism with six dof is reduced to determining three unknowns, as one edge point of the output link is defined by the unknown angle ψ_j in polar coordinates. The vector loops close by introducing additional constraint conditions via the three constant sidelengths s of the equilateral triangular output link.

$$
\left|{}_{\mathbf{I}}\mathbf{r}_{\mathbf{OJ_{3,j}}} - {}_{\mathbf{I}}\mathbf{r}_{\mathbf{OJ_{3,j+1}}}\right|^2 = s^2 \tag{12}
$$

The three link pair equations thus result in the following three equations of three unknowns.

$$
\left.\begin{aligned}
&K_{1,j} + K_{2,j}\cos\psi_j + K_{3,j}\sin\psi_j + K_{4,j}\cos\psi_{j+1} \\
&+K_{5,j}\sin\psi_{j+1} + K_{6,j}\cos\psi_j\cos\psi_{j+1} \\
&+K_{7,j}\cos\psi_j\sin\psi_{j+1} + K_{8,j}\sin\psi_j\cos\psi_{j+1} \\
&+K_{9,j}\sin\psi_j\sin\psi_{j+1} = 0
\end{aligned}\right\} \tag{13}
$$

Still the unknowns are functions of $\sin\psi_j$ and $\cos\psi_j$. To transform the set of trigonometric equations into a set of polynomial

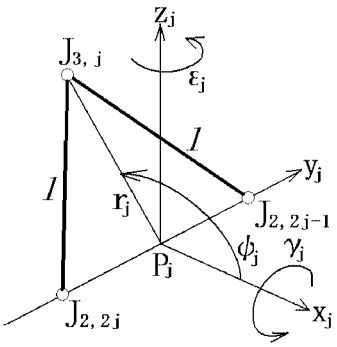

Figure 4: Definitions of radius r_j and angles ψ_j, γ_j and ϵ_j

equations, the half-tan relations are applied.

$$\sin\psi_j = \frac{2x_j}{1+x_j^2}; \quad \text{and} \quad \cos\psi_j = \frac{1-x_j^2}{1+x_j^2} \tag{14}$$

Further transformation yields the coefficients $K_{1..9,j}$:

$$\left.\begin{aligned}
K_{1,j} &= (A_j - A_{j+1})^2 + (B_j - B_{j+1})^2 + (C_j - C_{j+1})^2 \\
&\quad + r_j^2 + r_{j+1}^2 - s^2 \\
K_{2,j} &= 2r_j\,\{(A_j - A_{j+1})D_j - (B_j - B_{j+1})F_j\} \\
K_{3,j} &= -2r_j\,\{(A_j - A_{j+1})E_j + (B_j - B_{j+1})G_j \\
&\quad -(C_j - C_{j+1})H_j\} \\
K_{4,j} &= 2r_{j+1}\,\{(A_j - A_{j+1})D_{j+1} + (B_j - B_{j+1})F_{j+1}\} \\
K_{5,j} &= -2r_{j+1}\,\{(A_j - A_{j+1})E_{j+1} + (B_j - B_{j+1})G_{j+1} \\
&\quad -(C_j - C_{j+1})H_{j+1}\} \\
K_{6,j} &= -2r_j r_{j+1}(D_j D_{j+1} + F_j F_{j+1}) \\
K_{7,j} &= 2r_j r_{j+1}(D_j E_{j+1} - F_j G_{j+1}) \\
K_{8,j} &= 2r_j r_{j+1}(E_j D_{j+1} + G_j F_{j+1}) \\
K_{9,j} &= -2r_j r_{j+1}(E_j E_{j+1} + H_j Hj + 1 + G_j G_{j+1})
\end{aligned}\right\} \tag{15}$$

With the coefficients from above the following polynomial equation of degree eight and of two unknowns x_j and x_{j+1} is yielded for one link pair (j=1,2,3):

$$\begin{aligned}
&\{(K_{1,j} - K_{5,j} - K_{2,j} + K_{6,j})x_{j+1}^2 + 2(K_{4,j} - K_{7,j})x_{j+1} \\
&+(K_{1,j} + K_{5,j} - K_{6,j} - K_{2,j})\}\,x_j^2 + \{(K_{3,j} - K_{9,j})x_{j+1}^2 \\
&+2K_{8,j}x_{j+1} + (K_{3,j} + K_{9,j})\}\,x_j + \{(K_{1,j} - K_{5,j} + K_{2,j} \\
&-K_{6,j})x_{j+1}^2 + 2(K_{4,j} + K_{7,j})x_{j+1} + (K_{1,j} + K_{5,j} + K_{6,j} \\
&+K_{2,j})\} = 0
\end{aligned} \tag{16}$$

4 FDA-Equations

The set of three nonlinear polynomial equations already includes all solutions in closed-form. By Sylvester's dialytical elimination method the set of polynomial equations is reduced to a 16th order polynomials in one unknown. In contrast to the Stewart-Platform (Nanua,*et al.* 1990), also uneven terms are part of the polynomial in one unknown. As in case of the Stewart-Platform the base points of all links are element of one plane there exists a solution symmetric to the base plane for every FDA-solution. Therefore the 16th order FDA-polynomial for the classic Stewart-Platform only includes even terms. In case of the 6-3 crank-type mechanism, the link base points are determined by the crank input angles. Therefore only for special input configuration all base points are part of one plane: For identical input angles for all cranks the uneven terms vanish in the set of equations due to symmetry.

4.1 Numerical Examples

All solutions of the 16th order polynomial can be determined numerically with the Newton-Raphson algorithm. By reducing the polynomial degree after a solutions has been calculated (Deflation), it can be guaranteed, that every solution is calculated just once and that all solutions are determined. In the examples the Newton-Raphson algorithm is first applied to the polynomials in one unknown in order to determine all roots. The set of polynomial equations above is used in the next step for determining, which of the independently calculated 16 solutions in variables x_j belong together, thus defining an FDA solution. For numerical calculus the kinematic parameters are defined by the data provided below, which correspond to our worktable (Takeda,*et al.* 1999) :

$l = 529.3, f = 244.3, s = 423.14$mm
$J_{1,1}$: (265.405,-185.839, 0) mm
$J_{1,2}$: (265.405, 185.839, 0) mm
$J_{1,3}$: (28.239, 322.767, 0) mm
$J_{1,4}$: (-293.644, 136.928, 0) mm
$J_{1,5}$: (-293.644,-136.928, 0) mm
$J_{1,6}$: (28.239,-322.767, 0) mm

For $\boldsymbol{\theta} = [11.9981, 0, 26.1679, 26.5506, 32.4917, 11.8672]$ [deg], we obtained the following three polynomials of 16th order.

$$\left.\begin{aligned}
&1.488x^{16} - 6.005x^{15} + 115.814x^{14} - 93.119x^{13} \\
&-78.517x^{12} + 61.794x^{11} - 35.560x^{10} + 23.224x^9 \\
&+25.314x^8 - 12.676x^7 + 5.207x^6 - 2.933x^5 - 2.420x^4 \\
&+0.495x^3 - 0.519x^2 + 0.099x - 0.004 = 0 \\
&\\
&0.547y^{16} + 10.763y^{15} + 155.814y^{14} + 73.558y^{13} \\
&-122.629y^{12} - 52.902y^{11} - 29.268y^{10} - 14.724y^9 \\
&+30.366y^8 + 8.904y^7 + 3.721y^6 + 1.769y^5 - 2.312y^4 \\
&-0.264y^3 - 0.384y^2 - 0.049y - 0.001 = 0 \\
&\\
&0.462z^{16} - 2.284z^{15} + 135.536z^{14} + 50.909z^{13} \\
&-124.806z^{12} - 33.271z^{11} - 20.733z^{10} - 9.529z^9 \\
&+32.751z^8 + 5.685z^7 + 2.942z^6 + 1.135z^5 - 2.728z^4 \\
&-0.150z^3 - 0.428z^2 - 0.027z + 0.0002 = 0
\end{aligned}\right\} \tag{17}$$

4.2 Solution Analysis

In the numerical example both real and complex solutions of the equation system are determined, as the behaviour of all solutions are to be analyzed. For the crank input angles $\theta_{1..6}$ real and complex solutions have been numerically determined. Furthermore the real solutions are represented by the poses depicted in Figure 5. The coordinates of the vertices of the equilateral triangle output link are calculated as follows.

[1] [231.4,-15.9,-281.9][-122.2,211.1,-233.2][-142.1,-211.3,-244.9]
[2] [222.6,-15.7,-278.8][-126.7,218.9,-235.4][24.9, 2.3, 94.8]
[3] [221.2,-15.7,-278.2][11.0,-18.3, 88.9][-147.7,-220.3,-247.2]
[4] [16.9, 6.7, 83.5][-109.0,190.7, 443.1][-74.6,-230.4, 421.8]
[5] [19.1, 7.3, 94.7][-129.7,224.1,-236.7][-134.3,-198.9,-241.3]
[6] [261.2, 21.9, 341.3][-111.1,194.4, 444.5][-72.2,-226.1, 420.4]
[7] [294.3, 22.2, 347.5][7.7,-12.7, 38.1][-58.9,-201.8, 410.8]
[8] [309.6, 22.3, 349.2][-86.2,151.3, 424.4][18.6, 2.1, 42.6]

Complex solutions are simultaneously calculated as follows($[\psi_1, \psi_2, \psi_3]$, in rad.).

[9] [0.0163-0.5284*i, -0.0054- 0.4902*i, 2.646+16.99*i]
[10] [0.0163+0.5284*i, -0.0054+ 0.4902*i, 2.646-16.99*i]
[11] [0.0220-0.5235*i, -0.0082- 0.4968*i,-0.0132-0.5037*i]
[12] [0.0220+0.5235*i, -0.0082+ 0.4968*i,-0.0132+0.5037*i]
[13] [0.0496-0.5164*i, -9.549+13.55*i,-0.0420-0.5150*i]
[14] [0.0496+0.5164*i, -9.549-13.55*i,-0.0420+0.5150*i]
[15] [1.587-8.558*i, -0.0362+ 0.5068*i, 0.0125+0.4941*i]
[16] [1.587+8.558*i, -0.0362- 0.5068*i, 0.0125-0.4941*i]

It is obvious that the number of real solutions of the polynomial equation (system) depends on the six input angle values, which determine the polynomial coefficients. For fixed given input angles the solutions have already been calculated (see above). Keeping five input angles fixed one input angle (here:) θ_2 is constantly increased and the resulting FDA is calculated as well.

4.3 Sort Algorithm

It is important to know, if two given poses for different input angles are achievable by an identical assembly mode. In case of a single input crank being infinitesimally changed there exist 16 FDA solutions $S_{1..16}(\theta+\Delta\theta)$, which are infinitesimally changed to the solutions $S_{1..16}(\theta)$ of the original input values. As we assume continuously connected FDA solutions for changing input values, it is possible to determine, which $S_x(\theta+\Delta\theta)$ belongs to any solution of the original set $S_{1..16}(\theta)$. As solutions and poses of an identical path are closest to each other among both solution sets, the following statement holds true:

$$\left.\begin{array}{l} S_x(\theta+\Delta\theta) \in S_a \\ \text{if} \\ \text{Min}(|\ S_x(\theta+\Delta\theta) - S_a(\theta)|) = \\ \text{Min}(|S_{\psi 1,x}(\theta+\Delta\theta) - S_{\psi 1,a}(\theta)| \\ +|S_{\psi 2,x}(\theta+\Delta\theta) - S_{\psi 2,a}(\theta)| \\ +|S_{\psi 3,x}(\theta+\Delta\theta) - S_{\psi 3,a}(\theta)|) \\ (x = 1, 2, \cdots, 16) \end{array}\right\} \quad (18)$$

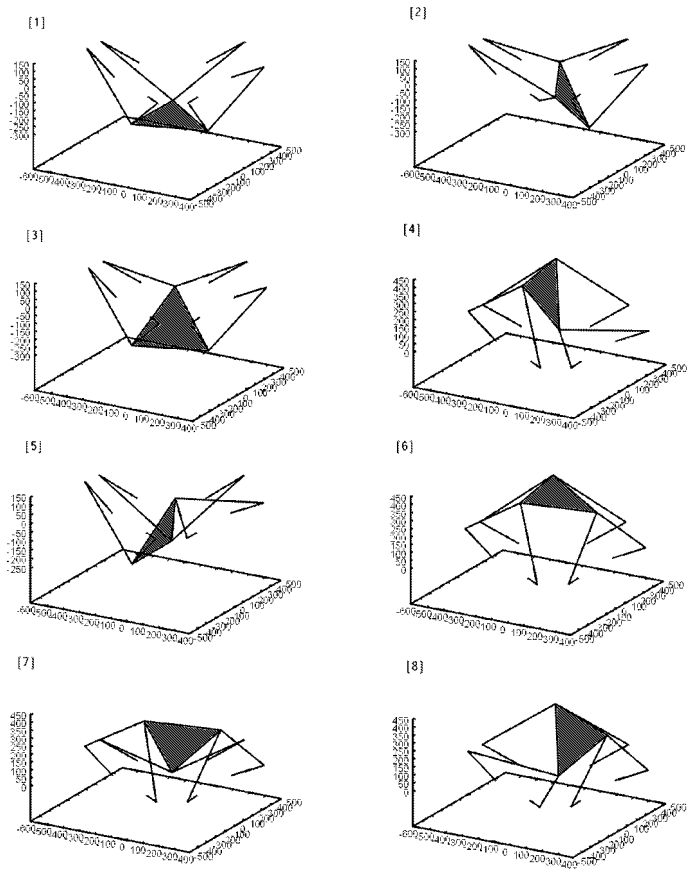

Figure 5: Real Solutions

Thus a solution is considered as adjacent, if the difference in all three variables $\psi_{1..3}$ reaches its minimum. For correct sorting the step size $\Delta\theta$ has to be small enough, so there exists no non-adjacent solution closer to the original solution:

$$\left.\begin{array}{l} \Delta\theta_{max} < \sqrt{(\Delta\theta(S_a, S_b)^2 + \text{Min}(|S_b - S_a|)^2} \\ \text{with } a \notin b \end{array}\right\} \quad (19)$$

4.4 Singularities and Root Diagrams

A set of three diagrams is introduced depicting both real and complex roots of the FDA polynomials for one crank input angle constantly increased as shown in Figures 6 $\sim$ 8. In the figures, the root-curves are shown that have been obtained by the proposed sort algorithm in the previous subsection. Both the polynomial real roots and the real part of the complex solutions are re-transformed into angle ψ_j using relation $\psi_j = \sin^{-1}\{(2x_j)/(1+x_j^2)\}$, thus making evident the relation between solutions and their effect on mechanism behavior with respect to the interaction between complex and real solutions. The complex parts of complex roots, which remain untransformed, are depicted separately.

In case of one input crank moved the diagrams show, that

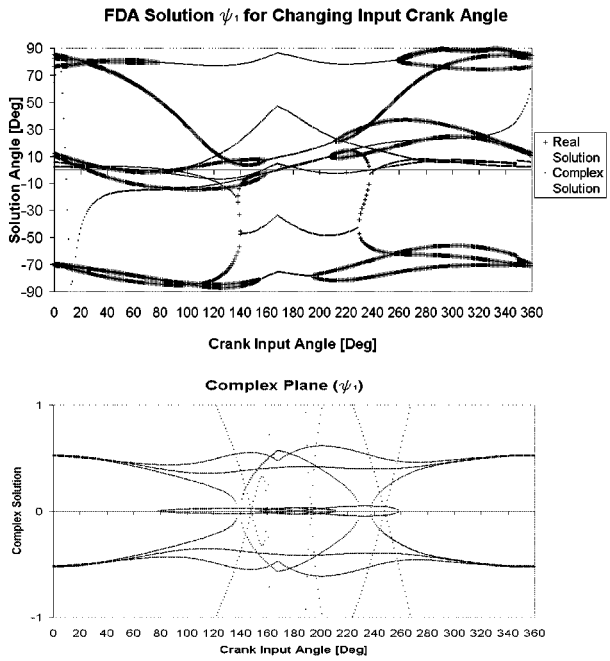

Figure 6: Root diagram for ψ_1

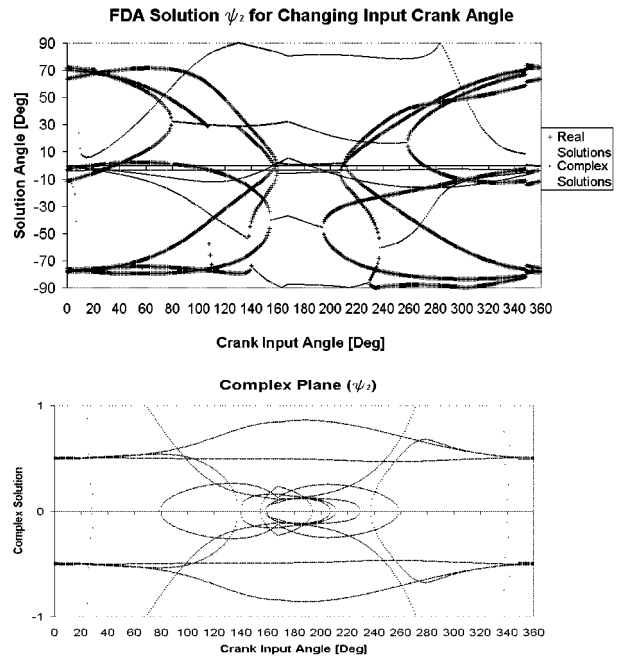

Figure 7: Root diagram for ψ_2

two solutions for different input angles belong to the same assemly mode, as they are connected by a continuous curve of solutions. As the total number of both real and complex solutions is constant for a polynomial of constant order, the decrease of real solutions is accompanied by an increase of complex solutions and vice versa. The change of number of real solutions is shown in Figure 9. The diagrams in figures(6 $\sim$ 9) prove, that for the three FDA-solution angles $\psi_{1..3}$ the number of real and complex solutions is always 16. For a solution set there is a simultaneous change in real solutions in all three variables. Furthermore solution sets $\psi_{1..3}$ consisting of both real and complex solutions, are not observed.

Below the identification of a forward kinematic singularity by the root diagram is proved with both the determinant of the Jacobian and the transmission index TI (Takeda,*et al.*1995). In case of a forward kinematic singularity(FKS) the dof of the mechanism increases. The additional dof corresponds to an infinite gradient, which is also expressed by the Jacobian, in the root diagrams. For defined input crank angles the output link can still move within the boundaries of the infinite (high) gradient. E.g. for the input angles from above and the moved crank angle $\theta_2 \approx 80°$ forward kinematic singularities are identified. The set of root diagrams for changing input angle shows special spots, where two real solutions coincide with a high gradient and become a pair of complex solutions. Both the determinant of the Jacobian and the TI in Figure 10 detect a singularity for the given input angles. Though only the example of one real solution is shown in the figure, similar cases were observed, where real solutions join to become complex at the singular point. Jacobian

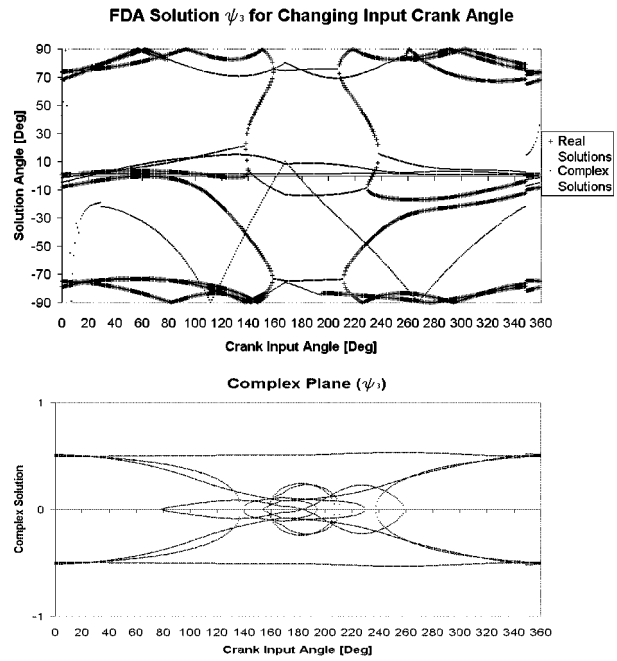

Figure 8: Root diagram for ψ_3

and TI verify that FKS appear with characteristics in the root diagrams as follows:

1. At least two solutions become identical for identical crank input.

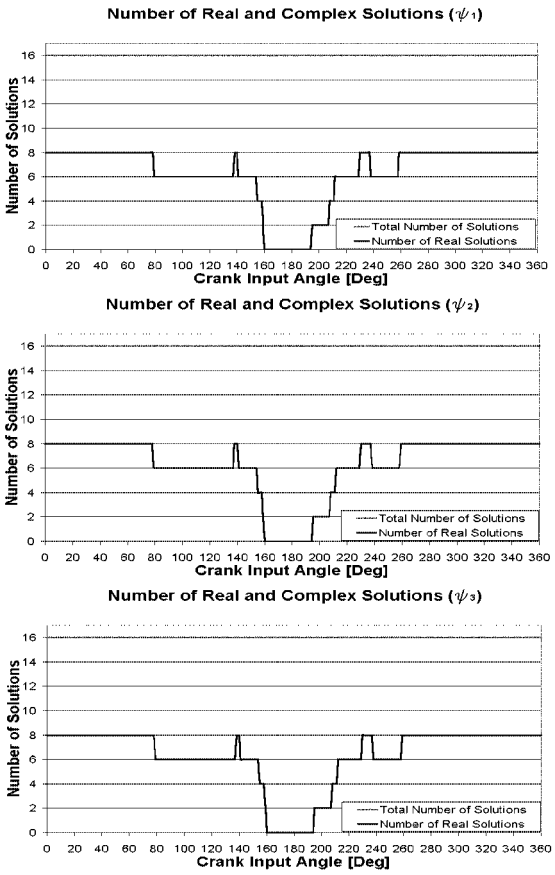

Figure 9: Total number of real and complex solutions for changed crank input

2. High gradient close to singularity.

3. Interaction with the complex plane.

4. For given θ_i singularity patterns show up in all three root diagrams.

The set of root diagrams indicates singularities, e.g. by a high gradient, graphically, whereas the Jacobian is a mathematical means for expressing the same relation differently. The Jacobian so far only provides information for a given posture; the root diagrams also provide information about the neighborhood of the pose to be analyzed and also shows the behavior of all solutions. The diagrams make evident that FKS, which are to be avoided due to the additional dof offer the possibility to switch from one configuration mode to a different one, if two real solutions coincide and if an additional actuator is provided. Thus the parallel mechanism becomes a more flexible tool, which can quickly switch between different working spaces.

The introduced method for determining FKS is based on mathematical considerations and is due to its mechanism independence also applicable to other types of parallel mechanisms, if the according FDA can be performed as well.

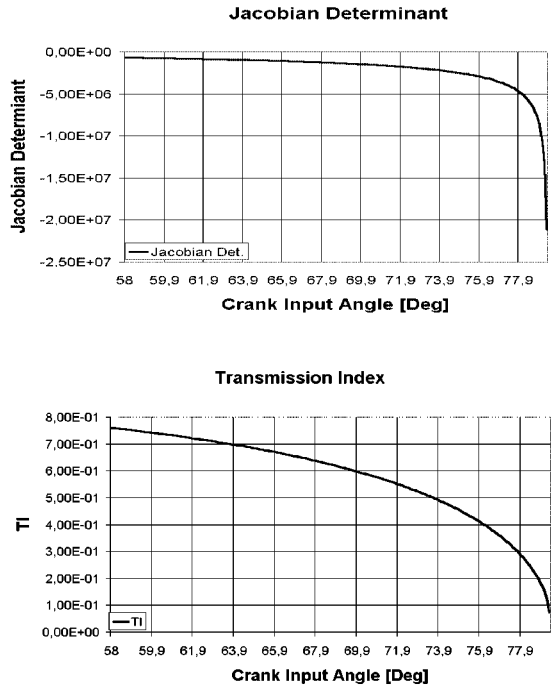

Figure 10: Singularity at $\approx 80^0$ for real solution branch at $\psi_1 \approx 80^0, \psi_2 \approx 38^0, \psi_3 \approx 80^0$

5 Conclusions

In this paper we present a forward kinematic analysis for a crank-type 6-3 mechanism. It is shown that the resulting polynomial with difference to the Stewart-Platform also includes uneven terms. All 16 solutions, including real postures as well as complex solutions, are determined for given input angles. A sort algorithm is introduced, which determines, if two solutions for different input belong to the same working space and assembly mode or not. For a single crank performing a full 360° turn the changing real and complex solutions are compiled in a set of three root diagrams. The newly introduced diagrams are discussed on their ability to determine forward kinematic singularities.

For further research, which will be focused on both forward and inverse kinematic singularities the analysis of the polynomial coefficients for changing input angles will provide further theoretical data on mechanism behavior. Real time FDA and singularity identification still remains an important goal for mechanism control and will enable a wider range of applications.

References

[Arai,*et al.*1996] Arai,T., Tanikawa,T., Merlet,J.P. and Sendai,T., 1996, "Development of a New Parallel Manipulator with Fixed Linear Actuator", *Proc. Japan-USA*

Symp. on Flexible Automation, pp.145-149.

[Arai,*et al.* 1997] Arai,T.,Funabashi,H., Nakamura,Y., Takeda,Y. and Koseki,Y., 1997, "High Speed and High Precision Parallel Mechanism", *Proc. IROS97*, pp.1624-1629.

[Bonev,*et al.* 2000] Bonev,I.A. and Gosselin,C.M., 2000, "A Geometric Algorithm for the Computation of the Constant-Orientation Workspace of 6-RUS Parallel Manipulators", *Proc. ASME 26th Biennial Mechanisms and Robotics Conference*, in CD-ROM.

[Funabashi,*et al.* 1991] Funabashi,H., Horie,M., Kubota,T. and Takeda,Y., 1991, "Development of Spatial Parallel Manipulators with Six Degrees of Freedom", *JSME International Journal, Series III*, Vol.34, No.3, pp.387-392.

[Gosselin,*et al.* 2000] Gosselin,C.M. and Wang,J., 2000, "Static Balancing of Spatial Six-Degree-of-Freedom Parallel Mechanisms with Revolute Actuators", *Journal of Robotic Systems*, Vol.17, No.3, pp.159-170.

[Griffs,*et al.* 1994] Griffs,M., Crane,C. and Duffy,J., 1994, "A Smart Kinestatic Interactive Platform", *Proc. ARK1994*, pp.459-464.

[Griffs,*et al.* 1989] Griffs, G., and Duffy,J., 1989, "A Forward Displacement Analysis of a Class of Stewart Platforms", *Journal of Robotic Systems*, Vol.6, No.6, pp.703-720.

[Hunt,1983] Hunt,K.H., 1983, "Structural Kinematics of In Parallel Actuated Robot Arms, *Trans. ASME, J. of Mechanisms, Transmissions and Automation in Design*, Vol.105, pp. 505-712.

[Husty,1996] Husty,M.L., 1996, "An Algorithm for Solving the Direct Kinematics of General Stewart-Gough Platforms", *Mechanism and Machine Theory*, Vol.31, No.4, pp.365-380.

[Innocenti,2001] Innocenti,C., 2001, "Forward Kinematics in Polynomial Form of the General Stewart Platform", *Trans. ASME, Journal of Mechanical Design*, Vol.123, pp.254-260.

[Kim,*et al.* 2001] Kim,J. and Park,F.C., 2001, "Direct Kinematic Analysis of 3-RS Parallel Mechanisms", *Mechanism and Machine Theory*, Vol.36, pp.1121-1134.

[Kong,*et al.* 2001] Kong,X. and Gosselin,C.M., 2001, "Generation and Forward Displacement Analysis of Two New Classes of Analytic 6-SPS Parallel Manipulators", *Journal of Robotic Systems*, Vol.18, No.6, pp.295-304.

[Lee,*et al.* 2001] Lee,T.Y. and Shim,J.K., 2001, "Forward Kinematics of the General 6-6 Stewart Platform Using Algebraic Elimination", *Mechanism and Machine Theory*, Vol.36, pp.1073-1085.

[Merlet,1992] Merlet,J.P., 1992, "Direct Kinematics and Assembly Modes of Parallel Manipulators", *International Journal of Robotics Research*, Vol.11, No.2, pp.150-162.

[Nanua,*et al.* 1990] Nanua,P., Waldron, K., J. and Murthy,V., 1990, "Direct Kinematic Solution of a Stewart Platform", *IEEE, Trans. on Robotics and Automation*, Vol.6, No.4, pp.438-444.

[Ota,*et al.* 2000] Ota, H., Shibukawa,T., Tooyama,T. and Uchiyama,M., 2000, "Forward Kinematic Calibration Method for Parallel Mechanism Using Pose Data Measured by a Double Ball Bar System", *Proc. PKM-2000*, pp.57-62.

[Selfridge,*et al.* 2000] Selfridge,R.G. and Mattew G.K., 2000, "Forward Analysis of Some Special Stewart Platforms", *Journal of Robotic Systems*, Vol.17, No.10, pp.517-526.

[Stewart,1965] Stewart,D., 1965, "A Platform with 6 Degrees of Freedom", *Proc. of the Institution of Mechanical Engineers*, Vol.180(Part 1, 15), pp.371-386.

[Takeda,*et al.*1995] Takeda, Y. and Funabashi, H., 1995, "Motion Transmissibility of In-Parallel Actuated Manipulators", *JSME International Journal, Series C*, Vol.38, No.4, pp.749-755.

[Takeda,*et al.* 1996] Takeda, Y. and Funabashi, H., 1996, "Kinematic and Static Characteristics of In-Parallel Actuated Manipulators at Singular Points and in Their Neighborhood", *JSME International Journal, Series C*, Vol.39, No.1, pp.85-93.

[Takeda,*et al.* 1997] Takeda, Y., Funabashi, H. and Ichimaru, H., 1997, "Development of Spatial In-Parallel Actuated Manipulators with Six Degrees of Freedom with High Motion Transmissibility, *JSME International Journal, Series C*, Vol.40, No.2, pp.299-308.

[Takeda,*et al.* 1999] Takeda, Y., Funabashi, H., Kimura, M., and Hirose, K., 1999, "Development of a Spatial Six-Degree-of-Freedom In-Parallel Actuated Worktable with Rolling Spherical Bearings", *Proc. 9-th ICAR*, pp.551-556.

[Takeda,*et al.* 1999JRM] Takeda, Y. and Funabashi,H., 1999, "Kinematic Synthesis of In-Parallel Actuated Mechanisms Based on the Global Isotropy Index", *J. of Robotics and Mechatronics(JRM)*, Vol.11, No.5, pp.404-410.

[Takeda,*et al.* 2000] Takeda,Y., Funabashi,H., Shen,G., Ichikawa,K. and Hirose,K., 2000, "Stiffness Analysis of a Spatial Six-Degree-of-Freedom In-Parallel Actuated Mechanism with Rolling Spherical Bearing", *Proc. PKM-2000*, pp.264-273.

[Uchiyama,*et al.* 1992] Uchiyama,M., Iimura,K., Pierrot,F., Unno,K. and Toyama,T., 1992, "Design and Control of a Very Fast 6-dof Parallel Robot", *Proc. of IMACS/SICE International Symposium on Robotics, Mechatronics and Manufacturing Systems '92 Kobe*, pp.473-478.

Proceedings of the WORKSHOP on
Fundamental Issues and Future Research Directions for Parallel Mechanisms and Manipulators
October 3–4, 2002, Quebec City, Quebec, Canada
Clément M. Gosselin and Imme Ebert-Uphoff, editors

DUAL QUATERNION SYNTHESIS OF A 2-TPR CONSTRAINED PARALLEL ROBOT

ALBA PEREZ
Robotics and Automation Laboratory
Department of Mechanical and Aerospace Engineering
University of California
Irvine, California 92697
Email: maperez@uci.edu

J. M. MCCARTHY*
Robotics and Automation Laboratory
Department of Mechanical and Aerospace Engineering
University of California
Irvine, California 92697
Email: jmmccart@uci.edu

Abstract: *This paper presents the dual quaternion synthesis methodology for constrained parallel robots. This methodology uses the dual quaternion form of the kinematics of supporting serial chains as design equations. Given a set of goal positions that define the desired workspace, we solve these design equations to determine the dimensions of the constrained parallel robot. The structure of these dual quaternion design equations allows a systematic elimination of the joint parameters. This methodology results in multiple solutions that are combined to form parallel robots. Here we formulate and solve the design equations for a 2-TPR parallel robot.*

1 Introduction

This paper presents a new formulation for the kinematic synthesis of constrained parallel robots. A constrained parallel robot is one in which each supporting chain imposes a kinematic constraint on the workpiece. These systems provide structural support in certain directions while allowing freedom of movement in others. Our synthesis methodology uses a set of goal positions that describe the workspace of the constrained parallel robot. The dual quaternion kinematic equations of the supporting chains are evaluated each of these goal positions to obtain the design equations, which are solved to obtain their physical dimensions.

This synthesis methodology is an extension of the kinematic synthesis of linkages (McCarthy (2000b)), which is based on finding the geometric constraints of the serial chain. The advantage of an approached based on the expression of the kinematic equations is that it can be applied systematically to serial chains with up to five degrees of freedom and joint axes. Multiple solutions obtained with this method can be combined to create a parallel robot.

The synthesis of parallel robotic systems has focussed on optimization strategies that allow the workpiece full mobility. Chedmail (1998) and Gosselin (1998) present optimization techniques for design serial and parallel robotic system, respectively, that provide desired properties of the workspace. Murray (2000) presents a similar methodology applied to planar platforms, and also Merlet (1997) presents an approach for six-degrees of freedom platforms that combines the geometric synthesis to enclose a given workspace and conditions to take into account joint limits and interferences. This paper focusses on a design methodology that results in a robotic system that guides a workpiece with less than full mobility.

2 Literature Review

Spatial linkage synthesis uses the geometric properties of a serial chain to formulate algebraic equations that must be satisfied at each of a discrete set of positions in the workspace (Suh and Radcliffe (1978)). This yields algebraic equations that are solved to determine the dimensions of the chain. Also see McCarthy (2000). Examples of this are the synthesis of spatial RR chains (Tsai and Roth (1973), Perez and McCarthy (2000)), spatial CC chains (Chen and Roth (1969), Huang and Chang (2000)) and SS chains (Innocenti (1994), Liao and McCarthy (1998)). Larochelle (2000) uses planar quaternion optimization for the approximate synthesis of planar one degree-of-freedom linkages.

Recently, Mavroidis and Lee (2001) used the kinematics equations of the spatial RR and RRR robots to formulate their design equations. This approach introduces the joint parameters of the chain at each of the goal positions as additional variables in the design equations, see also Lee and Mavroidis (2002). The advantage is that it can be systematically applied to a broad range of robotic systems.

In this paper, we follow Mavroidis' basic ideas, however, we use successive screw displacements (Gupta (1986), Tsai (1999)) formulated in terms of dual quaternions to represent the kinematics equations of the robot. Dual quaternions were introduced to

*Address all correspondence to this author.

linkage analysis by Yang and Freudenstein (1964). They form an eight dimensional Clifford algebra that contains a subset, known as unit dual quaternions, which is isomorphic to the group of spatial displacements (McCarthy (1990)). Also see Angeles (1998).

There are two advantages in this formulation. The first is that successive screw displacements provide a convenient formulation for the kinematics equations in terms of the joint axes directly. Secondly, it reduces the number of equations obtained in each goal position from 12 to 8.

3 Supporting Chain Kinematics Equations

The kinematics equations of the robot equate the 4×4 homogeneous transformation $[D]$ between the end-effector and the base frame to the sequence of local coordinate transformations along the chain (Craig (1986)),

$$\begin{aligned}[D] =&[G][Z(\theta_1, d_1)][X(\alpha_{12}, a_{12})][Z(\theta_2, d_2)] \dots \\ &\dots [X(\alpha_{n-1,n}, a_{n-1,n})][Z(\theta_n, d_n)][H].\end{aligned} \tag{1}$$

The parameters (θ, d) define the movement at each joint and (α, a) are the length and twist of each link, collectively known as the Denavit-Hartenberg parameters. The transformation $[G]$ defines the position of the base of the chain relative to the fixed frame, and $[H]$ locates the tool relative to the last link frame.

3.1 Successive Screw Displacements

These kinematics equations can be transformed into successive screw displacements by choosing a reference position $[D_0]$. Let $[D_i]$ be the homogeneous matrix describing the transformation from the fixed frame to a moving frame F_i. We can compute $[D_{0i}] = [D_i][D_0]^{-1}$, that is,

$$\begin{aligned}&[D_{0i}] = [D_i][D_0]^{-1} = \\ &([G][Z(\theta_{1i}, d_{1i})] \dots [Z(\theta_{ni}, d_{ni})][H]) \\ &([G][Z(\theta_{10}, d_{10})] \dots [Z(\theta_{n0}, d_{n0})][H])^{-1}.\end{aligned} \tag{2}$$

This can be viewed as

$$[D_{0i}] = [T(\Delta\theta_1, \mathsf{S}_1)] \dots [T(\Delta\theta_n, \mathsf{S}_n)], \tag{3}$$

where

$$\begin{aligned}&[T(\Delta\theta_1, \mathsf{S}_1)] = [G][Z(\theta_{1i}, d_{1i})][Z(\theta_{10}, d_{10})]^{-1}[G]^{-1}, \\ &[T(\Delta\theta_2, \mathsf{S}_2)] = ([G][Z(\theta_{10}, d_{10})][X(\alpha_{12}, a_{12})][Z(\theta_{2i}, d_{2i})]) \\ &\quad ([G][Z(\theta_{10}, d_{10})][X(\alpha_{12}, a_{12})][Z(\theta_{20}, d_{20})])^{-1}, \\ &\vdots \\ &[T(\Delta\theta_n, \mathsf{S}_n)] = ([G][[Z(\theta_{10}, d_{10})] \dots) \\ &\quad [Z(\theta_n, d_n)][Z(\theta_{n0}, d_{n0})]^{-1}([G][[Z(\theta_{10}, d_{10})] \dots)^{-1}.\end{aligned} \tag{4}$$

The displacements $[T(\Delta\theta_i, \mathsf{S}_i)]$ are the relative rotations about and translations along the joint axes S_i of the robot from the chosen reference configuration. Notice that by expressing them in this way, the initial transformation $[G]$ is absorbed in the first joint axis and the final transformation $[H]$ disappears from the expression.

3.2 Dual Quaternion Kinematics Equations

The workspace of the robot can also be expressed by using the Clifford algebra of the *dual quaternions*. A spatial displacement can be represented as a dual quaternion,

$$\hat{Q}(\hat{\theta}) = \sin(\frac{\hat{\theta}}{2})\mathsf{S} + \cos(\frac{\hat{\theta}}{2}), \tag{5}$$

where $\mathsf{S} = \mathbf{s} + \epsilon\mathbf{s}^0$, with $\epsilon^2 = 0$, is the screw axis of the transformation. The dual numbers $\cos(\frac{\hat{\theta}}{2}) = \cos\frac{\theta}{2} + \epsilon(-\frac{d}{2}\sin\frac{\theta}{2})$ and $\sin(\frac{\hat{\theta}}{2}) = \sin\frac{\theta}{2} + \epsilon(\frac{d}{2}\cos\frac{\theta}{2})$ contain the information about the rotation about and the displacement along the screw axis. The components of the dual quaternions can be easily computed from the homogeneous matrix transformation.

The spatial displacements can be represented as the set of points $\mathbf{Z} = (\mathbf{Z}, \mathbf{Z}^0)$ in $\mathbf{R}^8$ which are subject to two constraints: $\mathbf{Z}\cdot\mathbf{Z} = 1$ and $\mathbf{Z}\cdot\mathbf{Z}^0 = 0$. Then the workspace can be represented as lying on a six-dimensional submanifold of $\mathbf{R}^8$.

The dual quaternion form for the kinematics equations of the robot are obtained by transforming eq.(3) into

$$\hat{D}^i = \hat{S}_1(\Delta\hat{\theta}_1^i) \dots \hat{S}_n(\Delta\hat{\theta}_n^i), \tag{6}$$

where $\hat{D}^i$ is the dual quaternion for $[D_{0i}]$ and $\hat{S}_j$ is the dual quaternion for $[T(\Delta\theta_j, \mathsf{S}_j)]$.

This approach yields the kinematics equations as successive screw transformations from the reference position. It is a useful formulation from the synthesis point of view because the components of each axis appear explicitly in the base frame coordinates.

4 Constrained Parallel Robot Synthesis

The dual quaternion methodology for the synthesis of constrained serial chains yields multiple solutions. These solutions can be combined to form a parallel robot. It is also possible to design a different seral chain for the same set of goal positions and add this to the parallel robot. The operation of assembling the end-effectors of several serial chains ensures that the parallel robot will reach each of the goal positions of the supporting serial chains.

It is useful to note that the constraints on the workpiece of the combined system may not allow smooth movement through all of the goal positions. This is a performance issue that requires additional analysis. Other performance concerns are to accommodate joint limits as well as the potential for interference between links. Other performance factors can be included in the design process, such as dexterity, mechanical advantage, forces at the joints, the effect of tolerances, and positioning errors.

In this paper, we focus on the geometric problem of ensuring that the constraints imposed by each supporting chain are satisfied at each of the desired goal positions of the workpiece.

4.1 Design Equations for Supporting Serial Chains

Let $[T(\theta_1, \ldots, \theta_k)]$ be the kinematics equations of a serial robot, and let a discrete approximation of the desired workspace be given in the form of n goal transformations $[D_i], i = 0, \ldots, n-1$. The synthesis problem consists of solving the n matrix equations

$$[T(\theta_{1,i}, \ldots, \theta_{k,i})] = [D_i], \quad \imath = 0, \ldots, n-1. \tag{7}$$

We now transform these equations to successive screw displacements in dual quaternion form. Equating the $n-1$ goal positions $\hat{D}^i, i = 1, \ldots, n-1$ to the kinematics equations $\hat{Q}(\hat{\theta}_1, \ldots, \hat{\theta}_k)$, we obtain the $n-1$ equations

$$\hat{Q}_i(\hat{\theta}_1^i, \ldots, \hat{\theta}_k^i) = \hat{D}^i, \quad i = 1, \ldots, n-1 \tag{8}$$

For each of the $n-1$ positions we define eight component equations. However, due to the structure of the dual quaternions, only six of them are independent. For a unit dual quaternion, the 2-norm of the first vector is equal to one and the dot product of the first times the second vectors is equal to zero.

Assume for the moment that the robot chain can be represented by an equivalent series of j revolute joints. Each of these joints has an axis which is defined by six Plucker coordinates, which yields $6j$ unknowns. The j joint variables take different values at each of the $n-1$ positions, which add $j(n-1)$ unknowns. This yields $6j + j(n-1)$ unknowns.

Two constraint equations are associated with Plucker coordinates arise for each joint axis. For each of the $n-1$ goal positions we obtain eight equations, which can be reduced to six. Thus, we have $2j + 6(n-1)$ equations.

Equating the number of unknowns to the number equations, we obtain

$$6j + j(n-1) = 6(n-1) + 2j. \tag{9}$$

Solving for n

$$n = \frac{3j+6}{6-j}, \tag{10}$$

we have that $2R$, $3R$, $4R$ and $5R$ spatial chains require 3, 5, 9, 21 positions, respectively. However, we need to consider some limitations. In eq. (9) we equate dual quaternions component by component. As the rotations operate independently in spatial displacements, the number of spherical positions we can reach will be limited by this fact, while the number of spatial translations is computed in general. Hence, to compute complete spatial positions, first we need to check how these are limited by the maximum number of spherical positions we can reach. To separate rotations from translations, assume our robot consists of l rotational joints and k translational joints. We therefore need two equations; the first one equating rotational joint directions with rotation components of the dual quaternion,

$$3l + l(n_R - 1) = 3(n_R - 1) + l \tag{11}$$

and the second equating both rotational and translational joints to the whole quaternion,

$$6(l+k) + (l+k)(n-1) = 6(n-1) + 2l + k. \tag{12}$$

From the rotation equation,

$$n_R = \frac{3+l}{3-l}. \tag{13}$$

Notice that this coincides with the results for spherical robots: for one revolute joint we obtain finite number of solutions for two positions, this means we can reach one relative rotation. For two revolute joints we have finite number of solutions for $n_R = 5$, while for three we get infinity, which means that we can reach any orientation. The formula stops making sense after this. The maximum number of complete positions we can reach will be restricted by n_R, and if in the second formula we obtain more than that, the rest will be just translational components of dual quaternions in which rotations will have to be bounded to the given workspace.

Notice also that here we assume that the axes of the rotational and translational joints are not related, but it is easy to adapt the formula to particular cases in which the joints are constrained.

4.2 Solving the Design Equations

The design equations for constrained robots contain joint variables and the kinematic parameters defining the joint axes. Our goal is to eliminate the joint variables, if possible, and solve for the parameters of the axes, which define the physical dimensions of the robot.

In order to eliminate the joint parameters, we consider the equations for each position independently. We call this process "implicitization" of the parametric equations, see Cox (1998). The first step in this implicitization process uses the semi-direct product structure of the group of spatial displacements captured by the algebra of dual quaternions, which separates the composition of rotations in the real part from a combination of translations and rotations in the dual part. In the dual quaternion product the first four components are never mixed with the last four in any computation.

The four rotational components of the dual quaternion equation are parameterized only by the revolute joint variables,

$$\hat{Q}_{rot}(\theta_1, \ldots, \theta_k) = \begin{Bmatrix} q_x(\theta_1, \ldots, \theta_k) \\ q_y(\theta_1, \ldots, \theta_k) \\ q_z(\theta_1, \ldots, \theta_k) \\ q_w(\theta_1, \ldots, \theta_k) \end{Bmatrix} = \begin{Bmatrix} p_x \\ p_y \\ p_z \\ p_w \end{Bmatrix} \tag{14}$$

This can always be transformed to a linear system that allows to solve for two of the revolute joint variables as a function of the joint axes and the rest of revolute variables,

$$[R(\theta_3,\ldots,\theta_k)]\begin{Bmatrix}\cos\frac{\theta_1}{2}\sin\frac{\theta_2}{2}\\ \sin\frac{\theta_1}{2}\cos\frac{\theta_2}{2}\\ \sin\frac{\theta_1}{2}\sin\frac{\theta_2}{2}\\ \cos\frac{\theta_1}{2}\cos\frac{\theta_2}{2}\end{Bmatrix}=\begin{Bmatrix}p_x\\ p_y\\ p_z\\ p_w\end{Bmatrix} \tag{15}$$

where the matrix $[R(\theta_3,\ldots,\theta_k)]$ is invertible for non-degenerated cases. Degenerated cases are those in which the axes of the variables we are solving for are parallel, for instance solutions in which the serial chain is not spatial but planar. We can assume the matrix is compatible when the axes are a solution for the design problem. Also notice that the matrix in Eq. (15) is orthogonal for the cases in which the axes of the variables that we are solving for are perpendicular.

This allows us to eliminate linearly two of the rotational parameters in the form of a vector of sine and cosines. We can then substitute these expressions in the second four components of the dual quaternion,

$$\hat{Q}_{trans}(\theta_3,\ldots,\theta_k,d_1,\ldots,d_l)=$$
$$=\begin{Bmatrix}q_x^0(\theta_3,\ldots,\theta_k,d_1,\ldots,d_l)\\ q_y^0(\theta_3,\ldots,\theta_k,d_1,\ldots,d_l)\\ q_z^0(\theta_3,\ldots,\theta_k,d_1,\ldots,d_l)\\ q_w^0(\theta_3,\ldots,\theta_k,d_1,\ldots,d_l)\end{Bmatrix}=\begin{Bmatrix}p_x^0\\ p_y^0\\ p_z^0\\ p_w^0\end{Bmatrix}. \tag{16}$$

As a general rule, we can eliminate the last equation in Eq.(16), as we can see that in equating a robot $\hat{Q}$ to a goal dual quaternion $\hat{P}$, the equation $q_w^0=p_w^0$ does not add anything to the set of solutions,

$$\begin{aligned}&(q_x^0-p_x^0)p_x+(q_y^0-p_y^0)p_y+(q_z^0-p_z^0)p_z+(q_w^0-p_w^0)p_w-\\&(p_x-q_x)q_x^0-(p_y-q_y)q_y^0-(p_z-q_z)q_z^0-\\&(p_w-q_w)q_w^0+(q_x^0q_x+q_y^0q_y+q_z^0q_z+q_w^0q_w)=0.\end{aligned} \tag{17}$$

To this set of equations we need to add any condition on the additional joint variables that is implicit in the solution for the rotations. The subsequent joint variables can be eliminated sequentially in a similar fashion, but the procedure is different from case to case. The parameters corresponding to revolute joints appear as quadratic sine and cosine functions, while the parameters corresponding to prismatic joints appear linearly.

To the final set of equations free of joint variables we need to add the Plucker conditions for each joint axis $\mathsf{S}_i=\mathbf{s}_i+\epsilon\mathbf{s}_i^0$; in fact, these equations are the ones that allow us to disregard two equations for each dual quaternion equality.

$$\begin{aligned}\mathbf{s}_i\cdot\mathbf{s}_i&=1,\quad i=1,\ldots,k+l\\ \mathbf{s}_i\cdot\mathbf{s}_i^0&=0,\quad i=1,\ldots,k\end{aligned} \tag{18}$$

In the example below the process is illustrated for a TPR chain.

5 Design of the 2-TPR Constrained Parallel Robot

The 2-TPR robot consists of an end-effector supported by two TPR serial chains. Each supporting TPR serial chain imposes two constraints on the end-effector, which means that the resulting system has two degrees of freedom.

The TPR serial chain is a four-degree of freedom robot. The base joint T consists of two revolute joints about perpendicular axes. This joint is also called U-joint for universal joint. The fixed axis G_1 allows rotation of angle θ_1 about it. Located at 90° and intersecting G_1 is the second revolute axis, G_2, which allows rotation of angle θ_2. This is followed by a translation d along an arbitrary direction H and finally a rotation of angle ϕ about an arbitrary axis W, see Figure 1.

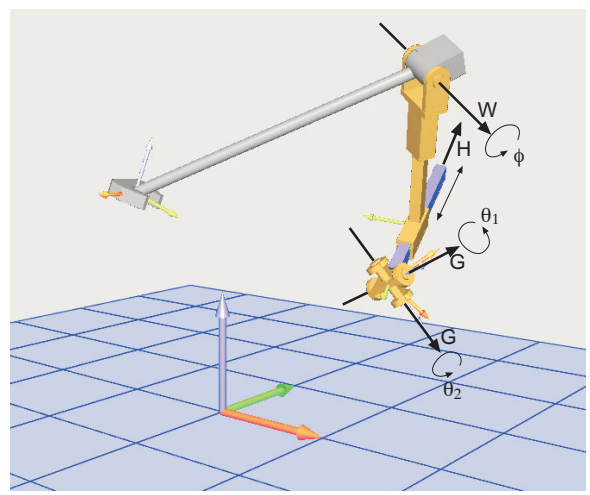

Figure 1: The spatial TPR robot

We call **c** to the intersection point of the two rotation axes G_1 and G_2. Notice that the location of the prismatic joint is immaterial and has been assigned in the drawing to the same intersection point.

The dual quaternion representation for the relative displacements of the chain is given by

$$\hat{Q}_{TPR}=\hat{G}_1(\theta_1,0)\hat{G}_2(\theta_2,0)\hat{H}(0,d)\hat{W}(\phi,0), \tag{19}$$

When applying the dual quaternion product we obtain the expression $\hat{Q}_{TPR}=Q^0+\mathsf{Q}$, where the point is

$$\begin{aligned}Q^0=&\,c\frac{\theta_1}{2}c\frac{\theta_2}{2}c\frac{\phi}{2}-s\frac{\theta_1}{2}c\frac{\theta_2}{2}s\frac{\phi}{2}\mathsf{G}_1\cdot\mathsf{W}\\&-c\frac{\theta_1}{2}s\frac{\theta_2}{2}s\frac{\phi}{2}\mathsf{G}_2\cdot\mathsf{W}-s\frac{\theta_1}{2}s\frac{\theta_2}{2}s\frac{\phi}{2}(\mathsf{G}_1\times\mathsf{G}_2)\cdot\mathsf{W}\\&-\epsilon\frac{d}{2}\Big(s\frac{\theta_1}{2}c\frac{\theta_2}{2}c\frac{\phi}{2}\mathsf{G}_1\cdot\mathsf{H}+c\frac{\theta_1}{2}s\frac{\theta_2}{2}c\frac{\phi}{2}\mathsf{G}_2\cdot\mathsf{H}\\&+c\frac{\theta_1}{2}c\frac{\theta_2}{2}s\frac{\phi}{2}\mathsf{H}\cdot\mathsf{W}+s\frac{\theta_1}{2}s\frac{\theta_2}{2}c\frac{\phi}{2}(\mathsf{G}_1\times\mathsf{G}_2)\cdot\mathsf{H}\\&+s\frac{\theta_1}{2}c\frac{\theta_2}{2}s\frac{\phi}{2}(\mathsf{G}_1\times\mathsf{H})\cdot\mathsf{W}+c\frac{\theta_1}{2}s\frac{\theta_2}{2}s\frac{\phi}{2}(\mathsf{G}_2\times\mathsf{H})\cdot\mathsf{W}\\&+s\frac{\theta_1}{2}s\frac{\theta_2}{2}s\frac{\phi}{2}((\mathsf{G}_1\times\mathsf{G}_2)\times\mathsf{H})\cdot\mathsf{W}\Big),\end{aligned} \tag{20}$$

and the dual vector,

$$
\begin{aligned}
\mathsf{Q} &= s\frac{\theta_1}{2}c\frac{\theta_2}{2}c\frac{\phi}{2}\mathsf{G}_1 + c\frac{\theta_1}{2}s\frac{\theta_2}{2}c\frac{\phi}{2}\mathsf{G}_2 \\
&+ c\frac{\theta_1}{2}c\frac{\theta_2}{2}s\frac{\phi}{2}\mathsf{W} + s\frac{\theta_1}{2}s\frac{\theta_2}{2}c\frac{\phi}{2}\mathsf{G}_1 \times \mathsf{G}_2 \\
&+ s\frac{\theta_1}{2}c\frac{\theta_2}{2}s\frac{\phi}{2}\mathsf{G}_1 \times \mathsf{W} + c\frac{\theta_1}{2}s\frac{\theta_2}{2}s\frac{\phi}{2}\mathsf{G}_2 \times \mathsf{W} \\
&+ s\frac{\theta_1}{2}s\frac{\theta_2}{2}s\frac{\phi}{2}(\mathsf{G}_1 \times \mathsf{G}_2) \times \mathsf{W} \\
&+ \epsilon\frac{d}{2}\Big(c\frac{\theta_1}{2}c\frac{\theta_2}{2}c\frac{\phi}{2}\mathsf{H} \\
&+ s\frac{\theta_1}{2}c\frac{\theta_2}{2}s\frac{\phi}{2}((\mathsf{G}_1 \times \mathsf{H}) \times \mathsf{W} - (\mathsf{G}_1 \cdot \mathsf{H})\mathsf{W}) \\
&+ c\frac{\theta_1}{2}s\frac{\theta_2}{2}s\frac{\phi}{2}((\mathsf{G}_2 \times \mathsf{H}) \times \mathsf{W} - (\mathsf{G}_2 \cdot \mathsf{H})\mathsf{W}) \\
&+ s\frac{\theta_1}{2}c\frac{\theta_2}{2}c\frac{\phi}{2}\mathsf{G}_1 \times \mathsf{H} + c\frac{\theta_1}{2}s\frac{\theta_2}{2}c\frac{\phi}{2}\mathsf{G}_2 \times \mathsf{H} \\
&+ s\frac{\theta_1}{2}s\frac{\theta_2}{2}c\frac{\phi}{2}(\mathsf{G}_1 \times \mathsf{G}_2) \times \mathsf{H} + c\frac{\theta_1}{2}c\frac{\theta_2}{2}s\frac{\phi}{2}\mathsf{H} \times \mathsf{W} \\
&+ s\frac{\theta_1}{2}s\frac{\theta_2}{2}s\frac{\phi}{2}(((\mathsf{G}_1 \times \mathsf{G}_2) \times \mathsf{H}) \times \mathsf{W} - ((\mathsf{G}_1 \times \mathsf{G}_2) \cdot \mathsf{H})\mathsf{W})\Big).
\end{aligned} \tag{21}
$$

The expansion of this equations componentwise leads to a set of equations in the components of the axes. The T-joint axis is formulated so that the coordinates of the intersection point $\mathbf{c}$ appear explicitly, as the point is also a design parameter,

$$
\begin{aligned}
\mathsf{G1} &= (g_{1x}, g_{1y}, g_{1z}) + \epsilon((c_x, c_y, c_z) \times (g_{1x}, g_{1y}, g_{1z})) \\
\mathsf{G2} &= (g_{2x}, g_{2y}, g_{2z}) + \epsilon((c_x, c_y, c_z) \times (g_{2x}, g_{2y}, g_{2z})).
\end{aligned} \tag{22}
$$

The moving prismatic axis has direction $\mathbf{h} = (h_x, h_y, h_z)$ and arbitrary location that will not appear in the design equations. The moving rotation axis is expressed in Plucker coordinates, $\mathsf{W} = (w_x, w_y, w_z) + \epsilon(w_x^0, w_y^0, w_z^0)$.

The number of positions needed to obtain finite number of solutions is calculated as explained in the previous section. As we have three rotational joints, the robot will be able to reach any orientation and the orientation does not limit the number of complete positions to reach. We have $18 + 4(n-1)$ unknowns, corresponding to the direction $\mathbf{G}_1$, the point $\mathbf{c}$, the direction $\mathbf{G}_2$, the direction $\mathbf{h}$ and the line W, plus the joint variables for the $n-1$ relative transformations. We have $6 + 6(n-1)$ equations, corresponding to the unit vector conditions for all directions, the perpendicularity condition between $\mathbf{G}_1$ and $\mathbf{G}_2$ and the moment condition for W, plus the six independent equations per goal dual quaternion . Therefore we need to define $n = 7$ positions.

5.1 The Design Equations

To create the design equations we equate the expanded eqs.(20, 21) to the goal dual quaternion $\hat{P}$, that is,

$$\hat{Q}_{TPR}(\theta_1^i, \theta_2^i, d^i, \phi^i) - \hat{P}^i = \vec{0}, \tag{23}$$

to obtain one of the sets of design equations. After equating for all the relative dual quaternion transformations, we obtain six sets of dual quaternion equations. However, to eliminate the joint parameters we work with only a generic set and apply the results to each relative position.

To eliminate the joint parameters we consider the separation between rotations and translations. It is easy to solve for two of the rotational joint parameters as shown in Eq.(15). Every direction will be reached by moving the rotation axes accordingly to the third rotation parameter as appears in the solution of the linear system,

$$[R(\phi)] \begin{Bmatrix} \cos\frac{\theta_1}{2}\sin\frac{\theta_2}{2} \\ \sin\frac{\theta_1}{2}\cos\frac{\theta_2}{2} \\ \sin\frac{\theta_1}{2}\sin\frac{\theta_2}{2} \\ \cos\frac{\theta_1}{2}\cos\frac{\theta_2}{2} \end{Bmatrix} = \begin{Bmatrix} p_x \\ p_y \\ p_z \\ p_w \end{Bmatrix}, \tag{24}$$

with

$$[R(\phi)] = \begin{bmatrix} \mathbf{v}_1 & \mathbf{v}_2 & \mathbf{v}_3 & \mathbf{v}_4 \\ s_1 & s_2 & s_3 & s_4 \end{bmatrix}. \tag{25}$$

The column vectors in $[R(\phi)]$ are

$$
\begin{aligned}
\mathbf{v}_1 &= \cos\frac{\phi}{2}\mathbf{g}_2 + \sin\frac{\phi}{2}\mathbf{g}_2 \times \mathbf{w} \\
\mathbf{v}_2 &= \cos\frac{\phi}{2}\mathbf{g}_1 + \sin\frac{\phi}{2}\mathbf{g}_1 \times \mathbf{w} \\
\mathbf{v}_3 &= \cos\frac{\phi}{2}\mathbf{g}_1 \times \mathbf{g}_2 + \sin\frac{\phi}{2}((\mathbf{g}_1 \times \mathbf{g}_2) \times \mathbf{w} - (\mathbf{g}_1 \cdot \mathbf{g}_2)\mathbf{w}) \\
\mathbf{v}_4 &= \sin\frac{\phi}{2}\mathbf{w}
\end{aligned} \tag{26}
$$

and the last row is composed of the scalars

$$
\begin{aligned}
s_1 &= -\sin\frac{\phi}{2}\mathbf{g}_2 \cdot \mathbf{w} \\
s_2 &= -\sin\frac{\phi}{2}\mathbf{g}_1 \cdot \mathbf{w} \\
s_3 &= -\cos\frac{\phi}{2}\mathbf{g}_1 \cdot \mathbf{g}_2 - \sin\frac{\phi}{2}(\mathbf{g}_1 \times \mathbf{g}_2) \cdot \mathbf{w} \\
s_4 &= \cos\frac{\phi}{2}.
\end{aligned} \tag{27}
$$

The matrix $[R(\phi)]$ is an orthogonal matrix when solving for the joint variables θ_1, θ_2 corresponding to the T-joint. The solution for the angles is

$$\begin{Bmatrix} \cos\frac{\theta_1}{2}\sin\frac{\theta_2}{2} \\ \sin\frac{\theta_1}{2}\cos\frac{\theta_2}{2} \\ \sin\frac{\theta_1}{2}\sin\frac{\theta_2}{2} \\ \cos\frac{\theta_1}{2}\cos\frac{\theta_2}{2} \end{Bmatrix} = [R(\phi)]^T \begin{Bmatrix} p_x \\ p_y \\ p_z \\ p_w \end{Bmatrix} \tag{28}$$

The solution always exists for directions $\mathbf{g}_1, \mathbf{g}_2$ and $\mathbf{w}$ and angles ϕ such that the system is solvable, which we can assume will be given by the solution of the design equations. In this case there is not planar degeneracy if we consider the constraint for

$\mathbf{g}_1$ and $\mathbf{g}_2$ to be at right angles. The angle ϕ is constrained by the relation among the four variables we are solving for,

$$\cos\frac{\theta_1}{2}\sin\frac{\theta_2}{2}\cdot\sin\frac{\theta_1}{2}\cos\frac{\theta_2}{2}=\cos\frac{\theta_1}{2}\cos\frac{\theta_2}{2}\cdot\sin\frac{\theta_1}{2}\sin\frac{\theta_2}{2}, \quad (29)$$

obtaining the condition for ϕ,

$$A_0\cos^2\frac{\phi}{2}+B_0\sin^2\frac{\phi}{2}+C_0\cos\frac{\phi}{2}\sin\frac{\phi}{2}=0. \quad (30)$$

The solutions for the θ_1, θ_2 angles are substituted in the three first moment equations of the dual quaternion. We obtain three equations which are linear in the prismatic joint variable d and quadratic in the revolute joint variable ϕ, and that we denote by

$$\begin{aligned}&(A_{1i}d+A_{0i})\cos^2\frac{\phi}{2}+(B_{1i}d+B_{0i})\sin^2\frac{\phi}{2}+\\&(C_{1i}d+C_{0i})\cos\frac{\phi}{2}\sin\frac{\phi}{2}+D_{0i}=0, \quad i=1,\dots,3\end{aligned} \quad (31)$$

To eliminate ϕ, we add the previously obtained angle condition, eq. (30), to create the homogeneous system

$$\begin{bmatrix} A_{11}d+A_{01} & B_{11}d+B_{01} & C_{11}d+C_{01} & D_{01}\\ \vdots & \vdots & \vdots & \vdots\\ A_{13}d+A_{03} & B_{13}d+B_{03} & C_{13}d+C_{03} & D_{03}\\ A_0 & B_0 & C_0 & 0\end{bmatrix}\begin{Bmatrix}\cos^2\frac{\phi}{2}\\ \sin^2\frac{\phi}{2}\\ \cos\frac{\phi}{2}\sin\frac{\phi}{2}\\ 1\end{Bmatrix}=\vec{0} \quad (32)$$

For the system to have solutions, the determinant must be equal to zero. The determinant is a quadratic equation in the prismatic joint variable d.

We can obtain the subspace of solutions from the matrix corresponding to the first three rows. By solving linearly in this system for the variables $\cos^2\frac{\phi}{2}$, $\sin^2\frac{\phi}{2}$ and $\cos\frac{\phi}{2}\sin\frac{\phi}{2}$, we obtain expressions as a function of the prismatic joint variable d. The relations between these three solutions,

$$\begin{aligned}&\cos^2\frac{\phi}{2}+\sin^2\frac{\phi}{2}=1\\&(\cos^2\frac{\phi}{2})(\sin^2\frac{\phi}{2})=(\cos\frac{\phi}{2}\sin\frac{\phi}{2})^2\end{aligned} \quad (33)$$

lead to two more equations in d, the first one being a cubic and the second one a quartic in d. We obtain the system of three equations

$$K_{4i}d^4+K_{3i}d^3+K_{2i}d^2+K_{1i}d+K_{0i}=0, \quad i=1,\dots,3. \quad (34)$$

Out of the system of three equations in d,

$$\begin{bmatrix} 0 & 0 & K_{21} & K_{11} & K_{01}\\ 0 & K_{32} & K_{22} & K_{12} & K_{02}\\ K_{43} & K_{33} & K_{23} & K_{13} & K_{03}\end{bmatrix}\begin{Bmatrix}d^4\\ d^3\\ d^2\\ d\\ 1\end{Bmatrix}=\begin{Bmatrix}0\\0\\0\\0\\0\end{Bmatrix} \quad (35)$$

we can eliminate the parameter d, for instance by direct substitution of the solution of d from the quadratic equation in the other two. We obtain two design equations per goal dual quaternion, which are free of joint variables and depend only on the coordinates of the joint axes. These 12 equations together with 6 constraints,

$$\begin{aligned}&g_{1x}^2+g_{1y}^2+g_{1z}^2=1,\\&g_{2x}^2+g_{2y}^2+g_{2z}^2=1, \quad g_{1x}g_{2x}+g_{1y}g_{2y}+g_{1z}g_{2z}=0\\&w_x^2+w_y^2+w_z^2=1, \quad w_xw_x^0+w_yw_y^0+w_zw_z^0=0\\&h_x^2+h_y^2+h_z^2=1\end{aligned} \quad (36)$$

allows us to solve for the 18 unknowns corresponding to the four joint axes.

5.2 Assemble the 2-TPR Constrained Robot

From the design equations for the TPR serial chain, we will obtain a certain number of solutions. The exact number of complex solutions can be known if we are able to reduce the polynomial system of design equations to a triangular system with one polynomial being univariate. In the case of the serial TPR chain, the only possibility of creating a parallel robot is to form a 2-TPR robot by joining the end-link of two of the solutions. The 2-TPR robot has two degrees of freedom, and notice that the 3-TPR platform is a structure. The 2-TPR robot will reach the set of seven positions, but nothing ensures that the movement of the robot will be smooth or even possible. The simplest strategy to choose a good design is to create all possible combinations of two solutions and to analyze their movement through the goal positions.

6 Numerical Example

We present an example for the design of the 2-TPR parallel robot. To pick up to seven positions in space, we can either generate them individually or perform dual quaternion interpolation between an initial position, an intermediate position and a final position McCarthy and Ahlers (1999). Each TPR serial robot will exactly hit the seven positions in the trajectory. Another option is to set some of the parameters of the TPR chain to desired values and solve for a smaller number of positions.

In our example we solve for the seven positions for the first TPR serial chain, and for the second chain we set both the directions of the rotations of the T-joint $\mathbf{g}_1$ and $\mathbf{g}_2$ to a specified value, which is equivalent to fix the plane of the rotation, and we also impose the condition that the moving revolute joint axis W must be perpendicular to the prismatic joint direction $\mathbf{h}$. Using the

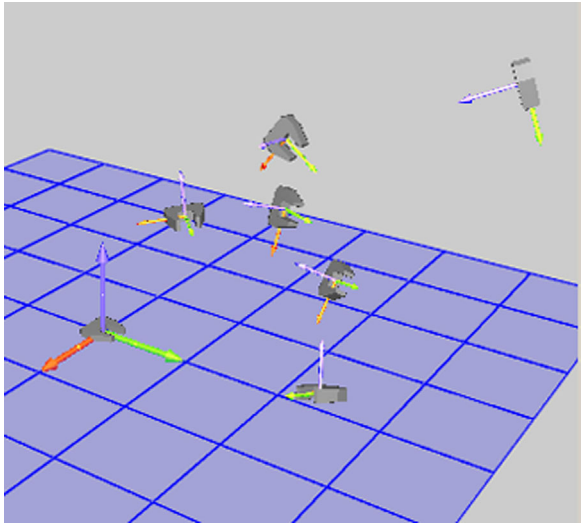

Figure 2: The seven initial positions

Table 1: THE GOAL POSITIONS

Pos.	*Axis*	*Rot.*	*Trans.*
1	$(1.0, 0.0, 0.0), (0.0, 0.0, 0.0)$	0°	0
2	$(0.5, 0.8, -0.4), (-1.8, 0.8, -0.7)$	68.9^o	0.32
3	$(-0.2, 0.9, -0.3), (-1.7, -0.3, 0.2)$	92.7^o	0.71
4	$(0.0, 0.8, -0.5), (-2.2, 0.0, 0.2)$	156.5^o	1.39
5	$(0.3, 0.9, -0.3), (-1.6, 0.5, -0.1)$	79.0^o	0.31

counting formula, we see that we can solve for a finite number of solutions for $n = 5$ positions.

On Table 1 and Figure 2 we define and show the specified positions.

We solve numerically the design equations using a Newton-Raphson type of solver. The design equations are very sensitive to the initial conditions, and in this particular case we could not find any good solution for the second chain, and the numerical solver led to a local minimum that hits four of the five positions. In Table(2, 3) we can see the obtained solutions. Figure 3 shows the parallel 2-TPR robot while reaching positions $1, 2$ and 5.

7 Conclusions

This paper introduces a new formulation for the kinematic synthesis of constrained parallel robots. While arbitrary serial chains can have up to six degrees of freedom, our focus is on chains with five or less degrees of freedom. These serial chains impose constraints on the workpiece of the parallel robot. These constraints can be used to provide structural support and enhance mechanical advantage.

The dual quaternion form of the kinematics equations of the supporting serial chain are evaluated at a set of goal positions to form design equations. These equations include both axis parameters that define the robot and joint parameters that define its configuration in a goal position. The structure of these equations provide a convenient strategy for the elimination of the joint parameters, which we demonstrate for the TPR serial chain. The parallel 2-TPR constrained robot is constructed by joining the end-links of two TPR solutions.

Table 2: THE JOINT AXES FOR FIRST TPR CHAIN

Joint Axis	*Direction*	*Moment*
G_1	$(0.52, 0.34, -0.78)$	$(-1.39, 1.06, -0.47)$
G_2	$(-0.41, 0.90, 0.11)$	$(-0.72, -0.48, 1.20)$
H	$(0.81, 0.46, 0.35)$	$(0.02, 0.54, -0.77)$
W	$(0.48, 0.86, -0.19)$	$(-1.83, 0.69, -1.49)$

Table 3: THE JOINT AXES FOR SECOND TPR CHAIN

Joint Axis	*Direction*	*Moment*
G_1	$(1.0, 0.0, 0.0)$	$(0.0, 0.98, -2.15)$
G_2	$(0.0, 1.0, 0.0)$	$(-0.98, 0.0, 1.0)$
H	$(-0.68, -0.33, 0.66)$	$(1.74, -1.33, 1.12)$
W	$(0.49, -0.87, 0.08)$	$(1.29, 0.58, -1.75)$

Our goal is to expand this approach to a systematic design procedure for a wide range of constrained parallel robotic systems. So far, we have results for the RR, RP, RPR, RRR, CC, and TS serial chains. In addition, we look forward to formulating the design equations for the TPT serial chain. The main challenge is the increasing complexity of the joint parameters in the design equations. We also look forward to incorporating performance measures such as speed ratios and mechanical advantage in order to rate resulting designs.

8 Acknowledgements

The authors gratefully acknowledge the support of the National Science Foundation and discussions with Dr Curtis Collins, Haijun Su and Dr Bruce Bennett.

References

Angeles, J., 1998, "The application on dual algebra to kinematic analysis," *Computational Methods in Mechanical Systems, NATO ASI Series* (ed. J. Angeles and E. Zakhariev) Springer, Berlin.

Bottema, O., and Roth, B., 1979, *Theoretical Kinematics,* North-Holland. (reprinted by Dover Publications, 1990).

Chen, P., and Roth, B., 1969, Design Equations for the Finitely and Infinitesimally Separated Position Synthesis of Binary Links and Combined Link Chains, *ASME J. Eng. Ind.* 91(1):209219.

Chedmail, P., 1998, "Optimization of multi-dof mechanisms," *Computational Methods in Mechanical Systems, NATO ASI Series* (ed. J. Angeles and E. Zakhariev) Springer, Berlin.

Cox, D., Little, J. and O'Shea, D., 1998, *Using Algebraic Geometry*, Springer, New York.

Craig, J., 1986, *Introduction to Robotics*, Addison-Wesley.

Gosselin, C. M., 1998, "On the design of efficient parallel mechanisms," *Computational Methods in Mechanical Systems, NATO ASI Series* (ed. J. Angeles and E. Zakhariev) Springer, Berlin.

Gupta, K.C., 1986, "Kinematic Analysis of Manipulators Using Zero Reference Position Description", *Int. J. Robot. Res.*, 5(2):5-13

Hunt, K.H., 1978, *Kinematic Geometry of Mechanisms*. Clarendon Press.

Huang, C., and Chang, Y.-J., 2000, Polynomial Solution to the Five-Position Synthesis of Spatial CC Dyads via Dialytic Elimination, *Proceedings of the ASME Design Technical Conferences*, September 1013, 2000, Baltimore MD, Paper Number DETC2000/MECH-14102.

Innocenti, C., 1994, "Polynomial Solution of the Spatial Burmester Problem." *Mechanism Synthesis and Analysis, ASME DE* vol. 70.

Larochelle, P., 2000, "Approximate motion synthesis via parametric constraint manifold fitting," *Advances in Robot Kinematics* (eds. J. Lenarcic and M. M. Stanisic) Kluwer Acad. Publ., Dordrecht.

Lee, E., and Mavroidis, D., 2002 (in press), "Solving the Geometric Design Problem of Spatial 3R Robot Manipulators Using Polynomial Homotopy Continuation," *ASME J. of Mechanical Design*.

Liao, Q. and McCarthy, J.M., 1998, "On the seven position synthesis of a 5-SS platform linkage", *ASME Journal of Mechanical Design*.

Mavroidis, C., Lee, E. and Alan, M. 2001, "A New Polynomial Solution to the Geometric Design Problem of Spatial R-R Robot Manipulators Using the Denavit and Hartenberg Parameters," *ASME J. of Mechanical Design* 123(2):58-67.

McCarthy, J.M., 1990, *Introduction to Theoretical Kinematics*. The MIT Press.

McCarthy, J.M., 2000, *Geometric Design of Linkages*. Springer-Verlag.

McCarthy, J. M., 2000, Mechanisms Synthesis Theory and the Design of Robots, *Proceedings of the 2000 IEEE International Conference on Robotics and Automation*, April 2428 2000, San Francisco, CA.

McCarthy, J.M. and Ahlers, S., 1999, "The dimensional synthesis of an spatial RR robot to provide a specified end-effector trajectory", *9th International Symposium of Robotics Research*, Snowbird, Utah, 1999.

Merlet, J.P., 1997, "Designing a parallel manipulator for a specific workspace", *Int. J. of Robotics Research*, 16(4):545-556.

Murray, A., and Hanchak, M. 2000, "Kinematic Synthesis of Planar Platforms with RPR, PRR and RRR Chains", *Advances in Robot Kinematics* (eds. J. Lenarcic and M. M. Stanisic) Kluwer Acad. Publ., Dordrecht.

Perez, A., and McCarthy, J. M., 2000, Dimensional Synthesis of Spatial RR Robots, Advances in Robot Kinematics, Lenarcic, J., ed., Piran-Portoroz, Slovenia, June 2630, 2000.

Suh, C.H. and Radcliffe, C.W., 1978, *Kinematics and mechanisms design*. John Wiley & Sons.

Tsai, L.W. and Roth, B., 1973, "A Note on the Design of Revolute-Revolute Cranks". *Mechanisms and Machine Theory*, 1973, Vol.8, pp 23-31.

Tsai, L.W., 1999, *Robot Analysis*. John Wiley and Sons, New York.

Yang, A.T., and Freudenstein, F., 1964, "Application of Dual-Number Quaternion Algebra to the Analysis of Spatial Mechanisms", *ASME Journal of Applied Mechanics*, June 1964, pp.300-308.

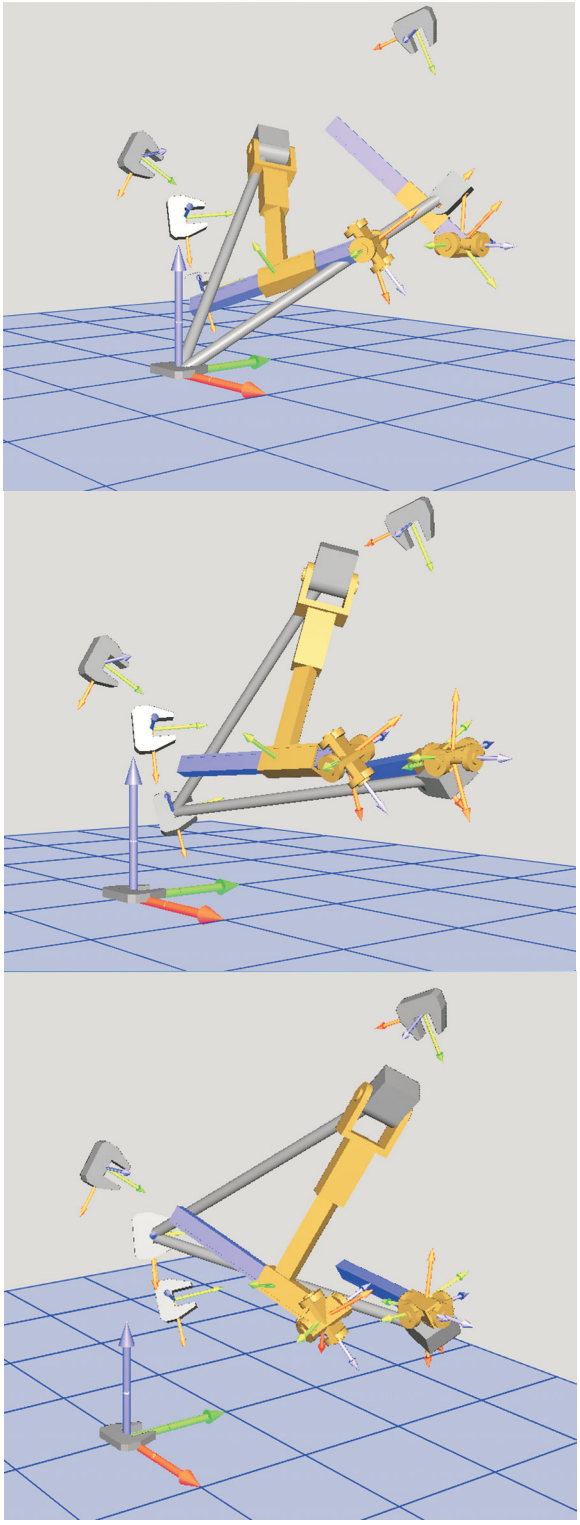

Figure 3: The 2-TPR robot reaching positions 1, 2 and 5

Keynote Address III

Friday, October 4, 2002, 8:30AM

Jorge Angeles

McGill University, Montreal, Canada

"The Qualitative Synthesis of Parallel Manipulators"

Proceedings of the WORKSHOP on
Fundamental Issues and Future Research Directions for Parallel Mechanisms and Manipulators
October 3–4, 2002, Quebec City, Quebec, Canada
Clément M. Gosselin and Imme Ebert-Uphoff, editors

The Qualitative Synthesis of Parallel Manipulators

JORGE ANGELES
Department of Mechanical Engineering
& Centre for Intelligent Machines
McGill University, Montreal
angeles@cim.mcgill.ca

Abstract: *As shown in this paper, when designing parallel manipulators for tasks involving less than six degrees of freedom, the topology can be laid out by resorting to qualitative reasoning. More specifically, the paper focuses on cases whereby the manipulation tasks pertain to displacements with the algebraic structure of a group. Besides the well-known planar and spherical displacements, this is the case of displacements involving: rotation about a given axis and translation in the direction of the same axis (cylindrical subgroup); translation in two and three dimensions (two- and three-dimensional translation subgroups); three independent translations and rotation about an axis of fixed direction, what is known as the* Schönflies subgroup*; and similar to the Schönflies subgroup, but with the rotation and the translation about the axis of rotation replaced by a screw displacement. For completeness, the fundamental concepts of motion representation and groups of displacements, as pertaining to rigid bodies, are first recalled. Finally, the concept of* Π*-joint, introduced elsewhere, is generalized to two and three degrees of freedom, thereby ending up with the* Π^2*- and the* Π^3*-joints, respectively.*

li·ai·son 1: a binding or thickening agent used in cooking
2a) a close bond or connection : INTERRELATIONSHIP
b): an illicit sexual relationship : AFFAIR

Merriam Webster's Collegiate Dictionary, Tenth Edition
(C)1997,
1996 Zane Publishing, Inc.

Qui pourrait ne pas frémir en songeant aux malheurs
que peut causer une seule liaison dangereuse!

Lettre CLXXV. Madame DE VOLANGES
à Madame DE ROSEMONDE (de Laclos, 1782)

1 Introduction

As robot designers realized the immense possibilities offered by parallel manipulators, the variety of designs has not ceased to grow. It would not be exaggerated to say that we are living an era of robot design comparable to the Cambrian period of natural history. Indeed, the number of novel designs either published in conference proceedings and archival journals or disclosed in patent files is too rich to be recorded exhaustively. We thus not aim here at a comprehensive account of all work currently known, but rather a representative sample of this work. The motivation behind the intense work in parallel manipulator design is equally rich, mostly pertaining to applications areas such as: a) machine-tool design, whereby parallel manipulators are termed *Parallel-Kinematics Machines* (PKM); b) robot-assisted surgery; c) surveillance; d) telescope design; and e) motion simulation. In virtually all these areas it has been realized that a full six-degree-of-freedom capability is not necessary; in some tances, all six degrees of freedom are sometimes even undesirable. This is the case, for example, in the assembly of electronic boards, with an essentially planar geometry, whereby any rotation about an axis lying in the plane of the board is to be prevented; else, the assembly will not be successful and the board can be even damaged.

Work on parallel robot design outside six-degree-of-freedom (six-dof) systems can be traced back to Hunt (1983). Later work focused mostly on planar and spherical manipulators (Gosselin and Angeles, 1987; Craver, 1989). An architecture that received special attention involves three legs of the revolute-prismatic-spherical type, producing two rotations and one translation of its moving platform (Lee and Shah, 1987; Lee and Arjuman, 1991; Agrawal, 1991; Pfreundschuh, Kumar and Sugar, 1991).

Of special interest is the design of three- and four-dof manipulators for the production of either pure translations or displacements of the Schönflies type, respectively. The latter consist of three independent translations and one rotation about an axis of fixed direction. A first manipulator of the pure-translation type

was disclosed in (Clavel 1990). Although the foregoing patent file claims a possible rotation about an axis of fixed direction, for the production of Schönflies displacements, this rotation is achieved by means of a motor mounted on top of the moving platform, and hence, the device is not a Schönflies-motion generator, properly speaking. Brogårdh (2001) discloses a parallel array that is capable of three-dof translations and can produce Schönflies motions by the addition of one motor at its end plate, similar to Clavel's. Other instances of three-dof translational manipulators are those proposed in (Hervé and Sparacino, 1992; Arai, Hervé and Tanikawa, 1996). A fully-parallel Schönflies-motion generator was disclosed fairly recently in (Company, Pierrot, Shibukawa and Koji, 2001).

2 Kinematics Background

The concepts, and to a great extent the notation and nomenclature that follow, are taken from (Hervé, 1978).

The kinematics of machines is studied via their underlying *kinematic chains*. A kinematic chain is the result of the coupling of rigid bodies, called *links*. Upon coupling *two* links, a kinematic pair is obtained. When the coupling takes place in such a way that the two links share a common surface, a *lower kinematic pair* results; when the coupling takes place along a common line or a common point of the two links, a *higher kinematic pair* is obtained.

Lower kinematic pairs deserve special attention for various reasons: One is that they model fairly well the mechanical couplings in a variety of machines; one more is that they are known to occur in exactly six types, to be described presently. Higher kinematic pairs occur in the coupling by cam-follower mechanisms and by gears, in which contact occurs along common lines or common points of the coupled bodies.

We shall denote with lower-case boldfaces all vectors; with upper-case boldfaces all matrices. Sets will be denoted with calligraphic fonts, e.g., $\mathcal{A}$, $\mathcal{B}$, etc., while lower kinematic pairs are denoted with *sans-serif* upper cases: R, P, H, C, E, and S denote the six pairs of interest (Denrit and Hartenberg, 1964), which are recalled below:

(i) The *revolute pair* R allows a relative rotation through an angle ϕ about one axis $\mathcal{A}$ passing through a point A of position vector **a** and parallel to the unit vector **e**;

(ii) The *prismatic pair* P allows a relative translation u in the direction of a unit vector **e**;

(iii) The *screw pair* H allows both a relative rotation through an angle ϕ about an axis $\mathcal{A}$ passing through a point A of position vector **a** and parallel to the unit vector **e**, and a relative translation u in the direction of **e**. However, the rotation and the translation are not independent, for they are related by the *pitch* p of the pair: $u = p\phi$;

(iv) The *cylindrical pair* C allows both a relative rotation through an angle ϕ about an axis $\mathcal{A}$ passing through a point A of position vector **a** and parallel to the unit vector **e**, and a relative translation in the direction of **e**, with rotation and translation being independent;

(v) The *planar pair* E allows two independent translations t_u and t_v in the directions of the *distinct* unit vectors **u** and **v**, respectively, and a rotation ϕ about an axis normal to the plane of these two vectors; and

(vi) The *spherical pair* S, allowing one independent rotation about each of three noncoplanar axes concurrent at a point O. The relative motions allowed by S are thus characterized by point O, and are associated with an axis parallel to the unit vector **e** and with the angle of rotation ϕ about this axis, as per Euler's Theorem (Angeles, 1982).

Remark: While the R, H and C pairs are characterized by an axis, the P pair is characterized by a *direction* alone; not by an axis!

3 Groups of Displacements

In the sequel, we shall resort to the algebraic concept of *group*. A group is a set $\mathcal{G}$ of elements related by a *binary operation* $\star$ with four properties:

(a) if a and $b \in \mathcal{G}$, then $a \star b \in \mathcal{G}$;

(b) if a, b, and $c \in \mathcal{G}$, then $a \star (b \star c) = (a \star b) \star c$;

(c) $\mathcal{G}$ contains an element ι called the *identity* of $\mathcal{G}$ under $\star$, such that $a \star \iota = \iota \star a = a$; and

(d) for every $a \in \mathcal{G}$, there exists an element a^{-1}, called the *inverse of* a *under* $\star$ such that $a \star a^{-1} = a^{-1} \star a = \iota$.

If the elements of a set $\mathcal{D}$ are the displacements undergone by a rigid body, then we can define a binary operation $\odot$—read "o-dot"—of displacements as the *composition* of displacements: As the body undergoes first a displacement d_a and then a displacement d_b, taking the body, successively, from pose $\mathcal{B}_0$ to pose $\mathcal{B}_a$, and then to pose $\mathcal{B}_b$, it is intuitively apparent that the composition of the two displacements, $d_a \odot d_b$, is in turn a rigid-body displacement. Hence,

(a) $d_a \odot d_b \in \mathcal{D}$;

(b) given d_a and d_b as introduced above, we define a third displacement d_c carrying $\mathcal{B}$ from pose $\mathcal{B}_b$ to pose $\mathcal{B}_c$. Then, $d_a \odot (d_b \odot d_c) = (d_a \odot d_b) \odot d_c$;

(c) under no motion, any pose $\mathcal{B}$ of a rigid body is preserved, the motion undergone by the body then being represented by a displacement ι that can be defined as the *identity element* of $\mathcal{D}$, such that, for any displacement d, $d \odot \iota = \iota \odot d = d$; and

(d) for any displacement d carrying the body from pose $\mathcal{B}_0$ to pose $\mathcal{B}$, the *inverse displacement* d^{-1} is defined as that bringing back the body from $\mathcal{B}$ to $\mathcal{B}_0$, and hence, $d \odot d^{-1} = d^{-1} \odot d = \iota$.

From the foregoing discussion it is apparent that the set of rigid-body displacements $\mathcal{D}$ has the algebraic structure of a group. Henceforth, we refer to the set of displacements of a rigid body as *group* $\mathcal{D}$. The interest in studying rigid-body displacements as algebraic groups lies in that, on the one hand, $\mathcal{D}$ includes interesting and practical subgroups that find relevant applications in the design of production-automation and prosthetic devices. On the other hand, the same subgroups can be *combined* to produce novel mechanical layouts that would be insurmountably difficult to produce by sheer intuition. The combination of subgroups, in general, can take place via the standard set operations of *union* and *intersection*. As we shall see, however, the set defined as that comprising the elements of two displacement subgroups is not necessarily a subgroup, and hence, one cannot speak of the union of displacement subgroups. On the contrary, the intersection of two displacement subgroups is always a subgroup itself, and hence, the *intersection of displacement subgroups* is a valid group operation.

Rather than the union of groups, what we have is the *product* of groups (Macdonald, 1968). Let $\mathcal{G}_1$ and $\mathcal{G}_2$ be two groups defined over the same binary operation $\star$; if $g_1 \in \mathcal{G}_1$ and $g_2 \in \mathcal{G}_2$, then the product of these two groups, represented by $\mathcal{G}_1 \bullet \mathcal{G}_2$, is the *set* of elements of the form $g_1 \star g_2$, where the order is important, for commutativity is not to be taken for granted in group theory. That is, in general, $\mathcal{G}_1 \bullet \mathcal{G}_2 \neq \mathcal{G}_2 \bullet \mathcal{G}_1$.

The intersection of the two foregoing groups, represented by the usual set-theoretic symbol $\cap$, i.e., $\mathcal{G}_1 \cap \mathcal{G}_2$, is the group of elements g belonging to both $\mathcal{G}_1$ and $\mathcal{G}_2$, and hence, the order is not important. Thus, $\mathcal{G}_1 \cap \mathcal{G}_2 = \mathcal{G}_2 \cap \mathcal{G}_1$.

3.1 Displacement Subgroups

A *subgroup* $\mathcal{G}_s$ of a given group $\mathcal{G}$ is a set with two properties: (a) its elements belong to $\mathcal{G}$, although some elements of $\mathcal{G}$ may not belong to $\mathcal{G}_s$, and (b) $\mathcal{G}_s$ has the algebraic structure of a group. Therefore, a subgroup $\mathcal{D}_s$ of the group of rigid-body displacements $\mathcal{D}$ is itself a group of displacements, but may lack some rigid-body displacements.

The six lower kinematic pairs can be regarded as *generators* of displacement subgroups. We thus have:

(i) The revolute pair R of axis $\mathcal{A}$ generates the subgroup $\mathcal{R}(\mathcal{A})$ of rotations about $\mathcal{A}$. Each element of this group is characterized by the angle ϕ of the corresponding rotation;

(ii) the prismatic pair in the direction $\mathbf{e}$ generates the subgroup $\mathcal{P}(\mathbf{e})$ of translations along $\mathbf{e}$. Each element of $\mathcal{P}(\mathbf{e})$ is characterized by the translation u along $\mathbf{e}$;

(iii) the screw pair of axis $\mathcal{A}$ and pitch p generates the subgroup $\mathcal{H}(\mathcal{A}, p)$ of rotations ϕ about $\mathcal{A}$ and translations u along the direction of the same axis, translations and rotations being related by the pitch p in the form $u = p\phi$, as described when the screw pair was introduced. Each element of $\mathcal{H}(\mathcal{A}, p)$ can thus be characterized either by u or by ϕ;

(iv) the cylindrical pair of axis $\mathcal{A}$ generates the subgroup $\mathcal{C}(\mathcal{A})$ of independent rotations about and translations along $\mathcal{A}$. Each element of $\mathcal{C}(\mathcal{A})$ is thus characterized by both the displacement u and the rotation ϕ;

(v) the planar pair generates the subgroup $\mathcal{F}(\mathbf{u}, \mathbf{v})$ of two independent translations in the directions of the *distinct* unit vectors $\mathbf{u}$ and $\mathbf{v}$, and one rotation about an axis normal to both $\mathbf{u}$ and $\mathbf{v}$. Each element of $\mathcal{F}(\mathbf{u}, \mathbf{v})$ is thus characterized by the two translations t_u, t_v and the rotation ϕ;

(vi) the spherical pair generates the subgroup $\mathcal{S}(O)$ of rotations about point O. Each element of $\mathcal{S}(O)$ is characterized by the axis of rotation passing through O in the direction of a unit vector $\mathbf{e}$ and through an angle ϕ. Alternatively, each element can be characterized by the independent rotations about three designated axes, e.g., the well-known Euler angles.

Besides the six foregoing subgroups, we can define six more, namely,

(vii) The *identity subgroup* $\mathcal{I}$, whose single element is the identity displacement ι introduced above;

($viii$) the *planar-translation subgroup* $\mathcal{T}_2(\mathbf{u}, \mathbf{v})$ of translations in the directions of the two distinct unit vectors $\mathbf{u}$ and $\mathbf{v}$. Each element of this group is thus characterized by two translations, t_u and t_v;

(ix) the *translation subgroup* $\mathcal{T}_3$ of translations in $\mathcal{E}$, each element of which is characterized by three independent translations t_u, t_v, and t_w;

(x) the subgroup $\mathcal{Y}(\mathbf{e}, p)$ of motions allowed by a screw of pitch p and axis parallel to $\mathbf{e}$ undergoing arbitrary translations in a direction normal to $\mathbf{e}$. Each element of this subgroup is thus characterized by the two independent translations t_u, t_v of the axis, and either the rotation ϕ about this axis or the translation t_w along the axis. Faute-de mieux, we shall call this subgroup the *translating-screw group*;

(xi) the subgroup $\mathcal{X}(\mathbf{e}) = \mathcal{F}(\mathbf{e}) \bullet \mathcal{P}(\mathbf{e})$, resulting of the product of the planar subgroup of plane normal to $\mathbf{e}$ and the prismatic subgroup of direction $\mathbf{e}$. Each element of this subgroup is thus characterized by the two translations t_u, t_v and the angle ϕ of the planar subgroup plus the translation t_w in the direction of $\mathbf{e}$. Moreover, note that $\mathcal{F}(\mathbf{e}) \bullet \mathcal{P}(\mathbf{e}) = \mathcal{P}(\mathbf{e}) \bullet \mathcal{F}(\mathbf{e})$. This subgroup is known as the *Schönflies subgroup*, and is generated most commonly by what is known as SCARA systems, for *Selective-Compliance Assembly Robot Arm*;

(xii) the group $\mathcal{D}$ itself. Each element of this subgroup is characterized by three independent translations and three independent rotations.

It is thus apparent that each subgroup includes a set of displacements with a specific degree of freedom. We shall need below an extension of the concept of dof, for which reason we term the dof of each subgroup its *dimension*, and denote the dimension of any subgroup $\mathcal{G}_s$ by $\dim[\mathcal{G}_s]$. Thus,

$$\dim[\mathcal{I}] = 0 \tag{1a}$$
$$\dim[\mathcal{R}(\mathcal{A})] = \dim[\mathcal{P}(\mathbf{e})] = \dim[\mathcal{H}(\mathcal{A}, p)] = 1 \tag{1b}$$
$$\dim[\mathcal{T}_2(\mathbf{u}, \mathbf{v})] = \dim[\mathcal{C}(\mathcal{A})] = 2 \tag{1c}$$
$$\begin{aligned}\dim[\mathcal{T}_3] &= \dim[\mathcal{F}(\mathbf{e})] = \dim[\mathcal{S}(O)] \\ &= \dim[\mathcal{Y}(\mathbf{e}, p)] = 3\end{aligned} \tag{1d}$$
$$\dim[\mathcal{X}(\mathbf{e})] = 4 \tag{1e}$$
$$\dim[\mathcal{D}] = 6 \tag{1f}$$

The foregoing list of displacement subgroups is *exhaustive*. The reader may wonder whether displacement products are missing from the list that might be subgroups. However, any displacement product not appearing in the list *is not a subgroup*, e.g.,

(a) $\mathcal{P}(\mathbf{e}) \bullet \mathcal{R}(\mathcal{A})$, with $\mathcal{A}$ defined as a line normal to the unit vector $\mathbf{e}$ and passing through a point O, is not a subgroup. This set of displacements is characterized by a translation t_e in the direction of $\mathbf{e}$ and a rotation about $\mathcal{A}$ through an angle θ, as depicted in Fig. 1. It should be apparent from this figure that this set of displacements does not form a group.

(b) $\mathcal{R}(\mathcal{A}) \bullet \mathcal{R}(\mathcal{A}')$ is not a subgroup, unless $\mathcal{A}$ and $\mathcal{A}'$ coincide. The reason here is that, assuming for example, that these two axes intersect at a point O, the composition $\mathcal{R}(\mathcal{A}) \bullet \mathcal{R}(\mathcal{A}')$ is, in general, equivalent to a new rotation, according to Euler's Theorem, about a third axis $\mathcal{A}''$, different from any of the first two axes, although still passing through O.

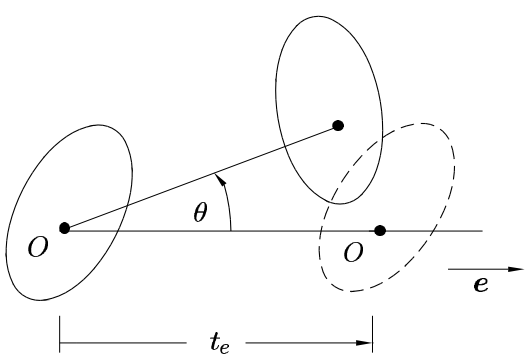

Figure 1: An instance of the $\mathcal{P}(\mathbf{e}) \bullet \mathcal{R}(\mathcal{A})$ set of displacements not constituting a group

4 Kinematic Bonds

Displacement subgroups can be combined to produce new sets of displacements that may or may not be displacement subgroups themselves. To combine subgroups, we resort to the group operations of product ($\bullet$) and intersection ($\cap$).

Now we recall the concept of *kinematic bond*, which is a generalization of kinematic pair, as first proposed by Hervé (1978), who called this concept *liaison cinématique* in French. This concept has been termed *kinematic liaison* (Angeles, 1982) or *mechanical connection* (Hervé, 1997) in English. Since "liaison" in English is usually applied to human relations, the term "bond" seems more appropriate, and hence, is adopted here.

We illustrate the concept with an example: Let us assume three links, numbered from 1 to 3, and coupled by two kinematic pairs generating the two subgroups $\mathcal{G}_1$ and $\mathcal{G}_2$, where these two subgroups are instanced by specific displacement subgroups below. We then have

$$\mathcal{G}_1 \bullet \mathcal{G}_2 = \mathcal{R}(\mathcal{A}) \bullet \mathcal{P}(\mathbf{e}) = \mathcal{C}(\mathcal{A}), \quad \mathbf{e} \parallel \mathcal{A} \tag{2a}$$
$$\begin{aligned}\mathcal{G}_1 \bullet \mathcal{G}_2 &= \mathcal{R}(\mathcal{A}) \bullet \mathcal{T}_2(\mathbf{u}, \mathbf{v}) = \mathcal{F}(\mathbf{e}), \\ &\qquad \mathbf{e} \quad \text{and} \quad \mathcal{A} \perp \mathbf{u} \quad \text{and} \quad \mathbf{v}\end{aligned} \tag{2b}$$
$$\mathcal{G}_1 \bullet \mathcal{G}_2 = \mathcal{R}(\mathcal{A}) \bullet \mathcal{R}(\mathcal{B}) = \mathcal{L}(1, 3) \tag{2c}$$
$$\mathcal{G}_1 \cap \mathcal{G}_2 = \mathcal{R}(\mathcal{A}) \cap \mathcal{C}(\mathcal{A}) = \mathcal{R}(\mathcal{A}) \tag{2d}$$
$$\mathcal{G}_1 \cap \mathcal{G}_2 = \mathcal{R}(\mathcal{A}) \cap \mathcal{S}(O) = \mathcal{R}(\mathcal{A}), \quad O \in \mathcal{A} \tag{2e}$$
$$\mathcal{G}_1 \cap \mathcal{G}_2 = \mathcal{R}(\mathcal{A}) \cap \mathcal{P}(\mathbf{e}) = \mathcal{I}, \quad \forall \quad \mathcal{A} \quad \text{and} \quad \mathbf{e} \tag{2f}$$

All of the above examples, except for the third one, amount to a displacement subgroup. This is why no subgroup symbol is attached to that set. Instead, we have used the symbol $\mathcal{L}(1, 3)$ to denote the kinematic bond between the first and third links of the chain. In general, a kinematic bond between links i and n of a kinematic chain, when no ambiguity is possible, is denoted by $\mathcal{L}(i, n)$. When the chain connecting these two links is not unique, such as in a closed chain, where these two links can be regarded as being connected by two possible *paths*, a subscript will be used, e.g., $\mathcal{L}_I(i, j)$, $\mathcal{L}_{II}(i, j)$, etc. A kinematic bond is, thus, a set of displacements, as stemming from a product of displacement subgroups, although the bond itself need not be a subgroup. Obviously, the 12 subgroups described above are themselves special cases of kinematic bonds.

The kinematic bond between links i and n can be conceptualized as the product of the various subgroups associated with the kinematic pairs between the ith and the nth links. To keep the discussion general enough, we shall denote the subgroup associated with the kinematic pair coupling links i and $i + 1$ as $\mathcal{L}(i, i + 1)$, with a similar notation for all other kinematic-pair subgroups, i.e.,

$$\mathcal{L}(i, n) = \mathcal{L}(i, i+1) \bullet \mathcal{L}(i+1, i+2) \bullet \cdots \bullet \mathcal{L}(n-1, n) \tag{3}$$

Thus, in a six-axis serial manipulator, we can set $i = 1$, $n = 7$, all six kinematic pairs in-between being revolutes of skew axes $\mathcal{R}(\mathcal{A}_1)$, $\mathcal{R}(\mathcal{A}_2)$, ..., $\mathcal{R}(\mathcal{A}_6)$. Then,

$$\mathcal{L}(1, 7) = \mathcal{D}$$

That is, the 6R manipulator is a generator of the general six-dimensional group of rigid-body displacements $\mathcal{D}$.

As an example of group-intersection, let us consider the *Sarrus mechanism*, which is depicted in Fig. 2.

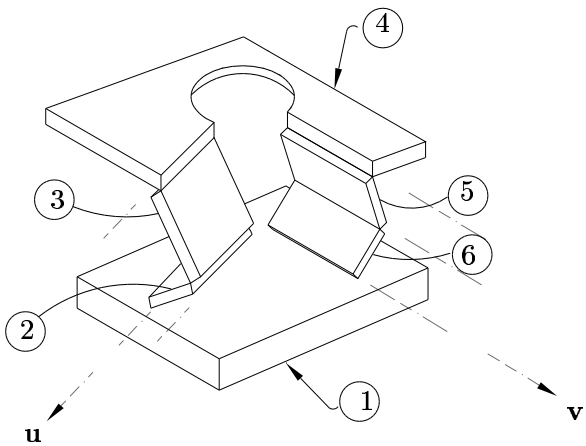

Figure 2: The Sarrus mechanism

In the Sarrus mechanism, we have six links, coupled by six revolute pairs. Moreover, the revolute pairs occur in two triplets, each on one leg of the mechanism. The axes of the three revolute pairs of each leg are parallel to each other. The bond $\mathcal{L}(1,4)$, apparently, is not unique, for it can be defi nedby traversing any of the two legs. Let the leg of links 1, 2, 3 and 4, coupled by revolutes of axes parallel to the unit vector **u**, be labelled I; the other leg, of links 4, 5, 6 and 1, coupled by revolutes of axes parallel to the unit vector **v**, is labelled II. It is apparent that, upon traversing leg I, we obtain

$$\mathcal{L}_I(1,4) = \mathcal{F}(\mathbf{u})$$

while, upon traversing leg II,

$$\mathcal{L}_{II}(1,4) = \mathcal{F}(\mathbf{v})$$

That is, leg I is a generator of the planar subgroup $\mathcal{F}$ of plane normal to vector **u**, while leg II is that of the subgroup $\mathcal{F}$ of plane normal to vector **v**. Therefore, $\mathcal{L}_I(1,4) \cap \mathcal{L}_{II}(1,4)$ is the set of displacements common to the two $\mathcal{F}$-subgroups, namely, the prismatic subgroup of translations in the direction $\mathbf{w} = \mathbf{v} \times \mathbf{u}$, i.e.,

$$\mathcal{L}_I(1,6) \cap \mathcal{L}_{II}(1,6) = \mathcal{P}(\mathbf{w})$$

The Sarrus mechanism is thus a revolute realization of the prismatic joint.

5 The Π Joint and Its Generalizations

The foregoing concepts are now applied to the *qualitative* synthesis of parallel robotic architectures. By qualitative we mean the determination of the topology of the kinematic chain, not including the corresponding dimensions. These dimensions are found at a later stage, by means of methods of *quantitative synthesis*. The full determination of the kinematic chain, including dimensions, yields what is known as the *architecture* of the robotic system at hand. Prior to the discussion of interest, we recall the Π joint, fi rst introduced by Hervé and Sparacino (1992).

5.1 The Π Joint

A four-bar linkage with its opposite links of the same length is known as a *parallelogram*. In the standard terminology, and referring to Fig. 3, the linkage is composed of: a) one fi xedlink, labelled 1; b) one input link, labelled 2; c) one coupler link, labelled 3; and one output link, labelled 4. In a parallelogram, the opposite links move with a relative pure translation, each point of one link describing a circular trajectory onto the other link. The linkage, shown in Fig. 3, thus provides a kinematic pair of the coupler link 3 with respect to the fi xedlink 1, which Hervé and Sparacino (1992) termed a Π joint. Notice that the four R joints of the parallelogram linkage can be paired so that each of the two pairs is either (a) fi xedto one single coupled link or (b) fi xedto different coupled links. In the linkage of Fig. 3, the pairs (R_1, R_4) and (R_2, R_3) are of the *first kind*. Correspondingly, (R_1, R_2) and (R_3, R_4) are of the *second kind*. Likewise, we distinguish two kinds of links, namely, the *coupled links* 1 and 3, and the *coupling links* 2 and 4.

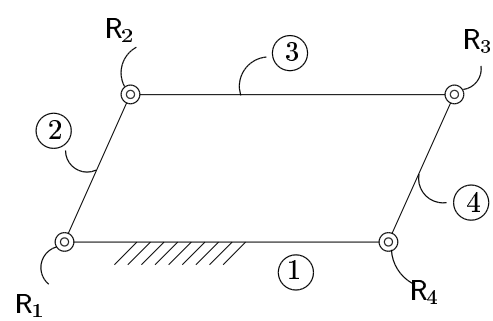

Figure 3: The Π joint, a four-bar parallelogram coupling links 1 and 3

Moreover, notice that the Π joint does not belong to any of the two classes of lower and higher kinematic pairs. Indeed, it couples two adjacent links by means of an infi nity of circular cylindrical surfaces of the same radius, but with axes at different locations normal to the plane of the parallelogram linkage. The Π joint is thus characterized by the unit vector **e** normal to the plane of the parallelogram and the radius R of its family of cylindrical surfaces. Therefore, R is nothing but the common length of the coupling links. In summary, the Π joint couples two links while allowing a relative translation along a circular trajectory.

While the Π joint is neither a lower nor a higher pair, we can

associate a kinematic bond to it. When combined with other kinematic pairs or other kinematic bonds, the Π joint can generate both $\mathcal{T}_3$ and Schönflies subgroups, as discussed in Section 6.

Below we introduce some extensions of the Π joint.

5.2 The R-Π Joint

Two kinds of joints are possible when a Π joint is concatenated with a R joint of axis lying in the plane of the Π joint. The difference lies on whether the axis $\mathcal{A}$ of the new R joint is the common normal to the axes of two parallelogram joints of the first kind or is normal to the plane of these joints, as depicted in Figs. 4a and b, respectively.

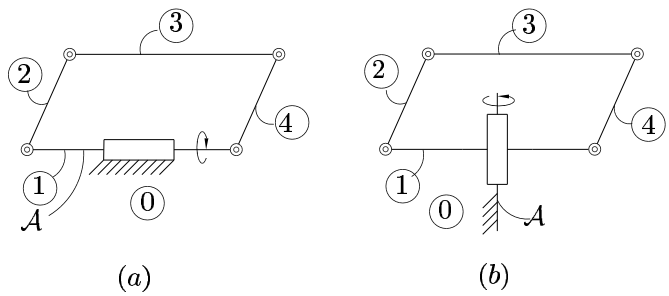

Figure 4: The two kinds of R-Π joints: (a) new R-axis lying along the common normal to two parallelogram R axes and (b) new R-axis normal to the plane of the two parallelogram axes of the first kind

We shall call the composite joints of Figs. 4a and b R-Π_a and R-Π_b, respectively. When two links, 0 and 3, are coupled by means of a R-Π_a or a R-$\Pi_b$joint, their points generate a family of tori of main axis $\mathcal{A}$.

5.3 The Π^2 Joint

It is apparent that, if the four joints of the parallelogram linkage of Fig. 3 are replaced by universal (U) joints, then the plane of the parallelogram undergoes a rotation about axis $\mathcal{A}$ of Fig. 4a. We recall here that a universal joint is the concatenation of two R joints intersecting at right angles. Moreover, by properly constraining the motion of link 3 with respect to link 1, it is possible to have link 3 still move with respect to link 1 with pure translation. In this case, the points of link 3 describe spheres of identical radii R equal to the length of the coupling links of the parallelogram.

Apparently, the constraint needed to produce the foregoing motion can be realized by coupling two identical parallelograms of parallel planes and sharing the same base link 1 and the same moving link 3. The result is displayed in Fig. 5.

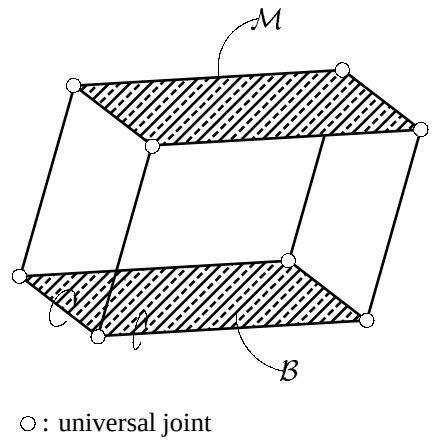

Figure 5: A Π^2 joint

The Π^2 joint thus generates two-dof displacements that can be represented by the bond $\mathcal{L}(\mathcal{B}, \mathcal{M})$. Moreover, these displacements are elements of the $\mathcal{T}_2$ subgroup characterized by the unit vector **e** normal to the plane of the R joints of the first kind of the given parallelograms. However, $\mathcal{L}(\mathcal{B}, \mathcal{M})$ does not constitute a subgroup.

5.4 The Π^3 Joint

We can go one more step and allow the coupled links of a Π^2 joint to undergo an additional pure translation in the direction of its coupling-link axes, as depicted in Fig. 6. In this figure, the four coupling links of the Π^2 joint of Fig. 5 have been replaced by P joints. By means of a suitable constraint, all four P joints can be made to undergo identical translations. We call this a Π^3 joint.

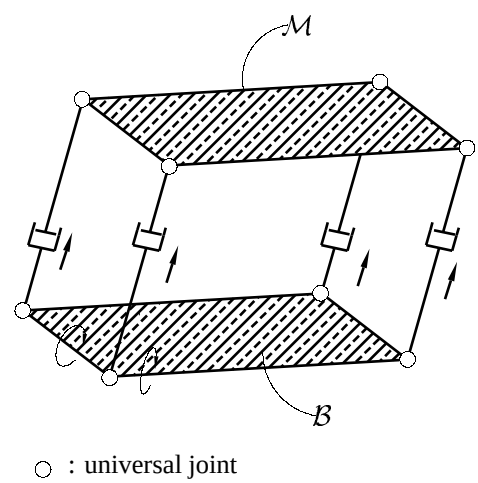

Figure 6: A Π^3 joint

The Π^3 joint thus generates the subgroup $\mathcal{T}_3$ of three-dof pure translations. Notice that a simple means of implementing a Π^3 joint is by cascading two Π^2 joints, upon attaching rigidly the moving link of one with the fixed link of the second one, as depicted in Fig. 7. In this layout, the two Π^2 joints are coupled by means of four R joints of parallel axes.

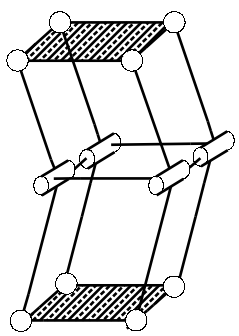

○: universal joint

Figure 7: A possible realization of a Π^3 joint

We illustrate below how the foregoing ideas can be used in the synthesis of parallel—and serial—manipulators.

6 The Synthesis of Serial and Parallel Robotic Architectures

The first parallel architecture with Π pairs was proposed by Clavel (1988), in what he called the *Delta Robot*. The kinematic chain of this robot is displayed in Fig. 8. This robot is a generator of the $\mathcal{T}_3(\mathbf{u})$ displacement subgroup. Delta is thus capable of three-dof translations.

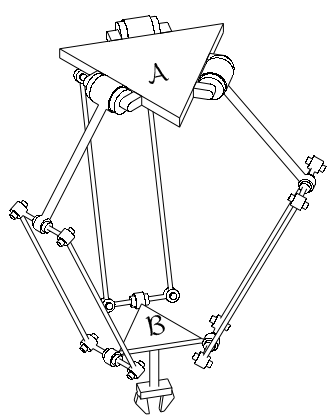

Figure 8: Kinematic chain of the Clavel Delta robot

The kinematic chain of the Delta robot is composed of two triangular plates, the top ($\mathcal{A}$) and the bottom ($\mathcal{B}$) plates. The top plate supports the three (direct-drive) motors, the bottom plate the gripper, and hence, constitutes the end-effector (EE) of the robot. The EE is capable of translating in 3D space with respect to the upper plate, which is considered fixed. The two plates are coupled by means of three legs, each with a RRΠR chain.

While Clavel did not cite any group-theoretical reasoning behind his ingenious design, an analysis in this framework will readily explain the principle of operation of the Delta robot.

The ith leg is a generator of the Schönflies $\mathcal{X}(\mathbf{e}_i)$ subgroup, with $\mathbf{e}_i$ denoting the unit vector parallel to the axis of the ith motor. That is, the ith leg generates a Schönflies subgroup of displacements comprising translations in 3D space and one rotation about an axis parallel to $\mathbf{e}_i$. The subset of EE displacements is thus the intersection of the three subgroups $\mathcal{X}(\mathbf{e}_i)$, for $i = 1, 2, 3$, i.e., the subgroup $\mathcal{T}_3$. Therefore, the EE is capable of pure translations in 3D space.

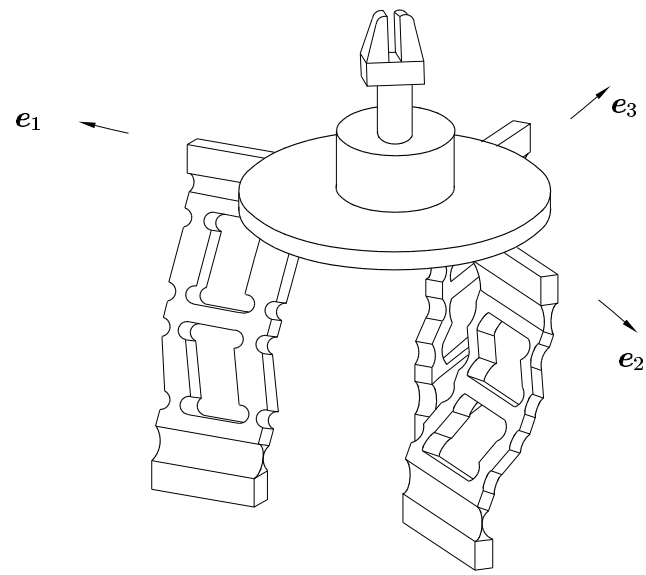

Figure 9: The MEL microfinger

One second applications example is the microfinger of Japan's Mechanical Engineering Laboratory (MEL) at Tsukuba (Arai, Hervé and Takinawa, 1996), as displayed in Fig. 9. In the MEL design, the inventors use a structure consisting of two plates that translate with respect to each other by means of three legs coupling the plates. The ith leg entails a R$\Pi\Pi$R chain, shown in Fig. 10, that generates the Schönflies subgroup in the direction of a unit vector $\mathbf{e}_i$, for $i = 1, 2, 3$. The three unit vectors, moreover, are coplanar and make angles of 120°. The motion of the moving plate is thus the result of the intersection of these three subgroups, which is, in turn, the subgroup $\mathcal{T}_3$. Moreover, the kinematic chain of each leg is made of an elastic material in one single piece, in order to allow for micrometric displacements.

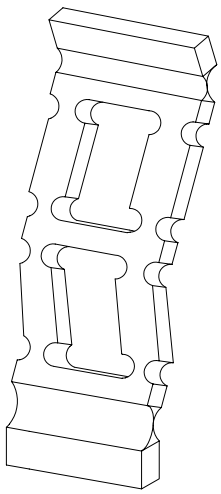

Figure 10: The ith leg of the MEL microfi nger

Yet another example is the Y-Tristar robot, developed at Ecole Centrale de Paris by Hervé and Sparacino (1992). Interestingly, the above instances of parallel manipulators using R-Π joints are capable of generating only the $\mathcal{T}_3$ subgroup. However, they are intended for Schönflies displacements. The inventors of these architectures have solved the problem of Schönflies-motion generation by cascading a fourth actuated axis to the parallel manipulator, thereby obtaining a hybrid parallel-serial one. An architecture realizing a Schönflies-motion generator is the linkage of Fig. 11. The Schönflies displacement subgroup is $\mathcal{X}(\mathbf{e})$, with $\mathbf{e}$ parallel to $\mathcal{L}$.

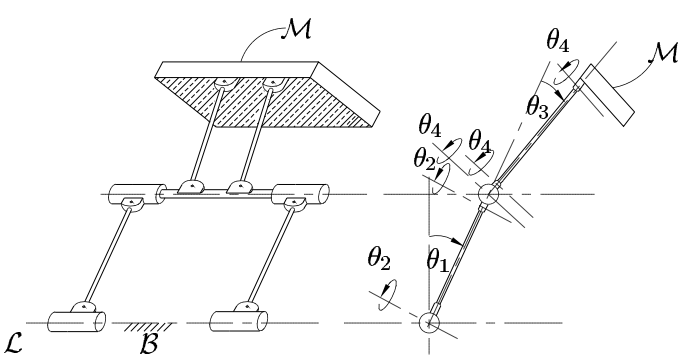

Figure 11: RΠRΠ kinematic bond generating Schönflies-motions

One more aplication of the same concepts is the serial Schönflies-motion generator proposed by Angeles, Morozov, and Navarro (2000). This robot entails a kinematic chain of the RΠRΠ type, as displayed in Fig. 12. In fact, the chain is the concatenation of two pan-tilt generating chains, each constituted by a R-Π_b joint, as displayed in Fig. 4b.

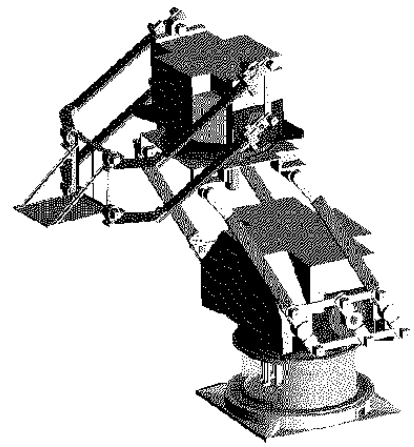

Figure 12: A serial Schönflies-motion generator

To be true, Company, Pierrot, Shibukawa and Koji (2001) dsiclosed a fully-parallel Schönflies-motion generator in European Patent 1084802. This robot comprises four legs, each being a Schönflies-displacement generator. Besides this manipulator, no other one is known with the same motion capabilities and a fully-parallel architecture. Nevertheless, the parallel robot of EP1084802 does not make proper use of Schönflies-motion generators. Indeed, this robot is the result of coupling two two-leg parallel manipulators, each leg being, in turn, the parallel array of two Schönflies-motion generators identical to those of the legs of the Delta robot. Such a parrallel array is displayed in Fig. 14, where it is apparent that two RRΠR legs generating Schönflies subgroups $\mathcal{X}(\mathbf{u})$ and $\mathcal{X}(\mathbf{v})$ are coupled by means of the end-effector 42, using the same notation as in the foregoing patent. Link 42, thus, undergoes the set of motions resulting from the intersection of the two Schönflies subgroups, namely,

$$\mathcal{X}(\mathbf{u}) \cap \mathcal{X}(\mathbf{v}) = \mathcal{T}_3$$

Thus, link 42 undergoes pure translations in three-dimensional space. However, the parallel array is supplied with only two actuators, one per leg, and hence, one translation is left uncontrolled, but this uncontrolled motion is exploited in producing Schönflies motions, as explained below.

What Company and his co-inventors did in order to produce the Schönflies subgroup was to couple the end-effectors of two identical parallel arrays like that displayed in Fig. 13 by means of revolutes of parallel axes, one normal to the $\mathbf{u}$ and $\mathbf{v}$ unit vectors, the other normal to the $\mathbf{u}'$ and $\mathbf{v}'$ vectors. Such a coupling is displayed in Fig. 14. In this coupling, the parallel axes of the rev-

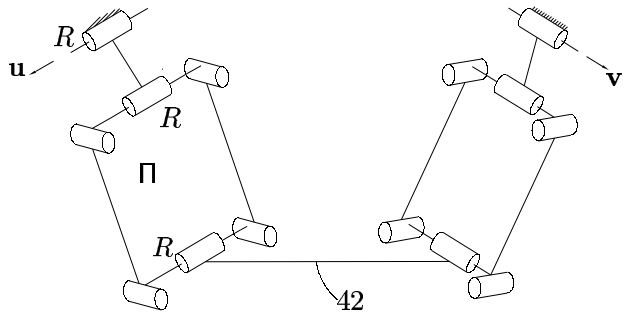

Figure 13: The coupling of two identical $\mathcal{T}_3$ generators

olutes of the end-effector 41 can translate freely in space, while keeping their parallel orientations. Such a motion is controlled by the actuators driving each of the two legs. Furthermore, the concatenation of one of the two revolutes of 41 with each $\mathcal{T}_3$ generator yields a hybrid parallel-serial generator of the Schönflies subgroup $\mathcal{X}(\mathbf{w})$, where $\mathbf{w} \equiv \mathbf{u} \times \mathbf{v} = \mathbf{u}' \times \mathbf{v}'$. The coupling of the two Schönflies-motion generators thus yields a set of displacements lying in the intersection of the two Schönflies subgroups, i.e.,

$$\mathcal{X}(\mathbf{w}) \cap \mathcal{X}(\mathbf{w}) = \mathcal{X}(\mathbf{w})$$

That is, the intersection of the two identical Schönflies subgroups is the same Schönflies subgroup.

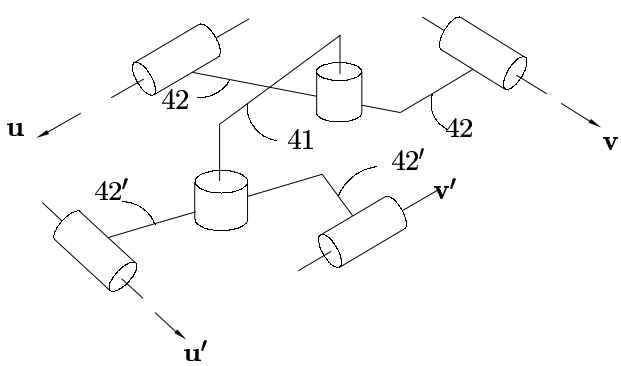

Figure 14: A parallel array of two Schönflies-motion generators

7 Conclusions

The use of qualitative reasoning in the synthesis of the topology of parallel manipulators was highlighted in this paper. The motivation behind is the design of parallel manipulators with three and four dof. To this end, the theory of groups, as first proposed by Hervé in 1978, was used extensively, and the concepts associated with kinematic chains in the same context were discussed. In this vein, various Schönflies-motion generators were recalled, and new kinematic bonds producing these were proposed. The concepts were illustrated with various examples.

Acknowledgements

The work reported here is being supported by NSERC (Canada's Natural Sciences and Engineering Research Council) under Strategic Project 215729-98.

References

Agrawal, S.K., 1991, "Study of an in-parallel mechanism using reciprocal screws," *Proc. 8th World Congress on TMM*, Prague, 26–31 Aug. 1991, pp. 405–408.

Angeles, J., 1982, *Spatial Kinematic Chains. Analysis, Synthesis, Optimization*, Springer-Verlag, New York.

Angeles, J., Morozov, A., and Navarro, O., 2000, "A novel manipulator architecture for the production of SCARA motions", *Proc. IEEE Int. Conf. Robotics and Automation*, San Francisco, pp. 2370–2375. CD-ROM 00CH37065C, April 24–28.

Arai, T., Hervé, J.M., and Tanikawa, T., 1996, "Development of 3 DOF micro finger," *Proc. IROS'96*, November 5–8, Osaka, pp. 981–987. Brogårdh, T., 2001, "Device for Relative Movement of two Elements," U.S Patent No. 6,301,988 B1 of October 16.

Clavel, R., 1988, "Delta, a fast robot with parallel geometry," *Proc. 18th Int. Symp. Industrial Robots*, Lausanne, pp. 91–100.

Clavel, R., 1990, *Device for the Movement and Positioning of an Element in Space*, U.S. Patent No. 4,976,582 of December 11.

Company, O., Pierrot, F., Shibukawa, T. and Koji, M., 2001, *Four-Degree-of-Freedom Parallel Robot*, European Patent EP1084802, March 21.

Craver, W.M., 1989, "Structural analysis and design of a three-degree-of-freedom roboic shoulder module," Master's Thesis, The University of Texas at Austin, Department of Mechanical Engineering, Austin.

Gosselin, C. and Angeles, J., 1987, "The optimum kinematic design of a spherical three-degree-of-freedom parallel manipulator", *Proc. 13th ASME Design Automation Conference*, Sept. 27–30, Boston, pp. 111–115.

Hartenberg, R.S. and Denavit, J, 1964. *Kinematic Synthesis of Linkages*, McGraw-Hill Book Company, New York.

Hervé, J.M., 1978, "Analyse structurelle des mécanismes par groupes de déplacements," *Mechanism and Machine Theory*, Vol. 13, pp. 437–450.

Hervé, J.M. and Sparacino, F., 1992, "Star, a new concept in robotics," *Proc. 3rd Int. Workshop on Advances in Robot Kinematics*, September 7–9, Ferrara, pp. 176–183.

Hunt, K.H, 1983 "Structural kinematics of in-parallel-actuated robot arms," *ASME Trans., J. Mech. Transmissions Automat. Design*, Vol. 105, pp. 705-712.

de Laclos, Ch., 1782, *Les liaisons dangereuses ou lettres recueillies dans une société, et publiées pour l'instruction de quelques autres*, Durand, Paris (the first edition seems to have been published in Amsterdam), 1907 edition by Maurice Bauche, Paris.

Lee, K,M., and Shah. D.K.,1987, "Kinematic analysis of a three-degree-of-freedom in parallel actuated manipulators," *Proc. IEEE Int. Conf. Rooties and Automation*, Vol. l, pp. 345-350.

Lee, K,M., and Arjuman, S., 1991, "A 3-DOF micromotion in-parallel actuated fnanipulator," *IEEE Trans. Robotics and Automation*. Vol. 7(5), pp. 634-640.

Macdonald, I.D., 1968, *The Theory of Groups*, Oxford University Press, London.

Pfreundschuh, G.H., Kumar, V,, and Sugar, T.H., 1991, "Design and Control of a Three-Degree-of-Preedom In-Parallel Actuated Manipulator," *Proc. IEEE Int. Conf. Robotics and Automation*, pp. 1659-1664.

Regular Papers: New Architectures and Wire-Driven Manipulators

Friday, October 4, 2002, 9:30AM

Session Chairs: V. Parenti-Castelli and Y. Takeda

1. X-J. Liu, J. Kim, J. Wang
   "Two Novel Parallel Mechanisms with Less than Six DoFs and the Applications".

2. J. Kim, J.C. Hwang, J.S. Kim, C.C. Iurascu, F.C. Park, Y.M. Cho
   "Analysis and Design of a New 6 D.O.F. Full Tilting Parallel Mechanism".

3. P. Lafourcade, M. Llibre, C. Reboulet
   "Design of a Parallel Wire-Driven Manipulator for Wind Tunnels".

4. A. Fattah, S.K. Agrawal
   "Design of Cable-Suspended Planar Parallel Robots for an Optimal Workspace".

Proceedings of the WORKSHOP on
Fundamental Issues and Future Research Directions for Parallel Mechanisms and Manipulators
October 3–4, 2002, Quebec City, Quebec, Canada
Clément M. Gosselin and Imme Ebert-Uphoff, editors

Two Novel Parallel Mechanisms with Less than Six DoFs and the Applications

XIN-JUN LIU
Robust Design Engineering Lab.
Seoul National University
Seoul, 151-742, Republic of Korea
xinjunl@yahoo.com

JONGWON KIM
Robust Design Engineering Lab.
Seoul National University
Seoul, 151-742, Republic of Korea
jongkim@snu.ac.kr

JINSONG WANG
Manufacturing Engineering Institute, Tsinghua University
Beijing, 100084, China. wangjs@tsinghua.edu.cn

Abstract: *Parallel mechanisms have been attracting more and more researchers' attention in the context of industrial application, especially, the parallel kinematics machine. This paper presents two novel parallel mechanisms with two and three degrees of freedom (DoFs) and their potential applications. The output of the two DoFs parallel mechanism is two planar translations of a rigid body. The architecture can be applied to the basic mechanism of a parallel kinematics machine with gantry structure, part handling, and mobile base for a spatial mechanism. The moving platform of the three DoFs parallel mechanism has two translational degrees of freedom and one rotational degree of freedom with respect to the base. The distinct advantage of the mechanism is that the mobility of the rotational DoF is very high, which means that the mechanism has the application advantage in the parallel kinematics machine and other manipulating devices. The results of the paper are very useful for the potential design conceive of parallel mechanisms and the applications.*

1 Introduction

The conceptual design of parallel mechanisms can be dated back to 1947, when Gough established the basic principles of a mechanism with a closed-loop kinematic structure (Gough, 1956), that allows the position and the orientation of a moving platform so as to test tire wear and tear. Stewart designed a platform mechanism for use as an aircraft simulator in 1965 (Stewart, 1965). In 1978, Hunt (1978) made a systematic study of the kinematic structure of parallel mechanisms, in which the planar 3-RPS parallel mechanism is a typically one. Since then, parallel mechanisms have been studied extensively by numerous researchers.

The most studied parallel mechanisms are with 6 DoFs. These parallel mechanisms posses the advantages of high stiffness, low inertia, and large payload capacity. However, they suffer the problems of relatively small useful workspace and design difficulties (Merlet, 2000). Furthermore, their direct kinematics is a very difficult problem, while the problem of parallel mechanisms with 2 and 3 DoFs can be described as closed forms (Liu, 2001). As well known, there are three kinds of singularity in parallel mechanisms (Gosselin and Angeles, 1990). Moreover, not all singularities of a 6-DoF parallel mechanism can be found out easily. But for a parallel mechanism with 2 and 3 DoFs, the singularities can always be identified readily. For such reasons, parallel mechanisms with less than 6 DoFs, especially 2 and 3 DoFs, have increasingly attracted more and more researchers' attention with respect to industry applications (Tonshoff et al., 1999; Siciliano, 1999; Tsai and Stamper, 1996; Ceccarelli, 1997; Xin-Jun Liu et al., 2001).

The existing planar 2-DoF parallel mechanisms (Asada and Kanade, 1983; McCloy, 1990; Gao et al., 1998) are the well-known five-bar mechanism with prismatic actuators or revolute actuators. In the case of the mechanism with revolute actuators, the mechanism consists of five revolute pairs and the two joints fixed to the base are actuated. In the case of the mechanism with prismatic actuators, the mechanism consists of three revolute pairs and two prismatic joints and the prismatic joints are actuated. The output of the

mechanism is the translational motion of a point on the end-effector but not a rigid body. Among the 3 DoFs parallel mechanisms, some (e.g. the 3-RPS parallel manipulator) have special kinematics characteristics (Huang and Fang, 1996). Some of them (e.g. DELTA (Clavel, 1988), Star like (Hervé, 1992) and spherical 3-DoF paralell manipulators (Liu et al., 2000a)) are with pure translational or orientational degrees of freedom. Some of them (e.g. planar 3-DoF parallel manipulator (Gosselin et al., 1996; Liu et al., 2000b)) are planar parallel manipulators. It is necessary to design a spatial three degree-of-freedom parallel manipulator combining spatial translational and orientational degrees of freedom in the context of industrial applications.

In this paper, two novel parallel mechanisms with two and three DoFs and their potential applications will be presented. The two DoFs parallel mechanism departs from the existing designs in that a parallelogram mechanism is adopted in each of the two legs. The motion of the platform is the planar translational motion of a rigid body but not a point. The architecture can be applied to the basic mechanism of a parallel kinematics machine with gantry structure, part handling, and mobile base for a spatial mechanism. The moving platform of the three DoFs parallel mechanism has two translational degrees of freedom and one rotational degree of freedom with respect to the base. The distinct advantage of the mechanism is that the mobility of the rotational DoF is very high, which means that the mechanism has the application advantage in manipulation a tool with high dexterity. The results of the paper are very useful for the potential design conceive of parallel mechanisms and the applications.

2 Description of the Mechanisms

2.1 The Two DoFs Parallel Mechanism

The novel 2-DoF parallel mechanism (Liu, 2001) is shown in Fig.1(a). A schematic of the mechanism is shown in Fig.1(b), where the base is labeled 1 and the moving platform is labeled 2. The moving platform is connected to the base by two identical legs. Each leg consists of a planar four-bar parallelogram: links 2, 3, 4, and 5 for the first leg; 2, 6, 7, and 8 for the second leg. In each planar four-bar parallelogram, the joints are all revolute pairs. Links 3 and 8 are actuated by prismatic actuators, respectively. Motions of the moving platform are achieved by the combination of movements of the links 3 and 8 that can be transmitted to the platform by the system of the two parallelograms. Due to the structure, one can see that the moving platform or the rigid body 2 has two pure translational degrees of freedom with respect to the base because of the planar four-bar parallelograms. What we should notice is that, to obtain two DoFs of a rigid body in this system, only one planar four-bar parallelogram is enough, as the mechanism shown in Fig.2. The reason to use two planar four-bar parallelograms is to increase the system's stiffness and make the system symmetry.

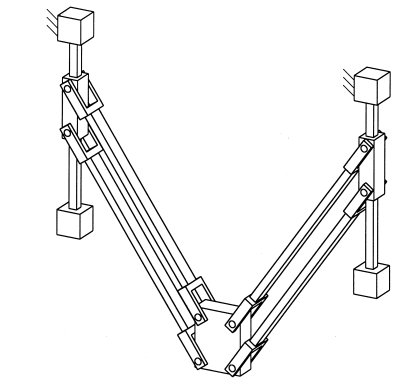

(a)

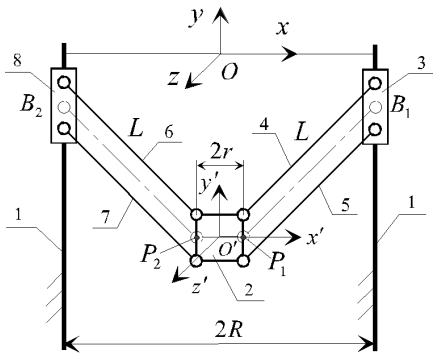

(b)

Fig.1 A novel planar 2-DOF parallel mechanism

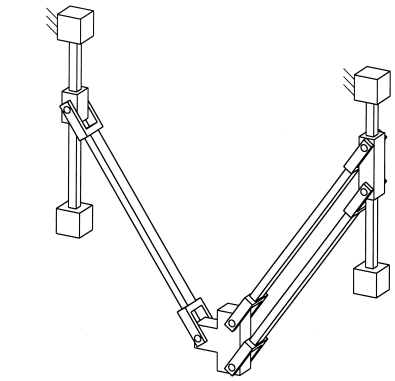

Fig.2 The 2-DOF parallel mechanism with one parallelogram

2.2 The Three DoFs Parallel Mechanism

2.2.1 Mechanism Structure

The spatial 3 DoFs parallel manipulator (Liu, 2001; Liu et al., 2001) is shown in Fig.3 (a), which consists of a base plate, a movable platform, and three legs that connect the

aforementioned two plates. Each connecting leg has four degrees of freedom. Two of the three legs have identical chains, each of which consists of a 2-DoF joint (or two 1-DoF joints) and two 1-DoF joints. The third one consists of a planar four-bar parallelogram and three 1-DoF joints. A 1-DoF joint for each of the legs is the actuated one.

The moving platform is an isosceles triangle. The vertices of this platform are connected to a fixed-base plate through three legs (1), (8) and (12). The legs (1) and (12) have identical chains, each of which consists of a constant link which is connected to a universal joint (or two revolute joints) (15) or (13) at the bottom end and a passive revolute joint (3) or (11) at the other. The revolute joint is then attached to an active slider (4) or (10), which is mounted on the guideway (2) or (9). The third leg (8) consists of a constant link, a planar four-bar parallelogram, which is connected to a revolute joint (16) at the bottom end and a passive revolute joint (5) at the other. The revolute joint is attached to an active slider (6), which is mounted on the guideway (7). The movement of the moving platform is accomplished by the slide of three sliders on the guideways.

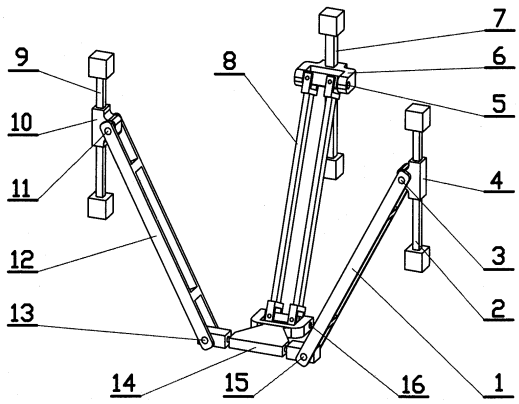

(a)

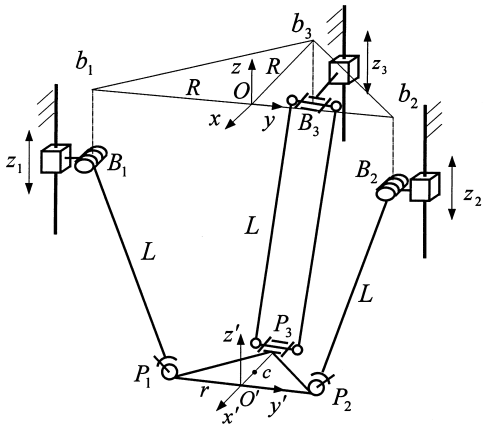

(b)

Fig.3 A new spatial 3-DOF parallel manipulator

2.2.2 Mechanism Capability

As described in last Section, the proposed manipulator is a general manipulation device that must have three degrees of freedom when the input elements are active. Due to the arrangement of the links and joints, as shown in Fig.3, two legs (1) and (12) provide two constraints on the rotation of the moving platform about the $z-$axis and the translation along $x-$axis. The two revolute joints (5) and (16) for the third leg (8) have parallel axes as shown in Fig.3 (a). The third leg can provide two constraints on the rotation of the moving platform about x and z axes. Hence, the combination of the three legs constrains the rotation of the moving platform with respect to x and z axes and the translation along $x-$axis. This leaves the mechanism with two translational degrees in $O-yz$ plane and one rotational degree of freedom about $y-$axis. Table 1 gives the description.

Table 1. The constraints and DoFs of the mechanism

Single leg			Combination of three legs	
No.	Chain type	Constraints	Constraints	Remained DoFs
1	$P_zR_xU_{x,y}$	$\{T_x, RO_z\}$	$\{T_x, RO_x, RO_z\}$	$\{T_y, T_z, RO_y\}$
2	$P_zR_xU_{x,y}$	$\{T_x, RO_z\}$		
3	$P_zR_yP^*_yR_y$	$\{RO_x, RO_z\}$		

where, P-prismatic joint, R-revolute joint, U-universal joint, P*-parallelogram, T-translation, RO-rotation, in each of which the suffix is the DoF.

2.3 Application of the Parallelogram in the Mechanical Design

The first design of parallel mechanism using parallelogram is the DELTA with three translational and one rotational degrees of freedom, which is proposed by Professor Clavel at EPFL in the early 1980's. A parallelogram allows an output link to remain at a fixed orientation with respect to an input link. The use of three such parallelograms restrain completely the orientation of the mobile platform, which remains only with three purely translational degrees of freedom. By now, the DELTA design has attracted great interest not only in industry but also in university labs (Bonev, 2001). Later, the design concept of parallelogram was applied to another three translational degrees of freedom parallel mechanism by Tsai (1996), which is also the first design to solve the puzzled problem of UPU chains. Parallelogram has been also used in the mechanical design of other parallel mechanisms, e.g., Star like parallel manipulator (Hervé, 1992), and CaPaman (Ceccarelli, 1997).

In our design, the parallelogram also plays its un-substitutable role in the mechanisms, respectively. It allows the moving platform of the two DoFs parallel mechanism to output two planar translational motions with respect to the base. And it remains axes of two revolute joints 5 and 16 of the three DoFs parallel mechanism, as shown in Fig.3(a), to parallel to each other permanently. For such reason, the moving platform cannot rotate with respect to the $x-$axis. We believe that the parallelogram will play more and more important role in the design of new parallel mechanisms, and will lead to some new parallel mechanisms.

3. Applications of the Mechanisms

The parallel kinematics machine (PKM) is a new type of machine tool which was firstly showed at the 1994 Internatinoal Manufacturing Technology Show in Chicago by two American machine tool companies, Giddings & Lewis and Ingersoll. These machine tools, named Hexpod, were based on the paradigm of the spatial 6-DoF parallel mechanism. The parallel kinematics machine technology promises to offer manufacturers a number of advantages relative to conventional machine tools, such as a higher stiffness-to-mass ratio, higher speeds, higher accuracy, reduced installation requirements, mechanical simplicity, and high flexibility.

The six DoFs Stewart platform is one PKM configuration that has been used in a number of new machine tool designs at the beginning of the born of PKMs. For machining applications, disadvantages of the Stewart platform include a complex workspace, limited orientation range of motion and a requirement of six actuators for a five degree-of-freedom task (milling, drilling, and similar operations). Moreover, there are some disadvantages with the parallel kinematics itself, such as the forward kinematics cannot be described in closed-form, the calibration is difficult, and so on. For these reasons, many researchers begin to pay their attentions to less than 6 DoFs PKMs (Liu, 2001; Liu et al., 2001; Moriwaki, 1999), especially hybrid PKMs (Tonshoff et al., 1999; Siciliano, 1999; Tsai, 1997), such as the Tricept HPI (Neos), Hexam (Toyoda), PA35 (Hitachi Seiki), Georg V (IFW-University of Hannover). PKMs with hybrid kinematics are always built as Tripod structures, for which all points within the workspace are reachable with high dynamics and high accuracy (Tonshoff et al., 1999) through the used parallel mechanism. By means of the two-axis wrist joint the end-effector gets the desired orientation in the workspace. By this arrangement of the kinematics the dexterity of the system can be increased compared to fully parallel kinematics (Hexapod systems). Another advantage to design a machine tool as hybrid structure based on a 3, or 4-DoFs parallel mechanism, to the author's knowledge there is no hybrid machine tool is based on a 2-DoF parallel mechanism, is that the stiffness can be improved by increasing redundant constraints.

3.1 Applications of the Two DoFs Parallel Mechanism

As described in Section 2.1, the output of the parallel mechanism is the planar translational motion of a rigid body but not a point. It can allow a rigid body to remain its orientation when the body is moving. Then, the mechanism has wide applications in the metal cutting, part handling, mobile bases for a spatial mechanism, etc.

Applying to the field of machine tool, a concept design of a PKM with hybrid kinematics based on the 2-DoF parallel mechanism presented in this paper is shown in Fig.4. In this design, the machine is a 5-axis system with gantry structure, that is three translations along x, y, and z axes, and two rotations about x and y axes. The planar 2-DoF parallel mechanism provides the machine tool with high stiffness and high speed. Especially, the upper and lower links of each of the two planar four-bar parallelograms are substituted by two plates, which can improve the system's stiffness. By means of the two-axis wrist joint the end-effector gets the desired orientation in the workspace, which provides it with high mobility. Only single DoF joints are used in the machine tool, which can increase the accuracy. The worktable can move freely along the $z-$axis, which endows the machine tool with the capability of manufacturing long components.

Additionally, in this design, width of each of the four plates is increasing from the bottom end to the top, which can also increase the system's stiffness. As shown in Fig.4, each leg consists of one four-bar parallelogram. Letting each leg comprise two or more four-bar parallelogram, i.e., increasing the system's redundant constraints, will improve the system's stiffness largely, at the same time the accuracy of manufacture is increased correspondingly. In order to avoid the interference between the upper plate and the lower plate, the moving platform is design as trapezoidal profile, as shown in Fig.4.

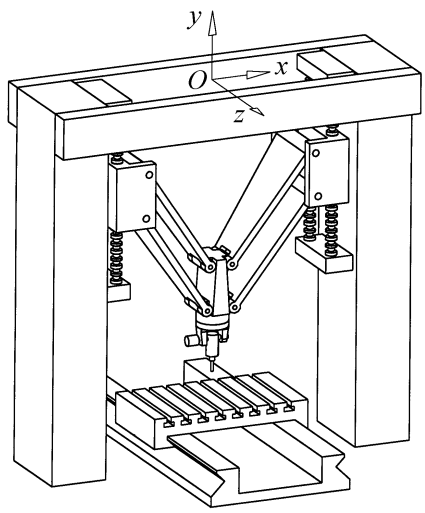

Fig.4 The concept design of a hybrid PKM

All in all, the advantages of the hybrid PKM with gantry structure are: (a) only single DoF joints are used; (b) high

speed and stiffness; (c) high mobility of the rotational DoF; (d) being capable of long components manufacturing. The machine tool will be developed, cooperated with the Second Machine Tool Factory in Qiqihaer, China, by the end of May 2002. The hybrid PKM can substitute for the traditional five-axis machine tool with bridging beam structure.

As mentioned above, the parallel mechanism can manipulate a rigid body in a plane without orientation. Therefore, if a tool is equipped on the moving platform, the parallel mechanism can be used as a two-axis horizontal PKM, which is characterized by high speed and stiffness, as shown in Fig.5.

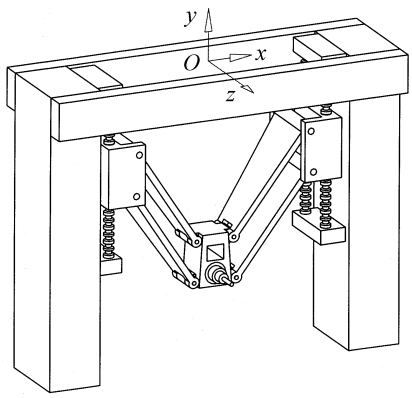

Fig.5 A horizontal two-axis device

3.2 Applications of the 3-DoF Parallel Mechanism

As described in Section 2.2, the advantages of the parallel mechanism are as following: (a) only single DoF joints are used; (b) combining spatial translational and rotational degrees of freedom in a spatial 3-DoF parallel manipulator; (c) high mobility of the rotational DoF (Liu, 2001; Liu et al., 2001)]. As analyzed in (Liu, 2001; Liu et al., 2001), the mobility of such a parallel mechanism can reach its maximum value $135.62°$, and minimum value $62.78°$, the value can be improved if advise the arrangement of the three legs.

For such reason, the parallel mechanism can be applied not only as the manipulating device with three DoFs but also as hybrid machines appending serial wrist and linear joints. Figure 6 shows an example of a device with four axes, which can manipulate a tool with high mobility. A horizontal device based on the parallel mechanism is shown as Fig.7. In these designs, the rotation DoF about $x-$axis is achieved by the parallel mechanism itself, which can reach the mobility $\pm 45°$ within the workspace. If additional movement of the worktable along $z-$axis is equipped on each of these two devices, the device will be an ideal five-axis one. From these devices, we can see that (a) only one-axis wrist joint is serial; (b) the rotation DoF about $x-$axis provide by parallel mechanism is higher, which are different from the existing tripod and hexapod PKMs.

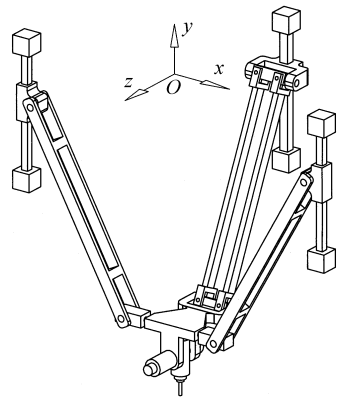

Fig.6 A hybrid device with four axes

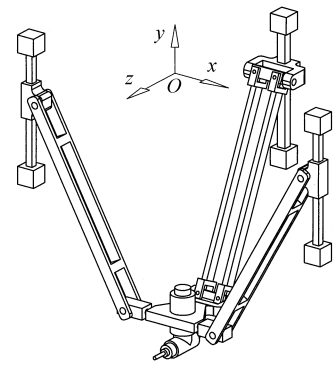

Fig.7 A horizontal hybrid 4-DoF device

4. Conclusions

This paper presents two novel parallel mechanisms and their potential applications. The moving platform of the new two-DoF parallel mechanism has two translational DoFs with the fixed base. The application in the field of PKM can provide high speed, high stiffness, and high mobility devices, which can substitute for the traditional five-axis machine tool with bridging beam structure. The output of the three-DoF parallel mechanism is two translational DoFs and one rotational DoF. The application of such mechanism in industrial world leads to a device manipulating a tool with high stiffness and high dexterity. The results of the paper are very useful for the potential design conceive of parallel mechanisms and the applications.

References

Asada, H. and Kanade, T., 1983, “Desgin of direct-drive mechanical arms”, ASME Journal of Vibration, Acoustics, Stress, and Reliability in Design, Vol.105 (3), pp.312-316.

Bonev, Ilian, 2001, “Delta parallel robot - the story of success”, http://www.parallemic.org/Reviews/Review002p. html.

Ceccarelli, M., 1997, “A new 3 D.O.F. spatial parallel mechanism”, Mechanism and Machine Theory, Vol.32 (8), pp.895-902.

Clavel, R., 1988, “DELTA: a fast robot with parallel geometry”, In 18th Int. Symp. on Industrial Robot, pp. 91-100.

Gao, F., Liu, Xin-Jun, and Gruver, W.A., 1998, “Performance evaluation of two degrees of freedom planar parallel robots”, Mechanisms and Machine Theory, Vol.33 (6), pp.661-668.

Gosselin, C.M. and Angeles, J., 1990, “Singularity analysis of closed loop kinematic chains”, IEEE Trans. on Robotics and Automation, Vol.6, No.3, pp.281-290.

Gosselin, C.M., Lemieux, S. and Merlet, J-P., 1996, “A new architecture of planar three-degrees-of- freedom parallel manipulator”, IEEE Int. Conf. on Robotics and Automation, pp.3738 –3743.

Gough, V. E., 1956, “Contribution to discussion of papers on research in automobile stability, control and tyre performance”, In: Proc Auto Div Inst Mech Eng, pp.392-395.

Hervé, J. M., 1992, “Group mathematics and parallel link mechanisms”, In IMACS/SICE Int. Symp. On Robotics, Mechatronics, and Manufacturing Systems, pp.459-464.

Huang, Z., and Fang, Y., 1996, “Kinematics characteristics of 3-DoF actuated pyramid mechanisms”, Mechanism and Machine Theory, Vol.31 (8), pp.1009-1018.

Hunt, K. H., 1978, “Kinematic geometry of mechanisms”, Oxford: Clarendon Press.

Liu, Xin-Jun, 2001, “Mechanical and kinematics design of parallel robotic mechanisms with less than six degrees of freedom”, Post-Doctoral Research Report, Beijing: Tsinghua University.

Liu, Xin-Jun, et al., 2000a, “Optimum design of 3-DoF spherical parallel manipulators with respect to the conditioning and stiffness indices”, Mechanisms and Machine Theory, Vol.35, pp.1257-1267.

Liu, Xin-Jun, et al., 2000b, “Performance atlases of the workspace for planar 3-DOF parallel manipulators”, Robotica, 18(5), pp.563- 568.

Liu, Xin-Jun, et al., 2001, “On the analysis of a new spatial three degrees of freedom parallel manipulator”, IEEE Transactions on Robotics and Automation, Vol.17, No.6, pp.959-968.

McCloy, D., 1990, “Some comparisons of serial-driven and parallel driven mechanisms”, Robotica, Vol.8, pp.355-362.

Merlet, J.-P., 2000, “Parallel robots”, London: Kluwer Academic Publishers.

Moriwaki, T., 1999, “Survey of R&D Activities Related to Parallel Mechanisms in Japan”, In: C.R. Boer, L. Molinari-Tosatti and K.S. Smith (editors), Parallel Kinematic Machines, Springer-Verlag London Limited, pp.431-440.

Siciliano, B., 1999, “The Tricept robot: inverse kinematics, manipulability analysis and closed- loop direct kinematics algorithm”, Robotica, Vol.17, pp.437-445.

Stewart, D., 1965, “A platform with six degrees of freedom”, In: Proc Inst Mech Eng, London, 180:371-386.

Tonshoff, H.K., Grendel, H. and Kaak, R., 1999, “Structure and characteristics of the hybrid manipulator Georg V”, In: C.R. Boer, L. Molinari- Tosatti and K.S. Smith (editors), Parallel Kinematic Machines, pp.365-376, Springer- Verlag London Limited.

Tsai, L. W., and Stamper, R., 1996, “A parallel manipulator with only translational degrees of freedom”, In: ASME 1996 Design Engineering Technical Conference, 96-DETC-MECH –1152, Irvine, CA.

Tsai, Lung-Wen, 1997, “Multi-degree-of-freedom mechanisms for machine tools and the like”, US Patent US5656905.

Proceedings of the WORKSHOP on
Fundamental Issues and Future Research Directions for Parallel Mechanisms and Manipulators
October 3–4, 2002, Quebec City, Quebec, Canada
Clément M. Gosselin and Imme Ebert-Uphoff, editors

Analysis and Design of a New 6 D.O.F Full Tilting Parallel Mechanism

JONGWON KIM*, JAE CHUL HWANG, JIN SUNG KIM, CORNEL C. IURASCU, FRANK C. PARK, AND YOUNG MAN CHO
School of Mechanical and Aerospace Engineering
Seoul National University
Seoul, Korea
* *jongkim@snu.ac.kr*

Abstract: *We present the analysis and design of a new six degree-of-freedom parallel mechanism, Eclipse-II, which can be used as a basis for general motion simulators. This mechanism allows x, y and z-axis translations and a, b and c-axis rotations. Most significantly, it presents the advantage of enabling continuous 360-degree spinning of the platform. We first describe the computational procedures for the forward and inverse kinematics of the Eclipse-II. Next, the complete singularity analysis is presented for the two cases of end-effector and actuator singularities. Two additional actuators are added to the original mechanism to eliminate both types of singularities within the workspace. Stiffness and workspace analysis are also performed and some practical aspects of the prototype development are introduced.*

1 Introduction

Motion simulators are virtual reality systems that assume the appearance of a real situation by using audio-visual effects and movements of a motion base. Such devices are used for many purposes, e.g., flight and driving simulators to name only a few. The former are used for pilot training by providing the pilot with motions that reflect the state of the aircraft while the later reproduce the actual driving conditions for vehicle design and human factors studies. Broadly speaking a motion simulator consists of an auditory system to generate sound, a visual system to display images, and a motion base system to generate movements as a result of motion cues.

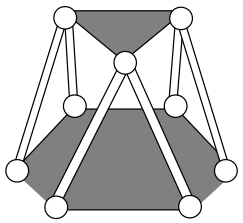

Fig. 1. Structure of Stewart-Gough platform

Most current simulators have adopted the Stewart-Gough platform shown in Fig. 1, as the motion base (see [1], [2], [3] and [4] for a survey on parallel mechanisms and list of references). This platform is a six degree-of-freedom parallel mechanism that permits both translational and rotational motions. The platform can only tilt as much as ±20-30 degrees and large motions, as the 360-degree platform overturn, are impossible. That is, the overturn motion of the aircraft or the 360-degree spin of the roller coaster cannot be reproduced by the Stewart platform.

Some other parallel mechanisms that display relatively large translational or rotational motions are the Delta robot [5] and the spherical parallel mechanism [6, 7]. Yet, the kinematic mobility of these mechanisms is not six and they are used either for positioning or orienting applications. Closer to the spirit of our design is the redundantly actuated Eclipse-I mechanism (see [8] and references cited therein), devised specifically for machining applications. This mechanism has a large workspace and all closed trajectories on five faces of a cube can be traced without breaking contact. Though the spindle can rotate 360 degrees around the fixed z-axis and tilt concomitantly, the tilting angle of the upper plate does not exceed 90 degrees with respect to the vertical. Hence, large overturn motions are impossible and motion simulation applications restricted.

The objective of the present research is to develop a mechanism capable of 360-degree tilting motion of the platform as well as translational motion. Fig. 2 shows the Eclipse-II mechanism and an example of its rotational motion capability. Since there are no limits in the rotational motion, it is possible to design a more realistic and higher fidelity motion simulator. This study emphasizes some of the practical aspects encountered when designing parallel mechanism and raises new and open research issues.

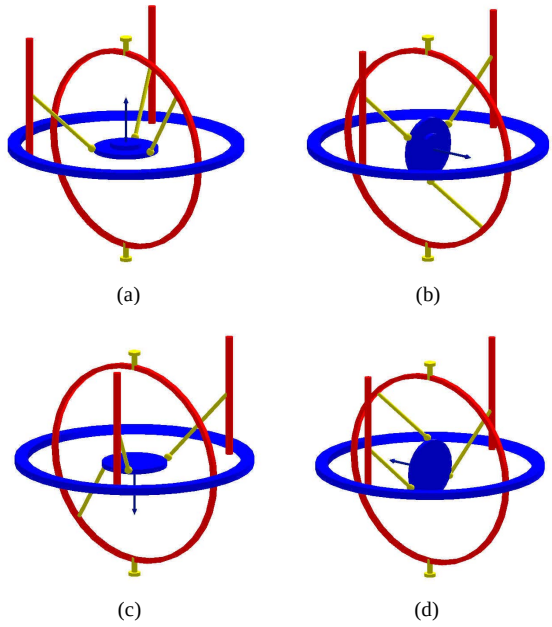

Fig. 2. Eclipse-II mechanism and its 360-degree continuous rotational motions: (a) Rotation angle 0°, (b) Rotation angle 90°, (c) Rotation angle 180°, and (d) Rotation angle 270°.

The paper is organized as follows. In Section 2, we describe the kinematic structure of the Eclipse-II, including the computational procedures for the forward and inverse kinematics. The singularity analysis and a method for eliminating the singularities are presented in Section 3. Section 4 presents the stiffness analysis while Section 5 describes the workspace analysis and presents a structure for maximizing the mechanism's workspace. In Section 6, the prototype Eclipse-II, which is currently being built at Seoul National University is depicted. Finally, some concluding remarks follow in Section 7.

2 Kinematics of the Eclipse-II

This section presents the architecture of the Eclipse II, followed by procedures describing the inverse and forward

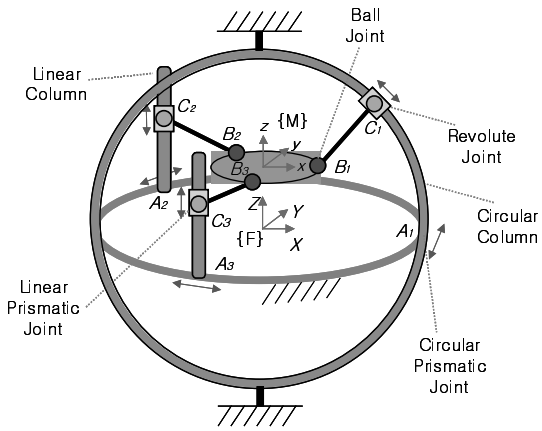

Fig. 3. Architecture of the Eclipse-II mechanism

kinematics. As shown in Fig. 3, the Eclipse-II consists of three *PPRS* serial sub-chains that move independently on a fixed circular guide. Here, *P*, *R*, and *S* denote prismatic, revolute, and spherical joints, respectively. The Eclipse-II has six degrees-of-freedom and six actuated joints. These joints are the three *A* joints (*P*) along the horizontal circular guide, the C_2 and C_3 joints (*P*) on the vertical columns and another *P* joint (C_1) on the vertical circular column. All six actuated joints can be found in Fig. 3, and are indicated by arrows. The connecting links, C_iB_i, are attached to the circular and vertical columns respectively through revolute joints. The other ends of these links are mounted to the moving platform via three, points B_i on the figure, ball-and-socket joints. Mounting one circular column and two linear columns on the circular guide results in the Eclipse-II having a large orientation workspace. Thus, the platform can rotate 360 degrees continuously about the *y*-axis in the moving frame {*M*} (center of the moving platform) and the *Z*-axis in the fixed frame {*F*} (center of the fixed horizontal track), respectively, as shown in Fig. 3. Coordinates and joint convention of the Eclipse-II are described in Fig. 4. The kinematic parameters of the mechanism are as follows: the fixed circular guide radius, r_a, the circular column radius, r_b, the radius of the moving platform, *r*, the length of the

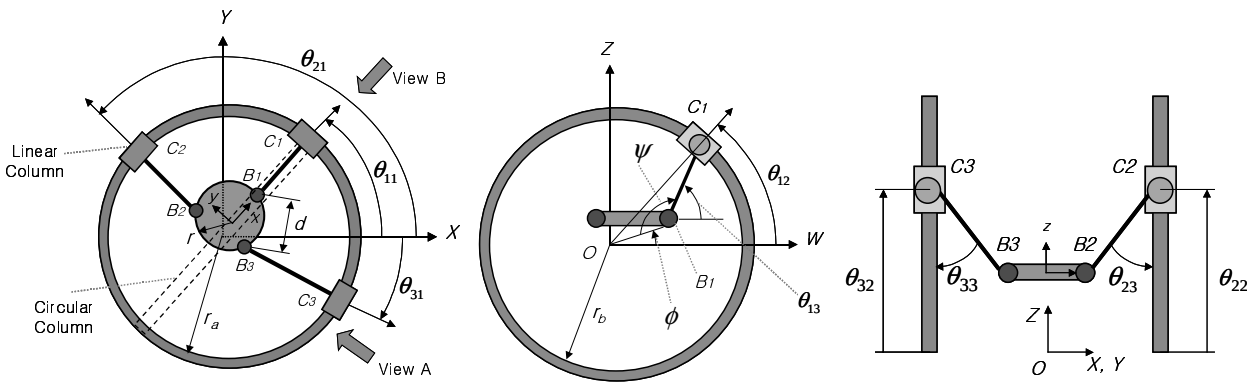

Fig. 4. Coordinate and joint convention: (a) Top view, (b) Side view A, and (c) Side view B

connecting C_iB_i links, L_i, and d, the distance between the spherical joints on the upper platform. The joint values are referred to as θ_{ij}, where i stands generally for the column index and j for the joint level (1 for the fixed circular guide, 2 for the circular and linear columns and 3 for the revolute joints on the same columns). For instance, θ_{32} refers to the prismatic joint on the third linear column.

2.1 Inverse Kinematics

The problem of inverse kinematics is to determine the values of the actuated joints from the position and orientation of the moving frame {M} attached to the moving platform. For the Eclipse-II mechanism, the inverse kinematics can be solved by successively solving the inverse kinematics of each sub-chain. The algorithm for solving the inverse kinematics is as follows:

1. Given the position $\vec{p}$ and orientation R of the moving platform in the fixed {F} frame, find the Cartesian position of the spherical joints:

$$\vec{b_i} = R\,{}^{M}\vec{b_i} + \vec{p} \tag{1}$$

where ${}^{M}\vec{b_i}$ is the vector of the ith spherical joint expressed in the moving frame coordinate. R, $\vec{p}$, and $\vec{b_i}$ are all expressed in the fixed frame coordinates.

2. The circular prismatic joint values (A_i) are calculated from the positions of the spherical joints as follows:

$$\theta_{i1} = \arctan_2(b_{iy}, b_{ix}) \tag{2}$$

where θ_{i1} is the ith circular prismatic joint value, and b_{ix} and b_{iy} are the x and y coordinates of $\vec{b_i}$, respectively.

3. Calculate the revolute joint value, θ_{13} (see Fig. 4b), on the vertical circular column:

$$\theta_{13} = 180° + \phi - \psi \tag{3}$$

where,

$$\phi = \arcsin\left(\frac{b_{1z}}{\left\|\vec{b_1}\right\|}\right)$$

$$\psi = \arccos\left(\frac{\left\|\vec{b_1}\right\|^2 + L_1^2 - r_b^2}{2\cdot\left\|\vec{b_1}\right\|\cdot L_1}\right)$$

and b_{iz} is the z coordinates of $\vec{b_i}$.

4. Determine the prismatic joint values, θ_{12}, on the vertical circular column:

$$\theta_{12} = \arctan_2(a_{1z}, a_{1w}) \tag{4}$$

where,

$$a_{1z} = L_1\cos\theta_{13} + \left\|\vec{b_1}\right\|\cos\phi$$
$$a_{1w} = L_1\sin\theta_{13} + \left\|\vec{b_1}\right\|\sin\phi,$$

5. Find the linear prismatic joint values, θ_{i2} (i = 2, 3), and the position of the revolute joints, θ_{i3} (i = 2, 3), on the vertical linear columns:

$$\theta_{i3} = \arccos\left(\frac{r_b - \sqrt{b_{ix}^2 + b_{iy}^2}}{L_i}\right) \tag{5}$$

$$\theta_{i2} = b_{iz} + L_i\sin\theta_{i3} \tag{6}$$

Note that the solution of θ_{i3} is in the range [0°, 180°].

2.2 Forward Kinematics

The problem of forward kinematics is to determine the position and orientation of the moving frame given the actuated joint values. Similar to many other parallel mechanisms the forward kinematics solution is not unique and finding a closed form solution is a difficult task. If all of the actuated and passive joint values are known, the forward kinematics can be solved from the forward kinematics of each serial sub-chain. Therefore, the first step in the forward kinematics solution is to numerically determine the passive joint values from the actuated joint values by using the kinematics constraint equations.

The following algorithm solves iteratively the forward kinematic using the Newton-Raphson procedure:

1. The constraint equation between the active and passive joint values is generated from the condition that the distances between the ball-and-socket joints of the moving platform are constant:

$$\vec{g}(\vec{\theta}_a, \vec{\theta}_p) = \vec{0} \tag{7}$$

where,

$$\vec{g}(\vec{\theta}_a, \vec{\theta}_p) = \begin{bmatrix} (\vec{b_1} - \vec{b_2})\cdot(\vec{b_1} - \vec{b_2}) - d^2 \\ (\vec{b_2} - \vec{b_3})\cdot(\vec{b_2} - \vec{b_3}) - d^2 \\ (\vec{b_3} - \vec{b_1})\cdot(\vec{b_3} - \vec{b_1}) - d^2 \end{bmatrix}$$

$$\vec{b_i} = \begin{cases} \begin{bmatrix} \cos\theta_{i1}(r_a\cos\theta_{i2} - L_i\cos\theta_{i3}) \\ \sin\theta_{i1}(r_a\cos\theta_{i2} - L_i\cos\theta_{i3}) \\ r_a\sin\theta_{i2} - L_i\sin\theta_{i3} \end{bmatrix} & (i=1) \\ \begin{bmatrix} \cos\theta_{i1}(r_a - L_i\sin\theta_{i3}) \\ \sin\theta_{i1}(r_a - L_i\sin\theta_{i3}) \\ \theta_{i2} - L_i\cos\theta_{i3} \end{bmatrix} & (i=2,3) \end{cases} \tag{8}$$

$$\vec{\theta}_a = [\theta_{11} \quad \theta_{12} \quad \theta_{21} \quad \theta_{22} \quad \theta_{31} \quad \theta_{32}]^T$$
$$\vec{\theta}_p = [\theta_{13} \quad \theta_{23} \quad \theta_{33}]^T$$

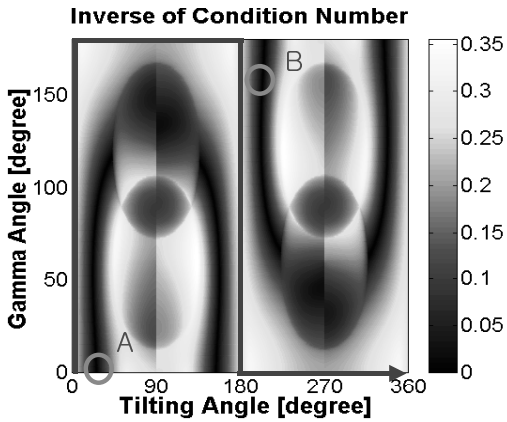

Fig. 5. Condition number plot of the actuator singularity configuration

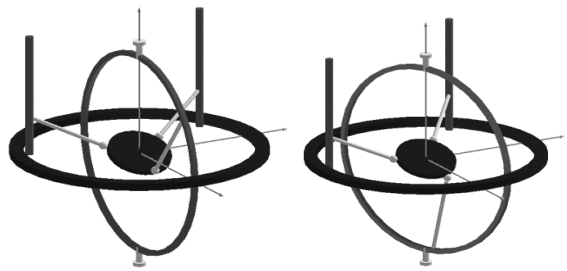

(a) (b)

Fig. 6. Examples of the actuator singular configurations: (a) Point A in Fig. 5, (b) Point B in Fig. 5

2. Given the actuated joint values, find the passive joint ones for which the kinematic constraint equation (7) is satisfied. Because analytic differentiation of (7) is quite simple, a numerical approach like the Newton-Raphson method can be easily applied [9, 10].

3. Determine the position and orientation of the moving frame from the forward kinematics equations for each sub-chain, equation (8), for the Cartesian coordinates of the spherical joints, and (9) and (10), from next section, for the position and orientation of the upper platform.

3 Singularity Analysis

Singularity refers to the configuration in which the number of degrees-of-freedom of the mechanism increases or reduces instantaneously. Since being close to one of the singularities can limit movement, disable control or break the mechanism, the singularity analysis is one of the most significant and critical problems in the design and control of parallel mechanisms.

Singularities of parallel mechanisms can be generally classified into two types: end-effector singularities and actuator singularities [4]. For the Eclipse-II mechanism, these two types of singularities co-exist in the workspace. In this section, the singular configuration of the Eclipse-II

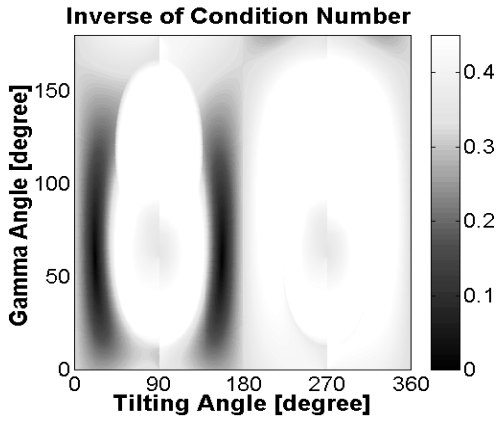

Fig. 7. Condition number plot of the actuator singularity configuration in the redundant case

mechanism and the method for eliminating singularities are described.

The kinematic parameters used for singularity analysis are specified as follows. The radius of the circular guide (r_a), circular column (r_b) and moving platform (r) are, respectively, 1000 mm, 1000 mm, and 300 mm. The lengths of the connecting link in the circular column (L_1) and of the connecting links in the linear column (L_2, L_3) are, respectively, 900 mm and 870 mm.

3.1 Actuator Singularity

At an actuator singularity, the mechanism gains one or more degrees-of-freedom of possible motion, i.e., a self-motion occurs. Actuator singularity configurations can be determined from the Jacobian of the constraint equations. In the case of the Eclipse-II, the Jacobian of the constraint equation can be found by differentiating the constraint equation (7):

$$\frac{\partial g}{\partial \theta_a}\dot{\theta}_a + \frac{\partial g}{\partial \theta_p}\dot{\theta}_p = 0 \tag{9}$$

where $\partial g / \partial \theta_p$ is a 3 × 3 matrix.

If the matrix $\partial g / \partial \theta_p$ is not of full rank, the passive joint values cannot be determined by the given active joint values, and then the mechanism is in one of the actuator singularity configurations.

Finding a closed form solution for the determinant roots (singularities) of the inverse of the Jacobian is a difficult task even when a specialized symbolic computational tool is available [12]. Besides this once the roots have been identified a different and even more challenging task is establishing what roots are within the workspace of the mechanism, i.e., joint values are within admissible motion range and link interferences are avoided. Another possibility for identifying the singularities of a parallel mechanism lies in the use of line geometry and screw theory [13], that is particularly suited for symmetric parallel platforms connected by six serial structures, in which the number of

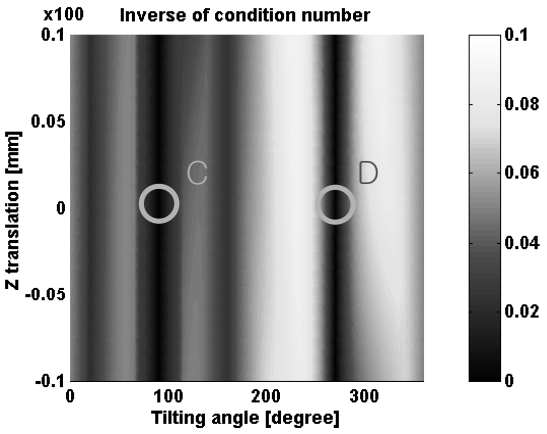

Fig. 8. Condition number plot of the end-effector singularity configuration

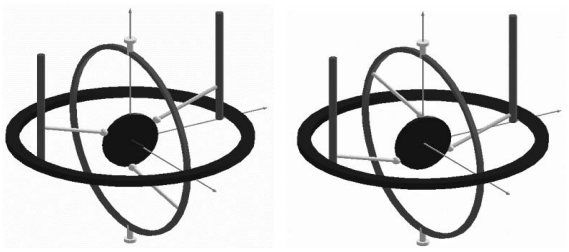

(a) (b)

Fig. 9. Examples of the end-effector singular configuration: (a) Point C in Fig. 8, (b) Point D in Fig. 8.

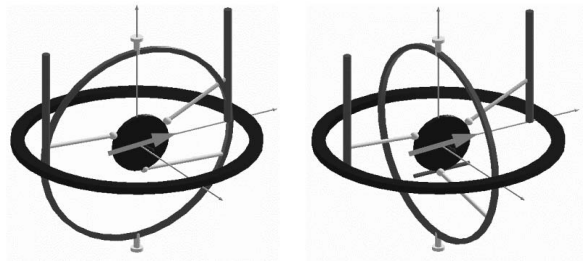

(a) (b)

Fig. 10. *Y*-direction motion of the Eclipse-II: (a) 6 d.o.f Eclipse-II and (b) 6+1 d.o.f Eclipse-II

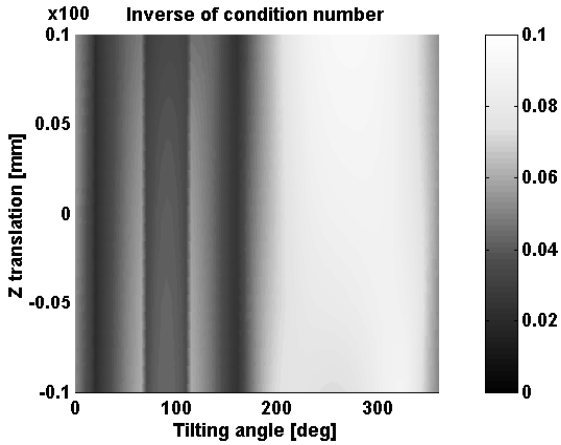

Fig. 11. Condition number plot of the end-effector singularity configuration of the 6+1 d.o.f Eclipse-II

actuators is equal to the kinematic degree of freedom of the platform. A different method, usually considered to be the simplest in the parallel mechanism literature, is to use a brute force algorithm and employ a numerical method that computes the condition number of the Jacobian at all points in the workspace. The condition number of Jacobian is defined as the ratio of the maximum singular value to the minimum singular.

Fig. 5 illustrates the condition number of $\partial g / \partial \theta_p$, while the platform tilts from 0° to 360°. The *x*-axis represents the tilting angle and the *y*-axis represents the rotation angle γ about the *z*-axis of the moving frame. As the condition number becomes larger, the mechanism moves nearer to an actuator singular configuration. For example, in the case of $\gamma = 0$, actuator singularities occur around tilting angles of 25° and 155°, the dark regions right above the tilting angle axis in the left side of the figure.

Fig.6 shows two examples (points A and B in Fig. 5) of actuator singular configurations of the Eclipse-II. In actuator singular configurations, two major problems exist. First, the platform cannot sustain its static equilibrium position in the presence of external force. In this case, the platform seems to have extra degrees of freedom. Second, the forward kinematic solutions are divided into two or more directions. Along the path crossing the actuator singular configuration, there exist multiple forward kinematic solutions with the same active joint values. Hence, there is a chance that the platform moves along an undesired direction.

One method for eliminating the actuator singular configurations is to redundantly actuate the mechanism by adding an actuator to one or more of the passive joints. In the case of Eclipse-II, an additional actuator is added to one revolute joint on one of the linear columns (thus $\partial g / \partial \theta_p$ reduces to a 3 × 2 matrix). Choosing one of the linear columns over the other one would only imply an upside-down turn of the figure. Comparing Fig. 7 with Fig. 5, it may be noted that the condition numbers reduced significantly and the majority of the actuator singular configurations are eliminated.

3.2 End-Effector Singularities

End-effector singularities are configurations in which the moving platform of the mechanism loses one or more degrees-of-freedom of possible motion. In this case the forward kinematic Jacobian loses rank. For Eclipse-II, the algorithm for solving the forward Jacobian is as follows:

1. The position of the moving platform $\vec{b}_c$ is the center of equilateral triangle determined by the three spherical joints.

$$\vec{b}_c = \frac{1}{3}(\vec{b}_1 + \vec{b}_2 + \vec{b}_3) \tag{10}$$

2. The rotational matrix representing the orientation of the moving platform is:

$$R = [R^x \quad R^y \quad R^z] \tag{11}$$

where,

$$R^x = \frac{1}{r}(\vec{b}_1 - \vec{b}_c),$$

$$R^y = \frac{1}{\sqrt{3}r}(\vec{b}_2 - \vec{b}_3),$$

$$R^z = R^x \times R^y.$$

3. In order to obtain the Jacobian matrix, equations (10) and (11) are differentiated:

$$\begin{bmatrix} v \\ w \end{bmatrix} = J\dot{\theta}, \; J \in R^{6\times 9} \tag{12}$$

Elements of the Jacobian, J, are as follows:

$$J_i = \begin{bmatrix} \frac{1}{3}\frac{\partial \vec{b}_i}{\partial \theta_i} \\ R^z \cdot \frac{\partial R^y}{\partial \theta_i} \\ -R^z \cdot \frac{\partial R^x}{\partial \theta_i} \\ -R^x \cdot \frac{\partial R^y}{\partial \theta_i} \end{bmatrix} \; (i = 1, 2, \cdots, 9)$$

where, $\vec{b}_1 = \vec{b}_4 = \vec{b}_7$, $\vec{b}_2 = \vec{b}_5 = \vec{b}_8$, $\vec{b}_3 = \vec{b}_6 = \vec{b}_9$, $\theta_1 = \theta_{11}$, $\theta_2 = \theta_{21}$, $\theta_3 = \theta_{31}$, $\theta_4 = \theta_{12}$, $\theta_5 = \theta_{22}$, $\theta_6 = \theta_{32}$, $\theta_7 = \theta_{13}$, $\theta_8 = \theta_{23}$, $\theta_9 = \theta_{33}$.

3. Equation (12) can be expressed as

$$\begin{bmatrix} v \\ w \end{bmatrix} = J_a\dot{\theta}_a + J_p\dot{\theta}_p \tag{13}$$

From equations (9) and (13), the relationship between the active joint velocity vector and the moving platform velocity vector can be expressed as

$$\begin{bmatrix} v \\ w \end{bmatrix} = J_f\dot{\theta}_a, \qquad J_f \in R^{6\times 6} \tag{14}$$

where, $J_f = J_a - J_p\left(\frac{\partial g}{\partial \theta_p}\right)^{-1}\frac{\partial g}{\partial \theta_a}$

Like the actuator singularities, end-effector singularities are established from the condition number of the forward kinematic Jacobian at all points in the workspace.

The results in Fig. 8 are based on this numerical method, and illustrate the condition number of the forward Jacobian, while Eclipse-II tilts from 0° to 360°. The *x*-axis and *y*-axis in Fig. 8 represent the tilting angle and translation along *Z*-axis in the fixed frame, respectively. The dark regions around 90° and 270° in the figure represent the singular configurations of J_f, which in-effect are end-effector singularities.

Fig. 9 shows two examples of the end-effector singular configurations of the Eclipse-II. The end-effector singular configurations occur in positions where, with the platform tilted at 90° or 270°, one of the spherical joints is located on the *Z*-axis of the fixed frame. If the platform reaches one of the end-effector singular configurations of the Eclipse-II, there exist infinite solutions for the inverse kinematics. With other words there exist infinite possible sets of active joint values for one specific end-effector configuration of the moving platform. Even if it is possible to select only one solution of the inverse kinematics while the platform tilts from 0° to 360°, either the joints have infinite velocity or one linear column and the circular column collide with each other. As a solution to this problem, it is possible to change the solution of the inverse kinematics at an end-effector singular configuration while avoiding columns or roads collisions.

However, there still remains a problem, as shown in Fig. 10(a). At this configuration, the platform cannot translate along the *y*-direction in the moving frame Therefore, an actuator is added to change the position of the spherical joint that is connected to the circular column; that is, one degree-of-freedom is added to the original Eclipse-II. With this addition, the platform can now move along the *y*-direction at an end-effector singular configuration by changing the position of the spherical joint along the linear guide, whereas it is not necessary for the circular column to move [see Fig. 10(b)]. The additional actuator results in the elimination of the end-effector singularity within the workspace of the mechanism. Fig. 11 shows that the condition number of the forward kinematics Jacobian (now $J_f \in R^{6\times 7}$) of Eclipse-II with the extra degree-of-freedom reduces significantly from that one corresponding to Fig. 8, at the tilting angles of 90° and 270°.

4 Stiffness Analysis

Any external forces applied to the end-effector will cause some deflections in the links and joints; if these deflections are significant they can seriously affect the overall accuracy of the mechanism. For this reason, a careful stiffness analysis of the mechanism is an integral part of the design process. Since the rods of the mechanism can be made arbitrarily stiff by increasing their radius, for most purposes it is sufficient to consider only the stiffness of the joints. If the spring constant of each joint is known, then joint stiffness can be analyzed via the virtual work approach (see [8]). The governing equations are

$$dX = CF \tag{15}$$

where $C = JH^{-1}J^T$ is the compliance matrix, and dX, F, J, and H are respectively the generalized displacement of the moving frame, the generalized force applied to the moving frame, the Jacobian of the forward kinematic map, and a diagonal matrix in which the ith entry is the spring constant of

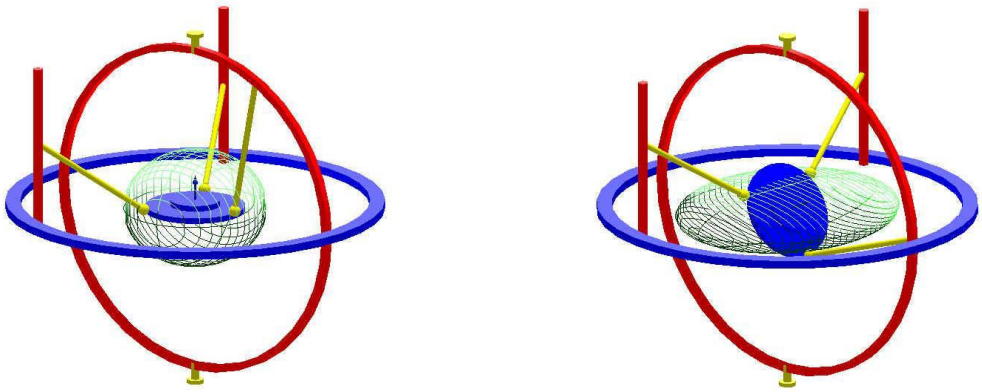

(a) (b)

Fig. 12. Stiffness ellipsoid: (a) Home position, (b) Tilting angle 60°

i^{th} joint. If all the actuators are identical, then the joint spring constant simply acts as a scaling factor for JJ^T.

The stiffness matrix K is defined to be C^{-1} (when it exists). The ellipsoid associated with the stiffness matrix K can be interpreted by finding stiffness ellipsoid of which the major and minor axes are given by the singular values and singular vectors of K, and indicate directions along which the mechanism as a structure is the most and least stiff. Since it is inconsistent to combine quantities with different physical units, we analyze the individual components of the stiffness ellipsoid separately, i.e., given

$$\begin{bmatrix} \vec{f} \\ \vec{m} \end{bmatrix} = \begin{bmatrix} K_{11} & K_{12} \\ K_{21} & K_{22} \end{bmatrix} \begin{bmatrix} \delta\vec{x} \\ \delta\vec{\theta} \end{bmatrix} \tag{16}$$

We examine the ellipsoids for each K_{ij} separately. Figure 12 illustrates the position force stiffness ellipsoid (i.e., the ellipsoid associated with K_{11}) of the Eclipse-II at its home position and tilting angle 60 degree, respectively; as seen from the figure the mechanism is stiffer to displacements in the horizontal direction at tilting angle 60 degree.

5 Workspace Analysis

The workspace of a mechanism is defined to be the set of all positions and orientations reachable by the moving platform. The workspace analysis of the Eclipse-II begins with a description of the moving frame orientation. Many parameterizations exist for describing orientation, e.g., Euler angles, fixed angles, exponential coordinates, etc. Due to the particular architecture of the Eclipse-II, we choose to describe the orientation of the mechanism using the *Z-Y-Z* fixed angles. In terms of these, the rotation matrix is given by

$$R = Rot_Z(\alpha)Rot_Y(\beta)Rot_Z(\gamma) \tag{17}$$

where, α, β and γ are the rotation angles, in succession, about the *Z*-, *Y*-, and *Z*-axis of the fixed frame. When the orientation of the moving platform is described as above, the characteristic of the Eclipse-II mechanism is that the tilting angle β can reach 360 degrees.

The actual Cartesian workspace is restricted by the following physical constraints on the mechanism:

(1) stroke limits of the linear prismatic joints;

(2) interferences between the vertical and/or circular columns;

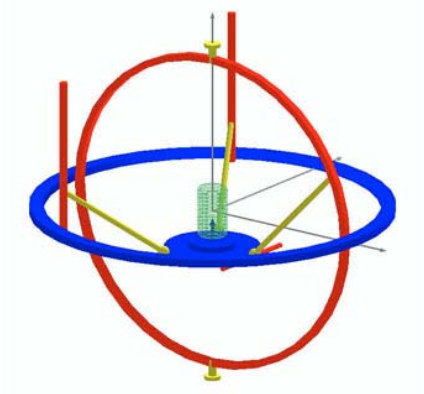

Fig. 13. Original workspace of the Eclipse-II mechanism

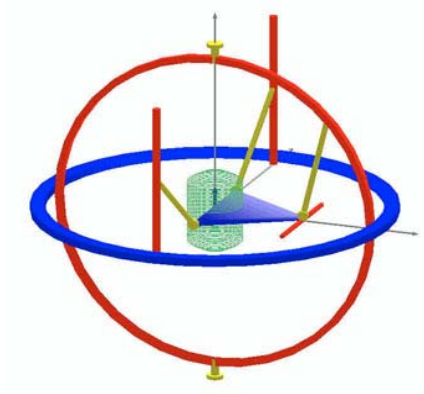

Fig. 14. Enlarged workspace of the Eclipse-II mechanism

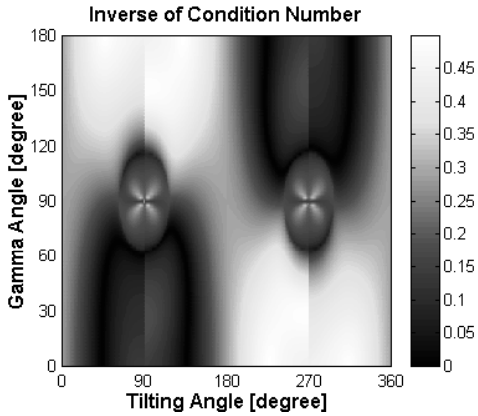

Fig. 15. Condition number plot of the actuator singularity configuration

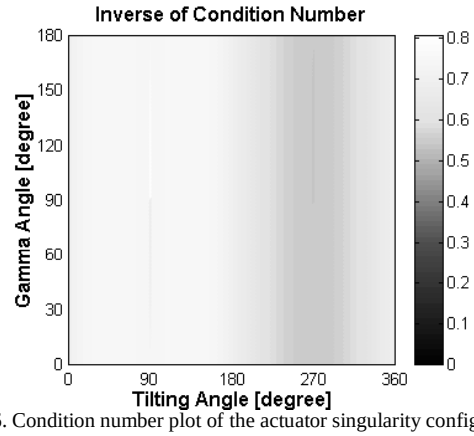

Fig. 16. Condition number plot of the actuator singularity configuration in the redundant case

(3) interferences between columns and rods;

(4) rotation limits of the spherical joints.

From the above restrictions the spherical joint limits are the most dominant. Fig. 13 and Fig. 14 display the workspace of the Eclipse-II original mechanism and modified one, respectively. The rotational limits of the spherical joints are assumed to be ±55 degrees. Under these circumstances the two rotational angles α and β can reach 360 degrees.

The kinematic parameters in Fig. 13 are the same as described in Section 3. The workspace has cylindrical shape, with the radius and height of 90 mm and 340 mm, respectively. For fixed radius of the circular guide and vertical column, the enlarged workspace of the mechanism is presented in Fig. 14. For this last case the spherical joints of the platform are placed at the apexes of an isosceles triangle, while for the original situation the ball and socket joints connect the apexes of an equilateral triangle. The lengths of the base and height of the isosceles triangle are 680 mm and 570 mm, respectively. The other kinematic parameters are the radius of circular guide and circular column, 1000 mm, and the length of the link in the circular column and of the links in the linear column, 700 mm and 840 mm, respectively. By simply modifying the shape of the moving platform and the lengths of the connecting links the radius and height of the workspace increase to 170 mm and 520 mm, respectively.

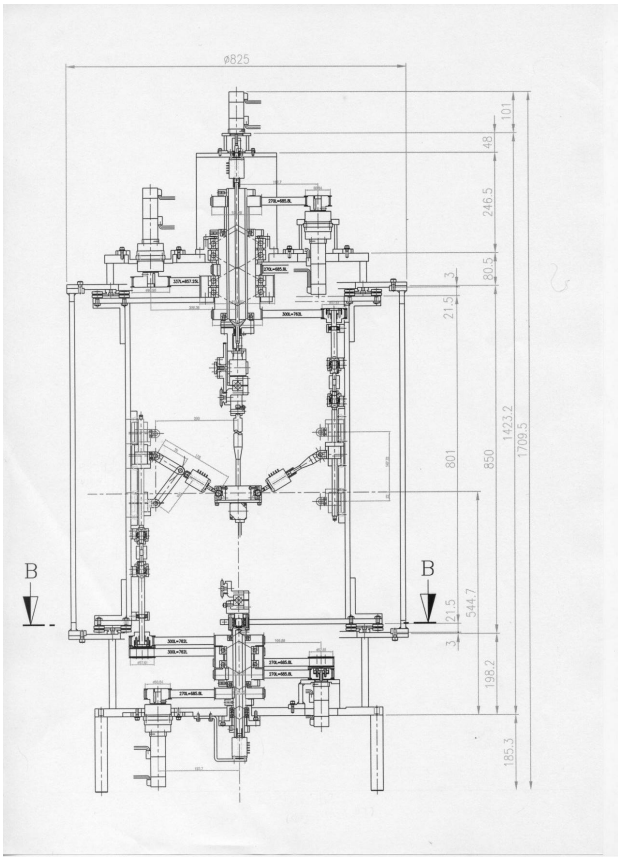

Fig.17. Layout of the prototype Eclipse-II

Because the link lengths and tool frame location are different from the original case we have to perform another singularity analysis of the mechanism. Figures 15 and 16 display the inverse of the condition number for actuator singularity analysis of the new mechanism in non-redundant and redundant actuated case, respectively. While the mechanism presents minor changes in the non-redundant option, as compared to Fig. 5, a substantial improvement is obtained in the redundant case, Fig. 7 and 16. Actuator singularities are not only completely removed but also the condition number for the whole mechanism workspace is closed to 1, i.e., the mechanism can be considered as being generally closed to an isotropic posture [14].

6 Development of the Prototype Eclipse-II

An experimental prototype, with layout presented in Fig. 17 and actuated by servomotors, is currently being developed to verify the motion performances of Eclipse-II architecture as a motion simulator. Table 1 describes specifications of the prototype. The structure consists of a fixed circular guide of radius of 200 mm, one circular column of the same radius and two vertical columns. Each of the columns glides independently on the circular guide and has a prismatic carriage that moves circularly and vertically, respectively. Fixed roads, of lengths of 140 mm for the circular column

and 178 mm for the other linear columns, are attached to the carriages using revolute joints. The connection to the upper platform is realized through spherical joints with angle limits of ±45 degrees. The spherical joints connect the tips of an isosceles triangle of base and height of 96 mm and 114 mm, respectively. The shape of the workspace is a cylinder of diameter and height of 52mm and 88 mm, respectively.

Table 1. Specifications of the prototype

Linear velocity of the platform	12m/min
Linear acceleration of the platform	0.1g
Rotational velocity of the platform	120deg/s
Rotational acceleration of the platform	500deg/s^2
Radius of circular guide	200mm
Rotational limit of spherical joint	±45deg
Workspace size	∅52 x 88 mm

Up to now the major design problem seems to be the wire connection for the encoder and power source of the redundant prismatic joint on the upper platform. Since the motion of the moving platform can reach tilting and turning angles of 360 degrees the electrical wires coil up around the roads and upper platform and jeopardize the motion of the mechanism. The only available technical possibility is to use one or two slip ring connectors on the mechanism frame and upper plate, respectively. A test bench to verify performances of the selected slip ring and evaluate design parameters related to the slip ring is currently being built while carrying the prototype design.

7 Conclusions

This paper deals with the analysis and design of a new redundant parallel mechanism, the Eclipse-II. The unique feature of this mechanism is that continuous 360-degree rotational motion of the platform is possible in addition to the translational motion. Results for the forward and inverse kinematics, the singular configuration analysis, stiffness and workspace evaluation are presented. The original Eclipse-II mechanism shows both end-effector and actuator singular configurations within its workspace. Hence, a linear guide, where one spherical joint moves, is added to the mechanism to eliminate the end-effector singularity. An actuator is also added to one of two passive revolute joints on the vertical columns to eliminate the actuator singularities. For full tilting and turning motions the mechanism display good manipulability and a singularity-free workspace. Currently, a prototype is being build at Seoul National University. Preliminary calculations indicate a maximum velocity of the platform of 12 m/min. and an acceleration of 0.1 g. The prototype Eclipse-II design confirms our practice that parallel mechanisms should be designed according to some task requirements and not as general parallel platforms.

Acknowledgements

This research was supported in part by the National Research Laboratory on Innovative Parallel Mechanism Platforms, and by the Brain Korea 21 program, both at Seoul National University.

References

[1] D. Stewart, "A Platform with six degrees of freedom," *Proc. Inst. Mech. Eng.*, Vol. 180, Part I, No.15, pp.371-386, 1966.

[2] J. S. Freeman, et al., "The Iowa Driving Simulator: An Implementation and Application Overview," *SAE Paper* 950174, 1995.

[3] G. P. Bertollini, et al., "The General Motors Driving Simulator," *SAE Paper 940179*, 1994.

[4] J. -P. Merlet, "Parallel Robots," *Kluwer Academic Publishers*, Dordrecht, Boston, London, 2000.

[5] R. Clavel, "Conception d'un robot parallèle rapide à 4 degrés de liberté," *Ph.D. Thesis*, EPFL, Lausanne, No. 925, 1991.

[6] C. M. Gosselin, E. St-Pierre, "Development and Experimentation of a Fast 3-DOF Camera-Orienting Device," *The Int. J. of Robotics Research*, Vol. 16, No. 5, pp. 619-630, October, 1997.

[7] J. M. Wiitala, M. M. Stanišić, "Design of an Overconstrained and Dextrous Spherical Wrist," *ASME J. of Mechanical Design*, Vol. 122, pp. 347-353, September 2000.

[8] J. Kim, F. C. Park, S. Ryu, J. Kim, J. C. Hwang, C. Park, C. Iurascu, "Design and Analysis of a Redundantly Actuated Parallel Mechanism for Rapid Machining," *IEEE Transactions on Robotics and Automation*, Vol. 17, No. 4, pp. 423-434, 2001.

[9] W. H. Press, S. A. Teukolsky, W. T. Vetterling, B. F. Flannery, "Numerical Recipes in C: The Art of Scientific Computing," *Cambridge University Press*, 1995, Second Edition, chapter 9.

[10] The MathWorks Inc., "Optimization Toolbox User's Guide," 1993.

[11] F. C. Park, J. W. Kim, "Singularity Analysis of Closed Kinematic Chains," *ASME J. of Mechanical Design*, Vol.121, pp.32-38, 1999.

[12] St. -O. B. Mayer, C. M. Gosselin, "Singularity Analysis and Representation of Spatial Six DOF Parallel Mechanisms," *Recent Advances in Robot Kinematics*, in J. Lenarčič and V. Parenti-Castelli, Editors, Kluwer, pp. 389-398, 1996.

[13] J. -P. Merlet, "Singular Configurations of Parallel Manipulators and Grassmann Geometry," The *Int. J. of Robotics Research*, Vol. 8, No. 5, pp. 45-56, October 1989.

[14] J. Angeles, "The Design of Isotropic Manipulator Architectures in the Presence of Redundancies," *The Int. J. Robotics Research*, Vol. 11, No. 3, pp. 196-201, 1992.

Proceedings of the WORKSHOP on
Fundamental Issues and Future Research Directions for Parallel Mechanisms and Manipulators
October 3–4, 2002, Quebec City, Quebec, Canada
Clément M. Gosselin and Imme Ebert-Uphoff, editors

Design of a Parallel Wire-Driven Manipulator for Wind Tunnels

PASCAL LAFOURCADE
DCSD ONERA-CERT
B.P. 4025, 2 avenue Edouard Belin,
31055 Toulouse cedex 4, France
pascal.lafourcade@cert.fr

MICHEL LLIBRE
DCSD ONERA-CERT
B.P. 4025, 2 avenue Edouard Belin,
31055 Toulouse cedex 4, France
michel.llibre@cert.fr

CLAUDE REBOULET
DCSD ONERA-CERT
B.P. 4025, 2 avenue Edouard Belin,
31055 Toulouse cedex 4, France
claude.reboulet@cert.fr

Abstract: *This paper deals with the design of a 6 d-o-f wire-driven manipulator. In the introduction we present its application field, why we chose a wire-driven manipulator and a short state of the art. In the second part we develop a geometrical approach for the architecture design. In the third part, we present a kinematic and dynamic model of the manipulator which is used to compute the manipulator workspace and we introduce the control principles.*

1 INTRODUCTION

1.1 SACSO goals

Our research on wire-driven manipulators takes place within the SACSO[1] project. This project deals with the study of aircraft behavior and more precisely with the identification of its aerodynamic coefficients. The study of aircraft flight has been a big part of ONERA research since its creation.

The free flight simulation concept in wind tunnels through an active suspension comes from the most recent robotic researches outcomes, and more specifically from the improvement in parallel manipulator and force control. Our experience in this domain at ONERA leads us to the conception of an active suspension to simulate free flight.

This suspension sustains a model-scale in a wind tunnel and has to reproduce propulsion forces and to create virtual mass and inertia in order to respect the similitude coefficients.

The suspension must have displacement capabilities for the model-scale installation and for standard tests purposes. It must have a high bandwidth force control to simulate the propulsion effects and to confer an artificial inertia to the model-scale. These two control capabilities have to be ensured along 6 d.o.f. to allow free flight. The suspension should not disturb the streamline flow and must be implemented in existing wind tunnels with little modification. Series type robot structures are too heavy and cumbersome to cope with theses constraints. For these reasons we choose a wire-driven suspension manipulator.

1.2 Wire-driven manipulator description

Wire-driven (or tendon-driven) mechanisms are mechanisms using wires (or tendons) to transmit effort or motion (figure 1[2]). We are not interested here in those using wires in addition to rigid links , which are generally serial type manipulators. The problems (especially the kinematics ones) they raise are quite different [1]. We are interested in the ones using exclusively wires. They are parallel mechanisms [2] [3]. Verhoven and Hiller speak about "Tendon-driven Stewart Platform" [4].

A first kind of application for wire-driven manipulators is robot cranes, e. g. in shipbuilding [5] [6]. These manipulators can be classified in the Incompletely Restrained Positioning Mechanism (IRPM) class. The number of wires is equal to the number of d.o.f.. A second kind of application is very fast manipulators. The FALCON-7 [7] and the WARP manipulator [8] belong to this application field. They can be classified in the Completely Restrained Positioning Mechanism (CRPM) class when

[1] Suspension ACtive pour SOufflerie

[2] these two figures come from Verhoeven web site

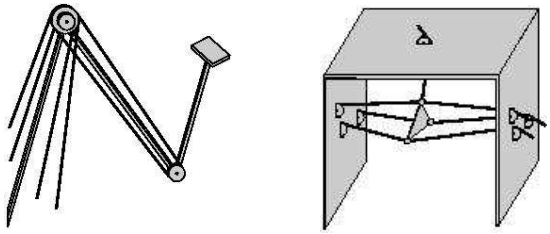

(a) Example of a tendon-driven serial manipulator

(b) Example of a tendon-driven Stewart Platform

Figure 1: The two types of wire-driven mechanisms

they use 7 wires or in the Redundantly Restrained Positioning Mechanism (RRPM) class when they use 8 wires [9] and more. With CRPM or RRPM, an another type of application is the virtual reality like virtual sport training [10].

2 GEOMETRICAL CONCEPTION OF A WIRE-DRIVEN MANIPULATOR

2.1 Introducing the method

We propose a geometrical approach to design wire-driven manipulators which use the designer experience. Although it is a very old method, it is the quickest one to obtain a preliminary architecture. In spite of those advantages, this approach does not seem to be used in this domain.

The fundamental principle of this approach lies in the fact that a tendon can only exert traction forces along its own direction.

In the following paragraphs we use this approach to design a manipulator whose workspace (according to Verhoeven definition of workspace [11]) is compatible with the application requirements.

We must keep in mind that the function of the wire driven manipulator is to sustain an aircraft model-scale in a wind tunnel. That implies that motion and clutter volumes are cylindrical.

In a first phase we design a 7-wire manipulator, but to increase substantially the workspace, we design, in a second phase, a 9-wire manipulator.

2.2 Application to the design of the parallel wire-driven manipulator SACSO-7

This first manipulator is a 7-wire parallel wire-driven mechanism. The mobile part is driven by seven wires anchored on it. They come from actuators and pass through pulleys, both are fixed on the stationary base frame.

Fixing the position and the orientation of a solid in a 3D coordinate frame requires the control of only three of its points which could be the wire anchorages on the mobile part. In our architecture, these three anchorages are the apexes of an isosceles triangle which is materialized by a T-cross (figure 2). The longitudinal rod controls the pitch and the course while the lateral one controls the roll[3]. Logically, the same symmetrical plans are taken for the aircraft model-scale and the suspension (particularly (O_x, O_z)). It gives the T-cross orientation in regards with the model-scale, and by extension with the wind tunnel and so with the stationary base frame. Positionning seven wires symmetrically on a T-cross at three points for a working solution does not offer a lot of possibilities. It is clear that four wires and more linked at the same anchorage point do not give more control than three. So, there are two possibilities : 1-3-3 and 3-2-2 (figure 2). Solution 1-3-3 does not work because an arbitrary torque around O_y cannot be made (torque can be made in only one way). It consequently leaves only one possibility: 3-2-2.

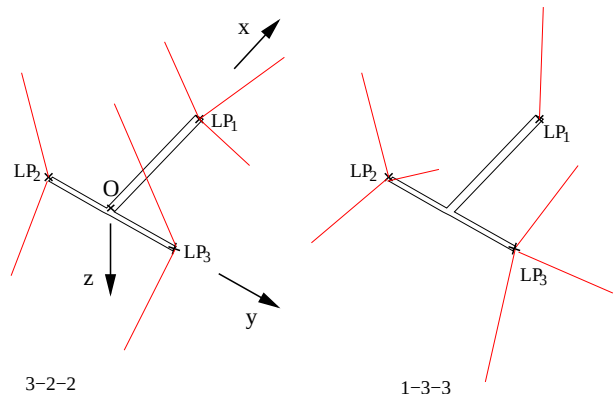

Figure 2: Only two possibilities for 7 wires linked on three points with no more than 3 wires on the same point

Wires linked on LP1 will be called front wires and those linked on LP2 and LP3 will be called back wires.

Now, pulleys locations on the stationary base frame have to be chosen. Tacpoint between wires and pulleys are approximated to fixed point. A wire can only pull. So, with a planar reasoning, LP1 must stay in the triangle described by the three front wire tacpoints on the base frame. To have the bigger surface, an equilateral triangle is chosen. In the case of the back wires, which transmit roll motion or effort (around O_x) the problem is different. Planar (plan (O_y, O_z)) reasoning and sketches are used to design and to study different solutions.

There are four back wires. The evident solution is a square (always the maximal surface for a quadrilateral in a circle). Planar translation motions are limited in this square. Figure 3 shows roll motion abilities. With this particular pose, wires 2 and 3 are aligned and only wires 1 and 4 can exert torques, and only in the negative direction. It is a singular pose, and if the roll increases beyond that limit, all wires would generate torques in negative direction. There would be one d.o.f. left.

[3] since the application is in the field of aeronautics, we use aeronautical references and angles

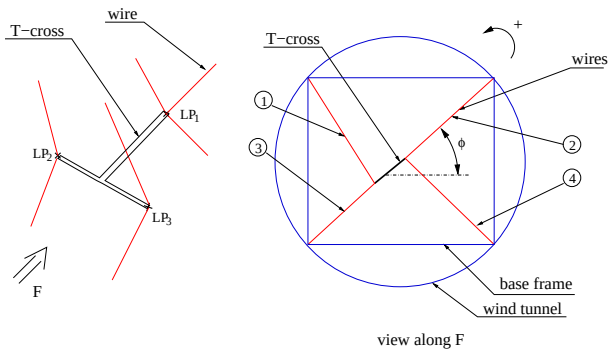

Figure 3: The square solution

Another solution, increasing roll abilities, is the diamond as shown on figure 4. Sketches show that the loss in O_Y motion abilities is greater than the gain in roll abilities. The maximum motion along O_Y is reached when wires 1 and 3 (or 2 and 4 as shown on the sketch) are aligned.

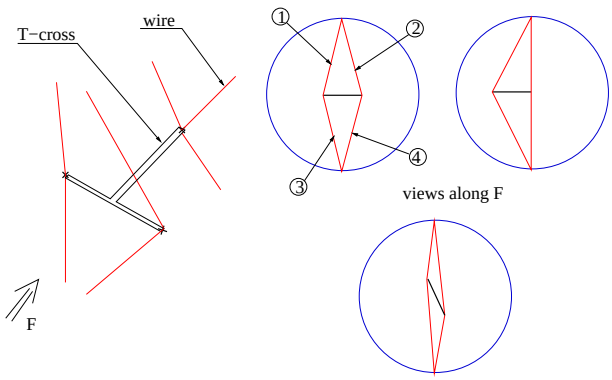

Figure 4: The diamond solution

To get the roll abilities of the diamond solution without its disadvantages, the principle of a "pendulum" is kept and an anchorage point is added. To respect symmetry, the point is added on the longitudinal rod. Tacpoints form an equilateral triangle on the stationary base frame. So the roll abilities are the same as those with the diamond solution and the planar motion surface is the triangle.

Pendulum solution is chosen, particularly for its roll abilities. As the (O_X, O_Z) reflective symmetry must be respected, there are two possibilities to merge the front wires solution and the back wires solution. They are shown on figure 6(a) and 6(b).

Starting with given roll and translation along O_Y specifications, we study geometrically the other motions to obtain the complete workspace. Top views and lateral views figures permit to study abilities in pitch motion (around O_y) and course motion (around O_z). It is not difficult to detect singular angular pose if the T-cross stays at the center of the base frame like it is shown

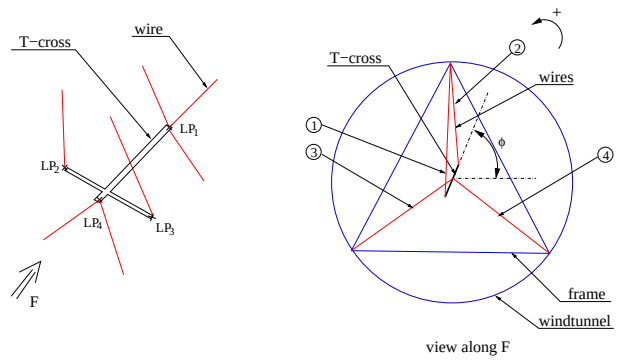

Figure 5: The pendulum solution

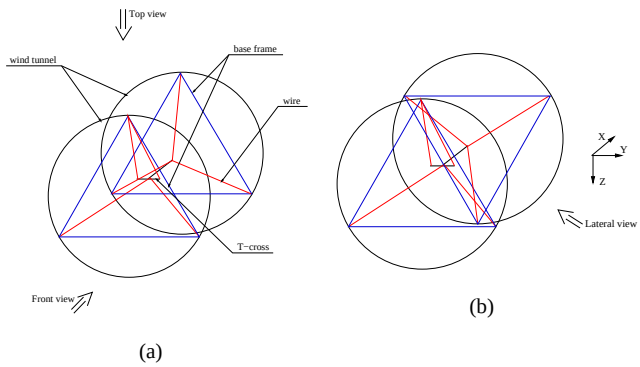

Figure 6: Two possibilities for SACSO-7

on figures 7(a) and 7(b). We can see that angular abilities decrease with the length of the stationary base frame, contrary to translations abilities along O_X which increase.

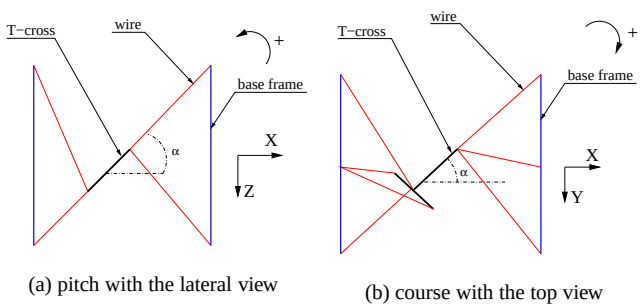

Figure 7: Singular angle pose at the center of the base frame

If the T-cross is not at the center, the analysis is more complex. For example, in figure 8(a), two wires (not really, some are coincident on the sketch) generate positive torque (around O_y), and two other ones generate negative torque; this pose is inside the workspace. On figure 8(c), all wires generate negative torque. This pose is outside the workspace. On figure 8(b),

one wire generate positive torque and the three others generate negative torque. It could works, but certainly badly, and T rod goes through a singular pose to reach it. It is certainly out of the workspace.

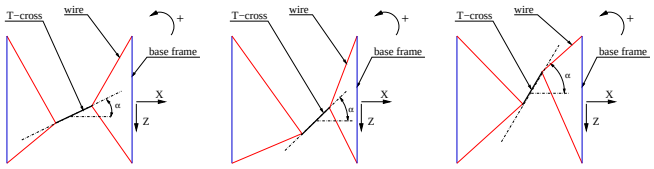

(a) case one, it works

(b) case two, it should not work

(c) case three, it does not work

Figure 8: graphical study of pitch limitation, mobile part not at the center of the base frame

Same type of analysis can be made for course abilities.

2.3 Operational workspace

Finally, with some geometrical considerations, we have got an idea of the workspace of the robot. In the two cases (6(a) & 6(b)) the 3D workspace in translation is not smooth enough. It is dangerous to ride near singularity and corner. Actually, the manipulator is not commanded in position and the aircraft model-scale behavior is not well monitored. So we decide to limit the workspace to a cylindrical base cylinder, like it is showed in figure 9. It is the same cylinder in both cases.

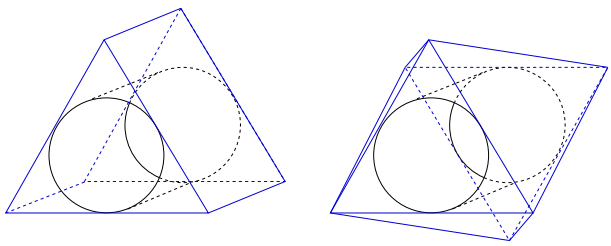

Figure 9: workspace is restricted to a cylinder

The problem is that this volume (and so the workspace) is too little. It is directly connected to the form described by the tacpoints on the stationary base frame. The surface of the circle inscribed in a square, itself inscribed in a circle, is twice bigger than the surface of the circle inscribed in a triangle, itself inscribed in the same external circle (figure 10). Next, we propose solutions with nine wires whose tacpoints describe two squares.

2.4 An evolution : SACSO-9

To design this RRPM[4] manipulator, we have kept the same concept as SACSO-7, with two square frames instead of triangular

[4]Redundantly Restrained Positioning Mechanism

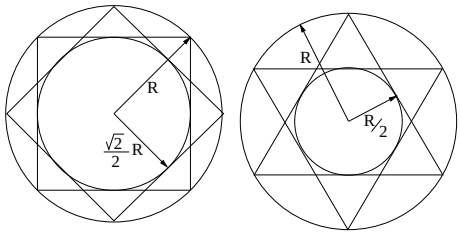

Figure 10: comparison of surfaces inside square or triangle

frames. So, we have kept the same rod, and have just added one front wire and two back wires.

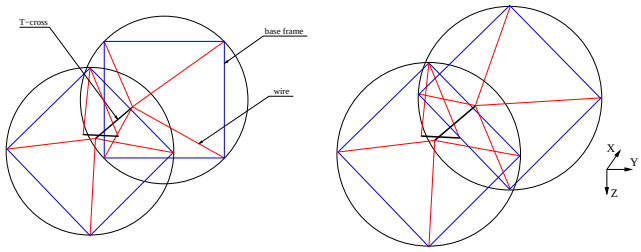

(a) solution 1

(b) solution 2

Figure 11: Two solutions for the 9-wire manipulator

Figure 11 shows two solutions : the one presented on figure 11(b) is not acceptable because there is a contact between front wires and wings. It lets solution figure 11(a). An OPENGL based visualization was developed. Figure 12 shows two view of the whole suspension.

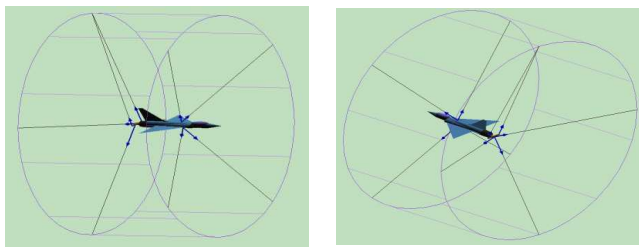

(a) 3/4 front view

(b) 3/4 back view

Figure 12: The manipulator with the model-scale

The same design principle conducts almost to the same rotational motion workspace. Its 3d workspace in translation are shown on figure 13. We again limit this workspace to the inside of the cylinder.

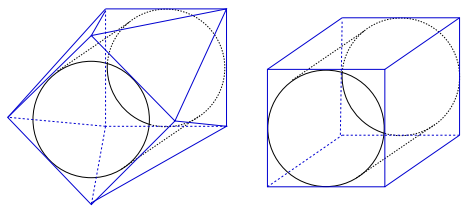

Figure 13: simplified figure of SACSO-9 displacement workspace

2.5 Conclusion on the method

The geometrical approach presented in this chapter gives just some ways and ideas for a first design of the manipulator. Of course, to obtain the complete workspace, it is necessary to use numerical method : including the study of the Jacobian and the study of wires tensions. In the following, we expose our modelisation and we explain our method to calculate wire tension and which is then applied to SACSO-7 and SACSO-9.

3 MODELISATION OF THE WIRE-DRIVEN MANIPULATORS

As shown on figure 14, let us note A_i the first contact points between wire and pulley on the fixed structure, B_i the anchoring points with the support(ed) model, $\vec{L}_i = \overrightarrow{B_iA_i}$, $l_i = \left\|\vec{L}_i\right\|$, $\vec{u}_i = \frac{1}{l_i}\vec{L}_i$ and t_i the tension in the cable i which exerts a force $\vec{T}_i = t_i\vec{u}_i$ on the support. G is the center of gravity of the scale model and $\vec{r}_i = \overrightarrow{GBi}$.

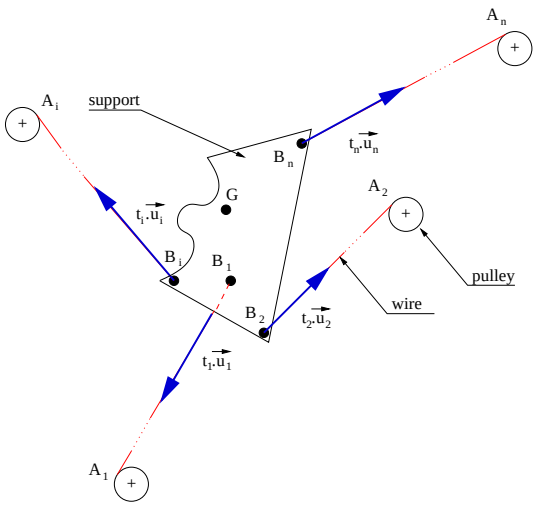

Figure 14: Sketch of a general parallel wire-driven mechanism

As far as notation is concerned, $\vec{V}$ is used for three components vectors like forces, torques, velocities, and $\mathbf{V}$ for other vectors (six components vectors) and matrices.

3.1 Kinematic and Static

We have $\dot{l}_i = \vec{u}_i \cdot \vec{V}_{B_i}$ and $\vec{V}_{B_i} = \vec{V}_G + \vec{\Omega} \times \vec{r}_i$ where $\vec{V}_G$ and $\vec{\Omega}$ are respectively the support translation and rotation velocities, so $\dot{l}_i = \vec{u}_i \cdot \vec{V}_G + \vec{u}_i \cdot \left(\vec{\Omega} \times \vec{r}_i\right)$. Permuting the triple scalar product yields to the well known form of the parallel manipulator Jacobian :

$$\dot{\mathbf{l}} = \mathbf{P}^{\mathsf{T}}\mathbf{W} \tag{1}$$

where $\dot{\mathbf{l}}$ is the l_i-component vector, $\mathbf{W}$ is the 6-component vector $\begin{pmatrix} \vec{V}_G \\ \vec{\Omega} \end{pmatrix}$ and $\mathbf{P}$ is given by :

$$\mathbf{P} = \begin{pmatrix} \vec{u}_1 & \cdots & \vec{u}_n \\ \vec{r}_1 \times \vec{u}_1 & \cdots & \vec{r}_n \times \vec{u}_n \end{pmatrix}$$

Let us note $\overrightarrow{F}$ the resultant force and $\overrightarrow{M_G}$ the resulting moment in G of the $t_i\vec{u}_i$. We have $\overrightarrow{F} = \sum_i t_i\vec{u}_i$ and $\overrightarrow{M_G} = \sum_i \vec{r}_i \times t_i\vec{u}_i$, so :

$$\mathbf{F} = \mathbf{PT} \tag{2}$$

where $\mathbf{T}$ is the t_i components vector and $\mathbf{F}$ is the 6 components vector $\begin{pmatrix} \overrightarrow{F} \\ \overrightarrow{M_G} \end{pmatrix}$.

Let us note $\mathbf{T_{eff}} = \mathbf{P}^{+}\mathbf{F}$ the minimal norm solution of (2), where $\mathbf{P}^{+}$ is the Moore-Penrose[5] inverse of $\mathbf{P}$, and $\mathbf{T_{nul}}$ a vector belonging to the null space $\mathcal{N}(\mathbf{P})$ of $\mathbf{P}$.

We can write the general solution in the form :

$$\mathbf{T} = \mathbf{T_{eff}} + \mathbf{T_{nul}} \tag{3}$$

Note that (1), (2), (3) and $\mathbf{P}.\mathbf{T_{nul}} = 0$ imply :

$$\mathbf{W} = \left(\mathbf{PP}^{\mathsf{T}}\right)^{-1}\mathbf{P}\dot{\mathbf{l}} \tag{4}$$

The model-scale speeds are obtained according to the wires speeds by the least squares inverse.

To maintain a minimal tension in the wires, we propose the following expression for $\mathbf{T_{nul}}$: $\mathbf{T_{nul}} = (\mathbf{I}_{n\times n} - \mathbf{P}^{+}\mathbf{P})\mathbf{T_{des}}$ where $\mathbf{T_{des}}$ is a desired value of $\mathbf{T}$ which is used as a control variable.

3.2 Dynamics

The dynamic model of the motors is written as :

$$\mathbf{T}_m + \mathbf{T}_f - \mathbf{T} = \mathbf{m}_m\ddot{\mathbf{l}} \tag{5}$$

where $\mathbf{T}_m$ is the vector of the driving forces, $\mathbf{T}_f$ is the vector of the friction forces and $\mathbf{m}_m$ is a diagonal matrix of motors inertias. The dynamic model of the scale-model is written as :

$$\frac{d}{dt}(\mathbf{A}_G\mathbf{W}) = \mathbf{F}_G + \mathbf{F}_A + \mathbf{F} \tag{6}$$

[5] $\mathbf{P}^{+} = \mathbf{P}^{\mathsf{T}}(\mathbf{PP}^{\mathsf{T}})^{-1}$

where $\mathbf{A}_G = \begin{pmatrix} m_A\mathbf{I}_{3\times3} & \mathbf{0}_{3\times3} \\ \mathbf{0}_{3\times3} & \mathbf{J}_G \end{pmatrix}$ is the matrix of inertia of the model-scale at its center of gravity, $\mathbf{F}_G = \begin{pmatrix} m_A\vec{g} \\ 0 \end{pmatrix}$ the torque of the forces of gravity, $\mathbf{F}_A$ the torque of the aerodynamic forces and $\mathbf{F}$ the torque exerted by the support. These two equations are connected by the relations (1) and (2).

The inertia of the engines seen by the model is obtained immediately by expressing the kinetic energy of the whole system according to the speeds model : $e = \frac{1}{2}\left(\mathbf{W}^\mathsf{T}\mathbf{A}_G\mathbf{W} + \dot{\mathbf{l}}^\mathsf{T}\mathbf{m}_m\dot{\mathbf{l}}\right)$. By using relation (1) we obtain :

$$\mathbf{A}_{Gtot} = \mathbf{A}_G + \mathbf{P}\mathbf{m}_m\mathbf{P}^\mathsf{T}$$

But to make the synthesis of the driving forces control correctors, we must estimate the inertia of the scale model seen by the motors. For that, we use relation (4). So :

$$\mathbf{m}_{mtot} = \mathbf{m}_m + \mathbf{P}^\mathsf{T}\left(\mathbf{P}\mathbf{P}^\mathsf{T}\right)^{-1}\mathbf{A}_G\left(\mathbf{P}\mathbf{P}^\mathsf{T}\right)^{-1}\mathbf{P}$$

4 WORKSPACE EXPLORATION WITH WIRE TENSIONS

4.1 Wire tension calculus

In order to get a satisfactory behavior of the mechanism and the actuators, we chose a desired tension in wires $\mathbf{T}_{des}$. For preliminary studies, the scheme to calculate tension is very simple. It consists in minimizing $\|\mathbf{T} - \mathbf{T_{des}}\|^2$ while respecting (2) and $min(\mathbf{T}) > t_{min}$. The proposed algorithm is :

Evaluating position
calculating $\mathbf{P}$
$\mathbf{T_{eff}} = \mathbf{P}^+\mathbf{F}$
$\mathbf{T_{nul}} = (\mathbf{I}_{n\times n} - \mathbf{P}^+\mathbf{P})\mathbf{T}_{des}$
$\mathbf{T} = \mathbf{T} + \mathbf{T}_{null}$
if $min(\mathbf{T}) < t_{min}$ then
  $\mathbf{T} = \mathbf{T} + \lambda\mathbf{T}_{null}$
  with $\lambda \mid min(\mathbf{T}) = t_{min}$
end if

4.2 Workspace capacities in displacement along O_Y and roll

Because of the complexity of the worspace (3 d.o.f. in displacement and 3 d.o.f. in orientation), it is quite difficult to represent it (so the sketches used in subsection 2.2). The calculus of the wire tensions for a given load will help us geting a more precise definition of this workspace.

For example, we studied in subsection 2.2 three types of 7-wires manipulators. We saw with a graphical approach that diamond and pendulum are better than square for roll motions, but diamond is quite bad in displacement along O_Y. We proposed section 2.4 the 9-wires manipulator SACSO-9, equal in roll capacities with pendulum but better in displacement along O_Y.

To confirm those feelings, we have calculated wires tensions during displacement along O_Y with other pose parameters equal to zero, and wires tensions during roll rotation with another parameters equal to zero[6]. The calculation scheme used is the one presented in subsection 4.1, with $t_{min} = 20N$ and $\mathbf{T}_{des} = \begin{pmatrix} t_{des} \\ \vdots \\ t_{des} \end{pmatrix}$, $t_{des} = 100N$. The load is equal to the weight of the model-scale, $50N$ and the drag, $10N$. The maximal tension in wires is $240N$. Dimensions of the T-cross are $0.6m \times 0.16m$ and the dimensions of the stationary base frame are $\phi = 3m \times L = 1.5m$.

Wires tensions along O_Y displacement are shown on figures 15 to 18, and wires tensions along roll rotation on figures 19 to 22. Lines with little circles[7] are for front wires and lines with little triangles[8] are for back wires.

Figures 15 to 18 confirm that roll abilities of the square solution ($\simeq \pm45^o$) is smaller than roll abilities of the other solution ($\simeq \pm90^o$). For tranlation abilities along O_Y , figures 19 to 22 show there are smaller in case of square solution, compared to the case of SACSO-9, despite the fact that back wires are linked on a similar square in both case. This is because front wires are linked on a triangle in one case and on a square in the other case.

5 CONCLUSION AND PERSPECTIVES

The work done in the frame of the SACSO project will lead to the build-up of a prototype of the wire-driven manipulator by the end of 2002. We already tested the control principles on a one degree of freedom setup, in which both tendons were force controlled (figure 23). We are now working, in a theoretical way, on an increase of the workspace of the manipulator through an optimization process and on the management of the multiple redundancies.

References

[1] Y. J. Ou and L.-W. Tsai. Theory of isotropic transmission for tendon-driven manipulators. In *Robotics: Kinematics, Dynamics and Control*, pages 53–61, Minneapolis, USA, 1994. ASME.

[2] A. Ming and T. Higuchi. Study on multiple degree-of-freedom positioning mechanism using wire-concept, design and control (part 1). *Intl. J. of the Japan Society for Precision*, 28(2):1331–138, juin 1994.

[3] A. Ming and T. Higuchi. Study on multiple degree-of-freedom positioning mechanism using wire-concept, part 2, development of a planar completely restrained position-

[6] the zero is where the middle of the T-cross is at the middle of the cylinder
[7] red
[8] green

ing mechanism. *Intl. J. of the Japan Society for Precision*, 28(3):235–242, septembre 1994.

[4] R. Verhoeven and M. Hiller. Estimating the controlable workspace of tendon-based stewart platforms. In *Proc. 7th Int. Symposium on Advances in Robot Kinematics"*, pages 277–284, 2000.

[5] J. Albus, R. Bostelman, and N. Dagalakis. The nist robocrane. *J. of Robotic Systems*, 1993.

[6] N. G. Dagalakis, J. S. Albus, B.-L. Wang, J. Unger, and J. D. Lee. Stiffness study of a parallel link robot crane for shipbuilding applications. *ASME Journal of Offshore Mechanics and Arctic Engineering*, pages 183–193, 1989.

[7] S. Kawamura, H. Kino, and C. Won. Hight-speed manipulation by using parallel wire-driven robots. *Robotica*, 18:13–21, 2000.

[8] K. Maeda, S. Tadokoro, T. Takamori, M. Hiller, and R. Verhoeven. On design of a redundant wire-driven parallel robot warp manipulator. In *International Conference on Robotics & Automation*, pages 895–900. IEEE, Mai 1999.

[9] S. Tadokoro, S. Nishioka, T. Takamori, and K. Maeda. On fundamental design of wire configurations of wire driven parallel manipulators with redundancy. In *Proceedings of Japan-U.S.A. Symposium on Flexible Automation*, volume 1, pages 151–158, 1996. Boston, U.S.A.

[10] T. Morizono, K. Kurahashi, and S. Kawamura. Realization of a virtual sports training system with parallel wire mechanism. In *Proc. of the 1997 IEEE International Conference on Robotics and Automation*, pages 3025–3030, Albuquerque, New Mexico, April 1997. IEEE.

[11] R. Verhoeven, M. Hiller, and S. Tadokoro. Worspace, stiffness, singularities and classification of tendon-driven stewart platforms. In *Proc. 6th Int. Symposium on Advances in Robot Kinematics*, pages 105–114, Strobl/Salzburg, Austria, 29 juin-4 juillet 1998.

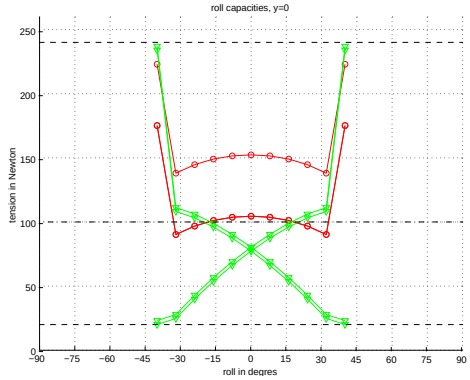

Figure 15: Square solution (figure 3). It is seen that roll max is under 45°

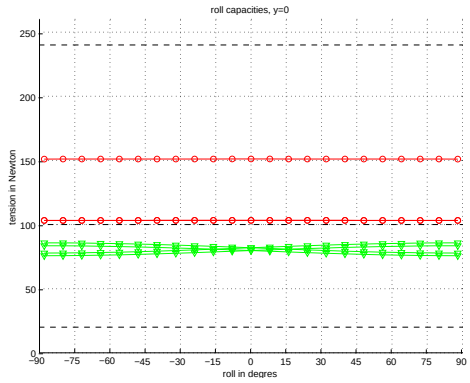

Figure 16: Diamond solution (figure 4). With the chosen load (no torque load), almost no limitation in roll

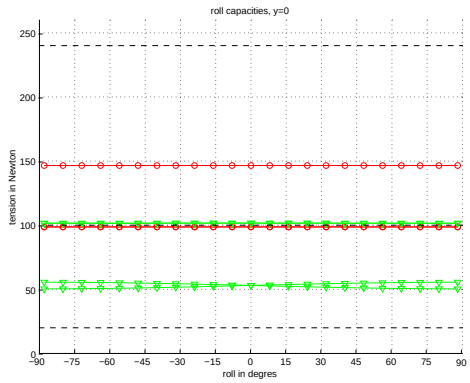

Figure 17: Pendulum solution (figure 5), same abilities than diamond solution

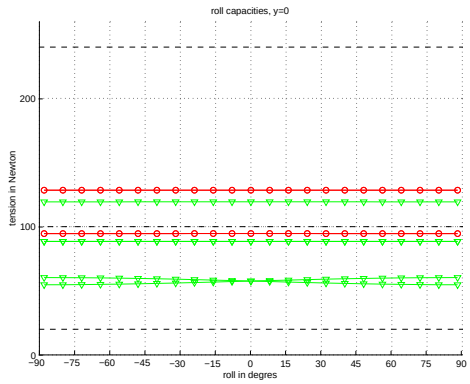

Figure 18: SACSO-9 (figure 11(a)) same abilities than diamond solution

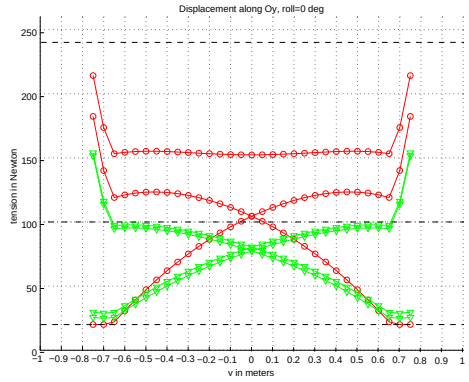

Figure 19: Square solution (figure 3). $y_{max} \simeq 0.75m$

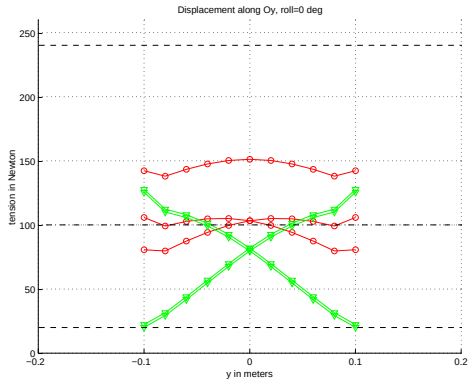

Figure 20: Diamond solution (figure 4). $y_{max} \simeq 0.1m \ < T - cross\ width$

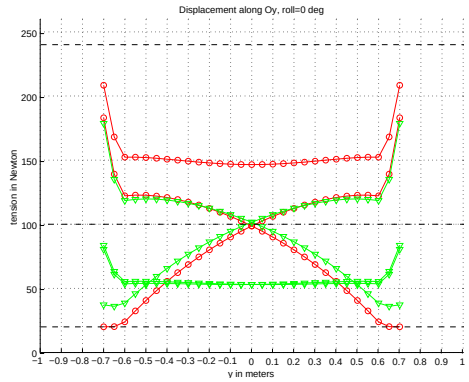

Figure 21: Pendulum solution (figure 5). $y_{max} \simeq 0.7m$

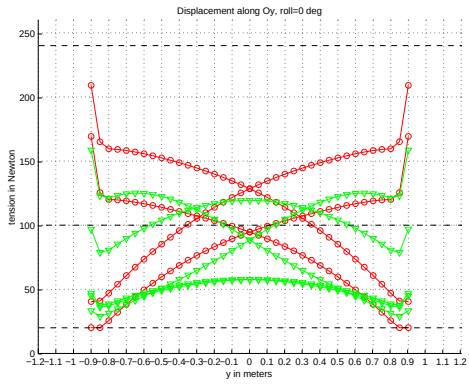

Figure 22: SACSO-9 (figure 11(a)). $y_{max} \simeq 0.9m$

Figure 23: One d.o.f. testing ground for control principle

Proceedings of the WORKSHOP on
Fundamental Issues and Future Research Directions for Parallel Mechanisms and Manipulators
October 3–4, 2002, Quebec City, Quebec, Canada
Clément M. Gosselin and Imme Ebert-Uphoff, editors

Design of Cable-Suspended Planar Parallel Robots for an Optimal Workspace

ABBAS FATTAH, Ph.D.
Visiting Professor
Department of Mechanical Engineering
University of Delaware, Newark, DE 19716, USA
fattah@me.udel.edu

SUNIL K. AGRAWAL, Ph.D.
Professor
Department of Mechanical Engineering
University of Delaware, Newark, DE 19716, USA
agrawal@me.udel.edu

Abstract: *In the design of cable-suspended parallel robots, the suspension points of the cables, size and shape of the moving platform are the design variables. In this paper, the workspace of a planar cable robot is characterized as the set of points where the centroid of moving platform can reach with tensions in all suspension cables. The workspace area and global condition index are used as the objective functions to optimize the design parameters. The global condition index is a measure of isotropicity of the manipulator. The design variables are determined for different numbers of cables using both methods.*

1 Introduction

Optimal design of parallel manipulators has been studied extensively over the last few years. Optimal design is aimed at finding the geometry of the manipulator to attain features such as largest workspace, best accuracy, isotropicity etc. The relevant literature includes work by Gallant and Boudreau (2002), Hong and Kim (2000), Fattah and Hadian Jazi (2001), Boudreau and Gosselin (1999), Merlet (1997), and Gosselin and Angeles (1989, 1991).

Optimal design of cable-suspended parallel robots (or cable robots) is also an important issue. The relevant literature on cable robots includes Albus et al. (1992), Bostelman et al. (1999), Kamamura it al. (1998), Verhoeven and Hiller (2000), Jeong it al. (1999), Alp and Agrawal (2002a, 2002b) and Baretle and Gosselin (2000). However, these papers address only limited issues such as workspace, singularities, and stiffness of the robots. Our paper focuses on optimal design of these robots.

Optimal design of cable-suspended robots is aimed at obtaining the size and geometry of the moving platform, suspension points of the cables and number of the cables. The goal of optimization is to maximize the workspace volume and the accuracy of the robot within this volume. The workspace area is characterized by the set of points where the center of mass of the moving platform can be positioned while all cables are in tension. Hence, the forces in the cables are derived using static equilibrium of the moving platform and conditions are imposed to have tension in the cables. A method to obtain this workspace efficiently was proposed by Fattah and Agrawal (2002). The accuracy of robot is described by the 'global condition index' (Gosselin and Angeles, 1989), which is a measure of kinematic dexterity of the robot over the whole workspace.

The organization of this paper is as follows: After a brief outline of the underlying models in Sections 2 and 3, the optimizations are performed for 3-cable and 6-cable planar parallel robots. A comparison of the results is presented at the end of the paper.

2 Modeling

Our model of a planar cable robot consists of a moving platform (MP) that is connected by n cables to a base platform shown in Fig. 1.

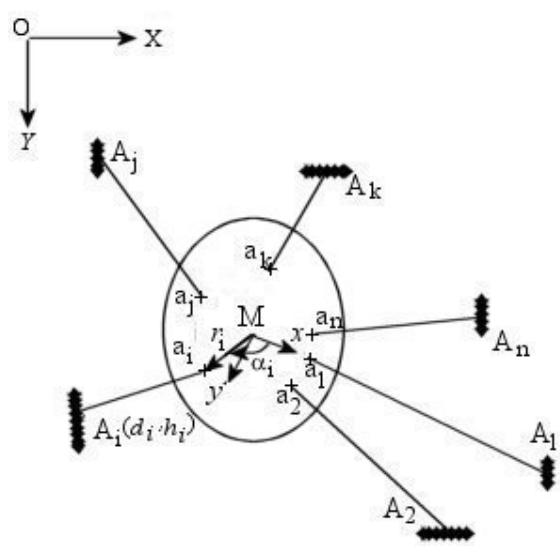

Fig. 1 A model of the planar cable robot

The cable i is connected to MP at a_i as shown in Fig. 1. The center of mass of MP is located at M. The cable separation angles on MP are denoted by α_i. An inertial reference frame $\mathcal{F}_O$ (XY) is located at O and a moving reference frame $\mathcal{F}_M$

(xy) is located on *MP* at its centroid *M*. The orientation of *MP* is specified by θ_e, the angle between *X* and *x* axis. The origin of $\mathcal{F}_M$ is given by the position vector from *O* to *M*, with x_e and y_e as components.
The position vector of point a_i with respect to $\mathcal{F}_M$ is written as

$$^{M}r_i = \begin{bmatrix} b_i c\alpha_i & b_i s\alpha_i \end{bmatrix}^T \tag{1}$$

where *c* and *s* stand for cos and sin, respectively and b_i is the distance between points M and a_i. The transformation matrix of frame $\mathcal{F}_M$ with respect to frame $\mathcal{F}_O$ can be readily obtained as

$$^{o}T_M = \begin{bmatrix} c\theta_e & -s\theta_e & x_e \\ s\theta_e & c\theta_e & y_e \\ 0 & 0 & 1 \end{bmatrix} \tag{2}$$

Therefore, the position vector of point a_i with respect to $\mathcal{F}_O$ is

$$\begin{bmatrix} ^{o}r_i \\ 1 \end{bmatrix} = {}^{o}T_M \begin{bmatrix} ^{M}r_i \\ 1 \end{bmatrix} \tag{3}$$

Upon substitution $^{o}T_M$ from Eq.(2) into Eq.(1), one leads to

$$^{o}r_i = \begin{bmatrix} x_e + b_i c\theta_e c\alpha_i - b_i s\theta_e s\alpha_i \\ y_e + b_i s\theta_e c\alpha_i + b_i c\theta_e s\alpha_i \end{bmatrix} \tag{4}$$

Moreover, the position vector of suspension point A_i of cable i with respect to reference point *O* is written as

$$^{o}p_i = \begin{bmatrix} d_i \\ h_i \end{bmatrix} \tag{5}$$

Hence, the vector $\overrightarrow{a_i A_i}$ for cable *i* is

$$l_i = {}^{0}p_i - {}^{0}r_i = \begin{bmatrix} l_{ix} \\ l_{iy} \end{bmatrix} = \begin{bmatrix} d_i - x_e - b_i c\theta_e c\alpha_i + b_i s\theta_e s\alpha_i \\ h_i - y_e - b_i s\theta_e c\alpha_i - b_i c\theta_e s\alpha_i \end{bmatrix}$$
(6)

The length of cable l_i is given by

$$\|l_i\|^2 = l_{ix}^{\ 2} + l_{iy}^{\ 2} \tag{7}$$

3 Static Equilibrium Equations

The static equilibrium equations of MP can be used to obtain the forces in the cables. The equilibrium equations for MP are

$$\begin{aligned} \Sigma F_x &= 0 \\ \Sigma F_y &= 0 \\ \Sigma M_M &= 0 \end{aligned} \tag{8}$$

Using Fig. 2, the equilibrium equations can be written as

$$\sum_{i=1}^{n} T_i c\theta_i = 0 \tag{9}$$

$$\sum_{i=1}^{n} T_i s\theta_i = -mg \tag{10}$$

$$\sum_{i=1}^{n} T_i s_i = 0 \tag{11}$$

where θ_i is the angle of cable i with respect to X axis of frame $\mathcal{F}_O$ and can be written using Eqs.(6) and (7) as

$$c\theta_i = \frac{l_{ix}}{\|l_i\|}, s\theta_i = \frac{l_{iy}}{\|l_i\|}, i = 1, \ldots, n \tag{12}$$

and s_i is the shortest distance of M to cable axis i and can be expressed using Fig.(2) as $s_i = b_i s(\theta_e + \alpha_i - \theta_i)$.

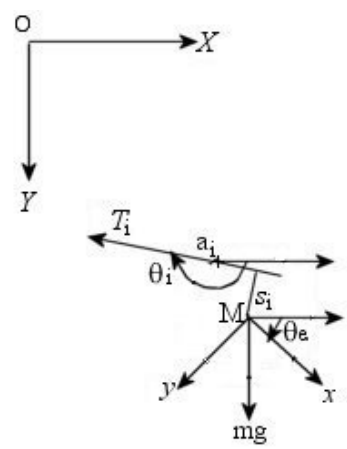

Fig. 2 Model of moving platform and cable *i*

Eqs. (9), (10) and (11) can be written in matrix form as

$$Ax = f \tag{13}$$

where

$$A = \begin{bmatrix} \frac{l_{1x}}{\|l_1\|} & \frac{l_{2x}}{\|l_2\|} & \cdots & \frac{l_{nx}}{\|l_n\|} \\ \frac{l_{1y}}{\|l_1\|} & \frac{l_{2y}}{\|l_2\|} & \cdots & \frac{l_{ny}}{\|l_n\|} \\ b_1 s(\theta_e + \alpha_1 - \theta_1) & b_2 s(\theta_e + \alpha_2 - \theta_2) & \cdots & b_n s(\theta_e + \alpha_n - \theta_n) \end{bmatrix}$$

(13-a)

and x and f are n-dimensional and 3-dimensional vectors, respectively as

$$x = [T_1, T_2, \ldots, T_n]^T \tag{13-b}$$

$$f = [0, -mg, 0]^T \tag{13-c}$$

The solution of Eq.(13) depends on number of cables. With 3 cables, Eq.(13) has 3 equations and 3 unknowns. If the three equations are linearly independent, there will be one solution for the problem. For more than 3 cables, Eq.(13) is an underdetermined system of equations and has many solutions if AA^T is invertible. This is the case for our problem if the three equations in Eq.(13) are linearly independent. The minimum norm solution for Eq.(13) can be derived using the generalized inverse of matrix A as

$$x = A^T (AA^T)^{-1} f \tag{14}$$

Eq. (14) gives one set of solution for the cable forces. The general solution for Eq.(13) can be expressed in the following form:

$$x = A^T (AA^T)^{-1} f + N(A)\beta \tag{15}$$

where $N(A)$ is the nullspace or kernel of matrix A and β is an $(n-r)$ dimensional arbitrary vector. Here, r is the rank of matrix A.

4 Workspace Area Optimization

In a given orientation of MP, by choosing a Cartesian grid of equally spaced points, the workspace area of the cable robot is given by the number of points where the center of mass of *MP* can be positioned while the cables are in tension. To this end, the following inequalities should be satisfied:

$$T_i \geq 0 \qquad i = 1, \ldots, n \tag{16}$$

The forces in the cables can be obtained by solving Eq.(13) over the grid of x_e and y_e in a specific orientation of MP. The points where the forces in all cables are in tension are feasible points of the workspace. The number of these points gives an estimate of workspace for the cable robot. There may be some configurations for the suspension points of the cables and cable attachment points to the MP where the workspace vanishes. In other words, we may not get any point inside the possible workspace with tension in cables at these configurations. Hence, it is necessary to study the optimal design of the cable-robot.

The objective is to determine the manipulator design variables to attain the maximum workspace. The manipulator design variables are size of *MP*, the suspension points of cables and cable attachment points to the MP, i.e., (d_i, h_i, b_i), the separation angles α_i and the number of cables. In order to assure practicality of the solution, the following constraints are imposed:

- The length of the cables are between given minimum and maximum values($l_{\min} < l_i < l_{\max}$).
- The cable forces are between given minimum and maximum values($T_{\min} < T_i < T_{\max}$).
- The manipulator workspace is singularity free.
- The workspace of the center of mass of *MP* is $0 < x_e < x_{\max}$ and $0 < y_e < y_{\max}$.
- The size of *MP* should not be lower than some specified values.
- The vector β in Eq.(15) is between the given minimum and maximum values($\beta_{\min} < \beta < \beta_{\max}$). The extreme values are chosen such that Eq.(15) gives all possible solutions for the optimal design.

After many optimizations runs, we found that when one of the cables is located at $O_1(d,0)$, it gave us the maximum workspace. Therefore, we assume that one cable is connected to origin O and a second cable is connected to point $O_1(d,0)$.

The other bounds are as follows:

$l_{\min} = 0.5$, $l_{\max} = 10$, $d = 10$, $x_{\min} = 0$, $x_{\max} = 10$, $y_{\min} = 0$, $y_{\max} = 10$, $T_{\min} = 0$, $T_{\max} = 50$

The optimization steps are outlined as follows:

1. Grid the design variables uniformly within their minimum and maximum values;
2. Specify a region as possible workspace for the center of mass of *MP* in an orientation and grid it uniformly;
3. At a grid point in step 2, perform the kinematic analysis and form the matrix A using Eq.(13-a);
4. Compute the cable forces using Eqs. (13) and (14). If the cable forces satisfy Eq.(16), i.e., $T_i \geq 0$ ($i = 1, \ldots, n$), one proceeds to step 6.
5. Use Eq.(15) to derive cable forces. To this end, by changing the arbitrary vector β, one can obtain tension forces in the cables.

6. Using the grid points in Step 2, compute all points where $T_i \geq 0$ ($i = 1, \ldots, n$). The total number of these points (WA) gives the workspace area;
7. Compute WA for different values of design variables using the grid points in Step 1;
8. Obtain the maximum workspace, i.e., the maximum of all WA's that are computed in Step 7, and the optimized design variables;
9. Draw the workspace for the optimized design in the frame XY.

The 3-cable and 6-cable robots are studied as numerical examples next using the procedures described above. In these examples, the shape of MP is assumed to be circle and the cables are connected to the MP on the circle. The center of mass of MP is located at the center of the circle. Moreover, the distance b_i in Eq.(1) is equal to *a*, i.e., radius of the circle. We considered the shape of the end-effector to be a circle in order to limit the number of design parameters. It is possible to use other shapes without any difficulty. Moreover, $\alpha_{i+1} - \alpha_i$ ($i = 1, \ldots, n-1$), is assumed to be equal.

4-1 3-Cable Robot

In this example, the three suspension points of the cables are $A_1(d,0), A_2(d_2, h_2), A_3(0,0)$. Therefore, the design parameters are a, d_2, h_2. The optimal design is obtained using the procedure described above. Since the optimal design is obtained by checking all points on the grids described in Steps 1 and 2, the solution is globally optimal. Here, we present the results for two orientations of *MP* as follows:

(i) $\theta_e = 30^\circ$: The optimal design parameters are $a = 1, d_2 = 3, h_2 = 1$ and the optimal workspace is shown in Fig. 3;

(ii) $\theta_e = 90^\circ$: The optimal solution is obtained for $a = 1, d_2 = 6, h_2 = 1$ and the optimal workspace is shown in Fig. 4.

From these plots, we see that the workspace for case (ii) ($\theta_e = 90^\circ$) is smaller than the workspace for case (i) ($\theta_e = 30^\circ$).

4-2 6-Cable Robot

In this example, the six cable suspension points are: $A_1(d,0), A_2(d_2, h_2), A_3(d_3, h_3), A_4(0,0), A_5(d_5, h_5)$, $A_6(d_6, h_6)$. The design parameters of the 6-cable robot are $a, d_2, h_2, d_3, h_3, d_5, h_5, d_6, h_6$.

The optimization problem is again solved for two specific orientations of MP: (i) $\theta_e = 30^\circ$, (ii) $\theta_e = 90^\circ$. The optimal design parameters for 6-cable robot with $\theta_e = 30^\circ$ are:

$a = 1, d_2 = 0, h_2 = 0, d_3 = 8, h_3 = 0, d_5 = 0, h_5 = 0,$
$d_6 = 4, h_6 = 0$.

The results for $\theta_e = 90^\circ$ are:

$a = 1, d_2 = 0, h_2 = 0, d_3 = 8, h_3 = 0, d_5 = 4, h_5 = 0,$
$d_6 = 4, h_6 = 0$.

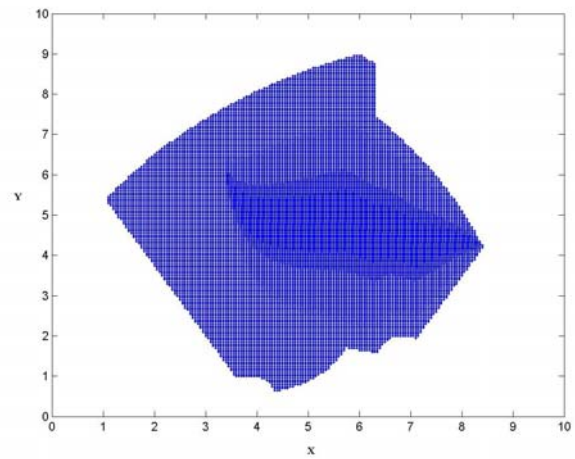

Fig.3 The optimal workspace for 3-cable robot at $\theta_e = 30^\circ$

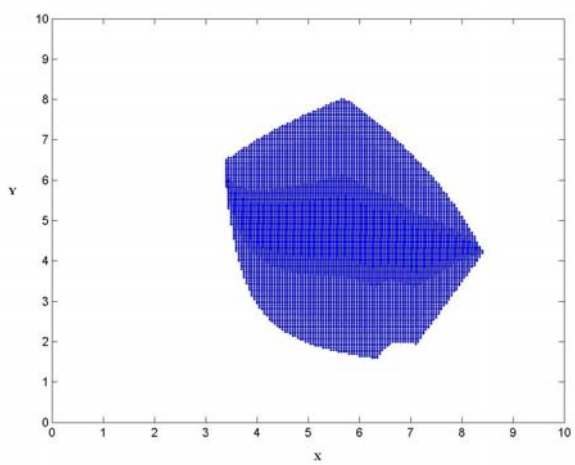

Fig.4 The optimal workspace for 3-cable robot at $\theta_e = 90^\circ$

Figs. (5) and (6) show the workspace for 6-cable robot with optimal design parameters at $\theta_e = 30^\circ$ and $\theta_e = 90^\circ$, respectively. From these plots, we can infer that the workspace for 6-cable robot is larger than the workspace for

3-cable robot. Therefore, by increasing the number of cables, the workspace increases.

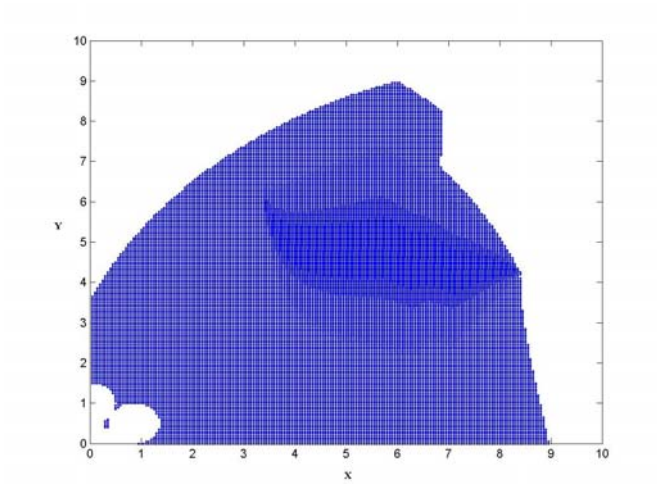

Fig.5 The optimal workspace for 6-cable robot at $\theta_e = 30^\circ$

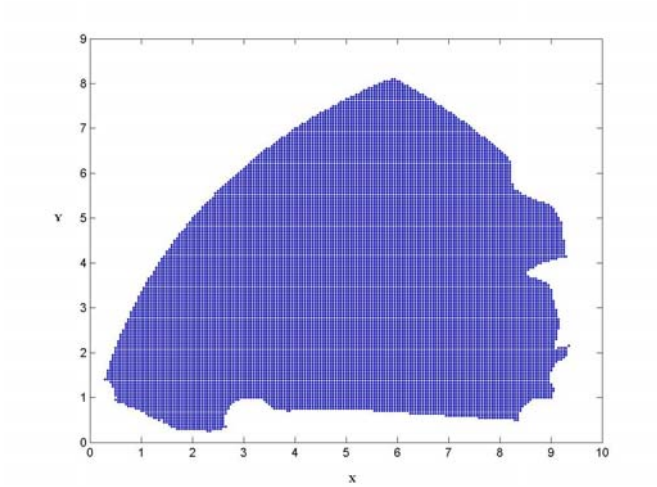

Fig.6 The optimal workspace for 6-cable robot at $\theta_e = 90^\circ$

5 Global Condition Index Optimization

The global condition index (GCI) measures how far away the robot is from being isotropic. Large values for *GCI* ensure good performance with respect to force and velocity transmission. Therefore, the objective function in this section is to maximize the global condition index over the workspace. The global condition index over the workspace is defined as

$$GCI = \int_w \frac{1}{k} dw \Big/ \int_w dw \tag{17}$$

where k is the condition number of the Jacobian matrix of the manipulator at a given position in the workspace and w is the workspace volume.

The condition number of a matrix is defined as

$$k = \frac{\sigma_{\max}}{\sigma_{\min}} \tag{18}$$

where $\sigma_{\min}$ and $\sigma_{\max}$ are the minimum and maximum singular values of the matrix (Gosselin and Angeles, 1989). The kinematic condition number varies between 1 and ∞ and thus $1/k$ bounds its variations between 0 and 1. The Jacobian matrix maps the Cartesian velocity t, i.e, the velocity and angular velocity of *MP* to cable length velocity vector $\dot{q}$ as

$$\dot{q} = Gt \tag{19}$$

where

$$\dot{q} = \left[\dot{l}_1, \dot{l}_2, \ldots, \dot{l}_n\right]^T \tag{19-a}$$

and

$$t = \left[\dot{x}_e, \dot{y}_e, \dot{\theta}_e\right]^T \tag{19-b}$$

Using the dual relation between kinematics and statics of robotic manipulators, the velocity Jacobian for the cable-robot is

$$G = A^T \tag{20}$$

where A is the $3 \times n$ matrix as defined in Eq.(13-a). The global condition index is computed by discretizing the workspace and computing $1/k$ at each point thus obtained. The average of $1/k$ over the workspace is computed as

$$GCI = \frac{1}{n_i} \sum_{i=1}^{n_i} \frac{1}{k_i} \tag{21}$$

where n_i is the number of points in the selected workspace where all cables are in tension.
In order to compute the condition number of Jacobian matrix, it should be homogenized. In other words, all elements of the

Jacobian matrix should have the same units. To this end, the third row of the matrix A in Eq.(13-a) is divided by the length L, the characteristic length (Angeles, 1997). The design parameters in this section are the same as Section 4 plus the characteristic length L. The objective function is subjected to the same constraints of Section 4. Also, the same sequence of steps is followed during the optimization process, except for a change in the cost.

Here, we use the same examples of Section 4 for comparisons. The following results were obtained using the global condition index as the optimization cost:

(i) 3-cable robot at $\theta_e = 30^\circ$: $a = 1$, $d_2 = 4$, $h_2 = 1$ and L=0.8;

(ii) 3-cable robot at $\theta_e = 90^\circ$: $a = 1$, $d_2 = 3$, $h_2 = 2$ and L= 0.8;

(iii) 6-cable robot at $\theta_e = 30^\circ$:

$a = 1, d_2 = 9, h_2 = 0, d_3 = 0, h_3 = 2, d_5 = 0, h_5 = 6,$
$d_6 = 3, h_6 = 6$ and L= 0.8;

(iv) 6-cable robot at $\theta_e = 90^\circ$:

$a = 1, d_2 = 3, h_2 = 6, d_3 = 0, h_3 = 6, d_5 = 9, h_5 = 4,$
$d_6 = 0, h_6 = 8$ and L=0 .8

The well-conditioned workspace for the above optimized design parameters are shown in Figs. 7 and 8 for 3-cable robot and Figs. 9 and 10 for 6-cable robot, respectively.

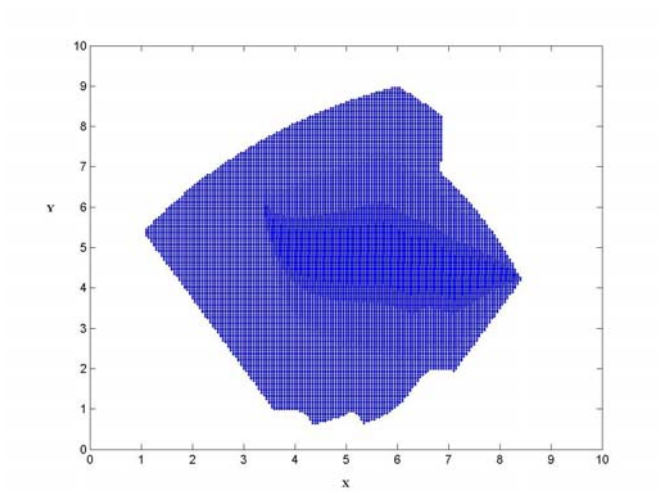

Fig.7 The optimal workspace for 3-cable robot at $\theta_e = 30^\circ$

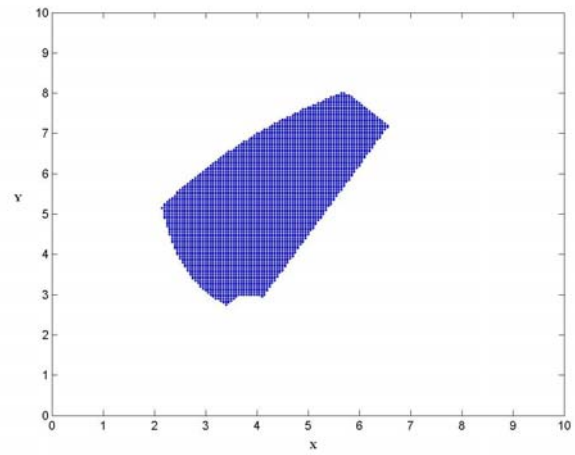

Fig.8 The optimal workspace for 3-cable robot at $\theta_e = 90^\circ$

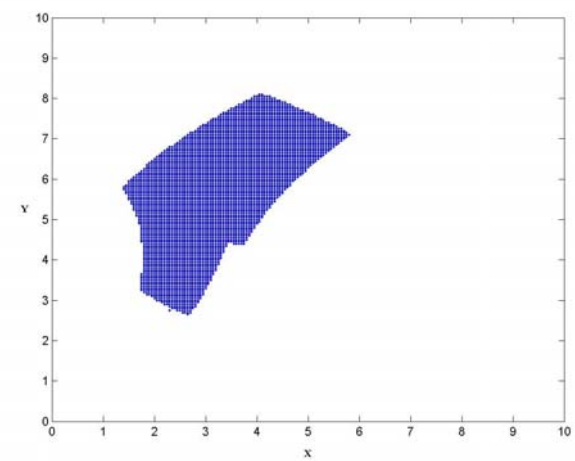

Fig. 9 The optimal workspace for 6-cable robot at $\theta_e = 30^\circ$

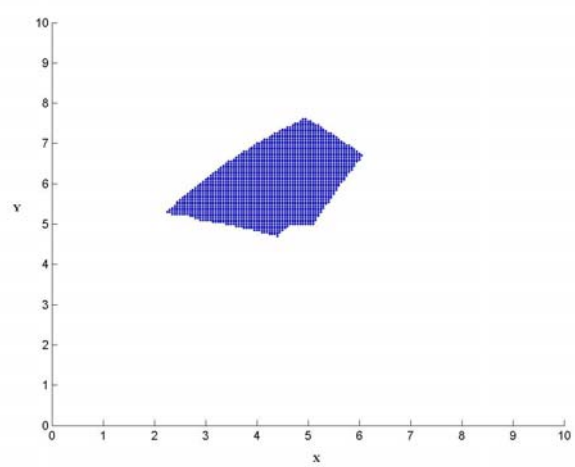

Fig.10 The optimal workspace for 6-cable robot at $\theta_e = 90^\circ$

6 Discussion of Results

As shown from the results, the workspace reduces when the global condition index is used as the cost for both 3-cable and 6-cable robots. It should be noted that it is difficult to attain a high GCI in the case of 3-cable robot because the number of design parameters is limited. However, the number of design variables in the 6-cable robot is much greater than in 3-cable robot. A comparison result of the two methods is shown in Tables (1) and (2) for 3-cable robot and in Tables (3) and (4) for 6-cable robot. As depicted from the results, it is possible to have high GCI in 6-cable robot but it reduces substantially the well conditioned workspace. It may be noted that the workspace and GCI optimization methods give the extreme boundaries for the workspace area. The practical optimal design should be somewhere between these two limits.

Table 1 Comparison of two optimization methods for 3-cable robot at $\theta_e = 30^\circ$

	Workspace area	GCI
workspace optimization	11358	0.4746
GCI optimization	11147	0.4800

Table 2 Comparison of two optimization methods for 3-cable robot at $\theta_e = 90^\circ$

	Workspace area	GCI
workspace optimization	8783	0.4390
GCI optimization	4792	0.5071

Table 3 Comparison of two optimization methods for 6-cable robot at $\theta_e = 30^\circ$

	Workspace area	GCI
workspace optimization	21688	0.4988
GCI optimization	4671	0.7213

Table 4 Comparison of two optimization methods for 6-cable robot $\theta_e = 90^\circ$

	Workspace area	GCI
workspace optimization	19364	0.4718
GCI optimization	2406	0.7737

7 Conclusions

Two optimizations for the design of cable suspended parallel robots were performed. The first method was based on maximizing the total area of manipulator workspace. The second method maximizes the global condition index of the robot over the whole workspace to achieve a well-conditioned workspace. The results of optimizations of both methods were shown graphically. It can be concluded from the discussion on results that by increasing the number of cables the workspace increases. Also, the workspace area increases by decreasing the size of moving platform. Moreover, more cables can result in a better performance for the robot.

Acknowledgment

We acknowledge research support of National Science Foundation Presidential Faculty Fellow Grant and Individual investigator grant IIS-0117733. The first author would also like to thank Isfahan University of Technology for its financial support during his sabbatical leave.

References

Albus, J., Bostelman, R. and Dagalakis, N., 1992, ``The NIST Robocarne``, Journal of Robotic Systems, 10(5), pp.709-724.

Alp, A. B. and Agrawal, S. K., 2002a, ``Cable suspended robots: Design, planning, and control``, Proceedings of IEEE International Conference on Robotics and Automation, Washington, D.C., May 11-15, pp.4275-4280.

Alp, A. B. and Agrawal, S. K., 2002b, ``Cable suspended robots: Feedback controllers with positive inputs``, Proceedings of the American Control Conference, Anchorage, AK, May 8-10, pp.815-820.

Angeles, J. , 1997, Fundamentals of Robotics Mechanical Systems, Springer, New York.

Barrette, G., Gosselin, C. M., 2000, ``Kinematic analysis and design of planar mechanisms actuated with cables``, ASME Design Engineering Technical Conference, DETC/MECH-14091, Baltimore, U.S.A.

Boudreau R. and Gosselin C. M., 1999, ``The synthesis of planar parallel manipulators with a genetic algorithm``, ASME Journal of Mechanical Design, 121, pp.533-537.

Bostelman, R., Jacoff, A., and Bunch, R., 1999, ``Delivery of an Advanced Double-Hull Ship Welding System Using Robocrane``, 3rd International ICSE Symposia on Intelligent Industrial Automation and Soft Computing, Genova, Italy.

Fattah A. and Agrawal, 2002,``Workspace and design analysis of cable-suspended planar parallel robots``, ASME Design Engineering Technical Conferences, 27th Biennial Mechanisms and Robotics Conference. DETC2002/MECH-34330, Montreal, Canada.

Fattah A. and Hadian Jazi, 2001, ``Optimal design of parallel manipulators``, Proceedings of the 10th International Conference on Advanced Robotics (ICAR 2001), Budapest, Hungary, Aug. 22-25, pp.645-650.

Gallant M. and Boudreau R., 2002, ``The synthesis of planar parallel manipulators with prismatic joints for an optimal, singularity-free workspace``, Journal of Robotic Systems, 19(1), pp.13-24.

Gosselin C. M. and Angeles J., 1989, ``The optimum kinematics design of a spherical three-degree-of-freedom parallel manipulator``, Journal of Mechanisms, Transmissions and Automation in Design, 111(2), pp. 202-207.

Gosselin C. M. and Angeles J., 1991, ``A global performance index for kinematic optimization of robotic manipulators``, ASME Journal of Mechanical Design, 113, pp. 220-226.

Hong Keum-Shik and Kim Jeom-Goo,2000, ``Manipulability analysis of a parallel machine tool: Application to optimal link length design``, Journal of Robotic Systems, 17(8), pp.403-415.

Jeong, J.W., Kim, S.H. and Kwak, Y.K., 1999, ``Kinematics and workspace analysis of a parallel wire mechanism for measuring a robot pose``, Mechanism and Machine Theory, 34, pp.825-841.

Kamamura, S., Choe, W., Tanaka, S. and Pandian, S.R., 1995, ``Development of an Ultrahigh Speed Robot FALCON using Wire Drive System``, IEEE International Conference on Robotics and Automation, Nagoya, Japan.

Merlet J.P., 1997, ``Designing a parallel manipulator for a specific workspace``, The International Journal of Robotic Research``, 16(4), pp. 545-556.

Verhoeven, R., and Hiller, M., 2000, ``Estimating the controllable workspace of tendon-based Stewart platforms, The ARK '00 (7th International Symposium on Advances in Robot Kinematics), pp. 277-284, Portoroz, Slovenia.

Regular Papers: Calibration and Applications

Friday, October 4, 2002, 11:00AM

Session Chairs: J. Herder and J.-P. Merlet

1. I. Fassi, G. Legnani
   "Automatic Identification of a Minimum, Complete and Parametrically Continuos Model for the Geometrical Calibration of Parallel Robots".

2. V. Parenti-Castelli, S. Venanzi
   "On the Joint Clearance Effects in Serial and Parallel Manipulators"

3. M. Krefft, M. Frindt, J. Hesselbach, F.M. Wahl
   "Robotic Systems for Handling and Assembly -- High Dynamic Parallel Structures with Adaptronic Components --".

Proceedings of the WORKSHOP on
Fundamental Issues and Future Research Directions for Parallel Mechanisms and Manipulators
October 3–4, 2002, Quebec City, Quebec, Canada
Clément M. Gosselin and Imme Ebert-Uphoff, editors

Automatic Identification of a Minimum, Complete and Parametrically Continuos Model for the Geometrical Calibration of Parallel Robots

Irene Fassi
Institute of Industrial Technology and Automation,
National Research Council
V.le Lombardia 20/A
20131 Milano - Italy
i.fassi@itia.mi.cnr.it

Giovanni Legnani
Dip. Ing. Meccanica – Università di Brescia
Via Branze 38
25123 Brescia – Italy
legnani@ing.unibs.it

Abstract: *The proposed paper concerns the development of a model for the kinematic description of parallel robots to be used for kinematic calibration. After a brief introduction to existing modelling techniques, some of them are reviewed, extended, and merged in order to obtain an innovative complete methodology that can be automatically applied to general PKMs. The proposed methodology can be applied both to the direct (external) and indirect (internal) calibration. The obtained model is minimum, complete and parametrically continuos (CPC). A general formula is also provided, to determine the total number of necessary parameters. Many application examples are given.*

1. INTRODUCTION

Many sources of error influence the motion accuracy of parallel robots, although composed by accurate mechanical components. Final position accuracy is mainly influenced by: kinematic inaccuracy (due to manufacturing and assembly errors in both actuated and passive joints), load deformation (due to external forces including gravity) and thermal deformation (Wildenberg F., 2001). Each of these factors should be addressed with an appropriate compensation or calibration methodology. This paper deals with kinematic inaccuracy, related to robot geometry.

One possibility to compensate for geometrical errors is to perform a *kinematic calibration*. The robot is requested to reach some *desired* poses and the reached *actual* poses are measured. Then, calibration is performed analysing the difference between the desired and the reached poses.

Different techniques are available to model and to compensate for the errors, they can be classified into two different families: parametric and non-parametric.

Parametric methodologies are based on a geometrical model of the robot in which all the possible sources of error are represented by a parameter. The structural parameters include link lengths, joint axes inclination and joint coordinate offsets. The calibration consists in identifying the value of all these parameters. Once this operation is performed, it is possible to predict the pose error for any robot configuration and so it is possible to compensate for them.

Conversely, non parametric methodologies do not try to identify the sources of error. The error is measured only in some poses of the workspace; in the other poses the error is predicted by interpolation. Non parametric calibration requires more simple models of the manipulator, but gives good results only in the working space where the robot has been calibrated.

This paper deals with parametric calibration and, more in detail, with the problem of constructing a suitable kinematic model of PKM (Parallel Kinematics Machines). An effective model for robot calibration must be *complete* and *proportional* (Mooring, Roth, Driels, 1991). Such a model is often referred as CPC (Complete and Parametrically Continuos) (Zhuang, Roth, 1992). This means that the model must describe all the possible sources of error and that, to avoid singularities, little geometrical errors must be described by small changes in the values of the corresponding parameters. Another useful property to simplify calibration is 'minimality'. A model is 'minimum' if different sources of inaccuracy, that produce indistinguishable pose errors on the gripper, 'collapse' in only one parameter. Methodology to automatically derive minimum CPC models for generic serial manipulators have already been developed in many versions (e.g. Mooring, Roth, Driels, 1991; Zhuang, Roth, 1992).

Many different calibration strategies have been proposed also for individual parallel manipulators, using both direct (e.g. Parenti-Castelli, *et al.*, 1995; Jokiel *et al*, 2000) and indirect or self calibration techniques (e.g. Neugebauer, 1999, Smollett, 1996), but a general methodology which derives a minimum CPC model for parallel robots has not been appeared yet.

This paper makes one significant step in this direction integrating available results with new ones and reordering

them in simple rules that can be automatically applied to any existing PKM with different kinematic chains. In all the cases a minimum and CPC kinematic model for geometrical calibration is automatically obtained.

Being aim of this work the analyses of geometrical errors, it will be assumed that the robot is composed by rigid links connected by "ideal" joints (without backlash).
It will be also assumed that actuators are directly connected to the manipulator joints and so errors in the transmission kinematics transmissions will be here neglected.
Calibration makes use of measures of the absolute gripper pose and/or the measure of some joint coordinates. Measures of joint coordinates include the motion of actuated joints and the motion of some non-actuated joints equipped with suitable sensors (called "extra sensors"). A joint whose motion is measured either because it is actuated or because it is equipped with an extra-sensor will be called *monitored* joint.
The paper is organized as follows: Section 2 presents the basic concepts for calibration of serial robots, that, properly adapted, will be used to determine the minimum CPC model for geometrical calibration of parallel manipulators, introduced in Section 3, where also a method to identify the total number of parameters is discussed. Section 4 presents some applications of the aforementioned method. In Section 5, an automatic algorithm to build the minimum CPC model for PKM is presented, while Section 6 shows some of its applications. In Section 7 a numerical methodology to obtain a reduced parameter set is introduced. Eventually, Section 8 draws the conclusions.

2. Methodological Bases (serial manipulators)

2.1 Introduction

When choosing a parameter set to describe errors in a manipulator geometry, two approaches can be followed.
In the first case, some parameters are chosen to describe the robot structure and errors are represented by variations of the parameters, as in the D&H approach (Denavit, Hartenberg, 1955). However, special care must be put when dealing with some situations. For example the base frame and the gripper frame must be properly chosen. More over, when prismatic frames are present, to achieve minimality, some parameters must be set to zero and when a link is composed by two parallel revolute joints modified D&H definitions must be adopted to avoid singularities (Hayti and Mirmirani, 1985).
In the second case, the nominal geometry of the robot is described by any parametric formulation without putting care in minimality and singularities. Errors are then represented by a suitable number of parameters describing the difference between the nominal manipulator and the actual one. This second set of parameters must be defined taking into account minimality and singularity issues.
The error parameters set considered in this paper falls into this second group and it's derived from Zhuang et al, 1992.

2.2 Geometrical parameter set

It has been proved for serial manipulators (Mooring, Roth, Driels, 1991) that a model to be complete must contain the following number of parameters:

$$N=4R+2P+6 \qquad (1)$$

being R and P the number of revolute and of prismatic joints in the kinematic chain. This formula is derived under the hypothesis that all the joints are actuated (and so their motion is monitored by the control system) and that a measuring device for all the 6 coordinates of the gripper is available.
When only a partial measure of the gripper pose is available, the number of the identifiable parameters is reduced accordingly (Omodei, Legnani, Adamini, 2001):

$$N=G+4R+2P \qquad (2)$$

being G the number of measurable coordinates of the gripper (G=<6). In milling applications, for example, the tool pose is identified by 5 coordinates, being the rotation about tool axis redundant.
Many methodologies to define the parameters to be included in the calibration process have been proposed. One of the more convenient is based on the observation that the location of revolute joints can be expressed in term of two translation and two rotations, while for the prismatic joints only their direction is relevant. Assuming that the kinematics is derived in term of 4*4 transformation matrices, that local frames are located with D&H like rules, assigning z axes to all the joint axes, the direct kinematics can be expressed as:

$$M=A_0\, A_1\, A_2 \ldots A_i \ldots A_n \qquad (3)$$

where M is the matrix describing the gripper pose with respect to the base frame, n is the number of DOF (Degrees of Freedom) A_0 is a constant matrix representing the location of the first joint with respect to the base frame, and A_i are matrices depending on the i-th joint coordinate and on the i-th link geometry.
The effect of the structure parameter errors can be expressed reformulating the equation (3) as

$$M=A_0\, B_0\, A_1\, B_1\, A_2\, B_2 \ldots A_i\, B_i \ldots B_{n-1}\, A_n\, C \qquad (4)$$

where B_i and C have the following form:

- $B_i=T(x,\Delta a_i)T(y,\Delta b_i)R(x,\Delta\alpha_i)R(y,\Delta\beta_i)$ if i+1 is a Rev. joint
  $R(x,\Delta\alpha_i)R(y,\Delta\beta_i)$ if i+1 is a Prism. joint
- $C=T(x,\Delta a_n)T(y,\Delta b_n)T(y,\Delta c_n)R(x,\Delta\alpha_n)R(y,\Delta\beta_n)R(z,\Delta\gamma_n)$

$R(u,\Delta\varphi)$ and $T(u,\Delta h)$ represent rotations and translations around axis 'u', while $\Delta\varphi$ and Δh ($\varphi=\alpha$, β or γ, h=a, b, c) are the parameters describing one of the robot kinematics errors.
B_i represents roto-translation errors in frame (i) while C is expressed in frame (n)[1].

[1] In this paper, we will use Δa, Δb, Δc to indicate translation along x, y, and z axes and $\Delta\alpha$, $\Delta\beta$, and $\Delta\gamma$ to describe rotations around x, y, and z; Δq will indicate a variation of a joint coordinate.

The set of the robot parameter errors is obtained collecting all the parameters (Δa_i, Δb_i, Δc_i, $\Delta\alpha_i$, $\Delta\beta_i$, and $\Delta\gamma_i$) of eq (4).

2.3 Joint offset

Offset errors in joint motions are not to be considered because it is possible to prove that their effect is un-distinguishable from that of some of the other parameters already included. However it is sometime requested to highlight the effects of the joint offset coordinates for example because their effect can be easily compensated by the robot controller simply adding a constant value to the joint coordinates. If the joint offset are introduced in eq(4), in order to avoid redundancy and preserve minimality in the parameters set, it is necessary to remove some of the parameters equivalent to them. This operation can be performed in two steps.
First of all equation (4) is modified introducing for each joint a matrix D_i describing the coordinate offset error:

$$M = A_0\, B_0\, D_1\, A_1\, B_1\, D_2\, A_2 \ldots D_n\, A_n\, C \qquad (5)$$

where D_i are defined as

- $D_i = R(z,\Delta q_i)$ if the i-th joint is Revolute
- $D_i = T(z,\Delta q_i)$ if the i-th joint is Prismatic

As a second step, equation (5) is analysed in order to remove from matrices B_i all the terms un-distinguishable from to the just introduced joint offset errors because they produce the same pose error on the links that follow. This elimination process can be performed utilising differential analyses (infinitesimal motions). After introducing matrices D_i and removing redundancy from B_i, the total number of parameters is unchanged.
Analytical methods to eliminate redundant parameters have been proposed by Khalil, et al, 1991, Meggiolaro and Dubowsky, 2000.

3. Parallel Manipulators

An analogous strategy can be followed for parallel manipulators, assumed that they have both actuated and not actuated, multi-dof joints, and that both direct or indirect calibration can be performed.

3.1. Indirect and external calibration

Indirect calibration (also called *internal* or *self* calibration) technique uses extra sensors to determine the unknown geometrical parameters (Parenti-Castelli, *et al.*, 1995; Ziegert, 1999, Weck, 1999), while *direct* calibration (also called *external* calibration) uses external devices, as theodolite and absolute measurement systems, to determine the kinematic error model (Neugebauer, 1999, Smollett, 1996).
External calibration mainly consists in calibrating the pose of the frame attached to the mobile base with respect to that of the fixed base, and it is similar to the calibration of serial manipulators. To perform it, it is necessary to use a suitable instrumentation able to measure the 6 coordinates (3 translation and 3 rotations) of the mobile base. When the used instrumentation measures less than 6 coordinates (e.g. when calibration is performed using a double ball bar - DBB), some of the robot parameters cannot be identified and a proper complete external calibration is not possible.
Indirect calibration is performed using the measure of extra-sensors that measure the relative motion between some robot links and comparing the sensor readings with the value predicted on the bases of the nominal manipulator kinematics. In these cases, some of the manipulator parameters cannot be identified and just a partial robot calibration can be performed.

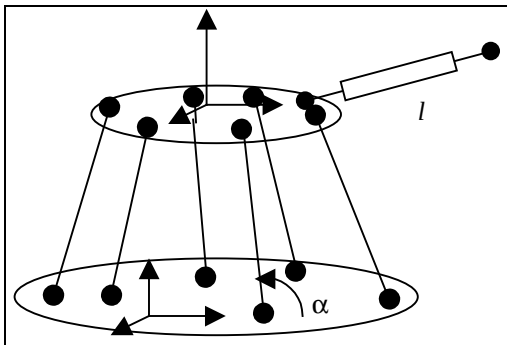

Fig. 1 - Calibration of a PKM using a double ball bar and extra-sensors.

An example is reported in figure 1 where calibration of an hexapod is performed on the basis of the length *l* measured by the DBB, and on the angle α (leg's inclination). Measures of α and *l* are useful to calibrate the relative poses between the joints, but are not suitable to determine the location of the bases frames.

3.2. Geometrical Parameters of a PKM

As a principle, the criterion developed for serial manipulators for the identification of the geometrical parameters described in Section 2 can be applied also to parallel manipulators, taking into account that PKMs make use of both actuated and not actuated joints, single-*dof* or multi-*dof*, as universal and spherical joints. Universal joints are kinematically equivalent to a sequence of 2 revolute joints, and can be modelled accordingly. To obtain a 3-dof joint, a third R joint, allowing a rotation about the leg axis, is added. Conversely, spherical (ball and socket) joints uncertainties depend only on the three coordinates of their center, while imperfections in the spherical motion are generally neglected. Thus, the minimum and complete parameter set is affected by the joint typology.

3.2.1 PKMs with R and P joints

When the mobile base is connected to the fixed base by 'L' legs, we can defined 'L' equivalent serial kinematic chains (one for each leg), all of them having in common the base

and the end effector. However, many joints are not actuated and the corresponding joint offsets should be neglected in defining the parameter set, at least if the corresponding joint coordinate is not measured by extra sensors. The correct number of parameters, for each leg, is then reduced and eq.(2) becomes:

$$N_L=G+3R_L+P_L+g_L \qquad (10)$$

where 'g_L' is the number of the *monitored* joint coordinates, R_L and P_L are the number of revolute and of prismatic joints of the leg, and G is the number of measured coordinates of the mobile base.
The parameters set can be obtained rewriting equation (5) for each leg and removing from them the matrices D_i associated to non monitored joints. We get

$$N_T=6(L-1)+3R_T+P_T+G+g_T \qquad (11)$$

where R_T and P_T are the total number of R and P joints of the PKM. The parameter set is minimum, complete, and continuous. For a general PKM, the number of parameters indicated by eq (11) is quite large, but some of them can be neglected because they have a very small effect on the PKM precision. This subject will be analysed in Sect. 7.

3.2.2 PKMs with R, P and S joints

Considering the case of actuated joints, equation (2) transforms as

$$N_T=G+4R_T+2P_T+3S_T \qquad (12)$$

where S is the number of the spherical joints. For the case of unactuated joints, one parameter for each dof must be eliminated; thus, equations (10) and (11) are still valid. As a result, in general, there is no explicit indication on the number of spherical joints in eq(11).
However, to take into account some "special" or "singular" cases described further in the paper (e.g. SS links), equations (10) (11) must be generalised as

$$N_L=G+3R_L+P_L+g_L+s_L \qquad (13)$$

$$N_T=6(L-1)+3R_T+P_T+G+g_T+s_T \qquad (14)$$

where s is the number of the singular links.

3.2.3 Indirect Calibration

As already mentioned, when indirect calibration is performed, the pose of the frames on the fixed and moving base cannot be determined and the number of the observable parameters is reduced by 6 (the DOFs of the frame) for each base; 12 for the whole manipulator. In fact in this case the bases' geometry is defined only by the relative positions of the joints and not by their absolute location with respect to the base frame. For instance, considering a general Stewart-Gough platform with 6 spherical joints for each base, we need 3 parameters to define the relative distance between the first three spherical joints plus 3 parameters for each other joint (the distance of the considered joint from the first three). In total we get 3+3(S-3)=3S-6 parameters for each base.

4. Identification of the total number of parameters: some applications

This section analyses some simple cases, in which the number of useful parameters for calibration is easily identified. These cases are used to clarify the presented methodology for the automatic identification of the parameter set.

4.1. Stewart-Gough platform 1: SPS

The parameters set of a standard Stewart-Gough platform can be identified as follows.

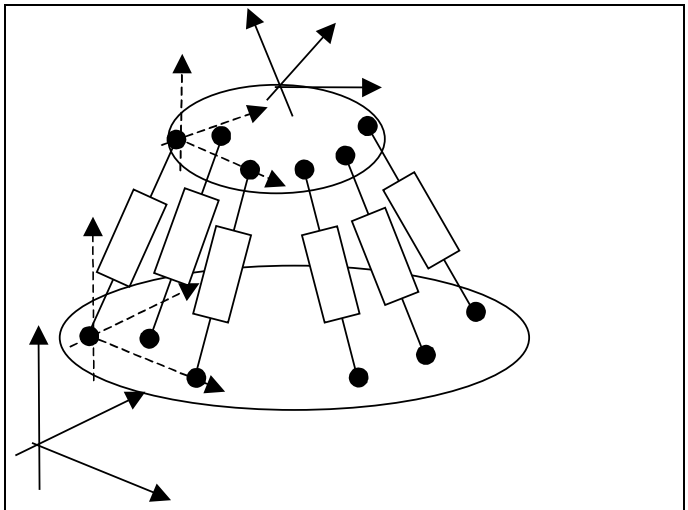

Fig. 2 – Stewart-Gough platform. Dashed frames are "intrinsic frames" defined on the joints, continuos frames are the "user frames"

Fixed base: A "user frame" is created on the fixed base and three parameters are necessary to define the location of each spherical joint. We get a total of 6*3 parameters.
Mobile base: As for the fixed base we get 18 parameters.
Legs: each leg is composed by two spherical joints connected by a prismatic joint. Each leg then requires 6+2P=8 parameters.

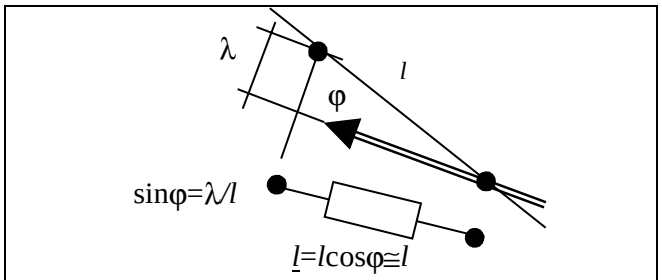

Fig. 3 - actuated SPS leg ($\lambda \ll l \rightarrow \cos(\varphi)\cong 1$)

Total number of parameters: N_T = 2*18+6*2 = 48

In this simple case, the same results can be obtained observing that we need 3 coordinates for each spherical joints (their coordinates on the bases) plus the prismatic joint offset and inclination error (λ in figure 3).
Generally, the angle φ is small (the nominal value is $\lambda=\varphi=0$), so this parameter can be ignored because its effect is numerically indistinguishable from the joint offset ($\sin\varphi\cong 0$), meaning that an error on φ doesn't significantly affect the distance between the two joints.

Total number of parameters: $N_T = 2*18+6*1 = 42$

This parameter set has been adopted during the external calibration of several PKMs (e.g., Jokiel, et al. 2000)

4.2. Stewart-Gough platform 2: URPU

Stewart-Gough platform is usually realised using universal joints in spite of spherical ones, due to their limited performance. Generally, the joints of one base are realised with universal joints plus rotational joints, while the others with universal joints. We assume that also in this case we are interested in representing the mobile base motion with respect to the fixed one in the more general case and so the user base frames can be freely assigned on them.
On each of the 6 legs there are 5 not actuated revolute joints and one actuated prismatic joint. We get $N_T=6*(G+3R_T+P_T+g_T)=6(6+15+1+1)=6*23=138$

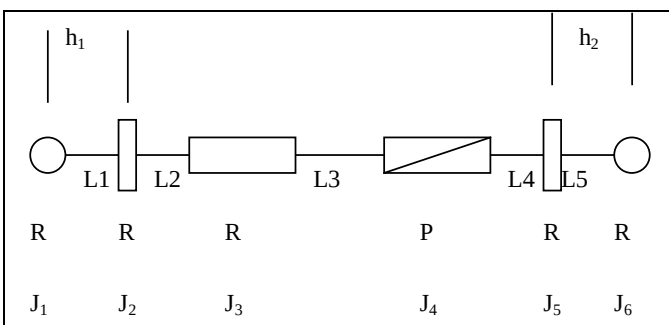

Fig 4 – a six-joints URPU leg

Calibrating a so large number of parameters can be a problem but some of them can be neglected because URPU legs are usually realised with intersecting and orthogonal joints axes (Fig.4); their nominal value is $h_1=h_2=0$, $\varphi=90°$ (Wang *et al*, 1993a, 1993b). In this case, little errors in many of the structural parameters do not affect significantly the mobile base pose (e.g. the relative orientation between joints J_1-J_2 or J_5-J_6). As a further example, if the joint inclination changes just a little during PKM operation, errors on h_i are un-distinguishable from the offset error of the P joint coordinate. These parameters are sometimes neglected during external calibration and the URPU leg is modelled as a SPS leg (Patel *et al*., 1997). This is not possible when indirect calibration is performed using extra-sensors on the same joints, because, for example, the value of the joint coordinate of J_2 is affected by its orientation with respect to J_1.

4.3. Stewart-Gough platform 3

Consider the SPS platform of par.4.1, assuming that calibration is performed by a double ball bar (Ryu *et al*, 2001). No user frames are defined on the fixed and mobile bases. The number of the parameters is then decreases by 12.
Errors can be also present in the DBB or in its connection to the bases. Therefore, 8 further parameters are needed (a DBB is cinematically equivalent to an actuated leg):
Total number of parameters: $N_T = 48-12+8=44$.
The parameter set is composed by the coordinates of the center of the spherical joints and by 2 parameters for each leg (joint offset and λ).
The number of parameters can be reduced with a proper choice of the reference frames on the bases: the origin is located on one sphere S_1, being the x axis directed toward a second sphere S_2, and y axis chosen in such a way that a third sphere S_3 lies in the x-y plane. As a results, the following coordinates error must be neglected: Δx, Δy and Δz for S_1, Δy and Δz for S_2 and Δz for S_3.

4.4. 6 dof PKM with fixed length leg: PSS

The analysed PKM is described in (Ryu *et al*, 2001). It is similar to platform 3, but the legs have constant length. The mobile base is actuated by moving the ends of the legs on prismatic joints of the fixed base.
For the external calibration 5 parameters are necessary to define the position of the moving end of each leg (4 to define the joint axis, 1 to define the position of the spherical joint on the line), 1 parameter is necessary for each leg (its length), 3 parameters are necessary for each spherical joint on the mobile base.
Total number of parameters: $N_T=6*(5+1+3)=54$.

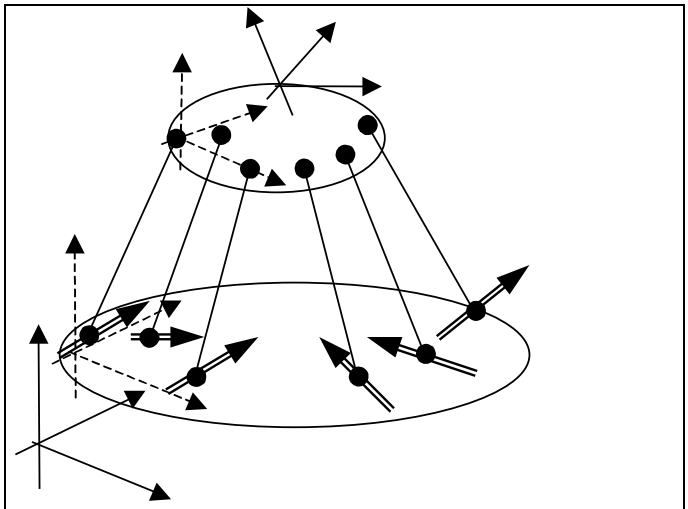
Fig. 5 – a-6 leg PSS PKM.

If indirect calibration is performed by a DBB, in analogy with the other cases, we get:
Total number of parameters: N_T=54-12+8=50.

5. General algorithm for the automatic identification of the parameters of a PKM

5.1. Introduction

The general concepts presented in the previous section can be systematised and an algorithm to automatically generate the parameter set for a general PKM in obtained.
The strategy will be based on the following steps:

1. On each kinematic train, as many frames as the joints number are created: one is the *intrinsic* frame while the others are called *auxiliary* frames.
2. If external calibration is performed, a second *user* frame is created on the fixed and the mobile bases. This frame is freely located on the bases according to the user needs.
3. For each leg, a matrix expression representing the pose of the mobile frame with respect to the fixed frame is generated by a multiplication of the transformation matrices associated to the link frames. For external calibration, the user frames of the bases are considered, while in indirect calibration the implicit frames will be considered.
4. Suitable matrices to describe the sources of errors will be then inserted.
5. The matrix equations will be analysed to extract the PKM parameters.

When applied to serial manipulators, the resulting methodology will be equivalent to those described in Sect. 2.

5.2. Definition of the intrinsic frames

To define the intrinsic frame of a link, firstly a suitable number of joints of the link are selected, to completely define the position and orientation of the frame. Many choices can be sometimes made, all resulting in different but equivalent parameters sets. Available cases are described in the following.
RR-links: two non parallel R joints can define the intrinsic frame as follows. One frame axis (e.g. z) is coincident with the first joint axis, while a second axis (e.g. x) is located on the common normal.
SSS-links: three spherical joints can define an intrinsic frame as follows. Origin in S_1. Axis x_i toward S_2, axis y_i in such a way that the z coordinate of S_3 is null.
PPS-link: origin of the frame in the spherical joints, axis z_i parallel one prismatic joint axis, axis x_i defined by cross product of the two prismatic joint axes.

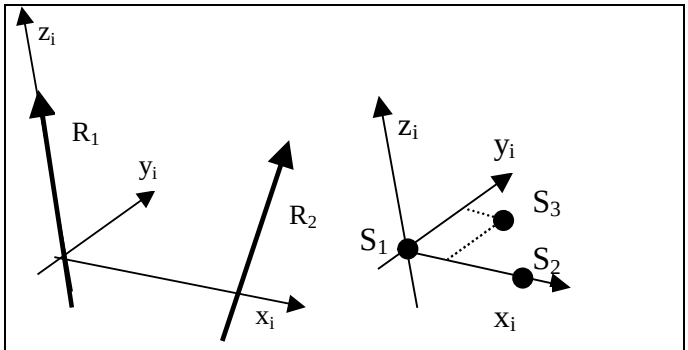

Fig 6 – Definition of intrinsic frames for RR and SSS links.

RS-link: axis z_i coincident with the revolute joint axis, axis x_i toward the spherical joint.
PSS-link: origin of the frame in one spherical joint, axis z_i parallel the prismatic joint axis, axis x_i laying in the plane passing through z_i and the second spherical joint.

When defining the intrinsic frame PS-joints can be considered as R joints. No parameters are defined in this case for the prismatic joint offset which is assumed null.

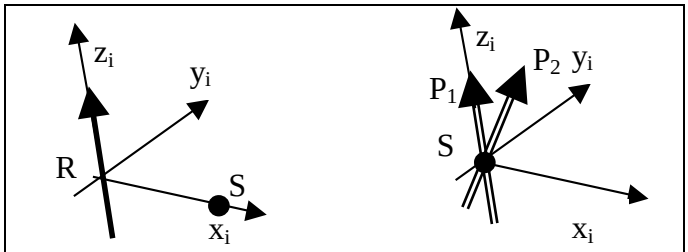

Fig 7 – Definition of intrinsic frames for RS and PPS links

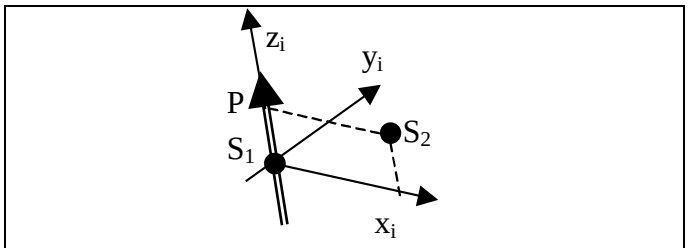

Fig. 8 – Definition of intrinsic frame for PSS links

Exceptions:
The geometry of some links does not allows a complete automatic definitions of an intrinsic frame. This case are the SS and the PS links.
SS-link: origin of the frame is S_1, axis z toward S_2, orientation of x and y axis arbitrary (but orthogonal to z axis).
PS-link: origin of the frame in S, axis z parallel to P, orientation of x and y axis arbitrary (but orthogonal to z axis).

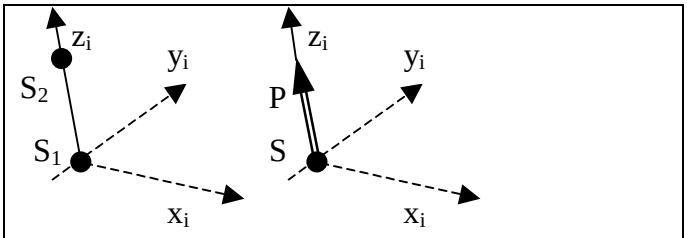

Fig. 9 – Definition of intrinsic frames for SS and PS links

Singular cases can also appear for particular joint alignments (e.g. for two parallel RR joints there are an infinitive number of common normals and the origin of the frame is not completely defined). In these cases, a different group of joints must be selected to define the intrinsic frame. If this is not possible, the intrinsic frame is constructed arbitrarily assigning one ore more of its 6 coordinates.

5.3. Definition of auxiliary joint frames

Although the construction of these frames is not mandatory, it can simplify the identifications of the parameters errors as well as the writing of the kinematics equations. One of these frames coincides with the intrinsic frame, while the others can be constructed using the following rules.

Frame of **revolute joints**: Axis z is the joint axes. Axis x is chosen to lay on the common normal to the joint axis and axis z of the intrinsic frame. As in the standard D&H methodology, if with nominal geometry the two mentioned axes are parallel to each other, the origin of the frame is freely translated along z.

Frame of **prismatic joints**: Axis z is parallel to the joint axes. axes x is defined as for revolute joints. As in the standard D&H methodology the origin of the frame can be translated in order that in the assembly configuration it coincides with the origin of the frame associated to the first revolute joints which follows it.

Frame of **spherical joints**: The origin of the frame coincides with the center of the joints and the frame axes are parallel to those of the intrinsic frame.

5.4. Joint assembly and joint motions

If all the mentioned joint frames are defined with the given rules, prismatic and revolute joints axes will coincide with the z axes of a local frames. The relative assembly of the two links can be then described simply by a rotation and/or a translation around this z axis. One of this rototranslation will coincide with the joint coordinate. Spherical joints will require a 3 dof rotation to describe the joint motion.

Joints assembly and motions will be then described by joint matrices G_i defined as

- $G_i=T(z, h_i)R(z,q_i)$ for revolute joints
- $G_i=T(z,q_i)$ for prismatic joints
- $G_i=R(x,y,z,q_i,q_{i+1},q_{i+2})$ for spherical joints

where $R(x,y,z,q_i,q_{i+1},q_{i+2})$ represents a 3 dof rotation matrix which is often represented by the product of three elementary rotations around concurrent axes $R(x,q_i)$ $R(y,q_{i+1})$ $R(z,q_{i+2})$; however this representation is not completely equivalent because a spherical joint allows three simultaneous rotations while the representations of a sequence of three elementary rotations is "asymmetrical" with respect to elementary rotations and is singular for $q_{i+1}=\pm\pi/2$.

All the mentioned matrices describe joint motions with the exception of the translation T(z,h) in the revolute joints which describe an assembly condition.

For each leg it is possible to express the pose of the mobile base with respect to the fixed one by the product of all the matrices describing its links geometry and its joint motion:

$$M=E_{f1}\, E_{f2}\, G_1\, H_1\, G_2\, H_2 \ldots G_n\, E_{m2}\, E_{m1} \qquad (15)$$

Where E_{f1} is the nominal pose of the intrinsic frame of the fixed base with respect to the user frame, E_{f2} is the nominal pose of the auxiliary joint frame on the base with respect to the intrinsic frame (Fig. 10), E_{m1} and E_{m2} have for the mobile base the same meaning that E_{f1} and E_{f2} have for the fixed one, H_i are "link" matrices describing the link geometry in term of the relative pose between the frames assigned to the involved joints (Fig. 11).

Since eq(15) must be rewritten for each leg, some matrices should have 2 subscripts (i.e. $E_{f2,k}$ $G_{i,k}$, $H_{i,k}$ and $E_{m2,k}$ for leg k) but for simplicity the second one is omitted. In contrast, E_{f1} and E_{m1} are identical for all the legs.

Equation (15) is for one leg of the PKM analogous to eq(3) for serial manipulator. Similarity is evident adopting the following corrispondence:

$A_0= E_{f1}\, E_{f2}$
$A_i= G_i\, H_i$
$A_n= G_n\, E_{m2}\, E_{m1}$

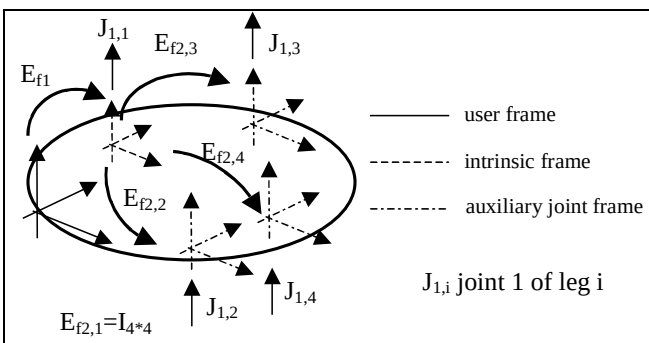

Fig. 10 – Transformation matrices between user, intrinsic and joint auxiliary frames for fixed base. Example for PKM with 4 legs. Mobile base is defined analogously.

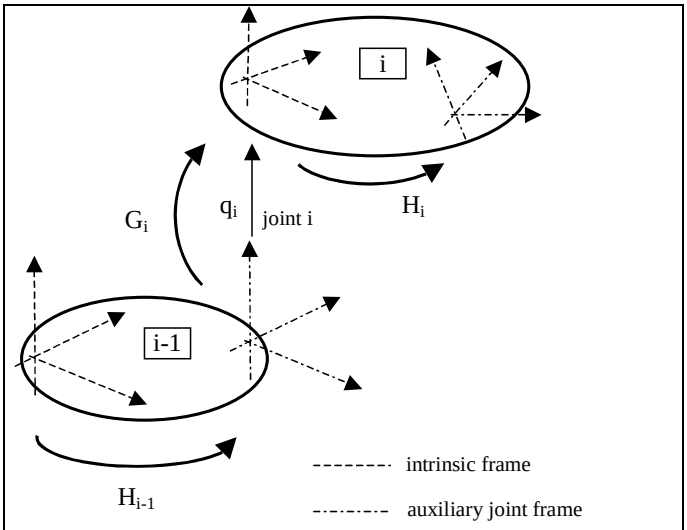

Fig. 11 – Transformation matrices between frames defined on links with 2 joints.

5.5. Description of geometrical error (parameter set)

Assuming that local frames are assigned in such a way that prismatic and revolute joints are directed as z axes, errors in the geometrical parameters for a general joint can be can be described generalizing the rules already given in section 2 for serial robots:

- $B_i=T(x,\Delta a_i)T(y,\Delta b_i)R(x,\Delta\alpha_i)R(y,\Delta\beta_i)$ for R joints
- $B_i=R(x,\Delta a_i)R(y,\Delta b_i)$ for P joints
- $B_i=T(x,\Delta a_i)T(y,\Delta b_i)T(z,\Delta c_i)$ for S joints
- $C_k=T(x,\Delta a_k)T(y,\Delta b_k)T(z,\Delta c_k)R(x,\Delta\alpha_k)R(y,\Delta\beta_k)R(z,\Delta\gamma_k)$ (k=f,m); for indirect calibration C_k is the identity matrix.

For each leg, equation (15) is then modified as:

$$M=E_{f1}\, C_f\, E_{f2}\, B_0\, G_1\, H_1\, B_1\, G_2\, H_2 \ldots \\ \ldots B_{n-1}\, G_n\, B_n\, E_{m2}\, C_m\, E_{m1} \qquad (16)$$

Eq. (16) is for one leg of the PKM analogous to eq. (4) for serial manipulator. Similarity is evident adopting the following corrispondence:

$A_0B_0= E_{f1}\, C_f\, E_{f2}\, B_0$	fixed base geometry and errors
$B_i=B_i$	link errors
$A_i= G_i\, H_i$	joint motion nominal links geometry
$A_nC= G_n\, B_n\, E_{m2}\, C_m\, E_{m1}$	mobile base geometry and errors

However, to avoid redundancy, on some legs not all the parameters of B_0 and B_n must be considered.
The parameters to be neglected are those utilized to define the intrinsic frame of the bases. For example if the intrinsic frame of the base is defined by SSS joints, no parameter error is defined for S_1, only $T(x,\Delta a_2)$ is defined for S_2 and only $T(x,\Delta a_i)T(y,\Delta b_i)$ for S_3. All the other joints will be given to full parameters set as described above.

As a further example, if the intrinsic frame of one base is described by RR joints, no parameter errors are defined for R_1 while for R_2 it is necessary to use $T(x,\Delta a_i)R(x,\Delta\alpha_i)$. All the other joints will have a full parameter set.
More over, if the intrinsic frame of one base is described by RS joints, no parameter errors are defined for R while for S it is necessary to use $T(x,\Delta a_i)$. All the other joints will have a full parameter set.
The general rule is that a parameter must be inserted only if its variation doesn't change the position or the orientation of the intrinsic frame of the base. When performing external calibration, an alternative equivalent formulation is also possible: all the joints of the bases are given the full set of parameters but the 6 parameters defining position and orientation error of the intrinsic frame with respect to the fixed one are neglected ($C_f=C_m=I_{4*4}$).

5.6. Extraction of the geometrical parameter set

If all the joints are monitored, then the list of the parameters contained in the matrices B_i and C_k described in the previous paragraph give a complete set of parameters describing geometrical inaccuracy. Otherwise, a list of the parameters is obtained applying the procedure already discussed in section 2. For each leg:

1. matrices D_i describing the joint offset errors are introduced in eq(16) as it was done in equation (5),
2. error undistinguishable from the joint offsets are removed
3. parameters describing joint coordinate offsets of non monitored joints are removed
4. the list of the error parameters is compiled collecting all the remaining parameters errors

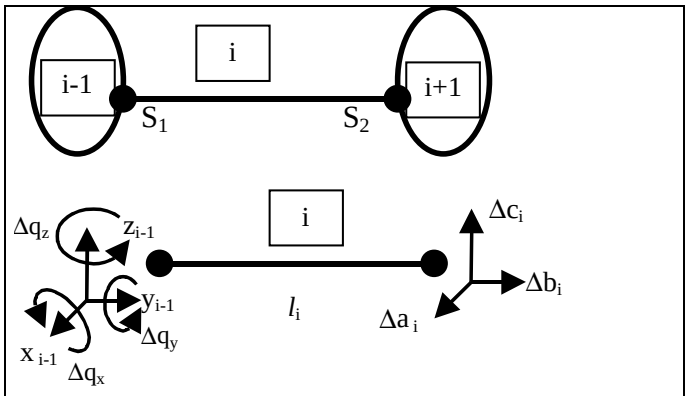

Fig. 12 – Analysis of the redundant parameters on a SS link

If the PKM doesn't contain S joints, the elimination process can be performed using the same algorithm proposed by Khalil et al, 1991, Meggiolaro et al, 2000, for serial robots.
While performing step 2, as already mentioned for the serial manipulators, a parameter error is generally removed for each joint offset parameter introduced in step 1 and the total number of parameters is so unchanged. This general rule is violated in some cases involving spherical joints when a

singular situation happen during the definition of the intrinsic frame of the link.
As an example, let us analyze the case of the SS link represented in Fig. 12. Since the three rotations of the joint are contemporary and not constrained by a particular sequence, they can be represented in a frame of arbitrary attitude: for simplicity they are represented in a frame having the y axis coincident with the link axis. An infinitesimal analysis of the error propagation in the kinematic chain leads to the following results. Error Δa_i is equivalent to $-\Delta q_{zi-1} l_i$ and Δc_i is equivalent to $\Delta q_{xi-1} l_i$; therefore, Δa_i and Δc_i must be ignored. Even if the effect of Δq_{yi-1} is not propagated to the gripper, this rotation error produces effects that are not equivalent to Δb_i or to any other parameters and so just two parameters (and not three) are eliminated; Δq_x, Δq_y, and Δq_z, are to be discharged because the joint is unactuated. As a result only Δb_i survives.

6. Final examples

6.1. Example 1: 6 RSS

Consider a generic 6RSS PKM, with rotational actuated joints. The *i*-leg is shown in Fig. 13 and fig. 14.

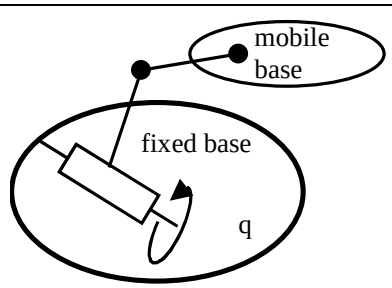

Fig. 13 – One leg of a PKM with RSS legs. Actuators are on R joints.

The complete transformation matrix M_i, describing the position and orientation of the gripper with respect to the reference frame, comprehensive of all possible geometrical and joint offset error parameters of the *i*-leg, is (Fig. 14):

$$M_i = E_{f1}\, C_f\, E_{f2,i}\, B_{0,i}\, D_{1,i}\, G_{1,i}\, H_{1,i}\, B_{1,i}\, D_{2,i}\, G_{2,i}\, H_{2,i} \cdot$$
$$\cdot\, B_{2,i}\, D_{3,i}\, G_{3,i}\, B_{3,i}\, E_{m2,i}\, C_m\, E_{m1}$$

If internal calibration is performed, some error parameters, modelled by matrices B and D, can be neglected, and $C_f = C_m = I_{4*4}$. The complete set of error parameters, both for external and internal calibration, is hereafter listed.

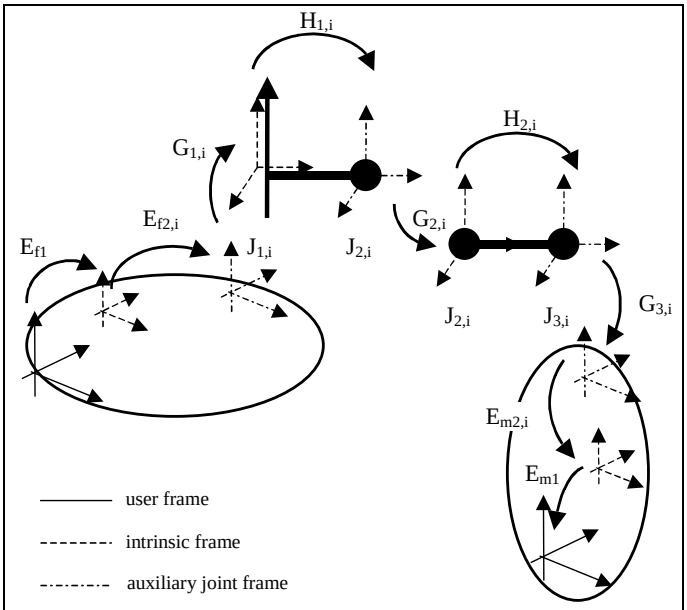

Fig. 14 - Reference frames and transformation matrices for nominal kinematics on leg *i* (RSS PKM).

Internal calibration

An intrinsic frame is defined on the fixed base considering the revolute joints of leg 1 and leg 2 and on the mobile base considering the spherical joints of legs 1, 2 and 3.
On the RS links an intrinsic frame is constructed with the above given rules. Parameter error Δa is the link length error and Δc is a translation along the revolute joint axis; Δb is discharged because it is redundant with Δq.
On the SS link only the link length error is to be considered.
Results, and corresponding error matrices, are presented in the following table.

leg	on fixed base	R joint	RS link	SS link	on mobile base
i	$\mathbf{B_{0,i}}$	$\mathbf{D_{1,i}}$	$\mathbf{B_{1,i}}$	$\mathbf{B_{2,i}}$	$\mathbf{B_{3,i}}$
1	-	Δq	Δc, Δa	Δa	-
2	$\Delta a, \Delta\alpha$	Δq	Δc, Δa	Δa	Δa
3	$\Delta a, \Delta b, \Delta\alpha, \Delta\beta$	Δq	Δc, Δa	Δa	$\Delta a, \Delta b$
4	$\Delta a, \Delta b, \Delta\alpha, \Delta\beta$	Δq	Δc, Δa	Δa	$\Delta a, \Delta b, \Delta c$
5	$\Delta a, \Delta b, \Delta\alpha, \Delta\beta$	Δq	Δc, Δa	Δa	$\Delta a, \Delta b, \Delta c$
6	$\Delta a, \Delta b, \Delta\alpha, \Delta\beta$	Δq	Δc, Δa	Δa	$\Delta a, \Delta b, \Delta c$

Further parameters must be also inserted in dependence on the measuring system used to collect data. For example if one or more DBB are utilised, as already mentioned, 8 further parameters are to be considered for each of them. Furthermore, if calibration is performed using extra-sensors on joints, their offset has to be considered as well.

External calibration

For external calibration, 12 more parameters are added to describe errors in the pose of the user frame with respect to the intrinsic frame (see the following table).

fixed base ($\mathbf{C_f}$)	$\Delta a, \Delta b, \Delta c, \Delta\alpha, \Delta\beta, \Delta\gamma$
mobile base ($\mathbf{C_m}$)	$\Delta a, \Delta b, \Delta c, \Delta\alpha, \Delta\beta, \Delta\gamma$

As a second alternative, we can omit to define the intrinsic frames on the two bases and errors of the joints can be defined with respect to the user frame (see the following tables and assume in this case $C_f=C_m=I_{4*4}$).

leg	on fixed base	R joint	RS link	SS link	on mobile base
i	$\mathbf{B_{0,i}}$	$\mathbf{D_{1,i}}$	$\mathbf{B_{1,i}}$	$\mathbf{B_{2,i}}$	$\mathbf{B_{3,i}}$
1	$\Delta a,\Delta b,\Delta\alpha,\Delta\beta$	Δq	Δc, Δa	Δa	$\Delta a,\Delta b,\Delta c$
2	$\Delta a,\Delta b,\Delta\alpha,\Delta\beta$	Δq	Δc, Δa	Δa	$\Delta a,\Delta b,\Delta c$
3	$\Delta a,\Delta b,\Delta\alpha,\Delta\beta$	Δq	Δc, Δa	Δa	$\Delta a,\Delta b,\Delta c$
4	$\Delta a,\Delta b,\Delta\alpha,\Delta\beta$	Δq	Δc, Δa	Δa	$\Delta a,\Delta b,\Delta c$
5	$\Delta a,\Delta b,\Delta\alpha,\Delta\beta$	Δq	Δc, Δa	Δa	$\Delta a,\Delta b,\Delta c$
6	$\Delta a,\Delta b,\Delta\alpha,\Delta\beta$	Δq	Δc, Δa	Δa	$\Delta a,\Delta b,\Delta c$

fixed base ($\mathbf{C_f}$)	– (none)
mobile base ($\mathbf{C_m}$)	– (none)

7. Identification of a suitable reduced set of parameters.

The algorithms described in the previous sections lead to a theoretically minimum and complete parametrically continuous set of parameters. For some PKM, the number of parameters can be very high. However, as already mentioned in the paper, with particular dimension of the links or when calibration is performed in a limited portion of the working area, some of the parameters may have a very limited effect on the mobile base motion and their value cannot be reliably identified by calibration. We will call them "unobservable" parameters. In other cases two or more parameters may have nearly the same effect on the collected data. In these cases it is not possible to separate their effects and estimate the correct value of all of them. One (or more) of these parameters is then "redundant".

It is in general advisable to remove unobservable and redundant parameters from the model to improve the calibration effectiveness because their presence degrades the identification of the numerical value of the parameters especially in presence of measuring noise or of not modeled sources of error.

In this paragraph a methodology to identify the undesirable parameters is summarized.

We will indicate with Λ the set of the geometrical parameters of the PKM, with Q the joint coordinates and with Φ the set of internal or external coordinates that are measured and used for calibration. On the bases of the PKM kinematics it is possible to write the calibration equations

$$\Phi=\Phi_n+\Delta\Phi =F(Q, \Lambda)= F(Q, \Lambda_n)+J\Delta\Lambda$$

with

$$\Delta\Phi=J\Delta\Lambda \qquad J= J(Q)=\partial\Phi/\partial\Lambda$$

where subscript n marks the nominal values, $\Delta\Phi$ is the difference between the measured value of Φ and the value predicted by the nominal geometry and $\Delta\Lambda$ represent the errors in the robot parameters to be estimated.

Collecting data for many PKM configurations (1, 2, … i, ..n), for each of them we can write

$$\Delta\Phi_i=J_i\,\Delta\Lambda$$

and, grouping equations of all the poses:

$$\Delta\underline{\Phi} = \begin{bmatrix} \Delta\Phi_1 \\ \vdots \\ \Delta\Phi_i \\ \vdots \\ \Delta\Phi_n \end{bmatrix} = \underline{J}\Delta\Lambda = \begin{bmatrix} J_1 \\ \vdots \\ J_i \\ \vdots \\ J_n \end{bmatrix}\Delta\Lambda$$

the value of $\Delta\Lambda$ can be esteemed with minimization techniques. Three of them are presented in (Omodei A., Legnani G., Adamini R:, 2001). For example, a recursive least squares algorithm leads to

$$\begin{aligned} \mathbf{\Delta\Lambda}_{i+1} &= \mathbf{\Delta\Lambda}_i + \boldsymbol{K}_i\left(\Phi_i - \boldsymbol{F}(\mathbf{Q}_i, \Lambda_i + \mathbf{\Delta\Lambda}_i)\right) \\ \boldsymbol{K}_i &= \mathbf{P}_i\boldsymbol{J}_i^T\left(\mathbf{R} + \boldsymbol{J}_i\mathbf{P}_i\boldsymbol{J}_i^T\right)^{-1} \qquad \mathbf{\Delta\Lambda}_0 = 0 \\ \mathbf{P}_{i+1} &= \left(\mathbf{1} - \boldsymbol{K}_i\boldsymbol{J}_i\right)\mathbf{P}_i \end{aligned}$$

where K_i is a so-called gain matrix, $\Delta\Lambda_i$ is the i-th estimate of $\Delta\Lambda$ after the i-th measure of $\Delta\Phi$ has been considered, R is the covariance matrix of Φ representing uncertainty in the measuring sensors and P_i is an estimation at the i-th step of the uncertainty of the parameters error $\Delta\Lambda_i$. P_0 should be initialized to suitable large values (Mooring et al, 1991).

Detection and elimination of the redundant parameters can be performed by analysis of matrix $\underline{J}$ (rank and null space), of matrix P_n or using iterative elimination. These procedures lead the identification of a reduced set of parameters that can be profitably used for the PKM in hand.

Numerical methods to eliminate redundant parameters have been presented also by Besnard et al, 2001, Khalil et al, 1991b.

8. Conclusions

The paper has presented a complete methodology for the identification of the geometrical parameter set necessary to describe inaccuracy in the kinematic structure of a generic PKM.

The methodology, that can be applied to any existing PKM, supplies a minimum, complete and parametrically continuous model of the manipulators. It can be applied both to intrinsic (internal) and extrinsic (external) calibration.
The methodology identifies the parameters describing geometric errors of the manipulator, joint offset errors and errors in external devices (e.g. double ball bar) used for calibration. Furthermore, a general formula to determine the total number of necessary parameters has been presented and discussed.
The paper shows how for some manipulators the number of parameters that are theoretically necessary to describe some PKM is quite large and a numerical methodology to remove the less significant is sketched.
The final methodology is general and it is an *algorithm*, this means that it can be automatically applied to any given PKM. Practical explicative examples are also given.

Acknowledgment

This research work has been partially supported by MIUR grants.

References

Besnard S, Khalil W. 2001 Identifiable parameters for Parallel Robots kinematic calibration, ICRA 2001, Seoul.

Denavit J., Hartenberg, 1955 R. S., Trans. ASME J. Appl. Mech. 22, 215 – 221, June 1955.

Hayti S., Mirmirani M., 1985, Improving the Absolute Positioning Accuracy of robot manipulators, J. Rob. Syst., vol.2, n. 4, pp. 397-413

Jokiel B., Bieg L., Ziegert J, 2000, Stewart Platform Calibration Using Sequential Determination of Kinematic Parameters, *Proc. of 2000-PKM-IC*, Ann Arbor, MI, USA, pp. 50-56

Khalil W., Gautier M., Enguehard Ch, 1991, Identifiable parameters and optimum configurations for robot calibration, *Robotica*, vol.9, pp. 63-70

Khalil W., Gautier M., 1991, Calculation of the identifiable parameters for robot calibration, IFAC 91, pp. 888-892

Mooring B.W., Roth Z.S., Driels M.R., 1991, "Fundamentals of manipulator calibration", John Wiley & Sons, Inc., USA.

Neugebauer R., Wieland F., Schwaar M., Hochmuth C., 1999, Experiences with a Hexapod-Based Machine Tool, in *Parallel Kinematic Machines: Theoretical Aspects and Industrial Requirements*, Springer-Verlag, C.R. Boër, L. Molinari-Tosatti, K. S. Smith (Eds), pp. 313-326

Omodei A., Legnani G., Adamini R:, 2001 "Calibration of a Measuring Robot: Experimental Results on a 5 DOF Structure", Journal of Robotic System 18(5), 237-250.

Parenti-Castelli V, Di Gregorio R 1995 Determination of the actual configuration of the general Stewart platform using only one additional displacement sensor. In: *Proc. of ASME Int. Mechanical Engineering Congress & Exposition*, Nov. 12-17, San Francisco, CA.

Patel A., Ehmann K.F., 1997, Volumetric Error Analysis of a Stewart Platform Based Machine Tool, *Annals of CIRP*, Vol.46/1, pag.287-290

Ryu J., Rauf A., 2001, Efficient Kinematic Calibration of Parallel Manipulators using a Double Ball Bar System, Proceedings of the 32nd International Symposium on Robotics, April 2001, Seoul, Korea

Smollett R., 1996, A method for Measuring the Position and Orientation of a Stewart Platform, *Proc. Of the 1996 Florida Conference on Recent Advances in Robotics*, pp.257-260

Wang J, O. Masory, H. Zhuang, 1993, On the Accuracy of a Stewart Platform-Part II: Kinematic Calibration and Compensation, *IEEE Int. Conf. on Robotics and Automation*, Atlanta, 2-6 Mai.

Wang J., Masory O., 1993, On the accuracy of a Stewart platform-Part I: The effect of manufacturing tolerances, *IEEE Int. Conf. on Robotics and Automation*, pp. 114-120, Atlanta, 2-6 Mai 1993.

Weck M., Giesler M., Meylahn A., Staimer D., 1999, Parallel Kinematics: the Importance of Enabling Technologies, in *Parallel Kinematic Machines: Theoretical Aspects and Industrial Requirements*, Springer Verlag, C.R. Boër, L. Molinari-Tosatti, K. S. Smith (Eds.), pp. 283-294

Wildenberg F., Calibrations for Hexapode CMW, *2nd Chemnitzer Parallelkinematik-Seminar: Working Accuracy of Parallel Kinematics*, 2000 Verlag Wissenschaftliche Scripten, pp.101-112

Zhuang H., Roth Z.S., 1992, "Robot calibration using the CPC error model" Robotics & Computer-Integrated Manufacturing, Vol 9, N.3, pp.227-237

J.C. Ziegert, B. Jokiel, C.-C. Huang, Calibration and Self-Calibration of Hexapod Machine Tools, 1999, in *Parallel Kinematic Machines: Theoretical Aspects and Industrial Requirements*, Springer Verlag, C.R. Boër, L. Molinari-Tosatti, K. S. Smith (Eds.), pp. 205-216.

Proceedings of the WORKSHOP on
Fundamental Issues and Future Research Directions for Parallel Mechanisms and Manipulators
October 3–4, 2002, Quebec City, Quebec, Canada
Clément M. Gosselin and Imme Ebert-Uphoff, editors

On the Joint Clearance Effects in Serial and Parallel Manipulators

VINCENZO PARENTI-CASTELLI
DIEM - Department of Mechanical Engineering
University of Bologna
Viale Risorgimento, 2, 40136 Bologna - Italy
vincenzo.parenticastelli@mail.ing.unibo.it

STEFANO VENANZI
DIEM - Department of Mechanical Engineering
University of Bologna
Viale Risorgimento, 2, 40136 Bologna - Italy
stefano.venanzi@mail.ing.unibo.it

Abstract: *This paper focuses on the effects of joint clearance on the end effector pose accuracy of serial and parallel manipulators. Despite the large number of papers devoted to the modelling of joint clearance, many questions dealing with its effect are still open. The paper reports simulation results of several serial and parallel manipulators with clearance in the joints, with the aim of comparing their positioning accuracy, answering some questions, and provoking further investigations and discussions on this still debated topic.*

1 Introduction

Joint clearance has been clearly recognized to play an important role in mechanisms and machines. Together with link elasticity it is considered one of the most important factors affecting positioning accuracy (Bodur and Derby, 1988; Kakizaki *et al.*, 1993; Wang and Roth, 1988b). It involves, however, contrasting features. On one hand it is a necessary requirement in order to assemble the mechanism and to allow a correct functioning of the pairing elements (and of the mechanism itself). On the other hand it deteriorates the mechanism performances generating pose (position and orientation) errors of the links, impacts of the pairing elements, vibrations and noise. Joint clearance can be eliminated by preloading the pairing elements. However, preloaded pairs may result in objectionable mechanism sound, higher power losses and wear, overheating, and overload bearing. Hence, joint clearance is preferred when zero clearance joints are not explicitly required. In any case, it is quite important to quantify the effects joint clearance has on the mechanism accuracy in order to define the minimum level of suitable tolerances that allows the mechanism to achieve the required performances: specifying unnecessarily close tolerances would increase the manufacturing cost of the mechanism. Moreover, interesting overconstrained mechanisms have been recently proposed as three-degree-of-freedom (dof) translational or orientational mechanisms (Gosselin and Angeles, 1989; Zhao and Huang, 2000). For these mechanisms joint clearance is unavoidable. This also calls for an accurate investigation of its effects on the mechanism kinematic performances. Nevertheless, it is the opinion of the authors that the influence of joint clearance is not given the attention it deserves, and its importance is not fully recognized - especially when performances of open (serial) and closed (parallel) chains have to be compared. In fact, while the influence of joint clearance on the accuracy of serial mechanisms has been widely investigated (Wang and Roth, 1988b; Waldron and Kumar, 1979; Kakizaki *et al.*, 1993), only few papers presented investigations on closed chain mechanisms (Xu, 1987; Innocenti, 1998; Tischler and Samuel, 1998), and comparative studies on serial versus parallel mechanisms are particularly lacking (Tlusty *et al.*, 1999). For instance, some papers credit parallel mechanisms to be superior to serial ones without presenting sound evidence. The importance of joint clearance is not properly considered also in the design of some spatial parallel mechanisms where, in spite of the innovative designs and excellent performances of the ideal clearance-free mechanisms, the unavoidable presence of joint clearance can compromise or at least dramatically reduce their kinematic performances (Carricato and Parenti-Castelli, 2002). The effect of clearance is inherently stochastic (Shi, 1997), but can be modelled as a deterministic one (Bodur and Derby, 1988). Many papers presented methods for evaluating the effects of joint clearance in planar mechanisms (Kolhatkar and Yajnik, 1970; Yin and Wu, 1990; Garrett and Hall, 1969; Biswas and Kinzel, 1998; Innocenti, 1999; Parenti-Castelli and Venanzi, 2002a) and only a few in spatial mechanisms (Innocenti, 1998; Tischler and Samuel, 1998; Parenti-Castelli and Venanzi, 2002b). Some of them deal with 1-dof planar and spatial mechanism (Horie *et al.*, 1985; Tavkhelidze *et al.*, 1979; Phillips, 1971); several, more recent, report effects of manufacturing and joint clearance on mechanisms with many dof (Innocenti, 1998; Bodur and Derby, 1988; Venanzi, 2000; Parenti-Castelli and Venanzi, 2002b). Most papers assume a rigid body model for the pairing elements and neglect friction.

The influence of joint clearance on the accuracy of the link of interest depends on many factors, such as the size of the mechanism links, the size of the pairing elements, the mechanism configuration, and the direction of the reaction the pairing elements mutually exchange. Conversely, the knowledge of joint clearance effects is relevant for the design of mechanisms and, in particular, for the optimal design of mechanisms geometry and the optimal tolerances allocation (Parenti-Castelli *et al.*, 2001), for the choice of the optimal configuration among those possible of a serial manipulator, and for the re-definition of the singularity loci. Only kinematic effects of joint clearance are investigated in this paper, dynamic effects (Dubowsky *et al.*, 1987) being beyond its scope. In particular, there are questions still to be answered such as which type of machine (serial or parallel) is superior. The question is difficult because of the inherent difference of these machines. Indeed, the comparison would imply consideration of many factors such as workspace, joint clearance, size of the machine links, mass of the machine, singularities, etc. (Wenger *et al.*, 1999). These parameters are difficult to compare, again because of the different nature of the two types of machines. In this context, then, it seems somehow useful to show, by means of examples, a comparative study on the influence of joint clearance on the accuracy of serial and parallel manipulators.

This paper presents the results of numerical simulations obtained by using an automatic code which can take into account the effects of joint clearance on the pose of any link of interest in spatial mechanisms (Parenti-Castelli and Venanzi, 2002b). The paper has a dual purpose. First, it represents a basis for showing and discussing clearance effects on the two types of mechanisms by means of examples, and second, it aims to somehow provoke a fertile debate and further studies on joint clearance for its importance in mechanism performances. The results of the simulations, in fact, will reveal contrasting effects of joint clearance for serial and parallel mechanisms. These effects are not yet clearly recognized in the current literature which, indeed, sometimes reports generic statements attributing a superior behavior to serial (Tlusty *et al.*, 1999) over parallel manipulators or viceversa (Patel and Ahmann, 1997), thus generating incorrect points of view.

2 Comparison between the PUMA Manipulator and the Generalized Stewart Platform (GSP)

This section will compare the behavior of a serial and a parallel manipulator, both affected by joint clearance. The two manipulators were chosen with similar dimensions, meaning that their overall size can be compared. Such a similarity criterium is not particularly significant, as the manipulator properties are very different: with similar overall size, the serial manipulator has a larger workspace, while the parallel one has a higher payload. However, this criterium was chosen because a choice providing the same workspace and payload for both the manipulators would have been unrealistic.

The PUMA manipulator was chosen to represent serial manipulators. It consists of an open chain formed by six binary links, interconnected by six controlled revolute pairs. Figure 1 shows the kinematic model of the manipulator in the reference configuration (henceforth, all lengths are in arbitrary length units). The manipulator has six dof, and the six revolute pairs control the position of the end effector (link 6) and its orientation. Moreover, the manipulator has a spherical wrist with center at point C, where the last three revolute pair axes intersect. The three revolute pairs close to the end effector control its orientation about the wrist center, whereas the remaining ones control the position of the wrist center itself. All the revolute pairs in the mechanism are affected by clearance. In order to evaluate the influence of clearance, a kinematic model providing the clearance-affected pair behavior is needed. A suitable model, presented in (Wang and Roth, 1988a), was chosen. The model describes the behavior of the clearance-affected revolute pair designed as journal bearing, like the one shown in Fig. 2. This model was chosen as representative of all the revolute pairs in the PUMA, even if the actual design of each pair is much more complex. In order to use this model, the geometric dimensions of each pair are

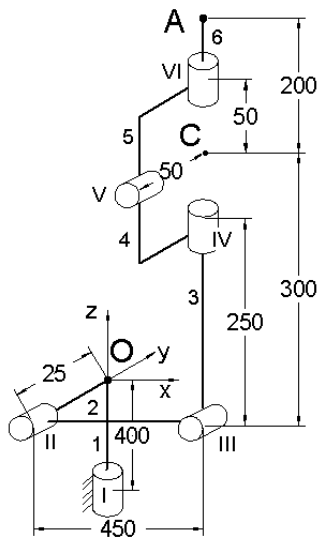

Figure 1: The PUMA manipulator

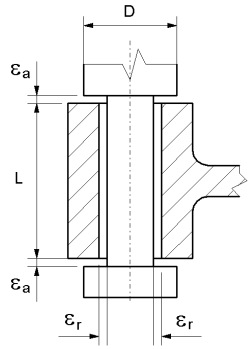

Figure 2: Kinematic model for the clearance-affected revolute pair

Table 1: Pair dimensions and clearance magnitude in the PUMA (arbitrary length units)

Pair Number	Diameter (D)	Length (L)	Radial Clearance (ε_r)	Axial Clearance (ε_a)
I	200	200	0.064	0.070
II	180	180	0.057	0.060
III	150	150	0.057	0.060
IV	120	120	0.049	0.050
V	80	80	0.042	0.050
VI	80	80	0.042	0.050

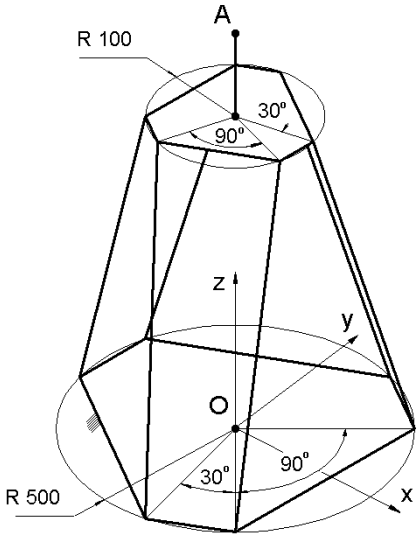

Figure 3: Generalized Stewart Platform

needed. With reference to Fig. 2, Table 1 reports the geometrical dimensions for each pair, together with the magnitude of clearance. As far as clearance magnitude is concerned, a coupling tolerance H6/g5 - as defined by the UNI ISO 286/1 Standard - was chosen for all the revolute pairs.

The Generalized Stewart Platform (GSP) was chosen to represent parallel manipulators (see Fig. 3). It comprises two platforms, one assumed as the frame (base), the other one movable (platform), interconnected by six serial chains (legs). Each leg is connected to the base by a universal joint and to the platform by a spherical pair. Because of design reasons, the spherical pairs are replaced by three revolute pairs with intersecting axes. Usually, two of the revolute pairs are realized so as to form a universal joint (see Fig. 4). In the inferior universal joint, the axis of the revolute pair consistent with the base is placed on a line tangent to the circle circumscribing the base itself. Similarly, in the superior universal joint the axis of the revolute pair consistent with the platform is placed on a line tangent to the circle circumscribing the platform. Each leg contains a prismatic pair. All the revolute pairs are idle, whereas the six prismatic pairs are controlled and provide the platform with six dof with respect to the base. All

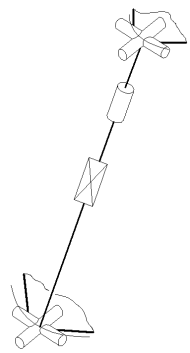

Figure 4: Leg of the Generalized Stewart Platform

the revolute pairs were considered affected by clearance, while clearance in the prismatic pairs was ignored. Clearance in the revolute pairs was modeled using the same kinematic models as in the previous manipulator. All the pairs where assumed identical; with reference to Fig. 2, their dimensions are $D = 20$, $L = 100$. As far as clearance is concerned, the same coupling tolerance H6/g5 was chosen (UNI ISO 286/1 Standard) and the values $\varepsilon_r = 0.030$ and $\varepsilon_a = 0.050$ were obtained.

In order to estimate the influence of clearance on the two manipulators a clearance evaluation technique was used. This technique, presented in (Parenti-Castelli and Venanzi, 2002b), is based on the Principle of Virtual Work. It directly provides the position and orientation (pose) error of the mechanism end effector under the action of an external load, once the mechanism configuration has been assigned. The end effector position error is intended as a three-component vector representing the difference between the theoretical and the actual position of a point of the end effector itself in the Cartesian space. In what follows, the norm of such a vector has been chosen as the index of the end effector position error. Similarly, the end effector orientation error is a three-component vector representing the difference between the ideal and the actual orientation of the end effector. The three components can be intended as three infinitesimal rotations - about three fixed axes - which are needed to rotate the end effector from the actual to the ideal orientation. The norm of such a vector has been used to represent the end effector orientation error.

The technique works when linearity conditions are satisfied, and the effects of clearance in the kinematic pairs can be linearly added. In order to have linearity conditions, the two following hypotheses have to be fulfilled:

- clearance magnitude has to be much smaller than the other pair dimensions;
- friction between the pairing elements can be ignored.

The two hypotheses are usually acceptable. The technique provides the end effector pose error when the mechanism configuration and the external load acting on it are given. In order to perform numerical simulations, an external load representing the

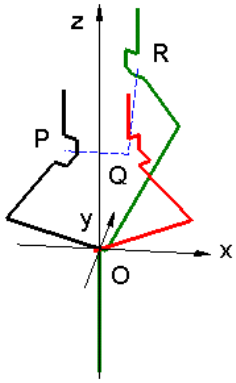

Figure 5: Path 1 for the PUMA

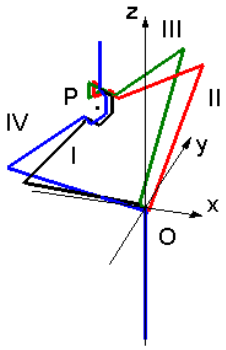

Figure 6: PUMA configurations at point P on path 1

gravity effect was chosen for both the mechanisms. Such an external load is along the z-axis and has its negative direction (in the two reference systems shown in Figs. 1 and 3) and is applied on the end effector (point A in Figs. 1 and 3). Its magnitude is not relevant since clearance behavior depends only on the load direction. After choosing the external load, the mechanism configuration has to be assigned. Two paths in the workspace were chosen instead of a particular configuration only.

2.1 Simulation 1

In the first case, with reference to system (x, y, z) centered in O shown in Fig. 5, the following path was chosen for the Puma: the center of the spherical wrist passes from point $P = (-100, -100, +350)$ to point $Q = (+100, -100, +350)$ and then to point $R = (+100, +100, +550)$. The orientation of the end effector is constant, and is the same as that shown in the reference configuration (see Fig. 5). The inverse position analysis of the PUMA provides, as known, eight possible configurations. In this first simulation four configurations only were considered. Figure 6 depicts the four configurations in the first point of the chosen path, when the wrist center is at point P. The first configuration is drawn in black, the second in red, the third in green and the fourth in blue.

The same path was chosen for the GSP, and is shown

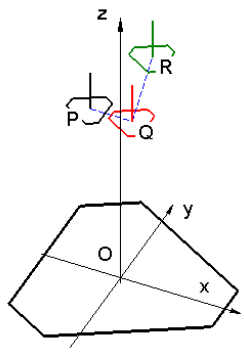

Figure 7: Path 1 for the Generalized Stewart Platform

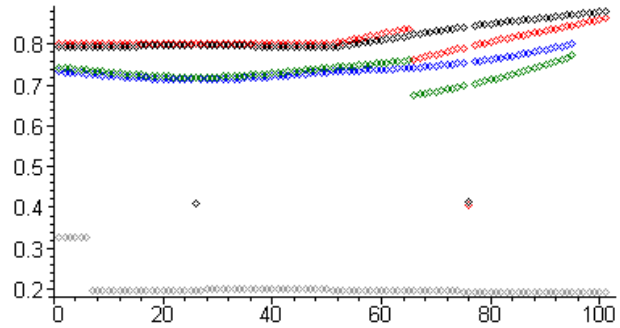

Figure 8: Position error (arbitrary length units) versus path 1

in Fig. 7 (for the sake of clarity, Fig. 7 shows the platform and the base only; the legs are not shown). The platform center passes from point $P = (-100, -100, +920)$ to point $Q = (+100, -100, +920)$, and then to point $R = (+100, +100, +1120)$. Point coordinates are expressed in the reference system shown in Fig. 7 and centered in O. The orientation of the platform is constant, and is the same as the orientation of the PUMA end effector.

Figure 8 shows the position error obtained with the first simulation. On the x-axis a label associated with the chosen path is reported (the path was split into 100 different positions); on the y axis the norm of the position error is reported. The light gray values represent the position error of the GSP, whereas the black, red, green and blue values are associated with the four chosen PUMA configurations. The colors are the same as those of Fig. 6. It clearly appears that the GSP behaves better than the PUMA, that is, clearance is less influent in the parallel mechanism. Moreover, it can be observed that configurations III and IV in the PUMA (green and blue values) are less error-affected than configurations I and II (black and red values).

Figure 9 shows the orientation error obtained with the first simulation. On the x-axis a label indicating the 100 positions the path was split into is shown. On the y axis the norm of the end effector orientation error is reported. The color association is the same as for Fig. 8: light gray for the GSP, black for the first, red for the second, green for the third and blue for the fourth PUMA configuration. On average, the GSP behaves better than

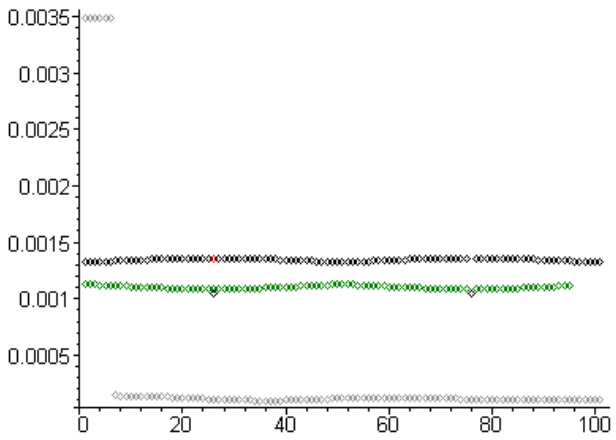

Figure 9: Orientation error (radians) versus path 1

the PUMA. However, it has to be noticed that at the beginning of the path the platform orientation error is much higher than in the remaining part of the path. This can be explained if the leg behavior is examined. In the central part of the path, where the platform is close to the central symmetry position, all the legs are compressed. Clearance in all the kinematic pairs is taken up in the same direction. Consequently, the platform displacement caused by clearance is almost a pure translation, and the orientation error is very small. On the contrary, when the platform is not close to the central symmetry position, some of the legs could be in tension and some other in compression. Clearance in the leg kinematic pairs is taken up in opposite directions. The platform displacement, then, is not a translation, and the orientation error is much higher than in the previous case. Figure 9 shows that the passage between these two situations is sudden. For the PUMA, it can be observed that the orientation error is almost constant. Configuration III gives the same orientation error as configuration IV (the blue points are fully covered by the green ones). Similarly, configuration II gives the same error as configuration I (the red points are fully covered by the black ones). Again, configurations III and IV behave better than configurations I and II.

2.2 Simulation 2

The second numerical simulation was performed with the same external load as in the first one. On the contrary, the mechanism path was slightly different. Figure 10 illustrates the PUMA path. The wrist center has the same position as in the first case, but the orientation of the end effector is different. With regard to the first case, the end effector was given a rotation of 45° about the y-axis. Its new orientation is kept constant along the whole path. In Fig. 10 one of the PUMA configurations is shown when the end effector center is at points P, Q, and R. Again, four possible configurations were considered. The four configurations are depicted in Fig. 11, the first one plotted in black, the second in red, the third in green and the fourth in blue. An identical path

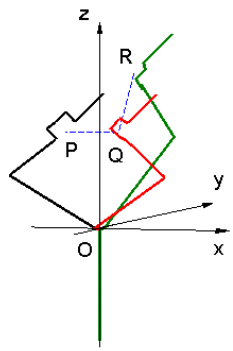

Figure 10: Path 2 for the PUMA

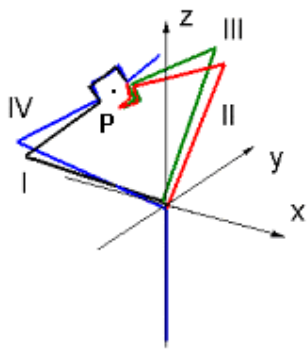

Figure 11: PUMA configurations at point P on path 2

was performed by the GSP (see Fig. 12). The platform center passes from point $P = (-100, -100, +920)$ through point $Q = (+100, -100, +920)$ to point $R = (+100, +100, +1120)$. Point coordinates are expressed in the reference system shown in Fig. 12 and centered in O. With respect to simulation 1, the platform here has been rotated of 45° about the y-axis, and its orientation is constant along the path (likewise the orientation of the PUMA end effector).

Figure 13 shows the simulation results for the position error of the end effector. As in the previous case, a label associated with the mechanism position along the path is reported on the x-

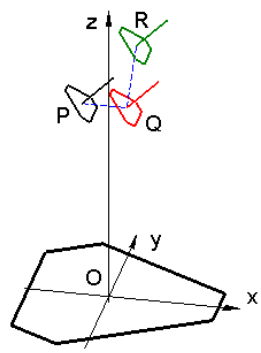

Figure 12: Path 2 for the Generalized Stewart Platform

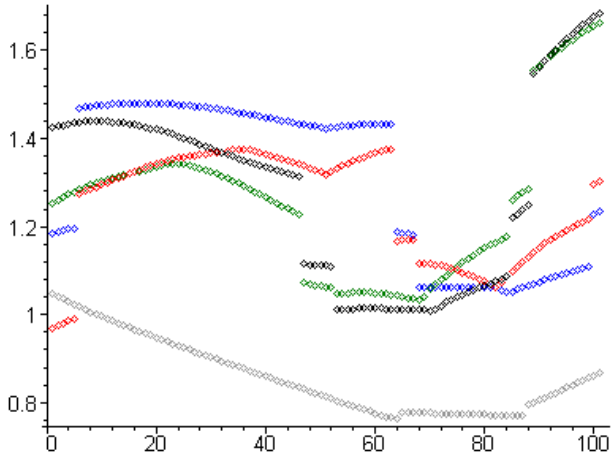

Figure 13: Position error (arbitrary length units) versus path 2

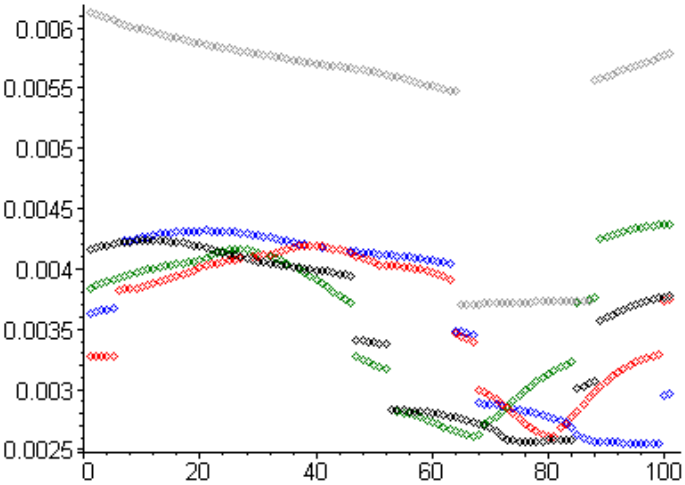

Figure 14: Orientation error (radians) versus path 2

axis, while the norm of the position error is shown on the y-axis. The light gray values are associated with the GSP, whereas the black, red, green and blue values refer to the four PUMA configurations I, II, III and IV respectively. Inspection of Fig. 13 shows that the GSP has a more regular behavior, and behaves definitely better than the PUMA. Its position error has two sudden variations (jumps), while all the PUMA configurations have four jumps. As in the previous case, the jumps are due to taking up clearance in different directions. Figure 14 shows that, when the orientation error is considered, the serial manipulator behaves better than the parallel for all the four configurations. With respect to Fig. 9, it can be noted that changing the platform orientation for the parallel manipulator causes a substantial reduction of the path portion where clearance is taken up in the same direction for all legs and the orientation error is lower. Anyway, even in that portion of the path the PUMA behaves better.

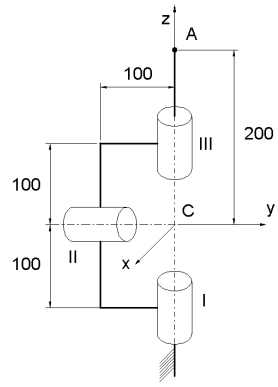

Figure 15: Serial Spherical Wrist

Table 2: Revolute pairs dimensions and clearance magnitude in the serial spherical wrist (arbitrary length units)

Pair Number	Diameter (D)	Length (L)	Radial Clearance (ε_r)	Axial Clearance (ε_a)
I	30	30	0.029	0.030
II	25	25	0.029	0.030
III	20	20	0.025	0.030

3 Comparison between a Serial and a Parallel Spherical Wrist

Finally, two other mechanisms were chosen to study the influence of clearance in the joints. The first one is a spherical wrist with serial structure. The mechanism is composed of two binary links, a frame, and the end effector, interconnected by three controlled revolute pairs (see Fig. 15). The revolute pair axes intersect in a common point, the wrist center (point C in Fig. 15). The mechanism has three dof, and the end effector orientation can be fully controlled by the three revolute pairs. The three revolute pairs are clearance-affected. Their behavior was studied using the pair kinematic model presented in (Wang and Roth, 1988a) (like in the previous examples). With reference to Fig. 2, the pair dimensions are reported in Table 2. The second mechanism is the parallel spherical wrist shown in Fig. 16. It consists of two equilateral triangles, one fixed (base) and one mobile (platform). Base and platform are connected by a spherical pair, centered at point C (see Fig. 16). The spherical pair is physically realized by a universal joint centered at C and a revolute pair located at the platform center, whose axis passes through point C. Three lateral legs are connected to the vertices of the base by a universal joint and to the vertices of the platform by a spherical pair, intended as the union of a revolute and a universal joint. Each lateral leg includes an actuated prismatic pair. The detailed model for the legs is shown in Fig. 4. The mechanism has three degrees of freedom, and the platform can fully rotate about the spherical wrist center. Its orientation is controlled by the length of the lateral legs. All

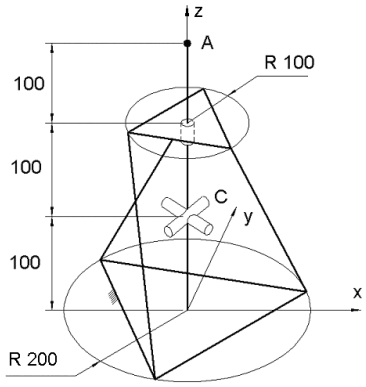

Figure 16: Parallel Spherical Wrist

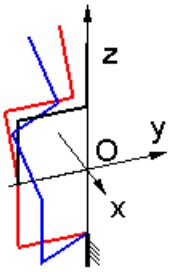

Figure 17: Path for the Serial Spherical Wrist

the revolute and universal joints are affected by clearance. The kinematic model for the clearance-affected pairs is the same as in the previous cases. All the pairs were considered to have the same dimensions; with reference to Fig. 2, $D = 10$, $L = 30$. The same coupling tolerance H6/g5 (UNI ISO 286/1 Standard) was considered, thus providing clearance magnitude $\varepsilon_r = 0.025$ and $\varepsilon_a = 0.030$.

The influence of clearance for these two mechanisms was evaluated using the same technique presented in (Parenti-Castelli and Venanzi, 2002b). The two mechanisms were loaded on a point of the end effector (point A in Figs. 15 and 16). The external load is along the z-axis and has its negative direction, and can be intended as the effect of gravity. Its magnitude is not relevant.

Figure 17 shows the serial mechanism at three positions on the performed path. The starting configuration is drawn in black. From the starting configuration, a first rotation of -30° was applied to the second revolute pair. The red configuration was obtained. Then, a further rotation of 30° was applied to the first revolute pair, and the blue configuration was the result. Last, a rotation of 30° about the third revolute pair was imposed. The same path was performed by the parallel mechanism. Figure 18 shows the first rotation: the mechanism passes from the black to the red configuration with a rotation of -30° about the y-axis. Figure 19 shows the second rotation in a top view: the mechanism passes from the red to the green configuration with a rotation of 30° about the z-axis. Figure 20 shows the final rotation of 30° about the platform axis: the mechanism passes from the

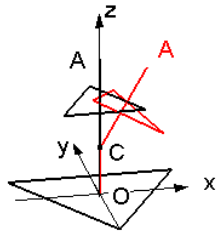

Figure 18: First rotation for the Parallel Spherical Wrist

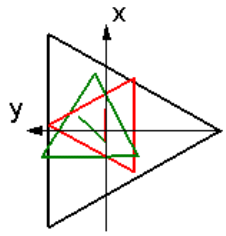

Figure 19: Second rotation for the Parallel Spherical Wrist

green to the blue configuration. The final configuration, drawn in blue in Fig. 20, is a singular configuration for the mechanism.

Numerical simulations were performed for the two mechanisms moving along the shown path. The results are illustrated in Fig. 21: on the x-axis there is a label associated with the mechanism configuration as it changes along the path (on which 61 representative points were chosen). On the y-axis the norm of the end effector orientation error is reported (in radians). In Fig. 21 the norm of such a vector is reported in blue for the parallel mechanism, in red for the serial one. Figure 21 reveals that the parallel mechanism gives better performances than the serial one, as its orientation error is always inferior. The only exception is in the last part of the path: when the parallel mechanism is close to singularity its orientation error suddenly grows. The orientation error for the parallel mechanism in the final point of the path is not reported, as the parallel mechanism is in a singularity configuration, and its orientation error cannot be defined. Similar results were obtained when the position error of point A was studied, and are shown in Fig. 22. The position error of point A is almost identical to the orientation error, as the former is almost completely caused by the latter. By knowing the orien-

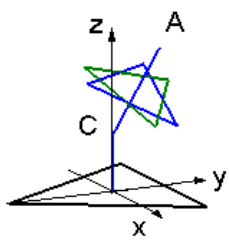

Figure 20: Third rotation for the Parallel Spherical Wrist

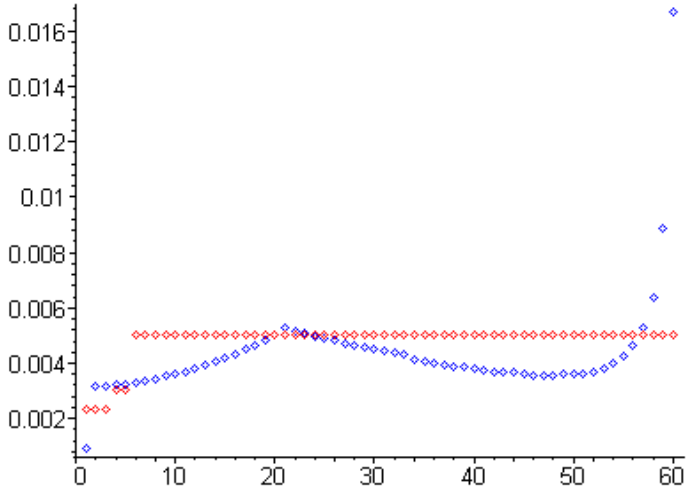

Figure 21: Orientation error (radians) for the serial (red) and the parallel (blue) spherical wrists versus path 1

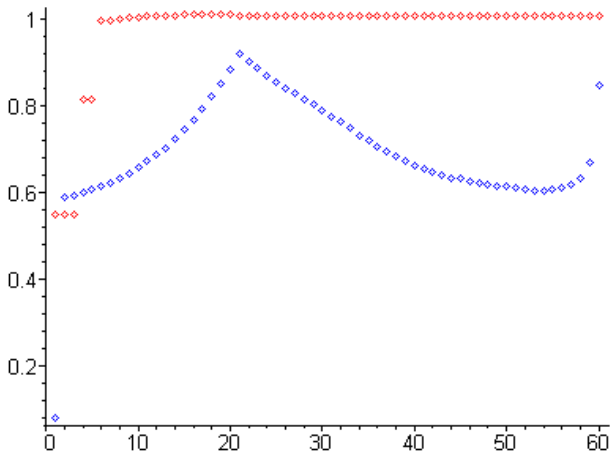

Figure 22: Position error (arbitrary length units) for the serial (red) and the parallel (blue) spherical wrists versus path 1

tation error and the position error of point A, the position error of the wrist center C could be obtained.

4 Conclusions

In this paper numerical simulations were performed on two serial and two parallel mechanisms, with the aim of evaluating joint clearance influence on the pose accuracy of the end effector. Based on the simulation results, the following considerations can be drawn:

- The influence of joint clearance has to be evaluated case by case. There is no a-priori evidence that serial manipulators are less or more sensitive to joint clearance than parallel ones.
- When comparing two mechanisms (serial and/or parallel), position and orientation errors may have contrasting values for the two mechanisms, i.e., one can have a better behavior as far as position, while the other can be better as far as orientation.

Acknowledgment

Funds by Italian MIUR and CNR are gratefully acknowledged.

References

Biswas, A., and Kinzel, G. L., 1998, ”An Iterative Kinematic and Force Solution Method for Revolute Joints with Clearance”, *Proceedings of 1998 ASME Design Engineering Technical Conference*, Paper DETC98/MECH-5491, Atlanta, USA.

Bodur, I. N., and Derby, S. J., 1988, ”Analysis and Modeling of the Positioning Inaccuracy of Industrial Manipulators in Off-Line Programming Part I: Due to Static Forces and Joint Clearances”, *Proceedings of ASME Conference*, Kissimmee, USA, pp. 383-391.

Broderick, P. L., and Cipra, R. J., 1988, ”A Method for Determining and Correcting Robot Position and Orientation Errors Due to Manufacturing”, *ASME Journal of Mechanisms, Transmissions, and Automation in Design*, vol. 110, pp. 3-10.

Carricato, M., and Parenti-Castelli, V., 2002, ”Singularity-Free Fully-Isotropic Translational Parallel Mechanisms”, *The International Journal of Robotics Research* (in press).

Dhande, S. G., and Chackraborty, J., 1978, ”Mechanical Error Analysis of Spatial Linkages”, *ASME Journal of Mechanical Design*, Vol. 100, pp. 732-738.

Dubowsky, S., Deck, J. F., and Costello, H., 1987, ”The Dynamic Modeling of Flexible Spatial Machine Systems with Clearance Connections”, *ASME Journal of Mechanisms, Transmissions, ad Automation in Design*, vol. 109, pp. 87-94.

Garrett, R. E., and Hall. A. S., 1969, ”Effect of Tolerance and Clearance in Linkage Design”, *ASME Journal of Engineering for Industry*, February 1969, pp. 198-202.

Gosselin, C., and Angeles, J., 1989. ”The Optimum Kinematic Design of a Spherical Three-degree-of-freedom Parallel Manipulator”, *ASME Journal of Mechanisms, Transmission and Automation in Design*, Vol. 111, No. 2, pp. 202-207.

Horie, M., Funabashi, H., Ogawa, K., and Kobayashi, H., 1985, ”A Displacement Analysis of Spatial Four-Bar Mechanisms”, *Bulletin of JSME*, vol. 28 No. 241, pp. 1535-1542.

Huang, Z., 1987, ”Error Analysis of Position and Orientation in Robot Manipulators”, *Mechanism and Machine Theory*, Vol. 22, pp. 577-581.

Innocenti, C., 1998, ”Kinematic Clearance Sensitivity Analysis of Spatial Structures with Revolute Joints”, *Proceedings of the 1998 ASME Design Engineering Technical Conference*, Paper DAC-8679, Las Vegas, USA.

Innocenti, C., 1999, ”A Static-Based Method to Evaluate the Effect of Joint Clearances on the Positioning Errors of Planar Mechanisms”, *Proceedings of the Tenth World Congress on the Theory of Machines and Mechanisms*, Oulu, Finland, pp. 650-655.

Kakizaki, T., Deck, J. F., and Dubowsky, S., 1993, ”Modeling the Spatial Dynamics of Robotic Manipulators with Flexible Links and Joint Clearances”, *ASME Journal of Mechanical Design*, vol. 115, pp. 839-847.

Kolhatkar, S. A., and Yajnik, K. S., 1970, ”The Effects of Play in the Joints of a Function-Generating Mechanism”, *Journal of Mechanisms*, Vol. 5, pp. 521-532.

Lakshminarayana, K., and Narayanamurthi, R. G., 1971, ”On the Analysis of the Effect of Tolerances in Linkages”, *Journal of Mechanisms*, vol. 6, pp. 59-67.

Parenti-Castelli, V., Venanzi, S., and Lenarcic, J., 2001, ”Influence of Geometry on the Kinematic Performances of a Humanoid Shoulder-Girdle Mechanism”, *Proceedings of 2001 IEEE/ASME International Conference on Advanced Intelligent Mechatronics Proceedings*, Como, Italy, pp. 260-265.

Parenti-Castelli, V., and Venanzi, S., 2002a, ”A New Technique for Clearance Influence Analysis in Planar Mechanisms”, *Proceedings of 2002 ASME Design Engineering Technical Conference*, Paper MECH-34318, Montreal, Canada.

Parenti-Castelli, V., and Venanzi, S., 2002b, ”A New Deterministic Model for Clearance Influence Analysis in Spatial Mechanisms”, *Proceedings of 2001 ASME International Mechanical Engineering Congress and Exposition*, Paper DSC-32485, New Orleans, USA.

Patel, A. J., and Ahmann, K. F., 1997, ”Volumetric Error Analysis of a GSP-Based Machine Tool”, *Annals of the CIRP*, vol. 46/1/1997, pp. 287-290.

Phillips, J., 1971, ”Geometry of Backlash in Spatial Mechanisms”, *Proceedings of the Third World Congress on the Theory of Mechanisms and Machines*, Paper H-25, Kupari, Yugoslavia, pp. 339-354.

Rehsteiner, F., Neugebauer, R., Spiewak, S., and Wieland, F., 1999, ”Putting Parallel Kinematics Machines (PKM) to Productive Work”, *Annals of the CIRP*.

Shi, Z., 1997, ”Synthesis of Mechanical Error in Spatial Linkages Based on Reliability Concept”, *Mechanism and Machine Theory*, vol. 32, No. 2, pp. 255-259.

Tavkhelidze, D. S., Davitashvili, N. S. and Demurishvili, N. V., 1979, ”The Determination of Technological Error in Spherical 4-Link Hinged Mechanism”, *Mechanism and Machine Theory*, vol. 14, pp. 43-59.

Tischler, C. R., and Samuel, A. E., 1998, ”Predicting the Slop of In-Series/Parallel Manipulators Caused by Joint Clearances”, *Advances in Robot Kinematics and Control*, (J. Lenarcic and M. L. Husty Eds.), Kluwer Academic Publishers, pp. 227-236.

Tlusty, J., Ziegert, J. and Ridgeway, S., 1999 (?), ”Fundamental Comparison of the Use of Serial and Parallel Kinematics for Machines Tools”, *Annals of CIRP*, pp. 451-456.

Venanzi, S., 2000, ”Influence of Kinematic Pair Clearance on the Configuration of Spatial Mecahnisms”, (in italian), Master Thesis, Bologna, Italy.

Waldron, K. J., and Kumar, A., 1979, ”Development of a Theory of Errors for Manipulators”, *Proceedings of the Fifth World Congress on Theory of Machines and Mechanisms*, Montreal, Canada, vol. 1 pp. 821-826.

Wang, J., and Masory, O., 1993, ”On the Accuracy of a Generalized Stewart Platform - Part I: The Effect of Manufacturing Tolerances”, *Proceedings of IEEE International Conference on Robotics and Automation*, Atlanta, USA, pp. 725-731.

Wang, H. H. S., and Roth, B., 1988a, ”Position Errors Due to Clearance in Journal Bearing”, *Proceedings of ASME Conference*, Kissimmee, USA, pp. 357-365.

Wang, H. H. S., and Roth, B., 1988b, ”Position Errors of Manipulators”, *Proceedings of RoManSy 7*, Krakow, Poland.

Wenger, P., Gosselin, C. and Maille, B., 1999, ”A Comparative Study of Serial and Parallel Mechanisms Topologies for Machine Tools”, *Proceedings of PKM’99*, Milano, Italy, pp. 23-32.

Xu, W., and Zhang, Q., 1987, ”On the Method of Combining Small Displacements in Studying the Kinematic Errors of Spatial Open - and Closed - Loop Linkages”, *Proceedings of the Seventh World Congress on the Theory of Machines and Mechanisms*, Sevilla, Spain, vol. 1, pp. 219-222.

Yin, Z. W., and Wu, J. K., 1990, ”An Optimal Synthesis of Linkages Considering Structural Error and Clearances”, *Proceedings of ASME Conference*, Chicago, USA, pp. 295-299.

Zhao, T. S., and Huang, Z., 2000, ”A Novel Three-DOF Translational Platform Mechanism and its Kinematics”, *Proceedings of 2000 ASME Design Engineering Technical Conference*, Paper MECH-14101, Baltimore, USA.

Proceedings of the WORKSHOP on
Fundamental Issues and Future Research Directions for Parallel Mechanisms and Manipulators
October 3–4, 2002, Quebec City, Quebec, Canada
Clément M. Gosselin and Imme Ebert-Uphoff, editors

Robotic Systems for Handling and Assembly
- High Dynamic Parallel Structures with Adaptronic Components -

MATHIAS KREFFT
Institute of Machine Tools and Production Technology
TU Braunschweig,Germany
m.krefft@tu-bs.de

MATTHIAS FRINDT
Siemens Dematic AG
München, Germany
matthias.frindt@mchrm.siemens.de

JÜRGEN HESSELBACH
Institute of Machine Tools and Production Technology
TU Braunschweig,Germany
j.hesselbach@tu-bs.de

FRIEDRICH M. WAHL
Institute of Robotic and Process Control
TU Braunschweig,Germany
f.wahl@tu-bs.de

Abstract: *Many applications in the field of production automation (material handling, assembly, etc.) require high operating speeds and accelerations. During the past years parallel robots proved to be an efficient and suitable supplement to serial robots. But for a better exploitation of the possibilities of these new types of robots the weak points of robots based on parallel structures have to be reduced as much as possible or – in the optimal case – completely extinguished. This is the starting point for a new research initiative with a multidisciplinary character, namely the Collaborative Research Centre 562 (SFB 562) "Robotic Systems for Handling and Assembly". The main goal of the Collaborative Research Centre 562 is to develop new types of robots based on closed kinematic chains to improve the structural and dynamic potential of such robots. The main focus is the modeling and control of new parallel structures and the consequent usage of new machine elements. In addition, by means of adaptronics it is possible to improve the dynamic and stiffness properties of parallel structures. The integration of active and multifunctional elements into lightweight links of parallel structures and suitable control concepts form an adaptive compound system minimizing movement oscillations for faster and more precise robot applications.*

1 Introduction

The usage of industrial robots is an important factor for economy. A survey of the International Federation of Robotics prognoses an annual growth rate of 15 %. In addition to a fortification of existing markets, such as automobile industry, the coverage of new application fields is of particular importance. In the future a great potential for robot systems is expected in particularly handling and assembly applications. The fast growing number of the installed industrial robots comes along with permanent increasing requirements on the dynamic performance. Economical as well as technological reasons require robot systems with improved efficiency data.

To reduce the sequence time for handling and assembly applications the most essential goal is to improve operating speeds and accelerations in the working space for given process accuracy. However, these increasing requirements end in a vicious circle (Fig.1):

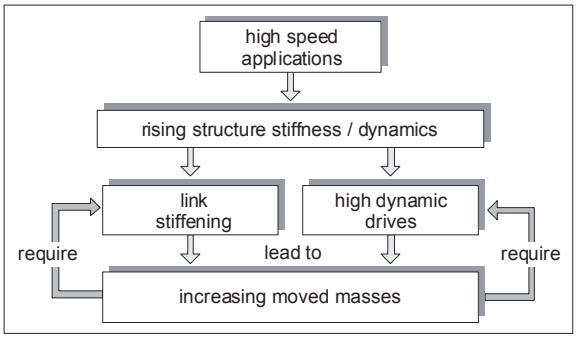

Fig. 1: Structural limits of industrial robot development

Corresponding author: Dipl.-Ing. Mathias Krefft, Institute of Machine Tools and Production Technology, Langer Kamp 19b, D-38106 Braunschweig, Germany, Phone: +49 531 / 391 – 7605, Fax: +49 531 / 391 – 2582, Email: m.krefft@tu-bs.de

The usage of high dynamic drives demands a higher stiffness of the links synonymous with rising moved masses. Due to that fact even higher dynamic drives are needed in order to move not only the handling objects but also the following links and drives. In other words: Both, the low stiffness and the high moved masses, cause oscillations that lead to a reduced quality of the products and shorten the life cycle of the whole mechanical system.

In addition, gear and joint backlash that are accumulated throughout the whole structure impair the positioning accuracy of the end effector. Supplementary, the necessity to lay the power supply and signal lines to each drive requires elaborate and not negligible engineering efforts.

Consequently, both contradictory goals, high operating velocity and high accuracy, cannot be achieved with conventional robots based on serial kinematic structures.

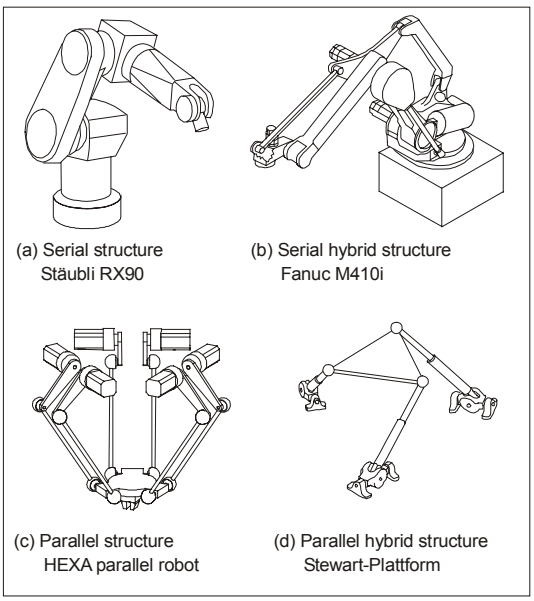

Fig. 2: Different types of robot structures

Under these circumstances the request of new robot systems is of major importance. During the past years parallel robots proved to be an efficient and suitable supplement to serial robots based on open kinematic chains (Fig. 2a). Compared to a conventional industrial robot, a parallel robot based on closed kinematic chains is a machine that consists of at least two driven guiding chains to guide a common working platform with a gripper or tool attached to it. Parallel structures can be realized with rotational or linear drives. Apart of these active joints, the parallel structures contain passive - not actuated - joints with one or more than one degree of freedom. Fully parallel structures are characterized by the fact that the amount of chains correspond to the degree of freedom of the structure. Well-known examples are the DELTA and HEXA robots (Fig. 2c) (Merlet, 2000). Combinations of serial and parallel structures are called hybrid structures, which unite certain advantages of these different structure types. It is important to distinguish between serial hybrid structures (FANUC M410I, Fig. 2b) and parallel hybrid structures (STEWART PLATTFORM, Fig. 2d) (Frindt, 2001, Hesselbach et al. 2001).

The possibility to mount all drives in the frame or near to the frame results in low moved masses allowing high operating speeds and accelerations. Due to the fact that the end-effector is supported by several guiding chains, further advantages are a high structural stiffness and a modular construction with standard elements. Even though parallel structures have significant disadvantages; first of all a poor workspace to construction room ratio combined with a limited movability in the workspace (particularly with regard to the orientation of the end-effector). Supplementary the passive joints with $f_i > 1$, e.g. cardanic or spherical joints, require considerable expenses.

2 Call for action

A commercial use of these new robot concepts will only be possible if the mathematical and mechanical design problems mentioned above are solved. Only a few robots come into a commercial operation. For example the 200I hexapod robot from FANUC or the FLEXPICKER DELTA robot from ABB FLEXIBLE AUTOMATION, which obtains an acceleration of 10 g and an accuracy of 0.5 mm. But despite of these promising machines showing the potential of parallel robots, these machines are single solutions for specific applications. Up to now comprehensive concepts for the development of parallel robots do not exist. A call for action for a better exploitation of the possibilities of these robots lies basically on this drawback. In the following the interdisciplinary fields of the call for action are defined:

- The present research activities are focused on a handful of symmetric kinematic structures, e.g. HEXAPOD, DELTA, PENTA or five joint robots (RP-1AH from MITSUBISHI) (Frindt, 1998). Still a lot of possible parallel structures remain unconsidered. A generic approach to structure synthesis in terms of given application has to be developed.

- Actually mainly conventional machine components are used. It is necessary to develop new solutions for the complex passive joints with two or more degrees of freedom. Ditto new technologies, e.g. using adaptronic elements for an active vibration damping, have met with no response. By means of adaptronics it is possible to improve the dynamics and the stiffness of parallel structures.

- Special characteristics of parallel structures however require new control functions, like working space survey or strategies for conflict situation escape. Considering the high dynamic applications new positioning and force control algorithms have to be developed. Especially the integrated adaptronic elements require special control solutions.

3 The SFB 562 - a new research initiative

3.1 Organization and main goals

In July 2000, the Deutsche Forschungsgemeinschaft (DFG) has established a new Collaborative Research Centre on "Robotic Systems for Handling and Assembly - High Dynamic Parallel Structures with Adaptronic Components" in Braunschweig, the SFB 562. Seven research institutes from the Technical University in Braunschweig and one institute from the German Aerospace Centre (DLR) are developing new methods and components related to new types of parallel robots. The members of the SFB 562 foundation belong to three faculties: i.e. mechanical (4 institutes) and electrical (2) engineers as well as computer scientists (2).

The main goal of the Collaborative Research Centre is the evolution of methodical and component related fundamentals for the development of robot systems based on closed kinematic chains in order to improve the promising potential of these robots, particularly with regard to high operating speeds and accelerations, which are essential for handling and assembly applications. In addition, the loading of machine tools belongs to the target application fields (Fig. 3).

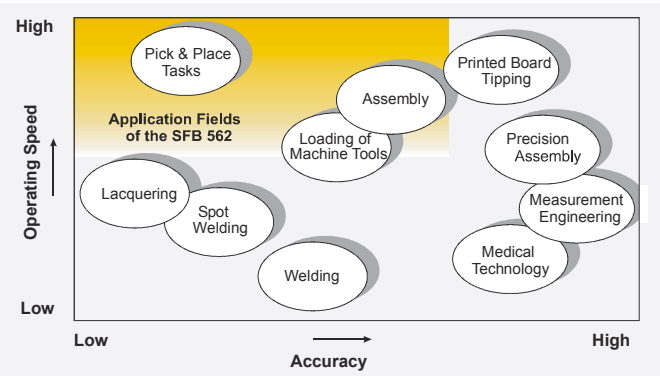

Fig. 3: Application fields of the SFB 562

Initial point of the investigations is the call for action (see chapter 2). A consequent exploitation is possible until the mentioned weak points are reduced as much as possible or – in the optimal case – completely extinguished. This is the motivation for the Collaborative Research Centre 562 working on the subsequent fields:

- Basic investigations for new structure and software concepts and the modeling of the kinematic and dynamic behavior with regard to the included components.
- Robot control and information processing with respect to integrated sensors and adaptronic elements; including modular software architecture and parallel specific robot programming.
- Development and optimization of single components of the mechanical structure.

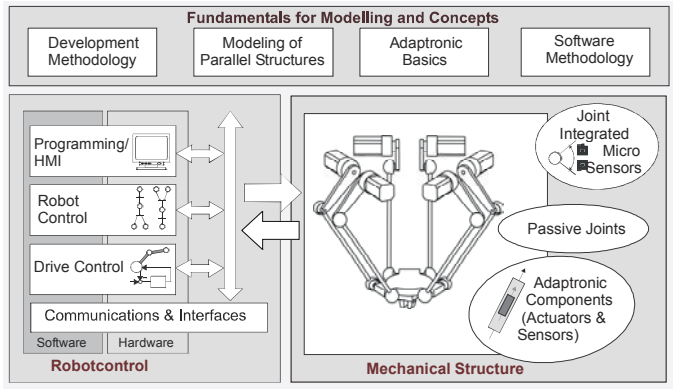

Fig 4: Research fields

The necessary investigations of the SFB 562 are demonstrated by means of Fig. 4. According to this the SFB 562 is subdivided into three project fields:

- Modeling
- Robot control and information processing
- New components

In the following three sections, the working fields, the basic ideas and approaches as well as first results are demonstrated in detail. Every section will start with the initial point and the resultant call for action. The outcomes of this are the intentions and approaches of the SFB 562.

4 Concepts and modeling

4.1 Initial point and call for action

In literature one will find a lot of various parallel structures. However, up to now there is no comprehensive systematic classifying and evaluating of parallel structures. Present approaches summarize known parallel structures or deal with special classes, particularly with symmetric structures with three or six degrees of freedom. Parallel structures with four degrees of freedom or hybrid structures have been almost ignored.

The dynamic behavior of parallel structures can be modeled with the existing mathematical and mechanical methods. To fulfill the requirements of the high dynamic applications the resulting equations have to be solved in real-time. Considering the varying payload during robot motion the equations of motion have to be prepared for adaptive control concepts.

4.2 Intentions and approaches

4.2.1 Structure synthesis and design methodology

The kinematic features of parallel robots strongly depend on their mechanical design, the arrangement of the joints within the chains and the geometrical dimensions. Starting point for a generic structure synthesis is a systematic classification of

parallel robots in consideration of the characteristic properties. These are for example the number of kinematic chains *k* or the dof *F* using Grüblers formula. This leads to a distribution of the joint dof intra the kinematic chains (Fig. 5). The structure synthesis will include extensions by additional branches for kinematic constraint conditions. These concepts are based on the idea to integrate plane substructures in spatial structures using parallelogram guidance mechanisms. Especially structures with the same kinematic chains belong to a special structure family. Thus a parameterization, i.e. definition of characteristic geometric parameters (e.g. link lengths, platform radius etc.), can be made very easily. This is very important for the structure analysis and optimization.

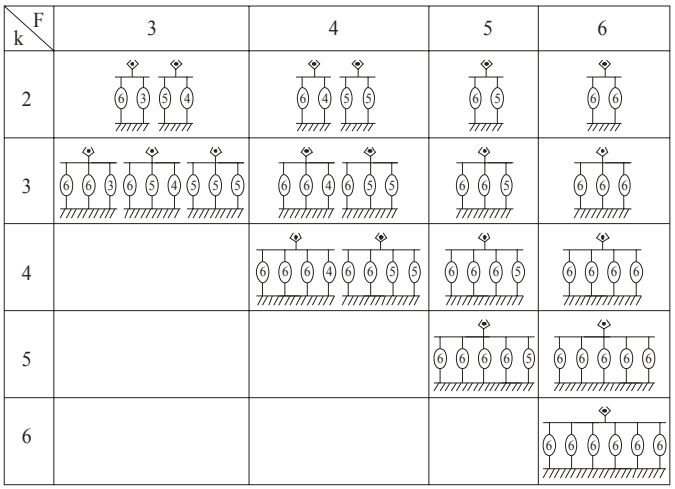

Fig. 5: Structure synthesis

Parallel robot development in SFB 562 is based on knowledge-based-methods. Therefore creating methodical information databases is a very important factor in structure synthesis. In contrast to existing design catalogues not only geometrical parameters but also operating procedures, machine parts modeled in UNIGRAPHICS (e.g. joints, sensors, links etc.) and style guides are included. Ditto it is important to classify structure performance criteria of available components in preliminary development phases. An internet based dynamic design catalogue EKAT as a modern data processing technology will increase the capability of information memories for the design process (Franke et al., 2001). In consideration of the modularity of parallel robots construction kits have to be developed. These extended design catalogues store technical information in a systematic and effective way. They allow a fast access to comprehensive and actual information sources. The knowledge is sorted systematically by a uniquely defined classification. Selected characteristics subclassify the stored knowledge and open a solution tree that separates the catalogues-objects clearly.

By using the knowledge-based-methods a methodical and complete classification of parallel robots and their components become possible. Another approach is to assort the demands of industrial applications, i.e. handling and assembly, in constraint networks. In order of an application-oriented development, the "robot catalogues" and the "application requirements" are linked together for finding an optimal solution.

4.2.2 Kinematic and dynamic modeling and analysis

The general basis for simulation, optimization and design layout according to given problems in the field of robot control is the preparation of the kinematic and dynamic models of the parallel robots. Intra the SFB 562 the multibody simulation tool SIMPACK is used, because the DLR was actively involved in its development. The included time integration algorithm ODASSL for solving differential algebraic equations is well suited for solving equations of motion of parallel structures (Führer, 1988).

The capability to generate a symbolic code of the equations of motion of multibody systems is a powerful tool since it allows a versatile means to include models in independent working environments. This is in view of simulation, performing optimization work as well as parameter identification, control and design an important property. Furthermore, the efficient programming of the equations of motion of complex multibody systems in SIMPACK has proven its ability to provide very good results for real-time computation. For modeling elastic and flexible bodies an interface to ANSYS FEM can be used.

This approach will allow to create a simulation and development environment for all types of parallel structures, e.g. to specify the drive performance or to identify the eigenmodes. In opposite to the present description of the kinematic and dynamic behavior of the parallel robots, the use of the multibody simulation tool SIMPACK allows a fast developing process. With respect to the modularity of parallel structures a SIMPACK library with different kinematic chains as well as frames and platforms with predetermined parameters is developed. With the help of this construction kit the modeling of new parallel structures in SIMPACK can be done very easily. Considering the parameterization of the kinematic chains and the platforms multiple variants of parallel robots can be simulated.

To provide the kinematics and dynamics for the robot control the equations of motion can be exported in a symbolic code description. By using the Newton-Raphson iteration method and the ODASSL time integration algorithm the equations of motion can be solved independently of SIMPACK in the different modules of the robot control, e.g. model-based force control or the inverse kinematic problem (IKP) and the direct kinematic problem (DKP) (Fig. 6).

Nevertheless, analytical kinematic and dynamic descriptions are not negligible. In addition to the multibody approach, a new schematic method for kinematic analysis and optimization is used. With respect to the modular structure of parallel robots, the computation is divided into a sequence of single steps according to the modular kinematic analysis of planar linkages as described in the guideline 'VDI-Richtlinie 2729'. This method is completed by a schematic procedure for deriving the general transmission matrix. This procedure is

founded on the idea of constraint conditions, which fix the geometry of single links and joints. By connecting all links, the corresponding conditions are summarized in the transmission matrix. The elements of the transmission matrix represent partial derivatives between all geometrical parameters and the coordinates of the joints thus forming a database with all kinematic information about the parallel structure. This is the starting point for optimization. There are different intentions for the structure synthesis and optimization of parallel robots. Especially, on the one hand a high velocity transmission, i.e. the Jacobian matrix J, is essential. On the other hand a good transmission of forces, i.e. $G = J^T$, is required. Both goals are contradictory. Usually, all kinematic performance criteria depend on the pose. In terms of significant structure criteria, pose independent key figures have to be determined. The approach for finding the optimal layout of a parallel structure with a particular degree of freedom emerging from a given application is as follows: First of all the application requirements have to be represented by mathematical performance criteria: The first criteria will be the workspace / construction room ratio. The shape of the workspace of a chosen structure is compared with simple geometrical bodies like: sphere, ellipsoid, cuboid, cylinder, prism, pyramid and torus for spatial structures. For plane structures rectangles, triangles, circles and ellipses are taken. Other criteria depending on the applications are for instance (Frindt, 2001, Gosselin, 1998, Schönherr, 1998): transmission quality, manipularibility, local dexterity and stiffness condition. The sum of the different mathematical criteria mentioned above multiplied (=assessed) with a weighting-factor represent the needful degree of performance of the underlying application requirements.

5 Robot control and information processing

5.1 Initial point and call for action

The promising possibilities of parallel structures cannot yield profit until the problems of the mechanical structure, e.g. singularities, collisions and the limited range of motion of the passive joints, have been solved by the robot control. Up to now there is no commercial robot control available fitting the requirements for all kind of parallel robots. This means that control functions of conventional robot control technology must be combined with parallel robot specific allocative functions (Hesselbach, Kusiek, 2000, Jansen, 1996).

The payload / robot mass ratio of parallel structures is even higher compared to serial robots, where the influence of the payload on the impedance of the robot is negligible. By use of direct drives the influence of a variable payload cannot be ignored. The adaptive control effort rises when parallel robot specific coupling terms have to be regarded in a model-based control and real-time requirements have to be fulfilled (Tsai, 1999, Sciavicco, Siciliano, 2000).

A survey of the Fraunhofer Institute of Production Technology and Automation discovered faults in the operator convenience of robot systems. Therefore further investigations for a HMI supporting the operator have to be done. A motion orientated robot programming language as well as visual aids are required.

Considering the use of adaptronic components (see chapter 6) additional sensor and actuator functions have to be implemented in the control and concatenate the corresponding hardware with a special communication system.

5.2 Intentions and approaches

5.2.1 Machine-orientated control functions

In order to take full advantage of the inherent structural possibilities of parallel robots new adapted machine-orientated control functions have to be included in the robot control architecture. One challenging task is the realization of efficient workspace monitoring concepts allowing the robot to move safely at arbitrary velocities within the whole workspace. The workspace monitoring has to prevent singular positions, collisions between structural elements, violation of passive joint angles etc.

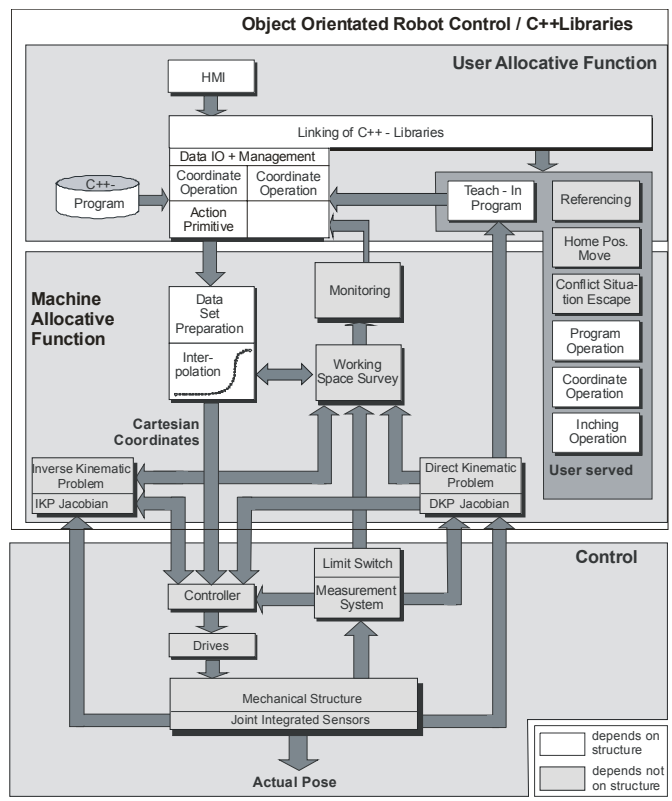

Fig. 6: The robot control functionalities

In contrast to serial robots, singularities of the 2nd type appear inside the workspace (Merlet, 2000). That means that the determinant of the Jacobian matrix of the DKP vanishes. In that case the robot obtains an additional degree of freedom and the structure can become uncontrollable as soon as a force is initiated to the platform and any further movement might

destroy the robot. In addition, the range of the passive joints must be taken into consideration. Thus a workspace survey module must be able to check the motion of the robot in real-time. The basis for monitoring the appearance of singularities is Grassmanns Theory (Gosselin, Angeles, 1990). This requires transformation equations of the DKP with reduced computing time. However, the DKP of parallel structures opposite to serial structures cannot be solved by an analytical way in general (Tsai, 1999). Rather iterative numeric procedures are necessary, which cannot guarantee numeric convergence or limited computation time. By integrating additional sensors into the passive joints, redundant information of the pose can be used for analytical equations of the DKP and monitoring of the passive joint states. Thus the moving into singularities can be prevented by the control system (Fig. 6, Hesselbach, Kusiek, 2000).Under these circumstances big efforts in developing joint integrated sensors have to be done. The sensor resolution has to match the accuracy of the robot in the whole workspace. In addition, the sensor information can be used for online calibration of the robot. The development of compact sensors for online monitoring is described in section 6.

Fig. 6 shows the structure of the robot control architecture which includes specific parallel robot functionality. If the parallel robot remains in a conflict situation, special strategies are needed to prevent the robot from damage. Because of the complex kinematic behavior this cannot be done by the operator. Therefore a special algorithm has to be developed for supporting the operator moving the robot out of the conflict situation. The corresponding algorithms are embedded in the blocks workspace monitoring and exeption handling. The exeption handling routines provide functions to remove the robot from inadmissible positions or to reach a safe starting position after the robot stopped manually or automatically.

5.2.2 Parallel robot programming

The development of a parallel robot specific programming language is divided into different tasks. Considering the assembly and handling applications there is a need for predefined motion commands for hybrid motion, i.e. force and/or position controlled motions of the robot.

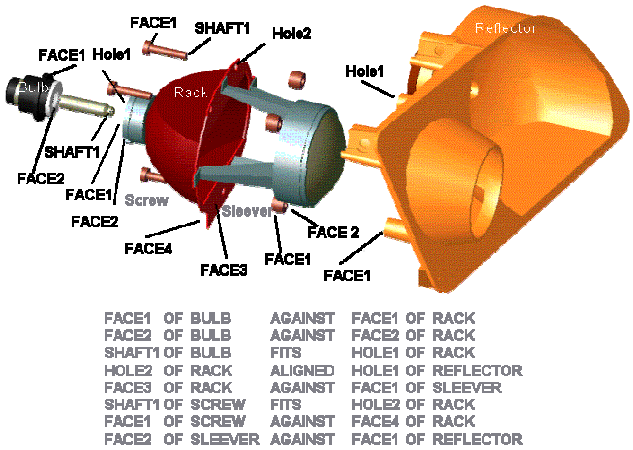

Fig. 7: Headlight assembly with SSrs

The basic idea of an automized generation of the robot program is the decomposition of an assembly task in standardized assembly functions like opening and closing of the gripper, transfer motion or contact with the environment. Therefore it is necessary to specify the relations of the parts to be assembled in a standardized way. The easiest way to generate symbolic spatial relations is to interactively let the design engineer model a virtual assembly of the product in the CAD environment in order to specify appropriate features and their suitable relations (Fig. 7). These symbolic spatial relations can be used for the automatic calculation of possible assembly plans and for an almost automated programming and execution of the assembly process (Fig. 8).

By using the HIGH LEVEL ASSEMBLY PLANNING SYSTEM *High*LAP and a CAD description of the assembly components sequence plans for the assembly strategies are provided. The robot programming system has to map the assembly task into a sequence of elemental robot operations automatically. In the different task-oriented commands the necessary motion oriented-commands are included.

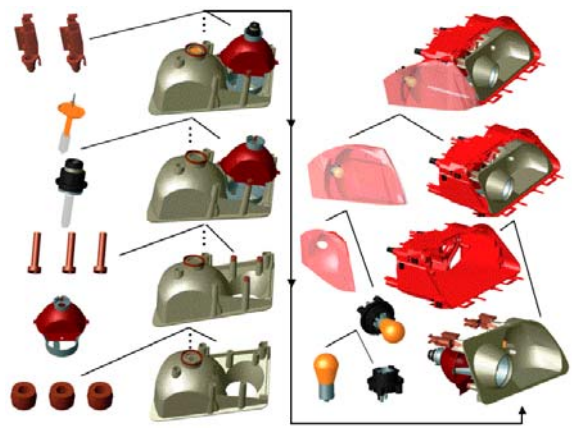

Fig. 8: Assembly plan

Due to uncertainities in the workspace during the assembly task operations the robot comes into contact with the environment. These contact states need to be represented in so called skill primitives. As mentioned above skill primitives can be considered as a sophisticated interface between the robot programming and the robot control and extend the known compliance frame concepts of Mason, 1981. In order to determine the robot motions, positions/orientations, velocities and forces/torques have to be specified in terms of a compliance frame matrix. Thus in case of a given assembly specification the program code will be generated automatically (Wahl, Thomas, 2001, Mosemann, Wahl, 2001).

The execution of automatically generated assembly programs is one key for a prosperous application of robots in industrial automation environment. In order to reach this goal a convenient Graphical User Interface supporting a task-orientated as well as a motion-orientated programming of the robot is needed. The HMI based on ROBCAD will consists of the following functions:

- a TeachIn-box for the interactive handling of the robot,
- workspace visualization tools to support the operator,
- modeling and animation of the robots the tools and the handling objects within the manufacturing cell,
- path planning tools with regard to the parallel kinematic disadvantages and
- a real-time simulation of the robot programs.

5.2.3 Position and force control

Considering the application fields of the SFB 562, e.g. joining process during assembly, position and force control concepts have to be developed. As mentioned above these so-called "compliant-motion" tasks could be presented in the compliance frame formulation. That means that the task can be translated in a positioning or force control problem in selected cartesian orthogonal directions within a transient cartesian coordinate system. The hybrid position/force control is perhaps the most widely adopted strategy within the compliance frame formalism. In this case controllers for position and force are designed independently with the force controller implementing a direct force control algorithm. As the compliance frame evolves accordingly with the description of the desired task selection matrices are used to bring the adequated controllers into the control loop, that is, in each frame direction a specific controller is chosen regarding the correct execution of position or force commands.

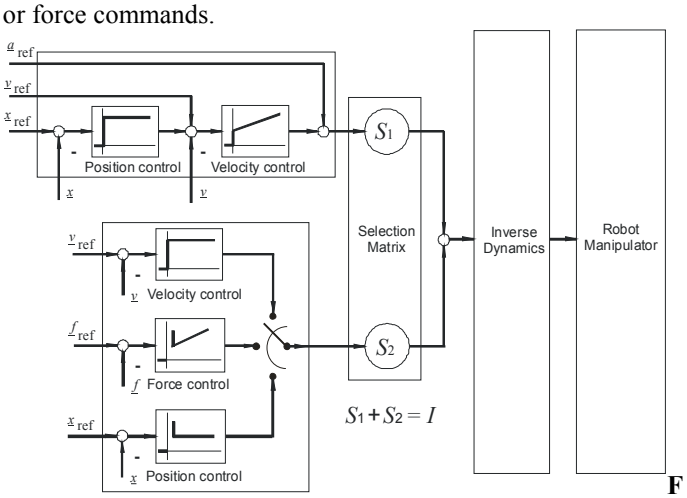

Fig. 9: Position and force control structure

These selection matrices, S_i, are diagonal matrices with a 1 or a 0 on the diagonal entries corresponding to the axes of the compliance frame and satisfy the equality, $\Sigma S_i = I$ where I is the identity matrix. Usually, a manipulator control system based on the position/force control approach has two feedback loops for an independent control of position and force with the actual positions and forces being measured (Fig. 9). One way to proof stability in switched systems is by using Lyapunov functions and to look if they -with the switching signal- lead to equilibrium points of the systems.

The increasing computational power allows a centralized controller concept. This concept is not only optimized for the drive but also for the entire robot system. Supplementary, additional sensors can be integrated easily. For these purposes task-space methods are preferable. The equations of motions are:

$$\underline{f} = J^{-T}\underline{\tau} = M_x(\underline{x})\ddot{\underline{x}} + C_x(\underline{x},\dot{\underline{x}})\dot{\underline{x}} + \underline{f}_g + \underline{f}_{reib} \qquad (1)$$

At the edge of the workspace the Jacobian matrix becomes singular. Thus some elements of the M_x and C_x including the inverse Jacobian matrix reach infinity values. To prevent unexpected strong fluctuations of the impedance and enhance the tracking behavior by compensating nonlinear dynamic effects feed-forward and computed torque are necessary (Kock, 2001, Kock, Schumacher, 1998).

In section 5.1 the fact is mentioned that by the use of direct drives the influence of the payload is not negligible. In order to determine the mass parameters (incl. the payload) in an adaptive control approach, it is worthwhile having linear dynamic parameters in the dynamic equations of the robot, like (Sciavicco, Siciliano, 2000):

$$\tau = Y(x,\dot{x},\ddot{x})\pi \qquad (2)$$

The structure-integrated adaptronic force sensors are used for the measurement of the contact forces as well as for payload estimation. The conventional force control based on the compliance principle, with fast and stiff force measurement and an inertial structure, cannot be used for parallel robots. The high stiffness of the structure and the use of direct drives lead to a system with low inertia. That means that the compliance of the sensors is equivalent to the compliance of the structure. Consequently new force control concepts have to consider this fact.

5.2.4 Architecture of a real-time communication network

Various sophisticated commercial robot control systems have been developed in the last 20 years. However these control systems often lack openness and flexibility and the implementation of new modules is complicated or impossible. Therefore the long term goal of the SFB 562 is to develop an own robot control for parallel robots. An object server middleware (Fig. 10) is organizing the communication between the allocative functions (Fig. 6), the controller and the bus. Thus the different modules communicate only with one partner. The communication between the modules and the object server consists of objects with a standardized format, containing messages, data, request, trigger signal, etc.. The interaction of the modules via the object server has the benefit that in a formal sense all modules are running autonomously (Finkemeyer et al., 2001). Thus the great advantage is that modules can be easily added or changed. The object server system is implemented on QNX neutrino OS on a PC. The realtime quality of the communication between processes can only be achieved by using synchronous data transmission without the object server as an intermediate station. This is achieved by using shared memory.

The effectively used communication systems, e.g. SERCOS and Profibus MC, provide the opportunity for

changing desired and actual values between the control and up to 16 servo drives. In these systems the nominal cycle time depends on the amount of peripheral units. Considering parallel robots with additional adaptronic elements, this bandwidth will not fit our real-time requirements. This is the starting point for the development of a new architecture for real-time communication for parallel robots. This new approach is based on the IEEE 1394 –FIREWIRE™ – standard, with a nominal cycle time of 125 µs, a transfer rate up to 400 Mbit/s, 63 user and isochronous as well as asynchronous transfer. The application of the IEEE 1394 in the field of industrial automation demands an additional communication protocol, namely the INDUSTRIAL AUTOMATION PROTOCOL (IAP) . The integration of the IAP manages isochronous and asynchronous transfer of data in the 125 µs cycle (Beckmann et al., 2001). That means the IAP realizes the coupling of external sensors and actuators via the FIREWIRE bus.

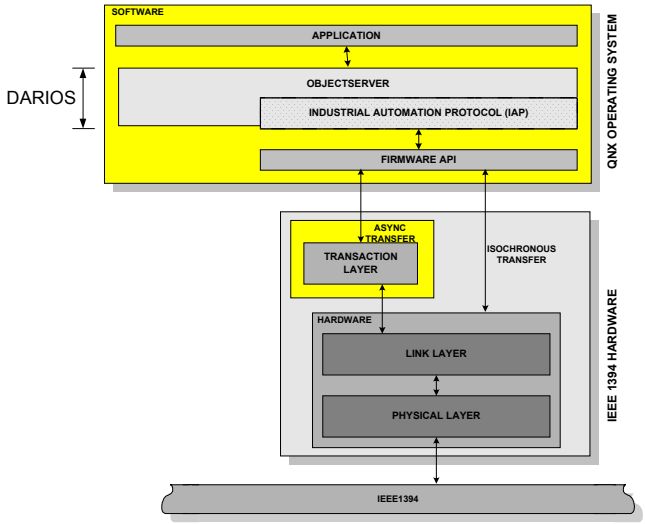

Fig. 10: Position of DARIOS in the layer model

The complete communication architecture is named DARIOS = Distributed Architecture for a Real-time Industrial Object Server (Fig. 10). Its characteristics offer following advantages:

- A consistent protocol for the transmission of process and parameter data within the robot system
- Free configuration of the data transfer for the consideration of different priorities and time requests of the processes
- Organization of the process and communication flow in order to ensure an unobstructed data transfer
- Fulfilment of realtime requirements of the processes through the use of shared memory and necessary memory protection mechanisms

5.2.5 Analysis of real-time systems modeled by UML

The complexity of the suggested modular control system necessitates software methodology for a straight and cost-efficient development of the whole robot control architecture. The complete architecture is modeled by using the visual notation UNIFIED MODELING LANGUAGE (UML). UML provides both, a high grade of clearness and correctness. Thus the semantic of the interactions of the mentioned modules, with regard to the priorities of the processes, the processes themselves and the data flow can be depicted in an easy way. The time-based semantic is transformed into a TIMED AUTOMATA SEMANTIC. For the validation of the developed system the verification tools RHAPSODY and UPPAAL will be used. In consideration of real-time requirements, deadlocks, bugs, and conflict states several scenarios will be used to verify and evaluate the functionality of the whole system (Firley et al., 1999). In this case study we illustrated the feasibility of a translation of UML-statecharts to timed automata. The translation of the object aerver shows that timed automata are an appropriate formalism to express behavior defined by UML-statecharts.

This case study is part of an effort to bring the advantages of formal methods to the application domain of real-time systems. The aim is to use UML as a user interface that hides the application of verification techniques.

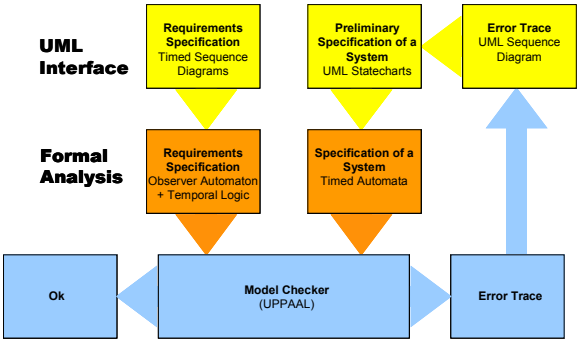

Fig. 11: Verification of the dynamic UML models

Fig. 11 shows the overall structure of the general approach. Part of this approach is to transfer UML statecharts automatically or (semi) automatically to timed automata. Additionally we need a description language of requirements. In Firley et al., 1999 UML sequence diagrams with timing annotations are proposed and a translation to timed automata is sketched. The model checking may then be performed by UPPAAL. A result could be an error trace referring to timed automata. Also this trace should be lifted to the UML level to hide the underlying formalism.

6 Components

6.1 Initial point and call for action

In every system with accelerated masses and finite stiffness mechanical vibrations occur. As well as the request for increasing operating speeds and accelerations rises mechanical vibrations attract the interests of robot engineers. The most

important goal is to lower the amplitudes of the oscillations of the structure in a short time.

The functional properties of mechanical systems such as parallel robots are significantly determined by the joints within the kinematic chains. Positioning accuracy depends on the quality of the joints. Hence, hysteresis and backlash must be prevented. Due to the high reaction forces and loads of the joints there is a demand for high stiffness and payload. However, present joint developments are not very helpful for application in parallel robots. Available standard joints for such purposes and with more than one degree of freedom are developed for machine tools and not for robots. The requirement on light parallel structures is inconsistent with the existing components (Franke, 1999).

For monitoring the dependent joint states of the passive joints of the robot and for an analytical real-time solution of the DKP internal sensors are needed. Conventional sensor technology will not fulfill the requirements, e.g. size, mass and resolution. By using new technologies, such as micro-technology, internal sensors have to be developed.

6.2 Intentions and approaches

6.2.1 The adaptronic approach = active vibration damping

In order to achieve an enlarged efficiency of parallel robots the consequent use of lightweight components is needed, because less moved masses lead to increased acceleration and velocity. With respect to their framework structure the use of rods made of carbon fibre materials is worthwhile for the design of link elements. This leads to problems like vibrational sensitivity due to low mass, tendency to buckling, and susceptibility to damage. Many approaches to reduce the amount of vibrations are known today. In addition to passive methods like reducing the accelerated masses or the integration of additional dampers, i.e. materials with high damping coefficients, active methods become more and more important. However, in many mechanical systems the possibilities of passive methods reducing or transforming the vibrational energy into a different type of energy come to a limit. In this case only additional active/adaptive systems, which consist of combined actuators, sensors and controllers, achieve a higher effectiveness on influencing the eigenmodes and eigenvalues of the system. Concerning the manufacturing technology, carbon fibre reinforced polymers (CFRP) are built up from fibres and epoxy resins to produce one material during the manufacturing process. This is a unique chance for adaptive technologies to embed multifunctional elements in load carrying structures in the sense of integral design.

The term *adaptronics* designates a system and its development process wherein all functional elements of a conventional regulator circuit are existent and at least one element is applied in multifunctional way. The conformity with a regulator circuit guarantees that the structure shows autonomic adaptive characteristics and can thus adapt itself to different conditions. Thus adaptronics allows the implementation of active elements made of multifunctional material with virtual properties such as changing stiffness, damping or mass distribution in real-time. In this way, structural elements (i.e. a combination of links and active elements, Fig. 13) can be developed which are not subject to any deformations as a result of external forces and, consequently, exhibit an apparently infinite stiffness. With this approach it becomes possible to equip optimized mechanical structural systems with structure-conforming integrated piezoceramic actuators and sensors as well as adaptive control systems offering real-time capability (Breitbach, 1997, Hesselbach, Helm, 2000). The main goal of the adaptronic approach intra the SFB 562 is to generate oscillations which are directly opposed to the structure vibrations. This leads to a compensation of the structure oscillations and a higher accuracy at the end-effector (Fig. 12).

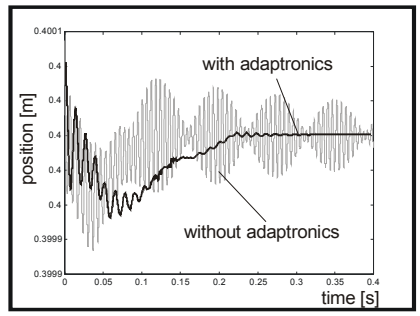

Fig. 12: Oscillation at the end-effector

In the field of adaptronics many multifunctional materials, such as piezoceramic fibers, patches, foils and stacks with adaptive controllers, magnetostrictiva, shape memory alloys and electrorheological fluids are developed. *Functional* means that the material will preserve the same functional property even when its volume is subdivided. *Multifunctional* means, that these elements satisfy both, load-bearing and actuatoric / sensoric tasks. Due to the fact that the piezoelectrical properties are inverse, the multifunctional material can be used for actuatoric as well as for sensoric tasks. By using these elements an internal force measurement for force control purposes becomes possible.

Owing to their construction by rod elements, which are poor in mass, parallel structures offer an ideal platform for an active vibration reduction. Thus it is possible to realize parallel robots with integrated active links based on multifunctional materials. For first experiments a five joint planar robot with two degrees of freedom as a test stand is used. The planar robot consists of two cranks made of CFRP panels using carbon fibre fabrics. The most important goal of this design is to achieve high bending stiffness and light weight. Thus active elements are integrated into the rods (Fig. 13, Sachau, 2001).

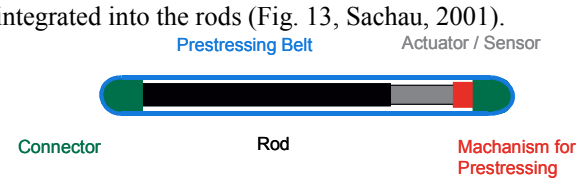

Fig. 13: Principle of the active rod

The active element is a piezoceramic stack actuator with one layer connected as a sensor. To prevent damage from the active element caused by tensile loads, the active elements have to be prestressed by a carbon fibre belt. By changing the length of the internal rod and the prestressing belt, this kind of active rod can be used for different types of parallel robots. By using direct drives the main goal of this demonstrator is to reach an acceleration of 10-20 g at the end-effector. In order to influence the impedance at the end-effector the right position of the actuators and sensors is a very important factor. Considering the classification of the structures (section 4) standardized methods for placing the adaptronic elements into the structure have to be developed. In addition to the actuators and the sensors the controller is an inherent part of an adaptronic system. Therefore three different controller concepts will be investigated: robust, model-based and adaptive controller. Supplementary, an observer for the determination of the internal states can be added to the control system.

6.2.2 Development of passive joints

Nevertheless, the accuracy of parallel robots depends directly on the quality of the passive joints. Joints for parallel kinematic machines and robots need to fulfill a specific set of requirements.

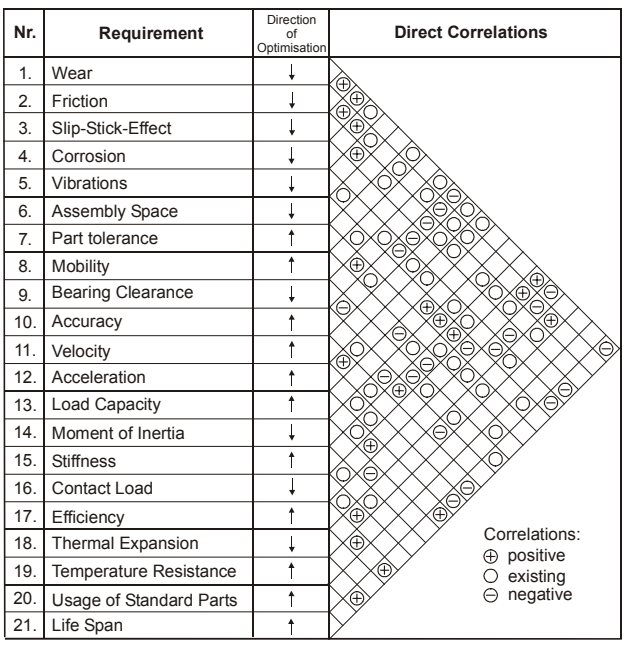

Fig. 14: Relevant joints requirements

The knowledge and documentation of these requirements are conditions for a reproducible design of new, well-adapted joints. Fig. 14 shows relevant requirements for joints and their mutual constructive and functional relationships. In order to fulfill this demand all joints should be designed in a lightweight way. On the other hand the joints have to accomplish high stiffness requirements. In addition the bearing slackness of the joints has to be minimized by preloading the components. In contrast to serial machines, parallel robots contain passive joints with more than one degree of freedom. These requirements ask for new design solutions. The use of design catalogues, which enable a comparison of available solutions, leads to a systematically development of new joints, e.g. with regard to shape variations and connections. Starting from existing design catalogues a selection of joint prototypes will be designed (Franke et al., 1999). In tribological tests the joint characteristics will be determined. According to the small slewing angles of the passive joints tribological problems in hydrodynamical bearings may arise. By using PVD-coated materials this problem could be resolved.

Intra the SFB a new HEXA parallel robot with 6 dof as a test stand will be developed. This robot requires joints with 2 or 3 dof. Fig. 15 shows modular joints for this new prototype. The angle ranges are 360° for the first axis, 270° for the second axis and 360° for the third axis. Particularly the value for the first axis may crucially depend on the platform or the arm to which the joint is mounted. E.g. used with the HEXA-platform the angle range for the first axis is 250°. The load capacity is 2.000 N and the FEM-calculated stiffness averages 32 N/µm for the joint with 2 DOF and 23 N/µm for the joint with 3 DOF. The weight is 202 g for the joint with 2 DOF and 290 g for the joint with 3 DOF.

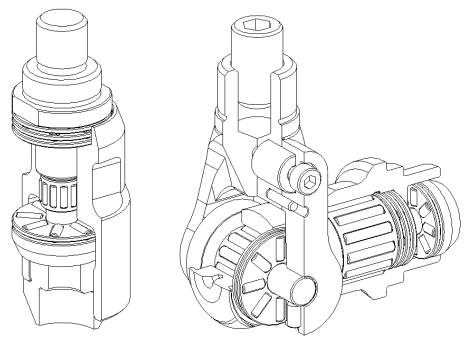

Fig. 15: Modular joints with 2 or 3 dof with needle roller bearings

6.2.3 Joint integrated micro senors

Nevertheless the small dimensions of the passive joints lead to problems with the integration of the sensors. By integrating the sensors into the joints further disturbance effects occur, which are harmful to the measurement quality: high accelerations, unsteady temperature, lubricant and dirt particle. In addition to the limited construction room these requirements must be fulfilled by the sensors. By means of micro-technology the fabrication of sensors with a high rate of miniaturization becomes possible. Utilizing UV-depth lithography enables high aspect ratio microcoil fabrication with of 5, 10 and 20 µm wide conductors and up to 100 windings (Fig. 17 (Ohnmacht et al., 2000, Seidemann, Büttgenbach, 2000). The measuring principle of the angular position is based on inductive scanning of a disk which carries a microscale with circular arranged grating structures consisting of alternative sections of different material properties.

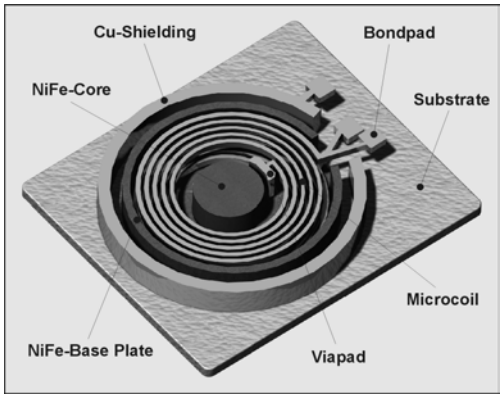

Fig. 16: Double layer microcoil with integrated NiFe-core and Cu-shielding.

These microcoils act as a scanning unit within the sensor. The mutual inductance is realized by linear or rotational micro-scales. Both types are modeled as incremental as well as encoded scales. The advantage of the encoded scales is the possibility of an absolute measurement.

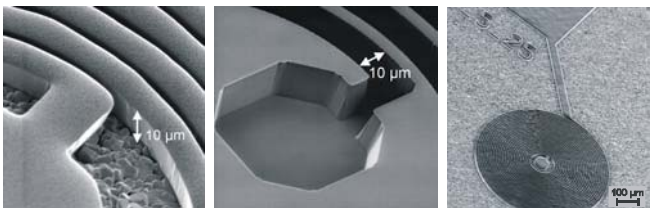

Fig. 17: Microcoils (Seidemann, Büttgenbach, 2000)

7 Conclusions

The integration of adaptronic components with special adaptive control concepts is a promising effective way to make robots both, more accurate and faster and consequently more productive (Fig. 18).

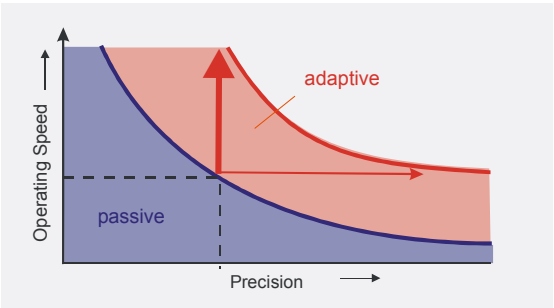

Fig. 18: Performance improvement

Only after having removed the fundamental disadvantages, an expansion of parallel robots to many applications in the field of handling and assembly is possible. Within the SFB 562 the basic research activities for the development of parallel robots are structured into three project fields, namely modeling, control and information technology and new components. In doing so, the interdisciplinary knowledge of mechanical and electrical as well as computer science will be synergetically combined for reaching one goal: The structural and methodical development of parallel robots for given applications. Thereby an important point is modularity not only with regard to the structure and its components but also in consideration of the control and information technology including the kinematic and dynamic equations.

Acknowledgment

In addition to the authors the following scientists participate in the Collaborative Research Center 562. The named persons are the chairmen of the different sub-projects within the SFB 562:

- Elmar Breitbach,
  Institute of Structural Mechanics **
- Stephanus Büttgenbach,
  Institute of Microtechnology *
- Hans-Joachim Franke,
  Institute of Engineering Design *
- Ursula Goltz,
  Institute of Software, Program Development Department **
- Michaela Huhn,
  Institute of Software, Program Development Department *
- Michael Rose,
  Institute of Structural Mechanics **
- Walter Schumacher,
  Institute of Control Engineering *
- Jörn-Uwe Varchmin,
  Institute of Electrical Measurement and Fundamentals of Electrical Engineering *

* Technical University Braunschweig, Germany
** German Aerospace Centre, Braunschweig, Germany

References

Beckmann, G.; Barklage, T.; Varchmin, J.-U., 2001, "FireWire - Hochgeschwindigkeit für die Automation", SPS/IPC/Drives 2001, Hüthig-Verlag, Heidelberg

Breitbach, E., 1997, "Adaptive Structural Concepts: State of the Art and Future". Proc. CFAS International Forum on Aerolasticity and Structural Dynamics, Rome

Finkemeyer, B.; Borchard, M.; Wahl, F., 2001, "A Robot Control Architecture Based on an Object Server" IASTED International Conference on Robotics and Manufacturing, Cancun, Mexico, May 2001, pp. 36-40.

Firly, T.; Huhn, M.; Diethers, K.; Gehrke, T.; Goltz, U.,1999 Timed Sequence Diagrams and Tool – Based Analysis – A Case Study, 2nd Int. Conf. on the Unified Modeling Language, Colorado

Franke, H.-J.; Hagemann, D.; Hagedorn, U., 1999, "Systematic Approach to the Design and Selection of Joints for Parallel Kinematic Structures with Design Catalogues", The International Workshop on Parallel Kinematic Machines (PKM '99), Mailand

Franke, H.-J.; Brey, M.; Jänicke, T., 2001, "eKat - Rechnerunterstütztes Konstruktionskatalogsystem", Manufacturing 01, Poznan, 8.-9.11.2001, (1) pp. 63-70

Frindt, M.; Kerle, H.; Plitea, N., 1998, "Penta – Vorstellung eines parallel Maschinenkonzepts mit fünf Bewegungsfreiheiten", VDI Berichte, Nr. 1427, VDI-Verlag Düsseldorf, pp. 15-34

Frindt, M., 2001, "Modulbasierte Synthese von Parallelstrukturen für Maschinen in der Produktionstechnik", Schriftenreihe des Instituts für Werkzeugmaschinen und Fertigungstechnik der TU Braunschweig, Vulkan Verlag, Essen

Führer, C., 1988, „Differential-algebraische Gleichungs-systeme in mechanischen Mehrkörpersystemen. Theorie, numerische Ansätze und Anwendungen." Technical report, TU München, Mathematisches Institut und Institut für Informatik.

Gosselin, C. M.; Angeles, J., 1990, "Singularity Analysis of Closed-Loop Kinematic Chains." IEEE Transactions on Robotics and Automation, Vol. 6, No. 3, pp. 281-289

Gosselin, C.M.1998, "On the Design of Efficient Parallel Mechanisms", Computational Methods in Mechanical Systems, Springer-Verlag, Berlin Heidelberg New York, pp. 68-96

Hesselbach, J.; Kusiek, A., 2000, "Control of Parallel Robots", Production Engineering, Vol. VII/1 (2000), pp. 83-86.

Hesselbach, J.; Helm, M., 2000, "Adaptronics in Machine Tools" Production Engineering, Vol. VII/1 (2000), pp. 91-94.

Hesselbach, J.; Kerle, H.; Frindt, M.; Pietsch, I., 2001, "PORTYS – A Machine Concept with Parallel Structure for Precise Pick & Place Operations at High Speed", Proc. 10th Intern. Workshop on Robotics in Alpe-Adria-Danube Region (RAAD ´01), Vienna (Austria), 6 pages

Jansen, D., 1996, "Objektorientierte Basisfunktionen für offene Steuerungen", Fortschritt-Berichte VDI, Reihe 8, Nr. 578, VDI Verlag Düsseldorf

Kock, S., 2001, "Parallelroboter mit Antriebsredundanz", Fortschritt-Berichte VDI, Reihe 8, Nr. 890, Dissertation, Braunschweig

Kock, S.; Schumacher, W., 1998, "A Parallel xy-Manipulator with Actuation Redundancy for High-Speed and Active-Stiffness Applications", Proc. IEEE Int. Conf. on Robotics and Automation, Leuven, Belgium, Vol. 3, pp. 2295-2300

Mason, M. T., 1981, "Compliance and Force Control for Computer Controlled Manipulators. IEEE Transactions on Systems, Man. And Cybernetics, Vol. 11, No. 6

Merlet, J.-P., 2000, "Parallel Robots", Solid Mechanics and its Applications, Kluwer Academic Publishers

Mosemann, H.; Wahl, F., 2001, "Automatic Decomposition of Planned Assembly Sequences into Skill Primitives", IEEE Transactions on Robotics and Automation, Vol. 17, No. 5, 2001, pp. 709-718.

Ohnmacht, M.; Seidemann, V.; Büttgenbach, S., 2000, "Microcoils and microrelays - an optimized multilayer fabrication process", Sensors and Actuators A83 (2000), pp. 124-129

Sachau, D.; Breitbach, E.; Rose, M.; Keimer, R., 2001, "An Adaptronic Solution To Increase Efficiency Of High Speed Parallel Robots", ICAST, 12th International Conference on Adaptive Structures and Technologies, College Park, Maryland, USA

Schönherr, J. 1998, "Bemessen, Bewerten und Optimieren von Parallelstrukturen", 1. Chemnitzer Parallelstruktur-Seminar, April 1998, Chemnitz

Seidemann, V.; Büttgenbach, S., 2000, "An Optimized Fabrication Process for Microcoils Utilizing UV-Depth-lithography and BCB", Proc. of the VDE World Microtechnologies Congress, Hannover, Vol. 1, pp. 69-72

Sciavicco, L., Siciliano, B., 2000, "Modelling and Control of Robot Manipulators", 2nd Edition, Springer London Berlin Heidelberg

Tsai, L.-W., 1999, "Robot Analysis – The Mechanics of Serial and Parallel Manipulators", John Wiley & Sons, Inc., NY Chichester Weinheim Brisbane Singapore

Wahl, F.M.; Thomas, U., 2001, "A System for Automatic Planning, Evaluation and Execution of Assembly - Sequences for Industrial Robots", International Conference on Intelligent Robots and Systems (IROS), Maui, Hawaii, USA, October 2001, pp. 1458-1464.

For further information of the subproject see the *Proceedings of the 1. International Colloquium of the Collaborative Research Centre 562 "Robotic Systems for Handling and Assembly"* / Mathias Krefft, Friedrich Wahl (edts.), Aachen, Shaker, 2002

Lunch with Panel on Education

Friday, October 4, 2002, 12:00PM

Session Chairs: J.L. Herder, J.M. McCarthy

J.L. Herder, *"Proposal for a Self-Developing Practical Course in Parallel Mechanisms"*.
(Additional details to be announced.)

Proceedings of the WORKSHOP on
Fundamental Issues and Future Research Directions for Parallel Mechanisms and Manipulators
October 3–4, 2002, Quebec City, Quebec, Canada
Clément M. Gosselin and Imme Ebert-Uphoff, editors

Proposal for a Self-Developing Practical course in Parallel Mechanisms

JUST L. HERDER
Delft University of Technology
Department of Mechanical Engineering
Section of HuMan-Machine Systems (mms.tudelft.nl)
Mekelweg 2, 2628 CD Delft, The Netherlands
j.l.herder@wbmt.tudelft.nl

Abstract: *This paper proposes a practical course in the education in parallel mechanism systems. The key issue of the set-up is that the students do not execute predefined projects of a yearly course but rather define and execute small, not previously conducted research or design projects in a larger innovative project. This is believed to be highly motivating for the students. However it also makes great demands on students and supervisors. Students are to define their own assignment and solve a problem with no known right-or-wrong answer, while supervisors must restrain themselves, and must judge work of different nature. Although many subjects qualify for being taught in this format, it is particularly suited for education in parallel mechanisms due to the many aspects involved in the design of these systems.*

1 Introduction

With good reason, parallel mechanisms and manipulators receive increasing attention, thanks to their specific qualities and the wide variety of architectures and applications (see for instance the websites listed in the reference section).

This paper presents a proposal for a practical course in parallel mechanisms which aims to let students discover the variety of architectures and applications and to allow them to gain experience in the analysis and design of parallel mechanism systems. In addition, this course aims to bridge the gap between regular courses and the graduation project by incorporating a fair amount of self-reliance. To achieve these goals, a practical course is proposed in which students do not execute predefined yearly repetitive projects but rather define and execute small, not previously conducted research or design projects within the framework of a larger, innovative project. Thus, two layers can be distinguished: a first one in which students complete their individual projects, and a second where their results add up to the progress of the overall project.

The course is intended to be self-developing in two senses. Firstly, this term emphasizes the responsibility of the students to acquire the appropriate knowledge. Secondly, it indicates that the content of the course is not a priori determined and that the students have a strong influence on their own education as well as on the direction of the development of the overall project.

The course is intended for students at early graduate level. Students will acquaint themselves with defining innovative projects within the larger framework of the overall goal, coping with responsibility for the project, and planning of their project, as well as acquiring knowledge on parallel mechanisms in general and at least one aspect of these in particular.

The remainder of this short paper will elucidate the intended set-up of the practical course, its supervision, the expectations, and provide an example which is to start running this year at Delft University of Technology.

2 Self-developing practical course

The subject of the practical course concerns parallel mechanisms, much else is not specified. An overall project goal will function as point of departure. Typically, this goal will concern an innovative project, the completion of which is evidently not attainable within the allotted time of the student's individual project.

The subsequent steps to be taken by the student are the following: (1) acquire background knowledge, (2) acquire project-specific knowledge, (3) formulate a well-defined problem statement for their own project considering allotted

time, (4) execute the project, (5) write a report, and (6) give a presentation. These steps will be discussed next.

(1) Background knowledge concerns general information on parallel mechanisms and manipulators, from books and internet, in order to acquire a general understanding of the subject. The student has the responsibility to locate and study appropriate material. Based on this information, students can select an aspect of their interest. Aspects of interest may include kinematics, dynamics, design, control, evaluation, psychophysical experiments, etc.
(2) Project-specific knowledge concerning the selected aspect of interest is needed as a preparation for the problem definition, and may include studying the reports written by previous students in the project.
(3) Formulating a problem statement is part of the student's effort. No prescribed assignments are available. The student may include preference in the consideration, but may also consider the progress of the project as a whole. The student will have to estimate whether the amount of work and the profundity of the work are at the right level. The allotted time should be taken into account.
(4) The self-determined assignment should be carried out with sufficient depth. Although the problem statement should be formulated accurately and agreed upon by the supervisor, it will generally prove necessary during the execution of the project to adjust the problem statement, for instance when it turns out to be too ambitious.
(5) A brief report must be made in the form of a two-page paper (including an introduction, background information, a problem definition, a main section, and a conclusion) and appendices (sufficient for successors to follow up on the work done, possibly including computer program code, technical drawings, design calculations, raw measurement data, etc).
(6) A ten to fifteen minute oral presentation on a mini-symposium concludes the project. This gives the student the opportunity to present their problem definition and discuss their findings with fellow students.

Thus, the students are self-developing in that they bear a great part of the responsibility for their project. They have a major say in the subject of their assignment as well as in the rigor of the execution. The course as a whole is self-developing in that the summation of individual student projects determines the direction of progress and adds up to the completion of the overall project. Starting the course, the image of the final outcome is unclear. It is felt that this is positively challenging for the students, and learns them to cope with uncertainty, as opposed to the process of taking courses and doing exams.

The course is additional to theoretical courses in the sense that students do not increase their proficiency in all the fields associated with parallel mechanisms. Furthermore, the course provides the opportunity not only to learn about state-of-the-art parallel mechanisms but also to improve existing designs or conceive new ones. A student who decides to investigate the dynamics of a new mechanical design may not improve on control implementation skills. However, the students will demonstrate their capability to specialize and to make their findings useful to fellow students who specialized in another aspect of the project. Inversely, they will learn from their fellow students' efforts.

Due to the wide field of aspects associated particularly to the design of parallel mechanisms, the format of the proposed course allows considerable transfer of knowledge and development of skills in limited time.

3 Supervision

It may seem from the above that supervision is not needed. This is neither true nor is it the intention of the course set-up. Indeed, also the supervisors will need to adapt. The course is not a collection of predefined projects which are carried yearly, nor is it to be regarded as a long term project broken down into small pieces of research and design which are carried out by a sequence of students. Both of these forms lack the prime feature of the proposed set-up, namely the responsibility of the students for their own project. It is the task of the supervisor to provide great latitude in project definition, yet to safeguard the quality level of the assignment.

At the start of each individual student project supervisors will check the initial problem statement on sufficient level, but must otherwise be reserved. Students should experience whether their problem statement suits the project term. Generally, after one third of the project term a workable problem statement should be defined.

	Student	Educator
Adv.	Personal interpretation of assignment Contribute to overall project. Preparation for graduation project.	Motivated students. Variety of work.
Disadv.	No off-the-shelf assignment. Responsibility for own project.	Balance between guide and let go. Close individual supervision on a variety of fields. Comparative marking difficult.

Table 1 Overview of some advantages and disadvantages of the self-developing course format.

4 Expectations

The increased responsibility and self-reliance are key features of the self-developing course. It is expected to stimulate motivation and therewith the transfer of knowledge. The fact that the students determine their own project is expected to result in high commitment. The perspective of the overall goal is expected to increase the perceived significance of the

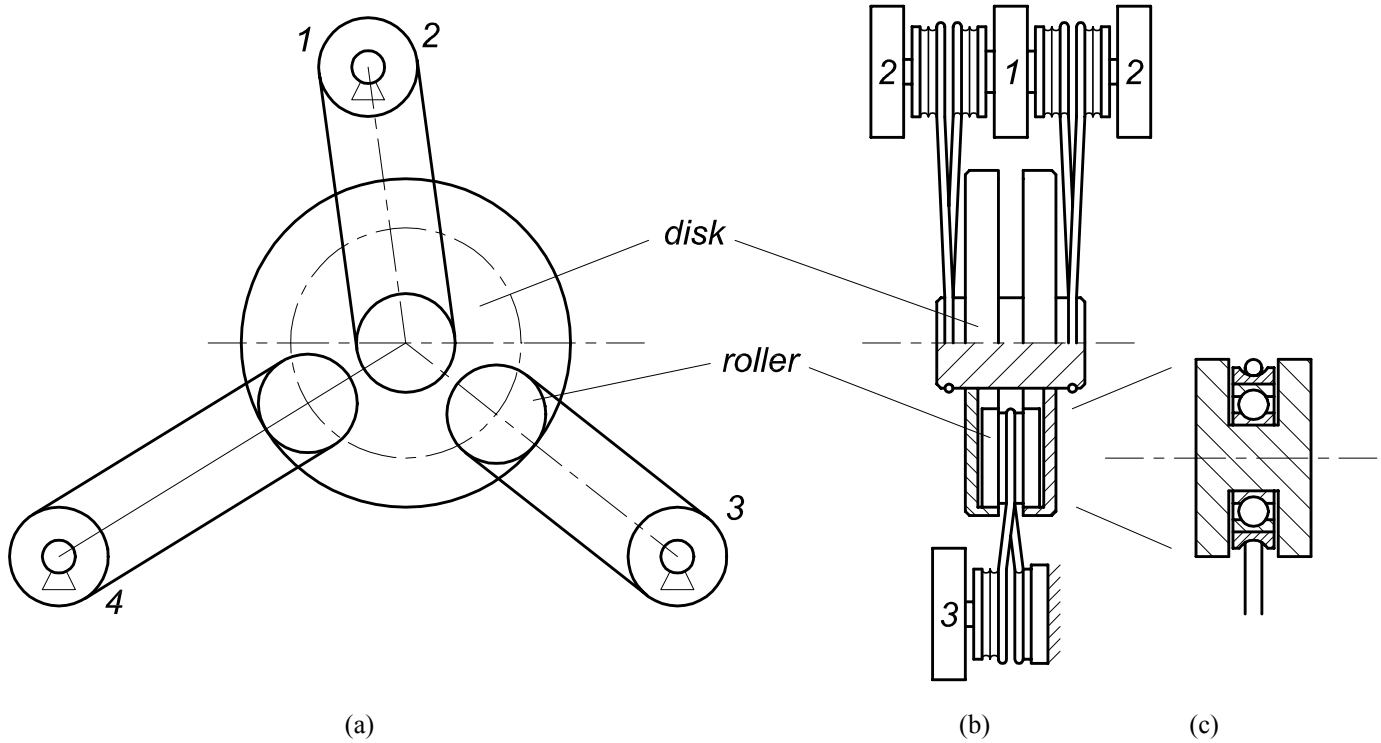

Figure 1 Design proposal for haptic input device: (a) schematic overview with exaggerated dimensions, (b) possible embodiment of central disk, partially in cross-sectional view, (c) enlarged view of roller.

student's individual project. Although no explicit element of competition is included, comparison of problem formulations and project results may incorporate a similar effect.

The students generally are interested in achieving evident result of their work, in this case their individual efforts as well as their combined work. It is therefore expected that the overall project will develop evenly. A missing link for the grand apparatus to work may well be regarded by a student as an opportunity to play an important role. Thus, apart from personal preference, factors such as expected impact may affect the choice of problem definition.

It will probably not be difficult to find new student projects in the framework of the overall project. Probably the greater challenge will be to define problem definitions that give satisfactory results within the project term. It is expected that a project term, which is the equivalent of six full-time weeks, is appropriate.

A summary of some advantages and disadvantages for student and educator respectively is given in table 1.

5 Example: master-slave system for microsurgery

Let us assume that the overall goal of the project is to develop a master-slave system for microsurgery. Such a project would include the design of a micromanipulator, a control device, and a control system. Furthermore, the human-machine evaluation and investigation of human psychophysics are needed to arrive at an optimal system. The field of application, surgery, places special demands on the design. The delicacy of the target object (tissue) may lead to the desire to provide the operator (surgeon) with force feedback. This requires sensors and actuators in both the micromanipulator (slave) and the master device, which in turn leads to special demands on the design of master and slave units. The master unit, for instance, should have high bandwidth to make a hard object in the micromanipulator feel hard to the operator. The micromanipulator on the other hand, may have to be precise but need not be able to generate large forces. The way the operator handles the different modi of feedback information is also an interesting aspect. The fundamental consideration of the design specifications and their dependency on the field of application is an essential part of each student's project.

A student may be interested in the mechanical design of a master unit. This student is supposed to come across a number of reports on this subject in literature (e.g. Birglen, 2002) and will find that parallel mechanisms in various forms are particularly suited to serve as (haptic) control interfaces, e.g. Melchiorri and Vassura (2001), Gallina and Rosati (2002), Williams and Gallina (2001). The student may be triggered by the problem of limited moment feedback in the design by Williams and Gallina, and may propose an alternative solution, which features full moment feedback, low friction, and results in straight-forward kinematics and control (figure 1).

In the proposed design, the cable system consists of three legs. The centerline of each leg passes through the center of a disk. The cable of one leg is wrapped around a pulley fixed to the disk, the cables of the other two legs are wrapped around rollers which roll on the inside of the disk circumference. The cables of the legs are fixed to ground and to the motors via pulleys. In the leg connected to the disk, each free end of the cable is wrapped around a pulley, each fixed to a separate motor (motor 1 and motor 2). In the other legs, the free ends of the cable are wrapped around pulleys, one of which is fixed to ground while the other is connected to a motor (motor 3, and motor 4, respectively). When the pulleys within each leg are of equal radius, the kinematics are the same as in a system where three cables are connected to a moving point via small bushes near the motors, as in Williams (2001). However, the fact that two motors are present in one leg allows rotation of the disk or the application of a moment to the disk without changing the position of the disk by simply giving opposite signals to motors 1 and 2.

The student may now decide, for instance, to optimize the design and elaborate until the phase of technical drawings, or perform kinematic and static analysis based on the schematic representation of the diagram, depending on preference and other considerations. It is also possible that several students work on the different aspects, such as the ones mentioned or other ones such as the flexibility of the wires, dynamic modeling, possibly including friction, etc.

Another student may find the design by Canfield et al. (2001) in literature and become interested in the application of compliant parallel mechanisms in the micromanipulator. This student will probably start with a type synthesis study, and, time permitting, proceed with dimensional design or pass this on to a subsequent student. Thus, the field of compliant mechanisms (e.g. Howell, 2001) is included in the course.

6 Conclusion

This short paper presented a proposal for a practical "self-developing" course in parallel mechanisms by letting students define their own project within the framework of a general overall goal. The course is self-developing in the sense that it emphasizes the responsibility of the students, and that it indicates that the students have a strong influence on their own education as well as on the direction of the development of the overall project. This approach aims to combine a broad perspective with concrete achievement, and therewith to increase students' awareness and enthusiasm for the subject of parallel mechanisms. The overall goal formulation provides sufficient latitude to allow the students to direct the course of the development. The students bear partial responsibility for the problem formulation and the depth of their work. Due to the variety of aspects associated particularly to the design of parallel mechanisms, the format of the proposed course allows considerable transfer of knowledge and development of skills in limited time. The approach is illustrated by an example that is to start shortly at Delft University of Technology: the design of a master-slave system for microsurgery.

Acknowledment
This paper was originally submitted as a short paper intended for presentation as a poster.

References

Birglen, L., 2002, "Haptic devices based on parallel mechanisms, state of the art", http://parallemic.org/reviews/review003p.html.

Birglen, L., Gosselin, C. M., Pouliot, N., Monsarrat, B., Laliberté, T., 2002, SHaDe, a new 3-dof haptic device, IEEE Transactions on Robotics and Automation, to appear.

Canfield S. L., Beard J. W., Parsons, R. D., Lobontiu, N., Paine, M., Paine, J., 2001, "Development of parallel architecture spatial compliant manipulators", *Proc. of the 2001 ASME Design engineering Technical Conferences*, DETC2001/DAC-21033.

Gallina, P., Rosati, G., 2002, "Manipulability of a planar wire driven haptic device", *Mechanism and Machine Theory,* 37(2002)215-228.

Howell, L. L., 2001, "*Compliant mechanisms*", John Wiley & Sons, Inc., New York.

Landsberger S. E., Sheridan, T. B., 1993, "A minimal, minimal linkage: the tension-compression parallel link manipulator", In: *Robotics, Mechatronics and Manufacturing Systems,* Takamori T., Tsuchiya K. (eds.), Elsevier Science Publishers B.V.

Melchiorri, C., Vassura, G., 2002, "Development and application of wire-actuated haptic interfaces", Journal of Robotic Systems, 18(12)755-768.

Williams II, R. L., Gallina P., 2001, "Planar cable-direct-driven robots, part I: kinematics and statics", *Proc. of the 2001 ASME Design engineering Technical Conferences*, DETC2001/DAC-21145.

Websites

Merlet: http://www-sop.inria.fr/coprin/equipe/merlet/merlet_eng.html.

ParalleMIC: http://parallemic.org

Laval University: http://wwwrobot.gmc.ulaval.ca

White Papers – Poster Session

Friday, October 4, 2002, 1:30PM

Session Chairs: C. Gosselin and I. Ebert-Uphoff

1. C. Lange, J-C Piedboeuf, E. Martin, J. Kövecses
   "Towards Docking Emulation using Hardware-in-the-Loop Simulation with Parallel Platforms".

2. R.L. Williams, II
   "Parallel Robot Projects at Ohio University".

3. B. Dasgupta
   "Redundancy Resolution Schemes for Parallel Manipulators with Force Redundancy".

4. K. Mianowski
   "On Some Properties of POLMAN-3L Parallel Manipulator to the Use as a 3-D Measuring System for Industrial/Educational Applications".

5. A.M. Hay, J.A. Snyman
   "Design of Parallel Manipulators for Optimal Conditioning Throughout a Prescribed Workspace".

6. Z. Huang, Q.C. Li
   "On the Type Synthesis of Lower-Mobility Parallel Manipulators".

7. J.M. Herve, M. Karouia
   "The Novel 3-RUU Wrist with No Idle Pair".

8. Y-Q Zheng
   "Workspace Analysis of a Six DOF Wire-Driven Parallel Manipulator".

9. Z. Xu, F. Xi, C.K. Mechefske
   "Kinetostatic Analysis and Optimization of a Tripod Attachment for Machine Tools".

10. P. Zsombor-Murray
    "Planar Point & Line Transformation with Blaschke-Grünwald Image Space Coordinates".

Proceedings of the WORKSHOP on
Fundamental Issues and Future Research Directions for Parallel Mechanisms and Manipulators
October 3–4, 2002, Quebec City, Quebec, Canada
Clément M. Gosselin and Imme Ebert-Uphoff, editors

Towards Docking Emulation using Hardware-in-the-Loop Simulation with Parallel Platforms

CHRISTIAN LANGE
Canadian Space Agency
Saint-Hubert, Quebec
Canada J3Y 8Y9
Email: Christian.Lange@space.gc.ca

ERIC MARTIN
Canadian Space Agency
Saint-Hubert, Quebec
Canada J3Y 8Y9
Email: Eric.Martin@space.gc.ca

JEAN-CLAUDE PIEDBŒUF
Canadian Space Agency
Saint-Hubert, Quebec
Canada J3Y 8Y9
Email: Jean-Claude.Piedboeuf@space.gc.ca

JÓZSEF KÖVECSES
Canadian Space Agency
Saint-Hubert, Quebec
Canada J3Y 8Y9
Email: Jozsef.Kovecses@space.gc.ca

Abstract: *In this paper a recent research project of the Canadian Space Agency in the field of satellite servicing is described. In particular, the hardware-in-the-loop simulation of a rendezvous-docking operation of a chaser and target satellite is targeted. The satellites and the controller will be modeled in software using Symofros, RT-Lab and Matlab/Simulink. A physical docking mechanism included in the loop will then be driven, depending on the satellites' relative motion, in a first phase of the project, by a serial manipulator and, in a second phase, by a parallel platform and a rail-mounted base. This project underlines the growing number of industry related applications for parallel platforms.*

1 Introduction

Satellite servicing capabilities render one key element for a substantial reduction in space system acquisition, launch and operations costs. In this setting the U.S. Air Force for instance targets within their Orbital Express Space Operations Architecture / ASTRO Program* to develop and demonstrate autonomous techniques for on-orbit re-supply, upgrading, refueling and reconfiguration of satellites. This and other similar programs aim not only to extend the life span but also to enable the capture and rescue of defective satellites as currently also investigated by the German Aerospace Center (DLR). The Japanese space agency (NASDA) is also very active in this field. Their ETS-7 spacecraft was launched on November 28, 1997. It is composed of a chaser satellite and a target satellite used to carry out experiments to confirm the basic technologies. In Canada, MD Robotics (MDR) is looking to the area of satellite servicing since a few years. They have already developed an intelligent vision systems (ORPE) and an end-effector for satellite servicing for CSA. They have also developed unmanned on-orbit operations capabilities through the Intelligent Interactive Remote Operations (IIRO) project with CSA participation.

As common to all space applications all tasks and procedures related to satellite docking require to be verified on earth prior to the execution in space. As the design and functionality of the actual docking mechanism, i.e., the satellite's end-effector, is crucial for the success or failure of the docking most reliable test facilities are needed. As an example, the state-of-the-art end-effector developed by MDR with its test-bed is shown in Figure 1. In this setup, the end-effector is mounted on a driven carriage. This carriage can be moved at various approach speeds in order to emulate the motion of the arm as the chasing spacecraft approaches the target spacecraft. On the other hand, the target spacecraft is floating on air-bearing pads, allowing for axial and lateral translation, and yaw rotation.

The rendezvous and docking operation test system (RDOTS) of NASDA is shown in Figure 2. This nine degrees-of-freedom system consists of a six degrees-of-freedom parallel platform and a rail-mounted chaser base with two additional degrees-of-freedom. With this system dynamic closed loop tests can be performed by attaching real sensors on a full-scale mock-up of the docking interfaces and feeding back the sensed data to the computers and software.

* www.darpa.mil/tto/PROGRAMS/astro.html

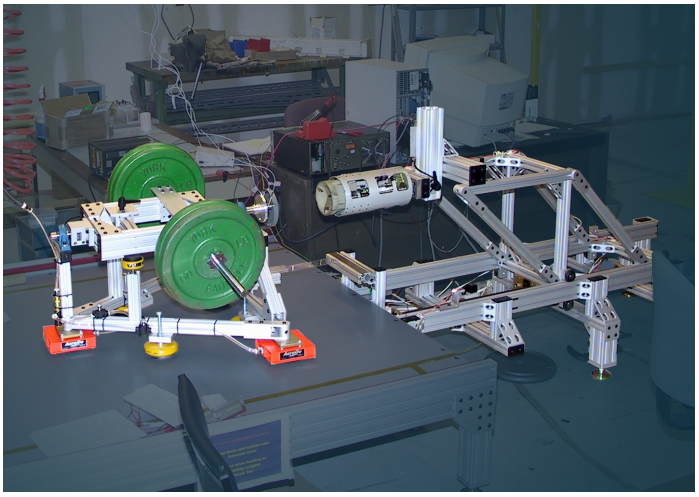

Figure 1: End-effector and test-bed developed by MD Robotics for the Canadian Space Agency

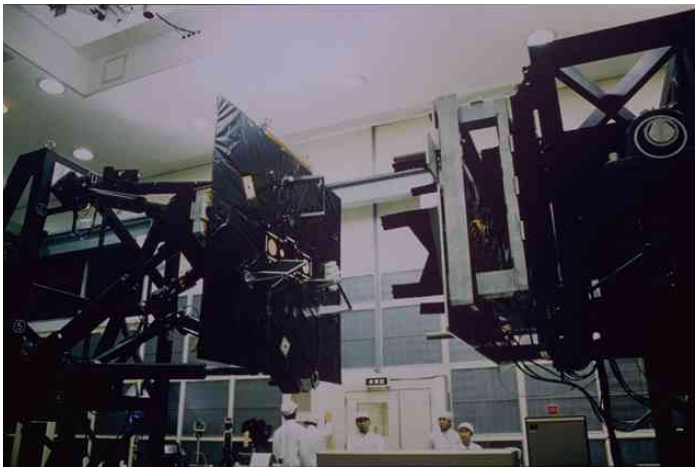

Figure 2: Rendezvous and docking operation test system (NASDA)

To allow for a most reliable docking simulation CSA targets in this project the utilization of hardware-in-the-loop simulation (HLS). Hereby, the satellites and their controller will be modeled in detail using Symofros (L'Archevêque et al. 2000) and the Matlab/Simulink environment. Since the modeling of the contact dynamics of the docking mechanism is very complex and strongly dependent on the contact parameter identification, real hardware will be included in the loop instead.

This concept was already successfully applied at CSA to verify insertion and extraction tasks of the Special Purpose Dextrous Manipulator as described in the next section. For the docking simulation the same serial robot will be used in a first phase of the project to perform this operation. After a verification of the overall concept with the SMT robot a parallel platform with a higher bandwidth will be used to perform the docking of the two spacecrafts with higher fidelity.

2 The STVF concept

As a partner in the International Space Station (ISS), Canada is responsible for the verification of all tasks involving the Special Purpose Dextrous Manipulator (SPDM) and its task verification facility, known as the SPDM Task Verification Facility (STVF) (Piedbœuf et al. 1999). The STVF Manipulator Test-bed (SMT), as shown in Figure 3, is used to refine the analysis of the contact portion of the task. It is a hardware-in-the-loop simulator consisting in a rigid robot with its control, a simulation of the Space Station Remote Manipulator Systems and the SPDM dynamics and a visualisation engine. An operator controls the motion of SPDM through a simulation engine which generates the endpoint motion of the SPDM. This commanded trajectory is then used as a setpoint for the robot controller which ensures that the robot endpoint follows the desired trajectory of the SPDM.

The contact forces are measured using force/moment sensors and fed back into the simulator to allow the dynamic simulation engine to react to external contact forces. This concept is very flexible since it can accommodate vibration of the space robot base or other phenomena. It can also be used to represent different space robots. The main difficulty with the HLS or, in general, with any master-slave type system with contact, is the trade-off between stability of the control loop and good performance. The control of robotic systems in contact has been the subject of research for several years. The HLS problem is a little different from the force-position control problem: the force to be applied is not known, it is the result of the hardware contact. In addition, for verification purposes, the ground robot controller cannot stabilize a space robot operation that is unstable in the reference scenario. Nor can it destabilize a stable operation. The performance of the HLS is measured in terms of dynamic equivalence to a reference dynamic system.

The ground robot control synthesis is of prime importance in the HLS concept. Since the idea is to replicate the dynamics of the space robot with the ground robot performing the contact task, the control algorithm shall be such that the controlled ground robot is transparent in the frequency band of interest for the analysis required. Two different control approaches can be applied. An intuitive approach consists of using the simulator to replicate the behaviour of the reference system subjected to input commands and contact loads, and to feed the ground robot with a reference position to track. Another approach consists of forcing the ground robot to behave like the simulated space robot by commanding its Cartesian acceleration. Cartesian position/velocity feedback is used in addition as a corrector to improve the system response within the bandwidth of interest. The behaviour of the ground robot above this bandwidth is solely dictated by the open-loop performance linked to the knowledge of the system parameters. This gives good performance and good stability. However, it requires a stiff robot with high tracking ac-

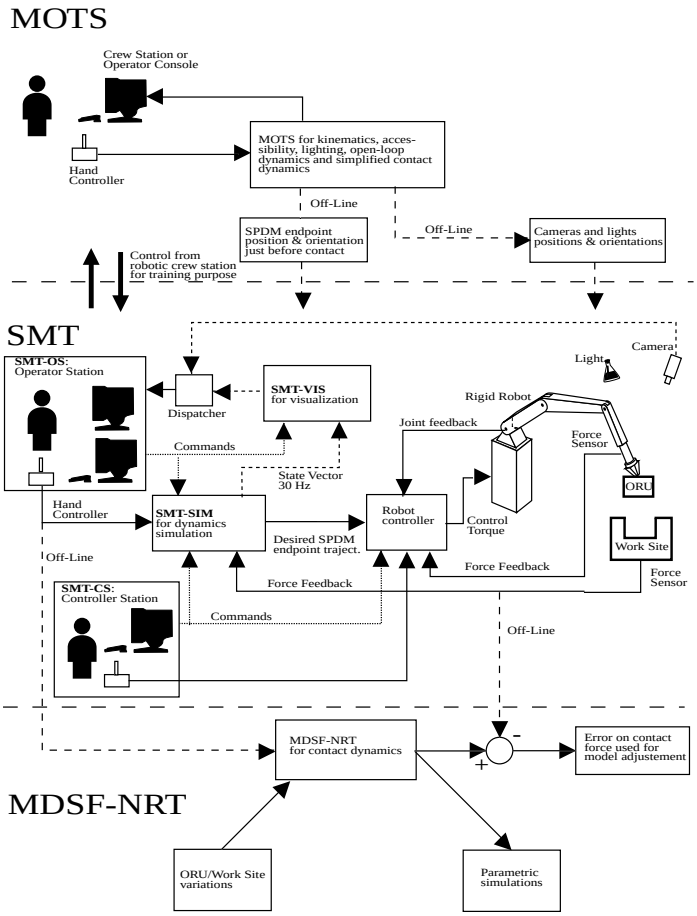

Figure 3: Hardware-in-the-Loop Simulation

curacy, a good torque controller and the ability to implement or access the robot controller at the lowest level to achieve a fast sampling time. To avoid exciting any higher, neglected dynamics in the ground robot, the acceleration command from the space robot simulator needs to be properly filtered.

The emulation of a space robot using a ground robot is done by ensuring that the ground robot extremity follows exactly the space robot extremity given by the simulation. From a dynamics point of view, we can see it as forcing a real robot to follow a virtual one. In some sense, it is similar to a master-slave control in which the master is a simulator.

The details of the controller design can be found in Aghili and Piedbœuf (2000). The base of the controller formulation is the application of constraints on the ground robot so it will follow the space robot. In dynamics, constraints are used to connect two parts of a system to close a kinematic loop. In our case, we put a constraint between the real robot and the virtual space robot. Using the Lagrange's multipliers approach, we obtain a controller that force the ground robot to follow the space robot. This controller ensures that the ground robot has the same acceleration as the space robot. Therefore, we do not control directly the position as proposed in other approaches but we use the acceleration. The controller is a model based Cartesian linearisation with acceleration input. To avoid the inevitable drift, we are adding a PD control on the Cartesian position and velocity. This is a complete analogy to the Baumgarte stabilisation used in constraint dynamical systems. Figure 4 illustrates this controller.

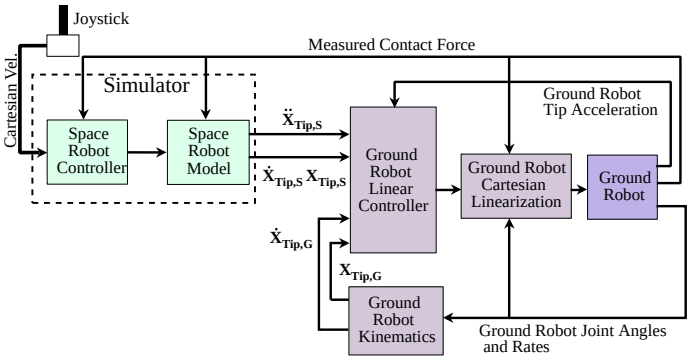

Figure 4: Cartesian Feedback Linearization with Acceleration Controller

3 The docking simulation

3.1 Docking simulation using the SMT robot

In the first part of the project, the SMT robot will be used to conduct an HLS simulation of a docking operation using the MDR end-effector. The MDR docking simulator and Symofros will be used as a basis to build the simulator of a chasing and target satellites. The end-effector will be mounted on the chasing satellite using a compliance mechanism that will emulate the elasticity of a robot arm. Since MDR has already performed studies with a similar model using their contact dynamics toolkit it is also targeted to identify the contact parameters to enable a pure simulation environment. For the experiment the simulator will be used to drive the SMT robot in HLS mode. The contact forces and moments will be measured with a force plate and applied as external perturbations to the satellites. Only the relative motion of the two satellites will be represent by the robot. Another experiment is planned where the end-effector will be installed on a manipulator mounted on the spacecraft.

3.2 Docking simulation using a parallel platform

In space robotics serial manipulators are widely used to perform many different tasks. There advantage is, among others, the large workspace. Significant drawbacks are the restriction on the position accuracy, payload and, most importantly, the small bandwidth, which is critical for HLS. The counterpart for these structures are parallel mechanisms. Here, the system forms one or more closed loops. Due to the loop-closing condition the resulting motion is constrained, allowing the generation of complex

transfer functions. Parallel platforms consists usually of a moving body (the platform) connected to a base via six legs, each leg being hinged at the base and the platform by a passive spherical joint. In between an active linear joint is mounted. Stewart and Gough were the first to propose to employ this structure to generate arbitrary rigid-body motion. Today, Stewart-Gough platforms are used in many fields of engineering, such as physical flight and vehicle simulators, robotics, machine tools, etc. The topology of parallel mechanisms allows for very accurate positioning, high payloads and yields a high bandwidth.

In this project, it is proposed to build or buy a COTS parallel platform that will be mounted on rails to increase its workspace. Since the platform will be used to develop advanced control schemes and for R&D work, it will need to be very well instrumented. Symofros will be used to build the model of the platform. This model will be needed to develop an advanced model-based real-time controller within the Matlab/Simulink environment that will be used to perform hardware-in-the-loop simulation. The HLS capability developed for serial manipulators during the STVF project, see Section 2, will be ported to parallel platforms using the same computer architecture than for the STVF project.

A main feature of the underlying concept is that the same inputs and outputs are used for both the real hardware and the simulation model. Hence, the user can readily switch between the two. It is thus possible to develop in a first step the necessary control schemes, monitoring and safety systems, state machines, etc. When the system is fully tested in simulation, in a second step, the same Simulink diagram can be distributed and compiled by a simple click of the mouse using RT-LAB† and run on a cluster of computers in real-time, driving the real hardware. This approach supports fully the concept of rapid prototyping and the testing of the final system is easily possible. It is also well suited for multi-users work. Newly developed kinematics and dynamics identification capabilities for Symofros will be used to identify the required model parameters.

The development and verification of hardware-in-the-loop capabilities will be done progressively using the following test cases: (a) Free motion test; (b) Constrained motion test; (c) Compliant contact test; (d) Peg on a surface test; (e) Peg in hole test; (f) Docking using MDR End-Effector.

The final testing of this HLS facility using parallel platforms will be done using the end-effector built by MD Robotics. This end-effector, weighing 4.6 kg, has already been tested on the test-bed of Figure 1 in MD Robotics facilities for approach velocities ranging from 10 to 65 mm/s. Although this test-bed is very good for preliminary testing, a facility to accommodate the relative six degrees-of-freedom motion of the two spacecrafts would increase the reliability of the results. The HLS setup proposed in this paper, using a parallel platform, should fulfill this objective.

Finally, since the architecture of Symofros and Matlab/Simulink described above will be used in the course of this project, any future collaboration with external partners that would be interested in the use of the platform will be easily possible.

† www.opal-rt.com

References

Aghili, F. and Piedbœuf, J.-C., 2000, "Hardware-in-loop simulation of robots interacting with environment via algebraic differetial equation, " *2000 IEEE/RSJ International Conference on Intelligent Robots and Systems*, Takamatsu , Japan, pp. 1590–1596.

L'Archevêque, R., Doyon, M., Piedbœuf, J.-C. and Gonthier, Y., 2000, "SYMOFROS: Sofware architecture and real time issues, " *DASIA 2000 - Data Systems in Aerospace*, Montreal, Canada.

Piedbœuf, J.-C., de Carufel, J., Aghili, F. and Dupuis, E., 1999, "Task verification facility for the Canadian special purpose dextrous manipulator, " *1999 IEEE International Conference on Robotics and Automation*, Detroit, Michigan, pp. 1077–1083.

Parallel Robot Projects at Ohio University

Robert L. Williams II

with graduate students:
John Hall, Brian Hopkins, Atul Joshi, Josh Collins, Jigar Vadia, Dana Poling, and **Ron Nyzen**

And Special Thanks to:
Dr. Paolo Gallina, Visiting Researcher, University of Trieste, Italy

Department of Mechanical Engineering
Ohio University
Athens, OH 45701

White Paper
Workshop on Fundamental Issues and Future Research Directions for Parallel Mechanisms and Manipulators
October 3-4, 2002, Quebec City, Canada

The purpose of this white paper is just a bit of the old show-and-tell. The following parallel manipulators and haptic interfaces have been designed, built, programmed, controlled, and evaluated at Ohio University by the author along with the listed graduate students and visiting researcher. Feel free to contact the first author for further discussions on these or any other parallel robot projects.

Contact information:

Robert L. Williams II
Department of Mechanical Engineering
Ohio University
phone: (740) 593-1096
email: williar4@ohio.edu

Associate Professor
257 Stocker Center
Athens, OH 45701-2979
fax: (740) 593-0476
URL: http://www.ent.ohiou.edu/~bob

Parallel Robot Projects at Ohio University

1. GPS/IMU Calibration Platform

The Department of Mechanical Engineering and the Avionics Engineering Center at Ohio University have developed an electromechanical system for the calibration of an inertial measurement unit (IMU) using global positioning system (GPS) antennas. The GPS antennas and IMU are mounted to a common platform to be oriented in the angular roll, pitch, and yaw motions. Vertical motion is also included to test the systems in a vibrational manner. A four-dof system based on the parallel Carpal Wrist (from Virginia Tech, in turn from NASA Langley Research Center's double-octahedral variable geometry truss) is used; the carpal wrist has three linear actuators and the entire system rotates on a turntable. High-accuracy positioning is not required from the platform since the GPS technology provides absolute positioning for the IMU calibration process.

2. 6-PSU Platform Manipulator

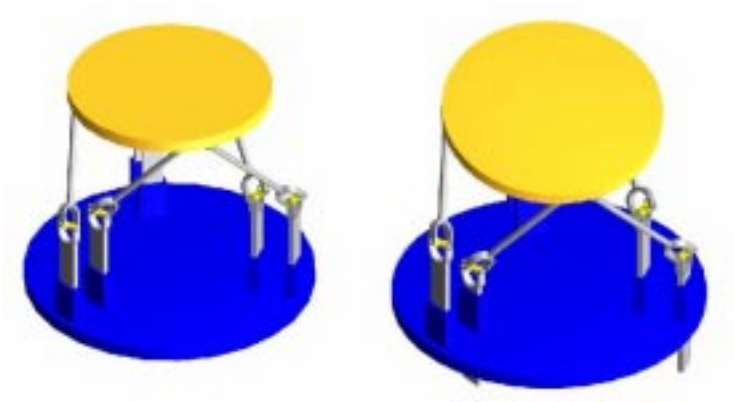

The Department of Mechanical Engineering at Ohio University has designed, constructed, and controlled a new 6-dof in-parallel-actuated platform, a combination and modification of existing designs. The 6-PSU platform consists of 6 legs with a prismatic joint, spherical joint, and universal joint connecting links in each leg which move the platform in the six Cartesian freedoms with respect to the base. The prismatic joint is actuated while the other two joints in each leg are passive. The six prismatic joints move vertically with respect to the base, which appears to be a big improvement over the standard Gough/Stewart platform. The base and moving platform joint locations are on concentric circles, which appears to have dexterity advantages over same-circle joint locations.

Our inspiration for this project comes from the Sandia Paradex, Merlet and Gosselin, Stoughton, Kozlowski, Wang et al., and Bonev and Ryu.

3. Pneumatic planar 3-RPR Robot

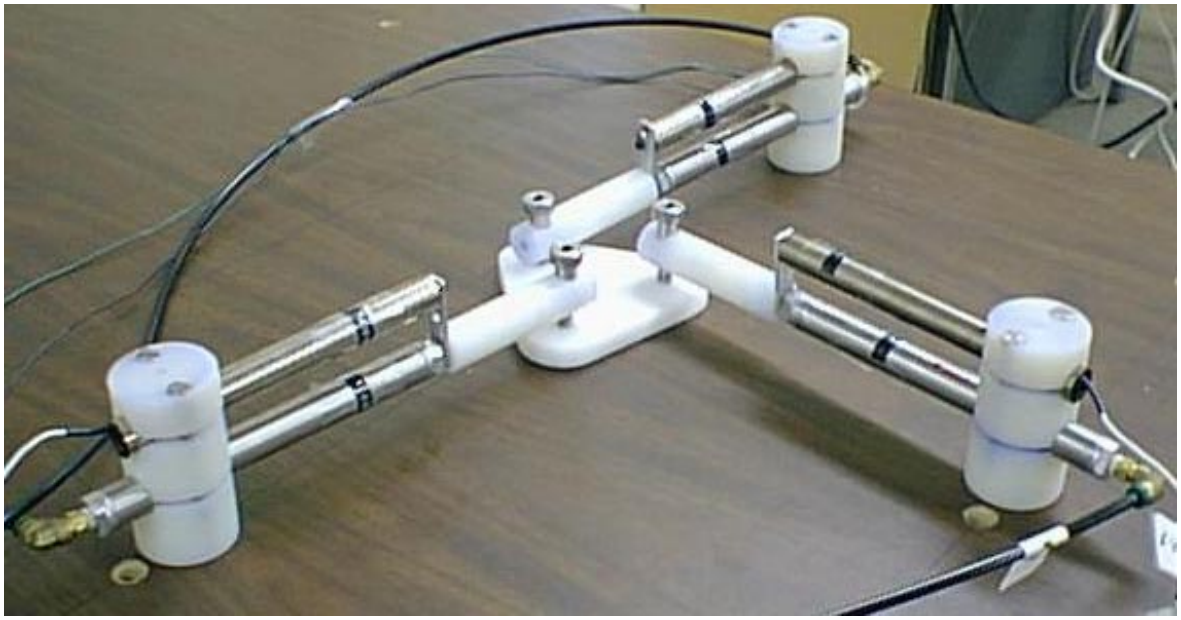

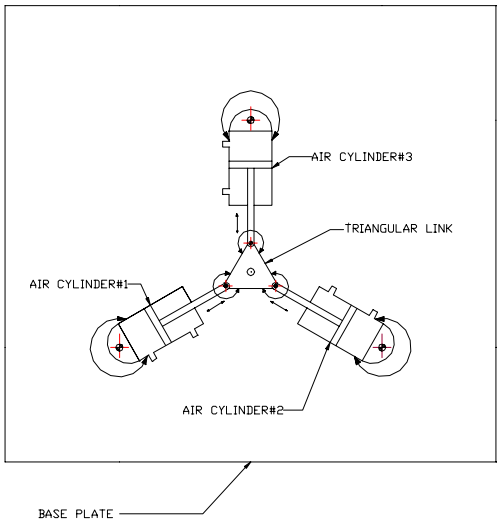

A planar three degree-of-freedom (dof) in-parallel-actuated manipulator has been designed, constructed, and controlled at Ohio University. The symmetric manipulator is composed of three identical legs connecting the fixed base to the end-effector triangle (see the figures). Each leg is of *RPR* design, with two passive revolute joints and an active prismatic joint in-between. Each prismatic joint is an actively controlled pneumatic cylinder. Using real-time closed-loop feedback control for each actuator length independently, we developed inverse pose and resolved-rate control for this manipulator. The objective of this work is to implement in hardware this 3-*RPR* manipulator design and to evaluate parallel manipulator control using pneumatics. This type of manipulator can be used for general tasks such as assembly and trajectory following. Since the workspace is smaller than an equivalent serial robot, we have considered workspace determination and design for this manipulator.

4. 8-dof spatial Cable-Suspended Haptic Interface (CSHI)

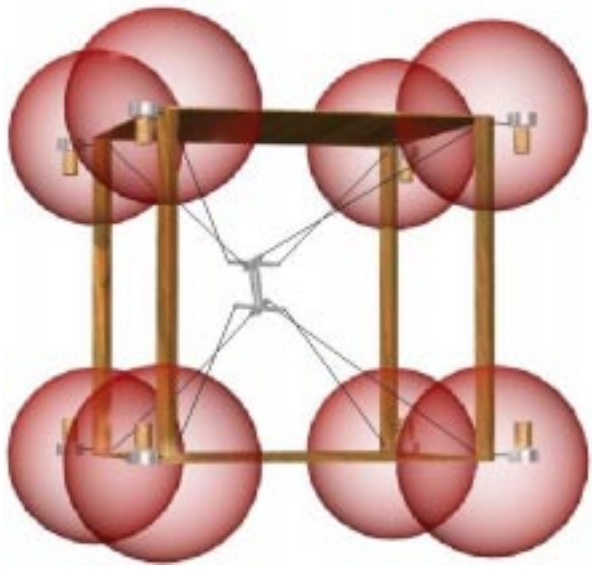

An 8-dof cable-suspended haptic interface (*CSHI*) has been designed and built at Ohio University. The goal is to create an input/output device to provide six-degree-of-freedom (dof) wrench (force and moment) feedback to a human operator in virtual reality or remote applications. Compared to commercially-available haptic interfaces for virtual reality applications, the present concept is striving for lighter, safer, crisper, more dexterous, and more economical operation. The first virtual environment programmed includes 8 one-eighth spheres with linear stiffness located at each corner of the frame, as shown above.

5. 4-dof planar Cable-Direct-Driven Robot (CDDR)

We have simulated the dynamics and control of a planar, translational cable-direct-driven robot (CDDR). The motivation behind this work is to improve the serious cable interference problem with existing CDDRs and to avoid configurations where negative cable tensions are required to exert general forces on the environment and during dynamic motions. Generally for CDDRs the commanded rotations are more demanding than commanded translations in terms of slack cable conditions. Therefore we provide a translational CDDR whose end-effector may be fitted with a traditional serial wrist mechanism to provide the rotational freedoms (assuming proper design to resist the rotational moments). We have simulated examples to demonstrate control including feedback linearization of the 4-cable CDDR (with one degree of actuation redundancy) performing a Cartesian task. An on-line dynamic minimum torque estimation algorithm has been developed to ensure all cable tensions remain positive for all motion; otherwise slack cables can result from CDDR dynamics and control is lost. We have built a planar 4-dof CDDR for experimental verification of our theoretical and simulation results.

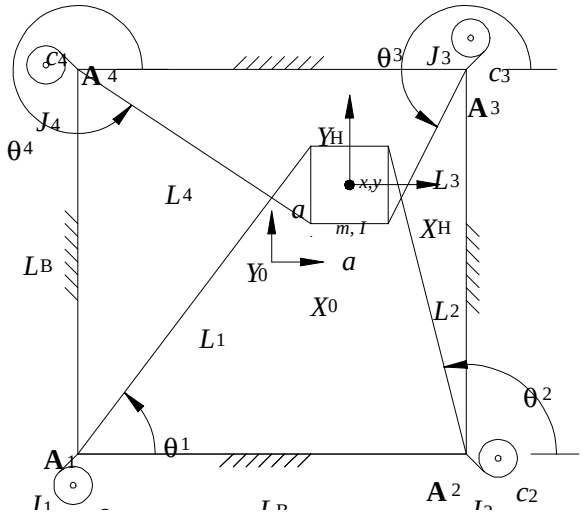

6. Spherically-Actuated platform Manipulators (SAM)

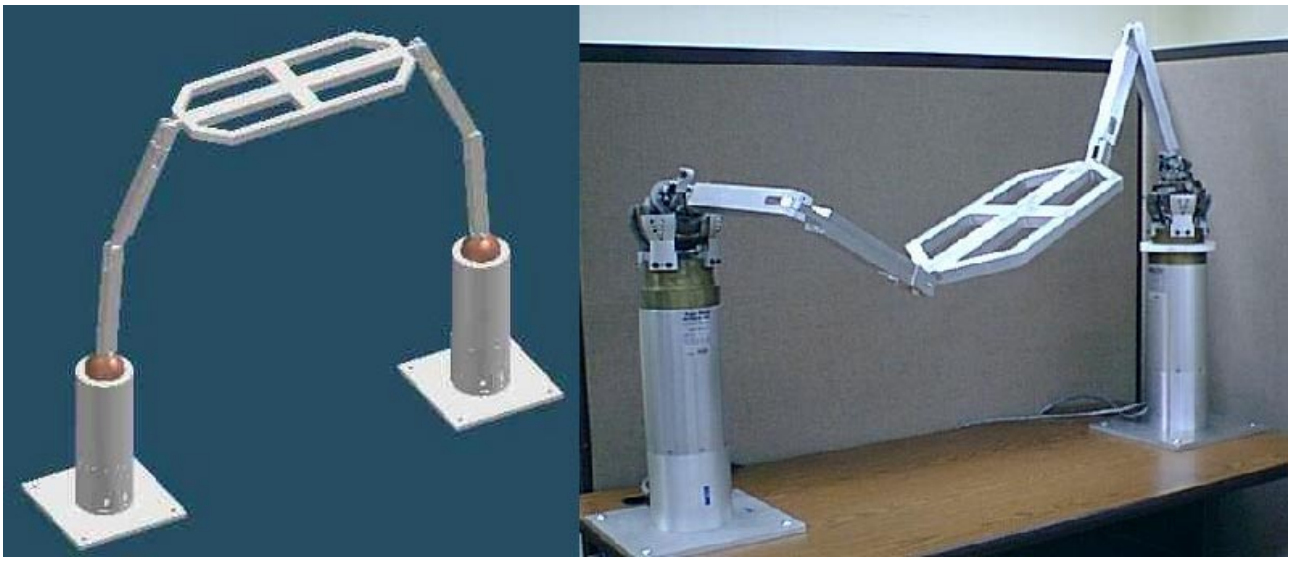

A novel 6-dof platform manipulator has been developed at Ohio University, actuated by two base-mounted spherical actuators. The moving platform is connected to the fixed base by two identical *SRU* serial chain legs. The *S*-joint is active, and the remaining two joints in each chain are passive. An analytical solution has been developed for the inverse pose kinematics problem, a semi-analytical solution is used for the rate kinematics problems, and the numerical Newton-Raphson technique has been employed to solve the forward pose problem. Unfortunately, the passive joint variables cannot be ignored in the kinematics solutions as they can for the Gough/Stewart platform. Experimental hardware has been built, using two Rosheim Omni-Wrists from NASA Langley Research Center as the spherical actuators.

An improved SAM is currently under development, wherein the serial chains are two identical *SPU* serial chain legs; that is, the passive revolute (*R*) joints will be replaced with passive prismatic (*P*) joints, see the CAD concept below. This change allows better singularity avoidance and better workspace.

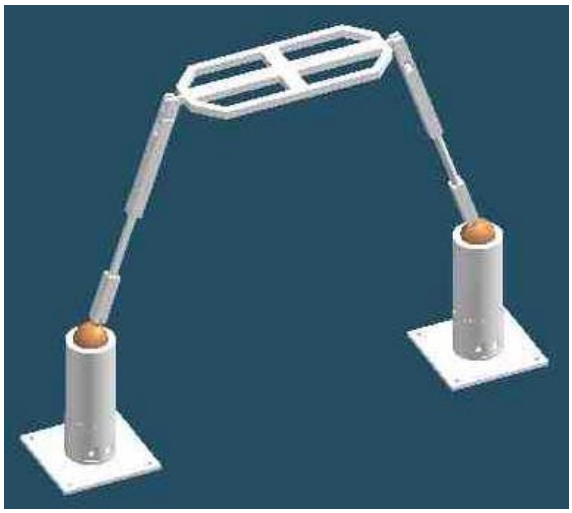

Related Ohio University References

Journal

B.R. Hopkins and R.L. Williams II, *"Design and Control of the 6-PSU Platform"*, submitted to **Industrial Robot: An International Journal**, November 2001.

R.L. Williams II and P. Gallina, *"Planar Cable-Direct-Driven Robots: Design for Wrench Exertion"*, **Journal of Intelligent and Robotic Systems**, final manuscript, October 2001.

R.L. Williams II and D.B. Poling, 2001, *"Spherically-Actuated Platform Manipulator"*, **Journal of Robotic Systems**, Vol. 18, No. 3, pp. 147-157.

J.J. Hall and R.L. Williams II, 2000, *"Inertial Measurement Unit Calibration Platform"*, **Journal of Robotic Systems**, Vol. 17, No. 11, pp. 623-632.

R.L. Williams II, 1998, *"Cable-Suspended Haptic Interface"*, **International Journal of Virtual Reality**, Vol. 3, No. 3, pp. 13-21.

Patent and Provisional Patents

R.L. Williams II, *"Active Scaffolding Systems"*, U.S. Patent No. 5,803,203, September 8, 1998.

R.L. Williams II, F. van Graas, and J.J. Hall, *"GPS/IMU Calibration Platform"*, Ohio University Provisional Patent, December, 1999.

R.L. Williams II, *"Cable-Suspended Haptic Interface"*, Ohio University Invention Disclosure, March, 1997, provisional status.

Conference

B.R. Hopkins and R.L. Williams II, *"Modified 6-PSU Platform"*, **CD Proceedings of the 2002 ASME Design Technical Conferences, 27th Biennial Mechanisms Conference**, **DETC2002/MECH-34245**, September 29-October 2, 2002, Montreal, Canada.

"Design and Control of the 6-PSU Platform", submitted to **Industrial Robot: An International Journal**, November 2001.

R.L. Williams II and P. Gallina, *"Planar Cable-Direct-Driven Robots, Part I: Kinematics and Statics"*, **CD Proceedings of the 2001 ASME Design Technical Conferences, 27th Design Automation Conference**, **DETC2001/DAC-21145**, Pittsburgh, PA, September 9-12, 2001.

R.L. Williams II and P. Gallina, *"Planar Cable-Direct-Driven Robots, Part II: Dynamics and Control"*, **CD Proceedings of the 2001 ASME Design Technical Conferences, 27th Design Automation Conference**, **DETC2001/DAC-21146**, Pittsburgh, PA, September 9-12, 2001.

J.J. Hall, R.L. Williams II, and F. van Graas, *"Cartesian Control for the Inertial Measurement Unit Calibration Platform"*, **CD Proceedings of the 2000 ASME Design Technical Conferences, 26th Biennial Mechanisms Conference**, **DETC2000/MECH-6508**, Baltimore, MD, September 10-13, 2000.

R.L. Williams II and D.B. Poling, *"Spherically-Actuated Platform Manipulator"*, **CD Proceedings of the 2000 ASME Design Technical Conferences, 26th Biennial Mechanisms Conference**, **DETC2000/MECH-6504**, Baltimore, MD, September 10-13, 2000.

R.L. Williams II, *"Planar Cable-Suspended Haptic Interface: Design for Wrench Exertion"*, **CD Proceedings of the 1999 ASME Design Technical Conferences, 25th Design Automation Conference**, **DETC99/DAC-8639**, Las Vegas, NV, September 12-15, 1999.

R.L. Williams II and B.H. Shelley, *"Inverse Kinematics for Planar Parallel Manipulators"*, **CD Proceedings of the 1997 ASME Design Technical Conferences, 23rd Design Automation Conference**, **DETC97/DAC-3851**, Sacramento, CA, September 14-17, 1997.

R.L. Williams II and J.B. Mayhew IV, *"Control of Truss-Based Manipulators using Virtual Serial Models"*, **CD Proceedings of the 1996 ASME Design Technical Conferences, 24th Biennial Mechanisms Conference**, **96-DETC/MECH-1169**, Irvine, CA, August 19-22, 1996.

R.L. Williams II, *"Survey of Active Truss Modules"*, **Proceedings of the 1995 ASME Design Technical Conferences, 21st Design Automation Conference**, Boston, MA, September 17-21, 1995.

R.L. Williams II and A.R. Joshi, *"Planar Parallel 3-RPR Manipulator"*, **Proceedings of the Sixth Conference on Applied Mechanisms and Robotics**, Cincinnati OH, December 12-15, 1999.

Proceedings of the WORKSHOP on
Fundamental Issues and Future Research Directions for Parallel Mechanisms and Manipulators
October 3–4, 2002, Quebec City, Quebec, Canada
Clément M. Gosselin and Imme Ebert-Uphoff, editors

Redundancy Resolution Schemes for Parallel Manipulators with Force Redundancy

BHASKAR DASGUPTA*
Technische Universität Berlin,
Institut für Technische Informatik und Mikroelektronik,
Sekretariat EN 10, Einsteinufer 17,
D-10587 Berlin, Germany.
dasgupta@cs.tu-berlin.de

Abstract: *This paper is intended to draw attention to the potential of static redundancy in parallel manipulators and the need to develop effective redundnacy resolution schemes specially suited for application in such robot manipulators. A few simple redundancy resolution schemes are discussed and compared with respect to their performance through an example. Minimization of a high-index norm is observed to yield a good solution for generic requirement of actuator force optimization. More studies may reveal suitable schemes for different kinds of constraints.*

1 Introduction

Parallel-actuated robot manipulators exhibit a duality and reciprocity against conventional serial manipulators, as detailed in a classic paper by Waldron and Hunt (1991). From the works on singularities of parallel manipulators, notably by Merlet (1989) and Gosselin and Angeles (1990), we find that the predominant kind of singularities in these manipulators are in force domain, rather than motion domain. Such singularities, hereafter referred to force singularities, manifest themselves in the inability of the actuators to sustain arbitrary loads in certain configurations and the resulting uncontrollability of the system.

As kinematic redundancy is found useful in avoiding kinematic singularity of serial manipulators, the natural kind of redundancy to avoid force singularity is force redundancy, with additional in-parallel supports, that has been analyzed as type III redundancy by Lee and Kim (1994). An elaborate treatment of the role of redundancy in parallel manipulators can be found in Merlet (1996). Dasgupta and Mruthyunjaya (1998a) showed that, through force redundancy, the singularities of parallel manipulators are not only avoided, but also reduced. This makes it a very attractive option for tackling the singularity problem in parallel manipulators.

However, it is important to devise effective redundancy resolution schemes to exploit the advantages of the force redundancy. Various such strategies are available (Nakamura , 1991), but mostly in the context of improving motion characteristics. In this paper, the question of redundancy resolution for force redundancy is considered and some simple force optimization strategies are explored as a beginning. Indeed, more research is needed in this direction for better utilization of force redundancy.

2 Force Redundancy

In this section, certain important implications of force redundnacy in parallel manipulators are summarized.

1. In parallel manipulators, the static or force redundancy is characterized by additional in-parallel chains (legs) to support the load more effectively.

2. With more legs, the direct (position and velocity) kinematics problems become over-specified and, therefore, easier to solve.

3. The inverse force transformation of statically redundant manipulators is under-specified, and has infinite solutions.

4. The workspace of the parallel manipulator gets more restricted due to the additional motion constraints of the redundant leg.

5. For every degree of redundancy, the manifold of the force singularities reduces by one in dimension, in general.

6. Redundancy resolution involves the selection of a set of *actuator forces/torques* out of infinite possible solutions.

These aspects have been analyzed in detail in an earlier work (Dasgupta and Mruthyunjaya , 1998a).

*Permanent address: IIT Kanpur, India. (dasgupta@iitk.ac.in)

3 Inverse Dynamics and Redundancy Resolution

As mentioned in section 2, determination of actuation forces for a statically redundant parallel manipulator involves the problem of redundancy resolution. Thus, forces required at the actuators can be optimized in some sense by selecting a particular solution of the inverse dynamics (or statics) problem.

The typical form of the dynamic equation of a parallel manipulator (Dasgupta and Choudhury , 1999) is given in the task-space as

$$\mathbf{H}\,\mathbf{F} = \mathbf{J}\begin{bmatrix} \ddot{\mathbf{t}} \\ \boldsymbol{\alpha} \end{bmatrix} + \boldsymbol{\eta} \tag{1}$$

where $\mathbf{J}$ is the inertia matrix, $\boldsymbol{\eta}$ represents other nonlinear components and $\mathbf{H}$ is the force transformation matrix mapping input forces ($\mathbf{F}$) to the task-space. Representing the right-hand-side of the equation by $\mathbf{T}$ (for inverse dynamics), we get

$$\mathbf{H}\,\mathbf{F} = \mathbf{T} \tag{2}$$

For a redundant manipulator, $\mathbf{H}$ is rectangular (with less rows than columns) and redundancy resolution would require a particular solution of equation 2.

The pseudoinverse $\mathbf{H}^{\#}$ gives the solution with minimum norm of $\mathbf{F}$ and is a good candidate for redundancy resolution, because that seems to require least effort[1] at the actuators. However, this may be inefficient in optimizing the force required from individual actuators. In order to meet actuator force constraints, a better choice can be the resolution of redundancy through a minimax solution of $\mathbf{F}$. If the null space of $\mathbf{H}$ is given by $\mathbf{F}_0$, then the general solution of equation 2 is given by

$$\mathbf{F} = \mathbf{H}^{\#}\mathbf{T} + \mathbf{F}_0\mathbf{u} \tag{3}$$

and a minimax solution will find the value of $\mathbf{u}$ by minimizing the maximum of $|F_i|$.

Though the minimax solution has the advantage over the minimum norm solution, of giving the utmost benefit of redundancy to the most severely loaded actuator, the force demands are discontinuous at instants when two legs have the maximum force magnitude, i.e. when there is a change of the 'most severely loaded actuator'. Relaxing the minimax criterion to some extent in such situations, the force demands can be made continuous.

Drawing from a more generalized norm

$$\|\mathbf{F}\|_k = \left[\sum_i |F_i|^k\right]^{1/k}, \tag{4}$$

the norm with a high even index (k = 6 or 8, for example) can be minimized to obtain solutions which give good trade-off between the minimization of the largest force and continuity. The results in the next section correspond to the norm for $k = 8$, apart from the pseudoinverse and the minimax solutions. Obviously, the pseudoinverse solution and the minimax solution can be viewed as special cases with $k = 2$ and $k = \infty$, respectively.

Thus, in different situations, one can prefer different strategies. If total power is the governing criterion, then one would choose the pseudoinverse solution. On the other hand, if the actuators are quite severely loaded and operating close to their capacity, then the greatest actuator force becomes the deciding factor. In that case, one may use the minimax solution, or the more practical solution given by a high-index norm (say the 8-norm). In some situations, a weighted norm may also be used, as in (Gonzalez and Sreenivasan , 2000), if actuators widely vary in their force/torque capability. Other redundancy resolution schemes are also possible. For example, a scheme may focus on fault-tolerance, in which the redundant actuations are reserved for use only when the regular ones fail to give the required resultant force (and moment) at the end-effector. In another situation, the redundancy could be in the form of passive compliant supports, in which case the redundancy resolution strategy has to consider both forces and motion at the same time for effectiveness. Evidently, a good deal of research is required to address all these issues in detail.

4 Example: A Redundant Stewart Platform

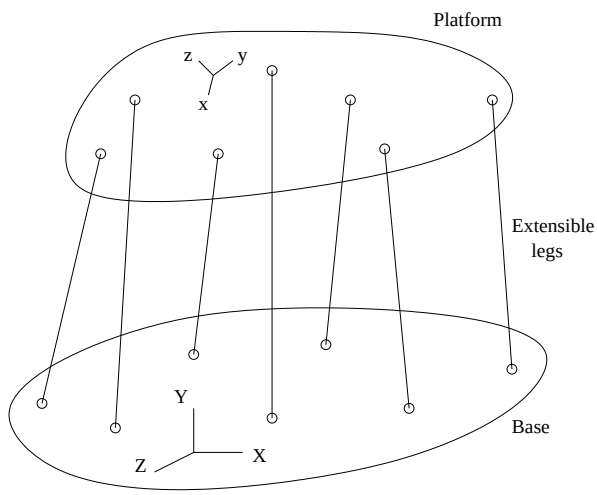

Figure 1: Redundant Stewart Platform with Seven Legs

As an example, let us consider a single degree of redundancy (one redundant leg) in a genaralized Stewart platform. The inverse dynamics of the resulting 7-legged manipulator (Figure 1) requires the solution of the 6×7 system given by equation 2.

The redundant Stewart platform studied here is essentially a 7-legged redundant version of the 'Test Manipulator' studied for inverse dynamics in (Dasgupta and Mruthyunjaya , 1998b). The inverse dynamics formulation is also similar to the one reported there[2]. The singular path studied there for the 6-legged

[1] e.g. minimum total power, for a given trajectory

[2] The datails of dynamic formulation are not very relevant for this paper.

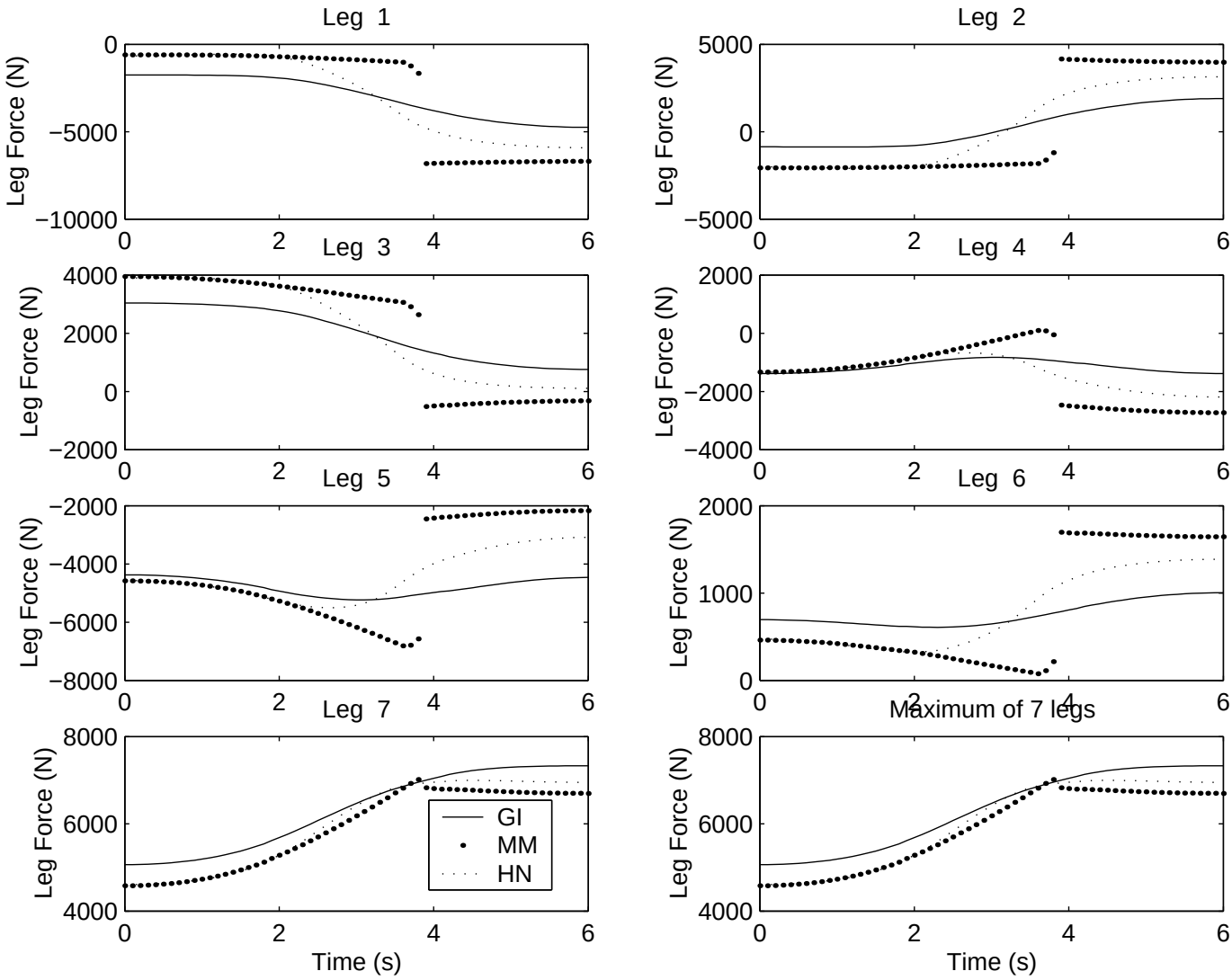

Figure 2: Redundant Stewart Platform — Leg Forces
(GI: Pseudoinverse, MM: Minimax, HN: High-index Norm)

non-redundant Stewart platform is taken up here for inverse dynamic analysis with respect to this redundant Stewart platform manipulator. The configuration of the manipulator is represented by the position vector $\mathbf{t} = [x\ y\ z]^T$ of the origin of the platform-frame and the RPY angles $\mathbf{\Theta} = [\theta_x\ \theta_y\ \theta_z]^T$ (with respect to the base-frame). The path is planned as a linear path with parabolic blends (having segments of constant acceleration, constant velocity and constant deceleration) in each of the six task-space coordinates between the initial pose

$$\mathbf{t}_0 = [0.4\ 1.4\ 1.2]^T, \qquad \mathbf{\Theta}_0 = [0.1\ 0.2\ 0.0]^T$$

and the final pose

$$\mathbf{t}_1 = [0.8\ 1.8\ 1.8]^T, \qquad \mathbf{\Theta}_1 = [0.3\ 0.4\ 0.0]^T$$

for a total period of 6 seconds and velocity constraints for linear motion as $V_{max} = 0.2$ and that for angular motion as $\Omega_{max} = 0.08$. (All data are in SI.)

The three redundancy resolution schemes discussed in the previous section are employed. The forces in all the seven legs and the greatest leg forces from the solutions are shown superimposed on one another in Figure 2, where the pseudoinverse (minimum norm) solution is shown by continuous line, the minimax solution by heavy dots and the solution minimizing the 8-norm by dotted line (with light dots). It is found that the 8-norm solution provides a good trade-off in this case. With an increase in the index k of the norm, the solution approaches the minimax solution more closely, and changes in the actuator force demands become sharper leading to a loss of continuity in a practical sense.

Comparison with results reported earlier (Dasgupta and Mruthyunjaya , 1998b) for the 6-legged non-redundant Stewart

platform manipulator (composed only of the first six legs from the current example), it is seen that the redundancy introduced by the seventh leg has eliminated the singularity of the path.

Another fact that is apparent from the plots is that, though singularity is eliminated by the redundancy, the ill-conditioning is still quite high, manifesting in large force magnitudes. An optimal placement of the seventh leg in the perspective of the other six legs or an optimal synthesis of connection-points for all the seven legs is expected to reduce the ill-conditioning as well.

5 Conclusions

The exploration of the potential of force redundancy has significant importance in the control and design of parallel manipulators. For control, redundancy resolution schemes need to be analyzed for optimizing performance and/or for satisfying operating constraints. In the current paper, a few simple schemes are demonstrated and compared. More detailed study will certainly be useful in developing effective control strategies for different situations. So far as the kinematic design of the manipulator is concerned, the placement of the redundant limb for optimal performance is also important.

References

Dasgupta, B., and Mruthyunjaya, T.S., 1998a, "Force Redundancy in Parallel Manipulators: Theoretical and Practical Issues", *Mech. Mach. Theory*, 33(6), 727-742.

Dasgupta, B., and Mruthyunjaya, T.S., 1998b, "A Newton-Euler Formulation for the Inverse Dynamics of the Stewart Platform Manipulator", *Mech. Mach. Theory*, 33(8), 1135-1152.

Dasgupta, B., and Choudhury, P., 1999, "A General Strategy Based on the Newton-Euler Approach for the Dynamic Formulation of Parallel Manipulators", *Mech. Mach. Theory*, 34(6), 801-824.

Gonzalez, L.J., and Sreenivasan, S.V., 2000, "Representational Singularities in the Torque Optimisation Problem of an Active Closed Loop Mechanism", *Mech. Mach. Theory*, 35(6), 871-886.

Gosselin, C., and Angeles, J., 1990, "Singularity Analysis of Closed-Loop Kinematic Chains", *IEEE Trans. Robot. Automn*, 6(3), 281-290.

Lee, S., and Kim, S., 1994, "Kinematic Feature Analysis of Parallel Manipulator Systems", *Proc. IEEE Int. Conf. Robot. Automn*, 77-82.

Merlet, J.-P., 1989, "Singular Configurations of Parallel Manipulators and Grassman Geometry", *Int. J. Robot. Res.*, 8(5), 45-56.

Merlet, J.-P., 1996, "Redundant Parallel Manupulators", *Lab. Robot. Automn*, 8(1), 17-24.

Nakamura, Y., 1991, "Advanced Robotics: Redundancy and Optimization", Addison-Wesley Publishing Company, Inc.

Waldron, K.J., and Hunt, K.H., 1991, "Series-Parallel Dualities in Actively Coordinated Mechanisms", *Int. J. Robot. Res.*, 10(5), 473-480.

Appendix

Kinematic and dynamic parameters of the 7-legged redundant Stewart platform (all in SI units):
Base points:

$$\begin{bmatrix} 0.6 & 0.1 & -0.3 & -0.3 & 0.20 & 0.5 & 0.5 \\ 0.2 & 0.5 & 0.3 & -0.4 & -0.30 & -0.2 & 0.0 \\ 0.0 & 0.1 & 0.1 & 0.0 & -0.05 & 0.0 & 0.0 \end{bmatrix}$$

Platform points (in platform frame):

$$\begin{bmatrix} 0.3 & 0.3 & 0.0 & -0.2 & -0.15 & 0.15 & 0.0 \\ 0.0 & 0.2 & 0.3 & 0.1 & -0.20 & -0.15 & -0.2 \\ 0.1 & 0.0 & 0.0 & -0.1 & -0.05 & -0.05 & 0.0 \end{bmatrix}$$

Mass of lower and upper part of each leg:

$$m_d = 3.0 \quad \text{and} \quad m_u = 1.0$$

Centres of gravity of lower and upper parts of each leg (in local frames):

$$\mathbf{r}_{d0} = [0.4 \;\; 0.14 \;\; -0.18]^T \quad \text{and} \quad \mathbf{r}_{u0} = [-0.6 \;\; -0.08 \;\; 0.08]^T$$

Moments of inertia of lower and upper parts of each leg (in local frames):

$$\mathbf{I}_{d0} = \begin{bmatrix} 0.010 & 0.005 & 0.007 \\ 0.005 & 0.002 & 0.003 \\ 0.007 & 0.003 & 0.001 \end{bmatrix}, \mathbf{I}_{u0} = \begin{bmatrix} 0.005 & 0.002 & 0.002 \\ 0.002 & 0.002 & 0.001 \\ 0.002 & 0.001 & 0.003 \end{bmatrix}$$

Platform mass (including payload): $M = 40.0$
Centre of gravity of the platform and payload (in platform frame):

$$\mathbf{R}_0 = [0.04 \;\; 0.03 \;\; -0.06]^T$$

Moment of inertia of platform and payload (in platform frame):

$$\mathbf{I}_p = \begin{bmatrix} 0.050 & 0.003 & 0.004 \\ 0.003 & 0.040 & 0.003 \\ 0.004 & 0.003 & 0.100 \end{bmatrix}$$

Proceedings of the WORKSHOP on
Fundamental Issues and Future Research Directions for Parallel Mechanisms and Manipulators
October 3–4, 2002, Quebec City, Quebec, Canada
Clément M. Gosselin and Imme Ebert-Uphoff, editors

On some properties of POLMAN-3L parallel manipulator to the use as a 3-D measuring system for industrial/educational applications.

K. MIANOWSKI
Institute of Aeronautics and Applied Mechanics
Warsaw University of Technology
Nowowiejska str. 24, 00-665 Warsaw, Poland
kmianowski@meil.pw.edu.pl

Abstract: *A new parallel manipulator POLMAN-3L for the use of the measurement applications is presented in the paper. It is parallel mechanical arragement with three degrees of freedom equipped with typical slide gauges and computer for acquisition of the data. Manipulator is consist of three properly situated serial chains connected in parallel way to end-element, which has the form of the platform with measuring probe. It is equipped with spherical joints and is attached to actuated mechanisms with using three identical rods. Because of good isotropy of the mechanical part, and homogenous space structure, mechanism has very good kinematic manipulability, and so the generated errors are similar in each direction in 3-D space and similar to errors of slide gauges. All gauges are connected with the base of the system. Manipulator can be use for the measure of smooth surfaces after technological operations. Because of special geometry some properties of its are similar to the cartesian manipulator. Adopted kinematic systems allows for easy solution of both inverse and direct kinematic tasks. Mechanical construction of the system are modular and very light, each elements are low cost in fabrication.*

1 Introduction

New technological applications of the robots need new approaches for the organization of its technological stands. Measuring the geometrical shape of the surface in order to prepare its mathematical model employing classical measurement methods is a very expensive task (high cost of machinery). For realizing milling and/or polishing with the use of some new kind of robots, it needs to use three-dimensional measuring systems for the measure worked-out surfaces exactly on the stand. In some applications considerable exactness measured in micrometers is not necessary (accuracy in 0.1 mm order is enough) but it would be desirable to have a measuring device portable and relatively cheap. Known from the literature laser scanning methods are rather very expensive, while typical measurement systems used in measurement machines are rather bulky and heavy, and so its applications on the stand with the robot can be very difficult. Because of that, last time it has been invented some new approaches for the solving such a difficult task. One of them is presented in this paper. The principle of such a measuring system was derived from the class of spatial manipulators typically used as mechanical arragements of very fast parallel robots [see Mianowski 1994, 2000]. Compared to serial manipulators, parallel systems have some advantages like a stiff mechanical structure and more precise positioning. Limited working area and reduced maneuverability of the end element are the main disadvantages of typical parallel manipulators of Stewart platform type. The main advantages of proposed system are simplicity and lightness of the construction with relatively high (good) stiffness of the mechanism, and clear concept of kinematic description of mathematical model. Adopted kinematic arragement has very good isotropic kinematic properties. Because of well-conditioned kinematic transformation between the input and output, obtained results of the measure have very clear interpretation.

2 Polman-3L manipulator for the measuring applications

Good isotropy of three DOF parallel manipulator can be achive when possible motion of the end element are determined by three identical orthogonal components of linear velocities [Mianowski 2000]. When the use three linear slides mounted to the base, and connected to them spatial moving mechanism, one of possible arragement of the manipulator could have a form shown in the general scheme in Fig. 1a.

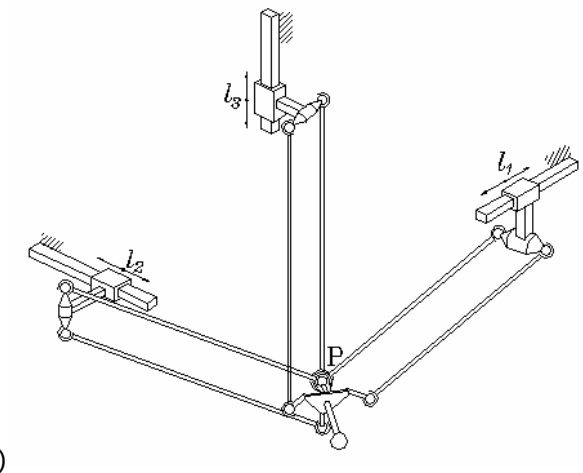

a)

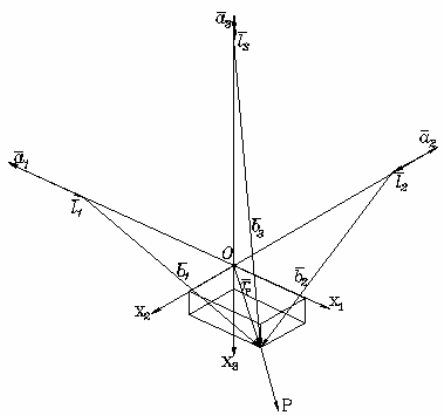

b)

Fig. 1. General scheme of POLMAN-3 manipulator for the measure of smooth surfaces
a) kinematic arragement, b) kinematic model for calculation of the position

Manipulator POLMAN-3L is consist of specially connected three typical slide gauges located in the base in such a way, that each one slide is perpendicular to two the others. Each slide can realize translational motion. The end element of the manipulator is connected to slides with the use six identical rods in such a way, that three of them are mounted to one special spherical joint on the platform. Three the other connecting rods are located in such a way, that moving platform has the form of spatial parallelogram, and so it can only realize translational motion in the space (without any rotations). Mechanical part of the system has very high (good) stiffness, and can assure very small mechanical hysteresis. The resolution of each slide is ±0.01mm, so the average resolution of the measure is no more then ±0.02mm (approx. ±0.015mm) in each direction in the space.

3 Kinematic model of the manipulator

Kinematic model of POLMAN-3L manipulator is derived with the use vector method. General scheme of kinematic model is shown in the Fig. 1b, where the vector $\overline{\mathbf{W}}$ is mean as $\mathbf{W}$. The basic absolute reference frame is a cartesian orthogonal dextrorotary $p_0(x_1, x_2, x_3)$. Current configuration of the mechanism can be described equivalently with the use vectors $\mathbf{r}_P = [x_{1P}, x_{2P}, x_{3P}]^T$, describing current location of point P in absolute reference frame, or $\mathbf{l} = [l_1, l_2, l_3]^T$, describing local coordinates of the moving tables of slide gauges. Vectors described coordinates of locations slide gauges are in the form:

$$\mathbf{a}_1 = a_1 \begin{bmatrix} -1 \\ 0 \\ 0 \end{bmatrix}, \ \mathbf{a}_2 = a_2 \begin{bmatrix} 0 \\ -1 \\ 0 \end{bmatrix}, \ \mathbf{a}_3 = a_3 \begin{bmatrix} 0 \\ 0 \\ -1 \end{bmatrix} \quad (1)$$

$$a_i = a_i(t), \quad a_i \in (a_{imin}, a_{imax}) \quad \text{where, } i=1,2,3,$$

Vectors $\mathbf{l_i}$ described current configuration of the manipulator in absolute reference frame:

$$\mathbf{l}_1 = l \begin{bmatrix} \cos x_1 \\ \cos h_1 \\ \cos z_1 \end{bmatrix}, \mathbf{l}_2 = l \begin{bmatrix} \cos x_2 \\ \cos h_2 \\ \cos z_2 \end{bmatrix}, \mathbf{l}_3 = l \begin{bmatrix} \cos x_3 \\ \cos h_3 \\ \cos z_3 \end{bmatrix} \quad (2)$$

Measured trajectory of the ball gauge while its moving with the contact with measured surface in absolute reference frame is a set of points in the form:

$${}^j\mathbf{r}_P = \begin{bmatrix} {}^jx_{1P} \\ {}^jx_{2P} \\ {}^jx_{3P} \end{bmatrix}, \text{ where } {}^jx_{iP} = {}^jx_{iP}(t), \quad (3)$$

The basic kinematic relation describing mathematical model of the manipulator is:

$$\mathbf{a_i}(t) + l_i + \mathbf{c} = \mathbf{r_P} \quad (4)$$

In more compact form it can be described:

$$\mathbf{r_P} = \mathbf{r_P}(a) \quad (5)$$

Where $\mathbf{r_P}$ in the form (5) is called now as manipulation vector, while $\mathbf{a}$ in the form $\mathbf{a} = [a_1, a_2, a_3]^T$ is a joint vector. Solution of equation (4) can be obtained as intersection of three spheres with constant radius of each l, and with the center in the point of the end of vector $[\mathbf{a_i}(t)]$, located away by vector $\mathbf{c}$ represent probe element on the end-effector with constant orientation. There exist two solutions of this task, and so it has to take only one for positive x_{iP}. Working space of the manipulator can be obtained by inspection of relations

(5) according to (1). It is area between six spheres with radius l each, which centers are located in points on the ends of slides in the base. Workspace of the manipulator is shown in the Fig. 2a.

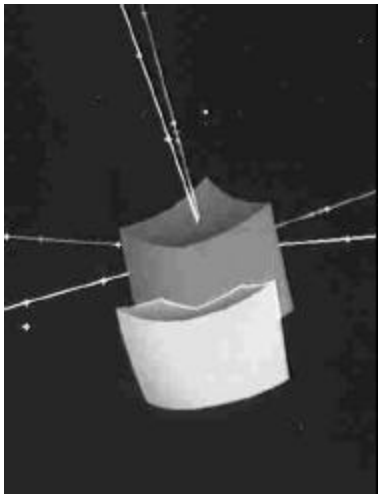

a)

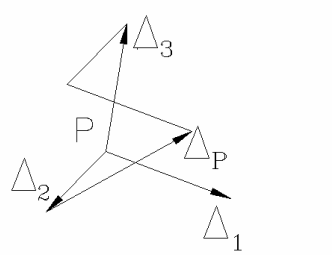

b)

Fig. 2. Basic features of the manipulator POLMAN-3L:
a) workspace, b) generated errors of the end-effector

Error of the position of the end-effector *P* is composed of three independent components generated in sliding gauges and transmitted to the end-effector. Appropriate its components can be derived from general form of differential equations (5) of kinematic model of the manipulator [6]:

$$d\mathbf{r_P} = \mathbf{J}(\mathbf{l})d\mathbf{l} \qquad (6)$$

in the form:

$$\Delta\mathbf{r_P} = \mathbf{J}(\mathbf{l})\Delta\mathbf{l} \qquad (7)$$

where matrix $\mathbf{J}(\mathbf{l})$ is the Jacobian matrix of the whole system d(.) is operator of differentiation, and Δ is the first difference of actual variable. Scalar value:

$$w = \sqrt{\det \mathbf{J}\mathbf{J}^{\mathrm{T}}} \qquad (8)$$

is defined to be the manipulability measure at state $\mathbf{l}$ with respect to the manipulation vector $\mathbf{r}_{\mathrm{P}}$. In investigated kinematic model of POLMAN-3 manipulator dimensions of vectors of input and output variables are the same, and equal to 3, so the manipulability measure is simply given by:

$$w = |\det \mathbf{J}| \qquad (9)$$

It means, that normalized error generated in the mechanism of POLMAN-3 manipulator can be simply obtained from equation (9) as euclidean norm of the determinant of Jacobian matrix. In 3-D space, this error can be interpreted as is shown in the Fig. 2b, where Δ_i are the vectors generated from sliding gauges seen in the end-effector, while Δ_P is produced error of the end-effector. By expecting equation (9) in working space, one can show, that produced error is not exceed ±0.02mm.

4 Initial results, applications

On the basis of the idea described in the paper a number of prototypes of similar measure systems has been designed and made. POLMAN-3L manipulator has been realized with the use electronic slide gauges with working range 300mm and measure resolution 0.01mm, They have been connected exactly to the computer. The other characteristic lengths of

a)

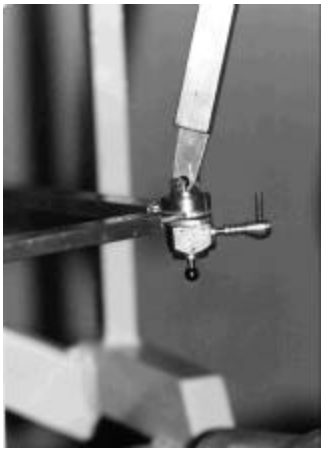

b)

Fig. 3. POLMAN 3L manipulator
a) general view, b) measuring probe,

the system are l=450mm. Ball multijoint of the structure has been mounted exactly to the tool at the end of the manipulator.

One of such a system with linear slide gauges mounted to the base with using ball joints and with three DOF's is shown in the fig. 3a.

POLMAN-3 manipulator can be used as a measuring machine for the measure of smooth surfaces after technological operations. It has been used in the stand with RNT robot. First applications was the measure probes after polishing realized with the use RNT robot shown in Fig. 4.

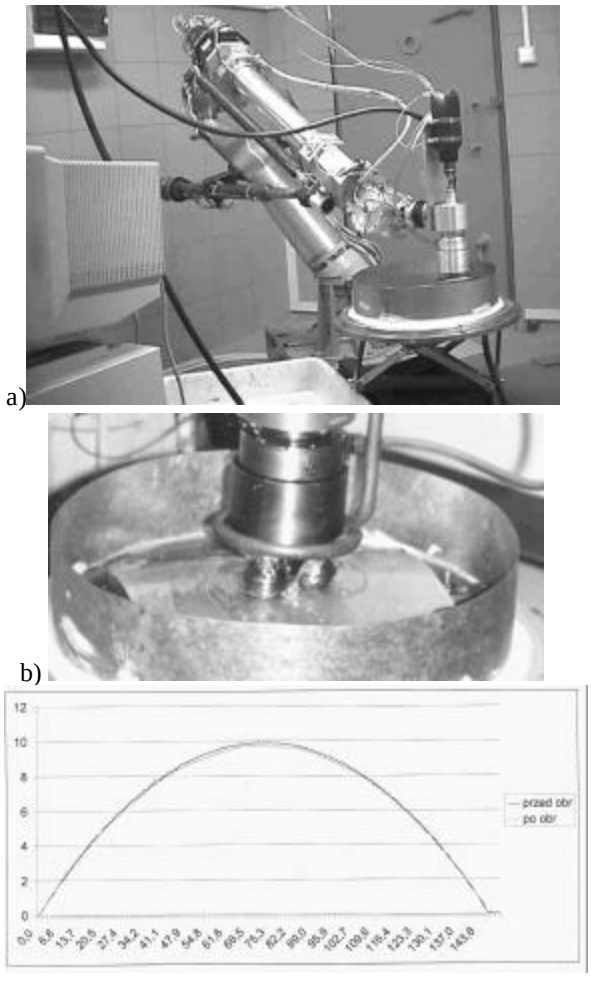

Fig. 4. Polishing operations realized with the use of RNT robot: a) general view of laboratory stand, b) polished surface, c) results of the measure

The other applications of POLMAN-3 manipulator was the measure of milled surfaces. It has been realized from point to point with actual acquisition of the data. In order to prepeare visualization and for calculate average errors, in the next step it have to be calculate new coordinates of the measuring surface by smoothing the data, and prepeare collection of coordinates of regular or irregular meshes for presentation on the monitor and for correction of the robot trajectory. It has been observed several conclusions:

(1) results of the measure are accurate and stable,
(2) proposed method is able to measure most items of the motion accuracy of the robot,
(3) measuring results characterized of good repeatability.

After a number of initial tests, it was decided to use this same arragement to on-line measure of the position of the end point of end-effector with ball in the place, where the tool is mounted as it is shown in Fig. 6. Procedure of local correction of kinematic model in such a case is based on

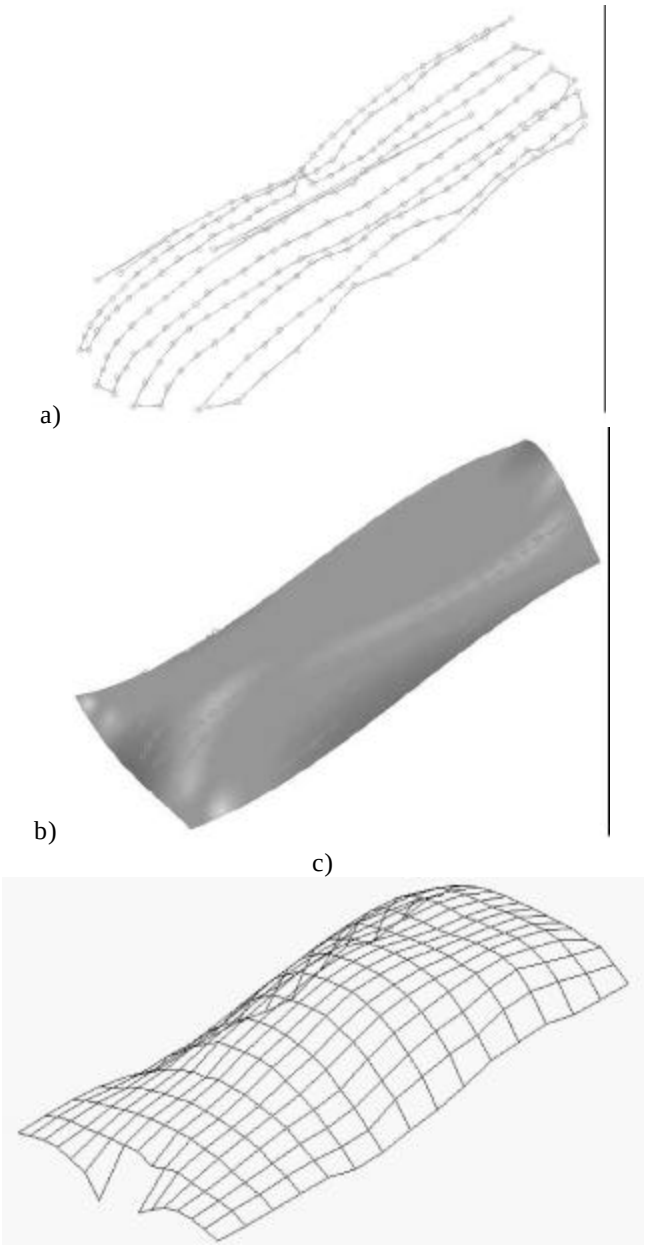

Fig. 5. Initial results of the measure smooth surfaces
a) measured points of human upper limb,
b) surface obtained in UNIGRAPHICS system,
c) grid model of human body destined for planning of surgical operations.

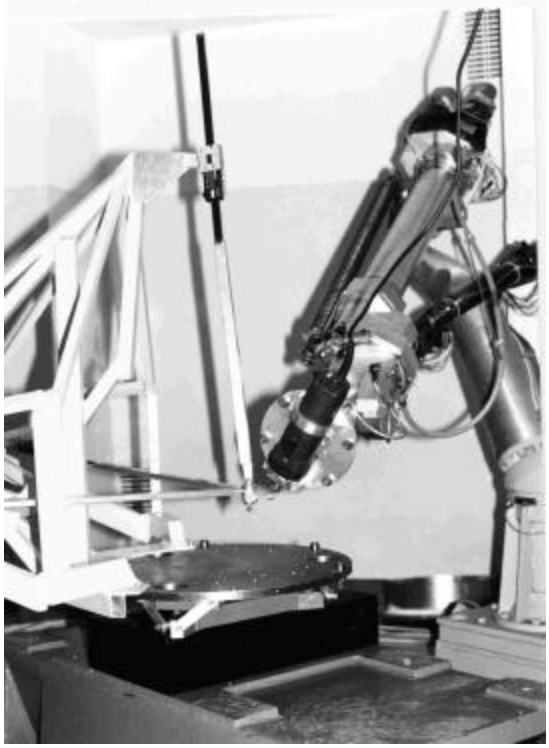

a)

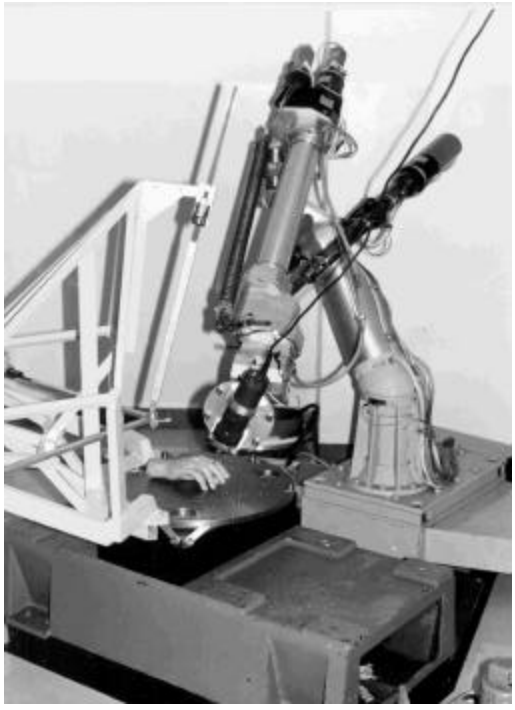

b)

Fig. 6. Manipulator POLMAN 3L on the stand with RNT robot: a) local correction of kinematic model, b) localization of the tool with respect to machining piece.

deriving and implementing an algorithm for improvement kinematic calculating of position and orientation of the robot. It was realized in such a way, that in investigated subspace of working space of the robot the vector of the difference between position and orientation calculated from corrected kinematic model and measured sized of them are minimal in the sense of its euclidean norm.

Manipulator has been used to the measure of the other models with smooth surfaces i.e. of human hand, as it is shown in Fig. 3a. Modified system has been used to the measure of the human body for computerized virtual model as it is shown in Fig. 5.

Some measure operations have to be realized in two steps:

- locating element should be measure in two locations, measured points are shown in two ways in Fig. 7a,
- selected trajectories are connected to closed curves as it is shown in Fig. 6b

Calculated model obtained with the use UNIGRAPHICS system is shown in Fig. 6c.

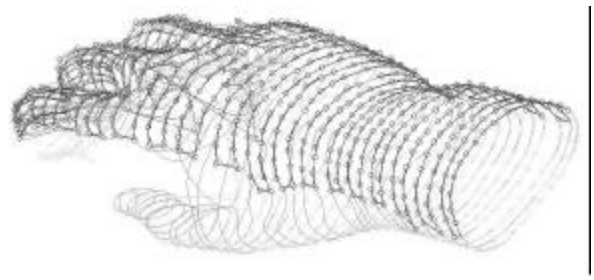

a)

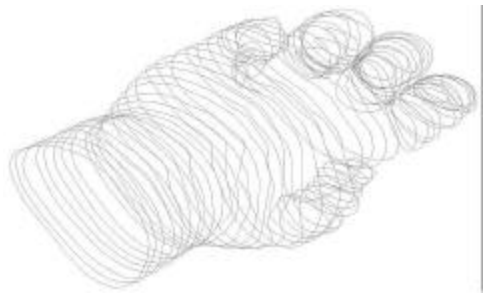

b)

c)

Fig. 7. Initial results of the measure surfaces obtained in two steps: a), b) grid of human hand, c) computer model,

For improving absolute accuracy of the measure it is profitable to equippe it with special calibration element in the form of spatial corner with very accurate measured distances. For achieve improved in such a way absolute accuracy of the system, special fixture has been designed and implemented. It has been shown, that because of good kinematic properties and enough accuracy, it can be implemented on the other real stands.

Worked-out parallel manipulator POLMAN-3L has been implemented in real stand with RNT robot. Obtained results can be summarized as follows:

- POLMAN 3L manipulator has a compact modular structure and relatively large working space with high resolution and very good isotropic kinematic properties, its cost is relatively very low,
- proposed method of the measure can be implemented exactly on the machining stand at the laboratory or in the workshop,
- generated errors are not exceed 0.02mm, while there is no any elastic deformations of the structure, and there is no any mechanical hysteresis,
- installation process of the manipulator on the stand is simple and reliable, and so measuring working is easy and convenient in actual measurement,
- because of modularity it is very easy to apply selected results to make portable system working on the base of this same idea,
- moving elements are very light and so it is very easy to apply driving systems to drive manipulator automatically for very fast and accurate motion.

4 Summary

Worked-out parallel manipulator POLMAN-3 for the measurement applications has been designed, constructed and built. Because of compact structure, good isotropic kinematic properties and good appropriate accuracy it can be used for some measurement applications after technological operations. With application of very simple driving system, it can be used as automatic measuring system. It is very convenient for the use it as a portable system. Manipulator can be use exactly in technological process without changing any its functional components. Mechanical part is modular and very simple, its cost is very low. Another advantage of the proposed solution is the fact, that it is easy to change parameters of the measurement system (e.g. characteristic linear or angular dimensions) for individual neccesity.

Acknowledgments

Results presented in the paper was partially supported by CATID programme at Warsaw University of Technology in 2002.

References

Bernier D., Castelain J-M., Xiaoming Li.: A new parallel structure with six degrees of freedom, Proc. Int. Congress TMM, Mediolan 1995, Vol. 4, pp.8-12,

Clavel R.: DELTA, a fast robot with parallel geometry, Proc. of the 18th Int. Sym posium on Industrial robots, IFR Publications, 1988, pp. 91-100,

Danescu G., Jacquet P., Dahan M.: The singular configurations of an unirotational manipulator, Proc. Int. Congress TMM, Mediolan 1995, Vol. 4, pp.1961-1965.

Fitzgerald J.M.: Evaluating the Steward Platform for Manufacturing, Robotics Today, Vol. 6, No. 1, 1993,

Jacket P., Danescu G., Carvalho J., Dahan M.: A spatial fully-parallel manipulator, Proc. Int. Symposium Ro.Man.Sy'92, Udine, Italy,

Matone R., Roth B.: Designing manipulators for both kinematic and dynamic isotropic properties, Proc. RoManSy'96,

Mianowski K.: Parallel mechanical system for 3-d measure of smooth surfaces, Proc. of XVI IMEKO World Congr. Vienna 2000

Mianowski K.: A 3-D Lever Parallel Mechanism of a Robot with 6 Degrees of Freedom, proc. of 6th Int. Symp. Measurement and Control in Robotics, Brussels 1996, pp. 104-109,

Mianowski K.: Parallel and Serial-Parallel Robots for the Use of Technological Applications, proc. Int. Workshop on Parallel Kinematic Machines, Milano 1999, pp. 39-46,

Mianowski K.: 3-D Lever Mechanism of a robot of 6 Degrees of freedom, app. to the proc. of Fifth World Conf. on Robotics Research, Cambridge, Mass. 1994,

Pierrot F., Daunchez P., Fournier A.: HEXA: a Fast six-DOF fully-Parallel Robot, IEEE Proc. 1991, Vol. 1, pp. 1158-1163,

Sorli M., Ceccarelli M.: On the workspace of a 6 D.O.F. platform with three articulated double-parallelograms, Proc. Int. Conf. ICAR'93,

Yoshikawa T.: Dynamic Manipulability of Robot Manipulators, Journal of Robotics Systems, 2(1), J. Wiley & Sons, Inc. 1985, pp. 113-124.

Proceedings of the WORKSHOP on
Fundamental Issues and Future Research Directions for Parallel Mechanisms and Manipulators
October 3–4, 2002, Quebec City, Quebec, Canada
Clément M. Gosselin and Imme Ebert-Uphoff, editors

Design of parallel manipulators for optimal conditioning throughout a prescribed workspace

ALEXANDER M. HAY
Department of Mechanical Engineering
University of Pretoria
Pretoria, 0002, South Africa

JAN A. SNYMAN
Department of Mechanical Engineering
University of Pretoria
Pretoria, 0002, South Africa
jan.snyman@eng.up.ac.za

Abstract: *The main objective of this paper is to find a fundamentally sound and robust numerical methodology for synthesizing parallel manipulators for desired workspaces. The method includes a constrained optimization formulation aimed at determining a manipulator design so that a prescribed workspace is both fully enclosed and well-conditioned with respect to some performance index. Dextrous requirements within the prescribed workspace may also have to be satisfied. The particular manipulator used to illustrate and evaluate the proposed method is a simple planar 3-dof parallel manipulator. Solutions to the manipulator design problems are found in an efficient and convincing manner.*

1 Introduction

It is well known that parallel manipulators possess a number of advantages over traditional serial manipulators (Merlet, 2000). One disadvantage of parallel manipulators is that the particular architecture of the manipulator results in smaller workspaces than their serial counterparts. Parallel manipulators can also be difficult to design, since the relationships between design parameters and the workspace, and behavior of the manipulator throughout the workspace, are not intuitive by any means. Indeed, Merlet (2000) argues that since the performance of parallel manipulators is so dependent on their dimensions, customization of these manipulators for each application is absolutely necessary. An effective way of performing this customization and of addressing the problems stated above is through the use of optimization techniques in the design process.

The constrained optimization formulation presented here is aimed at determining a manipulator design so that a prescribed workspace is fully enclosed and well-conditioned with respect to some performance index. Depending on the particular application, certain manipulator performance criteria may be of more importance than others. The performance measure used here is the condition number of the manipulator Jacobian, although a number of other performance measures could also have been used. The optimization method used in performing the optimization is the Dynamic-Q method (Snyman and Hay, 2000a).

In the next section the proposed optimization formulation is described. This formulation is then applied to a planar 3-dof planar parallel manipulator.

2 Optimization formulation

2.1 Definition of the workspace

As used by Haug *et al.* (1994), *generalized* coordinates $\mathbf{q} = [q_1, q_2, \ldots, q_{nq}]^T \in R^{nq}$ describe the motion of the manipulator. These generalized coordinates can be divided into *input* coordinates $\mathbf{v} = [v_1, v_2, \ldots, v_{nv}]^T \in R^{nv}$, used to control the manipulator, *output* coordinates $\mathbf{u} = [u_1, u_2, \ldots, u_{nu}]^T \in R^{nu}$, describing the functionality of the mechanism, and the remaining *intermediate* coordinates $\mathbf{w} = [w_1, w_2, \ldots, w_{nw}]^T \in R^{nw}$, where $nw = nq - nu - nv$. In the vicinity of an assembled configuration the input and output coordinates satisfy m independent kinematic constraint equations of the form

$$\mathbf{\Phi}(\mathbf{q}) = \mathbf{\Phi}(\mathbf{u}, \mathbf{v}, \mathbf{w}) = \mathbf{0} \tag{1}$$

where $\mathbf{\Phi} : R^{nq} \rightarrow R^m$ is a smooth function.

Limits imposed by the construction of the manipulator are described by means of inequality constraints placed on the input, or sometimes the intermediate coordinates. These respectively take the forms

$$\mathbf{v}^{\min} \leq \mathbf{v} \leq \mathbf{v}^{\max} \tag{2}$$

$$\mathbf{w}^{\min} \leq \mathbf{w} \leq \mathbf{w}^{\max} \tag{3}$$

These constraints, together with the geometry of the manipulator, determine the size and shape of the workspace A_c of the manipulator. The workspace is the set of points that can be

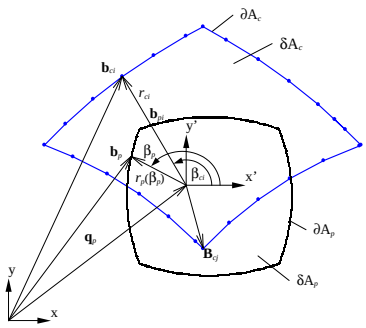

Figure 1: Prescribed and calculated workspaces

reached by the *working point* of the manipulator. The boundary ∂A_c of the workspace is defined as: (Snyman *et al.*, 2000)

$$\begin{aligned}\partial A_c = \{&\mathbf{u} \in R^{nu} : \mathbf{u} \in A_c \text{ and } \exists \text{ an } \mathbf{s} \in R^{nu} \text{ such that for}\\ &\mathbf{u}' = \mathbf{u} + \lambda \mathbf{s},\ \lambda \in R \text{ arbitrarily small and either}\\ &\text{positive or negative, no } \mathbf{v} \text{ and } \mathbf{w} \text{ exist}\\ &\text{that satisfies } \mathbf{\Phi}(\mathbf{u}', \mathbf{v}, \mathbf{w}) = \mathbf{0};\ \text{as well as}\\ &\text{inequalities (2) and (3)}\}\end{aligned} \tag{4}$$

There exist a number of different methods for determining workspaces of manipulators. In this study, an optimization method that is based on the above definition of the workspace is used. The particular optimization method used is the chord method (Snyman and Hay, 2000b). The optimization method uses the LfopC algorithm (Snyman, 2000) to determine discrete points $\mathbf{b}_{ci}, i = 1, 2, \ldots, n_{bc}$ along the boundary ∂A_c of the workspace A_c, as shown in Fig. 1.

2.2 Constrained optimization formulation

The problem studied here is to determine a manipulator design vector $\mathbf{d}$ which has a corresponding workspace A_c that fully includes a prescribed workspace A_p, and such that the included A_p is well-conditioned. As indicated in Fig. 1, the prescribed workspace is defined by polar coordinates (r_p, β_p) centered on a local coordinate system $x' - y'$ at $\mathbf{q}_p$. The boundary of the workspace A_c associated with design $\mathbf{d}$ may be defined in a similar manner (Fig. 1). Here the boundary point $\mathbf{b}_{ci}$, generated by the chord method (Snyman and Hay, 2000b), corresponds to angle β_{ci} and ray length r_{ci}.

The part of workspace A_p not intersecting A_c is denoted δA_p, and the part of workspace A_c not intersecting A_p is denoted δA_c. The calculation of approximations to the areas δA_p and δA_c is performed using a simple numerical scheme.

It is evident that for any prescribed workspace there is a very large number of manipulator designs which will result in a workspace that fully includes the prescribed one. Murray *et al.* (1997) and Merlet (2000) have proposed different methods for determining the set of manipulator configurations, the workspaces of which include prescribed points, or line segments. The most suitable manipulator with respect to some performance criterion or criteria can then be selected from this set. The method proposed here differs from these methods in that the optimum solution is obtained directly in one step. Thus the constrained optimization formulation, proposed here, is aimed at optimizing manipulators with respect to some performance index, subject to the constraint that the workspace of the optimal manipulator should include the prescribed workspace.

The specific performance measure chosen here is the inverse of the condition number of the Jacobian matrix of the manipulator. The accuracy of control of the manipulator is dependent on the condition number, denoted here by κ (Gosselin and Angeles, 1991). Since κ tends to infinity as the manipulator approaches a singular position, maximizing the inverse condition number, κ^{-1}, ensures that the manipulator remains far away from singular positions. For a parallel manipulator the inverse kinematics are easy to solve. From (1), an inverse transformation relating the input, output and intermediate velocities can be determined:

$$\mathbf{J}_\theta \dot{\theta} = -\mathbf{J}_\mathbf{v} \dot{\mathbf{v}} \tag{5}$$

where $\theta = [\mathbf{u}^T, \mathbf{w}^T]^T$ and $\mathbf{J}_\theta$ and $\mathbf{J}_\mathbf{v}$ are the respective constraint Jacobian matrices, containing the partial derivatives of the m kinematic constraints (1) with respect to the variables θ and $\mathbf{v}$. This can be rewritten as

$$\mathbf{J}\dot{\theta} = \dot{\mathbf{v}} \tag{6}$$

where $\mathbf{J} = -\mathbf{J}_\mathbf{v}^{-1}\mathbf{J}_\theta$. For the parallel manipulator studied here $m = n = nv = nu + nw$. The condition number κ of the $n \times n$ Jacobian $\mathbf{J}$ is defined as

$$\kappa = \|\mathbf{J}\|\|\mathbf{J}^{-1}\| \tag{7}$$

where $\|\cdot\|$ denotes any norm of its matrix argument. The norm adopted here is the same as that used by Gosselin and Angeles (1991), namely

$$\|\mathbf{J}\| = \sqrt{\text{trace}(\mathbf{J}\mathbf{W}\mathbf{J}^T)} \tag{8}$$

where $\mathbf{W}$ is defined as n^{-1} multiplied by the $n \times n$ identity matrix. The lower the condition number, the better the behavior of the manipulator, with the lowest possible value of κ being unity. The *inverse* of the condition number thus lies between 0 and 1, and is used in the objective function as it is bounded and better conditioned than the condition number itself.

The optimization problem is thus:

$$\begin{aligned}&\max_{\mathbf{d}} \left\{ \min_{\mathbf{u} \in A_p} \kappa^{-1}(\mathbf{d}, \mathbf{u}) \right\}\\ &\text{subject to the inequality constraint}\\ &c(\mathbf{d}) \leq 0\end{aligned} \tag{9}$$

where the vector of intermediate coordinates $\mathbf{w}$ is prescribed and fixed, and where the inequality constraint function $c(\mathbf{d})$ is defined as follows. The displacement vector between the prescribed workspace boundary and calculated workspace boundary, measured along a ray emanating from $\mathbf{q}_p$ at angles β_{ci} is

denoted by $r_i\mathbf{e}_i$, where $\mathbf{e}_i$ is a unit outward vector at angle β_{ci}. If $r_j = \min_i \{r_i, i = 1, 2, \ldots, n_{bc}\}$ then set $r = r_j$. The constraint function is now defined as follows:

$$c(\mathbf{d}) = \begin{cases} \delta A_p & \text{if } \delta A_p > 0 \\ -r^2 & \text{if } \delta A_p = 0 \end{cases} \tag{10}$$

This is done to improve the topography of the inequality constraint which in turn improves the behavior of the optimization algorithm.

The solution to optimization problem (9) seeks to improve the *single worst point* with respect to chosen performance measure, κ^{-1}, within the *prescribed* workspace, A_p. This philosophy differs from that proposed by Gosselin and Angeles (1991) and used by numerous other researchers where the *average* performance index over the *entire* workspace is optimized. Since in this case it is assumed that the manipulator's movements will be limited to the prescribed workspace it is only necessary to ensure good performance qualities within this workspace and thus it is better here to optimize the single worst value instead of the average.

One point which arises concerns the nested part of optimization problem (9) and the question of how to determine the smallest value of κ^{-1} over the set $\mathbf{u} \in A_p$. Since we only require the single lowest value of the inverse condition number, an efficient method for determining this value, based on the convexity of the condition number is proposed and used here. It can easily be shown, for a planar 2-dof manipulator studied previously (Hay and Snyman, 2001), that κ is convex over the plane R^2, and thus that the maximum value of κ (or minimum of κ^{-1}) will lie on the boundary ∂A_p of the prescribed workspace. Here an assumption is made that a similar result can be found for the particular 3-dof manipulator to be investigated here. The minimum value of the inverse condition number κ^{-1} can thus be approximated by calculating κ^{-1} at points $\mathbf{b}_{pi},\ i = 1, \ldots, n_{bc}$ simultaneously to the determination of the boundary points $\mathbf{b}_{ci},\ i = 1, \ldots, n_{bc}$. The overall minimum of the κ^{-1} values at these candidate points may then easily be determined. Based on the results presented later in this paper it appears that the above assumption is valid.

3 Three-dof planar parallel manipulator

The three-dof planar parallel manipulator taken from Haug *et al.* (1994) is shown in Fig. 2. The mechanism consists of a platform of length $2r$ connected to a base by three linear actuators of variable leg lengths l_1, l_2 and l_3. The actuators are joined to the base and platform by means of revolute joints $A - E$. It will be assumed that $y_C = y_D = y_E$. The coordinates of point P, the working point of the platform, are (x_P, y_P) and the orientation of the platform is ϕ_P. With reference to the definitions given in sections 2.1 and 2.2, the actuator leg lengths are the input variables, i.e. $\mathbf{v} = [l_1, l_2, l_3]^T$. The global coordinates of the working point P form the output coordinates, i.e. $\mathbf{u} = [x_P, y_P]^T$. The rotation angle of the platform is the only intermediate coordinate, i.e. $\mathbf{w} = w = [\phi_P]$. The generalized

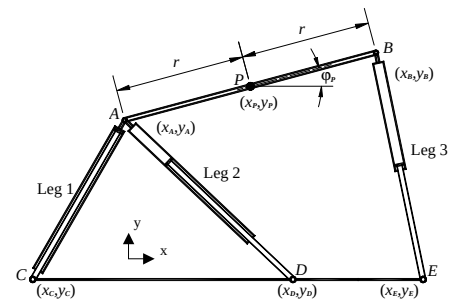

Figure 2: The 3-dof planar parallel manipulator

coordinates for the three-dof parallel manipulator are given by $\mathbf{q} = [\mathbf{u}^T, \mathbf{v}^T, \mathbf{w}^T]^T = [x_P, y_P, l_1, l_2, l_3, \phi_P]^T$. It is assumed the the actuators have been chosen and thus that the maximum and minimum leg lengths are predetermined. The remaining five design variables for the problem are thus

$$\mathbf{d} = [x_C, y_C, x_D, x_E, r]^T \tag{11}$$

Certain points arise now due to the platform's orientational ability. First amongst these is the fact that the Jacobian of the manipulator contains entries related to both translational and rotational abilities of the platform. The condition number will thus inherently contain a mix of these terms. It is thus important to normalize the translational terms of the Jacobian matrix so that translational and rotational abilities are equally represented by the condition number. Pittens and Podhorodeski (1993) and Stoughton and Arai (1993) note this occurrence and suggest that the best approach is to normalize the translational terms of the Jacobian with respect to the platform radius r, a suggestion which is adopted here.

The second point arising is that some strategy needs to be implemented for dealing with the fact that the condition number number needs to be minimized throughout the manipulator's three-dimensional (x, y, ϕ) workspace. Indeed, the prescribed workspace is also 3-dimensional. This point is addressed by evaluating the problem at various angular "slices" through the workspace. This is the approach used by Boudreau and Gosselin (2001) in an unconstrained case. Accordingly, in the example considered here, the minimization over $\mathbf{u} = [x, y]^T$ in (9) is carried out, not only for a single prescribed value of ϕ_P, but over three slices of the prescribed workspace corresponding to three fixed values of ϕ_P, namely $\phi_P = -5°, 0°, +5°$. In doing so the optimized design is expected to fulfill the dexterity requirement of operating over the range of $\phi_P = [-5°, 5°]$ within the prescribed workspace.

Optimization problem (9), now modified to allow for the optimization over the three values of $w = \phi_P$, was solved using the Dynamic-Q algorithm (Snyman and Hay, 2000a). In this method, the LfopC algorithm is used to solve successive spherical approximations of the optimization problem. During extensive testing of the method on a set of representative test problems, the solutions of the successive approximate subproblems

$P[i], i = 1, 2, \ldots$ invariably converged towards local minima (Snyman and Hay, 2000a).

The method described above has been applied to the 3-dof planar parallel manipulator for the prescribed workspace shown in Fig. 3. For the initial design vector $\mathbf{d}_0 = [-0.75, 0, 0.75, 1.5, 0.75]^T$, the manipulator workspaces for various constant orientations, as well as the corresponding inverse condition number contours for the respective orientations are shown in Fig. 3. Actuator limits were chosen as $l_i^{\min} = \sqrt{2}$, $l_i^{\max} = 2, i = 1, 2$ and $l_3^{\min} = 1$, $l_3^{\max} = \sqrt{2}$. The Dynamic-Q move limit used was $\triangle = 0.1$ and the chord length for calculating the workspace was 0.02.

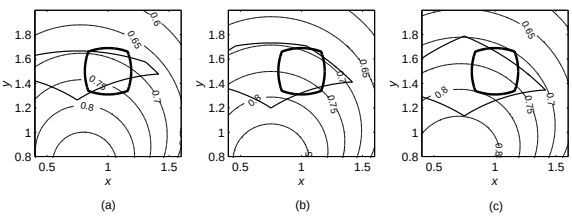

Figure 3: Prescribed workspace, starting manipulator workspace and κ^{-1} contours for (a) $\phi_P = -5°$ (b) $\phi_P = 0°$ and (c) $\phi_P = +5°$

For this optimization run, the number of gradient evaluations required for convergence was $n_{ge} = 33$, the function value increased from $f(\mathbf{d}_0) = 0.676$ to a converged objective function value of $f^* = 0.901$, the converged inequality constraint function value was $c^* = 0.204 \times 10^{-5}$ and the design vector at the solution was $\mathbf{d}^* = [-1.034, 0.2484, 1.331, 1.657, 0.8553]^T$. The workspaces and inverse condition number contours for the respective orientations and corresponding to this solution are shown in Fig. 4.

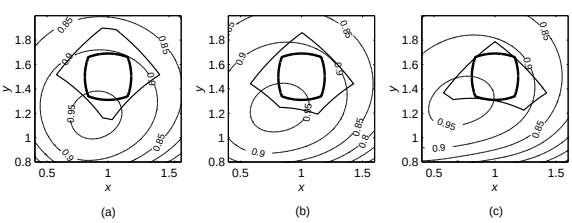

Figure 4: Prescribed workspace, manipulator workspaces and corresponding κ^{-1} contours for the optimal design at respectively (a) $\phi_P = -5°$ (b) $\phi_P = 0°$ and (c) $\phi_P = +5°$

4 Conclusion

For the 3-dof manipulator studied here the results obtained are extremely encouraging and accurate, with optimum solutions having been obtained with minimal computational effort. Although not reported here, the methodology has also been applied to simpler 2-dof planar manipulators with very good results. In each case the algorithm not only determines manipulator dimensions so that the prescribed workspace can be reached by the manipulator, but also places the calculated workspace so that the inverse condition number is as high as possible throughout the prescribed workspace. The proposed methodology produces convincing results, indicating it to be a stable and efficient method for designing planar parallel manipulators. The Dynamic-Q optimization algorithm used in the synthesis methodology exhibits high efficiency in solving the associated optimization problem. Although the application of this numerical methodology for synthesizing parallel manipulators, which is believed to be fundamentally sound and robust, has been restricted to the simple 2-dof and 3-dof manipulator cases, it nevertheless led to a scheme that appears to be general. It is hoped that the principles developed here can be extended to similar, but more complicated spatial manipulator problems.

References

Boudreau, R., and Gosselin, C.M., 2001, "La synthèse d'une plate-forme de Gough-Stewart pour un espace atteignable prescrit", *Mechanism and Machine Theory*, vol. 36, pp. 327-342.

Gosselin, C.M., and Angeles, J., 1991, "A global performance index for the kinematic optimization of robotic manipulators", *ASME Journal of Mechanical Design*, vol. 111, pp. 202-207.

Haug, E.J., Luh, C.M., Adkins, C.M., and Wang, J.Y., 1994, "Numerical algorithms for mapping boundaries of manipulator workspaces", *Concurrent Engineering Tools for Dynamic Analysis and Optimization: IUTAM Fifth Summer School on Mechanics*, Aalborg, Denmark.

Hay, A.M., and Snyman, J.A., 2001, "Methodologies for the optimal design of parallel manipulators", Submitted to *International Journal for Numerical Methods in Engineering*.

Merlet, J-P., 2000, "Parallel Robots", Kluwer Academic Publishers, Dordrecht, The Netherlands.

Murray, A.P., Pierrot, F., Dauchez, P., and McCarthy, J.M., 1997, "A planar quaternion approch to the kinematic synthesis of a parallel manipulator", *Robotica*, vol. 15, pp. 361-365.

Pittens, K.H., and Podhorodeski, R.P., 1993, "A family of Stewart platforms with optimal dexterity", *Journal of Robotic Systems*, no. 4, vol. 10, pp. 463–479.

Snyman, J.A., 2000, "The LFOPC leap-frog algorithm for constrained optimization", *Computers and Mathematics with Applications*, vol. 40, pp. 1085-1096.

Snyman, J.A., Du Plessis, L.J., and Duffy, J., 2000, "An optimization approach to the determination of the boundaries of manipulator workspaces", *ASME Journal of Mechanical Design*, vol. 122, pp. 447-455.

Snyman, J.A., and Hay, A.M., 2000a, "The Dynamic-Q method: An alternative to SQP?", *Proceedings of the International Workshop on Multidisciplinary Design Optimization*, Pretoria, South Africa, pp. 163-172.

Snyman, J.A., and Hay, A.M., 2000b, "The chord method for the determination of non-convex workspaces of planar parallel platforms", *Advances in Robot Kinematics*, Dordrecht, The Netherlands, Kluwer Academic Publishers.

Stoughton, R.S., and Arai, T., 1993, "A modified Stewart platform manipulator with improved dexterity", *IEEE Transactions on Robotics and Automation*, no. 2, vol. 9, pp. 166-173.

On the Type Synthesis of Lower-Mobility Parallel Manipulators

Z Huang. Q. C. Li

Robotics Research Center, Yanshan University

Qinhuangdao 066004, China

Email huangz@ysu.edu.cn

Tel. (86)335-8074709

Abstract: This paper introduces our study on type synthesis of the lower-mobility symmetrical parallel mechanisms. Some synthesized 3-, 4- and 5-DOF parallel symmetrical mechanisms are introduced including limb-symmetrical and mechanism-symmetrical and input-symmetrical parallel manipulators.

Keyword: parallel mechanism design theory mechanism synthesis

1. Introduction

In recent years, the use of lower-mobility parallel manipulators for many tasks requiring its mobility fewer than six have drawn a lot of interest. Because lower-mobility parallel manipulators comprise fewer links and actuators, developers stand a good chance of reducing the costs of design and manufacturing.

The majority of literatures on the symmetrical lower-mobility parallel manipulators dealt with the three-dimension translational parallel mechanisms[1-5] and the three-dimension rotational spherical parallel mechanisms[6-9]. A fast 3-DOF camera-orienting device was built based on the 3-DOF spherical parallel mechanism [10]. In addition, some 3-DOF cubic parallel mechanisms were introduced [11].

The number of lower-mobility parallel manipulators with 4 or 5 DOF is fairly small[12-14]. An interesting 4-DOF parallel manipulator proposed by Zlatanov and Gosselin(2001) has three rotational freedoms and one translational freedom.

Generally, the desired lower-mobility parallel mechanism should have prescribed mobility and property, should be symmetrical with identical limbs to meet the requirements of kinematic isotropy.

Research on parallel manipulators began about twenty years ago. The types of lower-mobility symmetrical parallel manipulators with 4- and 5-DOF are still deficient. Type synthesis of such a symmetrical parallel mechanism is rather difficult because of three existing problems. One is how to correctly calculate the mobility of lower-mobility parallel mechanisms by the common mobility formulas. The second is how to judge kinematic properties of the mobility, i.e., to determine whether they are rotational freedoms or translational freedoms. The third is how to keep the required mobility and properties after combining limbs and forming mechanism.

Lie group theory has been used to synthesize new parallel mechanisms[15]. We propose *the constraint-synthesis methodology*[16], which is described in detail in another paper accepted by the *International Jounral of Robotic Research.* The fundamental idea is that the required mobility of the moving platform will be the map of intersection of all limb constraint systems of the mechanism.

The constraint-synthesis method tries to simultaneously treat the type synthesis considering mobility, property and different kinematic pair combinations of limb. Using the method, we can get different limb architectures by different permutations of kinematic pairs, which means that there will be much more different mechanisms with the same mobility and the same property for further selection.

Using reciprocal screw system, we define the mechanism constraint system and the limb constraint system. We then investigate the relations between the mechanism constraint system and the limb constraint system under

different geometrical conditions. Based on the relations, we propose a constraint-synthesis method for type synthesis of symmetrical lower-mobility parallel manipulators. The *constraint synthesis* method is simple and effective. Here we will introduce some mechanisms we synthesized with 3-, 4- and 5-DOF[17]. The detailed analysis has been included in some papers for publication. Some of them have been filed for Chinese patents.

Generally, a lower-mobility parallel mechanism may have the following features:

1) Stably realize prescribed mobility number and properties, which means it can move with expectant rotation or translation freedoms.
2) Have identical limbs, which means the same number, kind and permutation of kinematic pairs in each limb.
3) Keep all limbs with symmetrical distribution on the base.
4) Have all actuators mounted in the same position of limbs on or nearby the fixed base, and each limb has one actuator.

Satisfying all the four conditions, it is a fully-symmetrical parallel mechanism[18]. Satisfying the first three conditions, it may be named as a mechanism-symmetrical parallel mechanism. Satisfying the first two conditions, it is a limb-symmetrical parallel mechanism. Satisfying the first two and the fourth conditions, it may be named as an input-symmetrical parallel mechanism. Satisfying only the first conditions, it is an asymmetrical parallel mechanism.

Type synthesis of such a symmetrical mechanism with expectant mobility and properties is difficult because of four existing problems. The first is how to correctly calculate the mobility of lower-mobility parallel mechanisms by the common mobility criterion. The second is how to judge kinematic properties of the mobility of a mechanism, i.e., to determine whether they are rotational freedoms or translational freedoms. The third is how to obtain the expectant mobility and properties of the synthesized mechanism. The most difficult problem, however, is how to obtain the fully-symmetrical parallel mechanism, especially, for the 5-DOF mechanism with three translational and two rotational freedoms.

Here we briefly introduce some mechanisms with 3-, 4- and 5-DOF we synthesized by this method. Some of them have been filed for Chinese patents. All of these synthesized mechanisms are checked and are not instantaneous.

Without loss of generality, we set the XY plane of the global frame, $O-XYZ$, coincident with the fixed platform plane, thus the Z axis of the global frame is perpendicular to the fixed platform plane and is upward. We set the z axis of limb frame, $o-xyz$, upward and parallel to the Z axis of the global frame of the mechanism, and the xy plane of the limb frame is coincident with the XY plane of the global frame. The x axes of the limb frames are not parallel to each other. Because the linear dependence of any screw system is independent with the selection of the reference system[19], so that we may choose the most convenient frame.

2.1 3-DOF Parallel Mechanisms

Fig.1 shows a 3-$\underline{\mathrm{RR(R}}\overline{\mathrm{R)R}}$ 3-DOF translational mechanism, where the line over or under R means that these revolute axes are parallel; (RR) denotes that the two revolute axes intersect each other. In each limb,

counting from the base, the first three revolute axes are parallel to the base plane, and the last two revolute axes are parallel to each other and not parallel to the platform plane. The fourth revolute axis intersects at a point on the third revolute axis. The limb twist system is

$$
\begin{aligned}
\$_1 &= (1\,0\,0\,;\,0\,0\,0) \\
\$_2 &= (1\,0\,0\,;\,0\,b_2\;c_2) \\
\$_3 &= (1\,0\,0\,;\,0\,b_3\;c_3) \\
\$_4 &= (l_5\;m_5\;n_5\,;\,a_6\;b_6\;c_6) \\
\$_5 &= (l_5\;m_5\;n_5\,;\,a_7\;b_7\;c_7)
\end{aligned}
\tag{1}
$$

The limb constraint system is

$$
\$_1^r = (0\,0\,0\,;\,0 - n_5\;m_5), \tag{2}
$$

which shows that the above $\underline{\mathrm{RR(R}}\overline{\mathrm{R)R}}$ limb exerts a constraint couple on the moving platform. The constraint couple is perpendicular to the plane determined by the third revolute axis and the fourth revolute axis. The mechanism constraint system contains three constraint couples and they are noncoplanar. Thus the three couples are linearly independent and constrain three rotations of the moving platform. Hence the mechanism has only three translational freedoms and it is a fully-symmetrical parallel mechanism. The mobility is not instantaneous as well.

Fig. 2 shows a 3-RPR$\underline{\mathrm{RR}}$ 3-DOF translational mechanism. In the above 3-$\underline{\mathrm{RR(R}}\overline{\mathrm{R)R}}$ 3-DOF translational mechanisms, we replace the second revolute pair by a prismatic pair in each limb. The prismatic pair is perpendicular to the first and the third revolute axis.

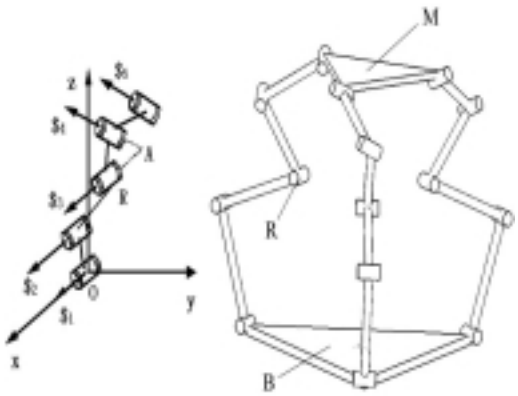

Fig. 1 3-DOF 3-$\underline{\mathrm{RR(R}}\overline{\mathrm{R)R}}$ translational parallel mechanism

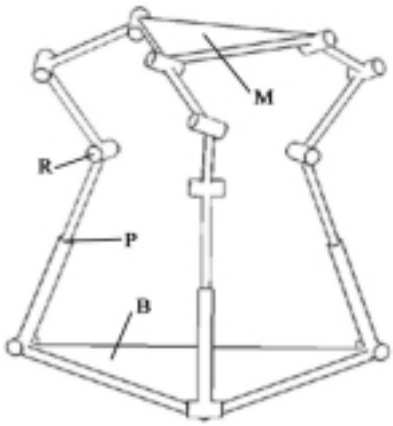

Fig. 2 3-DOF 3-RPR$\underline{\mathrm{RR}}$ translational parallel mechanism

Fig. 3 shows a 3-RPC 3-DOF translational mechanism. In each limb, counting from the base, the first revolute axis and the last cylindrical axis are parallel to the base plane. The second prismatic pair axis is perpendicular to the other two pairs. The limb twist system is

$$
\begin{aligned}
\$_1 &= (1\,0\,0\,;0\,0\,0) \\
\$_2 &= (0\ \ 0\ \ 0\,;0\ \ m_2\ \ n_2) \\
\$_3 &= (1\,0\,0\,;0\ \ b_3\ \ c_3) \\
\$_4 &= (0\,0\,0\,;1\ \ 0\ \ 0)
\end{aligned}
\quad . \tag{3}
$$

By calculating the screws reciprocal to equation (3), we can get the limb constraint system

$$
\begin{aligned}
\$_1^r &= (0\,0\,0\,;0\,1\,0) \\
\$_2^r &= (0\,0\,0\,;0\,0\,1)
\end{aligned}
\tag{4}
$$

Equation (4) shows that a single RPC limb exerts two constraint couples on the moving platform. The three RPC limbs exert 6 constraint couples on the moving platform, and they are linearly dependent and the maximum linear independent number of these 6 couples is 3. Thus the combined effect of the 6 constraint couples equals three linearly independent constraint couples, which restrict three rotations of the moving platform. It is a fully-symmetrical parallel mechanism.

Fig. 4 shows a 3-PRC 3-DOF translational mechanism. In each limb, the first prismatic pair axis is perpendicular to the base plane. The second revolute axis and the last cylindrical axis are perpendicular to the prismatic pair axis and parallel to the platform. It is also a fully-symmetrical parallel mechanism.

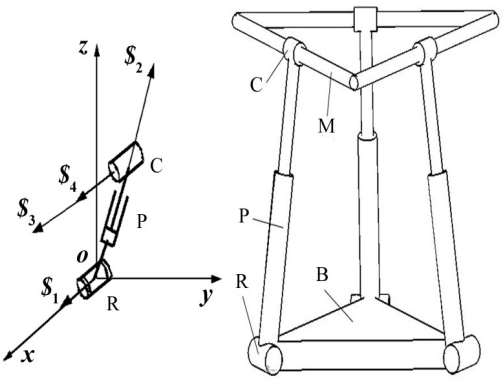

Fig. 3 3-DOF 3-RPC translational mechanism

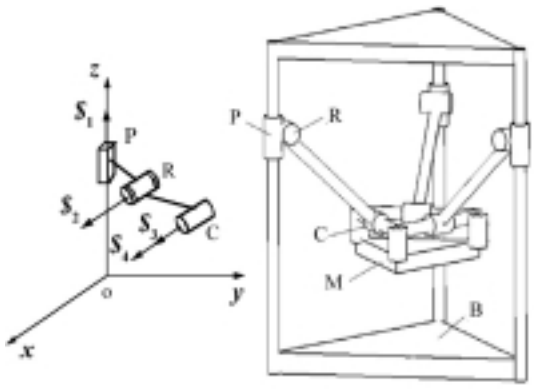

Fig. 4 3-DOF 3-PRC translational mechanism

2.2 4-DOF Parallel Mechanisms*

Fig. 5 shows a 4-UPU 4-DOF parallel mechanism, which has three translational freedoms and one rotational freedom. In each limb, counting from the base, the first revolute axis is perpendicular to the base plane. The last universal pair is perpendicular to the moving platform. The axes of two intermediate revolute axes are parallel to one another.

* This mechanism had been introduced in Laval University on Oct. 2000 and a similar mechanism has a Chinese patent.

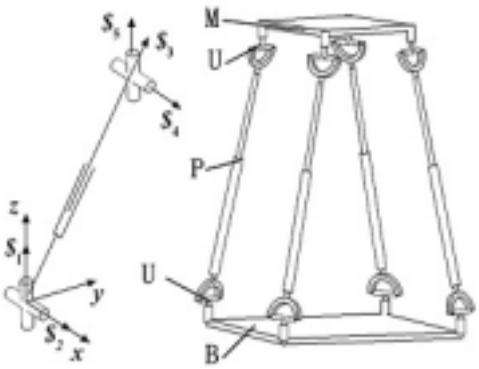

Fig. 5 4-DOF 4-UPU parallel mechanism

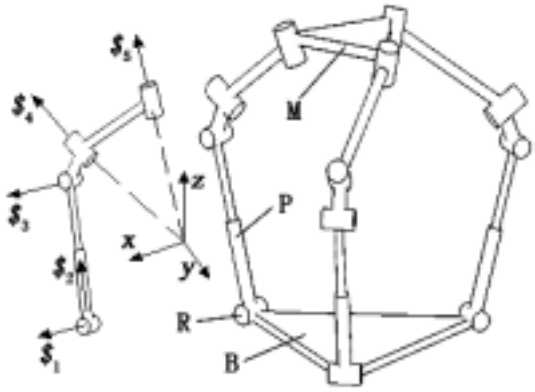

Fig. 6 4-DOF 3-RPR(RR) parallel mechanism

The limb twist system is

$$
\begin{aligned}
\$_1 &= (0\,0\,1\,;\,0\,0\,0) \\
\$_2 &= (1\,0\,0\,;\,0\,0\,0) \\
\$_3 &= (0\,0\,0\,;\,l_3\ m_3\ n_3) \\
\$_4 &= (1\,0\,0\,;\,0\ b_5\ c_5) \\
\$_5 &= (0\,0\,1\,;\,a_5\ b_5\ 0)
\end{aligned}
\tag{5}
$$

By calculating the screws reciprocal to equation (5), we can get the limb constraint system

$$\$_1^r = (0\,0\,0\,;\,0\,1\,0) \tag{6}$$

Equation (6) shows that a single UPU limb exerts one constraint couple on the moving platform along the normal of the crosshead plane. The four UPU limbs exert four constraint couples on the moving platform, and they are coplanar and linearly dependent. The maximum linear independent number of these four couples is two. Thus the combined effect of the four constraint couples equals two linearly independent constraint couples, which restrict two rotations of the moving platform. The axes of two rotations are all in XY plane. Thus the 4-UPU parallel mechanism has three translational freedoms and one rotational freedom about the Z axis. The mechanism is fully-symmetrical.

Fig. 6 shows a 4-DOF 3-RPR(RR) parallel mechanism. In each limb, counting from the base, the first revolute pair axis is parallel to the third revolute pair axis. The second prismatic pair axis intersects and is perpendicular to the adjacent revolute pairs, i.e., the first and the third. The fourth and the fifth revolute pair axes converge toward a common point, denoted by (RR). The common point is called as the central point. Note that in all of the three limbs, the fourth and the fifth revolute pair axes converge toward the same central point. The first revolute pair axes in all of the three limbs are in the base plane and set symmetrically. The limb twist system is:

$$
\begin{aligned}
\$_1 &= (1\,0\,0\,;\,0\ b_1\ c_1) \\
\$_2 &= (0\,0\,0\,;\,0\ m_2\ n_2) \\
\$_3 &= (1\,0\,0\,;\,0\ b_3\ c_3) \\
\$_4 &= (l_4\ m_4\ n_4\,;\,0\,0\,0) \\
\$_5 &= (l_5\ m_5\ n_5\,;\,0\,0\,0)
\end{aligned}
\tag{7}
$$

By calculating the screws reciprocal to equation (7), we have：

$$\$_1^r = (1\,0\,0\,;\,0\,0\,0) \tag{8}$$

Equation (8) shows that a single RPR(RR) limb exerts a constraint force on the moving platform. The constraint force, $\$_1^r$, passes the central point and parallel to the first revolute pair axis. The three limbs exerts three constraint forces on the moving platform, and the three forces are coplanar, in a plane parallel to the base plane, and intersecting at the central point.

Under this geometrical condition, the three constraint forces are linearly dependant and equal two linearly independent constraint forces in the plane parallel to the base plane. Consequently, the moving platform loses two translational freedoms parallel to the base plane. The 3-RPR(RR) parallel mechanism has three rotational freedoms and one translational freedom along the normal of the base plane. This mechanism is mechanism-symmetrical. This mechanism can also consists of four such RPR(RR) limbs, as shown in Fig. 7, which is fully-symmetrical.

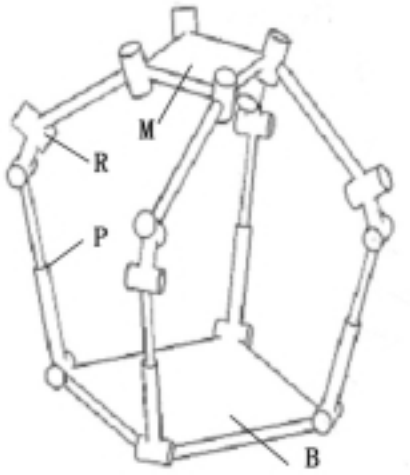

Fig. 7 4-DOF 4-RPR(RR) parallel mechanism

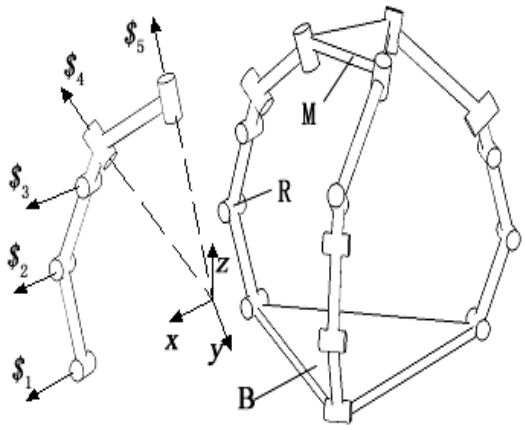

Fig. 8 4-DOF 3-RRR(RR) mechanism

Fig. 8 shows a 4-DOF 3-RRR(RR) parallel mechanism, which has the same mobility as the above 4-DOF 3-RPR(RR) parallel mechanism. It is mechanism-symmetrical. We replace the prismatic pair in the 3-RPR(RR) parallel mechanism by a revolute pair parallel to the adjacent revolute pairs. This mechanism can also consists of four such RRR(RR) limbs, as shown in Fig. 9, which is a fully-symmetrical.

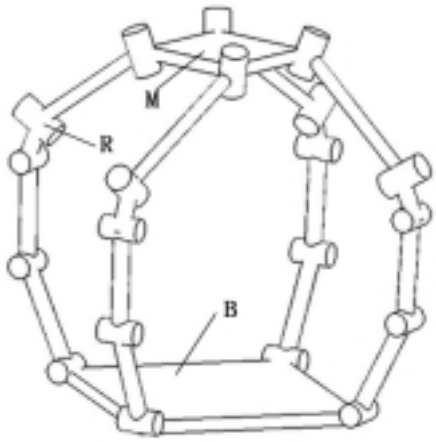

Fig. 9 4-DOF 4-RRR(RR) parallel mechanism

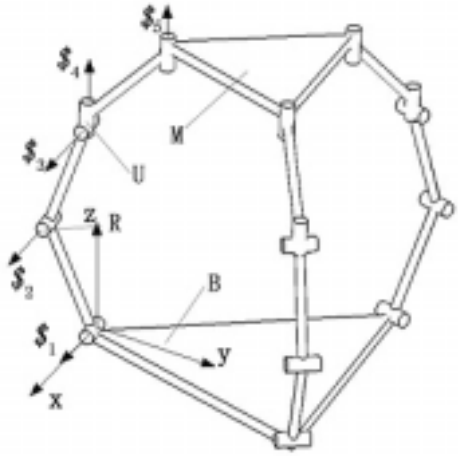

Fig. 10 4-DOF 3- RR(R$\overline{R}$)$\overline{R}$ parallel mechanism

Fig. 10 shows a 4-DOF 3-$\underline{\mathrm{RR(R}}\overline{\mathrm{R)R}}$ mechanism-symmetrical parallel mechanism. In each limb, the first three revolute axes are parallel to the base plane, and the last two revolute axes are also parallel to each other and normal of the platform plane. The third revolute axis and the fourth revolute axis intersect, and they form an crosshead plane, P_{34}. The kinematic chain is denoted as $\underline{\mathrm{RR(R}}\overline{\mathrm{R)R}}$. The crosshead in the parentheses can also be expressed as a universal pair. Each kinematic pair in a limb is expressed by a unit screw with respect to the limb twist system. In the initial configuration, as shown in Fig. 10, the limb twist system is

$$\begin{aligned}
\$_1 &= (1\,0\,0\,;0\,0\,0) \\
\$_2 &= (1\,0\,0\,;0\,b_2\;c_2) \\
\$_3 &= (1\,0\,0\,;0\,b_3\;c_3) \quad , \\
\$_4 &= (0\,0\,1\,;a_4\;b_4\;0) \\
\$_5 &= (0\,0\,1\,;a_5\;b_5\;0)
\end{aligned} \tag{9}$$

where $\$_1, \$_2, \$_3, \$_4, \$_5$ are linearly independent.

The limb exerts a constraint on the platform

$$\$_1^r = (0\,0\,0\,;0\,1\,0) \tag{10}$$

which is a constraint couple along the direction of y-axis reciprocal to all the five twists. Actually, it is normal to the plane P_{34}, i.e., normal to all the revolute axes. The three limbs exert three constraint couples on the moving platform, and the three couples are coplanar, in a plane parallel to the base plane.

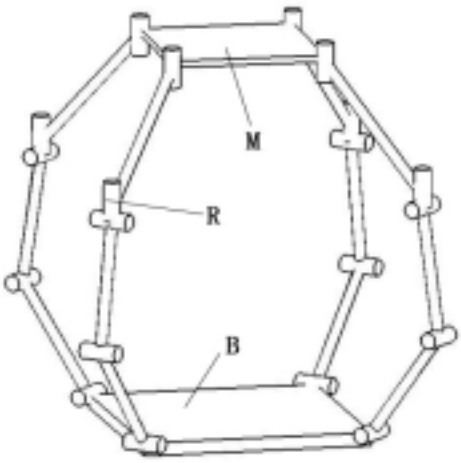

Fig. 11 4-DOF 4-$\underline{\mathrm{RR(R}}\overline{\mathrm{R)R}}$ parallel mechanism

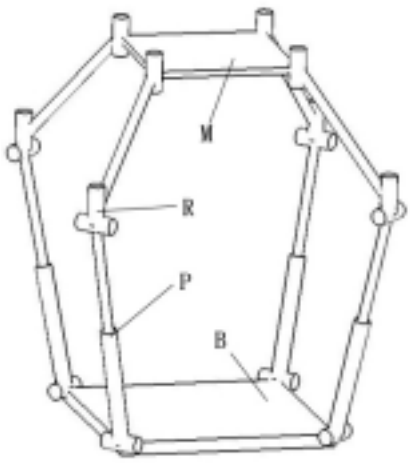

Fig. 12 4-DOF 4-$RP(\underline{R}\overline{\mathrm{R)R}}$ parallel mechanism

The three $\underline{\mathrm{RR(R}}\overline{\mathrm{R)R}}$ limbs exert three constraint couples on the moving platform, and they are coplanar and linearly dependent. The maximum linear independent number of these three couples is two. Thus the combined effect of the three constraint couples equals two linearly independent constraint couples, which restrict two rotations of the moving platform. The axes of two rotations are all in XY plane. Thus the 3－$\underline{\mathrm{RR(R}}\overline{\mathrm{R)R}}$ parallel mechanism has three translational freedoms and one rotational freedom about the Z axis. The

mechanism is mechanism-symmetrical. This mechanism can also consists of four $\underline{\mathrm{RR(R}}\overline{\mathrm{R)R}}$ limbs, as shown in Fig. 11, which is fully symmetrical.

Note that the second revolute pair in the 4-$\underline{\mathrm{RR(R}}\overline{\mathrm{R)R}}$ parallel mechanism can be replaced by a prismatic pair, as shown in Fig. 12, which is also fully-symmetrical.

2.3. 5-DOF Parallel Mechanisms

Fig. 13 shows a 5-DOF 3-RR(RRR) parallel mechanism. In each limb, counting from the base, the first two revolute axes are perpendicular to the base plane. The last three revolute axes converge toward a common point.

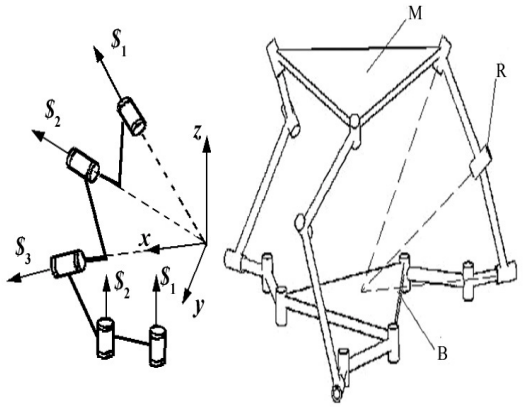

Fig. 13 5-DOF 3-RR(RRR) parallel mechanism

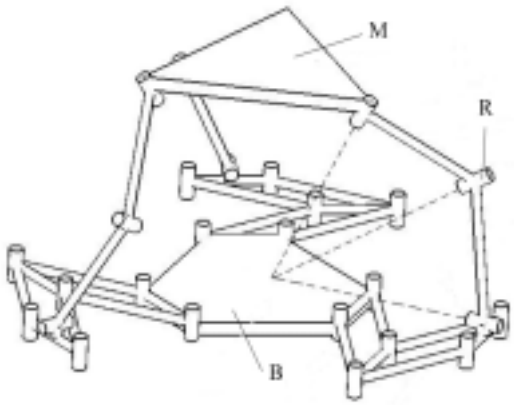

Fig. 14 5-DOF 3-$\overline{\overline{\mathrm{PP}}}$ (RRR) parallel mechanism

The limb twist system is

$$\begin{aligned}
\$_1 &= (0\,0\,1;\, a_1\ b_1\ 0)\\
\$_2 &= (0\,0\,1;\, a_2\ b_2\ 0)\\
\$_3 &= (1\ \ 0\ \ 0;\, 0\,0\,0)\\
\$_4 &= (l_4\ m_4\ n_4\,;\, 0\,0\,0)\\
\$_5 &= (l_5\ m_5\ n_5\,;\, 0\,0\,0)
\end{aligned} \quad . \tag{11}$$

By calculating the screws reciprocal to equation (11), we have

$$\$_1^r = (0\,0\,1;\, 0\,0\,0), \tag{12}$$

which shows that a single RR(RRR) limb exerts a constraint force on the moving platform. The constraint force passes the central point and lies along the Z axis. The three constraint forces of the mechanism constraint system are coaxial. They are linearly dependent and equal one constraint force restricting the translation of the moving platform along the Z axis. This mechanism has three rotational freedoms and two translational freedoms. This mechanism is only a mechanism-symmetrical.

Fig. 14 shows a 5-DOF 3-$\overline{\overline{PP}}$ (RRR) parallel mechanism, which has the same mobility as the above 5-DOF 3-RR(RRR) parallel mechanism. We replace the first two revolute pairs in each limb of the above 3-RR(RRR) parallel mechanism by two four-bar parallelograms, where the two four-bar parallelograms are denoted by $\overline{\overline{\mathrm{PP}}}$.

It is also a mechanism-symmetrical.

Fig. 15 shows a 5-DOF 3-RRR(RR) parallel mechanism. In each limb, counting from the base, the first three revolute axes are perpendicular to the base plane. The fourth and the fifth revolute pair axes converge toward a common point. The common point is called as the central point. In all of the three limbs, the fourth and the fifth revolute pair axes converge toward the same central point.

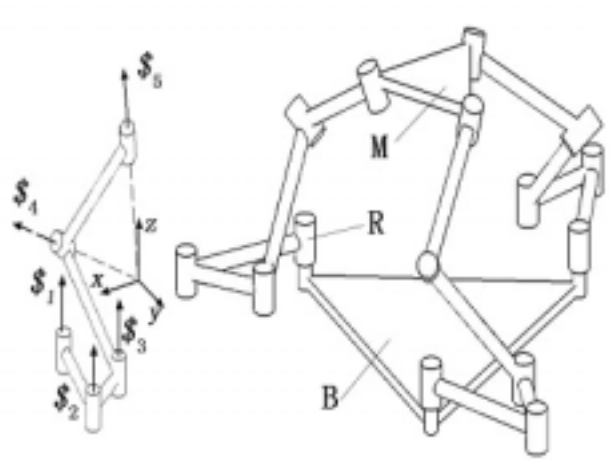

Fig. 15 5-DOF 3-RRR(RR) parallel mechanism

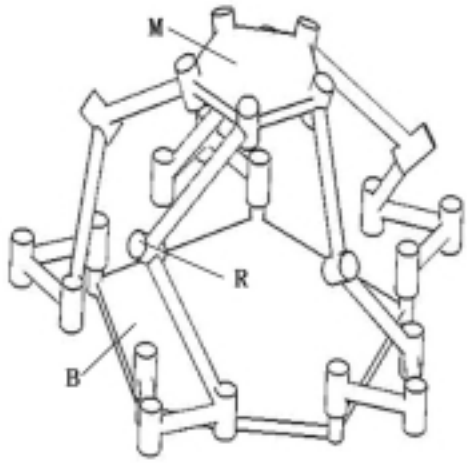

Fig. 16 5-DOF 5-RRR(RR) parallel mechanism

The limb twist system is

$$
\begin{aligned}
\$_1 &= (0\ 0\ 1;\ a_1\ b_1\ 0) \\
\$_2 &= (0\ 0\ 1;\ a_2\ b_2\ 0) \\
\$_3 &= (0\ 0\ 1;\ a_3\ b_3\ 0) \\
\$_4 &= (l_4\ m_4\ n_4\ ;\ 0\ 0\ 0) \\
\$_5 &= (l_5\ m_5\ n_5\ ;\ 0\ 0\ 0)
\end{aligned}
\tag{13}
$$

By calculating the screws reciprocal to equation (13), we have：

$$\$_{l1}^{r} = (0\,0\,1;0\,0\,0) \tag{14}$$

Equation (14) shows that a single RRR(RR) limb exerts the same constraint force on the moving platform as a single RR(RRR) limb. By similar analysis, it is easy to find this mechanism has the same mobility as the above 3-RR(RRR) parallel mechanism. It is mechanism-symmetrical. However, this mechanism can consist of five such RRR(RR) limbs and it is fully-symmetrical, as shown in Fig. 16. That is because the five line vectors are linearly independent, when locking all of the first revolute pairs of five limbs.

Fig. 17 shows a 5-DOF 3-RPR(RR) parallel mechanism, which has the same mobility as the above 5-DOF 3-RR(RRR) parallel mechanism. We replace the second revolute pair in each limb of the above 3-RRR(RR) parallel mechanism by a prismatic pair. The prismatic pair axis is parallel to the base plane. This mechanism can also consists of five such RPR(RR) limbs, as shown in Fig. 18, which is fully-symmetrical.

Fig. 19 shows a 5-DOF 3-$\underline{\mathrm{RR(R}}\overline{\mathrm{R)R}}$ limb-symmetrical parallel mechanism. In each limb, the first three revolute axes are parallel to the base plane, and the last two revolute axes are parallel to the moving platform plane. The third revolute axis and the fourth revolute axis intersect, and they form a crosshead plane, P_{34}. Note

that, the three first axes, $\$_1$, of three limbs are parallel to one another in the base. The three fifth axes, $\$_5$, of three limbs are also parallel to one another and mounded to the moving plate. The kinematic chain is denoted as $\underline{\mathrm{RR}}(\mathrm{R}\overline{\mathrm{R}})\mathrm{R}$. The crosshead in the parentheses can also be expressed as a universal pair.

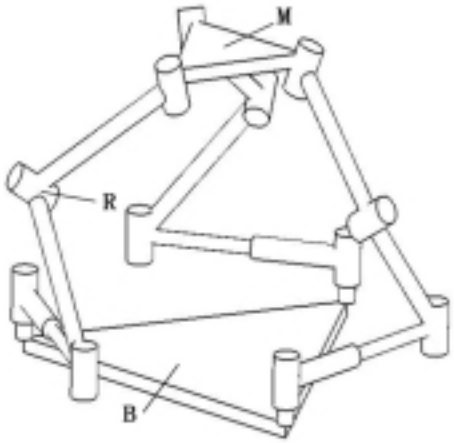

Fig. 17 5-DOF 3-RPR(RR) parallel mechanism

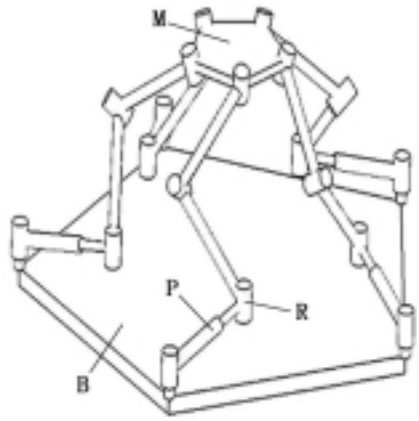

Fig. 18 5-DOF 5-RPR(RR) parallel mechanism

When each kinematic pair in a limb, as shown in Fig. 19, is expressed by a unit screw, for the initial configuration the limb twist system is

$$\begin{aligned}
\$_1 &= (1\,0\,0\,;0\,0\,0) \\
\$_2 &= (1\,0\,0\,;0\,b_2\;c_2) \\
\$_3 &= (1\,0\,0\,;0\,b_3\;c_3) \quad , \\
\$_4 &= (0\;m_5\;0\,;a_6\;0\;c_6) \\
\$_5 &= (0\;m_5\;0\,;a_7\;0\;c_7)
\end{aligned} \tag{15}$$

where they are linearly independent.. The limb exerts a constraint upon the platform

$$\$_1^r = (0\,0\,0\,;0\,0\,1), \tag{16}$$

which is a constraint couple perpendicular to the plane P_{34}.

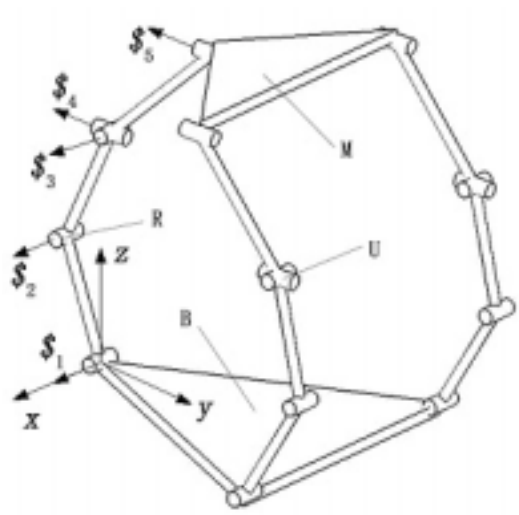

Fig. 19 5-DOF 3- $\underline{\mathrm{RR}}(\mathrm{R}\overline{\mathrm{R}})\mathrm{R}$ parallel mechanism

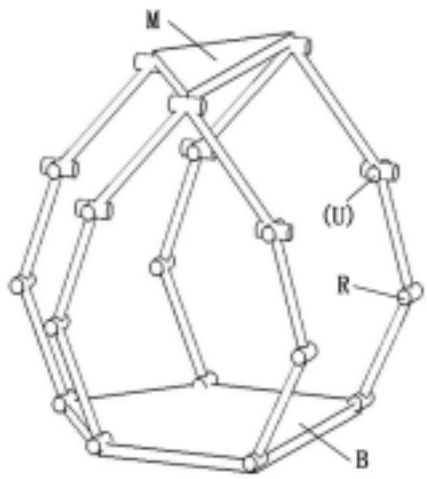

Fig. 20 5-DOF 5- $\underline{\mathrm{RR}}(\mathrm{R}\overline{\mathrm{R}})\mathrm{R}$ parallel mechanism

A single $\underline{RR(R}\overline{R)R}$ limb exerts a constraint couple on the moving platform, which is perpendicular to the crosshead plate. Three limbs exerts three constraint couples on the moving platform. Considering those three planes, P_{34}, of three limbs all are parallel to the moving platform plane, the three constraint couples are in the same direction and linearly dependent. They only equal one constraint couple perpendicular to the moving platform plane, restricting the rotation about the normal of the moving plane. Hence the mechanism has five degrees of freedom including three translational freedoms and two rotational freedoms.

Since the distribution of the first axis of each limb on the base is asymmetrical (parallel), so we may only name this mechanism as a limb-symmetrical parallel mechanism. This mechanism can also consist of five limbs, as shown in Fig. 20. It is only an input-symmetrical parallel mechanism.

4. Conclusion

The parallel mechanisms may be classified as fully-symmetrical, which means that both the mechanism and the input all are symmetrical; mechanism-symmetrical, which means that only the mechanism is symmetrical while the input is asymmetrical; limb-symmetrical, which means that the parallel mechanism consists of several the same limbs mounded on the base asymmetrically; input-symmetrical, which means it has symmetrical inputs and the same limb kinematic chains while the mechanism is asymmetrical. This paper introduced various different symmetrical parallel mechanisms.

Acknowledgements: This project is supported by NSFC under Grant No. 50075074.

References

1. Clavel R. Delta, a fast robot with parallel geometry. Proc. Of the Int. Symp. On Industrial Robot,Switzerland, 1988, pp. 91-100.
2. Tsai, L.W., and Stamper, R., 1996, "A Parallel Manipulator with Only Translational Degrees of Freedom," ASME 1996 Design Eng. Technical Conf., DETC96-MECH-1152, Irvine, CA.
3. Tsai Lung-Wen. The Enumeration of A Class of Three-Dof Parallel Manipulators, Proc of 10th IFToMM Conf. Vol 3, 1999, pp. 1123-1126.
4. R. Di Gregorio, V. Parenti-Castelli, Mobility analysis of 3-UPU parallel mechanism assembled for a pure translational motion, Proc of the 1999 IEEE/ASME International Conference on Advanced Intelligence Mechatronics, AIM'99, Atlanta (Georgia), 1999, pp. 520-525.
5. R. Di Gregorio. Closed-Form solution of the position analysis of the pure translational 3-RUU parallel mechanism, Proc of the 8th Symposium on Mechanisms and Mechanical Transmissions, MTM 2000, Timisoara (Romania), 2000, Vol. 1, pp. 119-124.
6. Cox D. and Tesar D. The Dynamic Model of a Three Degree of Freedom Parallel Robotic Shoulder Module. Advance Robotics, 1989 Proc. of the 4th Int. Conf. on Advanced Robotics. Ed. K.J. Waldron, Springer-Verlag, Berlin, 475-487
7. Gosselin C. M. and Angeles J. The Optimum Kinemaic Design of a Spherical 3-DOF Parallel Manipulator, ASME J.Mech. Trans. And Aut. In Des.1989, 111, pp. 202-207.
8. Gosselin C. M., Perreault L. and Vaillancourt Ch., Simulation and Computer-Aided Kinematic Design of Three-Degree-of Freedom Spherical Parallel Manipulators, J. of Robotic Systems, 1995, Vol.12(12), pp.

857-869.

9. R. Di Gregorio, Kinematics of a New Spherical Parallel Manipulator with Three Equal Legs: The 3-URC Wrist, Journal of Robotic Systems 18(5), 213-219, 2001.
10. Gosselin C. M., St-Pierre E., Development and Experimentation of a Fast 3-DOF Camara-Orienting Device, Int. J. of Robotics Research, 1997, Vol 16(5), pp. 619-630.
11. Huang Z and Fang Y F. Kinematic Characteristics Analysis of 3-DOF In-Parallel Actuated Pyramid Mechanisms. Mechanism and Machine Theory, 1996, 31(8), pp. 1009~1018.
12. Jean-Pierre MERLET, Parallel Robots: Open Problems INRIA, BP 93, 06902 Sophia-Antipolis, France
13. Clavel R, M. Bouri, S. Grousset, M. Thurneysen, A new 4 dof parallel robot: the Manta, Proc of the Int. Workshop on Parallel Kinematic Machines PKM'99, Milan (Italy), 1999, pp. 95-100.
14. Dimiter Zlatanov, Clement M. Gosselin, A New Parallel Architecture with Four Degrees of Freedom, the proccedings of the 2nd workshop on Computational Kinematics, May 19-22, 2001, Seoul, Korea, pp. 57-66.
15. J. M. Herve, The Lie group of rigid body displacements, a fundamental tool for mechanism design, Mechanism and Machine Theory 34 (1999) 719-730.
16. Z. Huang and Q. C. Li, General Methodology for Type Synthesis of lower-Mobility Symmetrical Parallel Manipulators and Several Novel Manipulators, Accepted by the *International Journal of Robotics Research*. Paper No. IJ1334
17. Z. Huang and Q. C. Li, Some Novel Lower-mobility Parallel Mechanisms, ASME DETC2002/MECH-34299, Montreal, Canada, September 29 - October 2, 2002
18. Mohamed M. G. and Duffy J. A Direct Determination of the Instantaneous Kinematics of Fully Parallel Robot Manipulators. ASME paper, 83-DET-114, 1984
19. Huang Z., Kong L. F. and Fang Y. F., The parallel Robot Mechanisms and control, China Machine Press, Beijing, 1997

Proceedings of the WORKSHOP on
Fundamental Issues and Future Research Directions for Parallel Mechanisms and Manipulators
October 3–4, 2002, Quebec City, Quebec, Canada
Clément M. Gosselin and Imme Ebert-Uphoff, editors

The Novel 3-RUU Wrist with No Idle Pair

JACQUES M. HERVÉ
Ecole Centrale Paris
92295 Chatenay-Malabry
France
jherve@ecp.fr

MOURAD KAROUIA
Ecole Centrale Paris
92295 Chatenay-Malabry
France
karouia@yahoo.fr

Abstract: *Most of the literature describes overconstrained parallel wrists. Such mechanisms have the essential drawback of sensitivity with respect to the geometrical conditions of the overconstrained mobility and therefore errors can produce uncheckable jamming effects or internal loads. In the classical* 3-RRR *parallel wrist, each leg generates three degrees of freedom instead of the required five degrees of freedom in an non-overconstrained 3-dof tripod. Then an immediate idea is to add two degrees of freedom in each leg by means of two revolute pairs for example. But generally these added pairs remain idle or undergo only small motions, which compensate the geometrical errors.*

Using equivalencies that result of the Lie group algebraic structure of the Euclidean displacement set, a new 3-RUU *wrist has been discovered. In each leg if the axes of two added R pairs intersect at one point on the fixed* R *axis of a classical* 3-RRR *wrist, the first three* R *pairs are equivalent to a spherical pair* S *and the whole mechanism becomes a* 3-SRR *wrist. Using again the equivalence of an* S *pair with a sequence* RRR *with converging axes, a new* 3-RUU *wrist with no idle pair is designed.*

1 Introduction

The classical 3-RRR overconstrained wrist (Figure 1) can work if and only if all R axes (R stands for revolute pair) are converging at the wrist centre O (Gosselin et al.,1989). Di Gregorio (2001) has described an non-overconstrained 3-RUU wrist (U stands for universal joint) by adding two R pairs that make up U joints with the end R pairs. However the original 3-RRR remains the active mechanism and the added R pairs are idle pairs or just compensate some errors in the axis convergence (Figure 2).

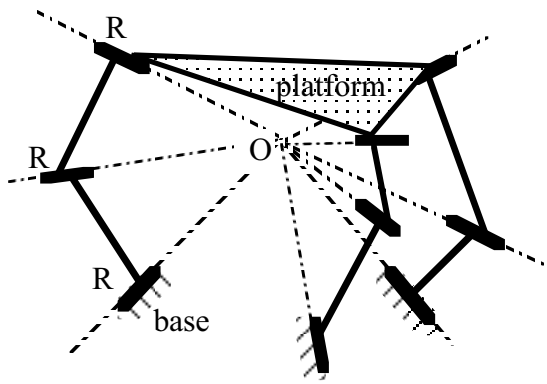

Figure 1: classical 3-RRR wrist

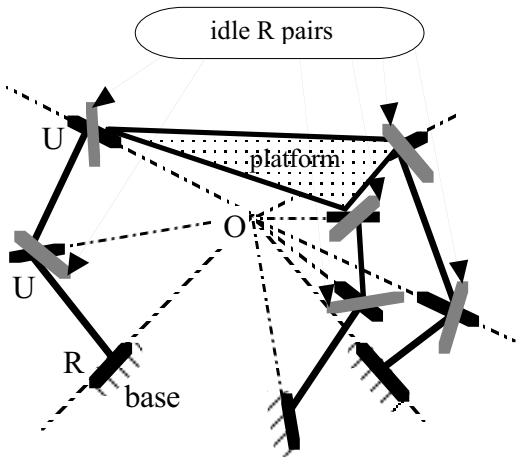

Figure 2: Di Gregorio 3-RUU wrist

Karouia and Hervé (2000, 2002) have proven that non-overconstrained orientational tripod can be designed without idle pairs by resorting on the Lie group algebraic structure of the set of Euclidean displacements (Hervé, 1978, 1999). As a matter of fact in an algebraic group the product of two elements belongs to the group. Otherwise the product is a closed product. One can readily verify that the product of two displacements is also a displacement. This essential property is still true for displacement subgroups. The set of spherical displacements $\{S(\mathrm{N})\}$ or orientational motions around a given point N is a subgroup of the displacement group $\{D\}$ (Hervé, 1978). Let **u** be a unit vector, (N,**u**) determines an axis of rotation as being a 1-dimensional frame of reference for an oriented straight line. The set of rotations around a given axis $\{R(\mathrm{N},\mathbf{u})\}$ is a subgroup of the subgroup $\{S(\mathrm{N})\}$. Let **u**, **v**, **w** be a vector base.

$\{R(\mathrm{N},\mathbf{u})\} \subset \{S(\mathrm{N})\}$

$\{R(\mathrm{N},\mathbf{v})\} \subset \{S(\mathrm{N})\}$

$\{R(\mathrm{N},\mathbf{w})\} \subset \{S(\mathrm{N})\}$

$\Rightarrow$

$\{R(\mathrm{N},\mathbf{u})\}\ \{R(\mathrm{N},\mathbf{v})\}\ \{R(\mathrm{N},\mathbf{w})\} \subseteq \{S(\mathrm{N})\}$

because of the closed product in the subgroup $\{S(\mathrm{N})\}$. The two sets are 3- dimensional. Considering only motion types and therefore neglecting the amplitude of the parameter variations, we can write

$\{R(\mathrm{N},\mathbf{u})\}\ \{R(\mathrm{N},\mathbf{v})\}\ \{R(\mathrm{N},\mathbf{w})\} = \{S(\mathrm{N})\}$

Furthermore it is a known fact (Hervé, 1982) that the sequence of three revolute pairs having axes (N,**u**), (N,**v**) and (N,**w**) generate a 3-dof kinematic bond represented by

$\{R(\mathrm{N},\mathbf{u})\}\ \{R(\mathrm{N},\mathbf{v})\}\ \{R(\mathrm{N},\mathbf{w})\}$

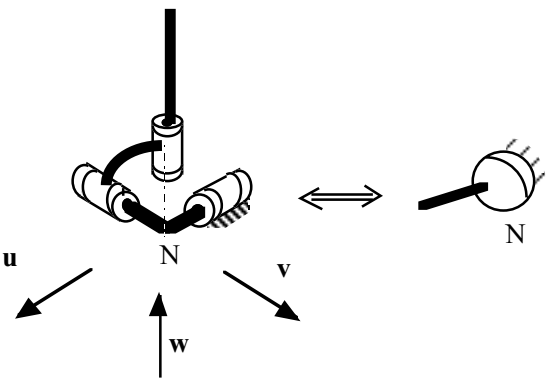

Figure 3: kinematic equivalence

By this reasoning, the equivalence between a serial arrangement of three R pairs with converging axes and a spherical pair S is now proven (Figure 3). This important property will be employed twice for the design of a novel 3-RUU wrist without idle pair.

2. Design of the new wrist

The design of the novel 3-RUU is obtained in two steps. In the first step we add two R pairs in each leg of a classical 3-RRR wrist. These idle R pairs can be introduced anywhere into any rigid body of each leg. Let N be a point on the fixed axis of a first leg. The choice of the added R pair axes is made in order to implement the previous equivalency: their axes intersect at N (Figure 4).

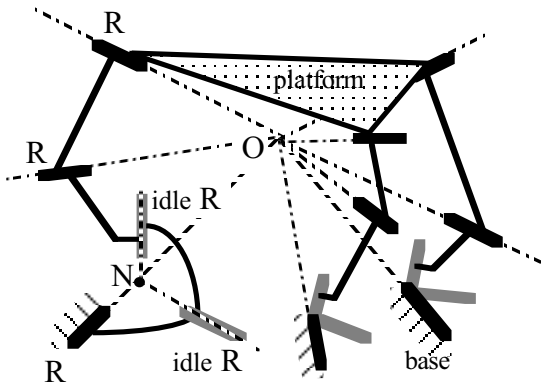

Figure 4: addition of idle R pairs.

A spherical pair S of centre N can replace the sequence of three R pairs whose axes converge at N, without modifying the platform mobility. The same process is done in the other two legs.

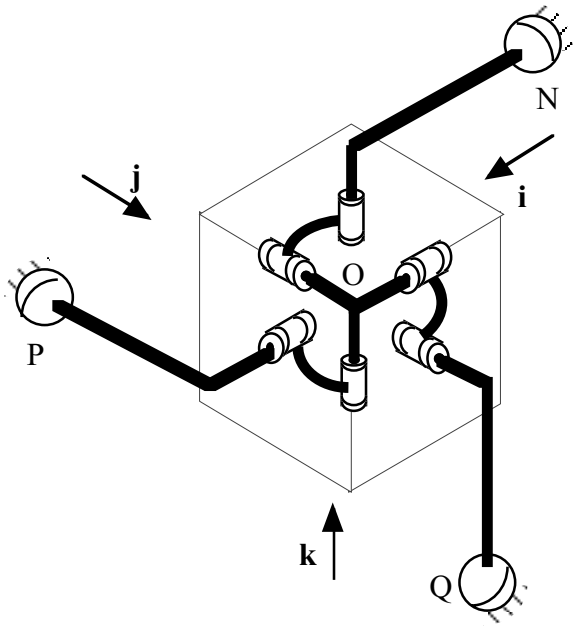

Figure 5: 3-SRR wrist

The figure 5 shows such a replacement result. It is a 3-SRR wrist of only theoretical interest because the fixed spherical pairs can't be easily actuated. In a special choice of mechanism, the two R pairs have perpendicular axes intersecting at O and then make up universal joints U. Thus a symbolic notation of this special parallel mechanism is 3-SU. The spherical joint centres are denoted N, P and Q

The second design step consists of the reverse change of the three S pairs by three sequences RRR whose axes converge at N, P and Q. But the first R axes of the three sequences don't intersect obligatorily at the centre O of the whole orientational parallel mechanism. The three fixed R pairs can

be actuated even though their axes don't converge at O and all R pairs undergo motions. In the special choice of perpendicular R pairs that consequently make up universal joints U, the mechanism is a parallel wrist of the 3-RUU type, which is not overconstrained and has no idle pairs (Figure 6).

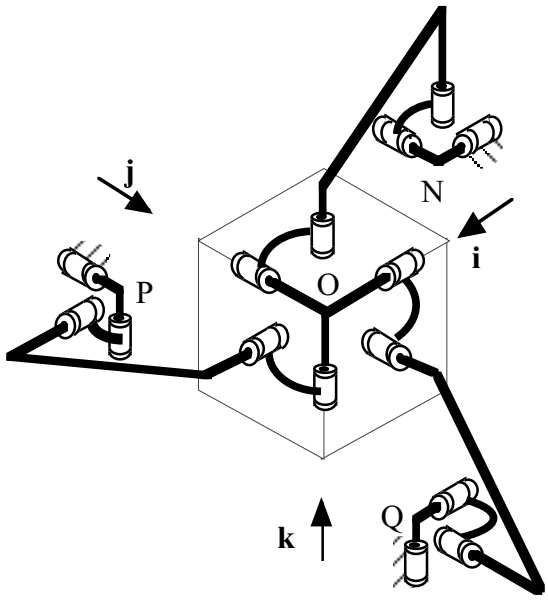

Figure 6: novel 3-RUU wrist without idle pairs.

Generally each of the four points O, N ,P and Q is the apex of a stiff tetrahedron. If this tetrahedron is flattened on a plane, the general stiffness is lost and the mechanism becomes singular and can't be used.

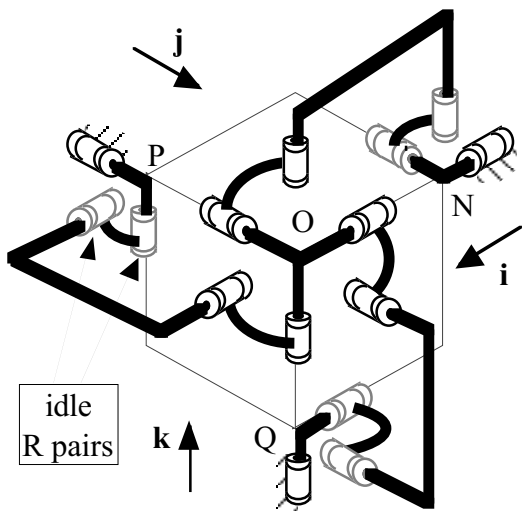

Figure 7: Special 3-RUU equivalent to 3-RRR wrist

It is worth noticing that in a special possible configuration, the fixed R axes converge at the mechanism centre O and then the second two R pairs are idle (Figure 7). Removing these idle pairs the wrist will be identical to the classical 3-RRR wrist.

3. Conclusion

A new 3-RUU parallel mechanism, which belongs to the large family of non-overconstrained orientational tripods (Karouia et al,. 2002b) has been described with more details than in previous publications. This mechanism can be regarded merely as the kinematic inversion of the simple 3-RRS wrist (Karouia et al.,2002a)

References

Gosselin C.M. and Angeles J., 1989,"The optimum kinematic design of a spherical three-degree-of-freedom parallel manipulator", ASME Journal of Mechanisms, Transmission and Automation in Design, 111(2), pp.202-207.

Di Gregorio R., 2001, "A new parallel wrist using only revolute pairs: the 3-RUU wrist", Robotica, 19,pp.305-309.

Karouia M., Hervé J.M., 2000,"A three-dof tripod for generating spherical rotation", Advances in Robot Kinematics, Kluwer ©2000, pp.395-402.

Karouia M., Hervé J.M., 2002 (a)," An orientational 3-dof parallel mechanism", Proceedings of PKS'2002, Chemnitz, Germany, April 23-25,2002.

Karouia M., Hervé J.M., 2002 (b)," A family of novel orientational 3-dof parallel robots ", Proceedings of RoManSy'2002, Udine, Italy, July 1-4, 2002.

Hervé J.M., 1978, "Analyse structurelle des mécanismes par groupe des déplacements", Mechanism and Machine Theory, 13, pp.437-450.

Hervé J.M., 1982, "Intrinsic formulation of problems of geometry and kinematics of Mechanisms", Mechanism and Machine Theory, 17, pp.179-184.

Hervé J.M., 1999, "The Lie group of rigid body displacements, a fundamental tool for mechanism design", Mechanism and Machine Theory, 34, pp. 719-730.

Proceedings of the WORKSHOP on
Fundamental Issues and Future Research Directions for Parallel Mechanisms and Manipulators
October 3–4, 2002, Quebec City, Quebec, Canada
Clément M. Gosselin and Imme Ebert-Uphoff, editors

WORKSPACE ANALYSIS OF A SIX DOF WIRE-DRIVEN PARALLEL MANIPULATOR

Applicant: Ya-Qing Zheng
Institute of Advanced Manufacturing Technology,
Huaqiao University, Quanzhou, Fujian, 362011, China
Tel: (86) 595-2691903 Fax: (86) 595-2686969
E-mail: yq-zheng@hqu.edu.cn

Supervisor: Prof. Dr. Xiong-Wei Liu
Institute of Advanced Manufacturing Technology,
Huaqiao University, Quanzhou, Fujian, 362011, China
Tel: (86) 595-2691903 Fax: (86) 595-2686969
E-mail: xwliu@hqu.edu.cn

Abstract: *This paper presented a novel six degrees of freedom (DOF) wire-driven parallel kinematic manipulator (PKM) with seven wires. In the proposed manipulator, one end of each wire is connected to the moving platform with a spherical joint and the other end is connected to a pulley which is driven by a servo motor. The authors investigated the workspace analysis of the six DOFs wire-driven PKM, including controllable workspace (WS) based on the concept of Vector Closure, workspace with tension conditions (WST) based on the Nullspace Method and workspace with stiffness conditions (WSS) based on the Eigenvalue Method. Finally, a case study was presented to demonstrate the application of the methodology to determine the controllable workspace, the WST and WSS using Monte-Carlo technique under the Matlab environment. The results show that the workspaces of different manipulators with different designing parameters differ vigorously from each other, and there is a little difference between the practical workspace and the theoretical one. If more randomly points are selected, the practical workspace will be closer to the theoretical one.*

1 Introduction

Wire-driven parallel kinematic manipulators (PKMs) have been given more and more attention in virtual reality [1], force display [2], ultra-high speed robots [3] in the last decade, due to their advantages comparing to strut supported PKMs, such as simple structure, low apparent mass/inertia, large workspace and high speed. The topics of the researches about wire-driven PKMs are mechanism configuration, workspace analysis, stiffness analysis, dynamic analysis and motion control [4~10]. A few manipulators have been designed and tested in the laboratories for potential application in crane robot, force reflecting joystick or haptic device, rehabilitation robot, positioning device, ultra-high speed robot, super large-scale light robot [2,3,5,8,10,11]. However there are still many problems to be sorted out before they are introduced into industrial application due to their extremely complexities both in theoretical and empirical aspects.

A novel six DOF wire-driven PKM with seven wires will be presented in this paper. In section 1, the mechanism configuration of the wire-driven PKM is described. Thereafter, the previous work about the approaches to analyze controllable workspace based on concept of Vector Closure, WST based on *Nullspace Method* and WSS based on *Eigenvalue Method* is outlined in section 2. Section 3 presents a case study to demonstrate the application of the approaches to workspace analysis using Monte-Carlo technique under the Matlab environment.

2 Mechanism Configuration

Figure 1 describes a six DOF wire-driven PKM. Its moving platform looks like a cylinder, which is driven by seven wires via spherical joints from different directions. The wires are connected to a base frame via pulleys, which are located at the base frame and form the two end circle boundaries of a large cylinder. Three of the seven spherical

joints are distributed uniformly on the front of the moving platform, and the other four of them are located at the rear of the platform uniformly. Three of the seven pulleys are distributed uniformly on the front of the base frame, and the other four of them are located at the rear of the base frame.

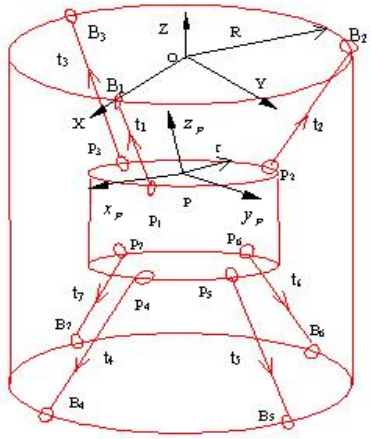

Figure 1: Structure model of the wire-driven PKM.

The locations of the connection points of wires on the base frame and the moving platform are shown in Figures 2 and 3 respectively. These locations are determined with consideration of geometric symmetry and simplicity that are typical requirements to robotic devices for general purposes. The moving coordinate system $P-x_P y_P z_P$ is fixed on the center of the moving platform. The position of the reference point of P is denoted by $P(X_P, Y_P, Z_P)$. The orientation of the moving platform is described by the roll, pitch and yaw angles ($\varphi_R, \varphi_P, \varphi_Y$) of the coordinate system $P-x_P y_P z_P$ to the fixed coordinate system $O-XYZ$. The positions of the connection points of the wires on the base frame are described in the fixed coordinate system $O-XYZ$ and are denoted by $B_i(X_{B,i}, Y_{B,i}, Z_{B,i})\,(i=1,2,3,\cdots,7)$. The positions of the connection points of the wires on the moving platform are described in terms of the moving coordinate system and are denoted by P_i ($x_{P,i}, y_{P,i}, z_{P,i}$) ($i=1,2,3,\cdots,7$). The coordinates of the connection points of wires are shown in Figures 2 and 3.

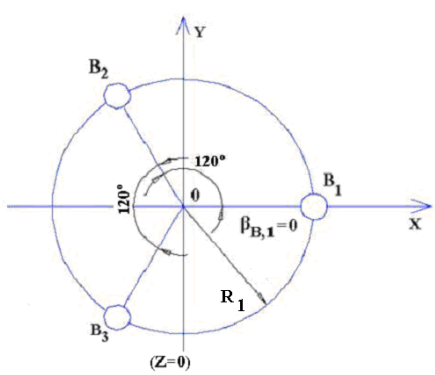

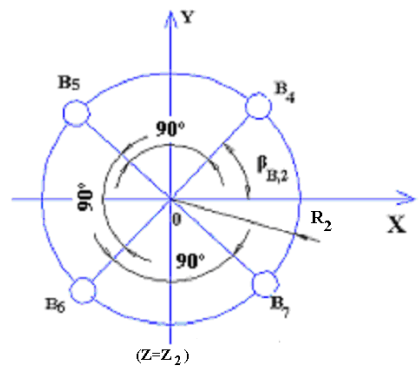

$Z_1 = 0, R_1, \beta_{B1} : B_i(X_{Bi}, Y_{Bi}, Z_{Bi})$ ($i=1,2,3$)

$B_1 : (R_1, 0, 0)$, $B_2 : (-\frac{R_1}{2}, \frac{\sqrt{3}R_1}{2}, 0)$, $B_3 : (-\frac{R_1}{2}, -\frac{\sqrt{3}R_1}{2}, 0)$

$Z_2, R_2, \beta_{B2} : B_i(X_{Bi}, Y_{Bi}, Z_{Bi})$ ($i=4,5,6,7$)

$B_4 : (R_2 \cos\beta_{B2}, R_2 \sin\beta_{B2}, -Z_2)$,

$B_5 : (R_2 \cos(\beta_{B2}+\pi/2), R_2 \sin(\beta_{B2}+\pi/2), -Z_2)$,

$B_6 : (R_2 \cos(\beta_{B2}+\pi), R_2 \sin(\beta_{B2}+\pi), -Z_2)$,

$B_7 : (R_2 \cos(\beta_{B2}+3\pi/2), R_2 \sin(\beta_{B2}+3\pi/2), -Z_2)$

Figure 2: Connection points of wires on the base frame.

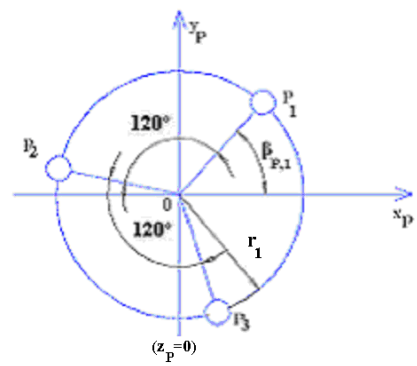

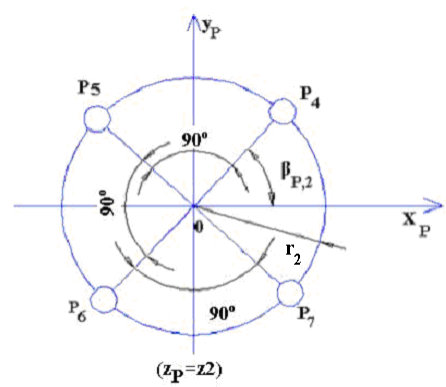

$z_1 = 0, r_1, \beta_{P1}, P_i : (x_{P,i}, y_{P,i}, z_{P,i})$ ($i=1,2,3$)

$P_1 : (r_1 \cos\beta_{P1}, r_1 \sin\beta_{P1}, 0)$,

$P_2 : (r_1 \cos(\beta_{P1}+2\pi/3), r_1 \sin(\beta_{P1}+2\pi/3), 0)$,

$P_3 : (r_1 \cos(\beta_{P1}+4\pi/3), r_1 \sin(\beta_{P1}+4\pi/3), 0)$

$z_2, r_2, \beta_{P2}, P_i : (x_{P,i}, y_{P,i}, z_{P,i})$ ($i=4,5,6,7$)

$P_4 : (r_2 \cos\beta_{P2}, r_2 \sin\beta_{P2}, -z_2)$,
$P_5 : (r_2 \cos(\beta_{P2} + \pi/2), r_2 \sin(\beta_{P2} + \pi/2), -z_2)$,
$P_6 : (r_2 \cos(\beta_{P2} + \pi), r_2 \sin(\beta_{P2} + \pi), -z_2)$,
$P_7 : (r_2 \cos(\beta_{P2} + 3\pi/2), r_2 \sin(\beta_{P2} + 3\pi/2), -z_2)$

Figure 3: Connection points of wires on the moving platform.

The transformation matrix of the moving coordinate system $P - x_P y_P z_P$ with respect to the fixed one is

$$T_{RPY} = T_Z(\varphi_Y) T_Y(\varphi_P) T_X(\varphi_R)$$
$$= \begin{bmatrix} c_Y & -s_Y & 0 \\ s_Y & c_Y & 0 \\ 0 & 0 & 1 \end{bmatrix} \begin{bmatrix} c_P & 0 & s_P \\ 0 & 1 & 0 \\ -s_P & 0 & c_P \end{bmatrix} \begin{bmatrix} 1 & 0 & 0 \\ 0 & c_R & -s_R \\ 0 & s_R & c_R \end{bmatrix}$$
$$= \begin{bmatrix} c_P c_R & c_R s_P s_Y - s_R c_Y & s_R s_Y + c_R s_P c_Y \\ c_P s_R & c_R c_Y + s_R s_P s_Y & s_R s_P c_Y - c_R s_Y \\ -s_P & s_Y c_P & c_P c_Y \end{bmatrix}$$

where
$c_R = \cos(\varphi_R), c_P = \cos(\varphi_P), c_Y = \cos(\varphi_Y),\ s_R = \sin(\varphi_R),$
$s_P = \sin(\varphi_P), s_Y = \sin(\varphi_Y)$, φ_R , φ_P and φ_Y are the roll, pitch and yaw angles respectively.

3 Workspace Analysis

3.1 Analysis of Controllable Workspace Based on Concept of Vector Closure

3.1.1 Concept of Vector Closure

In a 6 -dimensional space, a set of vector V is vector closure if and only if V has at least 7 vectors ($\omega_1, \omega_2, \cdots, \omega_7$) satisfying the following two conditions:

1. Each set of 6 vectors in this seven vectors ($\omega_1, \omega_2, \cdots, \omega_7$) are linearly independent.
2. $\sum_{i=1}^{7} \alpha_i \omega_i = 0$ ($\alpha_i > 0$ for any i)

As far as a six DOF wire-driven PKM is concerned, if we regard w_i and α_i as the wire direction vector and the wire tension of the ith wire, assuming no external force and torque acting on the moving platform, we can deduce that the equation $\sum_{i=1}^{7} \alpha_i w_i = 0$ is satisfied, according to the force and torque equilibrium of the moving platform; moreover each set of 6 vectors in all the seven wire direction vectors $(w_1, w_2, \cdots, w_7)$ are linearly independent, so the concept of Vector Closure can be introduced here.

One way proposed by Kawamura [5] to check whether the position and the orientation are not beyond singular points for a six DOF wire-driven PKM with six wires or not, is given by the relation as follows:

$$\tau = A^+ f + (I - A^+ A)k \qquad (1)$$

where $\tau = (\alpha_1 \alpha_2 \cdots \alpha_7)^T$ α_i :each wire tension;
$f(6\times1)$: force and moment vector acting on the moving platform;
A^+ : pseudo-inverse matrix of $A(6\times7)$;
k : an arbitrary vector (7×1)

The matrix A means the relation between wire tensions and the net force and moment on the moving platform. It is obtained by

$$f = A\tau \qquad (2)$$

The elements of matrix A are determined by the wire direction from the moving platform. If the second term in Eq.(1) becomes positive with sufficiently large value, all elements of the vector τ can become positive satisfying Eq.(2). Here, we remark that the vector k is an arbitrary vector and the matrix $(I - A^+ A)$ is non-negative. As the results, it is noted that if all elements of the matrix $(I - A^+ A)$ are positive, all elements $\tau_i (1 \le i \le 7)$ of the vector τ become positive. In other words, we should set positive elements in the matrix $(I - A^+ A)$ by changing the angles between the wires and the moving platform.

3.1.2 Procedure

Kawamura[5] introduced a simple algorithm to determine the controllable workspace of six DOF wire-driven PKMs with 7 wires, as follows:

Step 1: Set each wire direction vector $w_i(6\times1)(1 \le i \le 7)$,

$w_i = \begin{Bmatrix} \vec{f}_i \\ \vec{r}_i \times \vec{f}_i \end{Bmatrix}$, $\vec{f}_i = \begin{Bmatrix} f_{ix} \\ f_{iy} \\ f_{iz} \end{Bmatrix}$ ($f_{ix}^2 + f_{iy}^2 + f_{iz}^2 = 1$), $\vec{r}_i$ is a distance between the reference point P at the moving platform and the ith wire end , $\vec{r}_i = \begin{Bmatrix} r_{ix} \\ r_{iy} \\ r_{iz} \end{Bmatrix}$;

Step 2: Calculate a vector $r(6\times1)$ in the following way:
$r = -W^{-1} w_7$, where $W = (w_1 w_2 \cdots w_6)$;

Step 3: Check whether every element of the vector r is positive, If so, the second step of vector closure can be satisfied and meanwhile the pose of the moving platform is feasible;

Step 4:By using the above procedure, the positioning and orientation controllable workspace of the wire-driven PKM would be revealed.

3.2 Analysis of WST

3.2.1 Nullspace Method

Verhoeven and Miller [8] defined that the WST is the set of poses where a force and torque equilibrium can be obtained considering each wire tension must be greater than its pretension $\tau_{\min}$ and less than its maximum tension $\tau_{\max}$, and introduced an index $k_{\max}(=\tau_{\max}/\tau_{\min})$ for evaluating the ratio of $\tau_{\max}$ to $\tau_{\min}$. They [8] also introduced an analytical expression of the condition for the poses within the WST assuming no force and torque acting on the moving platform, as follows: $\frac{\max_{\mu=1,2,\cdots,7}|h_\mu|}{\min_{\mu=1,2,\cdots,7}|h_\mu|} \le k_{\max}$ (here, $h = N(A)$, $A = (w_1 w_2 w_3 w_4 w_5 w_6 w_7)$, is the Jacobian matrix of this wire-driven PKM) and presented the condition for the boundary of the workspace.

3.2.2 Procedure

1) Give a certain index $k_{\max}$;

2) Set each wire direction unit vector $w_i(6\times1)$ $(1 \le i \le 7)$, and determine A, the Jacobian matrix of this wire-driven PKM;

3) Calculate the nullspace of A, supposing that $h = N(A)$, if each element of is greater than zero and satisfies the inequality: $\frac{\max_{\mu=1,2,\cdots,7}|h_\mu|}{\min_{\mu=1,2,\cdots,7}|h_\mu|} \le k_{\max}$, then the pose is within the WST.

3.3 Analysis of WSS

3.3.1 Eigenvalues Method

For this wire-driven PKM, if $k_\mu(\mu = 1,2,3,\cdots,7)$ is the stiffness of the μth wire, and k' is the stiffness per reciprocal unit length of the wire, we have $k' = k_\mu \times l_{0\mu}$, here $l_{0\mu}$ is the original length of the μth wire. Using the stiffness matrix of conventional PKMs, Verhoeven and Miller [8] defined the WSS, of a six DOF wire-driven PKM with seven wires, is the set of poses where six positive eigenvalues $k_{ev}(1 \le v \le 6)$ of stiffness matrix are all not less than the allowable minimum stiffness, $k_{\min}$, of the wires.

3.3.2 Procedure

1) If k' is the stiffness per reciprocal unit length of the wire, $k_{\min}$ is the allowable minimum stiffness of the wire, and $l_{0\mu}$ is the original length of the μth wire. And $k_\mu(\mu = 1,2,3,\cdots,7)$ is the stiffness of the μth wire;

2) Set each wire direction unit vector $w_i(6\times1)$ $(1 \le i \le 7)$, and determine A, the Jacobian matrix of this wire-driven PKM;

3) Calculate the nullspace of A, supposing that $h = N(A)$;

4)Determine the stiffness matrix of this wire-driven PKM as $K = k' A L^{-1} A^T$,where $L_0^{-1} = diag(l_{0\mu}(1 + k'^{-1}\tau_\mu)$, in practice, the term $k'^{-1}\tau_\mu$ used to be <0.5%. Thus, stiffness properties must be achieved by the geometrical arrangement;

5) Calculate the six positive eigenvalues $k_{ev}(1 \le v \le 6)$ of the stiffness matrix K, if not only each element of h is greater than zero, but also $(\min_{1\le v\le 6} k_{ev}) \ge k_{\min}$ is satisfied, then the pose is within the WSS.

4. Case Study

Let us think of this wire-driven PKM mentioned in Figure 1, and a set of the following parameters of the manipulator: $R_1, R_2, \beta_{B,1}, \beta_{B,2}, Z_2$, r_1, r_2, $\beta_{P,1}$, $z_2, \beta_{P,2}$, are given. When the reference point P of the moving platform is located at $(0,0,Z_P,0,0,0)$, the manipulator is obvious singular because the rank of the Jacobian matrix at this pose is less than six. So, the home pose is defined as $X_P = Y_P = 5(mm), Z_P = Z_0$, $\varphi_R = 1^o$, $\varphi_P = \varphi_Y = 0$, where Z_0 is set as -30mm. Here the workspace includes the position workspace and the orientation workspace.

Let $Z_0 = -30$ mm, and give a set of the configuration parameters of the wire-driven PKM, which are denoted as Type 1 , as shown in Table 1.

Table 1: Type 1

z_1	0	Z_1	0
r	60mm	R	240mm
$\beta_{P,1}$	0	$\beta_{B,1}$	0
z_2	40mm	Z_2	240mm
$\beta_{P,2}$	0	$\beta_{B,2}$	0
z_2	40mm	Z_2	240mm
$\beta_{P,2}$	0	$\beta_{B,2}$	-30°

4.1 CASE 1：Determination of Controllable Workspace

As shown in Table 2 and Figure 5, the results are carried out by the programming using Monte-Carlo technique under the Matlab environment according to the procedure mentioned in Section 2.1 (N denotes the number of the selected sample points).

Table 2: Workspace ($TI_W > 0$) of Type 1

TI_W at the reference pose	0.5568
Workspace free from singularity	
Position workspace ($\varphi_R = 1^o, \varphi_P = \varphi_Y = 0$)	
$X(Y_P = 5, Z_P = Z_0)$	-40mm~40mm
$Y(X_P = 5, Z_P = Z_0)$	-40mm~40mm
$Z(X_P = Y_P = 5)$	-200mm~0
Orientation workspace ($X_P = Y_P = 5mm, Z_P = Z_0$)	
$\varphi_R(\varphi_P = \varphi_Y = 0)$	-25°~29°
$\varphi_P(\varphi_R = 1^o, \varphi_Y = 0)$	-50°~50°
$\varphi_Y(\varphi_R = 1^o, \varphi_P = 0)$	-70°~70°

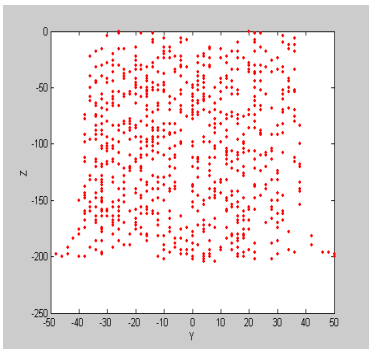

Y-Z Plane(N=12000)

(X_P =5, $\varphi_R = 1^o, \varphi_P = \varphi_Y = 0$)

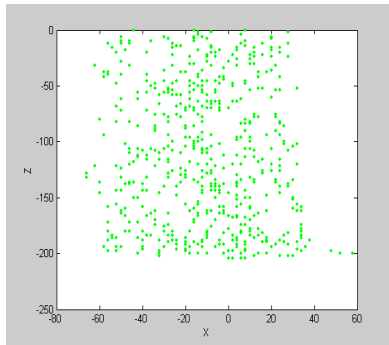

X-Z Plane(N=12000)

(Y_P =5, $\varphi_R = 1^o, \varphi_P = \varphi_Y = 0$)

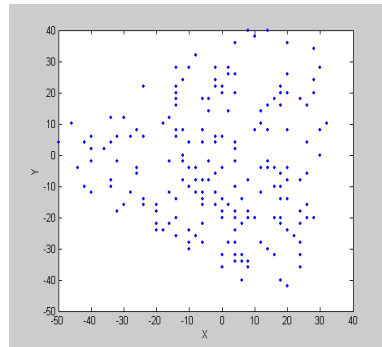

X-Y Plane (N=12000)

($Z_P = Z_0, \varphi_R = 1^o, \varphi_P = \varphi_Y = 0$)

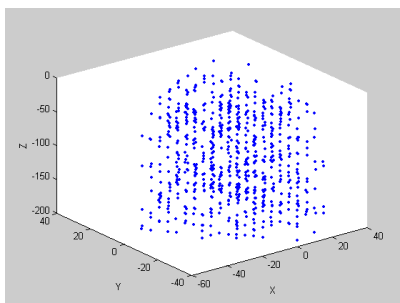

Position workspace (N=768000)

($\varphi_R = 1^o, \varphi_P = \varphi_Y = 0$)

Figure 5: The maps of controllable workspace

4.2 CASE 2: Determination of WST

Assuming $k_{\max} = \tau_{\max} / \tau_{\min} = 100$, the maps of position WST shown in Figure 6, are carried out by the programming using Monte-Carlo technique under the Matlab environment, according to the procedure mentioned in Section 2.2 (N denotes the number of the selected sample points).

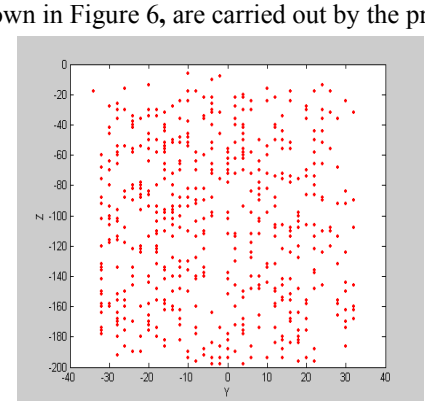

Y-Z Plane(N=12000)

(X_P =5, $\varphi_R = 1^o, \varphi_P = \varphi_Y = 0$)

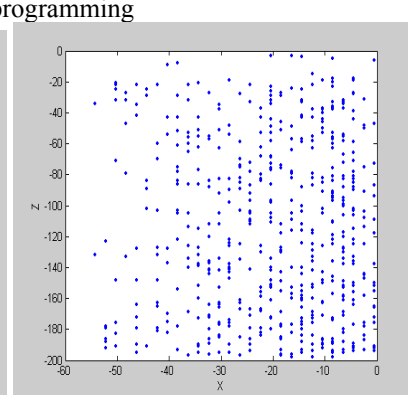

X-Z Plane(N=24000)

(Y_P =5, $\varphi_R = 1^o, \varphi_P = \varphi_Y = 0$)

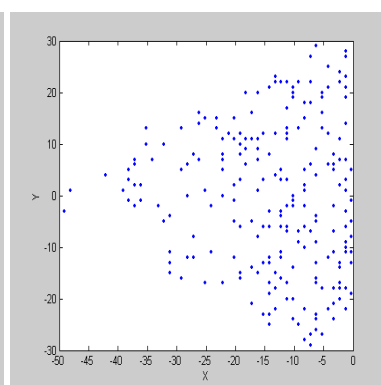

X-Y Plane(N=40000)

($Z_P = Z_0, \varphi_R = 1^o, \varphi_P = \varphi_Y = 0$)

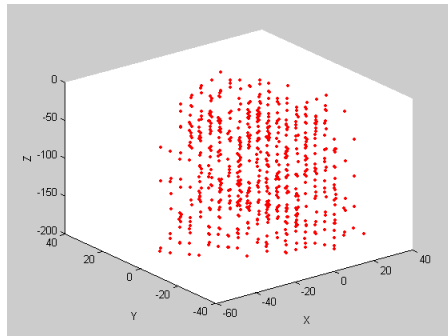

Position workspace (N=768000)

($\varphi_R = 1^o, \varphi_P = \varphi_Y = 0$)

Figure 6: The maps of WST

4.3 CASE 3：Determination of WSS

Assuming that $k' = 1000$ (N/mm), is the stiffness per reciprocal unit length of the wire, $l_{0\mu}$ ($\mu = 1,2,\cdots,7$) is the original length of the μth wire, 180mm,180mm,180mm, 197mm,197mm,197mm,197mm respectively. Then the average stiffness $k_a = k' \times l_{av}$ (l_{av} is the average original length of the seven wires). $k_{\min}$ is the allowable minimum stiffness of the wire, $k_{\min} = 0.10k_a$.

The maps of WSS shown in Figure 7 are carried out by the programming using Monte-Carlo technique under the Matlab environment, according to the procedure mentioned in Section 2.3(N denotes the number of the selected sample points).

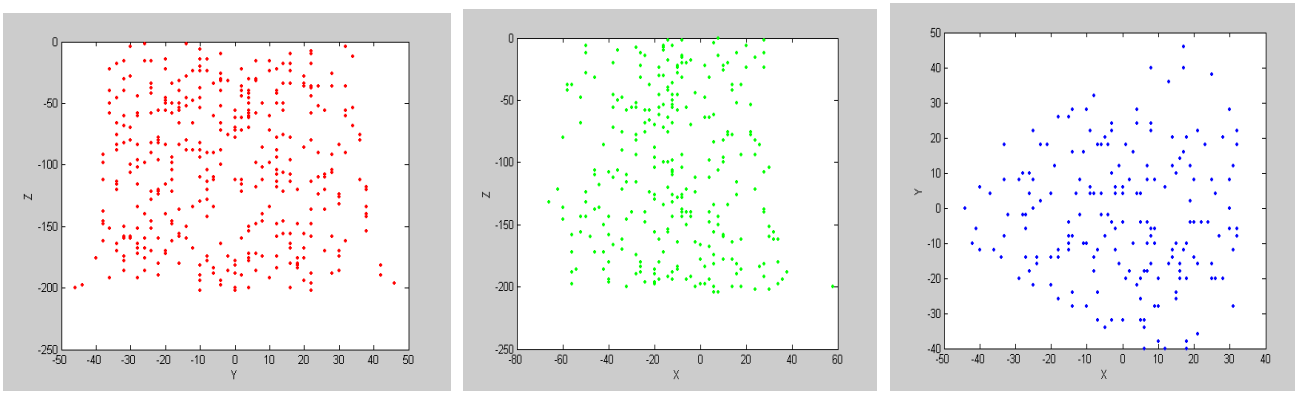

Y-Z Plane (N=12000) (X_P =5, $\varphi_R = 1^o, \varphi_P = \varphi_Y = 0$)

X-Z Plane (N=12000) (Y_P =5, $\varphi_R = 1^o, \varphi_P = \varphi_Y = 0$)

X-Y Plane (N=20000) ($Z_P = Z_0, \varphi_R = 1^o, \varphi_P = \varphi_Y = 0$)

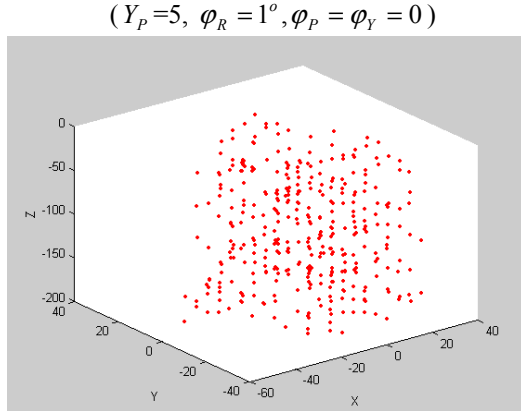

Position workspace (N=768000)

($\varphi_R = 1^o, \varphi_P = \varphi_Y = 0$)

Figure 7: The maps of WSS

The results, shown in the tables and figures mentioned above, demonstrate that the determination of controllable workspace base on concept of Vector Closure, WST based on Nullspace Method, and WSS based on Eigenvalues Method has been successfully carried out. In addition, in theory, the map of the WST is a closed set. But in practice, the map shown in Figure 6 is not the case, because the Monte-Carlo technique is an approximate algorithm. Meanwhile, if more random points are selected, the practical WS, WST and WSS will be closer to the theoretical ones. Also the fact is justified again that the maps of WST and WSS are indeed within those of the controllable workspace.

5 Conclusion

Mechanism design of this novel six degrees of freedom (DOF) wire-driven parallel kinematic manipulator(PKM) with seven wires was attained by changing several design variables. Workspace analysis of this six DOF wire-driven PKM was investigated in detail to show that controllable workspace based on concept of Vector Closure, WST based on Nullspace Method and WSS based on Eigenvalue Method. A case study was presented to demonstrate the application of the methodology to determine the controllable workspace, the WST and WSS using Monte-Carlo technique under the Matlab environment.

The results show that there is a little difference between the practical workspace and the theoretical one. If more randomly points are selected and a simplier algorithm is used, the practical workspace will be closer to the theoretical one.

If in the future work a required stiffness is reached by using internal forces among wires, the manipulator can be designed for large-scale flight simulators. A 3D CAD model of this manipulator is established by the authors, as shown in Figure 8.

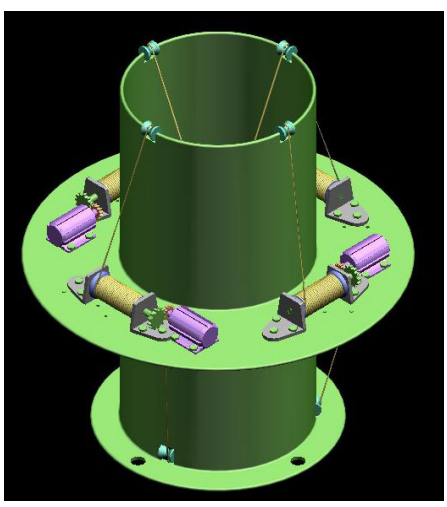

Figure 8: 3D CAD model of the wire-driven PKM

References

[1] Kawamura, S., Ida, M., Wada, T. and Wu, J.L. Development of A Virtual Sports Machine using A Wire Drive System-A Trial of Virtual Tennis. Proceedings of the 1995 IEEE/RSJ International Conference on Intelligent Robots and Systems, Pittsburgh(1995) pp.111-116.

[2] Morizono, T., Kurahashi, K. and Kawamura, S. Analysis and Control of A Force Display System Driven by Parallel Wire Mechanism. Robotica, Vol.16, pp.551-563, 1998.

[3] Kawamura, S., Choe, W., Tanaka, S. and Pandian, S. R. Development of an Ultrahigh Speed Robot FALCON Using Wire Drive System. Journal of the Robotics Society of Japan, Vol.15 No.1, 1997, pp.82-89.

[4] Tadokoro,S., Nishioka, S., Kimura,T., Hattori,T. , and Maeda,K. On Fundamental Design of Wire Configuration of Wire Driven Parallel Manipulators with Redundancy. In Proceedings of the Japan-U.S.A Symposium on Flexible Automation, pp.151-158, Boston, MA,USA,1996.

[5] Kino, H., Miyazono, H., Choe, W. and Kawamura, S. Realization of Large Work Space using Parallel Wire Drive Robots. Proceedings of 2nd Asian Control Conference, Vol.3, pp.591-594, Seoul, July, 1997.

[6] Kino, H., Yabe ,S., Shimamoto, T. and Kawamura ,S. Stiffness Increase Method of Wire Driven Systems using Interference of Wire Tension with Mechanical Constraint Directions, Proceedings of International Conference on Machine Automation, Osaka, September, pp.63-68, 2000.

[7] Kino, H. , Cheah, C. C. , Yabe, S., Kawamura, S. and Arimoto, S. A Motion Control Scheme in Task Oriented Coordinates and its Robustness for Parallel Wire Driven Systems, Proceedings of the Ninth International Conference on Advanced Robotics, pp.545-550, Tokyo, October 25-27, 1999.

[8]Verhoeven,R., Hiller,M. and Tadokoro S. Workspace, Stiffness, Singularities and Classification of Tendon-Driven Stewart Platforms. Proceedings of the ARK ’98 6th. International Symposium on Advances in Robot Kinematics, pp. 105~114, Strobl/Salzburg, Austria, June 1998.

[9] Verhoeven,R. and Hiller,M. Estimating the Controllable Workspace of Tendon-Based Stewart Platforms. Proceedings of the ARK '00 7th. International Symposium on Advances in Robot Kinematics, pp. 277~284, Portoroz, Slovenia, 2000.

[10] Jeong J.W., Kim S.H. and Kwak Y. K. Kinematics and Workspace Analysis of a Parallel Wire Mechanism for Measuring a Robot Pose. Mechanism and Machine Theory, 31(6): 825-841, April 1999.

[11] Bonivento, C., Eusebi, A., Melchiorri, C., Montanari, M., and Vassura, G. Wireman: A Portable Wire Manipulator for Touch-Rendering of Bas-Relief Virtual Surfaces, in:8th International Conference On Advanced Robotics, Proceedings ICAR’97 IEEE, New York, NY, USA, 1997, pp.13-18.

Kinetostatic Analysis and Optimization of a Tripod Attachment For Machine Tools

Zhengyi Xu
Department of Mechanical & Materials Engineering
The University of Western Ontario, London, Ontario, Canada

Fengfeng Xi,
Department of Mechanical, Aerospace and Industrial Engineering
Ryerson University, Toronto, Ontario, Canada

Chris K. Mechefske
Department of Mechanical Engineering
Queen's University, Kingston, Ontario, Canada

Abstract

Since most machining operations require a maximum of five axes, tripod design is becoming popular for the development of parallel kinematic machines (PKMs). The combination of a tripod with a gantry system forms a five-axis machine with both large workspace and dexterity. This paper is focused on kinetostatic analysis and optimization of a sliding-leg tripod unit. First, a parametric kinematic model is developed and constrained kinematic equations are derived. Based on this, a flexibility model is established considering the flexibility in the sliding legs and the actuators. A global index is introduced to characterize the tripod's compliance over the workspace. The method of Generic Algorithms is applied for structural optimization. Results of optimization show that a tripod unit with a smaller workspace would lead to a higher stiffness.

1. Introduction

The recent trend in manufacturing is moving towards high-speed machining (HSM). The main thrust behind this is to machine the part with a smooth surface finish. This would ultimately eliminate finishing processes such as grinding or polishing, and hence would improve productivity and reduce costs. For HSM, this requires the development of machine tools with high dynamic performance, improved stiffness and reduced moving mass.

Parallel mechanisms appear to be a good candidate and have been adopted to develop a new type of machine tools, called parallel kinematic machines (PKMs) [1-3]. Initial development of PKMs involved simply inverting the Stewart platform to have a hanging-down configuration. The Stewart platform based machine tools are called hexapods and they have six axes. Since most machining tasks require a maximum of five

axes, tripod designs with three axes are becoming popular. The combination of a tripod with a gantry system forms a five-axis machine with both large workspace and dexterity.

Several tripod units proposed in the literature have attracted attention from industry. The most successful one is Tricept [4] from Neos Robotics AB. This tripod unit is mainly designed for heavy-duty cutting applications. It can be mounted on different types of machine frames. The Z^3 Head [5] from Cincinnati Machine is another type of tripod unit designed for heavy-duty cutting applications. The difference is that the Tricept is designed with extensible legs while the Z^3 head is developed with fixed-length actuators. The Georg V [6] from University of Hannover is designed with fixed-length actuators for light-duty applications.

This paper is focused on kinetostatic analysis and optimization of a sliding-leg tripod unit developed at the Integrated Manufacturing Technologies Institute of National Research Council of Canada [7]. As shown in Figure 1, this unit was built in small scale as a toolhead to be attached to a basic machine such as a gantry system. In this paper, first, a parametric kinematic model is developed and constrained kinematic equations are derived. Based on this, a flexibility model is established considering the flexibility in the sliding legs and the actuators. A global compliance index is introduced to characterize the tripod's compliance over the workspace. The method of Generic Algorithms is applied for structural optimization. Results of optimization show that a tripod unit with a smaller workspace would lead to a higher stiffness.

2. Kinematic Modeling

Figure 2 shows the tripod unit under study, and it consists of three fixed-length legs that slide along the guideways. Each leg is connected on one end to the guideway by a revolute joint and on the other end to the moving platform by a spherical joint.

2.1 Kinematic Equations

As shown in Figure 2, the tripod has three independent kinematic loops. Each contains five vectors, $\mathbf{r}_i$ $\mathbf{h}$, $\mathbf{b}_i$, $\mathbf{s}_i$ and $\mathbf{l}_i$ and they satisfy the following equation

$$\mathbf{r}_i + \mathbf{h} = \mathbf{b}_i + \mathbf{s}_i + \mathbf{l}_i \qquad (1)$$

where $\mathbf{r}_i = \mathbf{R}\bar{\mathbf{r}}_i$, $\mathbf{R}$ is the rotation matrix, $\mathbf{h} = [x_c, y_c, z_c]^T$ is the vector representing the position of the moving platform, $\mathbf{b}_i$ is the vector representing the position of the lower end of the *i*th guideway attached to the base, $\mathbf{s}_i$ is the vector representing the displacement along the *i*th guideway, and $\mathbf{l}_i$ is the vector representing the *i*th sliding leg.

It is necessary to point out that for a spatial tripod, the degrees of freedom is 3, while the order of the system is 6. In other words, the tripod still has three linear and three angular movements. However, three of the six movements are dependent. Since the legs are constrained by the revolute joints, this generates three constraint equations, which may be expressed as [7]

$$\mathbf{x}_d = \mathbf{f}(\mathbf{x}_I) \qquad (2)$$

where $\mathbf{x}_I$ and $\mathbf{x}_d$ are independent and

dependent variables.

2.2 Inverse Kinematics

To solve the inverse kinematics, equation (1) is re-written as

$$\mathbf{R}\bar{\mathbf{r}}_i + \mathbf{h} - \mathbf{b}_i - s_i \mathbf{u}_i^s = l_i \mathbf{u}_i^l \qquad (3)$$

where $\mathbf{u}_i^s$ and $\mathbf{u}_i^l$ are the unit vectors of the guideway and leg, respectively. By applying the constraint of the fixed length of the sliding leg, the problem of inverse kinematics can be solved for the following equation

$$\left|\mathbf{R}\bar{\mathbf{r}}_i + \mathbf{h} - \mathbf{b}_i - s_i \mathbf{u}_i^s\right| = l_i \qquad (4)$$

2.3 Jacobian

Taking the time derivative of equation (1) yields

$$\dot{s}_i \mathbf{u}_i^s \cdot \mathbf{l}_i = [\mathbf{v} + (\omega \times \mathbf{R}\bar{\mathbf{r}}_i)] \cdot \mathbf{l}_i \qquad (5)$$

where $\mathbf{v} = [v_x, v_y, v_z]^T$ and $\omega = [\ \omega_x, \omega_y, \omega_z\ ]^T$. Let $\mathbf{t} = [v^T, \omega^T]^T$, equation (5) can be rewritten in the matrix form as

$$\mathbf{B}\dot{\mathbf{s}} = \mathbf{A}\mathbf{t} \qquad (6)$$

where $\dot{\mathbf{s}} = [\dot{s}_1, \dot{s}_2, \dot{s}_3]$ is the vector of the actuator speeds, and **A** and **B** are matrices representing the inverse and forward Jacobian of the mechanism and they are defined as

$$\mathbf{A} = \begin{bmatrix} (\mathbf{u}_1^l)^T & (\mathbf{R}\bar{\mathbf{r}}_1 \times \mathbf{u}_1^l)^T \\ (\mathbf{u}_2^l)^T & (\mathbf{R}\bar{\mathbf{r}}_2 \times \mathbf{u}_2^l)^T \\ (\mathbf{u}_3^l)^T & (\mathbf{R}\bar{\mathbf{r}}_3 \times \mathbf{u}_3^l)^T \end{bmatrix} \qquad (7)$$

$$\mathbf{B} = \mathrm{diag}(\mathbf{u}_1^a \cdot \mathbf{u}_1^l, \mathbf{u}_2^s \cdot \mathbf{u}_2^l, \mathbf{u}_3^s \cdot \mathbf{u}_3^l) \qquad (8)$$

Let

$$\mathbf{J} = \mathbf{B}^{-1}\mathbf{A} \qquad (9)$$

Equation (6) can be rewritten as

$$\dot{\mathbf{s}} = \mathbf{J}\mathbf{t} \qquad (10)$$

As mentioned before, the tripod has only 3 DOF, so this Jacobian **J** is 3 by 6 and cannot be inverted. To take into consideration the constraints, equation (2) is needed. It can be shown that the Jacobian pertaining to the independent variables is in the following form [9]

$$\mathbf{J}_I = \mathbf{B}^{-1}\mathbf{A}\mathbf{M}_1\mathbf{M}_2\mathbf{M}_3 \qquad (11)$$

where $\mathbf{M}_1$ is the transformation matrix between $\dot{\mathbf{x}}$ and **t**, $\mathbf{M}_2$ is a sorting matrix and $\mathbf{M}_3$ is the matrix that relates the dependent velocities to the independent velocities. Jacobain $\mathbf{J}_I$ is 3 by 3 matrix and can be inverted if not singular for the following equation

$$\dot{\mathbf{s}} = \mathbf{J}_I \dot{\mathbf{x}}_I \qquad (12)$$

3. Flexibility Modeling

It can be shown that the wrench **w** acting on the moving platform is related to the moving platform deformation $\delta\mathbf{x}$ as [8]

$$\mathbf{w} = \mathbf{K}\delta\mathbf{x} \qquad (13)$$

where the generalized stiffness matrix **K** is given as

$$\mathbf{K} = \mathbf{J}^T \overline{\mathbf{K}} \mathbf{J} \tag{14}$$

Equation (13) can be re-written in terms of compliance as

$$\delta \mathbf{x} = \mathbf{C}\,\mathbf{w} \tag{15}$$

where **C** is the generalized compliance matrix, and $\mathbf{C} = \mathbf{K}^{-1}$.

It should be noted that for the tripod under study, if there exist several types of flexibilities in the kinematic loops, their compliances should be additive, but not their stiffness. Suppose that stiffness were additive and one of the flexibilities under consideration were dropped, the total system stiffness would be infinite, which obviously is not true. On the other hand, under the compliance addition model, the total system compliance would be reduced, which is reasonable.

In this paper, three types of flexibilities are considered, including axial and bending flexibility in the sliding legs and flexibility in the actuators.

3.1 Leg Axial Compliance Matrix

The compliance matrix considering the leg axial deformation can be obtained as [9]

$$\mathbf{C}_a = \mathbf{J}_a \overline{\mathbf{C}}_a \mathbf{J}_a^{\,T} \tag{16}$$

where

$$\mathbf{J}_a = \mathbf{M}_2 \mathbf{M}_3 \left(\mathbf{J'}_a\right)^{-1} \tag{17}$$

$$\mathbf{J'}_a = \mathbf{A}\mathbf{M}_1\mathbf{M}_2\mathbf{M}_3 \tag{18}$$

$$\overline{\mathbf{C}}_a = \begin{bmatrix} 1/k_a & 0 & 0 \\ 0 & 1/k_a & 0 \\ 0 & 0 & 1/k_a \end{bmatrix} \tag{19}$$

and k_a represents the axial stiffness of the fixed-length leg.

3.2 Leg Bending Compliance Matrix

The compliance matrix considering the leg bending deformation can be obtained as [9]

$$\mathbf{C}_b = \mathbf{J}_b \overline{\mathbf{C}}_b \mathbf{J}_b^{\,T} \tag{20}$$

where

$$\mathbf{J}_b = \mathbf{M}_2 \mathbf{M}_3 \left(\mathbf{J'}_b\right)^{-1} \tag{21}$$

$$\mathbf{J'}_b = \mathbf{A}_b\mathbf{M}_1\mathbf{M}_2\mathbf{M}_3 \tag{22}$$

$$\overline{\mathbf{C}}_b = \begin{bmatrix} 1/k_b & 0 & 0 \\ 0 & 1/k_b & 0 \\ 0 & 0 & 1/k_b \end{bmatrix} \tag{23}$$

and k_b represents the bending stiffness of the fixed-length leg.

3.3 Actuator Compliance Matrix

The compliance matrix considering the actuator deformation can be obtained as [9]

$$\mathbf{C}_t = \mathbf{J}_t \overline{\mathbf{C}}_t \mathbf{J}_t^{\,T} \tag{24}$$

where

$$\mathbf{J}_t = \mathbf{M}_2 \mathbf{M}_3 \left(\mathbf{J'}_t\right)^{-1} \tag{25}$$

$$\mathbf{J'}_t = \mathbf{B}^{-1}\mathbf{A}\mathbf{M}_1\mathbf{M}_2\mathbf{M}_3 \tag{26}$$

$$\overline{\mathbf{C}}_t = \begin{bmatrix} 1/k_t & 0 & 0 \\ 0 & 1/k_t & 0 \\ 0 & 0 & 1/k_t \end{bmatrix} \tag{27}$$

and k_t represents the actuator stiffness.

3.4 Total Compliance Matrix

The total system compliance matrix is the addition of three compliance matrices

$$\mathbf{C} = \mathbf{C}_a + \mathbf{C}_b + \mathbf{C}_t \qquad (28)$$

3.5 Compliance Mapping

The compliance map shows the compliance changes over the workspace. Usually, the diagonal values of the compliance matrix are used which represent the deformation caused by the forces and moments along and about the Cartesian coordinates [8]. Figure 3 shows a typical compliance mapping of the tripod.

3.6 Global Compliance

The global compliance is characterized by an index over the entire workspace. Since the compliance changes inside of the workspace, the mean value and standard deviation of the trace of the compliance matrix may be used to evaluate the compliance and its variation over the workspace. These two measures are defined as

$$\mu = \text{mean}(\text{trace}(\mathbf{C})) \qquad (29)$$

$$\sigma = \text{std}(\text{trace}(\mathbf{C})) \qquad (30)$$

The mean value represents the average compliance of the tripod over the workspace, while the standard deviation indicates the compliance fluctuation relative to the mean value. In general, the lower the mean value the less deformation, and the lower the standard deviation the more uniform the flexibility distribution over the workspace.

4. Optimization

4.1 Generic Algorithms (GA)

For the tripod under study, optimization involved finding the optimal workspace and stiffness. The method of generic algorithms is applied for optimization.

Genetic algorithms start with a set of solutions (represented by chromosomes) called population. Solutions from one population are taken and used to form a new population. This is motivated by a hope that the new population will be better than the old one. The solutions chosen to form new solutions (offspring) are selected according to their fitness - the more suitable they are the better chances they will reproduce.

4.2 Basic Procedure of GA

Genetic algorithms consist of following basic operations:

1. *Initial population* - generate random population of n chromosomes (suitable solutions for the problem)
2. *Fitness* - evaluate the fitness of each chromosome in the population
3. *New population* - create a new population by repeating following steps until the new population is complete
4. *Selection* - select two parent chromosomes from a population according to their fitness (the better the fitness, the bigger chance to be selected)
5. *Crossover* - with a crossover probability, cross over the parents to form new offspring (children). If no crossover is performed, offspring are an exact copy of parents.
6. *Mutation* - with a mutation probability mutate new offspring at each locus (position in chromosome).
7. *Accepting* - place new offspring in a new

population
8. *Replacing* – use new generated population for a further run of algorithm
9. *Test* - if the end condition is satisfied, stop, and return the best solution in the current population
10. *Loop* - go to step 2

4.3 Implementation

There are five basic structural parameters for this tripod: base radius R_b, movable platform radius R_p, leg length L, guideway length S_{max}, and the angle between guideway and base β. In this optimization, R_b and S_{max} are fixed as constants (R_b = 141.76mm, S_{max} = 95.25mm), but R_p, L and β are variables. The vector of optimization variables is therefore

$$\mathbf{o} = [\, R_p, L, \beta \,] \qquad (31)$$

Their bounds are $R_p \in [75, 85]$ mm, $L \in [200, 230]$ mm, $\beta \in [65, 75]$ degree. There are three stiffness constants, $k_a = k_b = k_t = 1000$ N/mm.

The optimization variables are encoded into 30 bit binary numbers. The Roulette wheel method is adopted as the selection method. Crossover possibility P_c is 0.85, mutation possibility P_m is 0.0075, population size is 30 and maximum generation size is 100.

The objective of optimization is to achieve the maximum workspace and minimum compliance.

For workspace, the minimum reachable yaw angle [10] is chosen to evaluate the workspace size, since the tool attached to the tripod is required to orient freely in a cone with a certain apex angle. For compliance, the trace of the global compliance matrix is used. Combining the two, the fitness equation can be expressed as

$$f_i = W_\mu / \mu_i + W_\theta \theta_i \qquad (32)$$

where μ_i represents the average compliance trace for the *i*th population; θ_i represents the minimum reachable yaw angle for the *i*th population; and W_μ and W_θ are weighting factors.

If only the workspace is of concern, then $W_\mu = 0$. If only the stiffness is of concern, then $W_\theta = 0$.

4.4 Results

Table 1 shows the results of the compliance optimization. After adjustment of the structural variables, both the mean value and the standard deviation of the system compliance were reduced, meaning that the stiffness is increased and its variation over the whole workspace is decreased. The improvement of the stiffness is about 16%. However, the workspace after compliance optimization becomes smaller. Figure 4 shows the fitness statistics.

Table 2 shows the results of the workspace optimization. After adjustment of the structural variables, the workspace size is significantly enlarged, but the mean value and the standard deviation of the system compliance is increased. This indicates that the stiffness is decreased and its variation over the whole workspace is increased. The improvement of the workspace size is about 94%. Figure 5 shows the fitness statistics.

Though the workspace size and the stiffness can be improved, the workspace size is more

sensitive to structural parameters. The results also show that the workspace size and the stiffness cannot be optimized at the same time. Larger workspace always results in higher compliance (lower stiffness).

5. Conclusions

In this paper a parametric kinematic model is developed and constrained kinematic equations are derived. Based on this, a flexibility model is established considering the flexibility in the sliding legs and the actuators. A global index is introduced to characterize the tripod's compliance over the workspace. The method of Generic Algorithms is applied for structural optimization. Results of optimization show that a tripod unit with a smaller workspace would lead to a higher stiffness.

References

1. Lauffer, T. Hinnerichs, C. Kuo, P. Wada, B. Ewaldz, B. Winfough, and N. Shankar, 1996, "Milling Machine for the 21st Century - Goals, Approach, Characterization and Modeling," *Proceedings of SPIE – The International Society for Optical Engineering Smart Structures Technologies*, Vol. 2721, pp. 326-340.
2. J. Hollingum, 1997, "Features: Hexapods to Take Over?" *Industrial Robot*, Vol. 24, pp. 428-431.
3. M. Valenti, 1995, "Machine Tools Get Smarter," *ASME Journal of Mechanical Engineering*, Vol. 117, pp. 70-75.
4. D. Zhang and C.M. Gosselin, 2001, "Kinetostatic Analysis and Optimization of the Tricept Machine Tool Family," *Proceedings of Year 2000 Parallel Kinematic Machines International Conference*, Ann Arbor, Michigan, pp. 174-188.
5. J. Lewis, 2000, "Tripod-Mounted Spindle Targets Monolithic Parts," *Design News*, pp. 54-58.
6. H.K. Tünshoff, R. Grendel, and R. Kaak, 1999, *Structure and Characteristics of the Hybrid Manipulator Georg V, Parallel Kinematic Machines - Theoretical Aspects and Industrial Requirements*, edited by C.R. Boër, L. Molinari-Tosatti, and K.S. Smith, Springer, pp. 365-376.
7. F. Xi, W. Han, M. Verner, and A. Ross, 2000, "Development of a Sliding-Leg Tripod as an Add-on Device for Manufacturing," *Robotica*, Vol. 19, No. 3, pp. 285-294.
8. D. Zhang, 2000, *Kinetostatic Analysis and Optimization of Parallel and Hybrid Architectures for Machine Tools*, Ph.D. Thesis, Laval University.
9. Z. Xu, 2001, *Kinetostatic Analysis and Optimization of a Sliding-Leg Tripod*, M.E.Sc. Thesis, The University of Western Ontario.
10. T. Huang, J. Wang, C.M. Gosselin, and D.J. Whitehouse, 2000, "Kinematic Synthesis of Hexapods with Specified Orientation Capability and Well-Conditioned Dexterity," *SME Journal of Manufacturing Processes*, Vol. 2, No. 1, pp. 36-47.

Table 1. Compliance optimization results.

	Structural Variables			Workspace	Compliance	
	R_p (mm)	L (mm)	β (deg.)	θ (deg.)	μ (mm/N)	σ (mm/N)
Initial	75	200	65	35.0496	**0.006572**	**0.001443**
Optimized	84.2953	229.7621	74.9241	20.5907	**0.005545**	**0.000316**
Constraint	θ >20					

Table 2. Workspace optimization results.

	Structural Variables			Workspace	Compliance	
	R_p (mm)	L (mm)	β (deg.)	θ (deg.)	μ (mm/N)	σ (mm/N)
Initial	85	230	75	**17.0604**	0.005545	0.000316
Optimized	82.2788	225.3975	69.6152	**31.4749**	0.005552	0.000333
Constraint	μ<0.006					

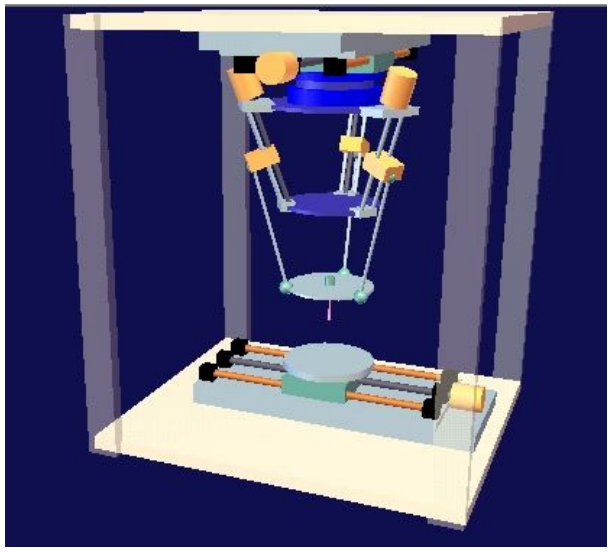

Figure 1 A hybrid machine combining a tripod with a gantry.

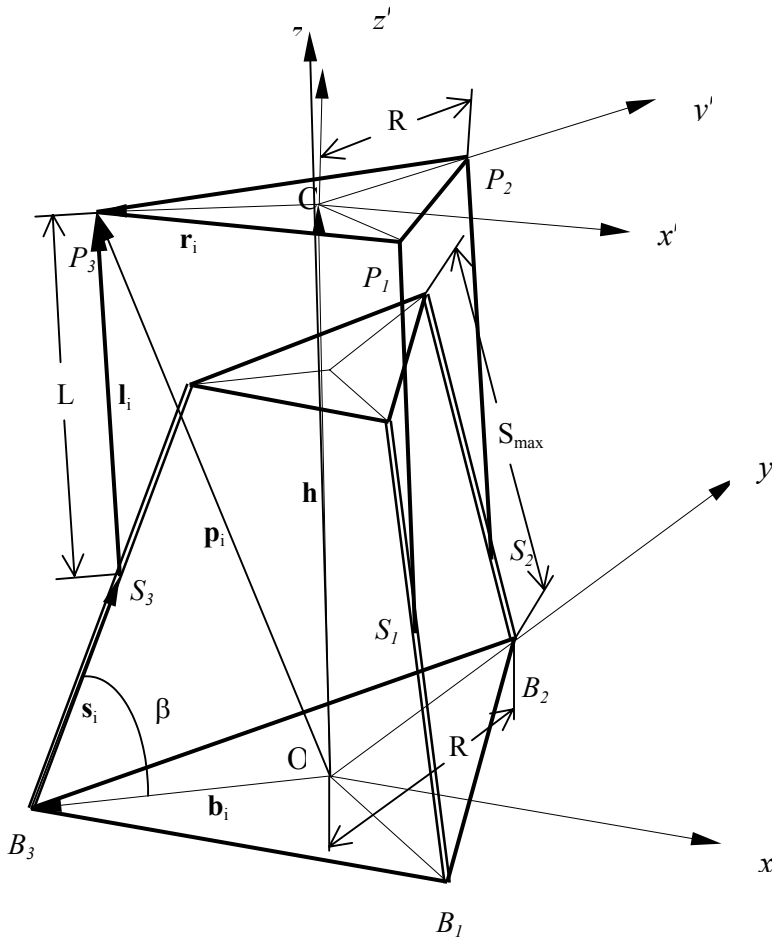

Figure 2 Schematic of a tripod

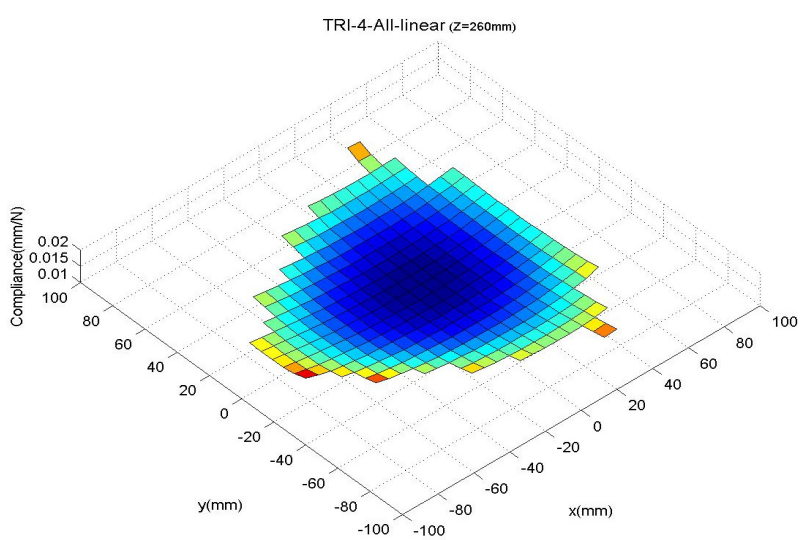

Figure 3 Compliance mapping

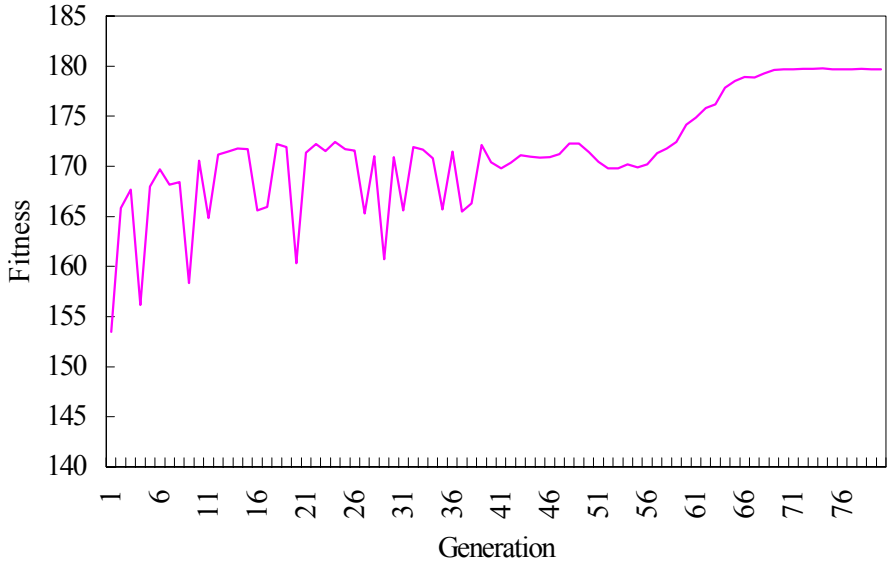

Figure 4 Fitness statistics for compliance optimization

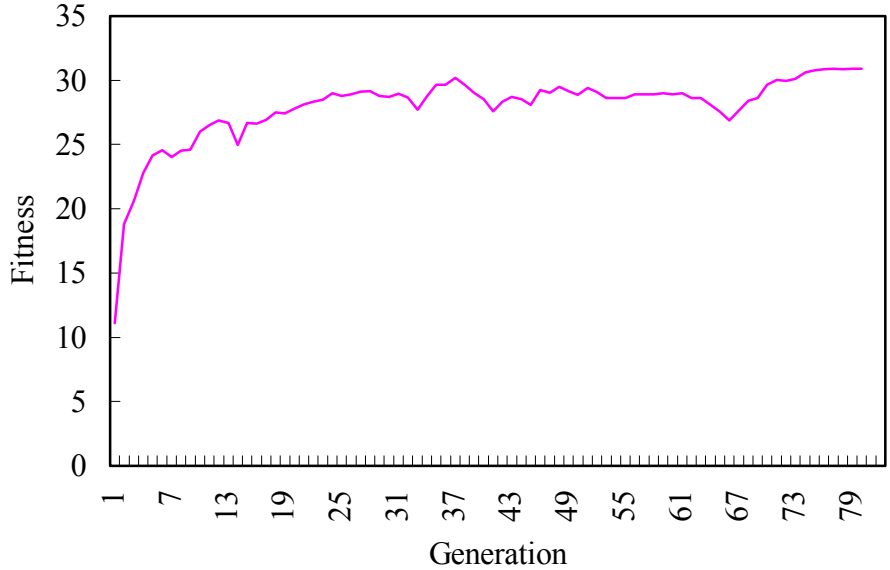

Figure 5 Fitness statistics for workspace optimization

Proceedings of the WORKSHOP on
Fundamental Issues and Future Research Directions for Parallel Mechanisms and Manipulators
October 3–4, 2002, Quebec City, Quebec, Canada
Clément M. Gosselin and Imme Ebert-Uphoff, editors

Planar Point & Line Transformation with Blaschke-Grünwald Image Space Coordinates

PAUL ZSOMBOR-MURRAY
Centre for Intelligent Machines and Department of Mechanical Engineering
Montréal, (Québec), Canada, H3A 2K6
paul@cim.mcgill.ca

Abstract:

This is very much a "work in progress". The intent is to explain, in a clear and simple way, what kinematic mapping is in terms of elementary homogeneous matrix transformations which "move" points and lines in the plane. Relationship of the image space coordinates to the pole of displacement, the invariant point of a planar motion, is derived.

1 Notions

For planar displacements consider the transformations which express the homogeneous coordinates of points and lines in the moving, end effector frame EE premultiplied by a transformation matrix and converted to their homogeneous coordinates in the fixed frame FF. Points are transformed as

$$\begin{bmatrix} w \\ x \\ y \end{bmatrix} = \begin{bmatrix} a_{11} & a_{12} & a_{13} \\ a_{21} & a_{22} & a_{23} \\ a_{31} & a_{32} & a_{33} \end{bmatrix} \begin{bmatrix} t \\ u \\ v \end{bmatrix}$$

Lines are transformed as

$$\begin{bmatrix} W \\ X \\ Y \end{bmatrix} = \begin{bmatrix} A_{11} & A_{12} & A_{13} \\ A_{21} & A_{22} & A_{23} \\ A_{31} & A_{32} & A_{33} \end{bmatrix} \begin{bmatrix} T \\ U \\ V \end{bmatrix}$$

The coefficients will be evaluated by using three ideal elements in the EE frames and their corresponding coordinates in FF. Then these coefficients will be converted and expressed in terms of four homogeneous Blaschke-Grünwald coordinates, a mapping in the kinematic image space. This is an abstract projective 3-space wherein a point represents a displacment of a rigid body in the plane.

$$\begin{aligned} &\{X_0 : X_1 : X_2 : X_3\} \\ \equiv\ &\{2\cos\frac{\phi}{2} : a\sin\frac{\phi}{2} - b\cos\frac{\phi}{2} : \\ &a\cos\frac{\phi}{2} + b\sin\frac{\phi}{2} : 2\sin\frac{\phi}{2}\} \end{aligned}$$

2 The Point Transformation

Ideal point elements are chosen as the origin,

$$\lambda \begin{bmatrix} 1 \\ a \\ b \end{bmatrix} = \begin{bmatrix} a_{11} & a_{12} & a_{13} \\ a_{21} & a_{22} & a_{23} \\ a_{31} & a_{32} & a_{33} \end{bmatrix} \begin{bmatrix} 1 \\ 0 \\ 0 \end{bmatrix} \Rightarrow$$

$$a_{11} = \lambda, \quad a_{21} = \lambda a, \quad a_{31} = \lambda b$$

the point at infinity which closes the x-axis,

$$\lambda \begin{bmatrix} 0 \\ \cos\phi \\ \sin\phi \end{bmatrix} = \begin{bmatrix} a_{11} & a_{12} & a_{13} \\ a_{21} & a_{22} & a_{23} \\ a_{31} & a_{32} & a_{33} \end{bmatrix} \begin{bmatrix} 0 \\ 1 \\ 0 \end{bmatrix} \Rightarrow$$

$$a_{12} = 0, \quad a_{22} = \lambda\cos\phi, \quad a_{32} = \lambda\sin\phi$$

and the point at infinity which closes the y-axis,

$$\lambda \begin{bmatrix} 0 \\ -\sin\phi \\ \cos\phi \end{bmatrix} = \begin{bmatrix} a_{11} & a_{12} & a_{13} \\ a_{21} & a_{22} & a_{23} \\ a_{31} & a_{32} & a_{33} \end{bmatrix} \begin{bmatrix} 0 \\ 0 \\ 1 \end{bmatrix} \Rightarrow$$

$$a_{13} = 0, \quad a_{23} = -\lambda\sin\phi, \quad a_{33} = \lambda\cos\phi$$

where λ is an arbitrary constant. Populating $[a_{ij}]$ with these results and making the tangent half-angle substitutions

$$\cos\phi = \frac{1-\tan^2\frac{\phi}{2}}{1+\tan^2\frac{\phi}{2}}, \quad \sin\phi = \frac{2\tan\frac{\phi}{2}}{1+\tan^2\frac{\phi}{2}}$$

and multiplying through by $(1+\tan^2\frac{\phi}{2})$, then by $\cos^2\frac{\phi}{2}$ produce

$$[a_{ij}] = \lambda \begin{bmatrix} (\cos^2\frac{\phi}{2}+\sin^2\frac{\phi}{2}) & 0 & 0 \\ a(\cos^2\frac{\phi}{2}+\sin^2\frac{\phi}{2}) & (\cos^2\frac{\phi}{2}-\sin^2\frac{\phi}{2}) & -2\cos\frac{\phi}{2}\sin\frac{\phi}{2} \\ b(\cos^2\frac{\phi}{2}+\sin^2\frac{\phi}{2}) & 2\cos\frac{\phi}{2}\sin\frac{\phi}{2} & (\cos^2\frac{\phi}{2}-\sin^2\frac{\phi}{2}) \end{bmatrix}$$

which becomes, after substitution for $\{X_0 : X_1 : X_2 : X_3\}$ and simplifying and dividing through by 4.

$$[a_{ij}] = \begin{bmatrix} X_0^2 + X_3^2 & 0 & 0 \\ 2(X_0X_2 + X_1X_3) & X_0^2 - X_3^2 & -2X_0X_3 \\ -2(X_0X_1 - X_2X_3) & 2X_0X_3 & X_0^2 - X_3^2 \end{bmatrix}$$

This is easily inverted and after multiplying by $(X_0^2 + X_3^2)^2$

$$[a_{ij}]^{-1} = \begin{bmatrix} X_0^2 + X_3^2 & 0 & 0 \\ -2(X_0X_2 - X_1X_3) & X_0^2 - X_3^2 & 2X_0X_3 \\ 2(X_0X_1 + X_2X_3) & -2X_0X_3 & X_0^2 - X_3^2 \end{bmatrix}$$

The metric is obtained as $[a_{ij}][a_{ij}]^{-1}$.

$$\begin{bmatrix} (X_0^2 + X_3^2)^2 & 0 & 0 \\ 0 & (X_0^2 + X_3^2)^2 & 0 \\ 0 & 0 & (X_0^2 + X_3^2)^2 \end{bmatrix}$$

3 The Line Transformation

Ideal line elements are chosen. The first is the invariant line at infinity.

$$\lambda \begin{bmatrix} 1 \\ 0 \\ 0 \end{bmatrix} = \begin{bmatrix} A_{11} & A_{12} & A_{13} \\ A_{21} & A_{22} & A_{23} \\ A_{31} & A_{32} & A_{33} \end{bmatrix} \begin{bmatrix} 1 \\ 0 \\ 0 \end{bmatrix} \Rightarrow$$

$$A_{11} = \lambda, \quad A_{21} = 0, \quad A_{31} = 0$$

Then the coordinates of the x-axis in FF are formed with the origin and the point at infinity.

$$\begin{vmatrix} w & x & y \\ 1 & a & b \\ 0 & \cos\phi & \sin\phi \end{vmatrix} \Rightarrow$$

$$\{a\sin\phi - b\cos\phi : -\sin\phi : \cos\phi\}$$

$$\lambda \begin{bmatrix} a\sin\phi - b\sin\phi \\ -\sin\phi \\ \cos\phi \end{bmatrix} = \begin{bmatrix} A_{11} & A_{12} & A_{13} \\ A_{21} & A_{22} & A_{23} \\ A_{31} & A_{32} & A_{33} \end{bmatrix} \begin{bmatrix} 0 \\ 0 \\ 1 \end{bmatrix} \Rightarrow$$

$$A_{13} = \lambda(a\sin\phi - b\cos\phi), \quad A_{23} = -\lambda\sin\phi, \quad A_{33} = \lambda\cos\phi$$

Finally the coordinates of the y-axis in FF are found with the origin and the point at infinity.

$$\begin{vmatrix} w & x & y \\ 1 & a & b \\ 0 & -\sin\phi & \cos\phi \end{vmatrix} \Rightarrow$$

$$\{a\cos\phi + b\sin\phi : -\cos\phi : -\sin\phi\}$$

$$\lambda \begin{bmatrix} a\cos\phi + b\sin\phi \\ -\cos\phi \\ -\sin\phi \end{bmatrix} = \begin{bmatrix} A_{11} & A_{12} & A_{13} \\ A_{21} & A_{22} & A_{23} \\ A_{31} & A_{32} & A_{33} \end{bmatrix} \begin{bmatrix} 0 \\ -1 \\ 0 \end{bmatrix} \Rightarrow$$

$$A_{12} = -\lambda(a\cos\phi + b\sin\phi), \quad A_{22} = \lambda\cos\phi, \quad A_{32} = \lambda\sin\phi$$

Note $U = -1$ making line normal in EE compatible with that in FF. Populating $[A_{ij}]$ with these results and making the tangent half-angle substitutions and multiplying through by $(1+\tan^2\frac{\phi}{2})$, then by $\cos^2\frac{\phi}{2}$ produce

$$[A_{ij}] = \lambda \begin{bmatrix} \cos^2\frac{\phi}{2} + \sin^2\frac{\phi}{2} & -a(\cos^2\frac{\phi}{2} + \sin^2\frac{\phi}{2}) + 2b\cos\frac{\phi}{2}\sin\frac{\phi}{2} & 2a\cos\frac{\phi}{2}\sin\frac{\phi}{2} - b(\cos^2\frac{\phi}{2} - \sin^2\frac{\phi}{2}) \\ 0 & \cos^2\frac{\phi}{2} - \sin^2\frac{\phi}{2} & -2\cos\frac{\phi}{2}\sin\frac{\phi}{2} \\ 0 & 2\cos\frac{\phi}{2}\sin\frac{\phi}{2} & \cos^2\frac{\phi}{2} - \sin^2\frac{\phi}{2} \end{bmatrix}$$

which, after substitution for $\{X_0 : X_1 : X_2 : X_3\}$, simplification and dividing through by 4, becomes

$$[A_{ij}] = \begin{bmatrix} X_0^2 + X_3^2 & -2(X_0X_2 - X_1X_3) & 2(X_0X_1 + X_2X_3) \\ 0 & X_0^2 - X_3^2 & -2X_0X_3 \\ 0 & 2X_0X_3 & X_0^2 - X_3^2 \end{bmatrix}$$

This is easily inverted and after multiplying by $(X_0^2 + X_3^2)^2$

$$[A_{ij}]^{-1} = \begin{bmatrix} X_0^2 + X_3^2 & 2(X_0X_2 + X_1X_3) & -2(X_0X_1 - X_2X_3) \\ 0 & X_0^2 - X_3^2 & 2X_0X_3 \\ 0 & -2X_0X_3 & X_0^2 - X_3^2 \end{bmatrix}$$

Then the metric

$$[A_{ij}][A_{ij}]^{-1} = [a_{ij}][a_{ij}]^{-1}$$

It is noted with satisfaction that $[A_{ij}] = [[a_{ij}]^{-1}]^T$.

4 Examples

Examining Fig. 1, one sees a coordinate frame pair with

$$a = 8, \quad b = 12, \quad \cos\frac{\phi}{2} = \sqrt{0.9}, \quad \sin\frac{\phi}{2} = \sqrt{0.1}$$

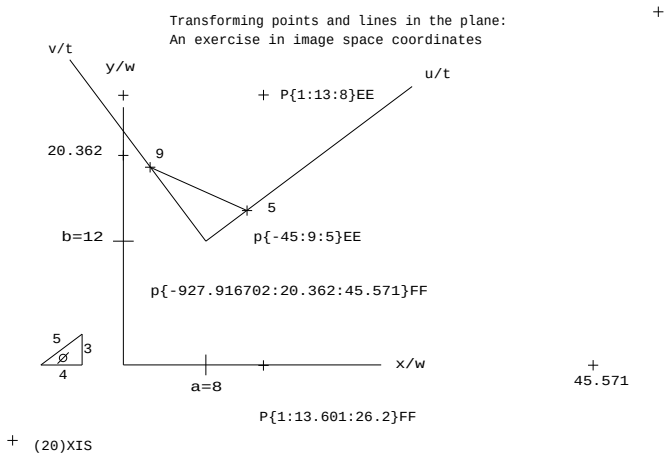

Figure 1: *Frames and Elements*

Substituting these in the definitions of the image space coordinates and dividing by $2\sqrt{0.1}$

$$\{X_0 : X_1 : X_2 : X_3\} = \{3 : -14 : 18 : 1\}$$

Then for the point P

$$[a_{ij}] = \begin{bmatrix} 3^2+1^2 & 0 & 0 \\ 2(3\times 18 - 14\times 1) & 3^2-1^2 & -2\times 3\times 1 \\ -2(-3\times 14 - 18\times 1) & 2\times 3\times 1 & 3^2-1^2 \end{bmatrix}$$

Calculating $[a_{ij}]$ and dividing by 2 and using the point P in frame EE

$$\begin{bmatrix} 1 \\ 13.6 \\ 26.2 \end{bmatrix} = \begin{bmatrix} 5 \\ 68 \\ 131 \end{bmatrix} = \begin{bmatrix} 5 & 0 & 0 \\ 40 & 4 & -3 \\ 60 & 3 & 4 \end{bmatrix} \begin{bmatrix} 1 \\ 13 \\ 8 \end{bmatrix}$$

Then for the line p

$$[A_{ij}] = \begin{bmatrix} 3^2+1^2 & -2(3\times 18 + 14\times 1) & 2(-3\times 14 + 18\times 1) \\ 0 & 3^2-1^2 & -2\times 3\times 1 \\ 0 & 2\times 3\times 1 & 3^2-1^2 \end{bmatrix}$$

Calculating $[A_{ij}]$ and dividing by 2 and using the line p in frame EE

$$\begin{bmatrix} -957 \\ 21 \\ 47 \end{bmatrix} = \begin{bmatrix} 5 & -68 & -24 \\ 0 & 4 & -3 \\ 0 & 3 & 4 \end{bmatrix} \begin{bmatrix} -45 \\ 9 \\ 5 \end{bmatrix}$$

5 Pole, Half-Angle and Image Space Coordinates

The homogeneous image space coordinates of planar kinematic mapping may be derived using the following parameters which descibe planar displacement of a rigid body. Refer to Fig. 2.

- Cartesian coordinates of a reference point, say, the origin $(0,0)$ in FF which is $(0,0)$ in EE and becomes (a,b) under displacement in FF and
- The angle ϕ between any line in FF and its image in EE after displacement

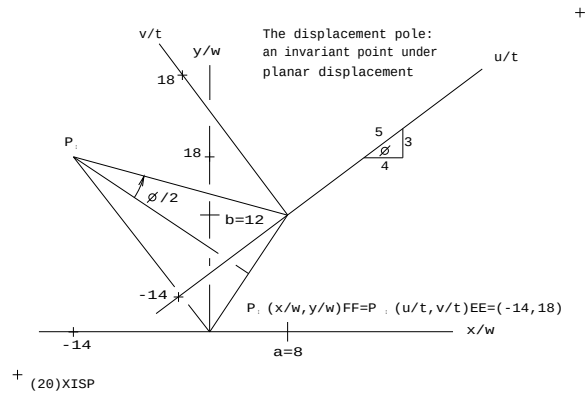

Figure 2:- *Displacement Pole, P_I*

Notice that the Cartesian coordinates of a point P_I, the displacement pole, may be expressed in terms of a, b, ϕ and these coordinates are identical in FF and EE.

$$P_I(x/w, y/w) = P_I(u/t, v/t) = \left(\frac{a}{2} - \frac{b}{2}\cot\frac{\phi}{2}, \frac{a}{2}\cot\frac{\phi}{2} + \frac{b}{2}\right)$$

The homogeneous coordinates of P_I in FF are $\{w : x : y\}$ and in EE they are $\{t : u : v\}$. In terms of a, b, ϕ the Cartesian coordinates of P_I may be homogenized as

$$\left\{\frac{a}{2} - \frac{b}{2}\cot\frac{\phi}{2} : \frac{a}{2}\cot\frac{\phi}{2} + \frac{b}{2} : 1\right\}$$

It does not matter that the ordering has been circular left shifted as $\{u : v : t\}$ and $\{x : y : w\}$ in the representation above. This reordering has been done to minimize subsequent sequence shuffling below while proceeding to the ultimate goal to present the homogeneous planar image space coordinates, ordered as they were initially introduced. But these are just the coordinates of an ordinary *point*. A point in the Cartesian kinematic image space, which must have three coordinates to represent the three degrees of freedom of displacement in the plane, is obtained by dividing by $\cot\frac{\phi}{2}$.

$$\left(\frac{a}{2}\tan\frac{\phi}{2} - \frac{b}{2}, \frac{a}{2} + \frac{b}{2}\tan\frac{\phi}{2}, \tan\frac{\phi}{2}\right)$$

To make this a projective 3-space, four homogeneous coordinates are required

$$\left\{1 : \frac{a}{2}\tan\frac{\phi}{2} - \frac{b}{2} : \frac{a}{2} + \frac{b}{2}\tan\frac{\phi}{2} : \tan\frac{\phi}{2}\right\}$$

Multiplying by $2\cos\phi$ produces the image space coordinates

$$\begin{aligned}&\{X_0 : X_1 : X_2 : X_3\}\\ \equiv\ &\{2\cos\frac{\phi}{2} : a\sin\frac{\phi}{2} - b\cos\frac{\phi}{2} :\\ &a\cos\frac{\phi}{2} + b\sin\frac{\phi}{2} : 2\sin\frac{\phi}{2}\}\end{aligned}$$

One may conduct the following simple verification upon the example shown in Fig. 2.

$$a = 8,\ \ b = 12,\ \ \cos\frac{\phi}{2} = \sqrt{0.9},\ \ \sin\frac{\phi}{2} = \sqrt{0.1},\ \ \cot\frac{\phi}{2} = 3$$

$$\left(\frac{a}{2} - \frac{b}{2}\cot\frac{\phi}{2}, \frac{a}{2}\cot\frac{\phi}{2} + \frac{b}{2}\right)$$

$$= \left(\frac{8}{2} - \frac{12}{2}\times 3, \frac{8}{2}\times 3 + \frac{12}{2}\right) = (-14, 18)$$

6 Conclusion

Recently planar kinematic mapping has been applied with very encouraging results to

- A unified approach to solving, in compact symbolic form, the direct kinematics of all posible varieties of three-legged parallel platforms, (Zsombor-Murray *et al.*, 2002),

- Solving the five precision pose design problem (Hayes & Zsombor-Murray, 2002) using a general algorithm which, when formulated in the projective image space, will reveal the mechanism, whether two-joint dyad, revolute four-bar, slider-crank or even elliptical trammel, without resort to separate formulation as documented in (McCarthy, 2000).

The purpose of this short article is to describe, once again, the nature of the projective planar image space; possibly in a more simple way, palatable to a wider audience of engineering kinematicians who are yet reluctant to adapt these methods to their own research and teaching. To those, who feel that the field of planar kinematics is a well worked over field with little new to offer, it is submitted that a similar rework of spherical and spatial mapping will help us to effectively attack more challenging problems.

Acknowledgment

This research is supported by grants NSERC 139964, National Sciences and Engineering Research Council and FCAR ER73234, Fonds pour la Formations des Chercheurs et l'Aide à la Recherche.

References

Zsombor-Murray, P.J., Chao, C. & Hayes, M.J.D., 2002, "Direct Planar Kinematic Mapping for General Planar Parallel Manipulators", *Proc. CSME Forum 2002*, abstract ISBN 0-9730900-0-6, p.24a and article CD ISBN 0-9730900-0-4, 8pp.

Hayes, M.J.D. & Zsombor-Murray, P.J., 2002, "Solving the Burmester Problem Using Kinematic Mapping", *Proc. ASME DETC/CIE'02*, 7.pp (accepted)

McCarthy, J.M., 2000, *Geometric Design of Linkages*, ISBN 0-387-98983-8, Ch.5, pp.86-115.

Regular Papers: Dynamics

Friday, October 4, 2002, 3:00PM

Session Chairs: J. McPhee and J. Angeles

1. Y. Wu, C.M. Gosselin
   "On the Synthesis of a Reactionless 6-DOF Parallel Mechanism Using Planar Four-Bar Linkages".

2. W.A. Khan, V. Krovi
   "Comparison of Two Alternate Methods for Distributed Forward Dynamic Simulation of a Four-Bar Linkage".

3. I. Ebert-Uphoff, K. Kozak
   "Review of the Role of Quasi-Coordinates for the Kinematic and Dynamic Modeling of Parallel Manipulators".

4. J. Kövecses, J-C. Piedboeuf, C. Lange
   "Methods for Dynamic Models of Parallel Robots and Mechanisms".

5. T. Geike, J. McPhee
   "On the Automatic Generation of Inverse Dynamic Solutions for Parallel Manipulators with Full and Reduced Mobility".

Proceedings of the WORKSHOP on
Fundamental Issues and Future Research Directions for Parallel Mechanisms and Manipulators
October 3–4, 2002, Quebec City, Quebec, Canada
Clément M. Gosselin and Imme Ebert-Uphoff, editors

ON THE SYNTHESIS OF A REACTIONLESS 6-DOF PARALLEL MECHANISM USING PLANAR FOUR-BAR LINKAGES

YANGNIAN WU
Département de Génie Mécanique
Université Laval
Québec, Québec, Canada, G1K 7P4
wu@gmc.ulaval.ca

CLÉMENT M. GOSSELIN
Département de Génie Mécanique
Université Laval
Québec, Québec, Canada, G1K 7P4
gosselin@gmc.ulaval.ca

Abstract: *This paper addresses the synthesis of a novel reactionless spatial 6-DOF parallel mechanism using four-bar linkages without any counter-rotations. The mechanism is first described and its kinematics is discussed. A numerical example of the reactionless 6-DOF mechanism is given in this paper and, with the help of the dynamic simulation software ADAMS, it is shown that the mechanism is reactionless for any trajectory.*

1 Introduction

Parallel mechanisms are defined as architectures in which the moving payload is connected to the fixed base by multiple kinematic chains. Each chain can be considered as one mechanism and is a system with several bars, joints and a base.

Parallel mechanisms are excellent candidates for advanced robotic applications by virtue of their low moving inertia, high stiffness, high dexterity, compact size and high power to weight ratio. However, similarly to other robotic devices, they exert forces and moments on their base while moving, causing fatigue, vibration, noise and perturbations in the supporting structure of the mechanism.

A mechanism is said to be *reactionless or dynamically balanced* if, for any motion of the mechanism, there is no reaction force and moment at its base at all times. Since dynamic balancing is always accompanied with static balancing, dynamic balancing means actually both static and dynamic balancing.

The balancing of mechanisms has been an important research topic for several decades (Berkof and Lowen, 1969; Lowen *et al.* , 1983; Dresig *et al.* , 1998; Kochev, 2000). Extensive studies on the dynamic balancing of planar linkages (Berkof, 1973; Kochev, 1990a; Bagci, 1992; Gao, 1989) and some research works related to the complete balancing of spatial linkages with only one degree of freedom (Bagci, 1983; Yu, 1987a,b) have been presented in the literature. Some authors have addressed the trajectory planning of manipulators in order to generate reactionless trajectories or minimize disturbances (Papadopoulos and Abu-Abed, 1996; Papadopoulos and Dubowsky, 1991; Kochev, 1990b; Dubowsky and Torres, 1991; Legnani *et al.* ,1999). However, the approaches based on trajectory planning are only suitable for some special applications. In order to obtain dynamically balanced mechanisms, some authors have used counter-rotations — additional mechanisms designed to balance the shaking moments of the mechanisms— such as additional balancing links (dyads, triads or idler loops), fixed-axis-gear-inertia counterweights and planetary-gear-train-inertia counterweights (Bagci, 1982, 1992; Yu, 1987a, 1988; Gao, 1989, 1991; Ye and Smith, 1994). However, adding counter-rotations to a mechanism increases its complexity and can reduce its practicality significantly. To avoid the use of counter-rotations for the complete balancing of parallel mechanisms, Ricard and Gosselin (2000) have focused on a planar 4-bar linkage and obtained the complete balancing of the linkage in the plane as a set of constraints on the geometric and inertial parameters of the links. The dynamically balanced 4-bar linkages without any counter-rotation have been stacked up to synthesize reactionless planar 3-DOF parallel mechanisms (Ricard and Gosselin, 2000) and reactionless spatial 3-DOF parallel mechanisms (Cote *et al.* , 2001). However, since the reactionless four-bar linkages are effective in a plane, the stacked reactionless mechanisms — used as legs to synthesize planar or spatial 3-DOF mechanisms — can only move in that plane. Hence, these reactionless four-bar linkages cannot be directly used to synthesize reactionless spatial 6-DOF mechanisms. Wu and Gosselin (2002) have obtained dynamically balanced four-bar linkages undergoing spatial motion and synthesized a reactionless spatial 3-DOF mechanism which can be used for the development of spatial reactionless multi-degree-of-freedom — having up to 6-DOF — mechanisms or manipulators.

In this paper, two basic reactionless planar four-bar linkage mechanisms are first introduced. A spatial 6-DOF parallel mech-

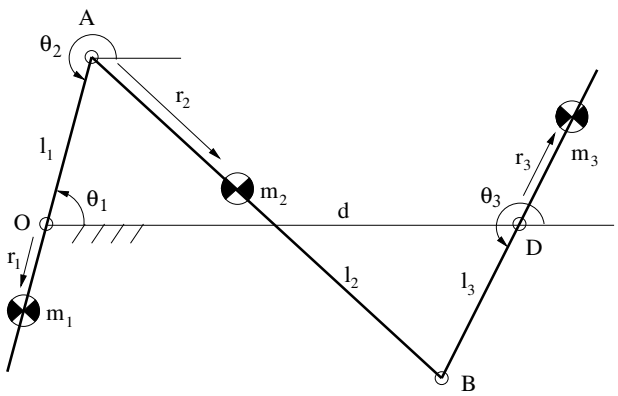

Figure 1: Planar reactionless four-bar linkage.

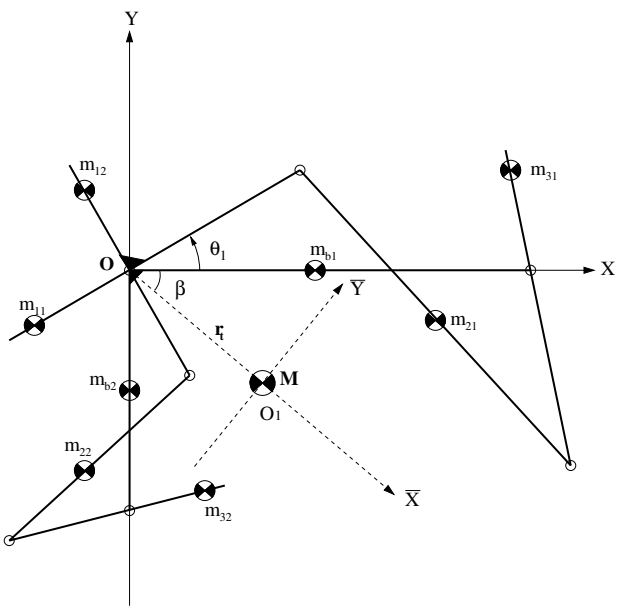

Figure 2: Composite mechanism with a pair of reactionless four-bar linkages.

anism using four-bar linkages without any counter-rotations is then synthesized. The geometry of the mechanism is briefly introduced and the solutions of its kinematic problems are outlined. Finally, a numerical example of the reactionless 6-DOF mechanism is given and the dynamic simulation software ADAMS is used to show the reactionless property of the mechanism.

2 Basic Reactionless Planar Four-Bar Linkage Mechanisms Without Counter-rotations

In the literature, two basic mechanisms — a single planar dynamically balanced four-bar linkage and a planar composite mechanism with a pair of dynamically balanced four-bar linkages — have been presented (Ricard and Gosselin, 2000; Wu and Gosselin, 2002). For a single planar four-bar linkage (Fig. 1), the conditions for dynamic balancing in the plane are written as follows:

$$\begin{aligned} \epsilon = -1,\ d = l_2,\ l_3 = l_1, \\ r_2 = l_2(1 - \frac{m_1 r_1}{m_2 l_1}),\ r_3 = \frac{m_2 r_2 l_3}{m_3 l_2}, \\ k_2 = \sqrt{\frac{m_2 r_2 (l_2 - r_2) - m_1 k_1^2 - m_1(r_1^2 + r_1 l_1)}{m_2}}, \\ k_3 = \sqrt{\frac{-m_3 r_3 (l_3 + r_3) + m_1 k_1^2 + m_1(r_1^2 + r_1 l_1)}{m_3}} \end{aligned} \quad (1)$$

where ϵ is the branch index (assembly mode) of the four-bar linkage, m_i and l_i are the mass and length of the ith bar and d is the distance between the two joints on the fixed base as indicated in the figure. The position of the center of mass of bar i is described by parameter r_i. Moreover, θ_i is the angular position of bar i with respect to the X axis, k_i is the radius of gyration of the ith bar with respect to its center of mass. Variables m_1, m_2, m_3, l_1, l_2, r_1 and k_1 (or k_2) are the independent design parameters for the reactionless four-bar linkages.

Additionally, from the kinematic constraint equations of the four-bar mechanism in Fig. 1, one can write the following equations which are used below.

$$\cos\theta_1 = \frac{(l_1^2 + l_2^2)\cos\theta_3 + 2 l_1 l_2}{l_1^2 + 2 l_1 l_2 \cos\theta_3 + l_2^2} \quad (2)$$

$$\sin\theta_1 = \frac{(l_1^2 - l_2^2)\sin\theta_3}{l_1^2 + 2 l_1 l_2 \cos\theta_3 + l_2^2} \quad (3)$$

$$\dot{\theta}_3 = \frac{\sin\theta_1 \cos\theta_2 - \cos\theta_1 \sin\theta_2}{\cos\theta_2 \sin\theta_3 - \sin\theta_2 \cos\theta_3}\dot{\theta}_1 \quad (4)$$

A reactionless four-bar linkage behaves as a rigid body moving in a plane. Hence, it can be mounted on the moving link (the third or first bar) of another planar four-bar linkage — taking the moving link as its base link — to synthesize a multi-degree-of-freedom reactionless planar mechanism. However, since single reactionless four-bar linkages are effective in the plane, the stacked reactionless mechanisms can only move in that plane. Furthermore, since it is impossible for a single planar dynamically balanced four-bar linkage to keep a constant inertia tensor while moving as a rigid body, it cannot be dynamically balanced for spatial motion (Wu and Gosselin, 2002). Therefore, a planar composite mechanism composed of a pair of planar dynamically balanced four-bar linkages has been introduced (Fig. 2) for this purpose. The two dynamically balanced four-bar linkages are arranged perpendicularly. The base links and the first bars of the two mechanisms are fixed perpendicularly respectively. Hence, the two mechanisms move simultaneously (namely with same values of θ_1, θ_2 and θ_3) if the lengths of the corresponding bars of the two mechanisms are equal or have the same ratio. This composite mechanism has one degree of freedom. In the notation of Fig. 2, the first index of the subscript is used for the number of the bar, while the second index for the number of the

mechanism. Clearly, the composite mechanism is reactionless in the plane if the base links are fixed to the ground. When the base links are free for spatial motion, the conditions for obtaining a composite mechanism with constant and principal inertia tensor relative to the local frame $\overline{X}$, $\overline{Y}$, $\overline{Z}$ with origin at its center of mass are written as follows.

$$l_{i2} = ul_{i1} \quad (5)$$

$$m_{i2} = vm_{i1} \quad (6)$$

$$v = \frac{1}{u^2} \quad (7)$$

$$I_{yytb} = I_{xxtb} \quad (8)$$

where u and v represent respectively the ratios of the lengths and masses of the corresponding bars of the two mechanisms, while I_{xxtb} and I_{yytb} stand for the total moments of inertia of the two base links relative to the global frame X, Y. The conditions (5)–(7) imply that the principal moments of inertia — relative to their center of mass — of the corresponding bars of the two mechanisms should be equal. The composite mechanism with a fixed center of mass and a constant and principal inertia tensor behaves as a rigid body while undergoing spatial motion.

In the above two basic mechanisms, there are no counter-rotations and only counterweights are required. With these two basic mechanisms, reactionless multi-degree-of-freedom mechanisms can be synthesized according to the synthesis principles and constraint conditions. When stacking the mechanisms, a reactionless four-bar linkage or a composite mechanism is mounted on the third bar of another four-bar linkage. In doing so, it is clear that in order to obtain a reactionless synthesized mechanism in the plane of the four-bar linkage, the resulting mass, center of mass and radius of gyration relative to the resulting center of mass of the attached mechanism and the third bar should meet the requirements of (1) and the resulting center of mass should be situated on the axis of the third bar of the four-bar linkage and in the plane. Fig. 3 schematically shows the synthesis of a reactionless spatial 3-DOF mechanism composed of these two kinds of mechanisms. Two planar four-bar linkages are stacked in the horizontal plane, while a composite mechanism is rigidly attached on the third bar of a planar four-bar linkage in the vertical plane.

3 Synthesis of a spatial 6-DOF mechanism using planar four-bar linkages

The spatial 3-DOF mechanism mentioned above can be used as a leg to synthesize spatial multi-degree-of-freedom — having up to 6-DOF — mechanisms or manipulators. The end-effector point of the 3-DOF mechanism is attached to the mobile platform using either a spherical or a Hooke joint, depending on the number of legs used and the desired number of degrees of freedom for the mechanism. These factors also determine the number of joints to be actuated for each leg. A 6-DOF manipulator or mechanism can be obtained using only three legs and two actuators for each leg and spherical joints to connect legs to the mobile platform. The 6-DOF mechanism is schematically represented in Fig. 4. The 6-DOF mechanism is composed of three identical legs connecting the base to a common thin platform. Each of the three legs is a spatial 3-DOF mechanism (Fig. 3).

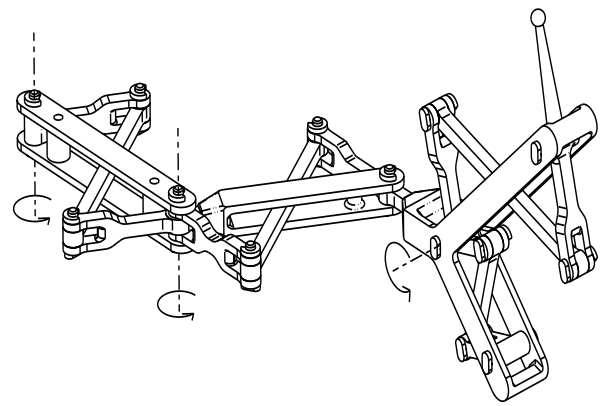

Figure 3: Synthesis of a spatial 3-DOF mechanism using four-bar linkages.

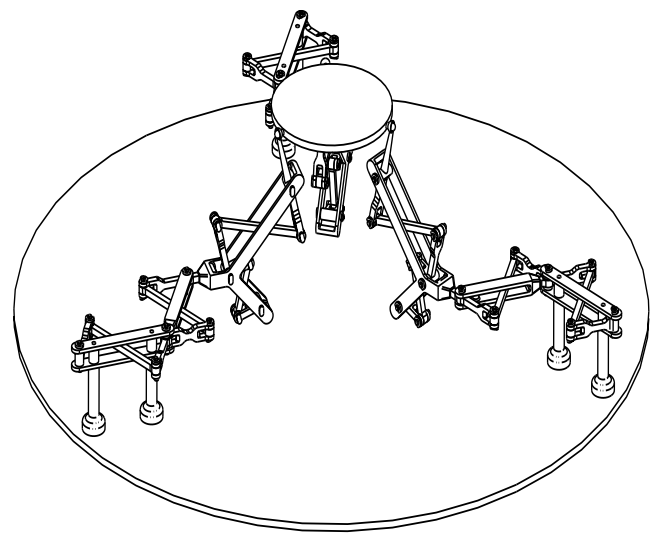

Figure 4: CAD model of a spatial 6-DOF parallel mechanism.

3.1 Inverse Kinematics

A fixed reference frame $O - xyz$ is attached to the base of the mechanism and a moving coordinate frame $O' - x'y'z'$ is attached to the moving platform (Fig. 5). Moreover, the points of attachment of the three legs to the base are noted B_i, $i = 1, 2, 3$ and the points of attachment of all legs to the platform are noted P_i, $i = 1, 2, 3$. One can then write

$$\mathbf{p}_i = \mathbf{p} + \mathbf{Q}\mathbf{p}'_i \quad (9)$$

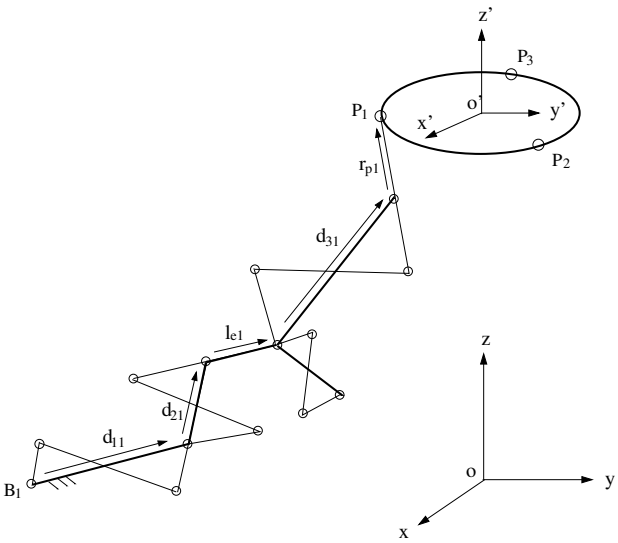

(a)

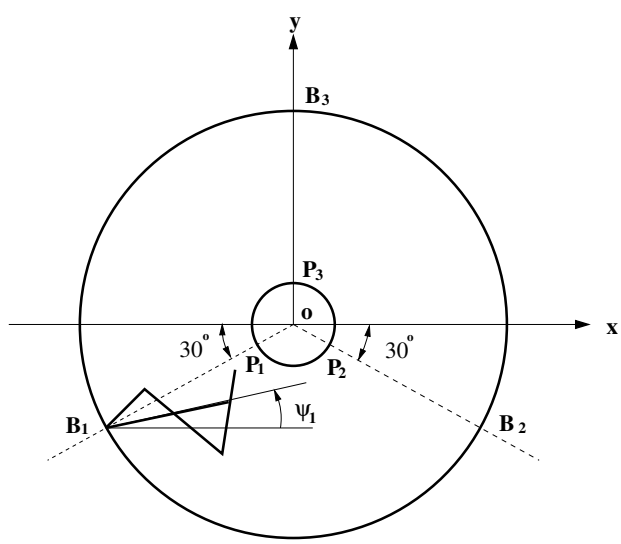

(b)

Figure 5: Schematic representation of one leg of the spatial 6-DOF parallel mechanism.

where $\mathbf{p}_i$ and $\mathbf{p}$ are respectively the position vectors of point P_i and O' expressed in the fixed coordinate frame. Furthermore, $\mathbf{Q}$ is the rotation matrix corresponding to the orientation of the platform of the mechanism with respect to the base coordinate frame — usually written as a function of the three Euler angles representing the three degrees of freedom in rotation of the platform — and the components of the above defined vectors are noted as

$$\mathbf{p} = \begin{bmatrix} x \\ y \\ z \end{bmatrix}, \quad \mathbf{p}_i = \begin{bmatrix} x_i \\ y_i \\ z_i \end{bmatrix}, \quad \mathbf{p'}_i = \begin{bmatrix} x'_i \\ y'_i \\ z'_i \end{bmatrix}, \quad i = 1, 2, 3 \quad (10)$$

Taking the ith leg mechanism into account, one can then write

$$\mathbf{p}_i = \mathbf{b}_i + \mathbf{d}_{1i} + \mathbf{d}_{2i} + \mathbf{l}_{ei} + \mathbf{d}_{3i} + \mathbf{r}_{pi} \quad (11)$$

with

$$\mathbf{b}_i = \begin{bmatrix} x_{0i} \\ y_{0i} \\ z_{0i} \end{bmatrix}, \quad \mathbf{d}_{1i} = \begin{bmatrix} d_1 \cos\psi_i \\ d_1 \sin\psi_i \\ 0 \end{bmatrix}, \quad \mathbf{d}_2 = \begin{bmatrix} -d_2 \cos\alpha_{1i} \\ -d_2 \sin\alpha_{1i} \\ 0 \end{bmatrix}$$

$$\mathbf{l}_{ei} = \begin{bmatrix} l_e \cos\alpha_{2i} \\ l_e \sin\alpha_{2i} \\ 0 \end{bmatrix}, \quad \mathbf{d}_{3i} = \begin{bmatrix} d_3 \cos\beta \cos\alpha_{2i} \\ d_3 \cos\beta \sin\alpha_{2i} \\ d_3 \sin\beta \end{bmatrix}$$

$$\mathbf{r}_{pi} = \begin{bmatrix} -r_p \cos\alpha_{3i} \cos\alpha_{2i} \\ -r_p \cos\alpha_{3i} \sin\alpha_{2i} \\ -r_p \sin\alpha_{3i} \end{bmatrix} \quad (12)$$

where

$$\alpha_{1i} = \theta_{31i} + \psi_i \quad (13)$$
$$\alpha_{2i} = \theta_{31i} + \theta_{32i} + \psi_i \quad (14)$$
$$\alpha_{3i} = \theta_{33i} + \beta \quad (15)$$

where β is the angular position of the center of mass of the composite mechanism shown in Fig. 2 and the first index of the subscript of a variable with three indexes of subscript (i.e., θ_{31i}) stands for the number of the bar, the second index for the number of the four-bar linkage and the third one for the ith leg. Substituting all the vectors in eq. (12) and eqs. (13) – (15) into eq. (11) leads to

$$\begin{bmatrix} x_{0i} + d_1 \cos\psi_i - d_2 \cos\alpha_{1i} + A_i \cos\alpha_{2i} \\ y_{0i} + d_1 \sin\psi_i - d_2 \sin\alpha_{1i} + A_i \sin\alpha_{2i} \\ z_{0i} + d_3 \sin\beta - r_p \sin\alpha_{3i} \end{bmatrix} = \begin{bmatrix} x_i \\ y_i \\ z_i \end{bmatrix} \quad (16)$$

where

$$A_i = l_e + d_3 \cos\beta - r_p \cos\alpha_{3i} \quad (17)$$

From the above equation, two solutions for α_{3i}, i.e., θ_{33i} — obtained from the z component — and four solutions for α_{1i} and α_{2i}, i.e., θ_{31i} and θ_{32i} are obtained. Then, from eqs. (2) and (3),

θ_{11i}, θ_{12i} and θ_{13i} — the joint coordinates of the first bars of the three four-bar linkages in the ith leg — are finally obtained.
For the velocity analysis, one can write

$$\dot{\mathbf{p}}_i = \mathbf{J}_i \dot{\boldsymbol{\theta}}_i \tag{18}$$

where $\dot{\boldsymbol{\theta}}_i = (\dot{\theta}_{11i}, \dot{\theta}_{12i}, \dot{\theta}_{13i})^T$ and $\mathbf{J}_i$ is the Jacobian matrix, which can be written as follows

$$\mathbf{J}_i = \begin{bmatrix} B_{1i}(d_2 s_{1i} - A_i s_{2i}) & -A_i B_{2i} s_{2i} & r_p B_{3i} c_{2i} s_{3i} \\ -B_{1i}(d_2 c_{1i} + A_i c_{2i}) & A_i B_{2i} c_{2i} & r_p B_{3i} s_{2i} s_{3i} \\ 0 & 0 & -r_p B_{3i} c_{3i} \end{bmatrix}$$

where c_{ji} and s_{ji} represent $\cos\alpha_{ji}$ and $\sin\alpha_{ji}$ respectively, and

$$B_{ji} = \frac{\sin\theta_{1ji}\cos\theta_{2ji} - \cos\theta_{1ji}\sin\theta_{2ji}}{\cos\theta_{2ji}\sin\theta_{3ji} - \sin\theta_{2ji}\cos\theta_{3ji}}, \quad j = 1, 2, 3$$

Hence the actuated joint velocities can be obtained by solving the linear system of equations given in eq. (18).

3.2 Direct Kinematics

The direct kinematic problem of the resulting 6-DOF parallel mechanism using planar four-bar linkages can be shown to be equivalent to direct kinematics of the existing parallel mechanisms or manipulators — e.g., mechanism with three prismatic legs (RRPS chains) and TSSM mechanism — for which the solution has been shown to be reducible to a 16th-order polynomial equation (Merlet, 1992; Nanua *et al.* , 1990; Ebert-Uphoff and Gosselin, 1998).

4 Design of a Reactionless Spatial 6-DOF mechanism Using Planar Four-bar Linkages

In order to simplify the design of reactionless spatial multi-degree-of-freedom parallel mechanisms, only dynamic balancing for each detached leg mechanism is considered independently, when the platform is replaced by point masses. The point masses must have the same mass, the same center of mass and the same moments of inertia with respect to any coordinate frame origin at its center of mass as the platform. For the spatial 6-DOF parallel mechanism of this paper, the mass and moments of inertia of the platform are distributed on each of the attachment points of the legs and replaced by three point masses m_{pm} symmetrically arranged on a plane (Fig. 6). It can be shown that the moments of inertia in any frame with the z axis orthogonal to the plane are equal and can be written as follows

$$I_{xx} = \frac{3}{2} m_{pm} r_{pm}^2 \tag{19}$$

$$I_{yy} = I_{xx} \tag{20}$$

$$I_{zz} = 3 m_{pm} r_{pm}^2 \tag{21}$$

where r_{pm} is the distance between the point mass and the centroid of the platform. Since m_{pm} is equal to one third of the mass of platform m_{pl}, r_{pm} is equal to the radius of gyration of the platform.

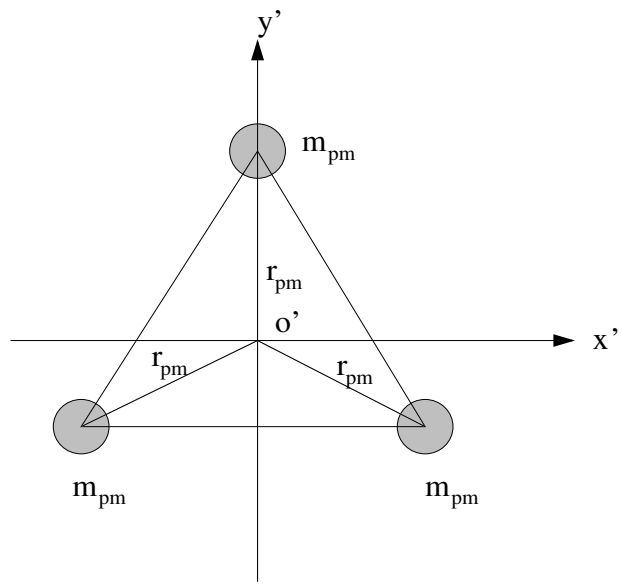

Figure 6: Determination of the three point masses.

From eqs. (19) – (21), it can be found that for any platform of symmetric thin flat plate, it can satisfy the conditions $I_{xx} = I_{yy} = \frac{1}{2} I_{zz}$ and can then be replaced by three point masses. However, if the platform has a certain thickness, it has to be replaced by four point masses on different planes. Namely, four legs must be used and the attachment points of the legs on the platform do not lie on one plane in order to obtain a reactionless 6-DOF parallel mechanism with thick or non-symmetric platform.

Therefore, by dynamically balancing each of the three legs — including the point mass — and attaching the legs — without the point masses — to a common platform satisfying the above conditions, a reactionless 6-DOF mechanism will be obtained. This result is correct because the redistribution of the internal forces due to the kinematic constraints induced by the platform do not affect the dynamic balancing. Indeed, dynamic balancing is a property of the moving masses only. Hence starting from this point mass, all the parameters of the bars of the four-bar mechanisms are chosen or calculated under the reactionless conditions. Finally a numerical example of the reactionless 3-DOF leg mechanism is given in Table 1 (point mass $m_{pm} = 0.1143kg$) where the lengths are in meters and masses in kilograms. Note that if a point mass, a four-bar linkage or a combination of mechanisms is attached on one element of another four-bar linkage, the parameters of this element in the table are actually the resulting parameters of the element and the attached mechanisms. For example, the parameters (m_{32}, r_{32}, k_{32}) in the table are resulting quantities of the third bar of the second four-bar linkage and the composite mechanism. Furthermore, $I_{xx1j} = I_{xx2j} = I_{xx3j} = I_{xxb3} = I_{xxb4} = 6 \times 10^{-6} kg \cdot m^2$,

Table 1: A numerical example of the reactionless spatial 6-DOF parallel mechanism.

Para.	1st Mech.	2nd Mech.	3rd Mech.	4th Mech.
m_{1j}	16.386	5	0.7	2.8
m_{2j}	30.178	5	0.5	2.0
m_{3j}	21.475	10.875	0.775	3.1
m_{bj}			0.4	0.2
l_{1j}	1.608	0.812	0.5	0.25
l_{2j}	5	2.5	1.0	0.5
l_{3j}	1.608	0.812	0.5	0.25
l_{bj}			1.0	0.5
r_{1j}	0.804	0.285	0.17446	0.08723
r_{2j}	3.64255	1.62254	0.5115	0.25575
r_{3j}	1.64619	0.2423	0.165	0.0825
r_{bj}			0.5	0.25
k_{1j}	2.673709	0.636766	0.197312	0.098656
k_{2j}	0.1	0.84	0.175	0.0875
k_{3j}	1.25593	0.273337	0.178106	0.089053

$I_{yyb3} = 0.033kg \cdot m^2$, $I_{yy1j} = I_{zz1j} = mk_{1j}^2$, $I_{yy2j} = I_{zz2j} = mk_{2j}^2$, $I_{yy3j} = I_{zz3j} = mk_{3j}^2$, $j = 1, 2, 3, 4$.

The verification of the reactionless property of the spatial 6-DOF parallel mechanism is performed using the dynamic simulation software ADAMS. For the above example mechanism, a simulation model is built using ADAMS (Fig. 7). Simulations have been performed for several arbitrary trajectories. The resulting reaction forces and moments on the base are illustrated in Fig. 8. The results clearly demonstrate that the resulting reaction forces and moments on the base are very small with respect to the joint forces and driving torques (with the ratio of 10^{-5} to 10^{-6}). Indeed, the reaction forces and moments obtained are most likely due to numerical simulation noise or small modeling errors. Hence, it is clearly demonstrated that the synthesized spatial 6-DOF mechanisms can be completely balanced. In other words, there are no reaction forces and moments on the base at all times and for any trajectory. These numerical simulation results support the formal mathematical proof provided in (Wu and Gosselin, 2002).

5 Conclusion

The design of a dynamically balanced spatial 6-DOF parallel mechanism using planar four-bar linkages has been presented in this paper. The geometric architecture and the inverse and direct kinematic problems have been solved. Then, reactionless spatial 6-DOF mechanisms using four-bar linkages have been synthesized. A numerical example of the reactionless spatial 6-DOF mechanisms has been given in this paper and with the help of the dynamic simulation software ADAMS it has been shown that the mechanism is reactionless for any trajectory and no torque

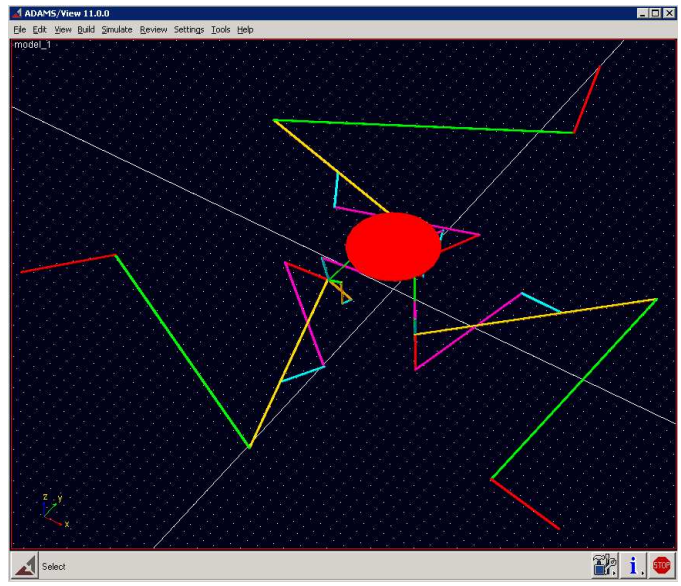

Figure 7: Modeling of reactionless 6-DOF mechanisms using ADAMS.

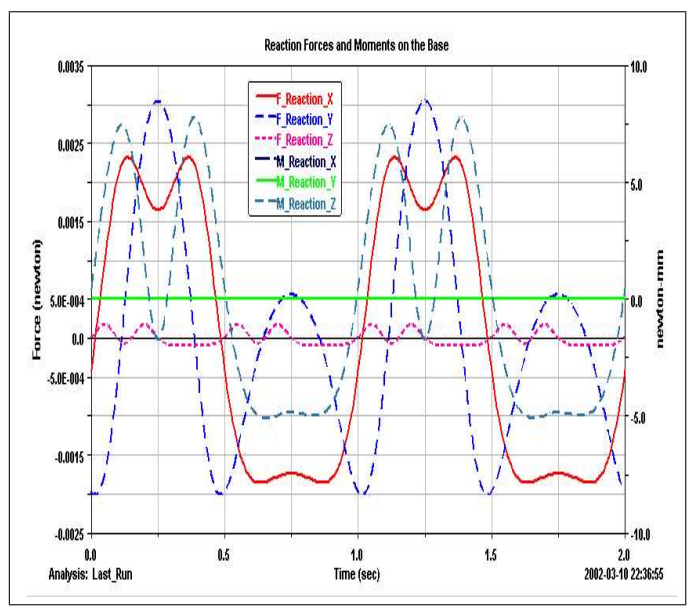

Figure 8: Verification of the reactionless property of the mechanisms.

is required at the actuators to maintain the mechanism in static equilibrium for any configuration.

Future work includes the optimal design and fabrication of prototypes of the reactionless spatial 6-DOF parallel mechanisms using planar four-bar linkages. Reactionless mechanisms are of interest to applications such as space robots or telescope mirror mechanisms.

Acknowledgments

The authors would like to acknowledge the financial support of the Natural Sciences and Engineering Research Council of Canada (NSERC) as well as the financial support of the Canada Research Chair Program. Pierre-Luc Richard is also acknowledged for his help with the CAD modeling of the mechanism.

References

Bagci, C., 1982, "Complete shaking force and shaking moment balancing of link mechanisms using balancing idler loops", *Journal of Mechanical Design*, Vol. 104, pp. 482–493.

Bagci, C., 1992, "Complete balancing of linkages using complete dynamical equivalents of floating links: CDEL method", *in DE Flexible Mechanisms, Dynamics, and Analysis, 22nd Biennial Mechanisms Conference*, DE–Vol. 47, pp. 477–488.

Bagci, C., 1983, "Complete balancing of space mechanisms – shaking force balancing", *ASME Journal of Mechanisms, Transmissions, and Automation in Design*, Vol. 105, No. 12, pp. 609–616.

Berkof, R.S. and Lowen, G.G., 1969, "A new method for completely force balancing simple linkages", *Journal of Engineering for Industry*, Vol. 91, No. 1, pp. 21–26.

Berkof, R.S., 1973, "Complete force and moment balancing of inline four-bar linkages", *Mechanism and Machine Theory*, Vol. 8, pp. 397–410.

Côté, G., Gosselin, C.M. and Vollmer, F., 2001, "Équilibrage dynamique et optimisation d'un mécanisme à quatre barres plan", *2001 CCToMM Symposium on Mechanisms, Machines, and Mechatronics*, Montréal, Québec, June 1, 2001

Dresig, H., *et al.* (VDI), 1998, "Dynamics of mechanisms – Rigid body mechanisms",VDI Richtlinien 2149 Part 1.

Dubowsky, S. and Torres, M.A., 1991, "Path planning for space manipulators to minimize spacecraft attitude disturbances", *IEEE International Conference on Robotics and Automation*, Sacramento CA, 1991, pp. 2522–2528.

Ebert-Uphoff, I. and Gosselin, C.M., 1998, "Kinematic study of a new type of spatial parallel platform mechanism", *ASME 1998 Design Engineering Technical Conference and Computers and Information in Engineering Conference*, Atlanda, Georgia, September 13–16, 1998.

Gao, F., 1989, "Complete shaking force and shaking moment balancing of four types of six-bar linkages", *Mechanism and Machine Theory*, Vol. 24, No. 4, pp. 275–287.

Gao, F., 1991, "Complete shaking force and shaking moment balancing of 17 types of eight-bar linkages only with revolute pairs", *Mechanism and Machine Theory*, Vol. 26, No. 2, pp. 197–206.

Kochev, I.S.,1990a, "General method for active balancing of combined shaking moment and torque fluctuations in planar linkages", *Mechanism and Machine Theory*, Vol. 25, No. 6, pp. 679–687.

Kochev, I.S., 1990b, "Full shaking moment balancing of planar linkages by a prescribed input speed fluctuation", *Mechanism and Machine Theory*, Vol. 25, No. 4, pp. 459–466.

Kochev, I.S., 2000, "General theory of complete shaking moment balancing of planar linkages: a critical review", *Mechanism and Machine Theory*, Vol. 35, No. 11 pp. 1501–1514.

Legnani, G., Zappa, B. Adamini, R. and Casolo, F., 1999, "A contribution to the dynamics of free-flying space manipulators", *Mechanism and Machine Theory*, Vol. 34, No. 3, pp. 359–372.

Lowen, G.G., Tepper, F.R. and Berkof, R.S., 1983, "Balancing of linkages – an update", *Mechanism and Machine Theory*, Vol. 18, No. 3, pp. 213–220.

Merlet, J-P., 1992, "Direct kinematics and assembly modes of parallel manipulators", *International Journal of Robotics Research*, Vol. 11, No. 2, pp. 150–162.

Nanua, P., Waldron, K.J. and Murthy, V., 1990, "Direct kinematic solution of a Stewart platform", *IEEE Transaction on Robotics and Automation*, Vol. 6, No. 4, pp. 438–444.

Papadopoulos, E. and Dubowsky, S., 1991, "Coordinated manipulator/spacecraft motion control for space robotic systems", *IEEE International Conference on Robotics and Automation*, Sacramento CA, 1991, pp. 1696–1701.

Papadopoulos, E. and Abu-Abed, A., 1996, "On the design of zero reaction manipulators", *Journal of Mechanical Design*, Vol. 118, No. 3, pp. 372–376.

Ricard, R. and Gosselin, C.M., 2000, "On the development of reactionless parallel manipulators", *ASME 2000 Design Engineering Technical Conference and Computers and Information in Engineering Conference*, Baltimore, Maryland, September 10–13,2000.

Wu, Y. and Gosselin, C.M., 2002, "On the synthesis of reactionless spatial 3-DOF mechanisms using planar four-bar linkages", *ASME 2002 Design Engineering Technical Conference and Computers and Information in Engineering Conference*, Montréal, Québec, September 30–October 2, 2002.

Ye, Z. and Smith, M.R., 1994, "Complete balancing of planar linkages by an equivalence method", *Mechanism and Machine Theory*, Vol. 29, No. 5, pp. 701–712.

Yu, Y.Q., 1987a, "Research on complete shaking force and shaking moment balancing of spatial linkages", *Mechanism and Machine Theory*, Vol. 22, No. 1, pp. 27–37.

Yu, Y.Q., 1987b, "Optimum shaking force and shaking moment balancing of the RSS'R spatial linkage", *Mechanism and Machine Theory*, Vol. 22, No. 1, pp. 39–45.

Yu, Y.Q., 1988, "Complete shaking force and shaking moment balancing of spatial irregular force transmission mechanisms using additional links", *Mechanism and Machine Theory*, Vol. 23, No. 4, pp. 279–285.

Proceedings of the WORKSHOP on
Fundamental Issues and Future Research Directions for Parallel Mechanisms and Manipulators
October 3–4, 2002, Quebec City, Quebec, Canada
Clément M. Gosselin and Imme Ebert-Uphoff, editors

Comparison of Two Alternate Methods for Distributed Forward Dynamic Simulation of a Four-Bar Linkage

WASEEM AHMED KHAN
Department of Mechanical Engineering
McGill University
3480 University Street, #421
Montreal, Quebec, Canada, H3A2A7
email: wakhan@cim.mcgill.ca
Web: http://www.cim.mcgill.ca/~wakhan

VENKAT KROVI*
Mechanical and Aerospace Engineering
State University of New York at Buffalo
318 Jarvis Hall
Buffalo, NY 14260
email: vkrovi@eng.buffalo.edu
Web: http://www.eng.buffalo.edu/~vkrovi

* Contact Author

Abstract: In this paper, we examine the modular development of two alternate methods for distributed computation of the forward dynamics simulations of constrained mechanical systems such as four-bar linkages. We exploit the natural spatial parallelism of closed-chain linkages, initially, for the modular development of overall dynamics and subsequently, for the distributed numerical simulation of the dynamics. Traditionally, the numerical simulation problem of constrained mechanical systems has been treated as two separate stages: the problem of algorithm development and the subsequent numerical problem of advancing the discretized differential equations in time. However the potential numerical instabilities arising from the formulation stiffness of the algorithm development stage has the potential to hinder the subsequent numerical integration stage. These aspects are also explored during the evaluation of the two alternative approaches for the distributed forward dynamics simulation of a four-bar linkage and preliminary results to quantify the *overall* computational efficiency and accuracy are presented.

1 Introduction

In the last quarter century, dynamics simulation tools have seen manifold increases in terms of their usage in the design, analysis, parametric refinement and ultimately model-based control of a variety of multibody systems such as vehicles, heavy machinery, spacecraft and robots. In the absence of efficient, general-purpose, closed-form analytical methods, numerical simulation methods have taken a premier position for simulation of such multibody systems. The interested reader may refer to a number of books on the subject (Ascher and Petzold, 1998; Garcia de Jalón and Bayo, 1994; Haug, 1989; Schiehlen, 1990; Shabana, 1989) for further details on the wide variety of formulations and computational methods that exist in the literature for numerical implementation of multibody simulations.

While efficient formulations exist for serial chain and tree structured multibody systems, the adaptation of these methods for the simulation of closed-chain linkages and parallel manipulators is relatively more difficult. Such systems possess one or more closed kinematic loops, requiring the introduction of algebraic (typically non-linear) constraints into the formulation. In our work, we will restrict our attention to the forward dynamic simulation of this class of constrained mechanical systems.

At the outset, we note that the configuration of such constrained multibody systems can be described by a variety of sets of coordinates. The suitable selection of a set of *configuration coordinates* is of particular importance due to its impact both on the ease of formulation and the subsequent computational efficiency. While the use of expanded sets of *dependent configuration coordinates* linked together by *constraining relations* is considered more appropriate for general-purpose analysis than the use of a minimal set of independent configuration coordinates, considerable variety and choice in selection of such sets exists. These choices may be broadly classified into: (i) relative; (ii) reference point and (iii) natural (or fully Cartesian), each bringing its corresponding share of advantages and shortcomings which are discussed in detail in Garcia de Jalón and Bayo (1994). In our case, we will focus our attention on the use of sets of *relative coordinates*, parameterizing the relative degrees of freedom at kinematic articulations. By facilitating direct control of joint-based actuators and enabling a minimal description of the configuration of open-chain systems, such sets of relative coordinates have found extensive use in the mechanisms and robotics community despite other

shortcomings in the form of creation of transcendental constraint relations or of relatively increased complexity of formulations of equations of motion.

In this paper, we examine both the development and performance-evaluation of two alternate methods for *modular and distributed forward dynamic simulations of constrained mechanical systems using such relative coordinates.* The emphasis on modular development is to promote reuse of existing components. Specifically, we will consider that the equations of motion of the individual subsystems/modules are well known and available and that an overall system may be composed of several serial or tree structured individual subsystems plus sets of holonomic constraints. In particular, we will examine exploiting the spatial parallelism (McMillan, 1994) that is inherent in closed kinematic chains to pursue a modular composition of the overall system dynamics. Such simulations are typically also computationally expensive and hence effective methods for distribution of computational load on multiple processors (associated with the composing subsystems) is attractive. The traditionally adopted solution approach is to: augment the unconstrained system dynamics with the differentiated constraints and Lagrange multipliers; convert the augmented system into a system of Ordinary Differential Equations (ODEs) by a variety of methods (to be discussed in the next section); which are then numerical integrated with appropriately applied stabilization or regularization techniques (Ascher and Petzold, 1998; Garcia de Jalón and Bayo, 1994). While good performance of such approaches has been reported for unified system solution, in our work we wish to their applicability and viability in the distributed computation domain.

Specifically, we will examine two approaches – a compliance-based method (e.g. Wang *et al.*, 2000) and a projection-based method (Yun and Sarkar, 1998) – from the viewpoint of *distributing the dynamics computation*. Compliance based methods use artificial mechanical compliance elements (virtual springs and dampers) to *approximate* the constraint forces. Such methods are attractive for distribution of the forward dynamics simulation because they permit explicit approximation of loop-closure constraint forces and can then effectively decouple the numerical integration of component dynamical sub-systems. In contrast, projection-based methods, require projection of the overall dynamics equations onto the feasible motion directions (the reduced-dimensional space of independent generalized velocities), which can add to the computation complexity. However, by permitting the inclusion of various stabilization and regularization methods, this latter approach shows considerable promise for ensuring consistency of the constraints over long periods of time in the presence of numerical disturbances.

Thus, in this paper, we wish to compare the compliance based and projection-based approaches focusing specifically on: (i) the modular development of dynamics formulation of an entire closed-loop manipulator by a composition of the dynamics of the component subsystems; (ii) re-distributing the computation of the forward dynamics simulations back to the individual subsystems; and (iii) quantifying the relative merits in terms of the relative computational efficiency and accuracy of the two approaches. These aspects will be studied in the context of the distributed forward dynamic simulation of a planar four-bar, whose overall dynamic equations are assumed to result from constraining the independent dynamics of a 2 degree-of-freedom (d.o.f.) left chain and a 1 d.o.f. right chain by means of holonomic constraints.

2 Background

One promising method to overcome the complexity of robotic systems consists of breaking down the system into independent subsystems, which can mapped onto distributed/parallel processing elements, at the algorithmic or natural body levels. Henrich and Höniger (1997) present a brief review and a preliminary taxonomy of the different levels of parallelism that have been explored in the context of robotic applications and note that parallelization at all levels may not be possible. Results obtained by parallelizing algorithms vary depending on the degree of dependency and coupling among the equations. While image processing problems (Chaudhary and Aggarwal, 1990) can be broken down quite well by dividing the image into smaller independent blocks, the problems of dynamic simulation of constrained mechanical systems is strongly coupled problem and the task is not trivially parallelizable (Fijany and Bejczy, 1992; Zoyama, 1993).

Fijany and Bejczy (1992) survey many of the methods developed for parallelization of dynamics algorithms, both at the algorithmic level and at the natural body level, for serial chain manipulators. Most work has focused on fine grain parallel algorithms for implementation on special purpose computational architectures (Lee and Chang, 1986; Lee and Chang, 1988; Sadayappan *et al.*, 1989). The primary motivation behind such methods is the desire to speed up computation to satisfy the required real-time constraints and not the requirement for modularity. In contrast, McMillan (1994) proposed and evaluated the use of a combination of spatial parallelism, based on the structural parallelism of a multi-arm or multi-legged system, and temporal parallelism, to compute the forward dynamics of individual chains, examining synchronization requirements and load balancing and our proposed distribution approach is more in this vein.

Several efficient algorithmic approaches have been developed for forward dynamics computation of *serial-chain* and *tree-structured* multibody systems. The two principal approaches are: Composite Rigid Body Methods (CRBM) (Walker and Orin, 1982) which have a computational complexity of $O(N^3)$ but are highly effective for typical robot arms; and Articulated Body Methods (ABM) (Featherstone, 1983) with fast recursive efficient algorithms of O(N) complexity for simulation of longer serial-chain and tree structured dynamic systems. Ascher *et al.*(1997) unified the two seemingly disparate methods by showing that the

different dynamics algorithms (ABM, CRBM) can be derived as different elimination methods for solving an augmented system of Differential Algebraic Equations (DAEs). They also highlight the potential numerical instabilities ("formulation stiffness") that can arise from separating the treatment of the forward dynamics problem of computing the system accelerations from the numerical integration problem of advancing the discretized differential equations in time and advocate a global, unified view.

The dynamics of *mechanical systems with closed loops* can be formulated as a system of ODEs whose solutions are required to satisfy additional holonomic (algebraic) equations resulting from cutting the loops (Featherstone, 1987). The dynamics of mechanical systems with holonomic constraints can be formulated as Lagrangian equations of the first kind (Arnold, 1989), as:

$$\dot{\mathbf{q}} = \mathbf{v} \tag{1}$$

$$\mathbf{M}(\mathbf{q})\dot{\mathbf{v}} = \mathbf{f}(\mathbf{q},\mathbf{v},t,\mathbf{u}) - \mathbf{A}(\mathbf{q})^T\boldsymbol{\lambda} \tag{2}$$

$$\mathbf{C}(\mathbf{q}) = \mathbf{0} \tag{3}$$

where

$\mathbf{q}$ is the *n*-dimensional vector of generalized coordinates.

$\mathbf{v}$ is the *n*-dimensional vector of generalized velocities.

$\mathbf{M}(\mathbf{q})$ is the $n \times n$ dimensional inertia matrix.

$\mathbf{f}(\mathbf{q},\mathbf{v},t,\mathbf{u})$ is the *n*-dimensional vector of external forces.

$\mathbf{u}$ is the vector of actuator forces/torques.

$\mathbf{C}(\mathbf{q})$ is a *m*-dimensional vector of holonomic constraints.

$\mathbf{A}(\mathbf{q}) = \dfrac{\partial \mathbf{C}}{\partial \mathbf{q}}$ is the $m \times n$ constraint Jacobian matrix.

$\boldsymbol{\lambda}$ is the *m*-dimensional vector of Lagrange multipliers.

The resulting formulations in non-minimal (redundant) sets of coordinates yields an often simpler, albeit larger, system of index-3 Differential Algebraic Equations (DAE). The development of such models for the entire system using augmented Lagrangian based models, initially in a redundant set of coordinates with a subsequent determination of the multipliers is also attractive since the given models can be used for both forward and inverse dynamics.

The solution of a system of index-3 DAEs by direct finite difference discretization is not possible using explicit discretization methods. The two principal approaches adopted for the forward dynamics simulation of such systems are: *(i) Direct elimination of the surplus variables* using the position-level algebraic constraints to explicitly reduce the index-3 DAE to an ODE in a minimal set of generalized coordinates (conversion into Lagrange's Equations of the 2nd kind). The resulting (smaller size) ODE can then be integrated using ODE methods without worrying about the stability issues. However, such a reduction cannot be done in general, and even when it can, the obtained differential equations are typically complicated (Kecskemethy *et al.*, 1997). (ii) *Converted ODE approach* wherein all the algebraic position and velocity level constraints are differentiated and represented at the acceleration level to obtain an augmented index-1 DAE (in terms of both the unknown accelerations and the unknown multipliers). Differentiating the position constraints, Eqn. 3, with respect to time, yields the velocity-level constraints:

$$\dot{\mathbf{C}} = \mathbf{A}(\mathbf{q})\mathbf{v} = 0 \tag{4}$$

and a further differentiation with respect to time yields the acceleration level constraints as:

$$\ddot{\mathbf{C}} = \mathbf{A}(\mathbf{q})\dot{\mathbf{v}} + \dot{\mathbf{A}}(\mathbf{q})\mathbf{v} = 0 \tag{5}$$

Thus, Eqn. 2 can then be written together with Eqn. 5 as an index-1 DAE as:

$$\begin{bmatrix} \mathbf{M} & \mathbf{A}^T \\ \mathbf{A} & \mathbf{0} \end{bmatrix}_{(n+m)\times(n+m)} \begin{bmatrix} \dot{\mathbf{v}} \\ \boldsymbol{\lambda} \end{bmatrix}_{(n+m)\times 1} = \begin{bmatrix} \mathbf{f} \\ -\dot{\mathbf{A}}(\mathbf{q})\mathbf{v} \end{bmatrix}_{(n+m)\times 1} \tag{6}$$

Such index-1 DAEs may be solved by: simply eliminating the Lagrange multipliers in favor of the unknown accelerations leaving a system of ODEs (Ascher and Petzold, 1998); explicitly computing the Lagrange multipliers by a projection into the constrained force space (Murray *et al.*, 1994); approximating the Lagrange multipliers using artificial compliance elements such as virtual springs and dampers (Wang *et al.*, 2000;); or projecting the equations of motion onto the tangent space of the constraint manifold in a variety of ways to obtain constraint-reaction free equations of motion (Garcia de Jalón and Bayo, 1994). These aspects will be explicitly discussed in the next section.

Some of the drawbacks of the converted ODE approach include the need to provide additional consistent initial conditions and the fact that the differentiated constraint manifold is mildly unstable resulting in drift of the state from the position constraint manifold. While the growth rate can be reduced by lowering the error tolerance and by using smaller step-sizes or greater numerical precision, this comes at the cost of longer and more expensive computations.

Hence, most constrained multibody methods also combine (one or more) of the following methods for improved numerical solution using explicit discretization methods (Ascher and Petzold, 1998): (a) Coordinate projection of the state of the system onto the constraint manifold at frequent intervals to ensure maintenance of the algebraic constraint; (b) Computing a local velocity-level parameterization and integrating the ODE on the constraint manifold (in the independent coordinates); or (c) Creation of an artificial first or second-order dynamical system which has the algebraic constraint as its attractive equilibrium configuration (Baumgarte, 1983). While Baumgarte's technique is very popular in the engineering application community, principally due to the resulting augmented ODE formulation, the practical selection of the parameters of the stabilization system depends both on the discretization methods and step-size and is widely regarded as an open research problem (Ascher *et al.*, 1995).

3 Converted ODE Approaches

Index-1 DAE systems resulting from the converted ODE apparoach are typically solved using one of the following three approaches: (a) direct Lagrange multiplier elimination;

(b) compliance-based; or (c) projection-based.

In the ***direct Lagrange multiplier elimination*** approaches, a simultaneous solution of the augmented linear system of equations in Eqn. 6 is possible at each time step. While we note that an explicit inversion of the augmented system may be avoided by adopting a Gaussian elimination method, the overall approach may still be denoted as:

$$\begin{bmatrix} \dot{\mathbf{v}} \\ \boldsymbol{\lambda} \end{bmatrix} = \begin{bmatrix} \mathbf{M} & \mathbf{A}^T \\ \mathbf{A} & \mathbf{0} \end{bmatrix}^{-1} \begin{bmatrix} \mathbf{f} \\ \varphi \end{bmatrix} = \begin{bmatrix} \mathbf{f}_1(\mathbf{q},\mathbf{v}) \\ \mathbf{f}_2(\mathbf{q},\mathbf{v}) \end{bmatrix} \tag{7}$$

Thus the overall system may now be written as a system of first order ODEs as:

$$\dot{\mathbf{x}}_{2\text{nx}1} = \begin{bmatrix} \dot{\mathbf{q}}_{\text{n}\times 1} \\ \ddot{\mathbf{q}}_{\text{n}\times 1} \end{bmatrix} = \begin{bmatrix} \mathbf{v} \\ \mathbf{f}_1(\mathbf{q},\mathbf{v}) \end{bmatrix} \tag{8}$$

which may then be integrated using standard codes. Note that, in principle, the index-reduced system Eqn. 8 needs more initial conditions than the original system Eqn. 1-3 to specify a unique solution. The main advantage is conceptual simplicity and simultaneous determination of the accelerations and the Lagrange multipliers by solving a *linear* system of equations. However, the constraint conditions may be progressively violated, especially in the presence of large step sizes, leading to unacceptably large errors even for short duration simulations.

In the ***compliance-based approaches***, the loop-closure constraints are *relaxed* and replaced using virtual springs and dampers. Using such virtual springs can be considered as a form of penalty formulation (see Section 5.1.4 of Garcia de Jalón and Bayo (1994)) which incorporates the constraint equations as a dynamical system penalized by a large factor. The Lagrange multipliers are *approximated* using a force-law (based the extent of the constraint violation and an assumed spring stiffness) and eliminated from the list of *n+m* unknowns leaving behind a system of *2n* first order ODEs. While the sole initial drawback may appear to be restricted to the numerical ill-conditioning due to selection of large penalty factors, it is important to note that penalty approaches only *approximate* the true constraint forces and can create unanticipated problems (as will be discussed later).

Finally, the class of ***projection-based approaches*** seek to take the constraint-reaction containing dynamical equations into the *orthogonal* and *tangent* subspaces of the vector space of the system's generalized velocities. Let $\mathbf{S(q)}$ be a $n\times(n\text{-}m)$ dimensional full rank matrix whose column space is in the null space of $\mathbf{A(q)}$ i.e. $\mathbf{A(q)S(q)} = \mathbf{0}$. The orthogonal subspace is spanned by the so-called constraint vectors (forming the rows of the matrix $\mathbf{A(q)}$) while the tangent subspace *complements* this orthogonal subspace in the overall generalized velocity vector space. All *feasible* dependent velocities, $\dot{\mathbf{q}}$, of a constrained multibody system necessarily belong to this tangent space, appropriately called the *space of feasible motions.* This space is spanned by the columns of $\mathbf{S(q)}$) and is parameterized by an *n-m* dimensional vector of independent velocities, $\boldsymbol{\upsilon}(\text{t})$, yielding the expression for the feasible dependent velocities as $\dot{\mathbf{q}} = \mathbf{S(q)}\ \boldsymbol{\upsilon}(\text{t})$.

It is very important to note two factors at this stage. *First*, the initial selection of the set of configuration coordinates plays an important role here. In particular, while it is always possible to create a Riemannian configuration space (and consequently vector spaces for the generalized velocities) using sets of relative coordinates, special care needs to be exercised when treating configuration spaces created with other sets of generalized coordinates (such as Cartesian coordinates of the bodies in SE(2) or SE(3)). This is because the generalized velocity space for Cartesian coordinates need not necessarily form a vector space and hence, the notion of orthogonal complement subspaces, which exist only in a Riemannian setting. needs to be examined carefully. For example, in Blajer *et al.* (1994), the local task-space coordinates (consisting only translations) form a Riemannian space permitting the orthogonal decomposition carried out. This is the other motivating factor for restricting ourselves to joint-based relative-coordinate descriptions of the configuration of the system. *Second*, a family of choices exists for the selection of projection between dependent and independent velocities (including the case where the set of independent velocities form a proper subset of the original set of dependent velocities) and each such choice can give rise to a different $\mathbf{S(q)}$. See Garcia de Jalón and Bayo (1994) for a description of the many possibilities as well as the determination of the projection matrices determining the transformations between dependent and independent velocities.

However, once a projection is selected, the dynamic equations of motion can now be projected on to the instantaneous feasible motion directions, to obtain the so-called the so-called constraint-reaction-free equations of motion. Pre-multiplying both sides of Eqn. 2 by $\mathbf{S^T}$ and noting that $\mathbf{S^T A^T} = \mathbf{0}$ we get:

$$\mathbf{S}^T\mathbf{M}(\mathbf{q})\dot{\mathbf{v}} = \mathbf{S}^T\mathbf{f}(\mathbf{q},\mathbf{v},t,\mathbf{u}) \tag{9}$$

Note that this is a system of *n-m* 2nd order differential equations in the *n* dependent accelerations. All further steps for the solution of this system of equations may be performed either in terms of *dependent* or *independent* coordinates, as discussed in Chapter 5 of Garcia de Jalón and Bayo (1994).

For example, the *m* acceleration-level constraints shown in Eqn. 5 may be appended to this system resulting in a system of *2n* first-order ODEs in the state vector consisting of the *n* dependent velocities and *n* dependent accelerations. Note that while the notion of dependent and independent velocities is not explicitly considered, this is implicit in the selection of $\mathbf{S^T}$. Alternatively, by explicitly considering the same local projection used to determine the feasible motion directions, the constraint-reaction-free equations of motion may be expressed in terms of the independent coordinates (Serna *et al.*, 1982). The final solution may be obtained either by numerically integrating a system of *2(n-m)* first-order ODEs in the (*n-m)* independent velocities and *n-m* independent accelerations and solving the position problem at each step or by numerically integrating a system of *2n-m* first-order ODEs in the *n* dependent velocities and *n-m*

independent accelerations. The benefits accumulate from two sources. *First*, since the feasible motion directions are guaranteed to be tangent to the holonomic constraint manifold, with an adequately small step size the resulting integrated solution is guaranteed to maintain the constraints. *Second*, the integration of reduced-order system of ODEs (with either *n-m* or *2n-m* states) also reduces the error that can 'creep in' due to numerical integration.

4 The Two Approaches Under Consideration

4.1 Compliance based Method (Method A)

In Wang *et al.* (2000), the Lagrange multiplier $\boldsymbol{\lambda}$ in Eqn. 2 is explicitly calculated as a restoring force provided by a virtual spring. This restoring force, proportional to the extent of constraint violation, can be expressed as $\lambda_i = K_i C_i(\mathbf{q})$ where K_i is the spring constant and $C_i(\mathbf{q})$ is the constraint violation in the direction of the respective λ_i. By substituting the value of $\boldsymbol{\lambda}$ in Eqn. 2, the final ODE system can be written as:

$$\dot{\mathbf{x}}_{2n\times 1} = \begin{bmatrix} \dot{\mathbf{q}}_{n\times 1} \\ \ddot{\mathbf{q}}_{n\times 1} \end{bmatrix} = \begin{bmatrix} \mathbf{v} \\ \mathbf{M}^{-1}(\mathbf{f}(\mathbf{q},\mathbf{v},t,\mathbf{u}) - \mathbf{A}(\mathbf{q})^T(\mathbf{K}\mathbf{C}(\mathbf{q}))) \end{bmatrix} \tag{10}$$

where $\mathbf{K} = diag[K_i]$ and $\mathbf{C}(\mathbf{q})$ is the vector of constraint violations.

4.2 Projection-based Method (Method B)

The derivation process discussed by Sarkar and Yun (1998) very closely resembles the work of Serna *et al*, (1982) but with the addition of Baumgarte stabilization. The formulation in terms of rheonomous constraints permits easy incorporation of Baumgarte stabilization and additionally can be easily specialized for the scleronomous case. The holonomic constraints $\mathbf{C}(\mathbf{q}) = \mathbf{0}$ are approximated by a first order system of the form:

$$\dot{\mathbf{C}}(\mathbf{q}) + \sigma\mathbf{C}(\mathbf{q}) = \mathbf{0}, \quad \sigma > 0 \tag{11}$$

where σ is the rate of convergence. The equilibrium condition for this first order system is the constraint manifold $\mathbf{C}(\mathbf{q}) = \mathbf{0}$ and for any initial condition $\mathbf{q}(0)$, which may not satisfy the holonomic constraint equation $\mathbf{C}(\mathbf{q}(0)) = \mathbf{0}$, the above first order equation guarantees exponential convergence of $\mathbf{C}(\mathbf{q}(t))$ to zero as the time *t* progresses. The rate of convergence will be determined by σ, which can be chosen based on specific application. By taking $\mathbf{A}(\mathbf{q})$ as the Jacobian of $\mathbf{C}(\mathbf{q})$, Eqn. 11 can be written as:

$$\mathbf{A}(\mathbf{q})\dot{\mathbf{q}} = -\sigma\mathbf{C}(\mathbf{q}) = \mathbf{a}(\mathbf{q}) \tag{12}$$

Then, the general solution of Eqn. 12 is given by:

$$\dot{\mathbf{q}} = \mathbf{v} = \mathbf{S}(\mathbf{q})\boldsymbol{\upsilon}(t) + \boldsymbol{\eta}(\mathbf{q}) \tag{13}$$

where $\mathbf{S}(\mathbf{q})$ is an $n\times(n\text{-}m)$ dimensional full rank matrix whose column space is in the null space of $\mathbf{A}(\mathbf{q})$ i.e. $\mathbf{A}(\mathbf{q})\mathbf{S}(\mathbf{q}) = 0$, $\boldsymbol{\upsilon}(t)$ is an *n-m* dimensional vector of independent velocities and $\boldsymbol{\eta}(\mathbf{q})$ is the *n*-dimensional particular solution of Eqn. 11. Differentiating once we get:

$$\dot{\mathbf{v}} = \mathbf{S}(\mathbf{q})\dot{\boldsymbol{\upsilon}}(t) + \dot{\mathbf{S}}(\mathbf{q})\boldsymbol{\upsilon}(t) + \dot{\boldsymbol{\eta}}(\mathbf{q}) = \mathbf{S}(\mathbf{q})\dot{\boldsymbol{\upsilon}}(t) + \boldsymbol{\gamma}(\mathbf{q},\boldsymbol{\upsilon}) \tag{14}$$

Pre-multiplying both sides of Eqn. 2 by $\mathbf{S}^{\mathbf{T}}$ and noting that $\mathbf{S}^{\mathbf{T}}\mathbf{A}^{\mathbf{T}} = \mathbf{0}$ we get:

$$\mathbf{S}^T\mathbf{M}(\mathbf{q})\dot{\mathbf{v}} = \mathbf{S}^T\mathbf{f}(\mathbf{q},\mathbf{v},t,\mathbf{u}) \tag{15}$$

By substituting $\dot{\mathbf{v}}$ from Eqn. 14 into Eqn. 15 and solving for $\dot{\boldsymbol{\upsilon}}$ we get

$$\dot{\boldsymbol{\upsilon}} = -(\mathbf{S}^T\mathbf{M}\mathbf{S})^{-1}(\mathbf{S}^T\mathbf{M}\boldsymbol{\gamma} + \mathbf{S}^T\mathbf{f}(\mathbf{q},\mathbf{v},t,\mathbf{u})) \tag{16}$$

The resulting overall system of ODEs may be expressed in state-space form as:

$$\dot{\mathbf{x}}_{(2n-m)\times 1} = \begin{bmatrix} \dot{\mathbf{q}}_{n\times 1} \\ \dot{\boldsymbol{\upsilon}}_{(n-m)\times 1} \end{bmatrix} = \begin{bmatrix} \mathbf{S}\boldsymbol{\upsilon} + \boldsymbol{\eta} \\ -(\mathbf{S}^T\mathbf{M}\mathbf{S})^{-1}(\mathbf{S}^T\mathbf{M}\boldsymbol{\gamma} - \mathbf{S}^T\mathbf{f}(\mathbf{q},\mathbf{v},t,\mathbf{u})) \end{bmatrix} \tag{17}$$

While this method would work for any projection that is independent of the existing constraints, the particular adopted projection (wherein the independent velocities are selected as a proper subset of the original set of dependent velocities) yields a simple and robust formulation.

5 Distributed Forward Dynamics for a Four-bar linkage

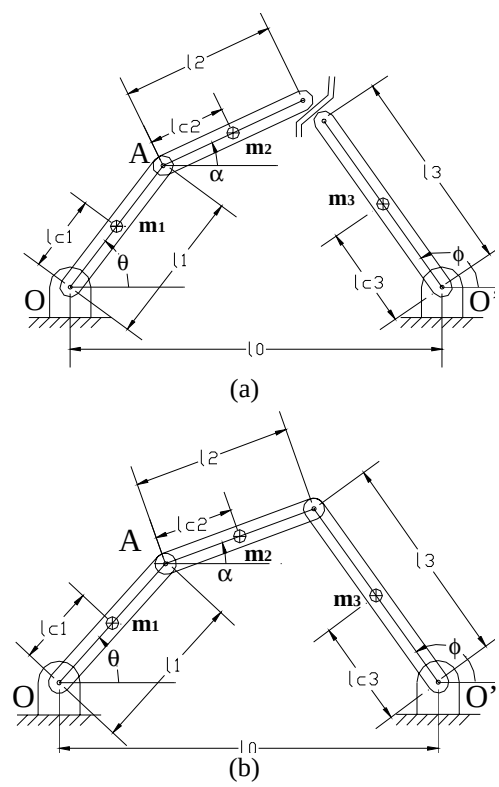

Figure 1. Representation of the four-bar linkage (a) Divided and (b) Composite models.

5.1 Lagrangian Modeling

The modeling process for the four-bar linkage considered here and the selected parameters are the same as in Wang *et al.* (2000) and are summarized here again for clarity. The four-bar linkage (Fig. 1) consists of three movable links (input, coupler link and the output links) of lengths l_1, l_2 and l_3 respectively whose orientation with respect to the horizontal can be denoted by angles θ, α and ϕ. The mass of each moving link of length l_i is m_i, and the moment of inertia of the moving link about the axis through the center of the mass and perpendicular to the plane of its motion is I_i, where i=1,2,3. The mass centers of each link is situated at a distance l_{ci} from the proximal joint of each link.

The equations of motion for the overall system are derived by treating the four-bar as being composed of a left chain (l_1+l_2) and the right chain (l_3), as shown in Fig. 1. The dynamic equations of each chain are derived independently by the Lagrange's method and the equations of the overall system written as an index-3 DAE as:

$$\begin{aligned} \dot{\mathbf{q}} &= \mathbf{v} \\ \mathbf{M}(\mathbf{q})\ddot{\mathbf{q}} + \mathbf{V}(\mathbf{q},\dot{\mathbf{q}}) + \mathbf{G}(\mathbf{q}) &= \mathbf{E}(\mathbf{q})\mathbf{u} - \mathbf{A}^T\boldsymbol{\lambda} \\ \mathbf{C}(\mathbf{q}) &= \mathbf{0} \end{aligned} \tag{18}$$

where:

$$\mathbf{M}(\mathbf{q}) = \begin{bmatrix} m_1 l_{c1}^2 + I_1 + m_2 l_1^2 & m_2 l_1 l_{c2}\cos(\alpha-\theta) & 0 \\ m_2 l_1 l_{c2}\cos(\alpha-\theta) & I_2 + m_1 l_{c2}^2 & 0 \\ 0 & 0 & m_3 l_{c3}^2 + I_3 \end{bmatrix} = \begin{bmatrix} [\mathbf{M}_A]_{2\times2} & \mathbf{0}_{2\times1} \\ \mathbf{0}_{1\times2} & [\mathbf{M}_B]_{1\times1} \end{bmatrix}$$

$$\mathbf{V}(\mathbf{q},\dot{\mathbf{q}}) = \begin{bmatrix} -m_2 l_1 l_{c2}\sin(\alpha-\theta)\dot{\alpha}^2 \\ m_2 l_1 l_{c2}\sin(\alpha-\theta)\dot{\theta}^2 \\ 0 \end{bmatrix} = \begin{bmatrix} [\mathbf{V}_A]_{2\times1} \\ [\mathbf{V}_B]_{1\times1} \end{bmatrix},$$

$$\mathbf{G}(\mathbf{q}) = \begin{bmatrix} m_1 g l_{c1}\cos\theta + m_2 g l_1\cos\theta \\ m_2 g l_{c2}\cos\alpha \\ m_3 g l_{c3}\cos\phi \end{bmatrix} = \begin{bmatrix} [\mathbf{G}_A]_{2\times1} \\ [\mathbf{G}_B]_{1\times1} \end{bmatrix},$$

$$\mathbf{q} = \begin{bmatrix} \theta \\ \alpha \\ \phi \end{bmatrix},\ \mathbf{u} = \begin{bmatrix} \tau_1 \\ \tau_2 \\ \tau_3 \end{bmatrix},\ \mathbf{E}(\mathbf{q}) = \begin{bmatrix} 1 & 0 & 0 \\ 0 & 1 & 0 \\ 0 & 0 & 1 \end{bmatrix}$$

The constraint equations are obtained from the requirement that the left and right chains to stay connected at the cut joint, which can be expressed in matrix form as:

$$\mathbf{C}(\mathbf{q}) = \begin{bmatrix} -l_1\cos\theta - l_2\cos\alpha + l_0 + l_3\cos\phi \\ -l_1\sin\theta - l_2\sin\alpha + l_3\sin\phi \end{bmatrix} = \begin{bmatrix} 0 \\ 0 \end{bmatrix} \tag{19}$$

5.2 Compliance-based Method (Method A)

By assuming that the state vector $\mathbf{q} = [\mathbf{q}_A^T \quad \mathbf{q}_B^T]^T$ has *a* state variables belonging to the chain-a and *b* state variables belonging to the chain-b and that *a* + *b* = *n*, the distributed model may be obtained in state-space form as:

$$\begin{aligned} [\dot{\mathbf{x}}_A]_{2a\times1} &= \begin{bmatrix} \dot{\mathbf{q}}_A \\ \ddot{\mathbf{q}}_A \end{bmatrix} \\ &= \begin{bmatrix} \mathbf{v}_A \\ \mathbf{M}_A^{-1}(\mathbf{E}_A\mathbf{u}_A - \mathbf{V}_A - \mathbf{G}_A - \mathbf{K}\mathbf{A}_A^T\mathbf{C}) \end{bmatrix} \\ [\dot{\mathbf{x}}_B]_{2bx1} &= \begin{bmatrix} \dot{\mathbf{q}}_B \\ \ddot{\mathbf{q}}_B \end{bmatrix} \\ &= \begin{bmatrix} \mathbf{v}_B \\ \mathbf{M}_B^{-1}(\mathbf{E}_B\mathbf{u}_B - \mathbf{V}_B - \mathbf{G}_B - \mathbf{K}\mathbf{A}_B^T\mathbf{C}) \end{bmatrix} \end{aligned} \tag{20}$$

where **K** is the compliance matrix and **C** represents the extent of the constraint violation.

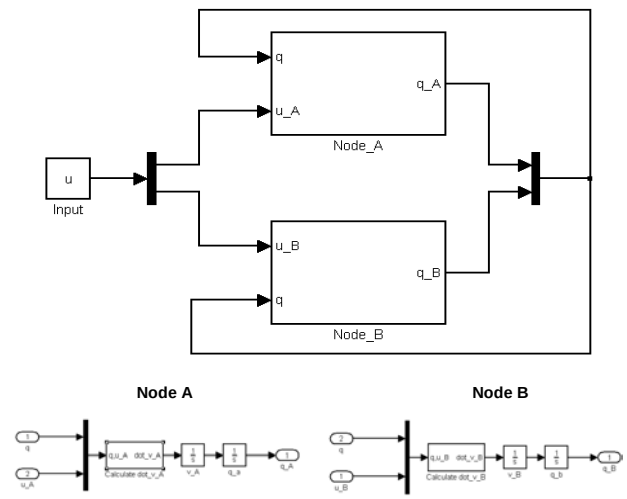

Figure 2: Distributed modeling for a four-bar linkage (Method A)

The two dynamic sub-systems, shown in Eqn. 20, can be simulated in a distributed manner if at every time step: (i) either the information pertaining to **C(q)**, the extent of the constraint violation, is made available explicitly or (ii) computed by exchanging state information between the two sub-subsystems. This suggests a way to distribute the computational load between two processors, as shown graphically in Fig. 2, wherein each independent sub-part can now be numerically integrated on a different processor. The sole coupling between the two sub-parts is due to the Lagrange multipliers, which are now explicitly calculated using the virtual spring. While this is shown for a "two part system", the process generalizes easily for "n-part" system.

5.3 Projection-based method (Method B)

Eqn. 17 may be converted into a suitable state-space form as:

$$\dot{\mathbf{x}} = \begin{bmatrix} \dot{\mathbf{q}} \\ \dot{\boldsymbol{\upsilon}} \end{bmatrix} = \begin{bmatrix} \mathbf{S}\boldsymbol{\upsilon} + \boldsymbol{\eta} \\ -(\mathbf{S}^T\mathbf{M}\mathbf{S})^{-1}(\mathbf{S}^T\mathbf{M}\boldsymbol{\gamma} + \mathbf{S}^T\mathbf{V} + \mathbf{S}^T\mathbf{G} - \mathbf{S}^T\mathbf{E}\mathbf{u}) \end{bmatrix} \tag{21}$$

By similarly assuming that the state vector $\mathbf{q}$ has *a* state variables belonging to the chain-A and *b* state variables

belonging to the chain-b with $a + b = n$ the projected dynamics equations may be partitioned as:

$$\begin{bmatrix}\mathbf{S}_A^T & \mathbf{S}_B^T\end{bmatrix}\begin{bmatrix}\mathbf{M}_A & 0\\ 0 & \mathbf{M}_B\end{bmatrix}\begin{bmatrix}\mathbf{S}_A\\ \mathbf{S}_B\end{bmatrix}\dot{\boldsymbol{\upsilon}}+\begin{bmatrix}\mathbf{S}_A^T & \mathbf{S}_B^T\end{bmatrix}\begin{bmatrix}\mathbf{M}_A & 0\\ 0 & \mathbf{M}_B\end{bmatrix}\begin{bmatrix}\boldsymbol{\gamma}_A\\ \boldsymbol{\gamma}_B\end{bmatrix} \tag{22}$$
$$+\begin{bmatrix}\mathbf{S}_A^T & \mathbf{S}_B^T\end{bmatrix}\begin{bmatrix}\mathbf{V}_A\\ \mathbf{V}_B\end{bmatrix}+\begin{bmatrix}\mathbf{S}_A^T & \mathbf{S}_B^T\end{bmatrix}\begin{bmatrix}\mathbf{G}_A\\ \mathbf{G}_B\end{bmatrix}=\begin{bmatrix}\mathbf{S}_A^T & \mathbf{S}_B^T\end{bmatrix}\begin{bmatrix}\mathbf{E}_A & 0\\ 0 & \mathbf{E}_B\end{bmatrix}\begin{bmatrix}\mathbf{u}_A\\ \mathbf{u}_B\end{bmatrix}$$

Multiplying we get:

$$\begin{aligned}&[\mathbf{S}_A^T\mathbf{M}_A\mathbf{S}_A+\mathbf{S}_B^T\mathbf{M}_B\mathbf{S}_B]\dot{\boldsymbol{\upsilon}}+[\mathbf{S}_A^T\mathbf{M}_A\boldsymbol{\gamma}_A+\mathbf{S}_B^T\mathbf{M}_B\boldsymbol{\gamma}_B]\\ &\quad+[\mathbf{S}_A^T\mathbf{V}_A+\mathbf{S}_B^T\mathbf{V}_B]+[\mathbf{S}_A^T\mathbf{G}_A+\mathbf{S}_B^T\mathbf{G}_B]\\ &\qquad=[\mathbf{S}_A^T\mathbf{E}_A\mathbf{u}_A+\mathbf{S}_B^T\mathbf{E}_B\mathbf{u}_B]\end{aligned} \tag{23}$$

Noting that the first part of Eqn. 23 is $(\mathbf{S}^T\mathbf{MS})$ and collecting terms we get:

$$\begin{aligned}\dot{\boldsymbol{\upsilon}}&=\left(\mathbf{S}^T\mathbf{MS}\right)^{-1}[\mathbf{S}_A^T(\mathbf{E}_A\mathbf{u}_A-\mathbf{M}_A\boldsymbol{\gamma}_A-\mathbf{V}_A-\mathbf{G}_A)]\\ &\quad+\left(\mathbf{S}^T\mathbf{MS}\right)^{-1}[\mathbf{S}_B^T(\mathbf{E}_B\mathbf{u}_B-\mathbf{M}_B\boldsymbol{\gamma}_B-\mathbf{V}_B-\mathbf{G}_B)]\end{aligned} \tag{24}$$

Thus, it is now possible to calculate the state vectors forming Eqn. 21 separately as:

$$\begin{aligned}\dot{\mathbf{x}}_A&=\begin{bmatrix}\dot{\mathbf{q}}_A\\ \dot{\boldsymbol{\upsilon}}_A\end{bmatrix}_{(a+n-m)\times 1}\\ &=\begin{bmatrix}\mathbf{S}_A\boldsymbol{\upsilon}+\boldsymbol{\eta}_A\\ -(\mathbf{S}^T\mathbf{MS})^{-1}(\mathbf{S}_A{}^T(\mathbf{M}_A\boldsymbol{\gamma}_A+\mathbf{V}_A+\mathbf{G}_A-\mathbf{E}_A\mathbf{u}_A)\end{bmatrix}\\ \dot{\mathbf{x}}_B&=\begin{bmatrix}\dot{\mathbf{q}}_B\\ \dot{\boldsymbol{\upsilon}}_B\end{bmatrix}_{(b+n-m)\times 1}\\ &=\begin{bmatrix}\mathbf{S}_B\boldsymbol{\upsilon}+\boldsymbol{\eta}_B\\ -(\mathbf{S}^T\mathbf{MS})^{-1}(\mathbf{S}_B{}^T(\mathbf{M}_B\boldsymbol{\gamma}_B+\mathbf{V}_B+\mathbf{G}_B-\mathbf{E}_B\mathbf{u}_B)\end{bmatrix}\end{aligned} \tag{25}$$

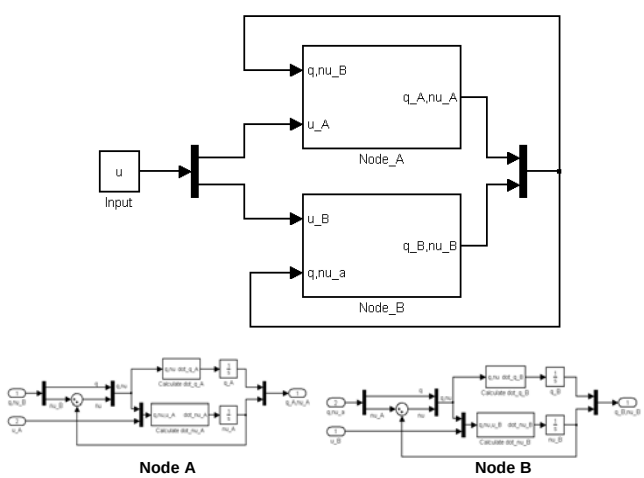

Figure 3: Distributed modeling of a four-bar linkage (Method B)

By examining Eqn. 25, we note that the overall system can be evaluated in a distributed manner if states $\mathbf{q}_i$ and $\boldsymbol{\upsilon}_i$ (i =a,b) are made available. This suggests a way to split the calculation of the dynamic equations, as depicted in Fig. 3. Each independent sub-part can now be numerically integrated on a different processor thereby permitting the distribution of the load. At each time-instant, the complete state of the system needs to be exchanged between the subparts. The coupling between the various sub-parts is due to the existence of the $(\mathbf{S}^T\mathbf{MS})^{-1}$. In the arrangement shown in Fig. 3, this matrix inverse needs to be computed on each and every processor (although we note that the explicit calculation of the inverse is typically avoided by using an optimal equation solver). Alternatively, state information from the slave processors could be collected by a master processor at each time instant, the $(\mathbf{S}^T\mathbf{MS})^{-1}$ could be computed once and the result subsequently propagated back to the slave processors where the actual numerical integration is performed.

6 Performance Evaluation

In the preceding section, we examined how both compliance-based and projection-based models of the four-bar were subdivided into two-part systems to be run in a distributed manner on separate processors, requiring only the exchange of state information at every time instant. This was implemented using RT-LAB, a commercial off-the-shelf system for distributing the computation and a series of tests were performed to evaluate the performance of both methods of simulation. The numerical parameters of the system were chosen as shown in Table 1. The two primary metrics of performance evaluation were: (a) extent of the constraint error; and (b) number of iterations/computational time required for each method. This performance was evaluated using two separate scenarios: adaptive time-stepping and fixed time-stepping.

Link lengths	l_1 = 1.0m	l_2 = 2.5m	l_3 = 3.0m
Distance of mass centers	$l_{c1} = l_1/2$	$l_{c2} = l_2/2$	$l_{c3} = l_3/2$
Link masses	m_1 = 1.0 Kg.	m_2 = 1.0 Kg.	m_3 = 1.0 Kg
Mass moment of Inertias	$I_1 = m_1 l_1^2/12$	$I_2 = m_2 l_2^2/12$	$I_3 = m_3 l_3^2/12$
Initial Conditions (q(0))	θ = pi/2	α = 0.35328	ϕ = 1.26486
Torque inputs (u)	τ_1 = 6.0Nm	τ_2 = 0.0Nm	τ_3 = 0.0Nm

Table 1: Relevant numerical parameters for the four-bar linkage (Wang *et al.*, 2000)

6.1 Adaptive Time-stepping Scenario

In this scenario, the relative tolerance was pre-specified and an adaptive timestepping scheme is used for the simulation. Four different relative tolerances, varying in orders of magnitude from 1e-3 to 1e-6, were examined in this scenario. Each method has one independent parameter that could potentially affect the performance of the method – the stiffness of the virtual spring (K) in the compliance-based approach and the convergence factor (σ) in the case of the projection-based method. In the plots that result, we examine: the role of the independent parameter on the constraint error; and the effect of the independent parameter on the number of time-steps required to simulate a fixed simulation duration.

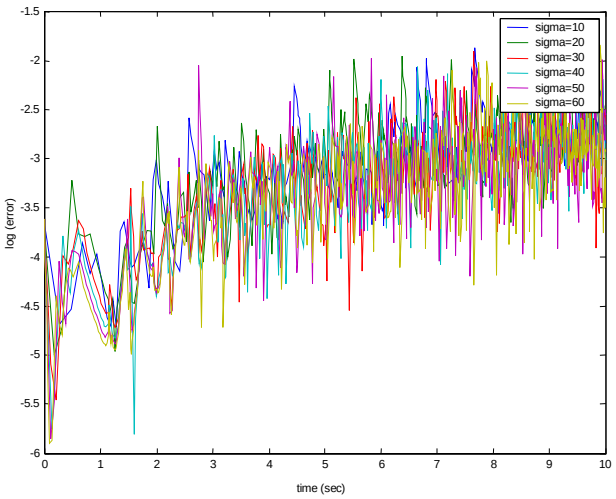

(a)

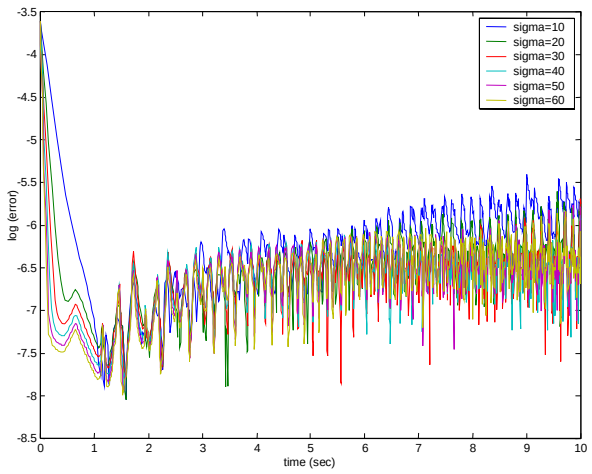

(b)

Figure 4: Constraint error in the projection-based approach using adaptive time-stepping for two sets of relative tolerances (a) 1e-3 and (b) 1e-6.

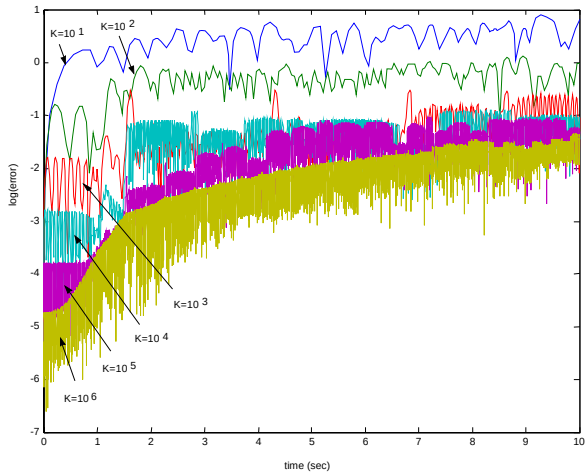

(a)

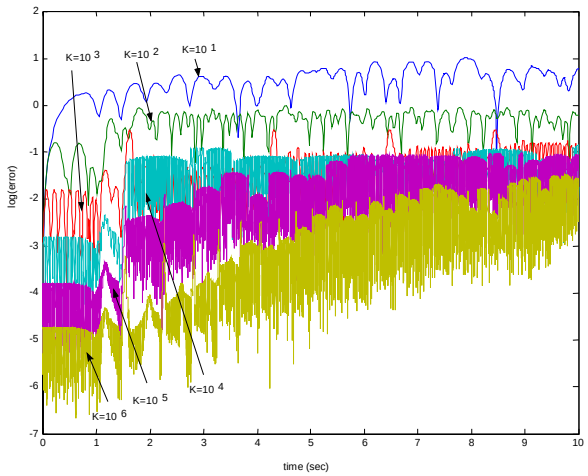

(b)

Figure 5: Constraint error in the compliance-based approach using adaptive timestepping for two sets of relative tolerances (a) 1e-3 and (b) 1e-6.

Figure 4 depicts the constraint error versus time for implementing the projection-based approach with different values of convergence factor (σ) for two sets of relative tolerances (1e-3 and 1e-6) using the ODE45 Dormand-Prince adaptive time step solver. As can be seen from the results, the convergence factor (σ) does not significantly affect the constraint errors and that the resulting relative constraint errors are representative of the selected relative tolerance settings.

Figure 5 shows the resulting constraint errors that result from implementing the compliance-based approach with different values of the spring constant (K) (varied in orders of magnitude from 1e1 to 1e6).

These were carried out for various settings of the relative tolerances of the adaptive time step solver but only shown here for two cases (1e-3 and 1e-6) in Fig. 5 (a) and (b) respectively. Qualitatively speaking, we note that decreasing the relative tolerance by three orders of magnitude did not affect the relative constraint errors, as can be seen by comparing Fig. 5 (a) and (b). However, within each graph, we note that the spring stiffness is increased, the constraint error drops commensurately but never attaining the performance levels of the projection-based method in Fig. 4.

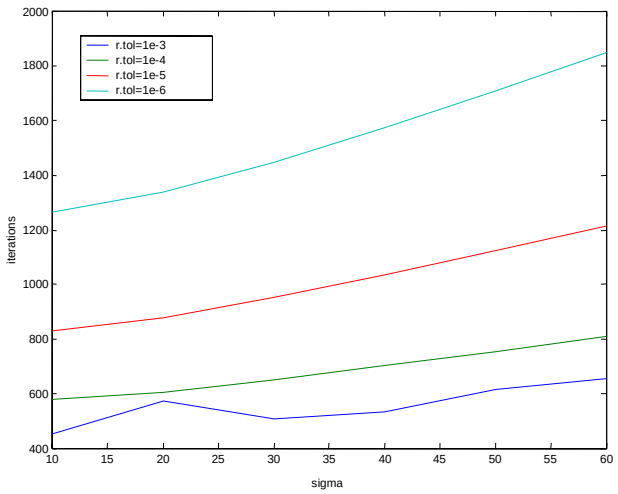

(a)

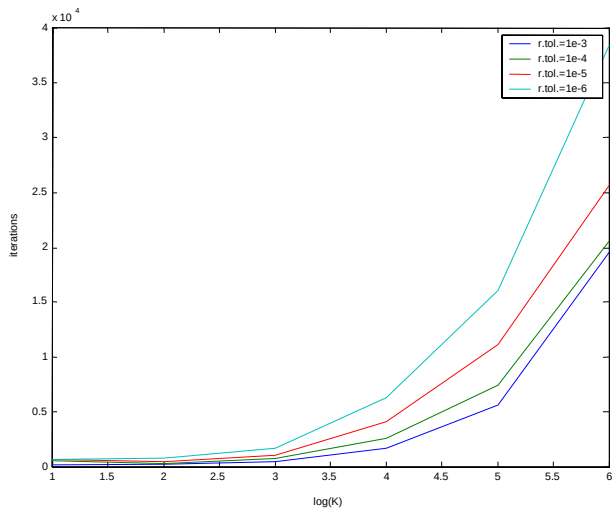

(b)

Figure 6: Number of iterations vs independent parameter for numerical integration of a 10 second duration with variable timestep for (a) Projection-based and (b) Compliance-based approaches.

To further compare the two methods in the adaptive time-stepping scenario, we examine the computational time required as measured in the number of discrete time-steps required to simulate 10 seconds. Figure 6 depicts the number of discrete time-steps of the adaptive time-stepping algorithm required to keep the constraint errors within the specified tolerances for different values of the parameters in each of the two methods. Two important features are to be noted: *First*, for increasing values of the parameter (σ or K) both methods show a distinct increases in the number of time-steps required to maintain a desired tolerance. However, while the rate of increase is linear in the case of the projection-based approach but tends to increase exponentially with increasing values of the spring stiffness in the compliance-based approach. *Secondly*, for a fixed value of

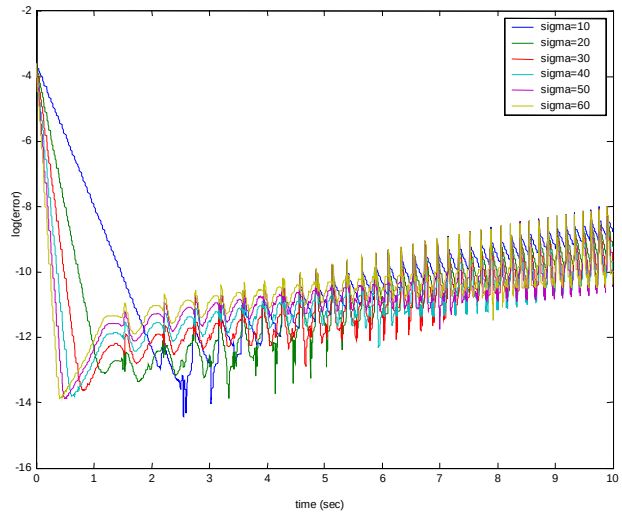

(a)

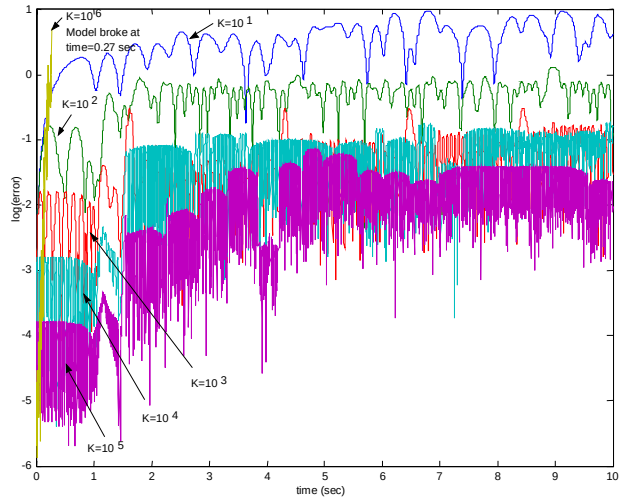

(b)

Figure 7: Constraint error for numerical integration with fixed timestep (1e-3 secs) for (a) Projection-based and (b) Compliance-based approaches.

the independent parameter, an exponential increase in the number of iterations can be seen with decreasing values of the relative tolerance in the compliance-based approach.

6.2 Fixed Time-stepping Case

This second scenario is more suited for real-time simulation and hardware-in-the-loop type simulation applications where deterministic time-stepping of the simulation is desirable. A number of simulations with different values for fixed time-steps (ranging from 1e-3 to 1e-6) were performed. However, only the resulting constraint errors from running the two simulation (compliance- and projection-based) schemes for a fixed step size of 0.001 seconds are shown in Fig. 7. In Fig. 7(a), we note that the selection of the value of the independent parameter (σ) only plays a minor role since regardless of the selected value the constraint error remains near about 1e-12. In contrast, in Fig. 7(b) we see that for

small values of the spring stiffness, considerable constraint error results which decreases as K is increased. While this constraint error reduces to the order of 1e-3 as the spring stiffness is increased to 1e6, this improvement is not comparable to the error magnitudes observed for the projection-based method.

7 Discussion

Schiehlen *et al.* (2000) performed a similar comparison by numerical simulation of a non-minimal description of a mechanical system obtained by coupling two or more minimal local subsystems with explicitly- or implicitly-stated holonomic constraints, with a variety of examples. They examined the effects of numerical integration with two similar classes of solution approaches, *i.e.* a so-called *force coupling approach*, which approximate the constraint forces by force laws proportional to the violation of coupling conditions; and the more traditional *differential algebraic approach*, using various integrators using projections on the position and velocity constraint manifold for stabilization.

As they note in their discussion, force coupled systems are especially sensitive to initial violations of the assembly conditions which may cause the coupling forces to create additional disturbances that excite the system. Further, such force-coupled systems can cause the dynamic behavior to be severely changed and even resulting in instability of the whole system. In contrast, they note that DAE description combined with integrators that use projection methods offer an efficient way of coupling local subsystems on the level of their equations of motion or for closing kinematic loops. Our own results, developed in the context of distributed computation of similar types of constrained dynamical systems match these observations.

In addition to the "natural" decoupling noted for the compliance-based formulation, several other advantages have been reported in the literature. These include the fact that appearance and disappearance of the constraints can be treated automatically and that the method performs robustly near kinematic singularity positions (Garcia de Jalón and Bayo, 1994). However, as noted by one of the reviewers, the Lagrange multipliers only form a part of the complete picture regarding the constraint forces. They represent the magnitude-type contribution while the other (and perhaps most important part) is the directional information that is embedded in the constraint Jacobian. The imperfect approximation of the Lagrange multipliers, coupled with the (artificial) relaxation of the constraints can over time lead to alternate configurations thereby indirectly affecting the directions of constraint vectors. Hence, not withstanding the small magnitudes of the constraint violations, the incorrect projection of the Lagrange multipliers would: yield seemingly correct but non-physical results; and additionally act as a continuous source of disturbance.

8 Summary

In this paper, we examined aspects of both the development and performance-evaluation of two alternate methods for distributed forward dynamics simulations of constrained mechanical systems exemplified by the four-bar linkage. Similar situations may also be encountered in other arenas where the governing equations take the form of sets of ODEs coupled together by algebraic constraints and solution of the combined system of DAEs needs to be found. We exploited the natural spatial parallelism of closed-chain manipulators initially for the modular development of overall dynamics and subsequently for the distributed numerical simulation of the dynamics. Traditionally, the numerical simulation problem has been treated as being composed of two more-or-less independent stages: an initial algorithm development stage followed by a numerical integration stage. While, the coupling of the two stages may not be as relevant for unconstrained mechanical systems, it plays a significant role for the simulation of constrained mechanical systems. Our preliminary results (examined in the context of four-bar linkage discussed in the previous section) indicates that a global unified view of the evaluation of the computational complexity of the simulation is advisable. Specifically, at an algorithmic development level, the compliance-based approach provides a seemingly natural method for decoupling and distributing the computation and has roughly one-third of the computational complexity of the projection-based approach. However, while the projection-based approach is computationally more expensive per time-step, fewer time-steps are required to maintain a desired relative constraint error tolerance leading to faster simulations.

Acknowledgements

We are indebted to the reviewers for their careful examination of the manuscript and their insightful comments that have helped to enhance the presented work. We would also like to acknowledge the support of the Natural Sciences and Engineering Research Council (NSERC) for support of this work.

9 References

Arnold, V. 1989, *Mathematical Methods of Classical Mechanics*, 2nd ed. New York: Springer-Verlag.

Ascher, U., Chin, H., Petzold, L., and Reich, S., 1995, "Stabilization of constrained mechanical systems with DAEs and invariant manifolds," *Mechanical Structures & Machines*, 23:135-158.

Ascher, U., Pai, D. K., and Cloutier, B., 1997, "Forward dynamics, elimination methods, and formulation stiffness in robot simulation," *The International Journal of Robotics Research*, 16(6):749-758.

Ascher, U., and Petzold, L., 1998, *Computer Methods for Ordinary Differential Equations and Differential-Algebraic Equations*, SIAM.

Ascher, U. and Lin, P., 1999, “Sequential regularization methods for simulating mechanical systems with many closed loops,” *SIAM Journal of Scientific Computing*, 21:1244-1262.

Baumgarte, J., 1983, “A new method of stabilization for holonomic constraints,” *ASME Journal of Applied Mechanics*, 50:869-870.

Blajer, W., Bestle, D., Schiehien W., 1994, "An orthogonal complement matrix formulation for constrained multibody systems," *ASME Journal of Mechanical Design*, Vol.116, pp. 423-428.

Chaudhary, V. and Aggarwal J. K., 1990, ”Parallelism in computer vision: A review”, in *Parallel Algorithms for Machine Intelligence and Vision*, Springer-Verlag:New York.

Featherstone, R., 1983, “The calculation of robot dynamics using articulated-body intertias,” *The International Journal of Robotics Research*, 2(1):13-30.

Featherstone, R., 1987, *Robot Dynamics Algorithms*, Kluwer.

Fijany, A. and Bejczy, A. K., 1992, *Parallel Computation Systems for Robotics: Algorithms and Architectures*, World Scientific, 1992.

García de Jalón, J., and Bayo, E., 1994, *Kinematic and Dynamic Simulation of Multibody Systems: The Real-Time Challenge*, Springer-Verlag, New-York.

Haug, E.J., 1989, *Computer-Aided Kinematics and Dynamics of Mechanical Systems*, Allyn and Bacon.

Henrich, D., and Höniger T., 1997, “Parallel processing approaches in robotics,” Proceedings of the *IEEE International Symposium on Industrial Electronics (ISIE'97)*, Guimaraes, Portugal, pp 702-707.

Kecskemethy, A., Krupp, T., and Hiller, M., 1997, “Symbolic processing of multi-loop mechanism dynamics using closed form kinematic solutions,” *Multibody System Dynamics*, 1(1):23-45.

Lee, C. S. G. and Chang, P. R., 1986, ``Efficient parallel algorithms for robot inverse dynamics computation,” *IEEE Transactions on Systems, Man, and Cybernetics*, 16:532-542.

Lee, C. S. G. and Chang, P. R., 1988, “Efficient parallel algorithms for robot forward dynamics computation,” *IEEE Transactions on Systems, Man, and Cybernetics*, 18:238-251.

McMillan, S., 1994, *Computational Dynamics for Robotic Systems on Land and Under Water*, Ph.D. Thesis, The Ohio State University, Columbus, OH.

Murray, R., Li, Z., and Sastry, S. S., 1994, *A Mathematical Introduction to Robotic Manipulation*, CRC Press.

Sadayappan, P., Ling, Y. L. C., Olson, K. W., and Orin, D. E., 1989, ``A restructurable VLSI robotics vector processor architecture for real-time control,” *IEEE Transactions on Robotics and Automation*, 5:583-599.

Serna, M.A., Avilés, R., and García de Jalón, J., 1982, "Dynamic Analysis of Plane Mechanisms with Lower-Pairs in Basic Coordinates", *Mechanism and MachineTheory*, Vol. 17, pp. 397-403.

Schiehlen, W., 1990, *Multibody Systems Handbook*, Springer-Verlag, Berlin.

Schiehlen W., Rukgauer A., and Schirle, Th., 2000, "Force Coupling versus Differential Algebraic Description of Constrained Multibody Systems", *Multibody System Dynamics*, 4(4):317-340.

Shabana, A.A., 1989, *Dynamics of Multibody Systems*, Wiley, New York.

Walker, M. W. and Orin, D. E., 1982, “Efficient dynamic computer simulation of robotic mechanisms,” *ASME Journal of Dynamic Systems, Measurement, and Control*, 104:205-211.

Wang, J., Gosselin, C.M. and Cheng, L., 2000, “Dynamic modeling and simulation of parallel mechanisms using the virtual spring approach”, Proceedings of *2000 ASME Design Engineering Technical Conferences*, Baltimore, Maryland, DETC2000/MECH-14107.

Yun, X. and Sarkar, N., 1998, “A unified formulation of robotic systems with holonomic and non holonomic constraints,” *IEEE Transactions on Robotics and Automation*, 14 (4): 640-650.

Zoyama A. B., 1993, *Modelling and Simulation of Robot Manipulators: a parallel processing approach*, Vol. 8, World Scientific Series in Robotics and Intelligent Systems. World Scientific.

Proceedings of the WORKSHOP on
Fundamental Issues and Future Research Directions for Parallel Mechanisms and Manipulators
October 3–4, 2002, Quebec City, Quebec, Canada
Clément M. Gosselin and Imme Ebert-Uphoff, editors

Review of the Role of Quasi-Coordinates for the Kinematic and Dynamic Modeling of Parallel Manipulators

IMME EBERT-UPHOFF
Woodruff School of Mechanical Engineering
Georgia Institute of Technology
Atlanta, GA 30332-0405, USA
ebert@me.gatech.edu

KRIS KOZAK
Woodruff School of Mechanical Engineering
Georgia Institute of Technology
Atlanta, GA 30332-0405, USA
gt3141a@prism.gatech.edu

Abstract:

This article discusses the role of quasi-coordinates for the kinematic and dynamic modeling of parallel manipulators. In contrast to serial manipulators, which do not require the use of quasi-coordinates for the dynamic modeling, quasi-coordinates are frequently used (implicitly) for parallel manipulators, but rarely ever discussed explicitly. Thus, there is very little discussion of quasi-coordinates in the general robotics literature. This paper seeks to close this gap, by providing specific references to classical dynamics literature on how to use quasi-coordinates for multibody systems such as parallel manipulators. The list of methods discussed in this paper, however, is by no means exhaustive and should only be seen as a starting point to make alternative dynamic modeling techniques more accessible to the parallel manipulator research community.

1 Introduction

This section seeks to answer two questions: (1) What is a quasi-coordinate and (2) why are quasi-coordinates important for the modeling of parallel manipulators? To answer the first question, the term quasi-coordinates can be defined as follows (Whittaker [1]):

Definition of a Quasi-Coordinate:
A quasi-coordinate, $\widetilde{p}$, is a coordinate for which only the time derivative, $\frac{d}{dt}\widetilde{p}$, must have a physical meaning. The quasi-coordinate $\widetilde{p}$ itself may not have a physical meaning. The time-derivative of a quasi-coordinate is called a quasi-velocity.

The most common occurrence of quasi-coordinates and *the only one of interest throughout this article* stems from the use of the angular velocity vector, $\mathbf{w}$, to describe the velocity of a rigid body, e.g. the end-effector of a parallel manipulator. $\mathbf{w}$ is a quasi-velocity, since it is well known that its integral generally does not have a physical meaning [2, 3], in the sense that the orientation cannot be retrieved from it (see Appendix). Note that within this manuscript, quasi-coordinates are always indicated with a tilde (e.g. $\widetilde{p}$), to emphasize that they may not have a physical meaning. In contrast a *true coordinate* is a coordinate with a clear physical meaning.

It remains to answer the second question: Why are quasi-coordinates important for the modeling of parallel manipulators? This question is answered in the following two subsections: Subsection 1.1 discusses the relevance of quasi-coordinates for velocity kinematics and Subsection 1.2 for the dynamic modeling.

1.1 What is the meaning of $\mathbf{x}$ in $\dot{\boldsymbol{\theta}} = \mathbf{J}\dot{\mathbf{x}}$?

The velocity kinematics of parallel manipulators with full six degrees-of-freedom is sometimes written in the form

$$\mathbf{J}_1\dot{\boldsymbol{\theta}} = \mathbf{J}_2\dot{\mathbf{x}}, \tag{1}$$

or, by defining $\mathbf{J} = \mathbf{J}_1^{-1}\mathbf{J}_2$,

$$\dot{\boldsymbol{\theta}} = \mathbf{J}\dot{\mathbf{x}}, \tag{2}$$

where $\boldsymbol{\theta}$ is the vector of actuated joint angles and $\mathbf{J}$ is the "geometric" Jacobian matrix of the manipulator (geometric and analytic Jacobian matrices are discussed in more detail in Subsection 2.2). Furthermore, $\dot{\mathbf{x}} = [\dot{r}_x, \dot{r}_y, \dot{r}_z, \omega_x, \omega_y, \omega_z]^T$ represents the linear and angular velocity of the end-effector, specifically, $[r_x, r_y, r_z]^T$ is the position of the mobile platform and $[\omega_x, \omega_y, \omega_z]^T$ is its angular velocity.

Since the integral of the angular velocity vector, $\mathbf{w} = [\omega_x, \omega_y, \omega_z]^T$, does not have a physical meaning, the question posed in this subsection's title about the meaning of $\mathbf{x}$ is somewhat ill-posed: $\mathbf{x}$ is a purely symbolic notation and its last three components, i.e. the integrals of $\omega_x, \omega_y, \omega_z$ do not have a physical meaning. In the language of analytical mechanics this

means that $\omega_x, \omega_y, \omega_z$ are quasi-velocities. The corresponding quasi-coordinates are denoted as $\widetilde{\boldsymbol{\pi}}$ in the following, where

$$\widetilde{\boldsymbol{\pi}} = \begin{bmatrix} \widetilde{\pi}_x \\ \widetilde{\pi}_y \\ \widetilde{\pi}_z \end{bmatrix} \quad \text{and} \quad \begin{bmatrix} \frac{d}{dt}\widetilde{\pi}_x \\ \frac{d}{dt}\widetilde{\pi}_y \\ \frac{d}{dt}\widetilde{\pi}_z \end{bmatrix} = \begin{bmatrix} \omega_x \\ \omega_y \\ \omega_z \end{bmatrix}.$$

$\mathbf{x}$ thus contains quasi-coordinates and should be written with a tilde:

$$\widetilde{\mathbf{x}} = [r_x, r_y, r_z, \widetilde{\pi}_x, \widetilde{\pi}_y, \widetilde{\pi}_z]^T. \tag{3}$$

However, even if $\mathbf{x}$ is replaced by $\widetilde{\mathbf{x}}$ in Equation (2), Equation (2) is still somewhat misleading[1]. Thus it is more appropriate and concise to write Equation (2) using a screw, $\$_t$, instead of $\dot{\widetilde{\mathbf{x}}}$:

$$\dot{\boldsymbol{\theta}} = \mathbf{J}\$_t \tag{4}$$

Similarly, Equation (1) then becomes $\mathbf{J}_1\dot{\boldsymbol{\theta}} = \mathbf{J}_2\$_t$.

1.2 Coordinates Used for the Dynamic Modeling of Serial and Parallel Manipulators

All of the comments from the preceding subsection apply equally to serial and parallel manipulators, the only difference being that for serial manipulators, the Jacobian matrix appears on the other side of Equations (2) and (4). Why then is it important to discuss the topic of quasi-coordinates for parallel manipulators, while it is of little relevance for serial manipulators?

The reason is that for serial manipulators it is not necessary to employ quasi-coordinates as generalized coordinates in the dynamic equations, since all terms can easily be described in the joint space. In contrast, for parallel manipulators, end-effector coordinates (or a combination of end-effector coordinates and other coordinates) are almost always the preferred choice to express the terms in the dynamic equations. This is discussed in more detail below.

- For serial manipulators, the set of actuated joint coordinates can always be used as a minimal set of generalized coordinates. These coordinates are automatically independent, since there are no closed kinematic chains. These generalized coordinates can then be used for example in Lagrange's equations or the principle of virtual work to derive the equations of motion. While the resulting expressions are generally far from trivial, each method is straightforward to apply.

- For parallel manipulators, the set of actuated joint coordinates can generally *not* be used as a minimal set of generalized coordinates. The reason is that since the forward kinematics can generally not be expressed in closed form, the position and orientation of the end-effector cannot be expressed in terms of only the actuated joint coordinates. Thus, writing the dynamic equations in terms of only these active joint coordinates is generally impossible. Since closed-form inverse kinematic expressions are often available for parallel manipulators, it is generally convenient to use the position and orientation of the end-effector instead as generalized coordinates. Furthermore, it is often convenient to use additional coordinates, e.g. to include the position and orientation of other parts of the manipulator to reduce the complexity of the expressions in the dynamic equations[2].

The fact that the orientation of the end-effector (and possibly of other moving bodies) is to be included in the generalized coordinates raises several questions: Which variables should be used to parameterize the orientation? Can quasi-coordinates be used for this purpose? Or is it necessary to use Euler angles?

Employing quasi-coordinates complicates the application of many methods from analytical mechanics, e.g. Lagrange's equations. Fortunately, the related issues are well known and well discussed in the general multibody dynamics literature. However, in spite of the fact that parallel manipulators are one instance of multibody systems, there is almost no discussion of these issues in the literature specifically dealing with parallel manipulators. In fact, textbooks on parallel manipulators discuss dynamic modeling only very briefly (Merlet [5]) and apply Lagrange's equations only for parallel manipulators with translation capabilities (Tsai [6]) and thus avoid having to deal with quasi-coordinates in Lagrange's equations or other methods.

This article seeks to provide additional references from the classical dynamics literature on how to deal with quasi-coordinates, in order to make this literature more accessible to the parallel manipulator research community.

1.3 Organization of This Article

The remainder of this article is organized as follows: Section 2 provides further background, including a more detailed discussion of quasi-coordinates, $\widetilde{\boldsymbol{\pi}}$, and the definition of the analytical and geometric Jacobian matrices. Section 3 reviews the use of quasi-coordinates for dynamic modeling using Newton-Euler, Virtual Work, Lagrange's Equations, the Boltzmann-Hamel Equations and the Gibbs-Appell Equations. While the comments in Section 3 are general, Section 4 derives the equations of motion of a simple parallel manipulator using each of the above methods. Section 5 summarizes the observations obtained in Sections 3 and 4. Section 6 presents conclusions.

2 Background

The issues discussed in this article are primarily of relevance for parallel manipulators satisfying both of the following assump-

[1] The authors find Equation (2) to be somewhat misleading, since it may give the impression that the taskspace (i.e. the position and orientation of the end-effector) can be parametrized by vector $\widetilde{\mathbf{x}}$. However, $\widetilde{\mathbf{x}}$ cannot be used to parameterize the taskspace as discussed in Subsection 2.1.

[2] Several articles have been published on selecting a suitable set of coordinates for the dynamic equations of parallel manipulators, see for example [4].

tions:

- **Assumption 1**: The forward kinematics of the manipulator cannot be expressed in closed form.
- **Assumption 2**: The end-effector has at least two degrees-of-rotation.

Manipulators that violate one of the above assumptions are generally simple enough not to require the use of quasi-coordinates. However, the majority of spatial parallel manipulators satisfy both assumptions.

The classic Gough-Stewart platform [7] is used as a pedagogical example throughout this article, because (1) this mechanism (and its dynamic modeling) is very well known and (2) it illustrates the common problems. The purpose of this article is not to find the simplest solution to modeling the Gough-Stewart platform, but to use it as example to highlight various alternatives for the dynamic modeling.

2.1 Relationships between $\boldsymbol{\phi}$ and $\widetilde{\boldsymbol{\pi}}$, $\dot{\boldsymbol{\phi}}$ and $\mathbf{w}$

The orientation of the end-effector is often denoted by Euler angles, ϕ_1, ϕ_2, ϕ_3. (It is of no importance in this context which Euler convention is used, e.g. ZYZ, etc.) The vector, $\boldsymbol{\phi} = [\phi_1, \phi_2, \phi_3]^T$, is introduced as a short notation for the set of Euler angles.

The velocity vectors $\dot{\boldsymbol{\phi}}$ and $\mathbf{w}$ can easily be related to each other by a configuration-dependent matrix. For example, if the ZYZ convention is used for the Euler angles, it holds [8] (page 102):

$$\begin{bmatrix} w_x \\ w_y \\ w_z \end{bmatrix} = \begin{bmatrix} 0 & -\sin(\phi_1) & \cos(\phi_1)\sin(\phi_2) \\ 0 & \cos(\phi_1) & \sin(\phi_1)\sin(\phi_2) \\ 1 & 0 & \cos(\phi_2) \end{bmatrix} \begin{bmatrix} \dot{\phi}_1 \\ \dot{\phi}_2 \\ \dot{\phi}_3 \end{bmatrix}, \tag{5}$$

which can be written as

$$\mathbf{w} \;=\; \mathbf{B}(\boldsymbol{\phi})\;\dot{\boldsymbol{\phi}}. \tag{6}$$

While the velocities, $\dot{\boldsymbol{\phi}}$ and $\mathbf{w}$, are directly related to each other by Equation (6), their integrals, i.e. $\boldsymbol{\phi}$ and $\widetilde{\boldsymbol{\pi}}$, cannot be related to each other. A simple example is provided in the Appendix that demonstrates this fact. That example clearly shows that it is *impossible* to recover the information of the orientation at the end of an arbitrary trajectory from the quantity $\widetilde{\boldsymbol{\pi}}(T) = \int_0^T \mathbf{w} dt$. **Thus it is impossible to establish a mapping from $\widetilde{\boldsymbol{\pi}}$ to $\boldsymbol{\phi}$, since information is lost in $\widetilde{\boldsymbol{\pi}}$. As a consequence it is also impossible to parameterize the taskspace, i.e. end-effector position and orientation, in terms of only $\mathbf{r}$ and $\widetilde{\boldsymbol{\pi}}$.**

2.2 Analytical and Geometric Jacobian Matrices

The Jacobian matrix of a manipulator can be defined in two ways, depending on whether $\mathbf{w}$ or $\dot{\boldsymbol{\phi}}$ is used to describe the angular velocity of the end-effector. Sciavicco and Siciliano [8] refer to these Jacobian matrices as *geometric Jacobian*, $\mathbf{J}_G$, or *analytical Jacobian*, $\mathbf{J}_A$, respectively. For parallel manipulators $\mathbf{J}_A$ and $\mathbf{J}_G$ can be defined as follows:

$$\dot{\boldsymbol{\theta}} = \mathbf{J}_G \begin{bmatrix} \dot{\mathbf{r}} \\ \mathbf{w} \end{bmatrix}, \qquad \dot{\boldsymbol{\theta}} = \mathbf{J}_A \begin{bmatrix} \dot{\mathbf{r}} \\ \dot{\boldsymbol{\phi}} \end{bmatrix}.$$

The two Jacobian matrices are related by matrix $\mathbf{B}(\boldsymbol{\phi})$ from Equation (6):

$$\mathbf{J}_A = \mathbf{J}_G \begin{bmatrix} \mathbf{Id}_{3\times 3} & \mathbf{0} \\ \mathbf{0} & \mathbf{B}(\boldsymbol{\phi}) \end{bmatrix},$$

where $\mathbf{Id}_{3\times 3}$ is the (3×3) identity matrix.

The challenge in the dynamic modeling arises from the fact that the vector of Euler angles, $\boldsymbol{\phi}$, is very suitable to express the orientation of the rigid body (mobile platform), but $\dot{\boldsymbol{\phi}}$ is not very suitable to describe its angular velocity. On the other hand, $\mathbf{w}$ is much more convenient to describe the angular velocity, but its integral, $\widetilde{\boldsymbol{\pi}}$, consists of quasi-coordinates.

3 Common Methods to Derive the Dynamic Equations

This section briefly describes the effect (if any) of quasi-coordinates on the modeling of the dynamic equations using (1) the method of Newton-Euler; (2) the principle of Virtual Work; (3) Lagrange's equations; (4) Boltzmann-Hamel Equations and (5) Gibbs-Appell Equations. Some of the descriptions in this section are kept rather short and are complemented by examples in Section 4 that further illustrate the key points.

3.1 Method of Newton-Euler

The method of Newton-Euler does not require the selection of generalized coordinates. As a consequence, there is no conflict in using $\boldsymbol{\phi}$ to describe orientation and $\mathbf{w}$ to describe angular velocity of any body in the system. Thus, the method of Newton-Euler is always a reliable way to determine the equations of motion of any parallel manipulator. While this method is not always the most computationally efficient, it is easy to understand and generally applicable. An example of its application is given in Subsection 4.1.

3.2 Virtual Work

The principle of virtual work has been successfully applied to parallel manipulators for several years [9, 10, 6, 11]. All of those articles employ quasi-coordinates to define virtual displacements, namely $\delta\mathbf{x}$, where $\mathbf{x}$ stands for $\tilde{\mathbf{x}} = [r_x, r_y, r_z, \widetilde{\pi}_x, \widetilde{\pi}_y, \widetilde{\pi}_z]^T$. Thus the use of $\delta\widetilde{\pi}_x, \delta\widetilde{\pi}_y, \delta\widetilde{\pi}_z$ is implicit in the formulation and not explicitly discussed. While this implicit use of $\delta\widetilde{\boldsymbol{\pi}}$ is permissible, it is not obvious *why* it is permissible. The purpose of this subsection is thus to review the reasons for the correctness of the use of $\delta\widetilde{\pi}_x, \delta\widetilde{\pi}_y, \delta\widetilde{\pi}_z$.

The formulation of the principle of virtual work in Lanczos [3] (pp. 74-79) for a mechanical system with external forces

$\mathbf{f}_1, \mathbf{f}_2, \ldots, \mathbf{f}_m$ acting at points $P_1, P_2, \ldots P_m$ of the system, respectively, serves as a starting point for the discussion. While the description focuses on the principle of virtual work for static equilibrium, the generalization to dynamics using the principle of d'Alembert is straight forward (for details see Lanczos [3]) and not discussed here. The virtual displacements of points, $P_1, \ldots, P_n$, are denoted as $\delta\mathbf{s}_1, \delta\mathbf{s}_2, \ldots, \delta\mathbf{s}_m$, respectively. The principle of virtual work can then be stated as follows:
The mechanical system is in equilibrium if and only if the total work of all impressed forces vanishes:

$$\delta W = \mathbf{f}_1 \cdot \delta\mathbf{s}_1 + \mathbf{f}_2 \cdot \delta\mathbf{s}_2 + \ldots + \mathbf{f}_m \cdot \delta\mathbf{s}_m = 0. \tag{7}$$

Standard Procedure:
When applying this principle to a given mechanical system, the typical next step is to select a convenient set of *true* coordinates as generalized coordinates, $q_1, q_2, \ldots, q_n$, and to express the position, $\mathbf{s}_k$, of point P_k as a function of those coordinates: $\mathbf{s}_k = \mathbf{s}_k(q_1, \ldots, q_n)$. The corresponding virtual displacement is $\delta\mathbf{s}_k = \sum_{j=1}^{n} \frac{\partial \mathbf{s}_k}{\partial q_j}\delta q_j$ and Equation (7) becomes

$$\begin{aligned} \delta W &= \sum_{i=1}^{m} \mathbf{f}_i \cdot \delta\mathbf{s}_i = \sum_{i=1}^{m} \mathbf{f}_i \cdot \left(\sum_{j=1}^{n} \frac{\partial \mathbf{s}_k}{\partial q_j}\delta q_j \right) \\ &= \sum_{j=1}^{n} \underbrace{\left(\sum_{i=1}^{m} \mathbf{f}_i \cdot \frac{\partial \mathbf{s}_k}{\partial q_j} \right)}_{Q_j} \delta q_j = \sum_{j=1}^{n} Q_j \; \delta q_j = 0, \end{aligned} \tag{8}$$

where Q_j is the generalized force (scalar) corresponding to generalized coordinate q_j. Equation (8) is a convenient form, because a system's motion can now be described in terms of any desired choice of generalized coordinates, rather than the explicit coordinates of m points. However, since the expression $\mathbf{s}_k = \mathbf{s}_k(q_1, \ldots, q_n)$, which was used in the derivation, only applies for true coordinates, the question arises whether Equation (8) applies if the q_j include quasi-coordinates, specifically $\widetilde{\pi}_x, \widetilde{\pi}_y, \widetilde{\pi}_z$.

Body-oriented Formulation:
To derive a formulation more suitable to parallel manipulators it is necessary to go back to Equation (7). What we really want for a multi-body system, such as a parallel manipulator, is to move from a point-oriented to a body-oriented description of the motion. Thus, let us assume that point P_k lies on body k and that the displacement and velocity of P_k can thus be expressed in terms of the motion of body k.

Let $\mathbf{r}_k$ denote the position of reference point R_k of body k, as shown in Figure 1, $\dot{\mathbf{r}}_k$ the linear velocity of point R_k, $\mathbf{w}_k$ the body's angular velocity and $\widetilde{\boldsymbol{\pi}}_k$ the corresponding quasi-coordinates. The velocity $\dot{\mathbf{s}}_k$ of point P_k can be expressed as:

$$\dot{\mathbf{s}}_k = \dot{\mathbf{r}}_k + \mathbf{w}_k \times \underbrace{(\mathbf{s}_k - \mathbf{r}_k)}_{\mathbf{c}_k} \quad \text{or} \quad \frac{d\mathbf{s}_k}{dt} = \frac{d\mathbf{r}_k}{dt} + \frac{d\widetilde{\boldsymbol{\pi}}_k}{dt} \times \mathbf{c}_k,$$

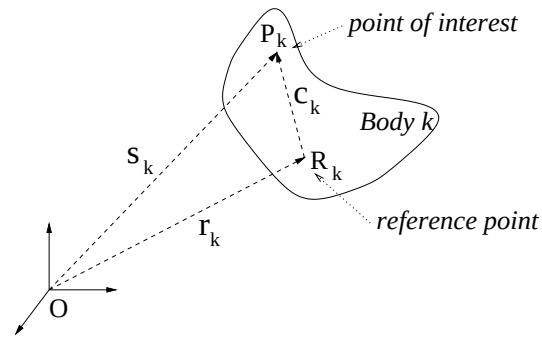

Figure 1: Point of interest, P_k, and reference point, R_k, on Body k.

where $\mathbf{c}_k = \mathbf{s}_k - \mathbf{r}_k$ is the vector from reference point R_k to point P_k (see Figure 1). Since only 1st order differentials are considered, $\mathbf{c}_k$ can be treated as constant, and we can multiply both sides by dt to obtain a relation between infinitesimal displacements (differentials):

$$d\mathbf{s}_k = d\mathbf{r}_k + d\widetilde{\boldsymbol{\pi}}_k \times \mathbf{c}_k. \tag{9}$$

To make the role of $d\widetilde{\boldsymbol{\pi}}_k$ above even more clear, it is helpful to look at a different way of deriving Equation (9). Instantaneously $\mathbf{w}_k$ can be described as $\mathbf{w}_k = \dot{\psi}_k \mathbf{e}_k$, where $\dot{\psi}_k$ is the angular speed and $\mathbf{e}_k$ (unit vector) its instantaneous axis of rotation, resulting in the same relationship as Equation (9):

$$\begin{aligned} d\mathbf{s}_k &= \dot{\mathbf{r}}_k \; dT + (\mathbf{w}_k \times \mathbf{c}_k) \; dT = \dot{\mathbf{r}}_k \; dT + \left(\dot{\psi} \; dT\right) \mathbf{e}_k \times \mathbf{c}_k \\ &= d\mathbf{r}_k + (d\psi \; \mathbf{e}_k) \times \mathbf{c}_k = d\mathbf{r}_k + d\widetilde{\boldsymbol{\pi}} \times \mathbf{c}_k. \end{aligned} \tag{10}$$

Equation (10) highlights that the first-order differential $d\widetilde{\boldsymbol{\pi}} = d\psi \mathbf{e}_k$ represents the rotation by angle $d\psi$ about a constant axis, namely the instantaneous axis of rotation, $\mathbf{e}_k$.

It only remains to relate the first-order differentials in Equation (9) to virtual displacements, and virtual work, respectively. As described in [12] (p. 241), the virtual displacement $\delta\mathbf{x}$ of any vector $\mathbf{x}$ can be seen as the first-order differential of $\mathbf{x}$ with time kept constant, $t =$ constant. Since Equation (9) is already independent of time, it suffices to replace all differentials d by virtual displacements δ:

$$\delta\mathbf{s}_k = \delta\mathbf{r}_k + \delta\widetilde{\boldsymbol{\pi}}_k \times \mathbf{c}_k. \tag{11}$$

Calculation of the desired virtual work term requires only simple algebraic transformations:

$$\begin{aligned} \delta W_k &= \mathbf{f}_k \cdot \delta\mathbf{c}_k = \mathbf{f}_k \cdot (\delta\mathbf{r}_k + \delta\widetilde{\boldsymbol{\pi}}_k \times \mathbf{c}_k) \\ &= \mathbf{f}_k \cdot \delta\mathbf{r}_k + \mathbf{f}_k \cdot (\delta\widetilde{\boldsymbol{\pi}}_k \times \mathbf{c}_k) \\ &= \mathbf{f}_k \cdot \delta\mathbf{r}_k + \delta\widetilde{\boldsymbol{\pi}}_k \cdot \underbrace{(\mathbf{c}_k \times \mathbf{f}_k)}_{\mathbf{m}_k} \\ &= \mathbf{f}_k \cdot \delta\mathbf{r}_k + \mathbf{m}_k \cdot \delta\widetilde{\boldsymbol{\pi}}_k, \end{aligned}$$

where $\mathbf{m}_k$ is the moment at point P_k resulting from force $\mathbf{f}_k$ applied at reference point R_k.

Thus Equation (7) can be written directly in the desired form, containing the quasi-coordinates:

$$\begin{aligned} \delta W &= \sum \mathbf{f}_k \cdot \delta \mathbf{r}_k + \mathbf{m}_k \cdot \delta \widetilde{\boldsymbol{\pi}}_k \\ &= \sum \begin{bmatrix} \mathbf{f}_k \\ \mathbf{m}_k \end{bmatrix} \cdot \begin{bmatrix} \delta \mathbf{r}_k \\ \delta \widetilde{\boldsymbol{\pi}}_k \end{bmatrix} = 0, \end{aligned} \tag{12}$$

where each term $\mathbf{f}_k, \mathbf{m}_k$ denotes a force and/or moment applied at body k and $\delta \mathbf{r}_k$ and $\delta \widetilde{\boldsymbol{\pi}}_k$ represent any motion of that body in accordance with the constraints. In summary, it is therefore permissible to use the quasi-coordinates, $\widetilde{\boldsymbol{\pi}}$, as virtual displacement $\delta \widetilde{\boldsymbol{\pi}}$ in the way indicated in Equation (12) and used by many authors [9, 10, 6, 11].

While the *use* of Equation (12) is straightforward and well discussed [9, 10, 6, 11], a simple example of its application is given in Subsection 4.2 for completeness.

3.3 Lagrange's Equations for True Coordinates (Standard Form)

To apply Lagrange's equations in the standard form, one must start out with a set of generalized coordinates, $\mathbf{q} = [q_1, \ldots, q_n]^T$, which may *not* include quasi-coordinates. One may choose to use position vector, $\mathbf{r}$, Euler angle vector, $\boldsymbol{\phi}$, plus, if desired, other coordinates:

$$\mathbf{q} = [r_x, r_y, r_z, \phi_1, \phi_2, \phi_3, \text{plus others as desired}]^T .$$

The well-known Lagrange's equations can then be written in vector form as follows:

$$\frac{d}{dt}\left(\frac{\partial T}{\partial \dot{\mathbf{q}}}\right) - \left(\frac{\partial T}{\partial \mathbf{q}}\right) + \left(\frac{\partial V}{\partial \mathbf{q}}\right) = \mathbf{Q} + \mathcal{B}^T \boldsymbol{\lambda}, \tag{13}$$

with constraint equation

$$\mathbf{c}(\mathbf{q}) = \mathbf{0}.$$

$\mathbf{Q}$ denotes the vector of generalized forces, $\boldsymbol{\lambda}$ are Lagrange multipliers and $\mathcal{B}$ is the constraint matrix. (Of course, $\boldsymbol{\lambda}$ and $\mathcal{B}$ appear only in Equation (13), if the number of generalized coordinates exceeds the number of degrees of freedom of the system. Matrix $\mathcal{B}$ is obtained from constraint vector $\mathbf{c}(\mathbf{q})$ as $\mathcal{B} = \frac{\partial \mathbf{c}}{\partial \mathbf{q}}$, which is also known as the Jacobian of $\mathbf{c}(\mathbf{q})$.)

However, taking derivatives, such as $\frac{\partial}{\partial \dot{\phi}_i}(T)$, where T now contains terms such as

$$\frac{1}{2}\, \mathbf{w}^T\, \mathbf{I}_{\text{PF}}\, \mathbf{w} = \frac{1}{2}\, \dot{\boldsymbol{\phi}}^T\, \mathbf{B}^T(\boldsymbol{\phi})\, \mathbf{I}_{\text{PF}}\, \mathbf{B}(\boldsymbol{\phi})\, \dot{\boldsymbol{\phi}},$$

and $\mathbf{I}_{\text{PF}}$ is the tensor of inertia of the body, leads to complex expressions. Taking these derivatives is not difficult, but handling the resulting terms is messy. (An example is given in Subsection 4.3.) Therefore, Lagrange's equations in standard form are rarely used to model parallel manipulators with full three degrees-of-orientation at the end-effector.

3.4 Lagrange's Equations for Quasi-Coordinates (Boltzmann-Hamel Equations)

Lagrange's equations can be modified to apply to quasi-coordinates, as described for example by Whittaker [1] (pp. 41-44) and by Meirovitch [13] (pp. 157-160). The resulting equations are often called the Boltzmann-Hamel equations [1]. Meirovitch [13] provides an excellent description of the derivation. While Lagrange's equations for true coordinates are discussed extensively in most dynamics textbooks, the Boltzmann-Hamel equations receive much less attention. Therefore they are discussed in this subsection in greater detail than some of the other methods.

Basically, one starts with Lagrange's equations for true coordinates in the form

$$\frac{d}{dt}\left(\frac{\partial T}{\partial \dot{\mathbf{q}}}\right) - \left(\frac{\partial T}{\partial \mathbf{q}}\right) + \left(\frac{\partial V}{\partial \mathbf{q}}\right) = \mathbf{Q}, \tag{14}$$

where $T = T(\mathbf{q}, \dot{\mathbf{q}})$ describes the system's kinetic energy in terms of generalized coordinates $\mathbf{q}$. The goal is to rewrite Equation (14) in terms of a new function, $\bar{T} = \bar{T}(\mathbf{q}, \dot{\tilde{\mathbf{p}}})$, which expresses the kinetic energy in terms of true coordinates $\mathbf{q}$ and quasi-velocities $\dot{\tilde{\mathbf{p}}}$. Here $\tilde{\mathbf{p}}$ may denote any vector of quasi-velocities that can be related to $\dot{\mathbf{q}}$ by an invertible matrix, $\boldsymbol{\mathcal{D}}$, as follows:

$$\dot{\tilde{\mathbf{p}}} = \boldsymbol{\mathcal{D}}^T \dot{\mathbf{q}}, \qquad \dot{\mathbf{q}} = \boldsymbol{\mathcal{D}}^{-T} \dot{\tilde{\mathbf{p}}}. \tag{15}$$

where matrix $\boldsymbol{\mathcal{D}} = \boldsymbol{\mathcal{D}}(\mathbf{q})$ is a function of $\mathbf{q}$.

The case of interest here is $\dot{\tilde{\mathbf{p}}} = \begin{bmatrix} \dot{\mathbf{r}} \\ \mathbf{w} \end{bmatrix}$, since the kinetic energy can then be written directly in the convenient form,

$$\bar{T} = \bar{T}(\mathbf{q}, \dot{\tilde{\mathbf{p}}}) = \bar{T}\left(\begin{bmatrix} \mathbf{r} \\ \boldsymbol{\phi} \end{bmatrix}, \begin{bmatrix} \dot{\mathbf{r}} \\ \mathbf{w} \end{bmatrix}\right).$$

Employing Equation (15) repeatedly to relate the partial derivatives of T to those of $\bar{T}$ (see [13] for details), leads to a first version of Lagrange's Equations for Quasi-Coordinates:

$$\boldsymbol{\mathcal{D}} \frac{d}{dt}\left(\frac{\partial \bar{T}}{\partial \dot{\tilde{\mathbf{p}}}}\right) + \boldsymbol{\mathcal{E}}\left(\frac{\partial \bar{T}}{\partial \dot{\tilde{\mathbf{p}}}}\right) - \left(\frac{\partial \bar{T}}{\partial \mathbf{q}}\right) + \left(\frac{\partial V}{\partial \mathbf{q}}\right) = \mathbf{Q}, \tag{16}$$

where matrix $\boldsymbol{\mathcal{E}}$ is defined in terms of its row vectors as

$$\boldsymbol{\mathcal{E}} = \begin{bmatrix} \left(\dot{\tilde{\mathbf{p}}}^T \boldsymbol{\mathcal{D}}^{-1}\right)\left(\nabla_{\mathbf{q}} \mathbf{d}_1 - \frac{\partial \boldsymbol{\mathcal{D}}}{\partial q_1}\right) \\ \hline \vdots \\ \hline \left(\dot{\tilde{\mathbf{p}}}^T \boldsymbol{\mathcal{D}}^{-1}\right)\left(\nabla_{\mathbf{q}} \mathbf{d}_n - \frac{\partial \boldsymbol{\mathcal{D}}}{\partial q_n}\right) \end{bmatrix},$$

wherein $\mathbf{d}_i$ denotes the ith vector of matrix $\boldsymbol{\mathcal{D}}$ and matrix $(\nabla_{\mathbf{q}} \mathbf{d}_i)$ denotes $\mathbf{d}_i$'s gradient with respect to $\mathbf{q}$. By multiplying Equation (16) by $\boldsymbol{\mathcal{D}}^{-1}$ from the left, one obtains the more common form:

$$\frac{d}{dt}\left(\frac{\partial \bar{T}}{\partial \dot{\tilde{\mathbf{p}}}}\right) + \boldsymbol{\mathcal{D}}^{-1}\boldsymbol{\mathcal{E}}\left(\frac{\partial \bar{T}}{\partial \dot{\tilde{\mathbf{p}}}}\right) - \boldsymbol{\mathcal{D}}^{-1}\left(\frac{\partial \bar{T}}{\partial \mathbf{q}}\right) + \boldsymbol{\mathcal{D}}^{-1}\left(\frac{\partial V}{\partial \mathbf{q}}\right) = \boldsymbol{N}, \tag{17}$$

where $\boldsymbol{N} = \boldsymbol{\mathcal{D}}^{-1}\mathbf{Q}$ are the generalized forces corresponding to $\dot{\tilde{\mathbf{p}}}$, just as $\mathbf{Q}$ are the generalized forces corresponding to $\dot{\mathbf{q}}$ in Equation (14). Equation (17) is known as Lagrange's equations for quasi-coordinates or as Boltzmann-Hamel equations.

For the case of interest, $\dot{\tilde{\mathbf{p}}} = \begin{bmatrix} \dot{\mathbf{r}} \\ \mathbf{w} \end{bmatrix}$, we get the following simplifications:

$$\begin{aligned} \boldsymbol{\mathcal{D}} &= \begin{bmatrix} \mathbf{Id}_{3\times 3} & \mathbf{0} \\ \mathbf{0} & \mathbf{B}(\boldsymbol{\phi})^T \end{bmatrix}, \\ \boldsymbol{\mathcal{D}}^{-1} &= \begin{bmatrix} \mathbf{Id}_{3\times 3} & \mathbf{0} \\ \mathbf{0} & \mathbf{B}(\boldsymbol{\phi})^{-T} \end{bmatrix}, \end{aligned} \tag{18}$$

and algebraic transformations yield

$$\boldsymbol{\mathcal{D}}^{-1}\,\boldsymbol{\mathcal{E}} = \begin{bmatrix} \mathbf{0} & \mathbf{0} \\ \mathbf{0} & \boldsymbol{\Omega} \end{bmatrix}, \tag{19}$$

where $\boldsymbol{\Omega}$ is the skew-symmetric matrix corresponding to angular velocity $\mathbf{w}$, i.e. $\boldsymbol{\Omega}\mathbf{y} = \mathbf{w} \times \mathbf{y}$ for any vector $\mathbf{y}$. Thus Equation (17) simplifies to a very convenient form:

$$\frac{d}{dt}\left(\frac{\partial \bar{T}}{\partial \dot{\tilde{\mathbf{p}}}}\right) + \begin{bmatrix} \mathbf{0} & \mathbf{0} \\ \mathbf{0} & \boldsymbol{\Omega} \end{bmatrix}\left(\frac{\partial \bar{T}}{\partial \dot{\tilde{\mathbf{p}}}}\right) - \boldsymbol{\mathcal{D}}^{-1}\left(\frac{\partial \bar{T}}{\partial \mathbf{q}}\right) + \boldsymbol{\mathcal{D}}^{-1}\left(\frac{\partial V}{\partial \mathbf{q}}\right) = \boldsymbol{N}. \tag{20}$$

Its use is demonstrated in Subsection 4.4.

3.5 Gibbs-Appell Equations for Quasi-Coordinates

Yet another tool from analytical mechanics that deals with quasi-coordinates in an effective way is the Gibbs-Appell Equations for quasi-coordinates, see for example [2] (pp. 347-364), which are also often referred to as Appell Equations [14]. For the Gibbs-Appell equations, one starts out with a set of generalized coordinates, $\tilde{\gamma}$, which may contain quasi-coordinates. The system is described in terms of the Gibbs-Appell function, S, (an expression which is often referred to as the 'energy of acceleration') and, similarly to Lagrange's equations above, the equations of motion are calculated by taking derivatives, and setting them equal to generalized forces $\boldsymbol{\Gamma}$:

$$\frac{\partial S}{\partial \ddot{\tilde{\gamma}}} = \boldsymbol{\Gamma}.$$

A significant difference, however, is that derivatives are only taken with respect to the quasi-accelerations, $\ddot{\tilde{\gamma}}$, but neither with respect to quasi-coordinates nor to quasi-velocities. Therefore this method is very suitable for application to quasi-coordinates. This method is illustrated in Section 4.5 below.

4 Application to Simplified Gough-Stewart Platform

This section derives the equations of motion using the previously described techniques for a simple example, namely a Gough-Stewart platform with the following assumptions:

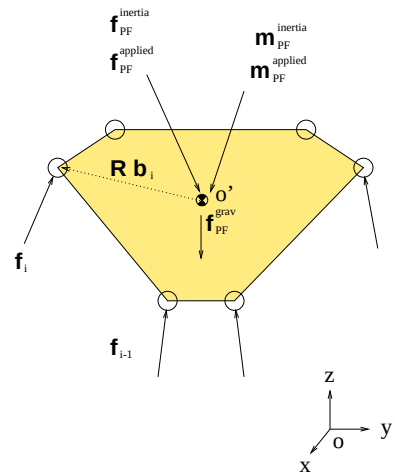

Figure 2: Free body diagram of the mobile platform

- The legs are massless, so that the only significant mass belongs to the moving platform.
- Consequently, inertia and gravitational forces and moments arise only from the moving platform.
- The origin of the body-fixed coordinate system on the moving platform is chosen to be at the center of mass of the platform. Thus, gravitational force and linear inertia do not cause any moment.
- The actuator torques in the legs are transferred as pure forces at the leg attachment points at the end-effector.
- An external force and moment is applied at the platform's center-of-mass.

While the leg masses are assumed negligible throughout this section for the sake of simplicity, comments are included on how to extend the model to incorporate the mass of any other moving bodies in the system (including leg masses).

The following variables are used throughout this section:

m, $\mathbf{I}_{\mathbf{PF}}$: Mass and inertia matrix of mobile platform;

$\mathbf{r}$: Location of center of mass of mobile platform;

$\boldsymbol{\mathcal{R}}$: Rotation matrix describing orientation of mobile platform;

$\mathbf{w}$: Angular velocity of mobile platform;

$\mathbf{b}_i$: Vector from platform's center of mass to attachment point of ith leg (in local platform coordinates);

$\mathbf{f}_i$: Actuator force in ith leg;

$\mathbf{f}_{\mathbf{PF}}^{\mathbf{grav}}$: Gravitational force of mobile platform;

$\mathbf{f}_{\mathbf{PF}}^{\mathbf{inertia}}$, $\mathbf{m}_{\mathbf{PF}}^{\mathbf{inertia}}$: Inertia force and moment of mobile platform at center-of-mass;

$\mathbf{f}_{\mathbf{PF}}^{\mathbf{applied}}$, $\mathbf{m}_{\mathbf{PF}}^{\mathbf{applied}}$: External force and moment applied at platform's center-of-mass.

4.1 Newton-Euler

Figure 2 shows a free-body diagram of the mobile platform. The balance of forces and moments at the platform results in two vector equations:

$$\begin{aligned}\underbrace{\mathbf{f}_{\text{PF}}^{\text{applied}} + \mathbf{f}_{\text{PF}}^{\text{grav}} + \mathbf{f}_{\text{PF}}^{\text{inertia}}}_{\mathbf{f}_{\text{PF}}} + \sum_{i=1}^{6} \mathbf{f}_i &= \mathbf{0} \\ \underbrace{\mathbf{m}_{\text{PF}}^{\text{applied}} + \mathbf{0} + \mathbf{m}_{\text{PF}}^{\text{inertia}}}_{\mathbf{m}_{\text{PF}}} + \sum_{i=1}^{6} (\boldsymbol{\mathcal{R}}\mathbf{b}_i) \times \mathbf{f}_i &= \mathbf{0}\end{aligned}$$

where

$$\begin{aligned}\mathbf{f}_{\text{PF}}^{\text{grav}} &= -m\, g\, \mathbf{e}_z \\ \mathbf{f}_{\text{PF}}^{\text{inertia}} &= -m\, \ddot{\mathbf{r}} \\ \mathbf{m}_{\text{PF}}^{\text{inertia}} &= -\left[\mathbf{I}_{\text{PF}}\dot{\mathbf{w}} + \mathbf{w} \times (\mathbf{I}_{\text{PF}}\mathbf{w})\right]\end{aligned}$$

and the terms $\sum_{i=1}^{6} \mathbf{f}_i$ and $\sum_{i=1}^{6} (\boldsymbol{\mathcal{R}}\mathbf{b}_i) \times \mathbf{f}_i$ can be related to the geometric Jacobian matrix, $\mathbf{J}_G$, as follows (based on the fact that leg inertia is ignored):

$$\begin{bmatrix} \sum_{i=1}^{6} \mathbf{f}_i \\ \sum_{i=1}^{6} (\boldsymbol{\mathcal{R}}\mathbf{b}_i) \times \mathbf{f}_i \end{bmatrix} = \mathbf{J}_G^T\, \boldsymbol{\tau}.$$

Thus the two vector equations can be combined into the following equation:

$$\begin{bmatrix} \mathbf{f}_{\text{PF}}^{\text{applied}} \\ \mathbf{m}_{\text{PF}}^{\text{applied}} \end{bmatrix} + \begin{bmatrix} -mg\mathbf{e}_z \\ \mathbf{0} \end{bmatrix} + \begin{bmatrix} -m\ddot{\mathbf{r}} \\ -\mathbf{I}_{\text{PF}}\dot{\mathbf{w}} - \mathbf{w} \times (\mathbf{I}_{\text{PF}}\mathbf{w}) \end{bmatrix} + \mathbf{J}_G^T\, \boldsymbol{\tau} = \mathbf{0}. \quad (21)$$

Summary for Newton-Euler: The method of Newton-Euler is straight-forward and does not employ quasi-coordinates in any way, although angular velocity vectors are used in the equations of motion.

Extension - If other moving bodies are to be considered: It is well known that the method of Newton-Euler extends easily to more complex cases, where the mass and inertia of many moving bodies is considered. For details, see for example [15, 6].

4.2 Virtual Work

The principle of virtual work is commonly written for simple parallel manipulators as follows:

$$\delta W = \begin{bmatrix} \mathbf{f}_{\text{PF}} \\ \mathbf{m}_{\text{PF}} \end{bmatrix}^T \delta\mathbf{x} + \boldsymbol{\tau}^T\, \delta\boldsymbol{\theta} = 0, \quad (22)$$

where $\mathbf{f}_{\text{PF}}, \mathbf{m}_{\text{PF}}$ denotes the sum of forces and moments acting on the mobile platform defined in Subsection 4.1. However, as we already know from Subsection 3.2, $\delta\mathbf{x}$ takes the role of vector $\delta\widetilde{\mathbf{x}} = \begin{bmatrix} \delta\mathbf{r} \\ \delta\widetilde{\boldsymbol{\pi}} \end{bmatrix}$. Equation (22) thus really implies:

$$\delta W = \begin{bmatrix} \mathbf{f}_{\text{PF}} \\ \mathbf{m}_{\text{PF}} \end{bmatrix}^T \underbrace{\begin{bmatrix} \delta\mathbf{r} \\ \delta\widetilde{\boldsymbol{\pi}} \end{bmatrix}}_{\delta\widetilde{\mathbf{x}}} + \boldsymbol{\tau}^T\, \delta\boldsymbol{\theta} = 0. \quad (23)$$

Substituting the terms for the forces and moments acting on the mobile platform yields

$$\delta W = \begin{bmatrix} \mathbf{f}_{\text{PF}}^{\text{applied}} & +\mathbf{f}_{\text{PF}}^{\text{grav}} & +\mathbf{f}_{\text{PF}}^{\text{inertia}} \\ \mathbf{m}_{\text{PF}}^{\text{applied}} & & +\mathbf{m}_{\text{PF}}^{\text{inertia}} \end{bmatrix}^T \begin{bmatrix} \delta\mathbf{r} \\ \delta\widetilde{\boldsymbol{\pi}} \end{bmatrix} + \boldsymbol{\tau}^T\, \delta\boldsymbol{\theta} = 0.$$

By substituting the relationship

$$\delta\boldsymbol{\theta} = \mathbf{J}_G \begin{bmatrix} \delta\mathbf{r} \\ \delta\widetilde{\boldsymbol{\pi}} \end{bmatrix}$$

and eliminating $\delta\mathbf{r}$, $\delta\widetilde{\boldsymbol{\pi}}$, we obtain the well-known relationship:

$$\begin{bmatrix} \mathbf{f}_{\text{PF}}^{\text{applied}} & +\mathbf{f}_{\text{PF}}^{\text{grav}} & +\mathbf{f}_{\text{PF}}^{\text{inertia}} \\ \mathbf{m}_{\text{PF}}^{\text{applied}} & & +\mathbf{m}_{\text{PF}}^{\text{inertia}} \end{bmatrix} + \mathbf{J}_G^T\, \boldsymbol{\tau} = \mathbf{0},$$

which, after substitution of all terms, is identical to Equation (21).

Summary for Virtual Work: The principle of virtual work is also straight-forward to apply and yields equations of the same form as the method of Newton-Euler. However, for this method it was necessary to employ quasi-coordinates for the virtual displacements. This is a subtle detail that is rarely mentioned and the proof of correctness of this approach is neither trivial nor completely obvious.

Extension – If other moving bodies are to be considered: It is well known that the principle of virtual work extends easily to more complex cases, where the mass and inertia of many moving bodies is considered. The equations are then written in the form:

$$\delta W = \begin{bmatrix} \mathbf{f}_{\text{PF}} \\ \mathbf{m}_{\text{PF}} \end{bmatrix}^T \delta\widetilde{\mathbf{x}}_{\text{PF}} + \sum_{j=1}^{J} \begin{bmatrix} \mathbf{f}_j \\ \mathbf{m}_j \end{bmatrix}^T \delta\widetilde{\mathbf{x}}_j + \boldsymbol{\tau}\, \delta\boldsymbol{\theta} = \mathbf{0},$$

where $\widetilde{\mathbf{x}}_j$ denotes the quasi-coordinates for the jth body, and $\mathbf{f}_j, \mathbf{m}_j$ denote the forces and moments acting on the jth body. The quasi-coordinates of the ith body are related to the quasi-coordinates at the end-effector through leg Jacobian matrices, $\delta\widetilde{\mathbf{x}}_j = \mathbf{J}_i \delta\widetilde{\mathbf{x}}$. For details, see [9, 10, 6, 11].

4.3 Lagrange's Equations for True Coordinates (Standard Form)

For the simplified Gough-Stewart platform considered here there is only one moving body, so the position and Euler angles can be used as a minimal set of generalized coordinates, $\mathbf{q} = \left[\mathbf{r}^T, \boldsymbol{\phi}^T\right]^T = [r_x, r_y, r_z, \phi_1, \phi_2, \phi_3]^T$. The potential energy results as:

$$V = mgr_z. \quad (24)$$

Employing the relationship $\mathbf{w} = \mathbf{B}(\boldsymbol{\phi})\dot{\boldsymbol{\phi}}$, the kinetic energy for the mobile platform can be expressed as

$$\begin{aligned} T &= \frac{1}{2}\, m\, \dot{\mathbf{r}}^T\, \dot{\mathbf{r}} + \frac{1}{2}\, \mathbf{w}^T\, \mathbf{I}_{\text{PF}}\, \mathbf{w} \\ &= \frac{1}{2}\, m\, \dot{\mathbf{r}}^T \dot{\mathbf{r}} + \frac{1}{2}\, \dot{\boldsymbol{\phi}}^T\, \mathbf{B}^T\, \mathbf{I}_{\text{PF}}\, \mathbf{B}\, \dot{\boldsymbol{\phi}}. \end{aligned} \quad (25)$$

Lagrange's equations take the form

$$\frac{d}{dt}\left(\frac{\partial T}{\partial \dot{\mathbf{q}}}\right) - \left(\frac{\partial T}{\partial \mathbf{q}}\right) + \left(\frac{\partial V}{\partial \mathbf{q}}\right) = \mathbf{Q},$$

or

$$\frac{d}{dt}\left(\frac{\partial T}{\partial \begin{bmatrix} \dot{\mathbf{r}} \\ \dot{\boldsymbol{\phi}} \end{bmatrix}}\right) - \left(\frac{\partial T}{\partial \begin{bmatrix} \mathbf{r} \\ \boldsymbol{\phi} \end{bmatrix}}\right) + \left(\frac{\partial V}{\partial \begin{bmatrix} \mathbf{r} \\ \boldsymbol{\phi} \end{bmatrix}}\right) = \mathbf{Q}. \qquad (26)$$

Based on Equation (25), the first term results in:

$$\begin{aligned} \frac{d}{dt}\left(\frac{\partial T}{\partial \begin{bmatrix} \dot{\mathbf{r}} \\ \dot{\boldsymbol{\phi}} \end{bmatrix}}\right) &= \frac{d}{dt}\begin{bmatrix} m\,\dot{\mathbf{r}} \\ \mathbf{B}^T\,\mathbf{I}_{\text{PF}}\,\mathbf{B}\,\dot{\boldsymbol{\phi}} \end{bmatrix} \\ &= \begin{bmatrix} m\,\ddot{\mathbf{r}} \\ \dot{\mathbf{B}}^T\mathbf{I}_{\text{PF}}\mathbf{B}\dot{\boldsymbol{\phi}} + \mathbf{B}^T\mathbf{I}_{\text{PF}}\dot{\mathbf{B}}\dot{\boldsymbol{\phi}} + \mathbf{B}^T\mathbf{I}_{\text{PF}}\mathbf{B}\ddot{\boldsymbol{\phi}} \end{bmatrix} \end{aligned}$$

The other terms result as:

$$\left(\frac{\partial T}{\partial \begin{bmatrix} \mathbf{r} \\ \boldsymbol{\phi} \end{bmatrix}}\right) = \begin{bmatrix} \mathbf{0} \\ \frac{1}{2}\,\dot{\boldsymbol{\phi}}^T\left(\frac{\partial}{\partial \boldsymbol{\phi}}\mathbf{B}\right)^T\mathbf{I}_{\text{PF}}\mathbf{B}\dot{\boldsymbol{\phi}} + \frac{1}{2}\dot{\boldsymbol{\phi}}^T\mathbf{B}^T\mathbf{I}_{\text{PF}}\left(\frac{\partial}{\partial \boldsymbol{\phi}}\mathbf{B}\right)\dot{\boldsymbol{\phi}} \end{bmatrix},$$

$$\left(\frac{\partial V}{\partial \begin{bmatrix} \mathbf{r} \\ \boldsymbol{\phi} \end{bmatrix}}\right) = \begin{bmatrix} m\,g\,\mathbf{e}_z \\ \mathbf{0} \end{bmatrix}$$

and

$$\begin{aligned} \mathbf{Q} &= \begin{bmatrix} \mathbf{Id}_{3\text{x}3} & \mathbf{0} \\ \mathbf{0} & \mathbf{B}^T \end{bmatrix}\begin{bmatrix} \mathbf{f}_{\text{PF}}^{\text{applied}} \\ \mathbf{m}_{\text{PF}}^{\text{applied}} \end{bmatrix} + \mathbf{J}_A^T\,\boldsymbol{\tau} \\ &= \begin{bmatrix} \mathbf{Id}_{3\text{x}3} & \mathbf{0} \\ \mathbf{0} & \mathbf{B}^T \end{bmatrix}\left(\begin{bmatrix} \mathbf{f}_{\text{PF}}^{\text{applied}} \\ \mathbf{m}_{\text{PF}}^{\text{applied}} \end{bmatrix} + \mathbf{J}_G^T\,\boldsymbol{\tau}\right). \end{aligned}$$

It remains to substitute the above terms into Equation (26), where some of the sub-terms actually cancel. However, the remaining terms are still of very high complexity.

Summary for Lagrange's Equations in Standard Form: This example demonstrates that while using the Euler angles as generalized coordinates in the standard form of Lagrange's equations is generally possible, it leads to unnecessarily complex equations that are unsuitable for the dynamic modeling of mechanisms of this type.

Extension – If other moving bodies are to be considered: If additional moving bodies are to be considered, it is often convenient to use more generalized coordinates than the number of degrees-of-freedom of the system, which can be handled through the use of Lagrange multipliers, see Equation (13).

4.4 Lagrange's Equations for Quasi-Coordinates (Boltzmann-Hamel Equations)

This subsection seeks to demonstrate that it is much more convenient to use Lagrange's Equations for Quasi-Coordinates for this problem, rather than Lagrange's Equations for true coordinates.

Euler angles are employed to describe the orientation of the moving platform, $\mathbf{q} = \begin{bmatrix} \mathbf{r} \\ \boldsymbol{\phi} \end{bmatrix}$, while in contrast to the preceding subsection, the angular velocity vector is used directly to describe the platform's velocity, $\dot{\tilde{\mathbf{p}}} = \begin{bmatrix} \dot{\mathbf{r}} \\ \mathbf{w} \end{bmatrix}$. Equation (20) from Subsection 3.4 thus directly applies and is repeated for convenience below:

$$\frac{d}{dt}\left(\frac{\partial \bar{T}}{\partial \dot{\tilde{\mathbf{p}}}}\right) + \begin{bmatrix} \mathbf{0} & \mathbf{0} \\ \mathbf{0} & \boldsymbol{\Omega} \end{bmatrix}\left(\frac{\partial \bar{T}}{\partial \dot{\tilde{\mathbf{p}}}}\right) - \boldsymbol{\mathcal{D}}^{-1}\left(\frac{\partial \bar{T}}{\partial \mathbf{q}}\right) + \boldsymbol{\mathcal{D}}^{-1}\left(\frac{\partial V}{\partial \mathbf{q}}\right) = \boldsymbol{N},$$

where $\boldsymbol{\mathcal{D}}^{-1}$ is given by Equation (18). The potential energy, $V(\mathbf{q})$, is given by Equation (24), and the kinetic energy is given by Equation (25), but the latter is now viewed as a function of $\mathbf{q}$ and $\dot{\tilde{\mathbf{p}}}$:

$$\bar{T}(\mathbf{q}, \dot{\tilde{\mathbf{p}}}). = \bar{T}\left(\begin{bmatrix} \mathbf{r} \\ \boldsymbol{\phi} \end{bmatrix}, \begin{bmatrix} \dot{\mathbf{r}} \\ \mathbf{w} \end{bmatrix}\right) = \frac{1}{2}\,m\,\dot{\mathbf{r}}^T\dot{\mathbf{r}} + \frac{1}{2}\,\mathbf{w}^T\,\mathbf{I}_{\text{PF}}\,\mathbf{w}.$$

The derivatives results as

$$\begin{aligned} \frac{\partial V}{\partial \mathbf{q}} &= \begin{bmatrix} m\mathbf{g}\mathbf{e}_z \\ \mathbf{0} \end{bmatrix}, \qquad \frac{\partial \bar{T}}{\partial \mathbf{q}} = \begin{bmatrix} \mathbf{0} \\ \mathbf{0} \end{bmatrix} \\ \frac{\partial \bar{T}}{\partial \dot{\tilde{\mathbf{p}}}} &= \begin{bmatrix} m\dot{\mathbf{r}} \\ \mathbf{I}\mathbf{w} \end{bmatrix}, \qquad \frac{d}{dt}\left(\frac{\partial \bar{T}}{\partial \dot{\tilde{\mathbf{p}}}}\right) = \begin{bmatrix} m\ddot{\mathbf{r}} \\ \mathbf{I}\dot{\mathbf{w}} \end{bmatrix}, \end{aligned}$$

and Equation (20) becomes

$$\begin{bmatrix} m\ddot{\mathbf{r}} \\ \mathbf{I}\dot{\mathbf{w}} \end{bmatrix} + \begin{bmatrix} \mathbf{0} & \mathbf{0} \\ \mathbf{0} & \boldsymbol{\Omega} \end{bmatrix}\begin{bmatrix} m\dot{\mathbf{r}} \\ \mathbf{I}\mathbf{w} \end{bmatrix} - \boldsymbol{\mathcal{D}}^{-1}\begin{bmatrix} \mathbf{0} \\ \mathbf{0} \end{bmatrix} + \boldsymbol{\mathcal{D}}^{-1}\begin{bmatrix} m\mathbf{g}\mathbf{e}_z \\ \mathbf{0} \end{bmatrix} = \begin{bmatrix} \mathbf{f}_{\text{PF}}^{\text{applied}} \\ \mathbf{m}_{\text{PF}}^{\text{applied}} \end{bmatrix} + \mathbf{J}_G^T\,\boldsymbol{\tau},$$

which simplifies further to

$$\begin{bmatrix} m\ddot{\mathbf{r}} + m\mathbf{g}\mathbf{e}_z \\ \mathbf{I}\dot{\mathbf{w}} + \mathbf{w} \times (\mathbf{I}\mathbf{w}) \end{bmatrix} = \begin{bmatrix} \mathbf{f}_{\text{PF}}^{\text{applied}} \\ \mathbf{m}_{\text{PF}}^{\text{applied}} \end{bmatrix} + \mathbf{J}_G^T\,\boldsymbol{\tau},$$

which is identical to Equation (21).

Summary for Boltzmann-Hamel Equations: Using the Boltzmann-Hamel Equations is a much more efficient way to deal with quasi-coordinates than using Lagrange's equations for true coordinates. Thus, out of these two, the Boltzmann-Hamel equations are the better choice to model general parallel manipulators.

Extension - If other moving bodies are to be considered: One possibility to include other moving bodies is to include include the corresponding variables for each body in vectors $\mathbf{q}$ and $\dot{\tilde{\mathbf{p}}}$. Constraint equations and Lagrange multipliers are then used to eliminate the additional degrees-of-freedom.

4.5 Gibbs-Appell Equations

For this simple example, the generalized coordinates can be chosen as $\widetilde{\gamma} = \begin{bmatrix} \mathbf{r} \\ \widetilde{\boldsymbol{\pi}} \end{bmatrix}$. The Gibbs-Appell function for a general rigid body is then applied to the mobile platform of the manipulator:

$$S = \frac{1}{2} m \, \mathbf{a}^T \mathbf{a} + \frac{1}{2} \boldsymbol{\alpha}^T \left(\mathbf{I}_{\text{PF}} \boldsymbol{\alpha} \right) + \boldsymbol{\alpha}^T \left(\mathbf{w} \times \mathbf{I}_{\text{PF}} \mathbf{w} \right),$$

where

$$\mathbf{a} = \begin{bmatrix} \ddot{r}_x \\ \ddot{r}_y \\ \ddot{r}_z \end{bmatrix}, \qquad \boldsymbol{\alpha} = \begin{bmatrix} \dot{\omega}_x \\ \dot{\omega}_y \\ \dot{\omega}_z \end{bmatrix}.$$

The Gibbs-Appell equations state that

$$\frac{\partial S}{\partial \ddot{\widetilde{\gamma}}} = \boldsymbol{\Gamma}, \tag{27}$$

where $\boldsymbol{\Gamma}$ corresponds to the generalized forces in the expression for virtual work given by $\delta W = \boldsymbol{\Gamma} \cdot \delta \widetilde{\gamma}$:

$$\boldsymbol{\Gamma} = \boldsymbol{\Gamma}_{\text{grav}} + \boldsymbol{\Gamma}_{\text{applied}} + \boldsymbol{\Gamma}_{\text{actuators}} = \begin{bmatrix} -mg\mathbf{e}_z \\ \mathbf{0} \end{bmatrix} + \begin{bmatrix} \mathbf{f}_{\text{PF}}^{\text{applied}} \\ \mathbf{m}_{\text{PF}}^{\text{applied}} \end{bmatrix} + \mathbf{J}_G^T \boldsymbol{\tau}.$$

Evaluating the derivative, $\frac{\partial S}{\partial \ddot{\widetilde{\gamma}}}$, leads to

$$\begin{aligned} \frac{\partial S}{\partial \ddot{\widetilde{\gamma}}} &= \frac{\partial}{\partial \begin{bmatrix} \ddot{\mathbf{r}} \\ \dot{\mathbf{w}} \end{bmatrix}} \left(\frac{1}{2} m \, \ddot{\mathbf{r}}^T \ddot{\mathbf{r}} + \frac{1}{2} \dot{\mathbf{w}}^T \left(\mathbf{I}_{\text{PF}} \dot{\mathbf{w}} \right) + \dot{\mathbf{w}}^T \left(\mathbf{w} \times \mathbf{I}_{\text{PF}} \mathbf{w} \right) \right) \\ &= \begin{bmatrix} m \, \ddot{\mathbf{r}} \\ \mathbf{I}_{\text{PF}} \dot{\mathbf{w}} + \mathbf{w} \times \mathbf{I}_{\text{PF}} \mathbf{w} \end{bmatrix}. \end{aligned}$$

Substituting the resulting terms for $\boldsymbol{\Gamma}$ and $\frac{\partial S}{\partial \ddot{\widetilde{\gamma}}}$ into Equation (27) yields:

$$\begin{bmatrix} m \, \ddot{\mathbf{r}} \\ \mathbf{I}_{\text{PF}} \dot{\mathbf{w}} + \mathbf{w} \times \mathbf{I}_{\text{PF}} \mathbf{w} \end{bmatrix} = \begin{bmatrix} -mg\mathbf{e}_z \\ \mathbf{0} \end{bmatrix} + \begin{bmatrix} \mathbf{f}_{\text{PF}}^{\text{applied}} \\ \mathbf{m}_{\text{PF}}^{\text{applied}} \end{bmatrix} + \mathbf{J}_G^T \boldsymbol{\tau},$$

which is also identical to Equation (21).

Summary for Gibbs-Appell Equations: The Gibbs-Appell equations provide another simple alternative to derive the equations of motion. A very interesting property of this method is that while it it employs quasi-coordinates as generalized coordinates, $\widetilde{\gamma}$, derivatives are only taken with respect to $\ddot{\widetilde{\gamma}}$. Thus quasi-coordinates can be used without any complication.

Extension - If other moving bodies are to be considered: Several techniques can be used to include the effects of the mass and inertia of other moving bodies in the equations. One method is to use Lagrange multipliers as follows: Extend the vector $\widetilde{\gamma}$ to also include the quasi-coordinates for the other moving bodies. Then account for the extra coordinates through the use of Lagrange multipliers:

$$\frac{\partial S}{\partial \ddot{\widetilde{\gamma}}} = \boldsymbol{\Gamma} + \boldsymbol{\mathcal{B}}^T \boldsymbol{\lambda}$$

with a constraint equation of the form

$$\mathbf{c}\left(\widetilde{\gamma}, \dot{\widetilde{\gamma}}, \boldsymbol{\phi} \right) = \mathbf{0}.$$

5 Discussion of Results

For a simplified Gough-Stewart platform, the method of Newton-Euler, the principle of virtual work, the Boltzmann-Hamel equations and the Gibbs-Appell equations were shown to yield the same equations of motion. The equations of motion obtained by applying Lagrange's Equations (in standard form) must theoretically result in equivalent equations of motion, but the equations actually obtained by that method, even for this simple example, were too complex to even be compared. Thus Lagrange's equations in their standard form appear to be less suitable due to greater complexity of the resulting expressions, but other methods, such as the Boltzmann-Hamel equations and the Gibbs-Appell equations appear to be more suitable.

There is one point that has been neglected in the derivation of the equations of motion that deserves special attention. For all of the formulations of the equations of motion that include $\mathbf{w}$ in the final expressions, i.e. for all of the formulations with the exception of Lagrange's equations for true coordinates, the forward dynamics are not uniquely solvable without additional equations. The additional set of required equations is given by the velocity relationship in (6). Therefore the actual equations of motion are those given in the previous sections plus the velocity relationships, Eq. (6). To evaluate the forward dynamics this full set of equations of motion can then be solved simultaneously using standard differential equation solution techniques.

6 Conclusions

This manuscript reviewed the role of quasi-coordinates for the kinematic and dynamic modeling of parallel manipulators. It was shown that quasi-coordinates play a central role for determining which methods of analytical mechanics can be applied to general parallel manipulators. Some of the key statements are:

- The principal of virtual work applies in spite of the fact that quasi-coordinates, rather than true coordinates, are used as virtual displacements;
- Lagrange's equations in their standard form are unsuitable due to unnecessary complexity, but other methods of analytical mechanics, such as the Gibbs-Appell equations and the Boltzmann-Hamel equations should be investigated further.

This manuscript only provides an overview of some of the methods and the reader is referred to the references for further

in-depth discussions and further examples. Furthermore, this list is certainly not complete (for example it did not include Jourdain's principle/Kane's method) and the authors would be grateful for references to additional techniques. Nevertheless, it is hoped that the discussion serves as a starting point to strengthen the connection between analytical mechanics and parallel manipulator research.

Acknowledgments

We would like to acknowledge our colleagues, Prof. Harvey Lipkin, Prof. John Papastavridis and Prof. Jerry Ginsberg (all at Georgia Tech), for their invaluable insight and references to relevant work. However, it is emphasized that the authors are solely responsible for any errors contained in this manuscript. Furthermore, we are grateful for the excellent feedback provided by the reviewers.

This work was partly supported by the National Science Foundation under CAREER Grant No. 9984279 and by an NDSEG doctoral fellowship awarded to the second author.

APPENDIX

This section provides a very simple counter example that demonstrates why the integral, $\widetilde{\boldsymbol{\pi}}$, of $\mathbf{w}$ can generally not be used to track the orientation of a moving body. Consider the following two trajectories:

- Trajectory 1: From an initial orientation, rotate a body about the global x-axis for 1 second at velocity $\omega_x = 90$ degrees/second. Then rotate the body for 1 second about the global y-axis at equal velocity, $\omega_y = 90$ degrees/second.
  Integration result: Integrating $\mathbf{w}$ over this trajectory results in $\widetilde{\boldsymbol{\pi}} = [90, 90, 0]$ degrees.

- Trajectory 2: From the initial orientation, proceed as in Trajectory 1, but with reversed order, i.e. rotate first about the global y-axis, then about the global x-axis.
  Integration result: Integrating $\mathbf{w}$ over this trajectory results in $\widetilde{\boldsymbol{\pi}} = [90, 90, 0]$ degrees.

Obviously, the orientation of the body at the end of Trajectory 1 differs from that of Trajectory 2. (Thus the Euler angles, ϕ, differ between the two cases.) However, $\widetilde{\boldsymbol{\pi}}$ is identical in both cases. Thus $\widetilde{\boldsymbol{\pi}}$ does not contain sufficient information to recover the orientation of the body, since the *order* of rotations taking place is lost.

A noteworthy exception to the above observation is the case of rotation about a single, constant axis. In that case, $\mathbf{w}(t)$ can be described as $\mathbf{w}(t) = \dot{\psi}\ \mathbf{e}$, where $\mathbf{e}$ is a constant unit vector denoting the axis of rotation and $\dot{\psi} = \dot{\psi}(t)$ is the angular speed. Integration results in $\int \mathbf{w}(t)dt = \int \dot{\psi}(t)\ \mathbf{e}dt = \psi(t)\ \mathbf{e}$, which of course is sufficient to denote the orientation and is known as exponential or axis-angle coordinates [16].

References

[1] E.T. Whittaker. *A Treatise on the Analytical Dynamics of Particles & Rigid Bodies*. Cambridge University Press, fourth edition, 1998.

[2] J.H. Ginsberg. *Advanced Engineering Dynamics*. Cambridge University Press, 2nd edition, 1998.

[3] C. Lanczos. *The Variational Principles of Mechanics*. Dover Publications, Inc., fourth edition, 1986.

[4] M.J. Winckler and C. Kraus. Simulation of hexapod machine tools by using natural coordinates. In *Year 2000 Parallel Kinematic Machines International Conference*, pages 109 – 117, Ann Arbor, MI, Sept 2000.

[5] J.-P. Merlet. *Parallel Robots*. Kluwer Academic Publishers, Dordrecht, The Netherlands, 2000.

[6] L.-W. Tsai. *Robot Analysis – The Mechanics of Serial and Parallel Manipulators*. John Wiley & Sons, 1st edition, 1999.

[7] V.E. Gough and S.G. Whitehall. Universal tyre test machine. In *Proceedings of the ninth Int. Technical Congress FISITA*, 1962.

[8] L. Sciavicco and B. Siciliano. *Modelling and Control of Robot Manipulators*. Springer, 2nd edition, 2000.

[9] A. Codourey and E. Burdet. A body-oriented method for finding a linear form of the dynamic equation of fully parallel robots. In *Proceedings 1997 IEEE International Conference on Robotics and Automation*, pages 1612–1618, April 1997.

[10] L.-W. Tsai. Solving the inverse dynamics of parallel manipulators by the principle of virtual work. In *1998 ASME Design Engineering Technical Conferences*, number DETC/MECH-5865, Sept 1998.

[11] I. Ebert-Uphoff and C.M. Gosselin. Dynamic modeling of a class of spatial statically-balanced parallel platform mechanisms. In *1999 IEEE International Conference on Robotics and Automation*, pages 881 – 888, Detroit, MI, May 1999.

[12] J.G. Papastravridis. A panoramic overview of the principles and equations of motion of advanced engineering dynamics. *ASME Applied Mechanics Review*, 51(4):239 – 265, April 1998.

[13] L. Meirovitch. *Methods of Analytical Dynamics*. McGraw Hill, 1970.

[14] F. Gantmacher. *Lectures in Analytical Mechanics*. MIR Publishers, Moscow, 2nd edition, 1975.

[15] C.M. Gosselin. Parallel computational algorithms for the kinematics and dynamics of planar and spatial manipulators. *Journal of Dynamic Systems, Measurement, and Control*, 118:22–28, March 1996.

[16] M.D. Shuster. A survey of attitude representations. *The Journal of Astronautical Sciences*, 41(4):439 – 517, Oct-Dec 1993.

Proceedings of the WORKSHOP on
Fundamental Issues and Future Research Directions for Parallel Mechanisms and Manipulators
October 3–4, 2002, Quebec City, Quebec, Canada
Clément M. Gosselin and Imme Ebert-Uphoff, editors

Methods for Dynamic Models of Parallel Robots and Mechanisms

JÓZSEF KÖVECSES
Canadian Space Agency
6767 Route de l'Aéroport, St-Hubert
Québec, Canada, J3Y 8Y9
Jozsef.Kovecses@space.gc.ca

JEAN-CLAUDE PIEDBŒUF
Canadian Space Agency
6767 Route de l'Aéroport, St-Hubert
Québec, Canada, J3Y 8Y9
Jean-Claude.Piedboeuf@space.gc.ca

CHRISTIAN LANGE
Canadian Space Agency
6767 Route de l'Aéroport, St-Hubert
Québec, Canada, J3Y 8Y9
Christian.Lange@space.gc.ca

Abstract: *Dynamic analysis is the basic element of mechanical design and control of mechanisms. This work intends to address dynamic methods relevant to parallel robots and mechanisms from a unified analytical point of view, which is based on differential variational principles. In this framework, many approaches can be discussed, and new directions can be highlighted that can contribute to the better understanding of dynamic behavior. The work intends to point out the areas and methods where further exploration is necessary to shed light on applications related to parallel machines. The paper also deals with some of the important problems in the dynamics of parallel robots in space applications.*

1 Introduction

Research on parallel manipulators have been mainly focused on kinematics related issues. As Tsai [18] noted, relatively fewer works are available on the dynamics of parallel robots. Textbooks discussing parallel systems have a relatively limited scope on dynamics of parallel robots. Dynamics effects and analysis are however the basis of design specifications and advanced control of parallel mechanical systems. Particularly, heavy duty applications (e.g. docking mechanisms and simulators, manufacturing machinery) have a high need for in-depth dynamics investigations. We feel that in order to increase the applications and practical use of parallel robots, the dynamics methods for such systems should receive more attention. There are current research activities at the Canadian Space Agency to address some of the problems of the dynamics of parallel structures. This paper intends to give a brief background on the dynamics methods and problems felt important and relevant to parallel systems.

In the analysis of robotic systems, it is usual to distinguish between inverse and forward dynamics. A significant portion of the published papers on dynamics of parallel robots deals with the inverse dynamics problem, e.g., Dasgupta and Mruthyunjaya [6], Geike and McPhee [9], Li et. al. [11], Tsai [18], Wang and Gosselin [21]. Inverse dynamics formulations are necessary for advanced model based control. The proposed approaches are usually effective, but they require a structure specific kinematic analysis, also the mass matrix is usually not expressed explicitly. In inverse dynamics, the explicit expression of the mass matrix is not required, but if we want to perform simulations and solve the forward dynamics problem then this quantity becomes necessary. Another important aspect that was addressed in Geike and McPhee [9] is the potential use of symbolic calculations in dynamic analysis. The generation of dynamic equations of parallel systems in symbolic form could be quite advantageous in both control and mechanical design related problems. The key for efficient handling of parallel systems dynamics lies in the in-depth understanding of constrained systems and methods.

In terms of modeling and analysis, the main difference between serial and parallel mechanisms is the presence of additional constraints, which ensure the forming of closed kinematic chains within the system. Handling constraints is the key issue in dynamics investigations of parallel systems (in both inverse and forward dynamics analysis of parallel structures). We intend to summarize some of the methodologies of constrained system dynamics that can be effectively used in parallel mechanical sys-

tems. We will follow a unified approach for discussing the methods. This approach is based on differential variational principles as fundamental physical laws of constrained systems.

2 Differential Variational Principles of Constrained Systems

Let us assume that we study a mechanical system that is subjected to bilateral constraints. The fundamental ideas of constrained systems can be briefly summarized by using the generic differential variational equation

$$\int \left[(dm\ddot{\vec{r}} - \vec{f}_{impressed} - \vec{f}_{constraint}) \cdot \delta\hat{\vec{r}} \right] = 0, \qquad (1)$$

where dm is a mass element of the constrained system, the sum $\vec{f}_{impressed} + \vec{f}_{constraint}$ represent the resultant force acting on the mass element, $\int[..]$ represents the summation (integration) over the mass elements of the system (discrete or distributed parameter systems [10]), and $\delta\hat{\vec{r}}$ will be called a kinematic variation. The physical definition of the kinematic variation can be done based on the particular differential variational principle applied: Lagrange's principle or the principle of virtual work (virtual displacements), Jourdain's principle (velocity variations or virtual velocities) or Gauss' principle (acceleration variations) (see e.g. Papastavridis [13] or Kövecses and Cleghorn [10] for further details and references). Virtual displacements represent infinitesimal coordinate variations that connect two configurations kinematically possible for the same time instant, velocity variations connect two velocity states of the system that are kinematically possible for the same time instant and configuration, and acceleration variations connect two acceleration states of the system that are both kinematically possible for the same time, configuration, and velocity state. Velocity and acceleration variations do not have to be infinitesimal quantities for linear velocity constraints. Detailed description of differential variational principles and kinematic variations can be found in Papastavridis [14].

A fundamental idea of constrained systems, as expressed in the above equation, is the decomposition of the forces acting on a mass element of the system to impressed and constraint forces (Papastavridis [14], Rosenberg [16]) . Impressed forces are also often called applied or active forces. Using this decomposition, the basic principle of constrained systems, which is the essence of differential variational principles, can be stated as: the totality of the products of constraint forces and kinematic variations admissible with the constraints vanishes. This product is usually equivalent to a variation (virtual change) in the power (or its time integral or differential depending on what definition is used for the kinematic variations) of the constraint forces. It can be expressed as

$$\int \left[\vec{f}_{constraint} \cdot \delta\hat{\vec{r}} \right] = 0. \qquad (2)$$

At a generic level and very briefly, these are the basic ideas necessary for the investigation of constrained systems. It is important to note the significance of the differential variational approach in constrained systems. In recent years, there have been several types of formulations proposed for constrained systems. It is, however, often forgotten that the basic law of constrained systems, as expressed by equation (2), originates from differential variational principles. Constraint forces do develop power in many cases (e.g. rheonomic, acatastatic constraints). It is the virtual change in this power (or in its time integral or differential) due to admissible kinematic variations, which vanishes for all types of constraints. To illustrate this, we can consider for example a simple system of a point mass, the motion of which is constrained to a predefined trajectory, $\mathbf{f}(t)$. This imposes holonomic, rheonomic constraints on the motion of the point mass. In this case, the constraint forces must develop power to move the point mass along this trajectory. But, it is relatively easy to show that the virtual change in this power (due to a Jourdainian velocity variation for instance) would always vanish. Further details on the actual and virtual power and work of constraint forces can be found in Bahar and Kwatny [4], and Papastavridis [14] for example.

Differential variational principles are necessary to develop a deeper understanding in constrained systems, and in the development of various methods for the analysis of these systems. Another important characteristic of differential variational principles is that they are invariant under transformations from one possible set of variables to another. Thus, these principles also give the means for transformation between the different sets of variables possible for the description of the system. In the following, we will apply these concepts to derive and characterize methods for general, parallel kinematic structures.

3 Fundamental Representation for Parallel Systems

A basic idea in parallel structures is that they can be composed of open-loop sub-systems that are connected to each other by constraints. The closed form system of dynamic equations of each open-loop sub-system can be derived using numerical or symbolic approaches (e.g., Piedbœuf [15]). They can include rigid or flexible bodies. Let us assume that this way the system comprises h open loops, and the total number of degrees of freedom of all these loops is n. The fundamental equation of differential variational principles can then be written for this *open-loop system* as

$$\begin{aligned} &\delta\hat{\mathbf{q}}^T \left(\mathbf{Q}_{inertial} - \mathbf{Q}_{impressed} \right) \\ &= \delta\hat{\mathbf{q}}^T \left(\mathbf{M}\ddot{\mathbf{q}} + \mathbf{C}(\dot{\mathbf{q}}, \mathbf{q}, t) - \mathbf{Q}_{impressed} \right) = 0, \end{aligned} \qquad (3)$$

where $\mathbf{Q}_{inertial}$ represents an $n \times 1$ array of the generalized inertial forces, $\mathbf{Q}_{impressed}$ is the $n \times 1$ array of the generalized impressed (or applied) forces of the system, $\mathbf{M}$ is the $n \times n$ mass matrix of the system, $\mathbf{q}$ is the $n \times 1$ array representing the generalized coordinates of the open-loop system, $\mathbf{C}$ is the $n \times 1$ array of the nonlinear inertial effects (Coriolis and centrifugal effects), $\delta\hat{\mathbf{q}}$ represents the $n \times 1$ array of generalized kinematic variations. As was mentioned in Section 2, kinematic variations

can be either virtual displacements (Lagrange's principle) or velocity variations (Jourdain's principle) or acceleration variations (Gauss' principle). The generalized impressed forces include the actuator forces or torques, external loads and potential friction effects in the joints. The decomposition of the generalized inertial forces $\mathbf{Q}_{inertial} = \mathbf{M}\ddot{\mathbf{q}} + \mathbf{C}(\dot{\mathbf{q}}, \mathbf{q}, t)$ does not always have to be done. For example, in inverse dynamics it can be more advantageous to establish and deal with $\mathbf{Q}_{inertial}$ directly without forming the mass matrix and calculating Coriolis and centrifugal effects separately. From the analytical mechanics point of view, the components of the generalized inertial forces can be represented as $\mathbf{Q}_{inertial_i} = \frac{d}{dt}\left(\frac{\partial T}{\partial \dot{q}_i}\right) - \frac{\partial T}{\partial q_i} = \frac{\partial G}{\partial \ddot{q}_i}$ $(i = 1, ..., n)$, where T is the kinetic energy function of the system and G is the Gibbs-Appell function.

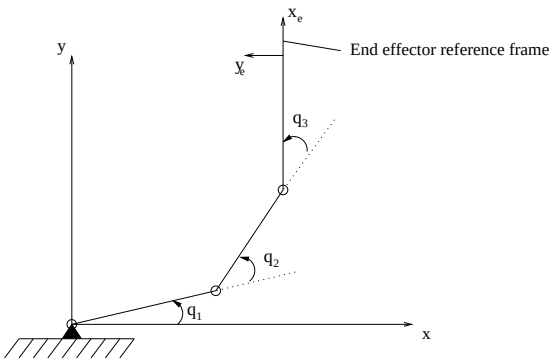

Figure 1: A three-link mechanism consisting of three beams connected by rotational joints

As an example for the generalized inertial forces, we can consider the three-link arm shown in Figure 1, and assume that the links are modeled as rigid beams. In this case,

$$\mathbf{Q}_{inertial} = \begin{bmatrix} Q_{inertial_1} \\ Q_{inertial_2} \\ Q_{inertial_3} \end{bmatrix} \tag{4}$$

and the three components of the generalized inertial forces can be obtained as

$$\begin{aligned}
&Q_{inertial_1} = \\
&\big[I_1 + m_2\ell_1^2 + 2m_2\ell_1 x_{CM_2}\cos(q_2) + I_2 + m_3\ell_1^2 \\
&+2m_3\ell_1\ell_2\cos(q_2) + m_3\ell_2^2 \\
&+ 2m_3\ell_1 x_{CM_3}\cos(q_2+q_3) + 2m_3\ell_2 x_{CM_3}\cos(q_3) + I_3\big]\,\ddot{q}_1 \\
&+ \big[I_2 + m_2\ell_1 x_{CM_2}\cos(q_2) + m_3\ell_1\ell_2\cos(q_2) + m_3\ell_2^2 + I_3 \\
&+m_3\ell_1 x_{CM_3}\cos(q_2+q_3) + 2m_3\ell_2 x_{CM_3}\cos(q_3)\big]\,\ddot{q}_2 \\
&+ \big[I_3 + m_3\ell_1 x_{CM_3}\cos(q_2+q_3) + m_3\ell_2 x_{CM_3}\cos(q_3)\big]\,\ddot{q}_3 \\
&+ (-m_2\ell_1 x_{CM_2} - m_3\ell_1\ell_2)\,(\dot{q}_1+\dot{q}_2)^2\sin(q_2) \\
&+ (m_2\ell_1 x_{CM_2} + m_3\ell_1\ell_2)\,\dot{q}_1^2\sin(q_2) \\
&+ \left(m_3\ell_1 x_{CM_3}\dot{q}_1^2 - m_3\ell_1 x_{CM_3}(\dot{q}_1+\dot{q}_2+\dot{q}_3)^2\right)\sin(q_2+q_3) \\
&+ \left(m_2\ell_2 x_{CM_3}(\dot{q}_1+\dot{q}_2)^2 - m_3\ell_2 x_{CM_3}(\dot{q}_1+\dot{q}_2+\dot{q}_3)^2\right)\sin(q_3),
\end{aligned}$$

$$\begin{aligned}
&Q_{inertial_2} = \\
&\big[I_2 + m_2\ell_1 x_{CM_2}\cos(q_2) + m_3\ell_1\ell_2\cos(q_2) + m_3\ell_2^2 + I_3 \\
&+m_3\ell_1 x_{CM_3}\cos(q_2+q_3) + 2m_3\ell_2 x_{CM_3}\cos(q_3)\big]\,\ddot{q}_1 \\
&+ \big[I_2 + m_3\ell_2^2 + I_3 + 2m_3\ell_2 x_{CM_3}\cos(q_3)\big]\,\ddot{q}_2 \\
&+ \big[I_3 + m_3\ell_2 x_{CM_3}\cos(q_3)\big]\,\ddot{q}_3 \\
&+ (m_2\ell_1 x_{CM_2} + m_3\ell_1\ell_2)\,\dot{q}_1^2\sin(q_2) \\
&+m_3\ell_1 x_{CM_3}\dot{q}_1^2\sin(q_2+q_3) \\
&+ \left(m_3\ell_2 x_{CM_3}(\dot{q}_1+\dot{q}_2)^2 - m_3\ell_2 x_{CM_3}(\dot{q}_1+\dot{q}_2+\dot{q}_3)^2\right)\sin(q_3),
\end{aligned}$$

$$\begin{aligned}
&Q_{inertial_3} = \\
&\big[I_3 + m_3\ell_1 x_{CM_3}\cos(q_2+q_3) + m_3\ell_2 x_{CM_3}\cos(q_3)\big]\,\ddot{q}_1 \\
&+ \big[I_3 + m_3\ell_2 x_{CM_3}\cos(q_3)\big]\,\ddot{q}_2 + I_3\ddot{q}_3 \\
&+m_3\ell_1 x_{CM_3}\dot{q}_1^2\sin(q_2+q_3) + m_3\ell_2 x_{CM_3}(\dot{q}_1+\dot{q}_2)^2\sin(q_3),
\end{aligned}$$

where m_1, m_2, m_3 are the masses of the links, I_1, I_2, I_3 are the moments of inertia of the links about the point where they are connected to the preceding link in the chain (this point is the origin of the local frame attached to the link, where the x_i axis of the local frame ($i = 1, ..., 3$) is directed parallel to the main axis of the beam), and x_{CM_1}, x_{CM_2}, x_{CM_3} are the locations of the center of mass of each link in the local coordinate frames. Instead of the center of mass, it is often useful to use $m_1 x_{CM_1}$, $m_2 x_{CM_2}$, $m_3 x_{CM_3}$ as dynamic parameters, which can be identified as the first moments of inertia about the origins of the local frames.

Since the system is first represented without the loop closure constraints, each of the arrays and matrices in (3) can be partitioned to h blocks representing the open-loop sub-system level models, for example

$$\begin{bmatrix} \mathbf{M}_1 & . & . \\ . & \mathbf{M}_2 & . \\ . & . & . \end{bmatrix}, \quad \begin{bmatrix} \mathbf{q}_1 \\ \mathbf{q}_2 \\ . \end{bmatrix}, \quad ..... \tag{5}$$

where $\mathbf{M}_i$, $\mathbf{q}_i$ represent the mass matrix and the generalized coordinates of the ith open-loop sub-system ($i = 1, ..., h$).

In order to form the model for the desired parallel system, *the closed-loop model*, the constraints representing the loop closures need to be imposed on (3). Assume that there are m constraints for the loop closures (m may be equal to h in certain cases). These constraints at the velocity level can be expressed usually as

$$\mathbf{A}(\mathbf{q}, t)\dot{\mathbf{q}} + \mathbf{b}(\mathbf{q}, t) = \mathbf{0}, \tag{6}$$

where $\mathbf{A}$ is the $m \times n$ constraint Jacobian matrix. The loop closure constraints in parallel systems are holonomic constraints, thus (6) can be integrated and expressed in the form of position constraints as

$$\mathbf{\Phi}(\mathbf{q}, t) = \mathbf{0}, \tag{7}$$

where $\mathbf{A} = \frac{\partial \mathbf{\Phi}}{\partial \mathbf{q}}$ and $\mathbf{b} = \frac{\partial \mathbf{\Phi}}{\partial t}$. For example, assume that we investigate the three-link mechanism shown in Figure 1, but instead of the open-loop structure we form a closed-loop system by joining the end effector frame to a point fixed in the global

coordinate system by employing a rotational joint. This loop-closure condition can be expressed by two holonomic constraint equations at the velocity level, where $\mathbf{b} = \mathbf{0}$ and

$$\mathbf{A} = \begin{bmatrix} A_{11} & A_{12} & A_{13} \\ A_{21} & A_{22} & A_{23} \end{bmatrix} \tag{8}$$

where

$$\begin{aligned}
A_{11} &= -\ell_1 \sin(q_1) - \ell_2 \sin(q_1 + q_2) - \ell_3 \sin(q_1 + q_2 + q_3), \\
A_{12} &= -\ell_2 \sin(q_1 + q_2) - \ell_3 \sin(q_1 + q_2 + q_3), \\
A_{13} &= -\ell_3 \sin(q_1 + q_2 + q_3), \\
A_{21} &= \ell_1 \cos(q_1) + \ell_2 \cos(q_1 + q_2) + \ell_3 \cos(q_1 + q_2 + q_3), \\
A_{22} &= \ell_2 \cos(q_1 + q_2) + \ell_3 \cos(q_1 + q_2 + q_3), \\
A_{23} &= \ell_3 \cos(q_1 + q_2 + q_3),
\end{aligned}$$

and these can be reduced to two geometric constraint equations at the configuration level, in the form

$$\begin{aligned}
\Phi_1 &= \ell_1 \cos(q_1) + \ell_2 \cos(q_1 + q_2) \\
&\quad + \ell_3 \cos(q_1 + q_2 + q_3) = 0,
\end{aligned} \tag{9}$$

$$\begin{aligned}
\Phi_2 &= \ell_1 \sin(q_1) + \ell_2 \sin(q_1 + q_2) \\
&\quad + \ell_3 \sin(q_1 + q_2 + q_3) = 0.
\end{aligned} \tag{10}$$

Constraints impose additional generalized forces, constraint forces, on the n degree of freedom open-loop system to transform it to the required closed-loop parallel system. These generalized constraint forces can be represented with an $n \times 1$ dimensional array, $\mathbf{Q}_{constraint}$, that needs to be added to the generalized forces, as per equation (1), and (3) becomes

$$\delta\hat{\mathbf{q}}^T \left(\mathbf{Q}_{inertial} - \mathbf{Q}_{impressed} - \mathbf{Q}_{constraint} \right) = 0 \tag{11}$$

If we require that the kinematic variations be admissible with the constraints that results in the interdependence between them in the form of

$$\mathbf{A}\delta\hat{\mathbf{q}} = \mathbf{0}. \tag{12}$$

This equation is of key importance in the dynamics investigations. It can be derived from equations (6) and (7) for all three cases of kinematic variations (virtual displacements, velocity variations, acceleration variations). For admissible kinematic variations,

$$\delta\hat{\mathbf{q}}^T \mathbf{Q}_{constraint} = 0, \tag{13}$$

which is the mathematical expression of the basic axiom of constrained systems, equation (2), for this formulation. Thus, equations (6), (11), (12) and (13) give the basis for the dynamics investigations of parallel structures, while equations (6) and (7) are necessary for the kinematics analysis.

The methods for the dynamic investigation of the parallel (constrained) system can be discussed and classified based on several criteria. Here, we discuss one approach that is based on the structure of the fundamental differential variational principles, that is represented by equations (3), (5) - (7), (11) - (13). This basically covers most of the approaches used in parallel structures, and opens up ways for developing new methods for the dynamics investigations. Geometrical representation of the above considerations and the methods discussed later is also possible by introducing the concept of the configuration manifold and tangent space, but in this paper we would like to carry out the discussion without differential geometric concepts.

As equation (11) shows, the variational principle can be expressed as product of generalized kinematic variations and generalized forces (inertial, impressed and constraint forces). For the open-loop, unconstrained system we have n generalized velocity components $\dot{\mathbf{q}}$ and n kinematic variations $\delta\hat{\mathbf{q}}$. Equation (11) is expressed in terms of these generalized variables of the open-loop system. For this form, we will say that the system is described using descriptor type variables.

The fundamental realm of the study of constrained system dynamics is the methods how constraint forces and kinematic constraints are handled and incorporated in the investigations. From the structure of equations (11) - (13), it can be seen that basically the kinematic variations and their interdependence determine the potential approaches for further dynamic analysis. Two major groups of approaches can be distinguished:

- Analysis using a new, independent set of kinematic variations, where the new set of variations is formed based on equations (11) - (13).

- Analysis using the original, descriptor type set of kinematic variations.

In the following we will briefly summarize methods pertaining to these groups, and highlight some of the features related to parallel systems. But, the detailed description and mathematical formulation of the methods cannot be included in this short paper (it will be available in a more detailed study).

3.1 Methods Using Independent Kinematic Variations

3.1.1 Independent Projections

Equation (12) imposes m constraints on the n kinematic variations. Thus, in general, it is possible to introduce $n - m = s$ new, independent kinematic variations so as

$$\delta\hat{\mathbf{q}} = \mathbf{B}\delta\hat{\mathbf{u}}, \tag{14}$$

where $\delta\hat{\mathbf{u}}$ is the $s \times 1$ array of new independent kinematic variations, and $\mathbf{B}$ is an $n \times s$ matrix describing the transformation between the original and new, minimum set of kinematic variations. The components of $\delta\hat{\mathbf{u}}$ can be linear combinations of the elements of $\delta\hat{\mathbf{q}}$. For example, for the loop closure equations of the three-link arm, as was detailed above, there is only one independent kinematic variation, and this can be selected as $\delta\hat{u} = \delta\hat{q}_1$

(Figure 1), and equation (14) for this case can be expanded as

$$\begin{bmatrix} \delta\hat{q}_1 \\ \delta\hat{q}_2 \\ \delta\hat{q}_3 \end{bmatrix} = \begin{bmatrix} 1 \\ \frac{-\ell_1 \sin(q_2+q_3)-\ell_2 \sin(q_3)}{\ell_2 \sin(q_3)} \\ \frac{\ell_1\ell_2 \sin(q_2)+\ell_1\ell_3 \sin(q_2+q_3)}{\ell_2\ell_3 \sin(q_3)} \end{bmatrix} \delta\hat{q}_1. \quad (15)$$

Equation (14) results in admissible kinematic variations that satisfy equation (12). Substituting (14) into equation (11) we obtain

$$\delta\hat{\mathbf{u}}^T \mathbf{B}^T \left(\mathbf{Q}_{inertial} - \mathbf{Q}_{impressed} - \mathbf{Q}_{constraint}\right) = 0, \quad (16)$$

and from this, using equation (13), the dynamic equations

$$\mathbf{B}^T \left(\mathbf{Q}_{inertial} - \mathbf{Q}_{impressed}\right) = 0 \quad (17)$$

are obtained. The major results with these transformations are the elimination of the constraint forces and the reduction of the number of dynamic equations to a minimum set. In multibody dynamics, equation (17) is often referred to as a projection equation or method. We can also call it the partial embedding of the constraints, since, independent kinematic variations are used, but $\mathbf{Q}_{inertial}$ is still based on the original descriptor set of variables ($\mathbf{q}$, $\dot{\mathbf{q}}$, $\ddot{\mathbf{q}}$). This may be advantageous in several cases when the selection and use of independent variables are cumbersome in establishing the generalized inertial forces. On the other side, however, because of the presence of the original, descriptor variables in the generalized inertial forces, equation (17) cannot be solved in itself. In addition, the constraint equations (6) and their time derivatives also need to be used to establish a complete set of equations that is solvable (forward dynamics problem). However, this approach can be useful in solving the inverse dynamics problem assuming that $\mathbf{q}$, $\dot{\mathbf{q}}$ and $\ddot{\mathbf{q}}$ are known. The generalized inertial forces, $\mathbf{Q}_{inertial}$, can be calculated and the equation (17) can be used to solve for the actuator forces or torques that are part of the array of impressed forces. Approaches pertaining to this class has been used by several researchers to solve inverse dynamics for specific kinematic structures utilizing virtual displacements as kinematic variations (principle of virtual work, e.g. Wang and Gosselin [21], Tsai [18]).

3.1.2 Independent Generalized Velocities

A further step can be to introduce a new set of independent variables, and embed the constraints into the expression of the generalized inertial forces, thus introduce a minimum number of components for the generalized forces. For this, constraint equations (6) and (7) need to be considered. For generic systems, it is usually more convenient to introduce the independent variables at the velocity level. The selection of new, independent generalized coordinates are generally quite difficult due to the nonlinear expression of the position level constraints (7). In some cases it is possible to find closed form relation between independent and dependent sets of coordinates using equation (7), in other cases only iterative solution is possible. However, we need to keep in mind that the dynamic equations are basically formulated to determine the rate of change of the velocity components. The coordinates describing the configuration are not the primary variables in dynamics. Thus, from the dynamic equations the velocity components can be determined and then, based on kinematic considerations, changes in configuration can be calculated using the relation between equations (6) and (7). This basically involves the integration of equation (6) to determine the changes in generalized coordinates.

Let us consider that we introduce a new set of independent velocity components based on equation (6). This will result in

$$\dot{\mathbf{q}} = \mathbf{B}\dot{\mathbf{u}} + \mathbf{d}(\mathbf{q}, t), \quad (18)$$

where $\dot{\mathbf{u}}$ is an $s \times 1$ dimensional array, and its components can be linear combinations of the elements of $\dot{\mathbf{q}}$, and $\mathbf{d}(\mathbf{q}, t)$ is present only if $\mathbf{b}(\mathbf{q}, t) \neq \mathbf{0}$ in equation (6). Here, we selected the new velocity components so as the matrix describing the transformation from the new set to the original descriptor set, $\mathbf{B}$, is identical to the one used in the selection of independent kinematic variations. This is usually convenient, but in principle, other selections of independent velocities would also be possible. Substituting equation (18) into equation (16) and considering the expression for the generalized inertial forces (3), we obtain

$$\begin{aligned} &\mathbf{U}_{inertial} - \mathbf{B}^T\mathbf{Q}_{impressed} \\ &= \mathbf{B}^T\mathbf{M}\mathbf{B}\ddot{\mathbf{u}} + \mathbf{B}^T\mathbf{M}(\dot{\mathbf{B}}\dot{\mathbf{u}} + \dot{\mathbf{d}}) + \mathbf{B}^T\mathbf{C}(\dot{\mathbf{u}}, \mathbf{q}, t) - \mathbf{B}^T\mathbf{Q}_{impressed} \\ &= \overline{\mathbf{M}}\ddot{\mathbf{u}} + \overline{\mathbf{C}}(\dot{\mathbf{u}}, \mathbf{q}, t) - \mathbf{B}^T\mathbf{Q}_{impressed} = \mathbf{0}. \end{aligned} \quad (19)$$

This is a minimum set of dynamic equations (s equation) expressed in independent velocity components. It can be solved for these velocity components (forward dynamics). Then the original set of generalized velocities can be calculated based on equation (18), and the kinematics level analysis can be carried out to determine changes in configuration. Generally, as shown in equation (19) the descriptor set of coordinates $\mathbf{q}$ still appears in the formulation at the displacement level due to the nonlinear nature of the loop-closure constraints. In specific cases, the introduction of independent coordinates ($\mathbf{u}$) can also be possible based on equation (7). For generic cases, the steps of the transformation described in equation (19) need to be followed, but for several concrete examples, the direct determination of $\overline{\mathbf{M}}$ and $\overline{\mathbf{C}}(\dot{\mathbf{u}}, \mathbf{q}, t)$ is also possible.

Using the minimum set of dynamic equations, the loop closure constraints are embedded at the dynamics level, the constraint forces are eliminated from the analysis, and the dynamic analysis is carried out in independent velocity components. For parallel manipulators, Angeles [2] introduced and discussed the natural orthogonal complement that belongs to this class of approaches, where the kinematic structure of the system investigated makes it possible to select matrix $\mathbf{B}$ in a relatively simple form. This form requires only one matrix inversion numerically to express the relation between $\dot{\mathbf{q}}$ and $\dot{\mathbf{u}}$.

This class of approaches also offers the possibility to generate the closed form minimum set of equations symbolically (using Maple or Mathematica), as can be done by manual derivations for specific systems (e.g., Stewart-Gough platform). The problem is generally, for both symbolic and numerical approaches, the efficient determination of the transformation between original, descriptor type and new, independent quantities (matrix $\mathbf{B}$). For general parallel systems, (that are usually considered for generation of computer codes) there is no methodology available for selecting the independent variables and forming the necessary transformations without numeric, linear algebraic manipulations. For an arbitrary parallel system, these manipulations are impossible to implement in symbolic form. However, there are some promising results available for certain classes of parallel manipulators (Geike and McPhee [9]). The applications of these approaches should be further explored for parallel systems. The possibility that independent kinematic variations and independent velocity components can be selected in different ways may also have interesting potentials (using active or passive joint variables and their combinations). Methods recently worked out for the Jacobian matrix of general parallel manipulators (Monsarrat and Gosselin [12]) may also be further extended to facilitate the symbolic "closed-form" determination of matrix $\mathbf{B}$.

3.2 Methods Using Descriptor Type Kinematic Variations

The use of the original descriptor type kinematic variations opens up two possibilities. One is to relax the constraints and then reinstate them by using explicit expressions for the constraint forces, and the other is to find a kinematically admissible set of kinematic variations using the decomposition of the original descriptor set. First, we will discuss two approaches pertaining to the relaxation of constraints: the Lagrangian multiplier method, and the so-called force coupling method.

3.2.1 Lagrangian Multipliers

The Lagrangian multiplier technique is perhaps the best known classical method to accommodate constraints using the original set of variables and using explicit expressions for the constraint forces. The constraint forces are expressed using the constraint Jacobian and the Lagrangian multipliers in the form (Rosenberg [16])

$$\mathbf{Q}_{constraint} = \mathbf{A}^T \boldsymbol{\lambda}, \tag{20}$$

where $\boldsymbol{\lambda}$ represents the $m \times 1$ array of the Lagrangian multipliers that are only time dependent. Using this explicit expression of the constraint forces, it is not necessary to employ admissible kinematic variations in equation (11), i.e., the constraints are relaxed in the differential variational principle. (Admissible kinematic variations are necessary only if we want to eliminate the constraint forces using the basic principle of equation (13).) Thus, from equation (11)

$$\mathbf{Q}_{inertial} - \mathbf{Q}_{impressed} - \mathbf{A}^T \boldsymbol{\lambda}$$

$$= \mathbf{M}\ddot{\mathbf{q}} + \mathbf{C}(\dot{\mathbf{q}}, \mathbf{q}, t) - \mathbf{Q}_{impressed} - \mathbf{A}^T \boldsymbol{\lambda} = \mathbf{0} \tag{21}$$

This set of equation still contains the multipliers as additional unknowns, and can be solved along with the time derivative of the constraint equations. This technique is frequently used in multibody software applications. It is, however, not very well suited for inverse dynamics and symbolic considerations. There are also several known problems with this approach for solving the forward dynamics problem. Methods have also been suggested to improve the computational performance (e.g. Baumgarte stabilization, penalty functions). The classical Lagrangian multiplier technique works only for independent constraints, where the constraint Jacobian matrix has a full row rank. An advantage of this method is its easy use and implementation.

3.2.2 Explicit Force Coupling

The second approach using the idea of relaxation of constraints is the so-called force coupling method (Schielen et al. [17], Wang et al. [22]), when the constraint forces are virtually replaced by impressed forces with the introduction of stiff springs and dampers instead of the loop closure equations. The explicit expression for the constraint forces can be expressed as

$$\mathbf{Q}_{constraint} = \mathbf{K}\mathbf{q} + \mathbf{D}\dot{\mathbf{q}}, \tag{22}$$

where $\mathbf{K}$ is an $n \times n$ stiffness matrix that is introduced by placing springs at the loop closure locations, and $\mathbf{D}$ is an $n \times n$ damping matrix. We keep the term constraint force, but as was noted these are basically impressed forces in this formulation that are introduced to attempt to realize the constraints. Since the constraints are fully relaxed, from equation (11), the dynamic equations for this case can be obtained as

$$\mathbf{Q}_{inertial} - \mathbf{Q}_{impressed} - \mathbf{K}\mathbf{q} - \mathbf{D}\dot{\mathbf{q}}$$

$$= \mathbf{M}\ddot{\mathbf{q}} + \mathbf{C}(\dot{\mathbf{q}}, \mathbf{q}, t) - \mathbf{Q}_{impressed} - \mathbf{K}\mathbf{q} - \mathbf{D}\dot{\mathbf{q}} = \mathbf{0}. \tag{23}$$

The springs are supposed to ensure that the constraints are maintained with reasonable accuracy, also, the springs make possible the explicit expression of the virtual work or power of the constraint forces. As was noticed in Wang et al. [22], this approach makes possible parallel computational implementation relatively easily. On the other hand, there can be several drawbacks. Some of the problems with this approach is the appropriate determination of the spring constants and the fact that the springs introduce high stiffness into the system that makes numerical solution difficult. Also, the determination of matrices $\mathbf{K}$ and $\mathbf{D}$ is difficult and cannot always be done in a closed form. The "artificial" springs also pose the danger that the constraint forces may become "active", i.e., influence the admissible motion of the system, which would be physically incorrect.

3.2.3 Decomposition of Kinematic Variations, Independent Projections in Descriptor Form

As was mentioned above, the second possibility for using the original descriptor type kinematic variations is to find a kinematically admissible set using the decomposition of the original,

descriptor set. Based on equation (12), it is possible to split the array of generalized kinematic variations, $\delta\hat{\mathbf{q}}$, into two parts

$$\delta\hat{\mathbf{q}} = \delta\hat{\mathbf{q}}_c + \delta\hat{\mathbf{q}}_a \tag{24}$$

where $\delta\hat{\mathbf{q}}_c$ is necessary to satisfy the constraints, and $\delta\hat{\mathbf{q}}_a$ is an array admissible with the constraints, i.e., from the purely kinematic point of view it can take non-zero values without violating the constraints. The elements of these two arrays are basically linear combinations of the original kinematic variations, $\delta\hat{\mathbf{q}}$, and these linear combinations can be determined based on the constraints (particularly the constraint Jacobian). This partition, and the expression of the two new arrays can be done as

$$\delta\hat{\mathbf{q}} = \mathbf{A}^{\dagger}\mathbf{A}\delta\hat{\mathbf{q}} + (\mathbf{I} - \mathbf{A}^{\dagger}\mathbf{A})\delta\hat{\mathbf{q}}, \tag{25}$$

where $\delta\hat{\mathbf{q}}_c = \mathbf{A}^{\dagger}\mathbf{A}\delta\hat{\mathbf{q}}$, $\delta\hat{\mathbf{q}}_a = (\mathbf{I} - \mathbf{A}^{\dagger}\mathbf{A})\delta\hat{\mathbf{q}}$, $\mathbf{I}$ is an $n \times n$ identity matrix, and $\mathbf{A}^{\dagger}$ represents a generalized inverse of $\mathbf{A}$. Here, the definition of the generalized inverse is closely related to the geometric representation of a dynamic system, and the interpretation of orthogonality for generalized vectors. In robotics and multibody dynamics, the Moore-Penrose pseudo-inverse is often used for the generalized inverse to perform decompositions similar to equation (25) (e.g. inverse kinematics of redundant robots). However, this pseudo-inverse is usually not associated with a physically meaningful, invariant norm of generalized vectors of dynamics (particularly the generalized velocity vector). This may lead to erroneous results in some cases (Duffy [8]). The physically meaningful and invariant norm of generalized vectors can be interpreted employing the mass matrix as metric for the tangent space of the configuration manifold. This leads to so-called mass-orthogonal formulations. The generalized inverse of the constraint Jacobian for this case can be derived as

$$\mathbf{A}^{\dagger} = \mathbf{M}^{-1}\mathbf{A}^{T}\left(\mathbf{A}\mathbf{M}^{-1}\mathbf{A}^{T}\right)^{-1}. \tag{26}$$

It is important to note that this expression can be derived based on pure physical considerations without algebraic manipulations. This definition of the generalized inverse can be further elaborated by decomposing $\mathbf{M}^{-1}$ as $\mathbf{M}^{-1} = \mathbf{M}^{-\frac{1}{2}}\mathbf{M}^{-\frac{1}{2}}$. Then, equation (26) can be understood as the Moore-Penrose pseudo-inverse of $\mathbf{A}\mathbf{M}^{-\frac{1}{2}}$, where the pseudo-inverse can be formed using singular value decomposition. The advantage of this transformation is that the generalized inverse can now be calculated for systems where the constraint Jacobian does not have a full row rank (e.g. over-constrained systems, singular systems). To illustrate the above decomposition, we can consider again the loop-closure of the three-link example (Figure 1). We present numerical values only, since the analytical expressions are too lengthy to include here. We assume that the joint angles are 15°, 20°, 25°, the links are beams with uniform mass distribution, and the mass and length of the links are 5 kg, 7 kg, 12 kg, 1 m, 2 m, 3 m. For this case and configuration, the constraints for the kinematic variations, equation (12), can be expressed as

$$\begin{bmatrix} -4.0040 & -3.7452 & -2.5981 \\ 4.1042 & 3.1383 & 1.5000 \end{bmatrix} \begin{bmatrix} \delta\hat{q}_1 \\ \delta\hat{q}_2 \\ \delta\hat{q}_3 \end{bmatrix} = \begin{bmatrix} 0 \\ 0 \\ 0 \end{bmatrix} \tag{27}$$

and, using equations (24) - (26), the decomposition can be performed as

$$\delta\hat{\mathbf{q}}_c = \begin{bmatrix} 3.2248 & 2.1852 & 0.7127 \\ -4.0861 & -3.0134 & -1.3090 \\ 2.4614 & 2.4176 & 1.7885 \end{bmatrix} \begin{bmatrix} \delta\hat{q}_1 \\ \delta\hat{q}_2 \\ \delta\hat{q}_3 \end{bmatrix} \tag{28}$$

and

$$\delta\hat{\mathbf{q}}_a = \begin{bmatrix} -2.2248 & -2.1852 & -0.7127 \\ 4.0861 & 4.0134 & 1.3090 \\ -2.4614 & -2.4176 & -0.7885 \end{bmatrix} \begin{bmatrix} \delta\hat{q}_1 \\ \delta\hat{q}_2 \\ \delta\hat{q}_3 \end{bmatrix} \tag{29}$$

As we can see, the elements of $\delta\hat{\mathbf{q}}_a$ can be non-zero, and for any arbitrary selection of the elements of $\delta\hat{\mathbf{q}}$, they are not influencing the satisfaction of the constraints.

Array $\delta\hat{\mathbf{q}}_a$ gives the admissible set of kinematic variations without the introduction of new, independent variations. Thus, based on the basic principle of constrained motion, equation (13),

$$\delta\hat{\mathbf{q}}_a^T\mathbf{Q}_{constraint} = 0. \tag{30}$$

Based on these considerations, by substituting the decomposition (24) into (11) we obtain the constraint force free equations as

$$\mathbf{P}^T\left(\mathbf{Q}_{inertial} - \mathbf{Q}_{impressed}\right) = \mathbf{0}, \tag{31}$$

where $\mathbf{P} = (\mathbf{I} - \mathbf{A}^{\dagger}\mathbf{A})$ can be considered as a projector operator. This equation can be seen as the counterpart of equation (17), but here the formulation is expressed in terms of n equations, using the descriptor set of variables. In the expression of the $\mathbf{Q}_{inertial}$, a decomposition similar to the above can also be done for $\dot{\mathbf{q}}$ and $\ddot{\mathbf{q}}$ using equation (6) and its time derivative. We do not give these detailed expressions here. But, the major physical idea and contribution is expressed by equation (31), which is clearly a consequence of the differential variational principles, as fundamental ideas of constrained systems. As we know, this is the first time that this general derivation based on the basic principles of constrained systems is presented. However, there are several works available in the literature where methods of this class of approaches are discussed. One of the first descriptions of this approach can be found in Brauchli [5], that was subsequently applied to model the dynamics of a parallel robot, the Delta robot, by Devaquet and Brauchli [7], with special attention to closed form inverse dynamics equations. This analytical technique was further considered and elaborated in Udwadia and Kalaba [19], [20]. Aghili and Piedbœuf [1] developed a method pertaining to this class of approaches for hardware-in-the-loop simulation of robotic systems interacting with the environment. With the exception of Devaquet and Brauchli [7], this approach has not really been applied to parallel systems yet. It should receive more attention since it can be used in both inverse and forward dynamics, and it has the great advantage that it can relatively simply work for singular cases when constraints become dependent ($\mathbf{A}$ does not have a full row rank) (Udwadia and Kalaba [19], Arabyan and Wu [3]. Redundant constraints can be especially important in modeling parallel manipulators (Devaquet

and Brauchli [7]). On the other hand, this technique is not very well suited for generic symbolic implementation since it requires to form and handle a generalized inverse, that usually cannot be carried out in symbolic form for an arbitrarily large system.

4 Some Interesting Areas in the Dynamics of Parallel Systems

Dynamics formulations usually have two main areas of applications: they are used in control, and in design analysis and operations. The methods summarized above can be advantageous in various problems of parallel systems dynamics. A few examples will be summarized here.

We already mentioned forward and inverse dynamics, and suitability for symbolic or numerical model developments. Forward dynamics is the essence of computer simulations. In the formulation of a model for simulations, it is of key importance how the loop closure constraints are handled. The methods presented in this paper should be further explored from the point of view of parallel structures, in order to develop the algorithms for efficient and tractable computer modeling. Efficient inverse dynamics solutions are required for advanced model based control of parallel systems. Inverse dynamics is, in a way, simpler because it does not require the solution for the accelerations. We would like to emphasize the potentials in symbolic model development. This offers more effective ways for controller development and also for further dynamic analysis. Symbolic methods can offer great advantages in the development of advanced numerical methods for the solution of the forward dynamics problem as well as in dynamic parameter identification.

Dynamic parameter identification is another area of great importance. In model based control, the knowledge of the accurate dynamic model is required. In simulations and detailed dynamic analysis of structures (e.g., analysis of constraint forces), good representation of the existing physical system is also necessary. The parameter identification of parallel systems is much more involved than that of serial arms (because of the presence of loop closure constraints). A detailed understanding of the constrained system dynamics and methods are necessary to advance the techniques for model identification of parallel structures.

In control, the user is often concerned only about the equations of motion of the system, where constraint forces are eliminated from the formulation. However, in design and operations of systems the constraint forces are of key importance. An example can be the Canadian space robotic system of the International Space Station, where the accurate knowledge of constraint forces in the system is of primary importance in assessing the feasibility and design of space operations. Constraint forces can even be important of advanced control of systems, for example, where friction effects are accounted for (in constrained systems, friction effects are usually dependent on constraint forces). The study of constraint forces and their optimum ”design” and distribution during dynamic loading should receive more attention in parallel systems.

Today, dynamic analysis is primarily based on simulations, i.e., the numerical solution of the system of dynamic equations. It would also be desirable to put more emphasis on qualitative methods that are not primarily based on simulation (numerical solution of differential equations with known initial values). But, instead they would rely on the study of the structure of the dynamic equations and the underlying physical phenomena, and the development of performance measures. This kind of approach can be particularly useful for example in case of interacting systems (e.g. docking mechanisms) where the numerical modeling and simulation of the contact dynamics effects are usually quite difficult. Also, it is of high importance to determine for example that how parallel systems can be optimally used (and designed for) to reduce contact dynamics effects in interacting systems. Redundant mechanisms can play a dominant role in these considerations.

References

[1] Aghili, F. and Piedbœuf, J.-C., Hardware-in-the-loop Simulation of Robots Interacting with Environment via Algebraic Differential Equations, *Proc. 2000 IEEE/RSJ Int. Conf. on Intelligent Robots and Systems*, Takamatsu, Japan, pp. 1590-1596, 2000.

[2] Angeles, J., *Fundamentals of Robotic Mechanical Systems* Springer-Verlag New York, 1997, pp. 398-409.

[3] Arabyan, A. and Wu, F., An Improved Formulation for Constrained Mechanical Systems, *Multibody System Dynamics*, Vol. 2, pp. 49-69, 1998.

[4] Bahar L.Y. and Kwatny H.G.: Extension of Noether's theorem to constrained non-conservative systems. *Int. J. Nonlinear Mechanics*, vol. 22, n. 2, pp. 125-138, 1987.

[5] Brauchli, H., Mass-Orthogonal Formulation of Equations of Motion for Multibody Systems, *J. Applied Mathematics and Physics (ZAMP)*, Vol. 42, pp. 169-182, 1991.

[6] Dasgupta, B. and Mruthyunjaya, T.S., A Newton-Euler Formulation for the Inverse Dynamics of the Stewart Platform Manipulator, *Mechanism and Machine Theory*, Vol. 33, No. 8, pp. 1135-1152, 1998.

[7] Devaquet, G and Brauchli, H., A Simple Mechanical Model for the DELTA-Robot, *Robotersysteme*, Vol. 8, pp. 193-199, 1992.

[8] Duffy, J., The Fallacy of Modern Hybrid Control Theory that is Based on 'Orthogonal Complements' of Twist and Wrench Spaces, *J. Robotic Systems*, Vol. 7, No. 2, pp. 139-144, 1990.

[9] Geike, T. and McPhee, J., Inverse Dynamic Analysis of Parallel Manipulators with 3 or 6 Degrees of Freedom, submitted to *Mechanism and Machine Theory*.

[10] Kövecses, J. and Cleghorn, W.L., Finite and Impulsive Motion of Constrained Mechanical Systems Via Jourdain's Principle: Discrete and Hybrid Parameter Models, *Int. J. Non-Linear Mechanics*, in press, to appear.

[11] Li, J., Wang, J. and Liu, X., An Efficient Method for Inverse Dynamics of Kinematically Defective Parallel Platforms, *J. Robotic Systems*, Vol. 19, No. 2, pp. 45-61, 2002.

[12] Monsarrat, B. and Gosselin, C.M., Jacobian Matrix of General Parallel and Hybrid Mechanisms with Rigid and Flexible Links: A Software-Oriented Approach, submitted to *2002 ASME Design Engineering Technical Conferences*, Montréal, Canada.

[13] Papastavridis, J.G., A Panoramic Overview of the Principles and Equations of Motion of Advanced Engineering Dynamics, *ASME Applied Mechanics Reviews*, Vol. 51, No. 4, pp. 239-265, 1998.

[14] Papastavridis, J.G., *Analytical Mechanics*, Oxford University Press, 2002.

[15] Piedbœuf, J.C., Recursive Modeling of Serial Flexible Manipulators, *J. Astronautical Sciences*, Vol. 46, No. 1, pp. 1-24, 1998.

[16] Rosenberg, R.M., *Analytical Dynamics of Discrete Systems*, Plenum Press, New York, 1977.

[17] Schielen, W., Rükgauer, A. and Schirle, TH., Force Coupling Versus Differential Algebraic Description of Constrained Multibody Systems, *Multibody System Dynamics*, Vol. 4, pp. 317-340, 2000.

[18] Tsai, L.-W., Solving the Inverse Dynamics of a Stewart-Gough Manipulator by the Principle of Virtual Work, *ASME J. Mechanical Design*, Vol. 122, pp. 3-9, 2000.

[19] Udwadia, F.E. and Kalaba, R.E., A New Perspective on Constrained Motion, *Proc. Royal Society Ser. A*, Vol. 439, No. 1906, pp. 407-410, 1992.

[20] Udwadia, F.E. and Kalaba, R.E., The Geometry of Constrained Motion, *Z. Angew. Math. Mech. (ZAMM)*, Vol. 75, No. 8, pp. 637-640, 1995.

[21] Wang, J. and Gosselin, C.M., A New Approach for the Dynamic Analysis of Parallel Manipulators, *Multibody System Dynamics*, Vol. 2, pp. 317-334, 1998.

[22] Wang, J., Gosselin, C.M. and Cheng, Li, Modeling and Simulation of Robotic Systems with Closed Kinematic Chains Using the Virtual Spring Approach, *Multibody System Dynamics*, Vol. 7, pp. 145-170, 2002.

Proceedings of the WORKSHOP on
Fundamental Issues and Future Research Directions for Parallel Mechanisms and Manipulators
October 3–4, 2002, Quebec City, Quebec, Canada
Clément M. Gosselin and Imme Ebert-Uphoff, editors

On the Automatic Generation of Inverse Dynamic Solutions for Parallel Manipulators

THOMAS GEIKE
Department of Mechanical Engineering
Technical University of Braunschweig, Germany
Thomas.Geike@gmx.de

JOHN MCPHEE
Systems Design Engineering
University of Waterloo, Canada
mcphee@real.uwaterloo.ca

Abstract: *An approach is presented for automatically generating inverse dynamic solutions for planar and spatial parallel manipulators, thereby eliminating the errors and tedium associated with hand derivations. Kinematic and dynamic equations are formulated using a combination of linear graph theory, the principle of virtual work, and symbolic programming. The formulation is first developed for spatial manipulators with 6 degrees of freedom (DOF) and planar manipulators with 3 DOF. Two examples, including a Gough-Stewart platform, are used to demonstrate the automated formulation and to compare the efficiencies of several different computer implementations. The method is extended to manipulators with less than 6 DOF, and demonstrated using a spatial 4-DOF manipulator as an example.*

1 Introduction

Merlet (2000) has defined a parallel manipulator as "a closed-loop kinematic chain mechanism whose end effector is linked to the base by several independent kinematic chains". In comparison with serial robots, parallel manipulators have very good performance in terms of rigidity, accuracy and dynamic characteristics. However, the closed chains in parallel manipulators lead to difficulties in obtaining the dynamic models needed for simulation, control, and design. Manual derivations may lead to very efficient solutions for the inverse dynamics, but they are very tedious and prone to errors for complex parallel manipulators. To quote Merlet, "one school of thought recommends that dynamic models should not be used because modelling errors are too numerous".

One of the most popular parallel manipulators is the Gough-Stewart platform, which has been the subject of three recent papers on manual derivations for the inverse dynamics. Dasgupta and Mruthynjaya (1998) use a Newton-Euler formulation to arrive at a system of six linear equations that are solved numerically for the six unknown driving forces. Tsai (2000) arrives at a similar system of equations, but uses the principle of virtual work to derive them. Wang and Gosselin (1998) also use the principle of virtual work, but their final equations are explicit in the driving loads so that the solution of linear systems is not required.

In multibody system dynamics (Schiehlen (1990)), a main goal is to develop formulations that automatically generate kinematic and dynamic equations. The approach taken by most commercial multibody computer programs, e.g. ADAMS, DADS, and Working Model, is to use absolute coordinates to represent the position and orientation of every body in the system (Haug (1989)). The result is very large systems of equations that are represented by abstract data structures; closed-form solutions for the inverse dynamics are not possible. The other common approach in multibody dynamics is to use the joint coordinates favoured by roboticists, in which the relative position and orientation of two adjacent bodies are represented by variables associated with the kinematic joint connecting the two bodies.

Shi and McPhee (2000) have used joint coordinates in a multibody formulation that combines graph-theoretic methods for kinematics with the principle of virtual work for dynamics. The formulation is implemented using computer algebra (Shi and McPhee (2002)), so that the equations of motion are automatically generated in symbolic form for systems with any number of open and closed chains of rigid or flexible bodies. Non-working reaction loads can be eliminated from the dynamic equations using coordinate partitioning and the principle of virtual work. The result is one dynamic equation per degree of freedom (DOF), in which the actuator loads appear explicitly. Assuming that there is one actuator per DOF, symbolic expressions for these actuator loads can be directly obtained. This represents an automated solution for the inverse dynamics of general multibody systems.

However, a problem arises when there are many closed kinematic chains, resulting in a large number of loop closure equations that are linear in joint velocities. The coordinate partitioning method requires the solution of these equations, but direct application of computer algebra to this large linear system will fail, or result in very large, unwieldy expressions. One can

take a combined symbolic/numeric approach, in which the linear equations from coordinate partitioning are solved numerically and substituted into symbolic expressions for the actuator forces. This approach was successfully applied to the Gough-Stewart platform (McPhee, Shi, and Piedboeuf (2002)). However, the efficiency of this approach is questionable, and the implementation of a linear equation solver may not be feasible in a real-time control application.

The purpose of this paper is to present a systematic method for generating inverse dynamic solutions for parallel manipulators, thereby eliminating the errors and tedium associated with hand derivations. By exploiting the decoupling of kinematic equations between independent chains of a parallel manipulator, symbolic solutions for the linear systems of loop closure equations are obtained. These solutions, for dependent virtual displacements in terms of independent virtual displacements, are then used to automatically generate closed-form expressions for the inverse dynamics.

For convenience, we refer to planar 3-DOF and spatial 6-DOF manipulators as having "full mobility", i.e. the end effector can be independently positioned and oriented within the limits of the workspace. A spatial (or planar) manipulator with less than 6 (or 3) DOF is defined as having "reduced mobility" because the end effector's position and orientation can not be controlled independently. The authors are very open to suggestions for a more appropriate terminology.

First, we present a formulation for planar and spatial manipulators with full mobility, in which there is one actuator per DOF. We have made no other assumptions regarding the number of legs or placement of actuators. Two examples, a planar RRR manipulator and the Gough-Stewart platform, are presented to demonstrate the features of this new formulation, and to draw conclusions regarding the efficiency of several different computer implementations. The method is then extended to parallel manipulators with reduced mobility, and demonstrated using a spatial 4-DOF manipulator as an example.

2 Multibody Dynamic Formulation

By representing the system topology by a linear graph and selecting a spanning tree, the n generalized coordinates $\mathbf{q}$ that appear in the kinematic and dynamic equations are defined (McPhee (1998)). One can use absolute or joint coordinates, or some combination thereof, but we will restrict ourselves to joint coordinates for the present paper. Complete details of the equation formulation process are given in Shi and McPhee (2000); a brief overview is presented here.

Each node in the linear graph represents a body-fixed reference frame, while each edge corresponds to a physical component such as a rigid or flexible body, kinematic joint, force, or torque. For each joint in the cotree (the complement of the tree), the graph-theoretic "circuit equations" are equivalent to the rotational and translational equations corresponding to loop closure. Combining these m nonlinear algebraic equations in a column matrix, one obtains:

$$\mathbf{\Phi}(\mathbf{q}, t) = \mathbf{0} \tag{1}$$

where $m = n - f$, and f is the DOF of the multibody system.

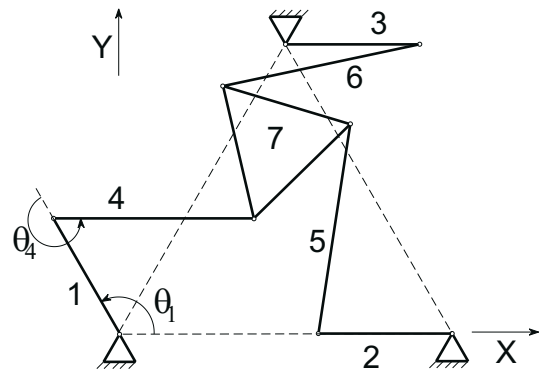

Figure 1: Planar Parallel 3-DOF Manipulator

To demonstrate, consider the 3-DOF planar parallel RRR manipulator from Ma and Angeles (1989), shown in Figure 1. The end effector (labelled 7) is an equilateral triangle with sides of length L_7, links 1, 2, and 3 have a length L_1, links 4, 5, and 6 have a length of L_4, and the three ground-fixed revolute joints form an equilateral triangle with sides of length L_0.

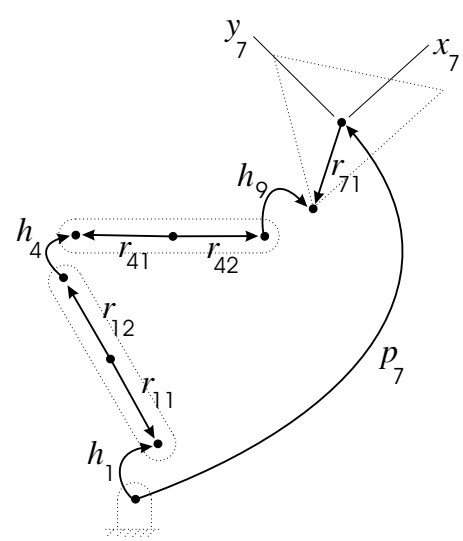

Figure 2: Linear Graph of Leg 1 of 3-DOF Manipulator

A linear graph representation of the first leg of the 3-DOF manipulator is shown in Figure 2. For clarity, the bodies are superimposed on the graph with dotted lines. The revolute joints are represented by edges h_1, h_4, and h_9, while a "virtual" planar joint p_7 represents the 3-DOF motion of the end effector relative to the ground. This virtual joint, sometimes called a free

joint, is included in the graph so that the position and orientation of the end effector frame ($x_7 y_7$ in Figure 2) can appear in the kinematic equations. The remaining edges r_{11}, r_{12}, r_{41}, r_{42}, and r_{71} represent body-fixed kinematic transformations between a reference frame (node) at the mass center and reference frames at the connection points between bodies. For simplicity, the dynamic elements corresponding to inertial and applied forces are not shown in the linear graph.

By selecting h_1, h_4, and p_7 into the spanning tree for this linear graph, the kinematic equations are automatically generated in terms of the corresponding "branch" coordinates θ_1, θ_4, x_7, y_7, and θ_7 (McPhee (1998)). Note that the tree is completed by the inclusion of the kinematic transformation elements r_{11}, r_{12}, r_{41}, r_{42}, and r_{71}. Joint h_9 must therefore be in the cotree; as a consequence, the corresponding joint coordinate is eliminated from all equations.

From the incidence matrix for this linear graph, one can systematically generate the circuit equation for cotree joint h_9:

$$\mathbf{r}_1 - \mathbf{r}_{11} + \mathbf{r}_{12} + \mathbf{r}_4 - \mathbf{r}_{41} + \mathbf{r}_{42} + \mathbf{r}_9 - \mathbf{r}_{71} - \mathbf{r}_7 = 0 \quad (2)$$

which clearly represents loop closure of translational displacement vectors. Into this circuit equation, the constitutive equations for individual components are substituted. For revolute joints, which do not admit any translations:

$$\mathbf{r}_1 = \mathbf{r}_4 = \mathbf{r}_9 = 0 \quad (3)$$

while the translational displacement vectors for the kinematic transformation elements and the planar joint are:

$$\begin{aligned} \mathbf{r}_{12} - \mathbf{r}_{11} &= L_1 c_1 \hat{\imath} + L_1 s_1 \hat{\jmath} && (4) \\ \mathbf{r}_{42} - \mathbf{r}_{41} &= L_4 c_{14} \hat{\imath} + L_4 s_{14} \hat{\jmath} && (5) \\ \mathbf{r}_{71} &= -\frac{L_7}{2}(c_7 \hat{\imath} + s_7 \hat{\jmath}) - \frac{\sqrt{3}}{6} L_7 (-s_7 \hat{\imath} + c_7 \hat{\jmath}) && (6) \\ \mathbf{r}_7 &= x_7 \hat{\imath} + y_7 \hat{\jmath} && (7) \end{aligned}$$

where $c_i \equiv \cos\theta_i$ and $s_{ij} \equiv \sin(\theta_i + \theta_j)$, etc, and $\hat{\imath}$ and $\hat{\jmath}$ are unit vectors parallel to the global X and Y axes, respectively. Note that θ_1 and θ_4 are measured as shown in Figure 1, and θ_7 is measured counter-clockwise from the global X axis to the x_7 axis. Substituting these constitutive equations (3-7) into the circuit equation (2), and projecting the result onto the reaction space ($\hat{\imath}$, $\hat{\jmath}$) for cotree joint h_9 (Shi and McPhee (2000)), one obtains 2 nonlinear algebraic equations in terms of the selected branch coordinates θ_1, θ_4, x_7, y_7, and θ_7.

Repeating this process for all three legs of the manipulator, one obtains the $m = 6$ kinematic constraint equations $\mathbf{\Phi} = \mathbf{0}$:

$$\left\{ \begin{array}{c} -x_7 + \frac{1}{2} L_7\, c_7 - \frac{\sqrt{3}}{6} L_7\, s_7 + L_1 c_1 + L_4 c_{14} \\ -y_7 + \frac{1}{2} L_7 s_7 + \frac{\sqrt{3}}{6} L_7 c_7 + L_1 s_1 + L_4 s_{14} \\ L_0 - x_7 - \frac{1}{2} L_7\, c_7 - \frac{\sqrt{3}}{6} L_7\, s_7 + L_1 c_2 + L_4 c_{25} \\ -y_7 - \frac{1}{2} L_7 s_7 + \frac{\sqrt{3}}{6} L_7 c_7 + L_1 s_2 + L_4 s_{25} \\ -x_7 + \frac{\sqrt{3}}{3} L_7\, s_7 + L_1 c_3 + L_4 c_{36} + \frac{1}{2} L_0 \\ -y_7 - \frac{\sqrt{3}}{3} L_7 c_7 + L_1 s_3 + L_4 s_{36} + \frac{\sqrt{3}}{2} L_0 \end{array} \right\} = \mathbf{0} \quad (8)$$

noting that θ_2, θ_3, θ_5, and θ_6 appear in the last four equations because the corresponding joint elements were selected into the spanning tree for the linear graph of the entire system. Given any 3 of the full set of branch coordinates $\mathbf{q} = [\theta_1, \theta_2, \theta_3, \theta_4, \theta_5, \theta_6, x_7, y_7, \theta_7]^T$, one can solve equations (8) for the remaining 6 coordinates, thereby effecting a kinematic analysis.

In anticipation of applying the principle of virtual work, $\mathbf{q}$ is partitioned into f independent coordinates $\mathbf{q_i}$ and m dependent coordinates $\mathbf{q_d}$. Taking the variation of equation (1), one obtains:

$$\mathbf{\Phi}_{\mathbf{q}_i} \delta \mathbf{q}_i + \mathbf{\Phi}_{\mathbf{q}_d} \delta \mathbf{q}_d = \mathbf{0} \quad (9)$$

where $\mathbf{\Phi}_{\mathbf{q}_i} = \partial \mathbf{\Phi} / \partial \mathbf{q}_i$ and $\mathbf{\Phi}_{\mathbf{q}_d} = \partial \mathbf{\Phi} / \partial \mathbf{q}_d$ is non-singular as long as the given physical constraints are not redundant. To eliminate all non-working reaction loads from the dynamic equations using the principle of virtual work, one needs to solve these linear equations (9) for the transformation from dependent to independent variations:

$$\delta \mathbf{q}_d = -\mathbf{\Phi}_{\mathbf{q}_d}^{-1} \mathbf{\Phi}_{\mathbf{q}_i} \delta \mathbf{q}_i = \mathbf{J}\, \delta \mathbf{q}_i \quad (10)$$

where the $m \times f$ matrix $\mathbf{J}$ is a nonlinear function of the joint coordinates.

To formulate the dynamic equations, the contributions of all working components to the system virtual work are summed. If there are n_T applied torques $\mathbf{T}$, n_F applied forces $\mathbf{F}$ (including weights), and n_R rigid bodies, one has:

$$\begin{aligned} \delta W &= \sum_{n_T} \mathbf{T}^T \delta\theta + \sum_{n_F} \mathbf{F}^T \delta \mathbf{r} \\ &\quad - \sum_{n_R} \left[m \mathbf{a}^T \delta \mathbf{r} + (\mathbf{I}\dot{\omega} + \omega \times \mathbf{I}\omega)^T \delta\theta \right] = 0 \quad (11) \end{aligned}$$

where $\delta\mathbf{r}$ and $\delta\theta$ are virtual translational and rotational displacements, respectively, m and $\mathbf{I}$ are the mass and inertia tensor of a rigid body, ω is its angular velocity, and $\mathbf{a}$ is the translational acceleration of its mass center. One of the attractive features of a virtual work approach is that flexible bodies can be included in the system model more easily than with a Newton-Euler approach (Shi and McPhee (2000)).

One can then use the graph-theoretic "branch transformation" equations to express all kinematic variables (e.g. ω, $\delta\mathbf{r}$) in terms of the coordinates $\mathbf{q}$ associated with joints in the tree. The easy and systematic generation of these transformations is one of the advantages of using linear graph theory for kinematic modelling. After applying these transformations, one has:

$$\delta W = \mathbf{Q}^T\, \delta \mathbf{q} = 0 \quad (12)$$

where $\mathbf{Q}$ are the n generalized forces corresponding to $\delta\mathbf{q}$. By treating these n variations as independent, one obtains n dynamic equations in which the m reaction forces and torques in cotree joints appear explicitly or as unknown Lagrange multipliers.

Assuming that we are not interested in these reaction loads, we can substitute equation (10) into the system virtual work expression (12) to get:

$$\delta W = \mathbf{Q}^T \begin{bmatrix} \mathbf{1} \\ \mathbf{J} \end{bmatrix} \delta \mathbf{q}_i = \mathbf{Q}_i^T \delta \mathbf{q}_i = 0 \tag{13}$$

where $\mathbf{Q}_i$ are the generalized forces associated with $\delta \mathbf{q}_i$. Since these variations are independent, each generalized force can be set to zero to obtain one dynamic equation per degree of freedom. In matrix form,

$$\widetilde{\mathbf{M}} \ddot{\mathbf{q}} = \widetilde{\mathbf{F}} \left(\mathbf{q}, \dot{\mathbf{q}}, t \right) \tag{14}$$

where $\widetilde{\mathbf{M}}$ is an unsymmetric $f \times n$ mass matrix. In a forward dynamic problem, (1) and (14) give $m + f$ equations that can be solved for the n coordinates $\mathbf{q}$. In an inverse dynamic problem for which $\mathbf{q}(t)$ is known, equation (14) can be solved for the f actuator loads. Note that the actuator loads will always appear linearly in $\widetilde{\mathbf{F}}$, which also contains external loads and quadratic velocity terms (Coriolis, centripetal). Furthermore, by choosing the actuated joint variables as the independent coordinates $\mathbf{q}_i$, the actuator loads will be decoupled in equation (14), i.e. exactly one actuator load appears explicitly in each equation. Hence, no matrix inversion is needed.

The systematic nature of this kinematic and dynamic formulation made it relatively easy to implement using the symbolic programming language Maple. Kinematic and dynamic equations are generated automatically in symbolic form by our program DynaFlex, given only a description of the system as input. Dynamic equations can be generated with or without Lagrange multipliers, as desired. However, the elimination of Lagrange multipliers requires equation (10), which in turn requires the solution of the linear equations (9).

3 Inverse Dynamics of Full-Mobility Parallel Manipulators

3.1 Pseudo-variable Approach

The direct application of symbolic programming to the solution of the linear equations (9) for the dependent variations will be called the *direct symbolical* approach. As discussed previously, this approach will fail when the number of loop closure equations is large, in which case the embedding formulation cannot be applied. In this section, we present a *pseudo-variable* approach to solving equation (9) in a way that exploits the special topology of parallel manipulators.

The set of coordinates are further partitioned as:

$$\mathbf{q} = \left(\mathbf{q}_i, \mathbf{q}_{dd}, \mathbf{q}_e \right) \tag{15}$$

where $\mathbf{q}_i$ are the independent variables (associated with the actuators), $\mathbf{q}_e$ are the end effector variables, and $\mathbf{q}_{dd}$ are the variables associated with the unactuated joints. The so-called pseudo-independent variables $\mathbf{q}_{pi}$ and pseudo-dependent variables $\mathbf{q}_{pd}$ are now introduced as follows:

$$\mathbf{q}_{pi} = \mathbf{q}_e \tag{16}$$

$$\mathbf{q}_{pd} = \left(\mathbf{q}_i, \mathbf{q}_{dd} \right) \tag{17}$$

where the number of pseudo-independent and end effector variables are both equal to f for manipulators with full mobility. This re-partitioning of the joint coordinates leads to a largely decoupled linear system of equations (9); this is the essential feature of the pseudo-variable approach.

To demonstrate, consider selecting the actuated joint angles θ_1, θ_2, and θ_3 as independent coordinates $\mathbf{q}_i$ for the planar 3-DOF manipulator. The partial derivatives (Jacobian matrices) of the loop closure equations (2) with respect to the dependent and pseudo-dependent variables have the structures:

$$\mathbf{\Phi}_{\mathbf{q}_d} = \begin{bmatrix} * & & & * & & * \\ * & & & & * & * \\ & * & & * & & * \\ & * & & & * & * \\ & & * & * & & * \\ & & * & & * & * \end{bmatrix} \tag{18}$$

$$\mathbf{\Phi}_{\mathbf{q}_{pd}} = \begin{bmatrix} * & & & * & & \\ * & & & * & & \\ & * & & & * & \\ & * & & & * & \\ & & * & & & * \\ & & * & & & * \end{bmatrix} \tag{19}$$

where an asterisk $*$ indicates a non-zero entry. One can clearly see the decoupling that is present in the Jacobian matrix $\mathbf{\Phi}_{\mathbf{q}_{pd}}$ for the pseudo-dependent variables. However, we don't want to use the end-effector variables as our independent variables, since we would end up with coupled dynamic equations to solve for the actuator loads. The approach presented in this section combines the advantages of selecting end effector variables as independent (Tsai (2000)) with the advantages of selecting the actuated joint coordinates as independent (Wang and Gosselin (1998)).

The transformation (4) from dependent to independent variations is obtained in a systematic manner by the following three steps:

1. First, the system of m linear equations

$$\mathbf{\Phi}_{\mathbf{q}_{pd}} \delta \mathbf{q}_{pd} + \mathbf{\Phi}_{\mathbf{q}_{pi}} \delta \mathbf{q}_{pi} = \mathbf{0} \tag{20}$$

is solved for $\delta \mathbf{q}_{pd}$

$$\delta \mathbf{q}_{pd} = \begin{bmatrix} \delta \mathbf{q}_i \\ \delta \mathbf{q}_{dd} \end{bmatrix} = \begin{bmatrix} \mathbf{J}_i \\ \mathbf{J}_{dd} \end{bmatrix} \delta \mathbf{q}_{pi} \tag{21}$$

where $\mathbf{J}_i$ is the "inverse Jacobian matrix" (Merlet (2000)).

2. In the second step, the first f equations of (21), which relate independent and pseudo-independent variables, are solved for the pseudo-independent variables:

$$\delta \mathbf{q}_{pi} = \mathbf{J}_i^{-1} \delta \mathbf{q}_i \tag{22}$$

The solution is obtained using a linear solver instead of inverting the matrix. It is evident from equation (22) that independent and pseudo-independent variables have to be equal in number (f).

3. In the third step, the relation obtained in the second step can be used to substitute in the remaining equations of (21) which leads to

$$\delta \mathbf{q}_{dd} = \mathbf{J}_{dd}\mathbf{J}_i^{-1}\delta \mathbf{q}_i \tag{23}$$

and hence

$$\delta \mathbf{q}_d = \begin{bmatrix} \mathbf{J}_{dd}\mathbf{J}_i^{-1} \\ \mathbf{J}_i^{-1} \end{bmatrix} \delta \mathbf{q}_i \tag{24}$$

This new procedure is advantageous, because (20) can be solved much easier than (9) due to a largely decoupled Jacobian matrix $\mathbf{\Phi}_{\mathbf{q}_{pd}}$. As an example, the Gough-Stewart platform requires solving a linear system with an 18×18 coefficient matrix. This is impossible using the direct approach as long as the actuator variables are treated as independent. It becomes feasible using the suggested 3-step procedure, since the 18×18-system is now largely decoupled. Tests with Maple showed that solving this system needs only seconds and little memory. The 6×6-system in the second step can be solved symbolically, but requires significantly more time and memory than solving the decoupled 18×18-system. In other words, the second step is now the bottleneck; however, the maximum number of linear equations to be solved is now only 6 (or 3, for planar manipulators).

3.2 Implicit Symbolical Approach

The Gough-Stewart platform requires, in the second step, a symbolic solution of a 6×6-system. This is feasible, but leads to very complex expressions for $\delta \mathbf{q}_{pi}$. Substituting these expressions into (23) and into the virtual work equation leads to even more complex expressions. So it might be desirable to use a symbolic dummy matrix for $\mathbf{J}$ in (10) and obtain expressions for the actuator loads in terms of the entries of $\mathbf{J}$. The matrix $\mathbf{J}$ itself can then be calculated as:

$$\mathbf{J} = \begin{bmatrix} \mathbf{J}_{dd}\mathbf{J}_i^{-1} \\ \mathbf{J}_i^{-1} \end{bmatrix} \tag{25}$$

The matrices $\mathbf{J}_i^{-1}$ and $\mathbf{J}_{dd}$ are saved by our symbolic program DynaFlex. Since later numerical inversion is not needed, this *implicit symbolical* approach gives a symbolic solution.

3.3 Combined Symbolic/Numeric Approaches

Instead of solving symbolically for the entries of $\mathbf{J}$, one might want to use numerical methods for linear systems. Two different approaches were added to the DynaFlex code. The first approach uses a dummy matrix for $\mathbf{J}$, leading to a solution for the driving loads in terms of the entries of $\mathbf{J}$. The $m \times f$-matrix $\mathbf{J}$ can be calculated by solving f linear systems

$$\mathbf{\Phi}_{\mathbf{q}_d}\mathbf{j}_k = -\varphi_k \quad , \quad k = 1 \ldots f \tag{26}$$

where $\mathbf{j}_k$ and φ_k are the k-th column of the matrices $\mathbf{J}$ and $\mathbf{\Phi}_{\mathbf{q}_i}$ respectively. This is greatly facilitated by a LU-decomposition of $\mathbf{\Phi}_{\mathbf{q}_d}$ prior to solving (26). Since LU-decomposition (done once) and forward/backward substitution (done f times) are of computational complexity m^2 and m respectively, this method will be more efficient than calculating $\mathbf{J}$ by the symbolic inversion shown in equation (10), which has a computational complexity of m^3.

The second symbolic/numeric approach, implemented only for comparison, uses a dummy for $\mathbf{\Phi}_{\mathbf{q}_d}^{-1}$, i.e. the dummy matrix used is then a $m \times m$-matrix. Calculating the driving loads requires numerical inversion of $\mathbf{\Phi}_{\mathbf{q}_d}$ for every time step. This second approach was used by McPhee et al. to solve for the inverse dynamics of the Gough-Stewart platform (McPhee, Shi, and Piedboeuf (2002)).

Since the matrix $\mathbf{\Phi}_{\mathbf{q}_d}$ is sparse, sparsity methods might be considered by the user.

3.4 End Effector Approach

In the previous approaches, the coordinates associated with the actuators were chosen to be independent. The approaches differ in the manner that they solve equation (3) to get the dependent variations $\delta \mathbf{q}_d$ as functions of the independent variations $\delta \mathbf{q}_i$. By selecting the actuator coordinates to be independent, the resulting dynamic equations are linear and decoupled in the actuator loads. Thus, explicit symbolic expressions for the actuator loads are generated.

For comparison purposes, we have also used an *end effector* approach in which the end effector variables are chosen to be independent. It was already shown that this choice leads to a largely decoupled system of linear equations (3) that are readily solved by Maple. However, the resulting dynamic equations are then coupled in the actuator loads τ:

$$\mathbf{C}\left(\mathbf{q}\right)\tau = \mathbf{c}\left(\mathbf{q},\, \dot{\mathbf{q}},\, \ddot{\mathbf{q}},\, t\right) \tag{27}$$

where the $f \times f$-matrix $\mathbf{C}$ is a function of displacements only. The right-hand side vector $\mathbf{c}$ contains all acceleration terms as well as quadratic velocity terms and external forces. Equation (27) can be solved symbolically as long as $f \leq 6$. Alternatively, the driving loads can be calculated by solving (27) numerically.

3.5 Formulation Time

Of all the symbolic approaches, the implicit symbolical approach is the fastest at generating the equations of motion because substitutions are avoided. On the other hand, this approach will lead to a less efficient numerical implementation when the symbolic expressions are converted to numeric form because optimization of the code conversion (e.g. `C(~,optimized)` in Maple) can work only on parts of the code at a time; this results in repeated evaluation of particular expressions. This could be partly overcome by revising the code afterwards and extracting common expressions.

The symbolic/numeric approaches will be even faster at generating equations, since solving (9) is done numerically during the actual simulation and not during the equation formulation.

Results of numerical simulations will be discussed in detail in the next section.

4 Full-Mobility Manipulator Examples

In this section, two examples of parallel manipulators with full mobility are considered. The main purpose is to show that the suggested approaches can automatically generate symbolic solutions for inverse dynamics. Furthermore, some statements are made about the relative computational efficiency of the different approaches.

The general procedure is always the same. Based on a description of the system, DynaFlex derives the dynamic equations. The symbolic expressions are transformed into Matlab-code, which is used in the numerical implementation. For the combined symbolic/numeric approaches, the linear system from the coordinate partitioning is solved using LU-decomposition.

4.1 Planar RRR 3-DOF Manipulator

For the planar RRR manipulator shown in Figure 1, the drivers given in Ma and Angeles (1989) were used:

$$\begin{aligned} \theta_1 &= \frac{1}{3}\pi + \frac{1}{6}\left(\frac{2\pi t}{T} - \sin\frac{2\pi t}{T}\right) \\ \theta_2 &= \frac{4}{3}\pi - \frac{1}{6}\left(\frac{2\pi t}{T} - \sin\frac{2\pi t}{T}\right) \\ \theta_3 &= \frac{11}{6}\pi + \frac{1}{12}\left(\frac{2\pi t}{T} - \sin\frac{2\pi t}{T}\right) \end{aligned} \tag{28}$$

where $T = 3\,s$. Note that these driver functions give zero velocity and acceleration at the start and end of the motion.

Prescribing the driver motion does not uniquely define the motion of the end effector (there are multiple solutions for the forward kinematics) as long as the initial configuration is not given. To calculate the actuator torques τ_1, τ_2, and τ_3 corresponding to the drivers θ_1, θ_2, and θ_3, we have used the initial configuration:

$$\begin{array}{lll} \theta_1 = \frac{1}{3}\pi & \theta_4 = -0.865 & x_7 = 0.728 \\ \theta_2 = \frac{4}{3}\pi & \theta_5 = -2.102 & y_7 = 0.233 \\ \theta_3 = \frac{11}{6}\pi & \theta_6 = -0.976 & \theta_7 = 3.916 \end{array}$$

Link i	L_i [m]	m_i [kg]	I_i [kg m^2]
1, 2, 3	0.4	3.0	0.04
4, 5, 6	0.6	4.0	0.12
7	0.4	8.0	0.0817

Table 1: Dimensions and inertia properties

The parameters used for the various links are shown in Table 1. In addition, $L_0 = 1.0$ m and gravity acts in the $-Y$ direction.

The resulting torques, shown in Figure 3, are identical to those derived by hand in Ma and Angeles (1989). Explicit expressions for the actuator torques are too lengthy to be displayed here[1].

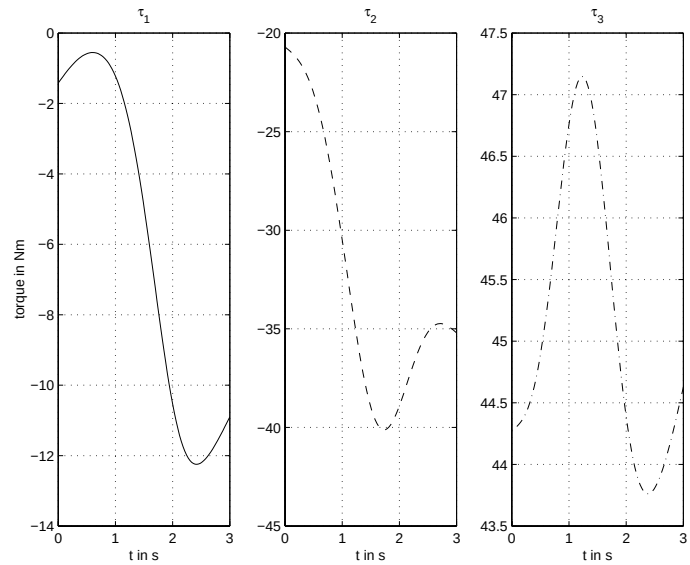

Figure 3: Driving torques for planar 3-DOF manipulator

Approach	Flops	CPU [ms]
direct symbolic	967	6.0
pseudo-variable	871	6.1
implicit symbolic	879	7.6
symbolic/numeric (dummy **J**)	923	15.4
symbolic/numeric (dummy $\mathbf{\Phi}_{\mathbf{q}_d}^{-1}$)	1235	19.8

Table 2: Computational efficiency: number of flops and CPU time for one inverse dynamic analysis (Pentium II, 333 MHz)

The computational efficiency was measured by means of the CPU time and the number of flops required for one inverse dynamic evaluation of the three driving torques; the results are summarized in Table 2. The kinematic solution, performed prior to the dynamic analysis, is not counted. It can be seen that the direct symbolic and pseudo-variable approaches are equivalent regarding the CPU time, while the implicit symbolic approach requires about 25% more CPU time than the first two symbolic approaches. The combined symbolic/numeric approach with a dummy for **J** needs more than twice the CPU time compared to the symbolic approaches. The discrepancy between the number of flops and the CPU-time might be explained by the way flops are counted, i.e. each operation is counted as one flop regardless of the time required to perform the operation.

[1] Available upon request from the authors, for both the 3-DOF RRR manipulator and the Gough-Stewart platform.

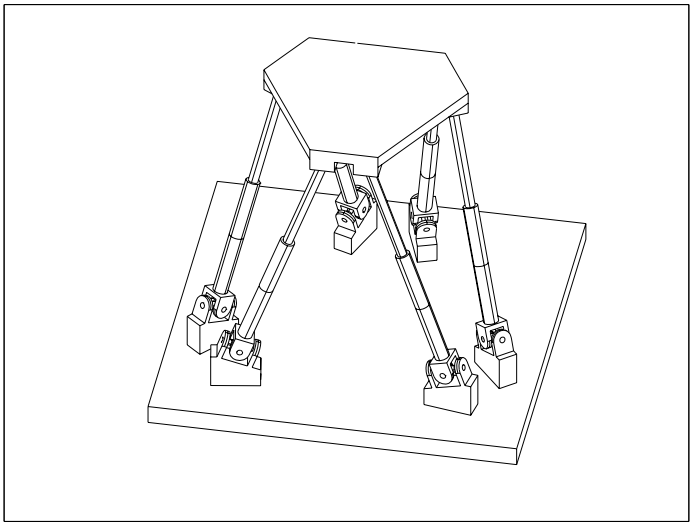

Figure 4: Gough-Stewart Platform

We can draw the conclusion that, for problems of this complexity, the symbolic approaches are preferred because they are faster than the numerical approaches. Furthermore, they do not need matrix manipulation capabilities — this is advantageous in microprocessor-based control applications.

4.2 Gough-Stewart 6-DOF Platform

The Gough-Stewart platform, shown in Figure 4, is a complex spatial parallel manipulator. An inverse dynamic analysis was carried out for the geometry given in Tsai (2000). The kinematic constraint equations associated with leg k are of the general form

$$\mathbf{\Phi}^k = \begin{bmatrix} \rho_k \cos\alpha_k \sin\beta_k - a_k\,(t) \\ \rho_k \sin\alpha_k \sin\beta_k - b_k\,(t) \\ \rho_k \cos\beta_k - c_k\,(t) \end{bmatrix} = \mathbf{0} \quad , \quad k = 1 \ldots 6 \tag{29}$$

where ρ_k is the actuated length of leg k, α_k and β_k are the angles of the universal joint between leg k and the ground, and $a_k\,(t)$, $b_k\,(t)$, $c_k\,(t)$ are known functions of the platform motion (McPhee, Shi, and Piedboeuf (2002)). With 3 joint coordinates per leg, and 6 end effector coordinates, there is a total of $n = 24$ variables. The trajectory from Tsai (2000) is used, in which the platform moves with constant orientation and a sinusoidal translation in each of the three Cartesian directions. With these 6 variables prescribed, one can solve the $m = 18$ kinematic constraint equations (29) for the joint coordinates associated with each leg.

As discussed previously, the direct symbolic approach is not feasible for this relatively large number of loop closure equations. The pseudo-variable approach without a dummy matrix is also not feasible on the computer used[2], because the expressions for $\mathbf{J}$ are too complex to substitute into the virtual work equation. However, the implicit symbolic approach provides a symbolic solution that does not require any algorithms for solving linear systems in the numerical implementation. To verify the implicit symbolic solution and to get information about the computational efficiency, the two combined symbolic/numeric approaches were also applied to the Gough-Stewart platform. Additionally, the approach that treats the end effector variables as independent and solves the final dynamic equations for the actuator loads was implemented, with equation (27) solved both symbolically and numerically.

[2] Pentium-II, 333 Mhz, 64 Mb Ram.

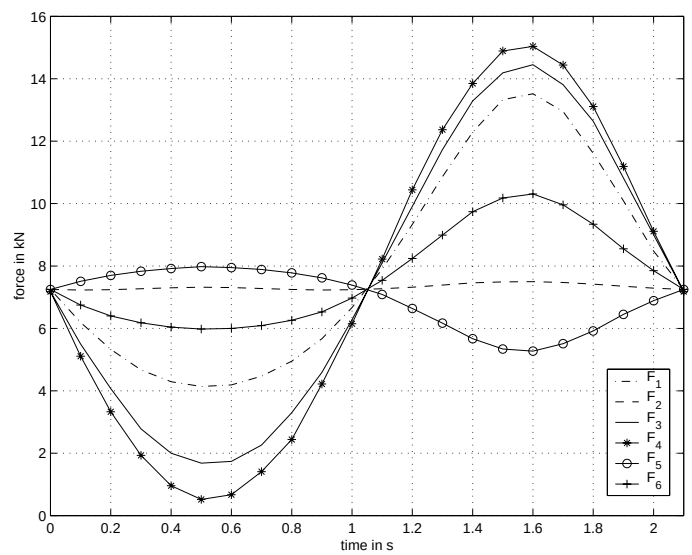

Figure 5: Driving forces for Gough-Stewart platform

In all five approaches, the calculated driving torques shown in Figure 5 are identical to those derived by hand in Tsai (2000).

As summarized in Table 3, the symbolic DynaFlex solutions (approaches 1 and 5) require between 60% and 75% more CPU time than the fastest numerical approach (approach 4). Note that approaches 4 and 5 correspond respectively to numeric and symbolic solutions of equation (27) in the end effector approach.

Approach	Without Sparsity	With Sparsity
1 – implicit symbolic	260	260
2 – symbolic/numeric (dummy $\mathbf{J}$)	195	82
3 – symbolic/numeric (dummy $\mathbf{\Phi}_{\mathbf{q}_d}^{-1}$)	305	90
4 – end effector, numeric	150	150
5 – end effector, symbolic	240	240

Table 3: Computational efficiency: CPU time [ms] for one inverse dynamic analysis (Pentium II, 333 MHz)

However, the symbolic approaches have the advantage of giving an explicit solution. Thus, no matrix manipulation ca-

pabilities (e.g. LU-decomposition) are required in the numeric implementation, which might be important when the inverse dynamic analysis has to be stored on a microprocessor. On the other hand, one has to take into account that the explicit expressions will be larger than the equations that are solved numerically. Hence, the memory savings by not implementing the matrix manipulation capabilities will be partly offset by larger program code for the explicit expressions.

The previous comments are based on calculations without sparsity methods. To investigate the influence of sparse matrix solution methods on the required CPU-time, the numerical calculation of $\mathbf{J}$ and $\mathbf{\Phi}_{\mathbf{q}_d}^{-1}$ was performed using Matlab's sparsity capabilities. The symbolic approaches and the numerical approach 4 cannot benefit from using sparsity methods. The faster of the two numeric/symbolic approaches described in Section 3.3 is about three times faster than the symbolic approaches when sparsity methods are employed.

5 Parallel Manipulators with Reduced Mobility

5.1 Modified Formulation

In the pseudo-variable approach presented in Section 3.1, it was assumed that the end effector variables are equal in number to the system DOF. Thus, this approach can only generate equations for parallel manipulators with full mobility, i.e. 6 DOF for spatial manipulators and 3 DOF for planar manipulators.

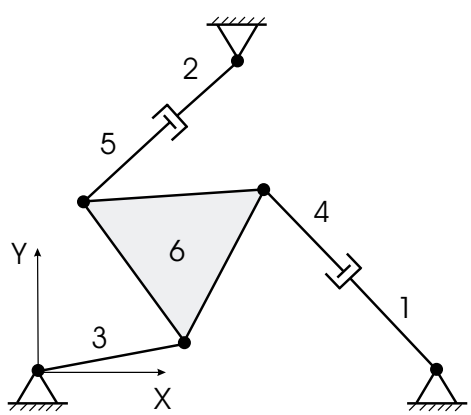

Figure 6: Planar 2-DOF manipulator

However, there are many practical applications involving parallel manipulators with reduced mobility, such as the planar manipulator shown in Figure 6. The end effector (body 6) has only two DOF, and so only two actuators are needed (e.g. in parallel with the two prismatic joints). Clearly, the three end effector coordinates $(x_6,\, y_6,\, \theta_6)$ cannot be treated as independent, as required by the first step of the pseudo-variable approach from Section 3.1. Thus, this approach cannot be used to generate an inverse dynamic solution for this relatively simple manipulator.

In this section, a modified pseudo-variable approach is presented, which will allow treatment of spatial manipulators with less than 6 DOF (and planar manipulators with less than 3 DOF) using the same basic steps as before, i.e.

1. select DOF of the end effector virtual displacements as pseudo-independent variables; for the topologies that are typical of parallel manipulators, this leads to a significant decoupling of the kinematic equations (20) that can be exploited during the solution of this (possibly large) linear system of equations.

2. solve for the pseudo-independent end effector variables as functions of the independent variables.

3. use the results from step 2 to obtain the desired relation $\delta\mathbf{q}_d = \mathbf{J}\delta\mathbf{q}_i$.

The method is explained using the 2-DOF planar parallel manipulator from Figure 6 as an example. The following $n = 8$ coordinates were chosen:

$$\mathbf{q} = (\rho_1,\, \rho_2,\, \theta_1,\, \theta_2,\, \theta_3,\, x_6,\, y_6,\, \theta_6)^T$$

where $\theta_1,\, \theta_2,\, \theta_3$ are the angles (measured from the positive X-axis) associated with the revolute joints that connect links 1, 2, 3 to the ground, and ρ_1, ρ_2 are the actuated lengths of legs 1+4 and 2+5, respectively. The end effector and the ground body are equilateral triangles with sides of length L_6 and L_0, respectively. From a linear graph representation of the system, the $m = n - f = 6$ kinematic constraint equations are systematically generated:

$$\mathbf{\Phi} = \left\{ \begin{array}{l} -x_6 - \frac{1}{2}L_6c_6 - \frac{\sqrt{3}}{6}L_6s_6 + \rho_1c_1 + L_0 \\ -y_6 - \frac{1}{2}L_6s_6 + \frac{\sqrt{3}}{6}L_6c_6 + \rho_1s_1 \\ -x_6 + \frac{1}{2}L_6c_6 - \frac{\sqrt{3}}{6}L_6s_6 + \rho_2c_2 + \frac{1}{2}L_0 \\ -y_6 + \frac{1}{2}L_6s_6 + \frac{\sqrt{3}}{6}L_6c_6 + \rho_2s_2 + \frac{\sqrt{3}}{2}L_0 \\ -x_6 + \frac{\sqrt{3}}{3}L_6s_6 + L_3c_3 \\ -y_6 - \frac{\sqrt{3}}{3}L_6c_6 + L_3s_3 \end{array} \right\} \tag{30}$$

where again, $s_j = \sin\theta_j$ and $c_j = \cos\theta_j$. The first variation of these equations has the general form:

$$\mathbf{\Phi}_{\mathbf{q}}\, \delta\mathbf{q} = \mathbf{0} \tag{31}$$

where the Jacobian matrix has the following structure:

$$\mathbf{\Phi}_{\mathbf{q}} = \left[\begin{array}{cccc|ccc} * & & * & & * & & * \\ * & & * & & & * & * \\ & * & & * & * & & * \\ & * & & * & & * & * \\ & & & * & * & & * \\ & & & * & & * & * \end{array} \right] \tag{32}$$

where $*$ is a non-zero entry. The Jacobian matrix shows that the end effector variables cannot be treated as independent; the columns associated with the legs do not give a square matrix that can be used in (20) to solve for the dependent variables.

The key idea in this modified approach is to reduce the linear system of equations (31) by eliminating one or more of the end effector variables. For example, the first row of equation (31) can be used to solve for δx_6 as a function of other virtual displacements. This allows the linear system of equations to be reduced by one (the amount by which the manipulator mobility is reduced from full mobility), resulting in:

$$\bar{\mathbf{\Phi}}_{\bar{\mathbf{q}}}\, \delta\bar{\mathbf{q}} = \mathbf{0} \tag{33}$$

where $\delta\bar{\mathbf{q}} = (\delta\rho_1, \delta\rho_2, \delta\theta_1, \delta\theta_2, \delta\theta_3, \delta y_6, \delta\theta_6)^T$ are the remaining variables, and the modified Jacobian matrix has the structure:

$$\bar{\mathbf{\Phi}}_{\bar{\mathbf{q}}} = \left[\begin{array}{ccccc|cc} * & & * & & & * & * \\ * & * & * & * & & & * \\ & * & & * & & * & * \\ * & & * & & * & & * \\ & & & & * & * & * \end{array}\right] \tag{34}$$

This reduced system of equations (33) can now be used as the starting point for the three-step procedure from Section 3.1.

The choice of which end effector variable to eliminate, and which equation to use, was found to be of minor importance as long as a translational virtual displacement (i.e. δx_6 or δy_6) was chosen. Looking at the Jacobian matrix (32), one can see that using the fifth row to eliminate δx_6 would lead to slightly simpler expressions in the (modified) third row compared to using the first row. Furthermore, the modified Jacobian $\bar{\mathbf{\Phi}}_{\bar{\mathbf{q}}}$ would have one less non-zero entry. In either case, though, Maple can readily solve the set of largely-decoupled equations, even for large problems. If a rotational variable (i.e. $\delta\theta_6$) were eliminated, the remaining equations would have a greater degree of coupling.

Comparing the Jacobian matrices (34) and (32), one can see that the reduction leads to a stronger coupling of the equations. However, a careful observation of (34) shows that solving the 5×5 system (consisting of the five leftmost columns) requires only solving one or two equations at a time. Computational tests showed that Maple can actually benefit from this structure; `linsolve` can solve this 5×5 system 10 times faster than a general 5×5 system.

The reduced system (33) can now be solved using the previous three-step procedure with the pseudo-independent variables $\delta\bar{\mathbf{q}}_{pi} = (\delta y_6, \delta\theta_6)^T$. One additional step is needed to calculate the eliminated variations (here δx_6) from the eliminated equations. The size of the associated linear system is given by the number of variables eliminated, usually only one or two.

By reducing the number of end effector variables to the DOF of the manipulator, the pseudo-variable approach can be applied to manipulators with reduced mobility. It should be mentioned that reducing the number of end effector variables to less than the DOF of the manipulator is not advantageous, since treating leg variables as pseudo-independent (combined with stronger coupling) will lead to systems that are more difficult to solve. Furthermore, it must be emphasized again that the introduced reduction of the linear system is only one more intermediate step in solving equation (9). All coordinates will appear in the final equations, i.e. eliminating δx_6 temporarily in the 2-DOF manipulator under study still gives dynamic equations that contain x_6 and its time derivatives. Therefore the user is not restricted in the choice of variables used to prescribe the motion. This falls under the domain of the kinematic analysis that precedes the inverse dynamic solution.

5.2 Spatial 4-DOF Manipulator Example

To demonstrate the capability of the modified approach, an inverse dynamic solution is generated for the spatial 4-DOF parallel manipulator shown in Figure 7, taken from Wang (1997).

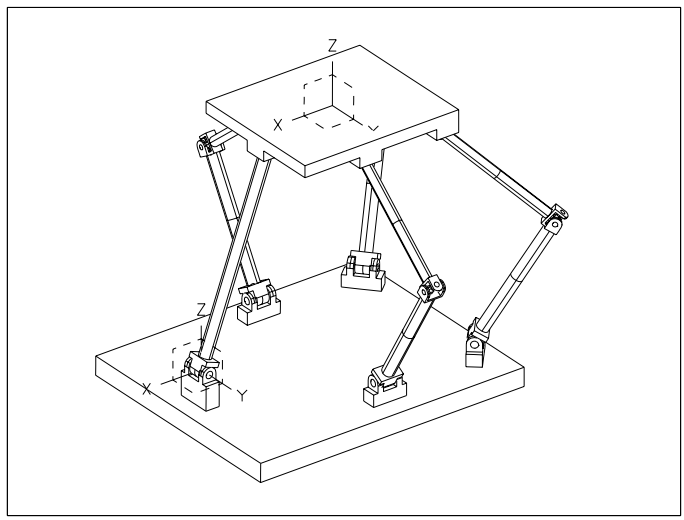

Figure 7: Spatial 4-DOF manipulator

The manipulator is composed of ten moving bodies and five legs. Four of these legs, numbered 1 to 4, consist of two links connected to each other by a universal joint. Leg number 5 consists of a single link. All five legs are connected to the ground by revolute joints, and to the moving platform by spherical joints. Legs 1 to 4 have the same geometric and inertia properties. The platform is considered to be the end effector, which undergoes a 4-DOF motion. The four revolute joints associated with legs 1 to 4 are assumed to be actuated, while leg 5 is unactuated. Gravitational forces act in the negative Z-direction.

Since the manipulator has only 4 DOF, the modified pseudo-variable approach was used to obtain an inverse dynamic solution for the actuator torques. The direct symbolic implementation is not feasible on the computer used, because the expressions for $\mathbf{J}$ are too complex to substitute in the virtual work equation. However, the implicit symbolic approach provides a symbolic solution that does not require any matrix operations in the numeric implementation. A dummy matrix $\mathbf{J}$ is used in the virtual work equation, and the symbolic expression for $\mathbf{J}$ is directly saved as Matlab code.

The manipulator is described using $n = 19$ coordinates: 6 absolute coordinates for the end effector position and orientation, and 13 joint coordinates for the revolute and universal joints. The $m = n - f = 15$ constraint equations are obtained from loop closure conditions (circuit equations) for the five spherical joints.

After reducing the system (31) by two of the end effector variables, the Jacobian matrix with respect to the pseudo-dependent variables (leg variables) is a 13×13-matrix that can be decomposed into five linear systems. These linear systems are not completely decoupled, but they can be solved one after the other, always using the results from the previous steps. Each system has a maximum number of three equations. Maple can easily solve this 13×13-system symbolically, because it recognizes and exploits the equation structure.

For large expressions in the coefficient matrix or the right-hand side vector, as they appear in this example, Maple runs out of memory even though the systems that have to be solved are only 3×3-systems. To overcome this computer implementation problem, a Maple procedure `solvelinearsystem` was written. In this procedure, a general linear system of the same size as the one to be solved is generated and all entries that are zero in the original system are set to zero in the general system. Non-zero entries are replaced by a single variable. In this way, complex expressions are avoided while the structure of the system is still recognized and exploited. The new system is now solved using `linsolve`. Finally, the non-zero entries from the coefficient matrix as well as the entries from the right-hand side vector are substituted into the general solution.

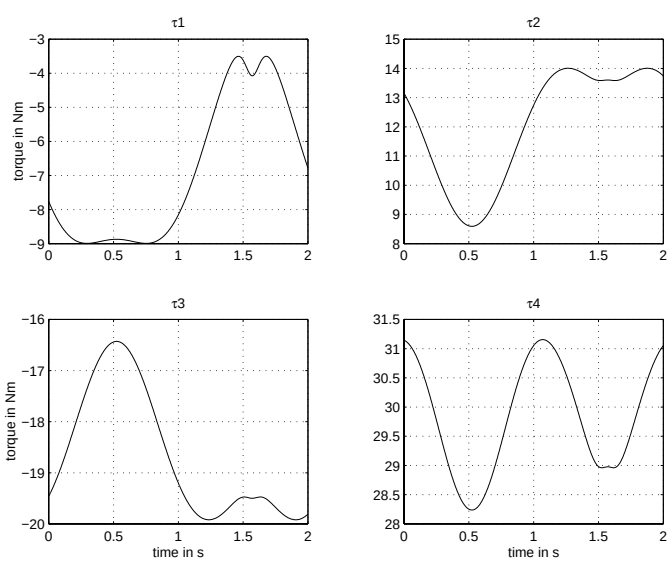

Figure 8: Driving torques for the 4-DOF manipulator

Figure 8 shows the actuator torques. In order to verify the implicit symbolic solution and to get information about the computational efficiency, the two symbolic/numeric implementations discussed in Section 3.3 and the natural orthogonal complement approach of Ma and Angeles (1989) are also used to generate an inverse dynamic solution. We could not use the results of Wang (1997) to validate our results, because we were unable to clearly identify the geometric parameters, reference frames, and initial configuration of the manipulator. However, the four different approaches that we have used all result in identical solutions for the actuator torques.

Table 4 gives an overview of the approaches used and the respective CPU time for one inverse dynamic analysis.

Approach	CPU [ms]
1 - implicit symbolic	60
2 - symbolic/numeric (dummy $\mathbf{J}$)	66
3 - symbolic/numeric (dummy $\bar{\mathbf{\Phi}}_{\mathbf{q}_d}^{-1}$)	107
4 - natural orthogonal complement	87

Table 4: Computational efficiency: CPU time for one inverse dynamic analysis (Pentium II, 333 MHz)

From Table 4 it can be seen that DynaFlex approaches 1 and 2 require almost the same CPU time. However, the purely symbolic approach (version 1) has the advantage of giving an explicit solution. Thus no matrix manipulation capabilities (e.g. LU-decomposition) are required, which might be advantageous when the inverse dynamic analysis has to be stored on a microchip. As for the Gough-Stewart platform, one has to take into account that the explicit expression for $\mathbf{J}$ will be larger than the expressions for $\bar{\mathbf{\Phi}}_{\bar{\mathbf{q}}_i}$ and $\bar{\mathbf{\Phi}}_{\bar{\mathbf{q}}_d}$ and therefore, the memory savings by not implementing the matrix manipulation capabilities will be partly offset by larger code for $\mathbf{J}$. For applications to the control of manipulators, it is interesting to note that the driving torques can be calculated about 16 times in one second using Matlab and a Pentium II (333 MHz). It would be interesting to investigate how these numbers would change if the routines were implemented in C on a microprocessor.

The natural orthogonal complement approach from Ma and Angeles (1989) was implemented to check the validity of our results for the actuator torques. Although our numeric implementation may not be the most efficient, it is clear that our automated symbolic approach is at least as efficient as the hand-derived model from the natural orthogonal complement approach.

6 Conclusions

Several approaches have been presented for automatically generating inverse dynamic solutions for planar and spatial parallel manipulators with full or reduced mobility. The automatic generation of driving loads eliminates the errors and tedium of manual derivations.

The kinematic and dynamic equations are formulated using a combination of linear graph theory, the principle of virtual work, and symbolic programming. Equations are formulated in joint coordinates for systems of rigid and flexible bod-

ies with open and closed kinematic chains. By selecting actuated joint coordinates as independent in an embedding formulation that eliminates non-working reaction loads from the dynamic equations, explicit expressions for driving loads are obtained. This direct approach will fail when the number of loop closure equations is large; we have presented alternative symbolic and symbolic/numeric approaches that exploit the special topology of parallel manipulators (with full or reduced mobility) to generate inverse dynamic solutions.

For a planar 3-DOF manipulator, the symbolic approaches out-performed the combined symbolic/numeric approaches in terms of computational efficiency. For the spatial 4-DOF manipulator, the symbolic approach is only slightly faster than the symbolic/numeric approach. However, for the spatial Gough-Stewart platform, a symbolic/numeric approach was the fastest at computing driving loads, especially when sparse matrix methods were employed. The latter may not be suitable for implementation on a microprocessor being used for real-time control. Considering that the implicit symbolical approach can generate the 6 driving loads at a rate of nearly 4 Hz in Matlab, it is likely that this automated approach would be more than adequate for a real-time control application if the symbolic expressions were exported in optimized C code, compiled, and downloaded onto a microprocessor.

7 Acknowledgements

Financial support for the exchange visit of the first author was provided by the Deutscher Akademischer Austauschdienst (DAAD). The second author gratefully acknowledges the financial support of this research by a Premier's Research Excellence Award, by Waterloo Maple Inc., and by the Natural Sciences and Engineering Research Council of Canada. The authors thank Professor Clément Gosselin of Laval University, Canada, and Dr. Jiegao Wang of MD Robotics, Canada, for providing the drawings of spatial parallel manipulators shown in Figures 3 and 6.

References

Dasgupta, B., and Mruthynjaya, T. (1998). A Newton-Euler Formulation for the Inverse Dynamics of the Stewart Platform Manipulator. *Mechanism and Machine Theory*, 33:1135–1152.

Haug, E.J. (1989) *Computer-Aided Kinematics and Dynamics of Mechanical Systems*. Boston, MA: Allyn and Bacon.

Ma, O., and Angeles, J. (1989) Direct Kinematics and Dynamics of a Planar 3-DOF Parallel Manipulator. In *Advances in Design Automation - 1989*, 3:313–320.

McPhee, J., Shi, P., and Piedboeuf, J.-C. (2002) Dynamics of Multibody Systems using Virtual Work and Symbolic Programming. To appear in *Mathematical and Computer Modelling of Dynamical Systems*.

McPhee, J. (1998) Automatic Generation of Motion Equations for Planar Mechanical Systems Using the New Set of "Branch Coordinates". *Mechanism and Machine Theory*, 33:805-823.

Merlet, J.-P. (2000). *Parallel Robots* Dordrecht, The Netherlands: Kluwer Academic Press.

Schiehlen, W., ed. (1990) *Multibody Systems Handbook*. Berlin: Springer-Verlag.

Shi, P., and McPhee, J. (2000) Dynamics of Flexible Multibody Systems using Virtual Work and Linear Graph Theory. *Multibody Systems Dynamics*, 4:355–381.

Shi, P., and McPhee, J. (2002) Symbolic Programming of a Graph-Theoretic Approach to Flexible Multibody Dynamics. *Mechanics of Structures and Machines*, 30:123–156.

Tsai, L.-W. (2000) Solving the Inverse Dynamics of a Stewart-Gough Manipulator by the Principle of Virtual Work. *Journal of Mechanical Design*, 122:3–9.

Wang, J., and Gosselin, C., (1998) A New Approach for the Dynamic Analysis of Parallel Manipulators. *Multibody System Dynamics*, 2:317–334.

Wang, J., (1997) Kinematic Analysis, Dynamic Analysis and Static Balancing of Planar and Spatial Parallel Mechanisms or Manipulators with Revolute Actuators. PhD Thesis, Université Laval, Canada.

AUTHOR INDEX

Agrawal, S.K..... 195
Angeles, J……..… 160
Brogårdh, T…….. 68
Ceccarelli, M…… 98
Chablat, D……..… 16
Cho, Y.M……..… 178
Clerc, J-P……..…… 34
Company, O……..…… 46
Dasgupta, B……..… 257
Ebert-Uphoff, I……....112, 328
Fassi, I……. 204
Fattah, A……...… 195
Frindt, M……...… 224
Funabashi, H……..… 142
Geike, T…… 348
Gil, J.J…… 12
Gosselin, C.M……..…… 25, 310
Hay, A.M……..…… 267
Hayes, M.J.D…….. 57
Herder, J.L……....…… 40, 238
Herve, J.M…… 284
Hesselbach, J…… 224
Huang, Z……...… 272
Husty, M.L……131
Hwang, J.C……178
Iurascu, C.C……..… 178
Jakobsen, O.G……...…. 86
Jimemez, J.M……..... 12
Karger, A…….....…131
Karouia, M……..... 284
Khan, W.A……...… 317
Kim, J……172, 178
Kim, J.S……..…178
Kong, X……..… 25
Kövecses, J……244, 339
Kozak, K……...… 112, 328
Krefft, M……..…… 224
Krovi, V……...… 317
Krut, S……..…46
Lafourcade, P…… 187
Lange, C……244, 339
Legnani, G……..…… 204
Li, Q.C……..… 272
Li, Z.X……..... 106
Liu, G.F…… 106
Liu, X-J…… 172
Llibre, M……...… 187
Martin, E……...… 244
McCarthy, J.M……..… 150
McPhee, J……..… 348
Mechefske, C.K……...… 294
Merlet, J-P…….....… 2
Meschini, A……..…… 120
Mianowski, K……261
Ottaviano, E…… 98
Parenti-Castelli, V……..…215
Park, F.C……...… 178
Perez, A……..…150
Petersen, H.G……...… 86
Piedboeuf, J-C……..… 244, 339
Pierrot, F……..…… 46
Pintor, J.M……..… 12
Pirrotta, S…….. 120
Reboulet, C……...…… 187
Ros, J…..……12
Ryu, J……...… 94
Sinatra, R……...……120
Singhose, W…….....…… 112
Snyman, J.A……..……267
Sorensen, A.S……....…… 86
Spaelter, U……..……142
Steinicke, J…….....… 86
Takeda, Y……..……142
Tol, U.A……..……34
Venanzi, S……..……215
Voglewede, P.A…… 112
Wahl, F.M……..…… 224
Wang, J……....… 172
Wenger, P……...…16
Wiens, G.J……...…34
Williams, II, R.L……...… 248
Wu, Y……...… 310
Xi, F……..… 294
Xu, Z……..… 294
Yoon, J…… 94
Zabalza, I…… 12
Zheng, Y-Q……...… 287
Zsombor-Murray, P……..... 304